N81-18045

U.S. DEPARTMENT OF COMMERCE
National Technical Information Service

N81-18045

DATA BASE FOR THE PREDICTION OF AIRFRAME/PROPULSION SYSTEM INTERFERENCE EFFECTS

O.J. McMillan, et al

National Aeronautics and Space Administration
Washington, D.C.

NOV 79

(NASA-CR-152316) DATA BASE FOR THE PREDICTION OF AIRFRAME/PROPULSION SYSTEM INTERFERENCE EFFECTS Final Report, 14 Feb. 1977 - 1 Jan. 1979 (Neilsen Engineering and Research, Inc.) 435 p HC A19/MF A01

N81-18045

Unclas
G3/05 16501

1 Report No NASA CR-152316	2 Government Accession No	3 Recipient's Catalog No
4 Title and Subtitle DATA BASE FOR THE PREDICTION OF AIRFRAME/PROPULSION SYSTEM INTERFERENCE EFFECTS		5 Report Date November 1979 6 Performing Organization Code 428/C
7 Author(s) Oden J. McMillan, Edward W. Perkins, Gary D. Kuhn, and Stanley C. Perkins, Jr.		8 Performing Organization Report No NEAR TR 187
9 Performing Organization Name and Address Nielsen Engineering & Research, Inc. 510 Clyde Avenue Mountain View, CA 94043		10 Work Unit No 11 Contract or Grant No NAS2-9513
12 Sponsoring Agency Name and Address National Aeronautics and Space Administration Ames Research Center Moffett Field, CA 94035		13 Type of Report and Period Covered Final Report 2/14/77 - 6/1/79 14 Sponsoring Agency Code
15 Supplementary Notes		

16 Abstract
Results are presented from a study to define and evaluate the data base for predicting certain aerodynamic interference effects associated with airframe/propulsion system integration. The study was conducted for supersonic tactical aircraft with highly integrated jet propulsion systems, although some information is included for supersonic strategic aircraft and for transport aircraft designed for high-subsonic or low-supersonic cruise. Primary attention is paid to those interference effects which impact the external aerodynamics of the aircraft; however, information on other effects such as inlet internal performance is collected and organized, but not analyzed.

The study consisted of a literature search, the development of a framework to organize the data base (which is considered to include theoretical and empirical prediction methods as well as experimental data), and the evaluation of the state-of-the-art for three interference effects: inlet external drag, afterbody drag, and the effects of the airframe on the inlet flow field. Adequacy of prediction methods is assessed through comparison with experimental data.

17 Key Words (Suggested by Author(s)) aerodynamic characteristics fighter aircraft engine inlets engine exhaust nozzles	18 Distribution Statement Unlimited	
19 Security Classif (of this report) Unclassified	20 Security Classif (of this page) Unclassified	21 No of Pages 436

*For sale by the National Technical Information Service, Springfield, Virginia

NOTICE

THIS DOCUMENT HAS BEEN REPRODUCED FROM THE BEST COPY FURNISHED US BY THE SPONSORING AGENCY. ALTHOUGH IT IS RECOGNIZED THAT CERTAIN PORTIONS ARE ILLEGIBLE, AND PAGE 217 IS NOT AVAILABLE, IT IS BEING RELEASED IN THE INTEREST OF MAKING AVAILABLE AS MUCH INFORMATION AS POSSIBLE.

TABLE OF CONTENTS

Preceding page blank NOT FI

TABLE OF CONTENTS (Continued)

TABLE OF CONTENTS (Concluded)

DATA BASE FOR THE PREDICTION OF AIRFRAME/PROPULSION SYSTEM INTERFERENCE EFFECTS

by

Oden J. McMillan, Edward W. Perkins, Gary D. Kuhn,
and Stanley C. Perkins, Jr.
Nielsen Engineering & Research, Inc.

SUMMARY

Results are presented from a study to define and evaluate the data base for predicting certain aerodynamic interference effects associated with airframe/propulsion system integration. The study was conducted for supersonic tactical aircraft with highly integrated jet propulsion systems, although some information is included for supersonic strategic aircraft and for transport aircraft designed for high-subsonic or low-supersonic cruise. Primary attention is paid to those interference effects which impact the external aerodynamics of the aircraft; however, information on other effects such as inlet internal performance is collected and organized, but not analyzed.

The study consisted of a literature search, the development of a framework to organize the data base (which is considered to include theoretical and empirical prediction methods as well as experimental data), and the evaluation of the state-of-the-art for three interference effects: inlet external drag, afterbody drag, and the effects of the airframe on the inlet flow field. Adequacy of prediction methods is assessed through comparison with experimental data.

1. INTRODUCTION

There continues to be concern in the aircraft industry and the military services about the difficulty encountered in developing aircraft that successfully achieve the performance predicted in design studies, particularly for mixed mission aircraft with highly integrated jet propulsion systems. Part of the problem is the lack of an adequate data base for the design studies which often leads to overly optimistic performance predictions. The broad mission requirements for high performance in the subsonic, transonic, and supersonic speed ranges, at high and low altitudes, create the need for an extensive body of data for use in mission performance studies. Of particular concern is the lack of adequate theoretical or engineering methods for predicting the airframe/propulsion system interference effects even though a significant body of performance data for isolated components (wings, fuselage, engines, etc.) is available.

Multi-mission aircraft configurations characteristically require that the airframe and propulsion system be closely coupled for both structural and aerodynamic efficiency. Consequently, there are large flow interference effects which significantly affect both lift and drag and therefore cannot be ignored in performance predictions. The current practice is to define these interference effects during development testing after selection of a basic configuration. Because these interference effects are large, and in most instances adversely affect performance, the codifying of methods for predicting interference effects should help in meeting performance goals and avoiding expensive and time-consuming redesign processes.

The selection of the "best" engine for a multi-mission aircraft is a difficult and important task. Because the time required to develop and qualify an engine is the same order as that for the airframe, it is essential that the engine selection be made early in the aircraft development cycle. Selection of the most effective engine cycle parameters (i.e., compression ratio, turbine inlet temperature, bypass ratio, etc.) is usually made on the basis of mission analysis studies. These studies draw heavily upon existing performance data to establish the best trade-offs for the most effective accomplishment of the desired mission. Consequently, it is important that an adequate "data bank" of component performance and related costs be used in these studies.

This report documents a study to define and evaluate the data base for predicting certain aerodynamic interference effects associated with airframe/propulsion system integration. Primary attention has been paid to interference effects which impact in an important way the external aerodynamics of the aircraft. For the sake of completeness, data for other effects which must be considered in predicting in-flight net thrust (e.g., inlet internal performance) have been collected and organized, but no analysis of this material is attempted. As used herein, the data base is considered to include theoretical and empirical prediction methods, as well as experimental data. This study is focused on interference effects for supersonic tactical aircraft with highly integrated jet propulsion systems, although some information is included for supersonic strategic aircraft and for transport aircraft designed for high-subsonic and low-supersonic cruise. No effort has been made to fully incorporate the substantial literature available for V/STOL aircraft, and hypersonic design point aircraft are specifically excluded.

In the first phase of this study, conducted under Contract NAS2-8874, a search of the classified and unclassified literature was made to identify the pertinent data. Use was made of the available indexing services, International Aerospace Abstracts (IAA), Scientific and Technical Aerospace Abstracts (STAR and CSTAR), the Government Reports Index (GRI), and the Technical Abstract Bulletin (TAB), as well as the computerized NASA RECON system. Searches were performed by the Defense Documentation Center. Additionally, letter and personal contacts were made with government and aerospace organizations actively engaged in the areas of interest. The latest available information pertaining to the F-14, F-15, and B-1 was obtained.

Also in the first phase, a framework to organize the data base was developed, and the information assembled in the ways described above was categorized using this framework. A preliminary evaluation of the suitability for preliminary design purposes of the data bases for two interference effects was conducted. These effects, inlet external drag and afterbody drag, are areas which exert a considerable influence on aircraft performance and where a significant need for correlation exists. The work conducted under the first phase was reported in reference 8.1.*

In the second phase of the study, conducted under Contract NAS2-9513, in-depth evaluation of the state-of-the-art was conducted for three interference effects: inlet external drag, afterbody drag, and the effects of the airframe on the inlet flow field. The literature search conducted in the first phase was updated and reports newly acquired were classified using the framework from the first phase. Additionally, existing empirically based techniques to predict nozzle/afterbody drag of single and twin engine installations were developed for implementation into the aerodynamic prediction computer program being developed by the NASA/Ames Research Center. This last work, and the evaluation of these nozzle/afterbody drag prediction techniques using data from the data base, is separately reported in ref. 8.2. The present report is the final report for Contract NAS2-9513 and documents the remainder of the work conducted in the second phase. Because a considerable amount of new material was generated in this phase, this report supersedes reference 8.1.

In sections 2, 3, and 4, the entire data base is presented and categorized by the type of interference effect treated and the general nature of the treatment used in each reference. The effects of interest are broken down into two main areas: those involving inlet/airframe integration (section 2) and those involving afterbody/airframe integration (section 3). Section 4 deals with some special topics. The documents cited in this report are categorized according to which of the areas (inlet or afterbody) is treated and appear in either the inlet/airframe reference list (Appendix A) or the afterbody/airframe reference list (Appendix B). The number assigned to a report in either of these

*References identified as 8.X are listed in section 8 of this report. The references comprising the data base appear in Appendices A and B and are identified as described later.

lists corresponds approximately to the order in which the report became available to us. A combined cross-index, alphabetized by author name, is contained in Appendix C. In this report, the list to which a particular reference number pertains is clear from the context in which it appears.

The remainder of the report consists of the analysis in some depth of three areas. Section 5 presents the data base for inlet external drag in more detail and contains an evaluation of its adequacy for preliminary design. Sections 6 and 7 similarly treat afterbody drag and the effects of the airframe on the inlet flow field, respectively.

LIST OF SYMBOLS

A	area
A/A^*	contraction ratio required to bring a reference flow to sonic velocity isentropically
A_c	inlet capture area - the frontal area of an inlet, projected in the free-stream velocity vector direction; for axisymmetric inlets, the area is bounded by the cowl leading edge, for others it is bounded by the cowl leading edge, side plate leading edges and initial ramp leading edge
A_e	area at nozzle exit plane
A_m	maximum fuselage cross-sectional area
A_{MI}	maximum projected frontal area of inlet
A_{MB}	cross-sectional area at metric-break station
A_p	projected frontal area
A_{SO}	total nozzle flow area plus base area at nozzle exit station (both nozzles)
A_t	area at nozzle throat
A_W	wing reference area
$C_D, \hat{C}_D$	boattail pressure drag coefficient, based on A_m and A_p, respectively [see eq. (27)]
C_{D_A} (†)	additive drag coefficient, $D_{add}/q_\infty A_c$
$C_{D_{BL}}$	bleed drag coefficient, based on A_c
$C_{D_{BLD}}$	boundary-layer-diverter drag coefficient, based on A_c
$C_{D_{BP}}$	by-pass drag coefficient, based on A_c
$C_{D_C}, \hat{C}_{D_C}$	cowl drag coefficient based on A_c and A_{MI}, respectively (see fig. 1)
$C_{D_{CALAC}}$	CALAC predicted aft end drag [see eq. (39)]
$\hat{C}_{D_{EB}}$	equivalent body pressure drag coefficient, based on A_p

† All drag coefficients are based on q_∞ and the indicated area.

$C_{D_{EXT}}$	inlet external drag coefficient, based on A_c (see fig. 1)
C_{D_I}	inlet external drag coefficient, based on A_W
$C_{D_{INT}}$	inlet interference drag coefficient, based on A_c
$C_{D_{NADC}}$	NADC predicted aft end drag [see eq. (39)]
$C_{D_{MB}}, \hat{C}_{D_{MB}}$	boattail pressure drag coefficient based on A_{MB} and $A_{P_{MB}}$, respectively [see eq. (26)]
$C_{D_{SP}}$	side-plate drag coefficient, based on A_c
$C_{D_{SPIL}}$	spillage drag coefficient, based on A_c (see fig. 1)
C_{D_W}	total drag coefficient (pressure, friction and base drag) on aft end of airplane configuration, based on A_W
ΔC_D	jet-off to jet-on drag coefficient increment, based on A_{SO} (fig. 57)
$\Delta \hat{C}_D$	pressure drag coefficient increment used in ESIP drag correlation (see figs. 52 and 53)
$\Delta C_{D_S}, \Delta C_{D_E}$	boattail drag increments due to plume shape and entrainment, respectively, based on A_m
ΔD	drag increment from design to operating pressure ratio [CALAC subsonic correlation, eq. (26)] or from jet-off to jet-on operation [CALAC supersonic correlation, eq. (27)]
C_{LS}	lip suction coefficient, based on A_c (see fig. 1)
C_p	pressure coefficient, $(P - P_\infty)/q_\infty$
C_T	nozzle thrust coefficient, ratio of actual gross thrust to ideal thrust, F_{ID}
D	fuselage maximum diameter
D_{add}	additive drag, $\int_\infty^{\text{cowl lip}} (P - P_\infty) dA_p$
D_m	maximum fuselage equivalent diameter, $\sqrt{4A_m/\pi}$
D_{MB}	metric break equivalent diameter, $\sqrt{4A_{MB}/\pi}$
$\overline{ER}$	nozzle expansion ratio, A_e/A_t

F_{ID}	nozzle ideal gross thrust based on the isentropic expansion of actual mass flow to free-stream pressure
$\overline{FR}$	boattail fineness ratio, L_A/D_m
H	height of nonaxisymmetric nozzle cross section
$\bar{h}$	nondimensional height above cone surface (see fig. 107)
IMS	integral mean slope: area-weighted average of the rate of change of nondimensional afterbody area distribution, based on A_m [see fig. 54(b)]
IMS_T	truncated integral mean slope: IMS which is determined using a maximum allowable slope which is a function of Mach number (see fig. 53)
IMSA	integral mean slope, based on A_{MB} [see fig. 54(a)]
K_{add}	additive drag correction factor [see eq. (3)]
K_1	drag coefficient parameter used in similarity correlation of jet-off boattail pressure drag [see eq. (26)]
K_2	drag coefficient parameter - increment in drag from design pressure ratio to operating pressure ratio [see eq. (26)]
K_3	drag coefficient parameter - increment in drag from jet-off to jet-on operations [see eq. (27)]
L_A	length of afterbody
L_N	length of nozzle
LE,TE	denotes wing leading and trailing edges, respectively (see figs. 112, 113)
M	Mach number
M_L	local Mach number
M_∞	free-stream Mach number
MFR	mass flow ratio - mass flow entering the inlet ratioed to free-stream flow through A_c

LIST OF SYMBOLS (Continued)

NPR	nozzle pressure ratio - ratio of nozzle total pressure to free-stream static pressure at nozzle exit
NSPR	nozzle static pressure ratio, p_e/p_∞
P,p	static pressure
P_b	base pressure
P_e	nozzle exit static pressure
P_p/P_{p_∞}	ratio of local to free-stream pitot pressure
P_{T_L}/P_{T_∞}	ratio of local to free-stream total pressure
P_t, p_t	total pressure
q	dynamic pressure
R	maximum body radius (see fig. 88)
Re	Reynolds number
r	radial distance from body centerline
$r_{\ell e}$	radius of the cowl lip leading edge
S/D	nozzle spacing ratio - ratio of nozzle centerline to centerline distance to equivalent diameter of nozzle at exit station
T	temperature
V_∞	free-stream velocity
$\frac{v}{V_\infty}$	local sidewash velocity (see Table XV)
W	width of nonaxisymmetric nozzle cross section
$\frac{w}{V_\infty}$	local upwash velocity (see Table XV)
X	axial distance along body or afterbody
Y	lateral distance from centerline of body (see fig. 97)
Z	distance below centerline of body (see fig. 97)

α	angle of attack
$\alpha_i (i=1,11)$	covariance coefficients, used in NADC extension of CALAC afterbody drag method [see eq. (39)]
α_L	local upwash angle (see Table XV)
β	angle of sideslip; also boattail trailing edge angle
β_L	local sideslip angle (see Table XV)
γ	ratio of specific heats
ϵ_L	local total-flow angle (see fig. 88)
θ	boundary-layer momentum thickness, or circumferential angle (see fig. 88)
θ_B	mean boattail angle - mean angle over a distance corresponding to one-third of nozzle exit radius
θ_{BTM}	maximum nozzle boattail angle
μ	viscosity
ρ	density
ϕ, ϕ_2, ϕ_B	velocity potentials associated with transonic equivalence rule (see fig. 110)
ϕ_L	local roll angle (see fig. 88)

<u>Subscripts</u>

B	referring to a basic configuration
corr	pertaining to the corrected value of nozzle pressure ratio [see eq. (12)]
e	referring to the nozzle exit
eff	effective
f.e.	pertaining to fully expanded flow in a nozzle
j	referring to conditions in a jet

LIST OF SYMBOLS (Concluded)

L	pertains to local conditions
ℓ	pertaining to the cowl lip plane
MB	referring to the metric break station
m	referring to the maximum cross-sectional-area station
p	referring to projected frontal area
ref	pertaining to the reference value
t	referring to the nozzle throat station
∞	free stream

2. INLET/AIRFRAME INTERACTION EFFECTS

In Table I, reports dealing with interactions of the inlet and airframe are categorized by the specific effect they treat and by report type, as described below.

2.1 Report Types

Review Papers attempt to enhance understanding of a given effect by analyzing in depth data first presented elsewhere, assessing the coherence of data from several sources, judging the applicability of existing prediction methods by drawing comparisons with data, etc. In short, they attempt to synthesize and analyze previously available information. Primary Data Sources are reports presenting detailed experimental data. What is meant by sources of Empirical Prediction Methods and sources of Theoretical Prediction Methods is clear once the (somewhat arbitrary) distinction is made between the approaches: empirical methods are based primarily on correlations of experimental data, and theoretical methods are taken to be solutions (finite difference, method of characteristics, integral, etc.), of the appropriate equations of motion. Theoretical methods may include combinations of several methods modified by and patched together with empirical considerations when the primary emphasis is on solution of the governing flow equations.

2.2 Definition of Effects

The inlet/airframe interaction effects appearing in Table I are defined in the following outline. In general, a reference is categorized under the lowest subdivision of an effect that is appropriate. If, however, the information in a reference is not sufficiently detailed, the reference is classified under a higher order heading. For example, if drag data were taken for an inlet that had an operating boundary-layer-control system and the drag associated with this boundary-layer control was not separated from the drag associated with mass spillage around the inlet, the reference is classified as one dealing with inlet drag, not with external or boundary-layer control drag.

I. Airframe Effects on Inlet "Free-Stream" Conditions

The flow entering an installed inlet may differ from the free stream in Mach number, angularity and stagnation pressure. In general, these differences may be ascribed to:

A. Forebody effects, for close-coupled inlets mounted forward of the wing, or

B. Forebody-wing effects, for under-wing-mounted inlets in the wing's compression field. References dealing with combined forebody-wing effects on an inlet are classified in this category.

II. Inlet Drag

The drag attributable to an installed inlet operating at an arbitrary Mach number and mass flow ratio (MFR) is broken down as follows:

A. External Drag ($C_{D_{EXT}}$) is defined to be the sum of the drag on the stagnation streamline, additive drag (C_{D_A}), the drag on the external surfaces of the cowl (C_{D_C}) and for two-dimensional inlets, the drag on the external surfaces of the side plates ($C_{D_{SP}}$). C_{D_C} and $C_{D_{SP}}$ are usually taken to be integrated pressure drag although some investigators include skin friction. The relationships of these quantities with the commonly used terms spillage drag and cowl-lip suction are schematically illustrated in Figure 1 for an axisymmetric inlet (thereby avoiding the complication of the side-plate drag). Spillage drag ($C_{D_{SPIL}}$) is shown to be the change in external drag as mass flow ratio is decreased from the reference value appropriate for the Mach number in question. Cowl lip suction (C_{LS}) is the decrease in cowl drag (C_{D_C}) as the mass flow ratio is decreased from this reference value. If a reference treats any of these inter-related terms, it is classified under external drag. Exactly which drag quantity is presented is described in a later section.

B. Bypass drag is defined to be that portion of inlet drag associated with the air passing through the bypass system. A bypass system provides an alternative to spillage for engine-inlet flow matching. Bypass drag results from the momentum loss of the bypassed air and the drag of any external surfaces installed for purposes of directing the bypassed air's exhaust.

C. Boundary-layer bleed drag is defined analogously to bypass drag except it is associated with the air removed from the inlet by porous surfaces or discrete holes or slots for the purpose of boundary-layer control.

D. Interference drag is the drag increment on airframe surfaces adjacent to the inlet that is a function of inlet mass flow ratio.

E. Boundary-layer diverter drag is the drag of the device provided to prevent the boundary layer developed on upstream surfaces (forebody or wing) from entering the inlet.

III. Inlet Internal Performance

The inlet exists to provide high-quality airflow to the engine throughout the flight envelope. This function must be, of course, accomplished while maintaining acceptable levels of drag and installed weight. The measures generally used for the quality of the internal airflow are.

A. Total pressure recovery; that is, how much of the free-stream total pressure is maintained through the diffusion process to the compressor face. Recovery and the level of distortion (discussed below) are enhanced by implementation of a boundary-layer bleed system. However, any improvement must be in the proper balance with the added complexity, weight and drag such a system entails.

B. Stable mass flow range. The inlet must be capable of providing the range of mass flows demanded by the engine. The low-flow limit for an inlet is set by either an engine maximum-allowable distortion criterion or the onset of an instability known as inlet "buzz". The high-flow limit is determined by engine distortion tolerance for inlet supercritical operation.

C. Distortion. There exists several definitions of terms used to quantify the nonuniformity (both stationary and dynamic) of the airflow in the inlet at the compressor face location. This measure of inlet performance is important because an engine will typically have limits specified in terms of one or more of these criteria above which stable operation is impossible. Even below this level, engine performance may be adversely impacted by some finite amount of distortion.

IV. Inlet Lift and Moment Effects

The aerodynamic forces acting on an inlet system can result in lift, pitching, yawing, and rolling moments as well as drag. The effects considered here are:

A. Inlet lift and moments due to airflow spillage.

B. Inlet lift and moments due to bypassed air.

C. Inlet lift and moments due to boundary-layer bleed flow.

D. Interference lift and moments. Analogously to interference drag, these are the increments on surfaces adjacent to the inlet and are functions of mass flow ratio.

V. Inlet Weight

While not strictly an interaction, this effect is considered because it is an important factor to be considered in evaluating inlet concepts. Sophisticated variable geometry inlets may enjoy benefits with respect to the previously listed effects, but if the accompanying weight penalty is too severe there is no net advantage to the integrated airframe/propulsion system.

3. AFTERBODY/AIRFRAME INTERACTION EFFECTS

In Table II, reports dealing with interactions of the afterbody (including the engine exhaust nozzles) with the airframe are categorized by the specific effects they treat and by report type in a manner similar to that of the inlet/airframe interaction effects in Table I.

3.1 Report Types

The report types are Review Papers, Primary Data Sources and Empirical and Theoretical Prediction Methods as in Table I.

3.2 Definition of Effects

The afterbody/airframe interaction effects appearing in Table II are defined in the following outline. The references generally fall within one of two general categories, those applicable to single-engine configurations and those applicable to twin-engine configurations. Within those two categories the references are classified as dealing with the effects of certain specific parameters. Some parameters such as nozzle pressure ratio are common to both types of configurations.

I. Single-Engine Configurations

The afterbody effects considered for single-engine configurations are associated with the effect of various parameters on the flow field around the afterbody, including the nozzle boattails.

A. Exhaust-plume effects are effects produced by the exhaust jet plume. The shape of the plume can create upstream disturbances which affect the flow field over the afterbody. Also, the velocity in the jet being higher than that of the surroundng flow results in flow entrainment which can also alter boattail flow fields. The specific effects considered are:

1. Nozzle-pressure-ratio effects are effects produced by the exhaust jet plume that can be attributed to the nozzle pressure ratio for a specific nozzle type.

2. Exhaust-temperature effects are effects produced by the exhaust jet plume that can be attributed to the exhaust jet temperature.

3. Miscellaneous other parameters or conditions may be capable of producing exhaust-plume effects. Included in this category are various methods of simulating an exhaust plume using solid stings, normal jet simulators, and other techniques.

B. Nozzle-type effects are the effects on afterbody drag which are attributable to the type of nozzle used. Any nozzle which can provide for efficient expansion of the exhaust gases at high pressure ratio can be designed to give good performance at a specified design condition. Thus, an optimum nozzle can be chosen for that design condition. However, the merit of any particular nozzle type frequently depends upon its ability to operate efficiently at conditions other than design. This requires comparison of the relative merits of different nozzles with regard to afterbody drag, nozzle weight and complexity and overall mission requirements. Papers in this category provide information toward this comparison.

C. Base-flow effects are effects associated with the existance of a finite base area as may occur with a truncated nozzle plug or when the afterbody boattail terminates with a cross-sectional area larger than the nozzle exit area.

D. Empennage interference effects are effects produced by the alterations of the flow field around an isolated afterbody when horizontal and/or vertical stabilizer surfaces or other external supporting structure are installed. An example of such an effect is the increase in afterbody pressure drag noted in reference 46 for twin vertical stabilizers on a twin-engine configuration compared with the drag for a single vertical stabilizer on the same configuration. The single vertical stabilizer exerts less influence on the afterbody flow field due to its location on the plane of symmetry.

E. Mach-number effects are the effects of compressibility on the afterbody flow fields. References in this category are primarily those which provide specific information about the effects of compressibility on afterbody drag for complete configurations. Other references in other categories may also provide such information with regard to partial configurations.

F. Angle-of-attack effects are changes in the afterbody drag due to changes in angle of attack.

G. In this category are listed references which provide information on the effects of Reynolds number over a wide range of Reynolds number. Reynolds-number effects are important for scaling wind tunnel test results to full-scale flight speeds.

H. Boattail shape effects are effects that can be specifically attributed to the particular shape of a boattail.

II. Twin-Engine Configurations

A. Exhaust-plume effects. References for this effect are those which apply specifically to twin-engine configurations.

B. Nozzle-type effects. As for single-engine configurations, references in this category deal with the afterbody-drag effects which are attributable to the type of nozzle used.

C. Nozzle-spacing effects arise due to the mutual interference between the two nacelles/nozzles of the twin-engine afterbody.

D. Nozzle-location effects are associated with the location of the nozzle exit relative to the terminus of the fuselage interfairing on the empennage.

E. Fuselage-interfairing effects are associated with various shapes of interfairing, and the manner in which they are applied to the twin nacelle/nozzle combination.

F. Empennage interference effects are associated with horizontal and/or vertical stabilizing surfaces or other supporting structures.

G. Mach-number effects are the effects of compressibility on twin-engine configurations.

H. Angle-of-attack effects.

I. Reynolds-number effects.

J. Boattail-shape effects.

4. SPECIAL TOPICS

In surveying the literature assembled in the course of this work, a few topics emerged which are of general interest to those concerned with the subject of airframe/propulsion system interactions. References which touched on these topics are identified in this section.

4.1 Thrust-Drag Bookkeeping

To assess the net propulsive force acting on an airplane, it is necessary to account for each thrust and drag component once and only once. The failure to comply in a straightforward manner with this seemingly obvious requirement has, however, resulted in needless confusion in more than one aircraft development program. Several references are listed in Table III which discuss the necessity of this procedure and which describe detailed schemes to account for each thrust and drag item. Reports from the reference lists for Inlet/Airframe Interaction and Afterbody/Airframe Interaction are included.

4.2 Test Techniques

The development of experimental procedures to allow accurate measurement of interaction affects is discussed in several references which also appear in Table III. Sophisticated techniques are required to allow the separation of the various interaction effects while minimizing the influence of undesirable interference effects brought about by partial, subscale model testing. Scale effects, simulation of the exhaust plume in afterbody testing, and modeling viscous effects are among the topics discussed.

4.3 Wind Tunnel to Flight Comparisons

An important means of assessing the success of test techniques is the comparison of wind-tunnel data to data obtained from actual flight vehicles. However, acquisition of accurate data for interference effects is particularly difficult and expensive in flight, so there are not a large number of such comparisons. Those comparisons we have uncovered appear in Table III.

4.4 Boundary Layer Methods

Many of the prediction methods in the data base use a particular boundary layer calculation method to account for viscous effects. The boundary layer methods so used are also listed in Table III.

4.5 Inviscid Flow Methods

Methods of calculating the inviscid flow about various kinds of bodies are also listed in Table III.

5. DATA BASE FOR INLET EXTERNAL DRAG AND THE EVALUATION OF ITS ADEQUACY FOR PRELIMINARY DESIGN

As previously shown in figure 1, inlet external drag* consists of the sum of integrated cowl pressure drag and additive drag:

$$C_{D_{EXT}} = C_{D_C} + C_{D_A} \tag{1a}$$

*For a nonaxisymmetric inlet, the drag on surfaces such as sideplates is sometimes treated independently or alternatively is included as part of C_{D_C}. The latter usage is adopted here for simplicity.

This relation can be expressed in a number of alternative ways, including

$$C_{D_{EXT}} = C_{D_A} - C_{LS} + \left(C_{D_C}\right)_{ref} \tag{1b}$$

$$= \left(C_{D_A}\right)_{ref} + \left(C_{D_C}\right)_{ref} + \int_{MFR_{ref}}^{MFR} \frac{\partial C_{D_{EXT}}}{\partial (MFR)}\, d(MFR) \tag{1c}$$

$$= \left(C_{D_A}\right)_{ref} + \left(C_{D_C}\right)_{ref} + K_{add}\left[C_{D_A} - \left(C_{D_A}\right)_{ref}\right] \tag{1d}$$

by incorporating the definitions for spillage drag

$$C_{D_{SPIL}} = C_{D_{EXT}} - \left(C_{D_{EXT}}\right)_{ref} \tag{2}$$

and the K_{add} factor

$$K_{add} = \frac{C_{D_{SPIL}}}{C_{D_A} - \left(C_{D_A}\right)_{ref}} \tag{3}$$

The data base for inlet external drag consists of experimentally determined values and theoretical or empirical prediction techniques for any of the quantities in Eqs. (1-3). In the following sections, we first present the applicable experimental data and describe methods ("Partial Prediction Methods") which result in the prediction of a component of $C_{D_{EXT}}$ (e.g., C_{LS} or $\frac{\partial C_{D_{EXT}}}{\partial (MFR)}$). We then present methods which result in the predicton of the detailed flow field about an inlet ("Flow-field Methods"), thereby allowing calculation of $C_{D_{EXT}}$ by simple quadrature. The requirements placed on the data base for use in preliminary design are discussed, and finally, the data base is evaluated with respect to these requirements.

5.1 Presentation of the Data Base

5.1.1 Experimental data

The experimental data base for inlet external drag is presented in Table IV. The types of inlets and ranges of test conditions are described for each set of data. The Primary Data Sources from Table I are included which present detailed experimental data for inlet external drag or a component (for example, additive drag or cowl drag). Also included are the data sources which are listed under Inlet Drag in Table I because the data presented are not further broken down into components.

Each inlet in Table IV is described by a string of characters, some of them subscripted, which represents the main characteristics of the inlet. These descriptors, and the characteristics they represent, are listed in Table V. Absence of a particular descriptor for a given inlet means that characteristic is not applicable to that inlet, or, as in the case of the design Mach number, that it was not reported. The items in Table V are self-explanatory, with the exception of the conventions for sideplate shape. These are schematically illustrated in the following sketches of the upstream portion of two-dimensional, external-compression inlets with two fixed horizontal ramps and a design Mach number of 2.4. Note that the absence of the descriptors for a bypass system and a boundary-layer-control system implies that these systems do not exist in these inlets.

$E_r H_{2f} S_r 2.4$

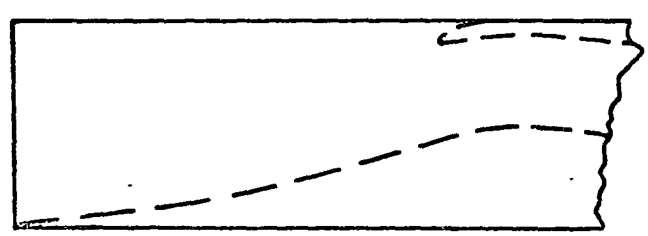

$E_rH_{2f}S_t2.4$

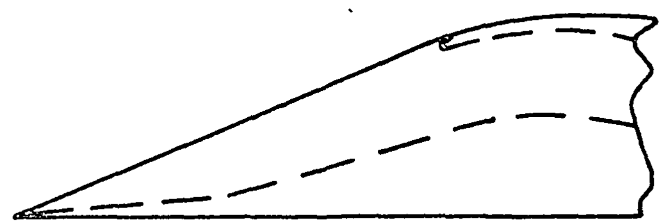

$E_rH_{2f}S_n2.4$

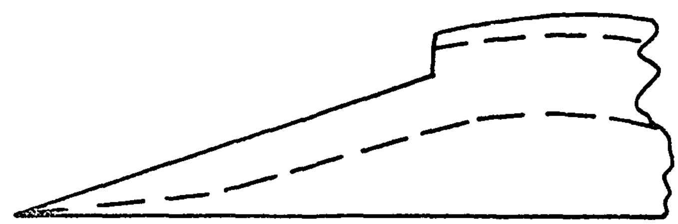

Other examples of this system are: the string $M_cC_{3v2}B_pBP2.5$ which describes an axisymmetric mixed-compression inlet with three conical external compression surfaces with two variable, a boundary-layer-control system consisting of porous elements, an operational bypass system, and a design Mach number of 2.5; and the string P_o which describes a pitot inlet whose capture area is neither circular nor rectangular.

The column in Table IV after the inlet characterization identifies the drag component(s) presented for that inlet in the reference in question. The next column shows the test configuration; that is, whether the inlet was tested alone or in the presence of a forebody, mounted on an entire fuselage, etc. Next come a series of columns containing the ranges of Mach number, unit Reynolds number, angle of attack and angle of sideslip covered for each inlet. Finally, the remaining columns show whether sufficient data exist to evaluate the separate effects of cowl shape, sideplate shape, ramp-angle or capture area variations on the drag component presented. Special circumstances are identified in the notes following Table IV.

5.1.2 Partial prediction methods

These methods, usually largely emprirical, result in predictions for one or more of the components of $C_{D_{EXT}}$ indicated in Eq. (1). Prediction methods of this type have been categorized in Table VI by the inlet type and the speed range (subsonic, transonic, supersonic) to which they apply. Inlet type in this table refers to a <u>pitot</u> inlet of either axisymmetric or two-dimensional shape, or an inlet which is either of <u>two-dimensional</u> or <u>axisymmetric</u> geometry with an external compression surface. Application of prediction methods of this class to an inlet of more complicated shape (e.g., "kidney", "chin", half-axisymmetric) must be done on an ad hoc basis; the methods are, in general, derived for the simple inlet shapes just described. In Table VI, if a reference is listed as predicting $\left[C_{D_A}\right]_{ref}$ or $\left[C_{D_C}\right]_{ref}$, then only the reference value of that quantity is predicted by the method in that reference. On the other hand, if a reference is listed as predicting C_{D_A}, then it is presumably valid at any mass flow (including the reference value).

A very brief description of some of the major features of each method shown in Table VI is contained in Table VII. For the convenience of the reader, the principal author's name is shown in parenthesis after the reference number. The information presented in Table VII does not, of course, allow for detailed understanding of the assumptions and limitations associated with each approach; for this purpose, the references themselves must be consulted. However, the general approach of each method is described, and important assumptions (such as independence of cowl lip geometry or a reference mass flow ratio of unity in lip-suction prediction methods) are shown. This allows essentially similar methods to be identified, a feature that is utilized in the comparison-to-data and evaluation processes to follow. For example, it is seen in Table VII that a number of references (21, 71, 102, 106) involve the "pitot inlet analogy", a method based on the observation made in reference 59 that for pitot inlets, if the additive drag occurring behind the normal shock for subcritical operation in a supersonic free stream is figured in a particular way, lip suction is implicitly accounted for and external drag may be predicted very simply.

It should be noted that the Partial Prediction Methods are in general derived for use at zero angles of attack and sideslip in a uniform free stream. Adaptation to more complicated situations is often required, of course, and schemes for accomplisning this exist (see, for example, ref. 4), but the approximations involved are over and above those fundamental to the methods themselves. The comparisons to data of predictions using these methods shown in a later section are largely for the case of a uniform free stream at zero angles of attack and sideslip because published comparisons have not been found for the more complicated situations.

5.1.3 Flow-field methods

A complete description of the flow field in the vicinity of the inlet is provided by these methods; external drag and its components are available by straightforward integration of the calculated pressure distribution. Methods of this type are shown in Table VIII, where in a fashion similar to Table VI, they are categorized by general approach and the geometry and speed range to which they apply. Major features of the methods are listed in Table IX.

A few general comments about these methods are in order. Firstly, we obviously have not acquired every implementation of each general approach listed in Table VIII, but it is felt that all the important general aproaches are represented. Secondly, all of the methods listed as applicable to 2-D geometries can handle non-zero angle of attack, but only two of the methods for other geometries (refs. 215 and 405) can do so. This is so because only these methods (intended for use with subsonic design-point inlets) are designed to handle a three-dimensional flow field. Calculation of three-dimensional inlet flow fields is only just beginning, and descriptions of this work are very scarce in the open literature. Finally, all of the methods except that of reference 274 are inviscid, whereas in reference 274 the inviscid streamtube curvature method is coupled to a boundary layer analysis. This is obviously an option available for use with all of the other methods, but this refinement is a separate problem not discussed in the published accounts nor in this report. Analysis of the boundary layer methods available for use in inlet calculations and an evaluation of their success is clearly beyond the scope of the present work.

5.2 Evaluation of the Adequacy of the Data Base for Preliminary Design

5.2.1 Requirements

The functional dependence of external drag on geometry and average local flow conditions can be represented as

$$C_{D_{EXT}} = f(\text{Inlet Geometry}, M_L, \alpha_L, \beta_L, Re_L, MFR) \tag{4}$$

where the specification of Inlet Geometry includes such general features as inlet type (pitot, external- or mixed-compression), inlet shape (two-dimensional, axisymmetric, quarter round, etc.), and design Mach number as well as details such as required capture area, compression surface angles, and cowl and sideplate (if applicable) external profile and leading-edge radius. Even this complicated relationship has been simplified if the inlet is located in a nonuniform flow field (caused by forebody precompression, for example) by the assumption that the external drag may be related to the average local conditions.

In the preliminary design process, external drag must be evaluated for various candidate inlet concepts, usually not defined in total detail, to allow the most promising of them to be selected for continued development in depth. The criterion for selection is some ranking in terms of overall best performance for a specified mission where drag level is traded off against internal performance, complexity and weight. To be useful for preliminary design, a data base must therefore satisfy three requirements:

1. Breadth. The range of applicability of the data or methods must be sufficiently wide to allow rational evaluation of a variety of inlet designs.

2. Ease of application. The time and expense required must be consistent with consideration of a large number of candidates.

3. Accuracy. The methods or data used must accurately reflect differences in the candidates considered.

In the following sections, the experimental data and prediction methods that exist for inlet external drag are evaluated with respect to these requirements.* First, however, a few additional remarks are in order about the level of accuracy required. Even at the preliminary design stage, exact solutions for the various effects would be useful if they were compatible with allowable levels of cost and effort. This is essentially never possible, however. The usual situation is that these constraints force the designer towards the use of methods on the other end of the scale; that is, methods that barely possess the required accuracy. It is also true that no simple, general statement of the accuracy required can be made. That is, it is not possible to say that the methods or data must be accurate to within ± X percent or ± Y drag counts. This is so because the minimum drag increment that causes a

*An exception: the accuracy of all the assembled experimental data is not evaluated.

meaningful change in airplane performance is very much a function of the detailed nature of the application (mission) considered.

Some calculations of the sensitivity of airplane performance to inlet external drag for specific applications exist in the assembled literature. References 29, 68, 94, 103, 114, and 115 address this question in different ways for various configurations of a supersonic transport. For example, in reference 114, for a supersonic transport powered by afterburning turbojet engines, a change in inlet-external-drag coefficient of 0.01 (~10 percent) results in a change in range of about 41 n.mi. (~1 percent). References 115 assesses this sensitivity for a similar application in a different way. At Mach 1.2, an increase of 0.06 (33 percent) in $C_{D_{EXT}}$ decreased the payload capacity of an SST with 3,500 n.mi. range by two passengers (~1 percent). This leverage can be considerably greater for supersonic tactical aircraft flying so-called "mixed missions" (combinations of supersonic and subsonic portions). References 2, 8, 10, 27, 29, 365, and 380 address this point. In reference 8, for example, a 30 percent increase in $C_{D_{EXT}}$ is shown to reduce mission range by about 10 percent if the drag increase occurs in a transonic portion of the mission. In reference 2, differences in $C_{D_{EXT}}$ for candidate inlet designs for such an aircraft are shown to result in differences in range of up to 200 n.mi. This magnified sensitivity is caused by the fact that the inlet drag is a considerable portion of the total airplane drag under some situations (up to 30 percent at cruise; reference 27). A similar strong dependence is demonstrated for the B-1 in reference 380. Thus, while no general statement can be made for the required accuracy of a preliminary design method, it is clear that inlet external drag exerts a powerful influence on airplane performance. If differences caused by different inlet configurations are not adequately represented, proper decisions for further development effort cannot be made.

5.2.2 Experimental data

Given the complicated functional dependence of inlet external drag on the large number of independent variables and parameters represented in Eq. (4), it is obvious that experimental treatment can never be "complete" or adequate for design in itself. All of the possible combinations of the controlling quantities cannot possibly be experimentally studied. What is required to fill in the gaps is an interpolative and extrapolative procedure. This procedure can be a simple curve-fit to data or it can consist of an assumed Taylor's series representation with the "partial derivatives" in this series being evaluated from the data. The notion of such a series expansion is simple enough to be useful only if the mixed and higher-order derivatives are negligible.

Empirically based Partial Prediction Methods are a means of interpolating in and extrapolating the existing experimental data base and are discussed in the next section. In this section, the adequacy for preliminary design of the "Taylor's series" representation is briefly reviewed. It is shown that external drag is sufficiently configuration dependent (that is, it depends on geometric detail to such a degree) that the Taylor's series representation is useful only for very limited excursions from the original data.

The experimental data base (Table IV) represents a formidable amount of information, even if those investigations where external drag is not explicitly available are excluded. However, most of the remaining investigations represent at most small perturbations around a specific design point, since they were a part of a particular airplane development program or were aimed at the optimization of a specific inlet. That is, the great majority of the references listed in Table IV report studies that are too specialized and too unsystematic to be useful as the basis for a design methodology of any generality. There do exist, however, a few serious attempts at systematic variations of the controlling quantities of sufficient scope to allow evaluation of the practicality of the "Taylor's series" approach. The investigations of references 33, 107 and the combined investigation of 52 and 108 as reviewed in 27 are useful in this regard.

The change in $C_{D_{EXT}}$ as the cowl contour is changed from some reference shape (with all other variables fixed) is one of the many "partial derivatives" that would have to be ascertained in the Taylor's series approach. Figures 2 through 4 are extracted from those references and show this dependence for the extremely simple case of a one-external-compression-surface inlet in a uniform free stream at zero angle of attack and sideslip.

Figure 2 shows the variation of $C_{D_{EXT}}$ with mass flow ratio for a two-dimensional inlet with six different sharp-leading-edge cowls at two Mach numbers. Similarly, each part of Figure 3 compares external-drag variations for two members of a family of elliptical cowls with constant leading-edge radius. These data are from reference 107 and are also for a single ramp, two-dimensional external-compression inlet. Finally, Figure 4 shows $C_{D_{EXT}}$ versus MFR for a conical and an elliptical cowl of the same leading-edge radius at three different transonic Mach numbers from reference 27 for an axisymmetric, single-cone external-compression inlet.

Examination of these figures reveals that the affect of changing cowl shape on $C_{D_{EXT}}$ is substantial and that the quantitative effect of going from one cowl to another is different in magnitude (and in some cases in sign) depending on the value of the Mach number and the mass flow ratio. Effects of other variables (e.g., angle of attack, ramp angle) on the dependence of $C_{D_{EXT}}$ on cowl shape are not shown but cannot be assumed negligible. In short, this dependence is sufficiently complicated that the simple Taylor's series approach is not useful except for very small excursions from a known data point. It follows then, that the experimental portion of the data base, taken by itself, is adequate for preliminary design purposes only if the inlets under consideration are substantially the same and are to operate in essentially the same conditions as those for which data exist.

5.2.3 Partial prediction methods

To synthesize external drag with acceptable accuracy from the parts utilized in these methods (see Eqs. (1)-(3)), each of the parts must obviously be predicted accurately (omitting the possibility of compensating errors from further consideration). While some of the elements of these methods are straightforward, the critical one is that which deals with the change in cowl drag with reduced mass flow. This element is most often treated using C_{LS} or K_{add} factors, or by means of the "pitot inlet analogy" (see Table VII). The success of these approaches will be ascertained by examination of comparison of predictions made using these methods to experimental data. (Some of these comparisons are presented here for the first time, but for the most part, we must rely on comparisons found in the assembled literature.) Additionally, the prediction of additive drag will be briefly examined.

5.2.3.1 Cowl-lip suction (C_{LS} factors)

Five of the references accumulated propose empirical correlations for this effect: 10, 11, 32, 39, and 86. The treatment in reference 86 is one-dimensional and because it is specified by the author to be inapplicable to realistic lip shapes, it is not considered further. Three of the remaining methods, 10, 11, and 39, have a reference mass flow ratio of unity. This presents special problems and these methods will be discussed together.

Methods with MFR_{ref} = 1.- Cowl lip suction in these methods is defined as

$$C_{LS} = C_{D_C}\ (MFR = 1) - C_{D_C} \tag{5}$$

In reference 10, correlations for the quantity C_{LS}/C_{D_A} are presented as a function of (local) free-stream Mach number, with C_{D_A} as a parameter. Two correlations are given, one for two-dimensional inlets, the other for axisymmetric inlets. The two-dimensional correlation is assumed to include the effects of suction on the lips of the sideplates. The data used to generate these correlations are neither identified nor shown. Implicit in this approach is the idea that inlets exhibiting the same levels of additive drag at a given Mach number will have the same C_{LS}. That is, all the dependence of C_{LS} on detailed geometry is in this method contained in C_{D_A}. A number of investigators, however, have shown that additive drag is in fact relatively insensitive to variations in cowl geometry, while the variation in cowl drag with mass flow ratio is not. Based on these considerations, one would not expect particulary good agreement of this method with data. Nonetheless, it is very convenient to apply.

This point is investigated in figure 5 by comparing C_{LS}/C_{D_A} as a function of C_{D_A} for two different Mach numbers from the correlations for two-dimensional inlets in reference 10 with data for two different cowl designs from reference 33 (uniform free stream, angle of attack = angle of sideslip = 0). These data were derived from plots of $C_{D_{EXT}}$ and C_{D_C} + $C_{D_{SP}}$ using Eqs. (1a) and (5). Agreement of the correlation with the data is seen to be poor in both level and trend. As expected, the effect of cowl geometry is clearly not adequately represented by its effect on additive drag.

In the process of reducing the data in reference 33 to the form shown in figure 5, a major disadvantage of the representation of Eq. (5) became apparent. That disadvantage is the choice of unity as the reference mass flow ratio. Because inlets with external compression surfaces cannot in general achieve MFR = 1, extrapolations of data for C_{D_C} (C_{D_C} + $C_{D_{SP}}$ for two-dimensional inlets) are required to allow evaluation of C_{LS}. The extrapolations required for one of the Mach numbers in figure 5 are shown in figure 6. The uncertainties introduced into C_{LS} by this process can be substantial, making comparisons with data extremely difficult to interpret, or to put it another way, making correlations formulated in this way inaccurate in principle.

The correlation method of reference 11 is an improvement on that of reference 10 in that the effects of two geometric quantities are explicitly included. These quantities (defined in detail in reference 11) are effective cowl lip slope and capture-area ratio. C_{LS}/C_{D_A} is given as a function of these quantities and the (local) free-stream Mach number. However, because the reference mass flow ratio is unity for this method, the preceding remarks apply here as well and comparisons with data become moot. Similar comments apply to the method of reference 39, where C_{LS}/C_{D_A} is a function of cowl lip angle, camber, leading-edge radius, local free-stream Mach number and C_{D_A}.

A Method with $MFR_{ref} \neq 1$.- The difficulties resulting from the use of a reference mass flow ratio of unity are avoided by Osmon (ref. 32). This method is applicable to two-dimensional inlets and employs curve-fits of the lip-suction data from reference 33. The independent variable is a parameter depending on mass flow ratio, throat Mach number, capture-to-throat area ratio and the contraction ratio required to decelerate a reference flow to sonic velocity isentropically (A/A*). For subsonic flows, the reference flow is at the free-stream Mach number; for supersonic flows, A/A* is evaluated at the Mach number to which the flow is assumed to expand at the end of the cowl area change. The reference value of the independent variable (where lip suction is zero) is taken to be 0.8 for all Mach numbers. For subsonic, isentropic inlet flows, this implies that the reference state is that for which the throat Mach number is approximately 0.82. No such simple statement of the reference condition can be made for supersonic flows.

The dependent variable consists of the cowl lip-suction coefficient times effective thickness-to-chord ratios for the cowl and the ramp (each ratio raised to an exponent which is a function of free-stream Mach number), times the ratio of capture area to maximum projected inlet area, also raised to a Mach-number-dependent exponent. The curves relating the dependent and independent variables are also parametized on Mach number. Bands are displayed on these mean curves to show the limits within which about 95 percent of the data from reference 33 fall. This scatter represents, among other things, the effects of different sideplate geometry which is not explicitly treated in this approach.

This method is applied to a two-dimensional inlet with three different cowls and two different sideplate shapes (ref. 107) in figure 7. The comparisons are for a single external ramp (angle = 5°) at zero angle of attack for a free-stream Mach number of 0.8. The cowl drag measurements shown were derived in a uniform free stream and are normalized on maximum projected inlet area. The data in figure 7(a) are for an elliptical cowl with a leading-edge radius which is ~1 percent of the capture height and with full rectangular sideplates (see ref. 107 for details). The reference mass flow ratio shown is calculated using the criterion in reference 32 and is in excellent agreement with the maximum mass flow ratio from the data. Cowl-drag coefficients were calculated at two mass flow ratios by the method of reference 32 by applying the lip suction from that method to the extrapolated experimental cowl-drag coefficient at the reference mass flow ratio. Note that the extrapolation required by the reference mass flow ratio of this method is of a much more reasonable extent than for the methods previously mentioned with $MFR_{ref} = 1$. The predicted cowl drag at the high mass flow ratio is in excellent agreement with the data, but this is mostly due to the fact that a very small amount of lip suction is involved and the experimental reference cowl drag was used. At the lower mass flow ratio, where there is more lip suction, the agreement is not as good. A band is shown on the predicted value, reflecting the bands on the correlation bounding ~95 percent of the data from which it was derived. At this low mass flow ratio, the correlation considerably underpredicts the lip suction.

A possible contributing factor to this underprediction is the fact that the data from reference 107 came from a model with full rectangular sideplates which would essentially eliminate sidespill, enhancing the suction effects on the cowl. Although reference 33 includes some data for full rectangular sideplates, it is not clear if those geometries are included in the correlation of reference 32 (indeed it is not clear if the correlated data is for suction on the lips of the cowl or on the lips of the cowl and sideplates). If the correlation only includes the triangular sideplate geometries of reference 33, and if it is for lip suction on the cowl only, an underprediction for lip suction would be expected for the case of figure 7(a).

A portion of this uncertainty is eliminated for the case of figure 7(b), where the data are for the same cowl as figure 7(a), but where triangular sideplates were used. Note that the lip suction prediction, which differs from that for figure 7(a) only by being applied to a different reference cowl drag, is still less than that measured, although at the low mass flow ratio the agreement is improved.

Figure 7(c) shows the agreement for a cowl of the same shape as in figure 7(a), but for an increased leading-edge radius (2 percent of the capture height). The comparison is again for the full rectangular sideplates because that is the only case for which data exist in reference 107. The agreement is essentially the same as in figure 7(a) and the same comments apply. Figure 7(d) is for a cowl with the same leading-edge radius as figure 7(c), but of different shape (although it is still elliptical, the point of tangency with the leading-edge circle is different). Agreement is improved in figure 7(d). Although the data show a considerable affect of the detailed cowl shape, the correlation does not: the lip-suction predictions for the cases of figures 7(c) and (d) are essentially the same.

5.2.3.2 The K_{add} factor

Another means of accounting for the change in cowl drag with varying MFR is the K_{add} factor. Use of this factor is advantageous if some freedom from geometric detail is gained by presentation of spillage drag data in this form; that is, if K_{add} is a correlating parameter which achieves some "collapse" of the original data into a more generalized form. Note that such generality of K_{add} would require differences in spillage drag to be reflected in additive drag, just as in the lip suction methods discussed in the previous section. If, on the other hand, a different K_{add} is required for each inlet geometry, no real advantage exists for this approach as compared to using the original spillage drag data. This point is examined using the primary source for K_{add} factors, the previously mentioned systematic investigation of reference 33.

In this investigation, K_{add} was evaluated as in Eq. (3), using experimentally determined spillage drag and the additive drag increment as calculated using the theory presented in reference 33. Data are shown at six Mach numbers for external-compression, two-dimensional, two-ramp inlets with various combinations of ramp angles, four different sideplate shapes and six cowl designs, all measured in a uniform free stream at zero angles of attack and sideslip. Some of the K_{add} factors determined are shown as functions of mass flow ratio in figures 8(a) and (b). Figure 8(a) is for an inlet with a design Mach number of 3 tested at a Mach number of 0.7. The band identified as being due to variations in cowl shapes is for identical inlet geometry except for variations in the cowl external profile. The other K_{add} curves reflect changes in second-ramp angle and sideplate shape. Figure 8(b) shows some of the same effects at Mach number of 1.3. It is clear from these figures that independence from geometric detail is not achieved. If a correlation were to be forced onto these data (e.g., by using some average K_{add} to represent all the geometries), the deviations from this mean must clearly represent sizable uncertainty in evaluating the effects of inlet drag on airplane performance for applications where spillage is at all significant in comparison to total airframe drag.

5.2.3.3 The "Pitot Inlet Analogy"

Still another way of accounting for the change in cowl drag with MFR is by means of the "pitot inlet analogy". In this analogy, inlet external drag under spilling conditions for inlets with external compression surfaces is calculated in a manner similar to the simplified treatment for spilling pitot inlets generally attributed to Fraenkel (ref. 59). Fraenkel calculated the subcritical external drag of a pitot inlet in a supersonic free stream by simply multiplying the spillage area by the pressure rise across the normal shock. This approxmation underestimates the force on the subsonic deflected streamtube (the additive drag), but in this way approximates the effect of cowl lip suction. No allowance is made for details of cowl geometry.

The application of the method of reference 59 to pitot inlets can be quite successful, as is illustrated in figure 10. This figure is taken from reference 21 and shows predictions and data at three Mach numbers from reference 59 for two pitot inlets shown in figure 9. However, examples can be found where the assumption of independence from cowl geometrical detail is inadequate. An unfavorable comparison is contained in reference 376. In this reference, substantial differences in pitot-inlet cowl lip suction at a given free stream Mach number and mass flow ratio are shown to exist which are due to differences in detailed cowl shape but which obviously cannot be reflected in the analysis.

Fraenkel's analysis has been extended to axisymmetric inlets with centerbodies in reference 71, and to two-dimensional inlets with external compression surfaces in references 21, 102, and 106. These extensions require a means of defining the terminal normal shock location as a function of the inlet mass flow ratio. This has usually been done in the manner suggested by Moeckel (ref. 72). Moeckel's method has been applied to axisymmetric inlets in references 71 and 364 and to two-dimensional inlets in references 21, 32, 81, 106, and 364 (see Table VI). In reference 81, the adequacy of several of these approaches for the estimation of normal shock locations in two-dimensional inlets is examined, and for successful prediction the need to account for side spillage is emphasized. The effect of side spillage on terminal normal shock location is included in the empirical treatment of reference 32; an approximate analytical treatment is contained in reference 81.

Results of application of the pitot inlet analogy to two-dimensional inlets are shown in figures 11-15 and to axisymmetric inlets in figure 16-18. The comparisons shown encompass varying free stream Mach number, compression-surface geometry and details of cowl and sideplate shape. The level of agreement with experimental data illustrated is variable, but in general it is surprisingly good considering the simplicity of the approach. No dependence of the level of agreement on Mach number is evident, although the poorest agreement shown [fig. 12(b)] is for the case where the Mach number is so low that the wedge shock is detached.

5.2.3.4 Additive drag

As just explained, the pitot inlet analogy deals with inlet external drag as an entity. Returning to the approach wherein the cowl and additive drag components of external drag are predicted separately, the approximate methods for additive drag listed in Table VI will now be discussed. The calculation of additive drag by integration of the pressure along the stagnation streamline is treated in the section on Flow-field Methods; however, because it is a trivial matter in a supersonic free stream for geometries that allow all shocks to be attached, this is the procedure used to calculate $C_{D_{A_{crit}}}$ in the "approximate" methods of this section. Calculation of critical additive drag in other speed ranges or in geometries with detached shocks, and calculation of subcritical C_{D_A} under all circumstances is typically done by means of a one-dimensional momentum analysis on a control volume encompassing the captured airflow extending from free-stream conditions to the cowl lip plane. Such a control volume is illustrated in the sketch below for a two-dimensional inlet operating subcriticaly in a supersonic free stream. For simplicity, viscous forces have been neglected and the inlet is shown at zero angle of attack.

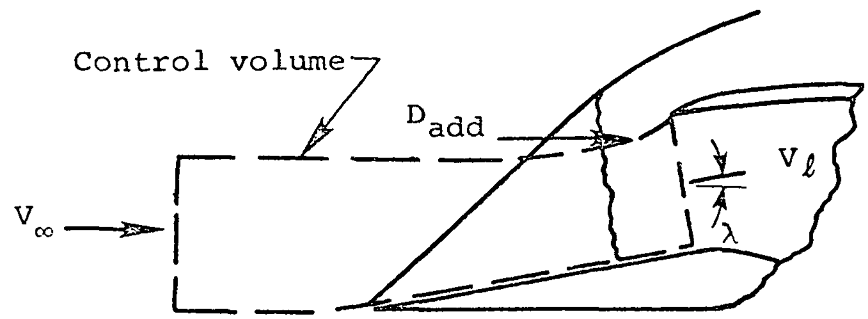

One-dimensional momentum analysis for this control volume gives

$$D_{add} = \int_\infty^\ell (P-P_\infty)dA_p = (P_\ell-P_\infty)A_\ell \cos\lambda + \int_{ramp} (P-P_\infty)dA_p$$

$$+ \rho_\infty A_\infty V_\infty (V_\ell \cos\lambda - V_\infty) \tag{6}$$

or in coefficient form,

$$C_{D_A} = \frac{(P_\ell-P_\infty)A_\ell \cos\lambda}{q_\infty A_c} + \int_{ramp} \frac{(P-P_\infty)}{q_\infty A_c} dA_p + 2(MFR)\left(\frac{V_\ell}{V_\infty} \cos\lambda - 1\right) \tag{7}$$

Calculation of C_{D_A} using this approach thus requires estimation of conditions in the cowl lip plane as well as the pressure force on the external compression surface. As is shown in this sketch, for subcritical operation of inlets with external compression surfaces in a supersonic free stream, the contribution of the integrated pressure drag of the external compression surface depends on the position of the terminal normal shock. Extimation of this position then becomes the critical item, and the methods used are those discussed previously in connection with the pitot inlet analogy.

The reported comparisons with data of additive drag predicted using the methods listed in Table VI (all for isolated inlets at zero angles of attack and sideslip, e.g., references 32, 47, 49, 90, 111, 372) tend to lead to contradictory conclusions. For example, for pitot inlets*, in references 49 and 111 it is shown that additive drag is accurately predicted using the one-dimensional momentum analysis. In reference 372, however, values calculated in this way are generally lower than the presumably more accurate values calculated using two-dimensional incompressible potential flow theory and the Lieblein-Stockman compressibility correction. Comparisons of predictions from these two theoretical approaches are shown for an axisymmetric pitot inlet over a range of subsonic free-stream Mach numbers (fig. 19). However, because no comparison with data for C_{D_A} was made in this reference, no definitive conclusions relative to the accuracy of either prediction method can be drawn.

For axisymmetric inlets with external compression surfaces, figure 20 from reference 49 shows comparisons with data of predictions for several inlets at two Mach numbers. The agreement is quite variable. These inlets had the same cowl and cone half angle, but the cone was extended by different amounts at each Mach number corresponding to three values of supercritical mass flow ratio (β in this figure). For the two-dimensional inlet shown in figure 21 the version of the momentum analysis expounded in reference 33 is shown in reference 47 to give very poor results (fig. 22). Figure 22(*a*) is for a case in which the ramp shock is detached; in reference 47 most of the disagreement is shown to be due to the ramp drag term. Measured ramp pressures are presented in reference 47 indicating a complicated viscous flow which is obviously not well

*In reference 90, an empirically derived curve is shown to adequately predict additive drag for some pitot inlets. However, no evaluation of the bounds of applicability of this method was conducted.

represented by inviscid one-dimensional theory. On the other hand, in figure 23, taken from reference 32, a momentum analysis (solid line), incorporating the normal-shock estimation procedure of reference 32 which has empirical allowance for the effects of sidespill is shown to give reasonably accurate predictions for the data from reference 33. The dashed line in that figure shows additive drag predicted using normal shock position estimated without allowance for sidespill (ref. 72) and agreement is degraded. Figure 23 and a comparison presented in reference 32 of measured normal shock position with predictions from the two methods used in figure 23 show that the sensitivity of additive drag prediction to normal shock position decreases with increasing Mach number. In spite of the success shown in figure 23 of the empirically based shock-location procedure, its applicability to geometries other than those of reference 33 (from which it was derived) is unknown.

The comparisons with data just discussed are inconclusive relative to the accuracy of the one-dimensional momentum approach to predicting C_{D_A}. There is, however, an additional consideration which reflects adversely on the potential accuracy of the method. At a given M_∞ and MFR, this method would predict the same additive drag for an axisymmetric inlet with conical centerbody of cone half-angle θ as for a two-dimensional inlet with the same throat-capture area ratio and a wedge angle of θ (excluding allowance for sidespill). However, it is well known (e.g., refs. 27 or 30) that the additive drag for two-dimensional inlets is higher than that for axisymmetric ones in this circumstance. This is due to the higher pressure force on the external compression surface caused by sharper curvature of the flow in the two-dimensional case. Inclusion of an allowance for sidespill in the prediction for a two-dimensional inlet (which lowers the predicted C_{D_A} as is shown in figure 23) does not help the situation.

5.2.4 Flow-field methods

In Table VIII, these methods have been divided into four classes: numerical solution of the unsteady Euler equations, finite-difference solution of the full potential equation, finite-difference solution of the incompressible potential equation with a compressibility correction, and the streamtube curvature approach.

By definition these methods provide a detailed description of the flow in the vicinity of the inlet, thereby allowing evaluation of all of the inlet drag terms. The price for this level of information is, of course, a computational cost that is increased substantially over that for the simple "partial" methods described earlier; in fact, in most implementations of these methods, the computational requirements are clearly in excess of what is reasonable for preliminary design purposes. In this section, a selection of the available comparisons with experimental data is presented to allow evaluation of the accuracy of the implementations of the basic approaches we have acquired. Also, to take account of the trade-off with computational costs, computer run times are given where they were reported. Because the numerical analysis and computer programming techniques used play a very important role in the implementation of flow-field methods, the accuracy and the computer cost demonstrated for a particular implementation may not apply to others of the same general approach. Thus, the conclusions drawn relative to speed and accuracy are usually applicable only to the particular implementation under discussion.

5.2.4.1 Unsteady Euler equations

In the class of flow-field methods consisting of numerical solution of the unsteady Euler equations, because of the details of the specific implementation, two of the methods are applicable only to pitot inlets in a supersonic free-stream (refs. 154, 354). In one of these, reference 154, the particular formulation of the boundary condition used resulted in numerical instabilities and insufficient accuracy to calculate pressure distributions on "thin cowls," although bow shock geometry could be predicted fairly well. Typical central processor unit (CPU) time for a converged solution is ~4 minutes on a CDC 7600 machine. In the other of these pitot-inlet methods, reference 354, fairly good agreement with an experimental cowl surface pressure distribution is demonstrated for $M_\infty = 1.14$, MFR = 0.98, and for bow-shock standoff distance for range of mass flow ratios at that Mach number using a relatively coarse computational grid. No integrated drag data are presented. For this method and grid, about 8 minutes on an IBM 370/158 is required for a converged solution.

Reference 19 presents an explicit finite-difference method of solution of the unsteady Euler equations which is valid for two-dimensional flow fields for two-dimensional or axisymmetric geometries in any speed range. The solution algorithm is briefly described, as is the formulation of the required boundary conditions and methods used to speed convergence of the solution. Interior points in the required computational mesh are automatically generated by the program from mesh coordinates specified on the boundaries. Solutions are presented and compared with data at two values of MFR for a two-dimensional three-ramp external-compression inlet at $M_\infty = 0.7$. Because the essential features of the comparison with data in both cases were the same, only one value of MFR (MFR = 0.5) will be discussed here. The geometry considered is shown in figure 24. Comparisons of calclated values with measured pressures on the ramp (fig. 25(a)), on the cowl external surface (fig. 25(b)), and on the cowl-lip internal surface (fig. 25(c)) are shown.

In these figures, good qualitative agreement is evident, but in reference 19 it is concluded that pressure level is not satisfactorily predicted. Drag computed from these pressure distributions would be considerably in error, particularly on the cowl external surface; the authors feel that improvement in this area would require a refined mesh structure. However, for the solutions shown, the full storage capacity of the available machine (a CDC 6600) was used, and approximately 5.6

hours of computer time were spent in the evolution of the flow field from the prescribed initial free-stream conditions. Although the solutions shown are not considered to be steady state (an additional 1.5 hours of computer time was estimated for full convergence), the calculated pressures are estimated to be near their final values; major improvement is felt to depend on mesh refinement.

5.2.4.2 Full potential equation

Finite-difference solution of the full potential equation is the second of the general classes of flow-field methods. These methods are valid up to free-stream speeds which result in local supersonic regions terminating in strong shocks. Various implementations of the basic approach have been made for pitot inlets and axisymmetric and two-dimensional inlets with external compression surfaces. Reference 215 is an example of an implementation of the general scheme valid for axisymmetric pitot inlets at angle of attack in a uniform subsonic free stream; note that this is one of the two flow-field methods we have acquired which can deal with a three-dimensional flow field. In reference 215, the solution method is described (including special handling of the circumferential derivatives), as are the boundary conditions and the initial field. Comparisons with measured surface Mach number are given for five pitot inlets operating in low-speed free streams ($M_\infty \lesssim .2$) at a variety of angles of attack and mass flow ratios (throat Mach numbers $\leq$ 0.86: at 0.86, the inlet was observed to be choked). Very good agreement with the data is demonstrated. No integrated drags were calculated. Typical run times for a converged solution are from 12 to 15 minutes on a CDC 6600 computer.

Another implementation of this class of methods is that of reference 37. The same implementation is also described in reference 52. This version allows solution of two-dimensional flow fields for inlets of either two-dimensional or axisymmetric geometry with external compression surfaces. The method is applied to two-dimensional inlets and is compared to data in references 63 and 224. Examples of these comparisons are given in figure 26 which is reproduced from reference 63. In this figure, fair agreement is shown for the drag slope but poor agreement is achieved for drag level. In reference 63, the disagreement is attributed to the existence of three-dimensional effects and shocks, and to inadequate grid resolution in the computation in regions of high gradients. Application of this technique to an axisymmetric inlet is shown in figure 27, taken from reference 37. Here, the level of $C_{D_{EXT}}$ has been adjusted by calculating additive drag using momentum analysis on the entering streamtube and replacing the stream thrusts generated by the method with one-dimensional values. The approach more typical in flow-field methods of integrating the pressure distribution on the stagnation streamline leads to erroneous C_{D_A} in this implementation. The discrepancy in level of additive drag observed here is claimed not to exist in the calculation for two-dimensional geometries. However, in the analysis of two-dimensional inlets, a problem with mass conservation in the calculation is indicated. This problem is obviously attributable to this specific implementation of the potential-equation method. That is, it is not a general characteristic of this class. However, because the implementation described in references 37 and 52 is the only application of the full potential equation to inlets with external compression surfaces we have been able to discover in the published literature, it is not clear whether the problem with additive drag level described above is a general one. Computational run times on the order of 15 seconds on a CDC 6400 computer are claimed.

5.2.4.3 Incompressible potential equation with compressibility correction

The third general class of method appearing in Table VIII is the solution of the incompressible potential equation with a compressibility correction. One implementation of this method we have acquired is described in reference 52, where the Douglas Neumann incompressible flow program (refs. 8.4-8.6) is coupled with either the

Prandtl-Glauert, Kármán-Tsein, Laitone, or Krahn compressibility correction. The method is applied to two-dimensional and axisymmetric inlets with centerbodies; in ref. 52, surface pressures on the cowl and centerbody are compared to data at $M_\infty = 0.7$, 0.9 and several mass flow ratios for the axisymmetric inlet shown schematically in figure 27. No integrated values of drag are given. The calculated pressure coefficients agree best using the Laitone correction.

The other implementation of the class of methods shown in Table VIII is that of reference 405. This is the second of the two Flow-field Methods we have acquired which can deal with a three-dimensional flow field. In this approach, the incompressible flow about a pitot inlet with or without a centerbody is solved using a panel method. Solutions for unit onset flows parallel to each of the coordinate axes are combined with a solution for static operation to result in a rigorous incompressible solution for an inlet at arbitrary angles of attack and yaw with arbitrary mass flow rate. Compressibility is accounted for by applying the Lieblein-Stockman correction (ref. 8.7). The method is applicable for subsonic free streams, but local regions of the flow may be supersonic although they should be shock-free. The geometry may be three-dimensional but it must exhibit a plane of symmetry. In reference 405, the method is applied to a subsonic-design-point axisymmetric pitot inlet at 75° angle of attack in a situation where the throat Mach number is 0.603 (the free stream velocity is not reported). Excellent agreement with data is shown for pressures on the internal and external cowl surfaces. Drag is not calculated. It is observed in reference 405 that panel methods usually require considerably less computer time than finite-difference methods; the superposition technique and compressibility correction used also lead to computational efficiency. Thus, it is claimed that the method of reference 405 is faster than a finite-difference method by two orders of magnitude.

5.2.4.4 Streamtube curvature analysis

The final general class of methods uses streamtube curvature (STC) analysis. This approach, as explained in reference 274, basically uses one-dimensional compressible flow analysis in a number of adjacent streamtubes; when taken together the entire flow field is simulated. Streamline positions are refined iteratively; in each iteration the momentum equation normal to the streamlines is integrated using calculated values of streamline curvature to obtain velocity, and the continuity equation is used to define a new streamline position. The iterative process is continued until streamline movement is less than a specified amount.

A characteristic of streamtube curvature methods, as discussed in reference 239, is that the method is extremaly sensitive to input geometry. As stated therein, "The difference between an aborted run and a successful run is usually a minute change in the geometric data." This extreme sensitivity is due to the need to calculate surface curvatures from input geometry and can make the method very troublesome to use. In reference 274, the method is applied to the pitot inlet shown in figure 28 for several Mach numbers and mass flow ratios. Calculated results accounting for viscous effects by means of the integral boundary layer method of Stratford and Beavers (ref. 8.8) are included. Sample comparisons with data from three circumferential positions identified in ref. 274 as "NASA-Langley Data, ATT Nacelle Inlet Test, 16 Foot Transonic Tunnel" are shown in figure 29. In figure 29(a), a fully subsonic case is shown and excellent agreement is obtained. At a higher value of free-stream Mach number, figure 29(b), increasing the number of grid points in the STC solution led to local oscillations in the inviscid solution which were claimed to be eliminated in the physical situation by "viscous effects". At a still higher Mach number, figure 29(c), predictions are included done with the boundary layer analysis (labeled STC-SAB) and without it (labeled STC). It is seen that neither one is in agreement with the data; separation over the initial portion of the cowl lip was observed experimentally at this condition, and the integral boundary layer method is inadequate in this situation. Cowl drag forces integrated from the predictions and data of figures 29(a), (b), and (c) are in reasonably good agreement (within .01 for $\hat{C}_{D_C}$), but at least in the case of figure 29(c), this must be attributable to compensating errors.

In reference 239, application of the streamtube curvature method to the B-1 external-compression inlet shown in figure 30 is made for free-stream Mach numbers of 0.7 and 0.85 for values of MFR of 0.55 and 0.75 and several positions of the variable ramps. Sample comparisons with data are shown in figures 31-33. All of these figures are for the ramp positions $R_B = 7.2°$, $H_L = 27.3$ and are for $M_\infty = 0.85$. Figure 31 shows the ramp and cowl pressures for MFR = 0.55, while figure 32 is for MFR = 0.75. Additive drag over a range of mass flow ratios is shown in figure 33 for this Mach number and geometry. The experimental data were obtained for an inlet mounted on a fuselage and stub wing assembly. Allowance for the angularity of the local inlet flow field was made by running the STC program using various incidence angles and selecting the incidence at each value of M_∞ that gave best agreement with the measured ramp pressures. Reasonable values of flow incidence resulted from this procedure and the agreement for ramp pressures in figures 31(a) and 32(a) is fairly good. Calculated cowl pressures agree poorly with the measurements, as shown in figures 31(b) and 32(b). This poor agreement is likely due to some combination of inadequate grid resolution and viscous effects, but further work would be required to ascertain this. However, additive drag is predicted with reasonable accuracy, as seen in figure 33; this positive result is possible because of the high degree of two-dimensionality of the inlet flow field indicated by the transverse taps in figures 31 and 32.

5.2.5 Concluding remarks

An evaluation of the adequacy for preliminary design (based on completeness, ease of application, and accuracy) of the data base for inlet external drag has revealed:

1. The sensitivity of airplane performance to inlet external drag is a strong function of the airplane's mission. Therefore, the required accuracy for preliminary design methods cannot be stated in general. However, *for aircraft with mixed missions, inlet external* drag exerts a powerful influence on the aircraft's performance and accurate predictions are required to allow for rational configuration definition.

2. Although a few systematic studies exist, the experimental data portion of the data base consists mostly of specialized studies of particular inlets. Because inlet external drag depends in an important way on geometrical details, this portion of the data base is adequate for prediction only for inlets not substantially different than those previously tested.

3. Calculation of cowl lip suction by methods with a reference mass flow ratio of unity are inaccurate because of the large extrapolation of data usually entailed.

4. Values of lip suction as calculated from the correlation of reference 32 for inlets reasonably similar to those from which the correlation was derived are in only fair agreement with data at low mass flow ratios. Because of its formulation, this method cannot predict experimentally demonstrated differences in lip suction resulting from changes in detailed cowl shape.

5. The K_{add} factor does not exhibit freedom from geometric detail. Its use is equivalent to using the original experimental data.

6. Use of the "pitot inlet analogy" to predict $C_{D_{EXT}}$ in a supersonic free stream leads to variable agreement with measurements (figs. 11-18). In this method, $C_{D_{EXT}}$ is again assumed to be independent of detailed cowl lip shape.

7. Prediction of additive drag using a one-dimensional momentum analysis leads to acceptable agreement with data only for the simplest possible configuration, i.e., a pitot inlet. Predictions in other situations are in general poor, although methods containing additional empiricism (e.g., for normal shock location) can give reasonable agreement in limited classes of geometries.

8. Some of the Flow-field Methods discussed herein can yield adequate results although the comparisons with data available do not allow for comprehensive evaluation of their limits of applicability. For those methods applicable to supersonic design-point inlets, the large computers and long run times required to achieve satisfactory agreement result in their being of limited usefulness for preliminary design.

6. DATA BASE FOR AFTERBODY DRAG AND THE EVALUATION OF ITS ADEQUACY FOR PRELIMINARY DESIGN

In this section, the part of the airframe/propulsion system interaction data base that is associated with afterbody drag is evaluated. Other aerodynamic interference effects associated with the afterbody will not be considered in detail in this report.

6.1 Requirements for Drag Prediction

The functional dependence of afterbody drag can be represented as

$$C_{D_{AB}} = f(\text{Afterbody Geometry},\ M_\infty,\ NPR,\ Re,\ \alpha) \tag{8}$$

where the specification of Afterbody Geometry includes such features as number of engines, interfairing type, engine nacelle spacing, empennage type and nozzle type. This relationship includes complex interaction effects due to the interference flow fields of the various constituents of the afterbody/airframe system as well as exhaust plume shape and entrainment effects. The total afterbody drag of a twin-engine fighter model can amount to 40 to 45 percent of overall zero-lift vehicle drag even though the afterbody portion of the vehicle may comprise only one-third of the total wetted area.

In the preliminary design process, this relationship must be evaluated for various candidate configurations to allow the most promising of them to be selected for development. To be useful for preliminary design, the afterbody/airframe data base must satisfy the same three requirements as for inlets, namely:

1. Breadth
2. Ease of application
3. Accuracy

In the following sections, the experimental data and prediction methods that exist for afterbody/drag are evaluated with respect to these requirements. Empirical prediction methods are generally found to be the easiest to apply but may be quite limited in the requirements of breadth and accuracy. Theoretical methods are more difficult to apply, may require costly computer time, and generally also suffer from lack of breadth and accuracy.

With regard to the accuracy required, it is clear that in a complex system such as a high performance fighter, the errors associated with each constituent of the overall system must be kept as small as possible. The general remarks made previously with regard to inlet external drag apply to the afterbody drag problem as well. That is, no simple general statement of the accuracy required can be made. The minimum drag increment that can be allowed is a function of the detailed nature of the mission considered.

Sensitivity of aircraft range to errors in predicted drag has already been discussed in section 5. The same considerations apply with regard to afterbodies since the afterbody drag can be a significant percentage of the total vehicle drag.

6.2 Empirical Prediction Methods

6.2.1 Single-engine configurations

The only comprehensive empirical method for single engine configurations is the Afterbody Drag Approximation Procedure (ADAP) of Bergman, et al., described in references 6, and 254-256. The method was adapted for use on a CDC 7600 computer by Kuhn (ref. 307). The ADAP calculates pressure drag for axisymmetric or non-axisymmetric (2-D) afterbody/nozzle configurations. The program is based on data correlations presented in references 254 and 255 for isolated bodies (no wing, tail, or 3-D fuselage effects) at subsonic speeds (Mach number less than approxmately 0.9) and, for purely axisymmetric configurations, at supersonic speeds (Mach numbers from 1.0 to 1.8). Base drag and friction drag are not included in the correlations.

6.2.1.1 Input parameters

The process of selecting geometric and flow-field parameters was described in reference 254. Because the intended use of the parameters was to relate experimental data, rather than for generating analytical solutions, they were selected to be somewhat generally descriptive instead of being extremely precise. Also, the input parameters were derived to be easily determined for a practical drag prediction procedure for preliminary design. The procedure applies to pressure drag only. Friction drag can be predicted separately and added to the pressure drag.

Geometric parameters.- Fuselage/nozzle afterbody geometry is described by non-dimensional parameters. The forebody is assumed to be a constant-area section extending upstream from the afterbody's maximum area. Afterbody geometry is simplified to the extent that protuberances such as horizontal and vertical tails are not included. Specifically, the type of afterbodies considered are those having smoothly contoured surfaces (no sharp corners) and negligible base areas (nozzle with thin trailing edges). The geometric parameters used in the ADAP are illustrated in figure 34. Note that fineness ratio and external area ratio (closure ratio) are used to define the afterbody rather than a detailed description of the surface contours. This approach was taken because it was found that smoothly contoured boattails such as those with circular arc or parabolic shapes exhibit roughly identical drag characteristics at subsonic Mach numbers. In contrast, contours having high slopes at the forebody/afterbody junction, such as conical afterbodies, usually create abnormally high drag levels and early drag rise. Such contours are excluded from the afterbodies used in the ADAP correlations.

Another geometric parameter that is related to afterbody drag is the nozzle expansion ratio. That parameter determines the exit flow Mach number and has a significant influence on the shape of the exhaust plume.

In summary, the geometric parameters required as input to the ADAP are as follows:

1. Fineness ratio, $L_A/D_m = \overline{FR}$
2. Nozzle expansion ratio, $A_e/A_t = \overline{ER}$
3. Boattail closure ratio, A_e/A_m

Flow-field parameters.- In addition to free-stream Mach number and Reynolds number, a parameter that has been found to be important in describing nozzle flow fields is the nozzle pressure ratio, defined as the exhaust-stream total pressure divided by the free stream static pressure. Another parameter that is useful in describing plume conditions is the ratio of exhaust-stream static pressure, at the nozzle exit, to the free-stream static pressure. This parameter can be derived from the nozzle pressure ratio, nozzle geometry and free-stream Mach number, and so is not an independent parameter.

The influence of Reynolds number on boattail drag has not been completely determined for bodies of the type used in the ADAP correlations. For the data used in the derivation of the ADAP, Reynolds number was not a significant parameter. Consequently, Reynolds number is not included in the input.

The flow field parameters required for input are:

1. Free-stream Mach number, M_∞
2. Nozzle pressure ratio, NPR, p_{t_j}/p_∞
3. Ratio of specific heats of the exhaust, γ

Additional parameters for two-dimensional nozzles.- The effect of non-axisymmetric nozzles was accounted for by assuming the maximum cross-sectional area is square and that two-dimensional effects are important only when the exit plane geometry is not square. The important parameters for two-dimensional nozzles are then:

1. Height ratio of nozzle, H_e/H_m
2. Width ratio of nozzle, W_e/W_m

6.2.1.2 Data correlation technique

Afterbody drag can be represented as a basic drag characteristic of the afterbody itself, plus the effects of exhaust plume interference. A jet-effects analysis conducted by General Dynamics resulted in the development of a methodology of dividing jet effects into components of plume-shape effects and entrainment effects. A more detailed account of the jet-effects analysis is found in reference 6. A pictorial description of the drag components is presented in figure 35. Notice that basic afterbody drag is defined as the drag which occurs if a semi-infinite cylinder extends downstream of the nozzle in place of a true plume.

For subsonic free-stream flow, jet-on afterbody drag was found to approximate basic drag (drag with a cylinder in place of a jet) when the plume's theoretical (1-D) fully-expanded area is roughly 9% larger (averaged value) than the nozzle exit area; that is, when nozzle flow is underexpanded by this amount. Examples of this phenomenon from references 6 and 46 are shown in figure 36. Therefore, at NPR conditions producing this amount of underexpansion, plume entrainment effect is equal in magnitude but opposite in sense to plume shape effect. Also, it can be assumed that entrainment effects are negligible when the plume momentum per unit area equals that of the free stream. For example, for an unheated plume, zero entrainment effect occurs when the NPR equals the free-stream total-to-static pressure ratio, that is when the Mach numbers of the jet and the free stream are equal. Although this low-NPR situation is unlike nozzle operation in flight, nozzle test data are sometimes taken at this condition.

For supersonic free-stream conditions, reference 256 points out that the plume underexpansion percentage is a function of afterbody/nozzle geometry. As a result, basic drag curves for supersonic flows were derived from a schedule defining the necessary plume expansion (in terms of nozzle pressure ratio, NPR_B) to approximate basic drag for different boattail geometries (fig. 37).

Basic afterbody drag can be predicted via configurations actually having long cylinders in place of plumes or by using the average 9 percent expanded-area criteria for subsonic flow or the appropriate expansion for supersonic flow. Plume entrainment effects were determined by measuring boattail drag with a solid, plume-shaped extension attached and then comparing the drag to the drag without the extension, but with the actual pressurized exhaust in its place. For supersonic flow, it was assumed that entrainment occurred at choked flow (NPR ≈ 2, $M_e = 1$ for a convergent nozzle) because of subsonic fow in the boundary layer being accelerated by the supersonic flow in the exhaust jet. Shape effects were assumed to occur when plume billowing began, that is, at NPR's greater than that required for fully expanded nozzle flow.

Therefore, given afterbody drag values for various geometry/flow field conditions, basic drags (C_{D_B}) and plume entrainment effects (ΔC_{D_E}) were determined (refs. 255 and 256). Accordingly, the equation

$$C_{D_{AB}} = C_{D_B} + \Delta C_{D_S} + \Delta C_{D_E} \tag{9}$$

presented in figure 35, was solved for ΔC_{D_S}, having determined the remaining terms. These drag components were then correlated such that their respective values for fuselage/nozzle geometry in general could be systematically predicted.

Basic afterbody drag.- The drag of smoothly contoured afterbodies (e.g., circular arc, parabolic) with cylinders in place of exhaust plumes was correlated by the use of fineness ratio and boattail closure ratio parameters. Typical correlations of basic afterbody drag are presented in figure 38. Reynolds-number effects on pressure drag coefficient are normally negligible at free-stream Mach numbers below drag rise (Mach numbers less than approximately 0.85) for turbulent boundary layers and smoothly contoured afterbodies--the situation being analyzed. Thus the drag coefficients presented are applicable to Reynolds numbers associated with turbulent boundary layer conditions.

Plume shape effect.- The maximum cross-sectional area to which an exhaust plume expands is a predominant factor influencing the plume interference effects on afterbody drag. External plume expansion will vary not only with nozzle pressure ratio, but also with nozzle internal area ratio. Unfortunately, the majority of available test data at subsonic Mach numbers are for afterbodies with convergent nozzles or only slightly convergent-divergent nozzles (i.e., $A_e/A_t \approx 1$). Therefore, generalized drag predictions for afterbodies with convergent-divergent nozzles were handled in a unique manner; in particular, the method used in the ADAP analysis was to transform the afterbodies with convergent-divergent nozzles into equivalent-drag afterbodies with convergent nozzles so that relatively abundant convergent nozzle data could be used. Specifically, an afterbody with a convergent-divergent nozzle is converted into an afterbody with a convergent nozzle which has an identical afterbody external shape and an identical plume external expansion. This approach is illustrated if figure 39. This necessitates that a "corrected", rather than true, nozzle static pressure ratio, p_j/p_∞, (NSPR) be used when analyzing the afterbody drag with a convergent-divergent nozzle. Corrected NSPR is that NSPR at which a convergent nozzle must operate to produce a plume with a maximum free-expansion area identical to that of the convergent-divergent nozzle in question. Note That the theoretical full-expansion area (from isentropic flow tables) is used as a quasi-average representation of the periodic behavior of the plume. Examples of the transformation from actual NSPR to corrected NSPR are given in figure 40.

The correlation of plume shape effect is presented in figure 41. As shown in these curves, a corrected NSPR equal to unity (i.e., no external expansion of the plume) produces no effect on basic drag. Basic drag can be described as the drag of an afterbody having a pseudo, cylindrically shaped nonentraining plume. The plume billows beyond the diameter of the nozzle exit at values of corrected NSPR greater than 1 and creates a drag-reducing effect.

Plume entrainment effect.- Plume entrainment, like flow separation, is a result of viscosity. Entrainment occurs because of the momentum differential between the plume and the external flow. The exhaust plume, having more momentum per unit area than the free stream entrains external flow.

The majority of subsonic test data used in the correlations pertain to free-stream Mach number between 0.4 and 0.85. However, more emphasis was placed on correlating the Mach 0.85 data since this is more representative of typical subsonic cruise conditions. The entrainment correlation is based on a jet momentum ratio given by

$$\theta = \frac{(\rho V^2)_e}{(\rho V^2)_\infty} = \frac{(\gamma p M^2)_e}{(\gamma p M^2)_\infty} \tag{10}$$

from which

$$\theta_{corr} = NSPR_{corr} \left(\frac{\gamma_e}{\gamma_\infty}\right)\left(\frac{M_{e_{ref}}}{M_{\infty_{ref}}}\right)^2 \frac{\left[1 + \frac{M-M_{ref}}{M_{ref}}\right]_e^2}{\left[1 + \frac{M-M_{ref}}{M_{ref}}\right]_\infty^2} \tag{11}$$

where $M_{e_{ref}} = 1$ and $M_{\infty_{ref}} = 0.85$

Thus,

$$\theta_{corr} = 1.384\ NSPR_{corr} \left(\frac{\gamma_e}{\gamma_\infty}\right)\left[\frac{1 + (M_e-1)^2}{1 - (1.176 M_\infty - 1)^2}\right] \tag{12}$$

The correlation of jet entrainment effects via the θ_{corr} momentum parameter is shown in figure 42. As expected, momentum ratios greater than unity produce a drag-increasing effect due to viscous pumping.

6.2.1.3 Calculation procedure for pressure drag on axisymmetric bodies

Equations used.- From the input quantities discussed in the previous section, the computer program calculates two parameters to obtain the plume shape and entrainment effects. These parameters are $NSPR_{corr}$, an effective nozzle static pressure ratio, and θ, the jet momentum ratio. NSPR is the nozzle static pressure ratio, as defined previously. $NSPR_{corr}$ is that NSPR at which a convergent nozzle must operate to produce a plume with a theoretical, maximum-free-expansion area, $(A_j)_{f.e.}$ identical to that of the convergent-divergent nozzle in question. The momentum ratio, θ, is the jet-momentum at the exit divided by the free stream momentum.

The calculation of $NSPR_{corr}$ is done in four steps by the ADAP procedure:

1. Knowing NPR, calculate correspondng $(A_j)_{f.e.}/A_t$.
2. Divide $(A_j)_{f.e.}/A_t$ by the expansion ratio, A_e/A_t.
3. Knowing $(A_j)_{f.e.}/A_e$, which is an area ratio, calculate corresponding p/p_t, the reciprocal of which is NPR_{corr}.
4. Multiply NPR_{corr} by p/p_t at $M_e = 1$ (convergent nozzle case) to obtain $NSPR_{corr}$.

The user inputs the expansion ratio, the nozzle pressure ratio, and γ into the ADAP, and the program internally performs these steps. The first step, from the Mach functions, is

$$\frac{(A_j)_{f.e.}}{A_t} = \frac{1}{\sqrt{\left(\frac{2}{\gamma-1}\right)\left(NPR^{\frac{\gamma-1}{\gamma}} - 1\right)}}\left[\frac{2}{\gamma+1}\left(NPR^{\frac{\gamma-1}{\gamma}}\right)\right]^{\frac{\gamma+1}{2(\gamma-1)}} \tag{13}$$

When considered relative to the nozzle exit station, this potential expansion is combined with the internal expansion ratio, thus yielding a relative expansion ratio defined by

$$\frac{(A_j)_{f.e.}}{A_e} = \frac{(A_j)_{f.e.}}{A_t} \bigg/ \frac{A_e}{A_t} \tag{14}$$

This parameter implies that a relative or corrected nozzle pressure ratio is needed to describe external plume expansion. This NPR_{corr} is the p_t/p that corresponds to the $(A_j)_{f.e.}/A_e$.

Mathematically, no closed-form solution exists for calculating a pressure ratio when given an area ratio. ADAP uses the Newton-Raphson method to find NPR_{corr} from the relations

$$f = \left(\frac{2}{\gamma+1}\right)^{\frac{\gamma+1}{\gamma-1}} \left(\frac{p_t}{p}\right)^{\frac{\gamma+1}{\gamma}} - \left(\frac{2}{\gamma-1}\right)\left(\frac{A_j}{A_e}\right)^2 \left(\frac{p_t}{p}\right)^{\frac{\gamma-1}{\gamma}} + \left(\frac{2}{\gamma-1}\right)\left(\frac{A_j}{A_e}\right)^2 \tag{15}$$

$$\frac{df}{d\left(\frac{p_t}{p}\right)} = f' = \left(\frac{2}{\gamma+1}\right)^{\frac{\gamma+1}{\gamma-1}} \left(\frac{\gamma+1}{\gamma}\right)\left(\frac{p_t}{p}\right)^{\frac{1}{\gamma}} - \left(\frac{2}{\gamma}\right)\left(\frac{A_j}{A_e}\right)^2 \left(\frac{p_t}{p}\right)^{-\frac{1}{\gamma}} \tag{16}$$

and the proper value of p_t/p is that value which causes $f(p_t/p) = 0$. $NSPR_{corr}$ is then found from

$$NSPR_{corr} = \frac{p_t}{p}\left[1 + \frac{\gamma-1}{\gamma}\right]^{\frac{\gamma}{1-\gamma}} \tag{17}$$

The momentum ratio, θ, is then calculated from

$$\theta = 1.384 \; (NSPR_{corr}) \; \frac{\gamma}{1.4} \left[\frac{1 + (M_e - 1)^2}{1 - (1.176 \; M_\infty - 1)^2} \right] \tag{18}$$

In the above equation, all of the variables, except M_e, are known. For ADAP, the exit Mach number is a function of expansion ratio and γ. Since there is no closed-form solution for Mach number given an expansion (area) ratio, the Newton-Raphson iterative technique is used to find M_e, where:

$$f = \left[\frac{2}{\gamma+1} + \frac{\gamma-1}{\gamma+1} M_e^2 \right]^{\frac{\gamma-1}{2(\gamma-1)}} - \left(\frac{A_e}{A_t} \right) M_e \tag{19}$$

$$\frac{df}{d(M_e)} = f' = M_e \left[\frac{2}{\gamma+1} + \frac{\gamma-1}{\gamma+1} M_e^2 \right]^{\frac{3-\gamma}{2(\gamma-1)}} - \frac{A_e}{A_t} \tag{20}$$

When f converges to 0, M_e is found. The momentum ratio, θ, is then calculated from Eq. (18).

Method of interpolation.- In the computational technique described in references 254, 255, 256, and 307, there are 174 parametric curves that define values necessary for computing the three drag components (basic pressure drag and the two corrections for plume shape and entrainment) of the axisymmetric afterbody/nozzle pressure drag. For the basic afterbody drag curves, for subsonic flows, 20 control points (points from ref. 354 curves, fig. 38) are used to define each curve. For the supersonic basic drag curves, the plume-shape-effect, and the plume-entrainment-effect curves, 6 control points are used for each curve (figs. 38(b), 41, and 42).

The appropriate data arrays containing control points necessary to describe specific curves for corresponding $NSPR_{corr}$ and θ at given $\overline{FR}$ are used during program execution. The 20 or 6 control points (depending on which curve type is called) are mathematically interpolated (curve-fit) with a 3rd-order, continuous-1st-and-2nd-derivative, natural-spline-function subroutine. When the control points are curve-fit, evaluation at any coordinate on the curve is available. For the interpolation between $NSPR_{corr}$, $\overline{FR}$, and θ curves, a linear interpolation is used.

An example is shown for illustration. For the case of $\overline{FR}$ = 2.3, A_e/A_m = .53, NPR = 6, $\overline{ER}$ = 1.1, and γ = 1.4, the plume shape effect is to be determined. The program would calculate $NSPR_{corr}$ = 2.6 and obtain the data arrays containing control points describing $NSPR_{corr}$ for $NSPR_{corr}$ = 2 and 3 at $\overline{FR}$ = 2 (see fig. 43). Then the spline-functions subroutine would evaluate ΔC_{D_S} at $NSPR_{corr}$ = 2 and 3 at A_e/A_m = .53. The program would then interpolate the plume-shape drag increment for $NSPR_{corr}$ = 2.6 from these two values. The above process would be repeated for the $\overline{FR}$ = 2.5 points. Once values at both $\overline{FR}$'s ($\overline{FR}$ = 2 and $\overline{FR}$ = 2.5) are calculated, linear interpolation can be used to produce the plume shape increment, ΔC_{D_S} at $\overline{FR}$ = 2.3.

To calculate the plume entrainment effect, the program would use the momentum ratio, θ as the correlating parameter (instead of $NSPR_{corr}$) and follow the same procedure.

6.2.1.4 Calculation procedure for subsonic pressure drag on non-axisymmetric bodies

Only a limited amount of data is presently available with regard to drag on non-axisymmetric nozzles. Consequently, there is great difficulty in defining an accurate generalized correlation of 2-D effects.

Published and unpublished test data from Pratt and Whitney Aircraft's isolated parametric 2-D nozzle tests (ref. 249) were incorporated by General Dynamics as the primary data source. These data, to be discussed in the following section, were employed in reference 255 to define relationships between axisymmetric and nonaxisymmetric nozzles that are used to calculate the 2-D nozzle pressure drag.

Experimental data.- Experimental data used to develop the correlation are shown in figure 44. The geometry is representative of single-engine installation, i.e., square at the forebody's maximum cross-sectional area. At the exit plane, the width is the same as the width at the afterbody maximum cross section (no side boattailing). Height at the exit plane is one-fourth the height at the maximum cross section. Therefore, the nozzle exit plane forms a 4:1 rectangle. The P&WA data was originally in the form of drag coefficients referenced to aft-facing projected area vs terminal boattail angles. The ADAP program calculates drag coefficients referenced to maximum cross-sectional area and calls for fineness and area ratios rather than boattail angles as the input quantities. Therefore, a conversion of $C_{D_{A_p}}$ to $C_{D_{A_m}}$, as well as D_e/D_m and boattail trailing edge angle, β to A_e/A_m and $\overline{FR}$ was performed using the following equations

1. $A_p = A_m - A_e$

2. $A_e = .25\ A_m$ since $H_e/H_m = .25$ and $W_e/W_m = 1$

3. $A_p = .75\ A_m$

Therefore

$$C_{D_{A_m}} = .75\ C_{D_{A_p}}$$

and

$$\overline{FR} = \frac{\frac{(1-D_e/D_m)}{\sin \beta} \pm \sqrt{\left[\frac{(1-D_e/D_m)}{\sin \beta}\right]^2 - (1-D_e/D_m)^2}}{2} \tag{21}$$

Correlation parameter.- A comparison, shown in figure 45, relates the 2-D drags to ADAP-predicted axisymmetric-nozzle drags based on the same nozzle-pressure and area ratios. The difference between the two drag levels is an incremental effect which is correlated and manipulated to convert axisymmetric nozzle predictions into those for 2-D nozzles. It was also reasoned in reference 255 that 2-D geometry predominantly affects the basic pressure drag (because of altered flow recompression) and entrainment drag increments (because of increased plume surface area) as opposed to affecting plume billowing. Consequently, this relationship was defined as

$$\Delta C_{D_{2-D}} \alpha \left[\frac{\Delta C_{D_{2-D}}}{\left(C_{D_B} + \Delta C_{D_E}\right)}\right]_{axi} \left(C_{D_B} + \Delta C_{D_E}\right)_{ADAP} \tag{22}$$

where the quantity $\Delta C_{D_{2-D}}/(C_{D_B} + \Delta C_{D_E})_{axi}$ is a function of fineness ratio and, as shown in figure 46, is stored via 10 control points in the ADAP program data files.

While the above relationship accounts for the geometric parameters of fineness ratio and A_e/A_m, it does not account for variations in sidewall boattailing; thus, the proportionality sign is employed. The P&WA data involves a 2-D nozzle having no sidewall boattailing. In order to investigate 2-D nozzles having some sidewall boattailing, a constant, ϕ, is used to include the effects of sidewall boattailing, so that

$$\Delta C_{D_{2-D}} = \phi \left[\frac{\Delta C_{D_{2-D}}}{\left(C_{D_B} + \Delta C_{D_E}\right)} \right]_{axi} \left(C_{D_B} + \Delta C_{D_E}\right)_{ADAP} \tag{23}$$

The parameter ϕ must be a function of the input 2-D geometry; ADAP uses the parameters W_e/W_m (exit width divided by max. afterbody width) and H_e/H_m (exit height divided by max. afterbody height). For the P&WA test, $W_e/W_m = 1$ and $H_e/H_m = .25$; however, one must recognize that for an isolated 2-D nozzle the flow field cannot distinguish the "side" of the nozzle from the "top"; hence, the data would be the same if $W_e/W_m = .25$ and $H_e/H_m = 1.0$. This evaluation is important because it restricts the possible relationships between ϕ and the 2-D geometric parameters. By assuming that for an isolated 2-D afterbody, the maximum cross-sectional area is square ($W_m/H_m = 1$), and then assuming that 2-D effects are significant only when the exit plane 2-D geometry is not square, the following equation was derived.

$$\phi = \left| \frac{(1 - W_e/W_m)(1 + H_e/H_m) - (1 + W_e/W_m)(1 - H_e/H_m)}{2\left[1 - \frac{W_e}{W_m}\frac{H_e}{H_m}\right]} \right| \tag{24}$$

The final equation, therefore, is a function of sidewall boattailing as well as upper- and lower-surface boattailing, fineness ratio, nozzle pressure ratio, and Mach number and is defined by the following relationship:

$$\Delta C_{D_{2-D}} = \left| \frac{\left(1 - \frac{W_e}{W_m}\right)\left(1 + \frac{H_e}{H_m}\right) - \left(1 + \frac{W_e}{W_m}\right)\left(1 - \frac{H_e}{H_m}\right)}{2\left(1 - \frac{W_e}{W_m}\frac{H_e}{H_m}\right)} \right| *$$

$$\left[\frac{\Delta C_{D_{2-D}}}{C_{D_B} + \Delta C_{D_E}}\right]_{axi} \left(C_{D_B} + \Delta C_{D_E}\right)_{ADAP} \tag{25}$$

6.2.1.5 Comparisons with experimental data

Several example cases were calculated to evaluate the prediction method. The first two examples, shown in figures 47 and 48, compare the predictions with data from references 249 and 36. The data were contained in the data base used by General Dynamics to derive the ADAP correlations. However, the calculations shown in figures 47 and 48 were performed using the FORTRAN version of the program developed by Kuhn (ref. 307). The agreement is excellent.

Other examples are shown in figures 49 and 50 which indicate more clearly the limitations of the predictive method. In figure 49 is shown the comparison between predicted drag coefficients and experimental values as functions of nozzle pressure ratio for various Mach numbers on several of the circular-arc boattails studied in reference 92. The values of the parameters covered in these figures are listed in the following table.

Figure	$\overline{FR}$	A_e/A_m	P_{t_j}/P_∞	M_∞
49a	0.8	0.25	1 - 6	0.4 - 1.3
49b	1.0	0.25	1 - 6	"
49c	1.768	0.25	1 - 6	"
49d	1.5	0.49	1 - 6	"
50a	0.8	0.25	3	"
50b	1.0	0.25	3	"
50c	1.768	0.25	3	"
50d	1.5	0.49	3	"

The data from reference 92 for supersonic Mach numbers were included in the ADAP data base. The subsonic data from reference 92 were not. Therefore, the subsonic data constitute an independent check of the prediction method. Also, it is noted that the ADAP correlations include fineness ratios from 1.0 to 4.0 for subsonic flows and 1.0 to 2.0 for supersonic flows. Thus, the body with fineness ratio of 0.8 requires extrapolation from the main data base in order to predict the drag. Another feature of the data is the existence of an extensive region of separated flow on the $\overline{FR}$ = 0.8 and 1.0 afterbodies as indicated by oil-flow studies discussed in reference 275. The agreement between the prediction and the data shown in figure 50 is good for the supersonic case for fineness ratios above 1.0. The predicted drag is generally somewhat lower than the data for all fineness ratios for the subsonic cases.

A better evaluation of the quality of the prediction can be seen in figure 50, where the drag coefficients are plotted as functions of Mach number for a single nozzle pressure ratio of 3.0. The first notable fact that can be observed from this comparison is that the ADAP does not predict the transonic drag rise. For subsonic flow best agreement for all the bodies occurs around a Mach number of 0.8. This is to be expected since the ADAP data correlation emphasized M_∞ = 0.85 data with some data between $M_\infty = 0.4$ and 0.85. It is not clear whether the lack of agreement shown in figure 50(a) for the $\overline{FR} = 0.8$ case can be attributed to the separation observed on that body or simply to the fact that such data were not included in the data base. Some improvement could probably be achieved in these predictions if the subsonic and transonic data from reference 92 were incorporated into the correlations.

6.2.2 Twin-engine configurations

All the remaining methods to be examined employ as a basic correlating parameter a projected-area-weighted average slope of the afterbody area distribution known as the Integral Mean Slope (IMS). This parameter has been found to correlate both twin-jet and single-jet parametric drag data (ref. 118).

The first method to be examined was developed by the Boeing Company and Pratt & Whitney Aircraft. The method is based on correlation of a large amount of data. However, it is limited to Mach numbers below 0.95. The second prediction method was developed by the Lockheed California Company (Calac) under an extensive program in which 92 aircraft configurations were tested over a wide range of Mach numbers, nozzle pressure ratios, and configuration variables. The third method, developed by the Naval Air Development Center, extends the Calac method to a broader base of experimental data by including all available afterbody drag data for twin-engine "fighter-type" configurations in a data base. A statistical method is then applied to develop a correcton for the Calac correlation.

6.2.2.1 ESIP twin-afterbody drag prediction method

The ESIP prediction method (ref. 24) deals with the pressure drag of the aft fuselage downstream from the maximum cross-sectional area for subsonic Mach numbers up to 0.95. The correlation covers configurations with horizontal interfairings. There is reason to believe it is also applicable to other interfairing concepts or even to single-engine configurations but data are not now available to verify this. The correlation accounts for the effects of either a single vertical stabilizer or twin vertical stabilizers extending radially from nacelle centerlines.

The correlation treats only the design-pressure-ratio case for which the nozzle-exit static pressure equals free-stream ambient pressure. Pratt & Whitney has developed a jet-plume parameter to help handle off-design conditions (ref. 113).

The ESIP correlation is based on the integral mean slope of an equivalent body of revolution representing the afterbody. However, in this correlation, an attempt has been made to account for the effects of separated flow. In the development of the method, studies indicated that the aft-end drag coefficient should correlate well with the IMS parameter. Other data, however, showed that the correlation broke down for afterbodies whose area plots involved regions of steep slopes. A modified IMS parameter called IMS_T was then developed to avoid a sensitivity to afterbody contours in regions which were likely to have separated flow. The IMS_T approach is based upon specifying a maximum slope of the nondimensional area distribution which can be used in the IMS calculation. The maximum slope is substituted for the real slope at each step of the IMS calculation for which the real slope exceeds the maximum slope. The best correlation was obtained by making the maximum slope a function of Mach number. The resulting correlation is shown in figure 51. Here $\hat{C}_D$ indicates the pressure drag coefficient based on projected frontal area of the afterbody. The data represent a wide range of aft-end geometries and nozzle types and both single- and twin-vertical-stabilizer configurations. The correlations for the two tail types were found to be nearly identical except that the single-vertical-tail data indicated a lower drag with a level shift of 0.006 in $\hat{C}_D$. Thus, the two correlations were combined into a single correlation in terms of $\hat{C}_D$ +

$\Delta\hat{C}_D$ where $\Delta\hat{C}_D = 0$ for centered-twin-vertical stabilizer configurations and 0.006 for single-vertical-stabilizer configurations.

Further studies of the correlation indicated that all of the data varied almost precisely as the IMS_T parameter raised to the 2.77 power. The IMS_T dependence was divided out to obtain a drag parameter which was a function of Mach number only as shown in figure 52.

The overall procedure for using the correlation in a prediction method for subsonic afterbody drag of twin-engine configurations is illustrated schematically in figure 53. The first step is to input the nondimensional afterbody area distribution. The area distribution together with the maximum slopes are then used to calculate the IMS values as a function of Mach numbers. The remaining calculations are then the determination of the drag parameter from the basic correlation curve and the inclusion of the appropriate drag increment for the tail type.

The limits of this correlation are as follows: The correlation does not extend below Mach numbers 0.7 because no data were obtaned there in the test program. However, extrapolation to Mach zero along a constant equal to the value of Mach 0.7 appears to be a reasonable approach due to the lack of a compressibility effect at Mach 0.7. Extrapolation in the other direction to Mach numbers greater than 0.95 would not be possible. Similarly, the data base for the correlation includes models with IMS_T values as large as about 1.1. The method should not be considered applicable to models with larger values of IMS_T. Finally, the correlations are based on a narrow range of afterbody shapes, with all data obtained with a wingless forebody. Since data presented in reference 45 indicate a rather significant effect of a wing on total aftend drag, application of the ESIP correlation to complete configurations should be done with caution. While the method may not predict the absolute level of drag accurately for a given configuration, it may be useful for a preliminary design analysis in comparing the relative merits of several candidate configurations.

6.2.2.2 Calac twin-nozzle/afterbody drag performance method

The twin-nozzle/afterbody drag performance method is described in reference 50, which is based on work described in references 44 and 46. It consists of a computer program for predicting twin-nozzle/afterbody drag and internal nozzle performance for fighter-type aircraft having twin buried engines and dual nozzles. The program is a revised version of that described in reference 45 and is capable of generating the installed thrust-minus-drag data required for conducting mission analysis studies of aircraft of this type. The configuration variables which can be analyzed include:

1. Nozzle type - convergent flap and iris
   convergent-divergent with and without secondary flow
   plug, both shrouded and unshrouded

2. Nozzle lateral spacing - narrow (S/D = 1.25)
   intermediate (S/D = 1.625)
   wide (S/D = 2.0)

3. Interfairing type - horizontal wedge
   vertical wedge

4. Vertical stabilizer type - single vertical for narrow, intermediate, and wide spacings
   twin vertical for wide spacing

The performance prediction methods are based almost entirely on empirical correlations. Correlations used in conjunction with one-dimensional flow relationships are employed for the prediction of the nozzle thrust and discharge coefficients, and correlations of wind-tunnel test data are employed for the effect of nozzle pressure ratio and flow separation on both internal and external nozzle surfaces. A schematic diagram of the method is presented in figure 54.

Boattail pressure drag.- Subsonic flow: For subsonic external flow, the prediction method begins with a basic correlation of the pressure drag on a twin afterbody aft of a certain reference station. For the wind-tunnel models used in developing the correlation, that station was the metric break station separating the part of the model on which aerodynamic loads were measured from the rest of the model. It is suggested that the appropriate station to be used for analysis of a new configuration is the axial location of the wing trailing edge. Input data for the computer program include quantities to account for the drag on the portion of the afterbody between this reference station and the maximum cross-sectional area station.

The boattail-drag coefficient referenced to the cross-sectional area at the metric break station is computed from the following empirical correlation of data.

$$\left.\begin{aligned} C_{D_{MB}} &= K_1 \left(\frac{IMSA}{M_\infty}\right)^{2/3} \frac{A_p}{A_{mb}} + \frac{K_2}{q_\infty}\frac{F_{ID}}{A_{mb}} \\ K_1 &= \hat{C}_{D_{MB}} \left(\frac{M_\infty}{IMSA}\right)^{2/3} \\ K_2 &= \frac{\Delta D}{F_{ID}} \end{aligned}\right\} \qquad (26)$$

The breakdown of Eq. (26) is as follows: The first term is the drag for the design pressure ratio, where the nozzle-exit static pressure equals the free-stream static pressure and a cylindrical exhaust plume is produced. The second term is the drag increment from the design pressure ratio to operation at a higher ratio.

A typical correlation for the design-pressure-ratio drag coefficient parameter, K_1, is shown in figure 55. Note that the equivalent base-to-metric-break area ratio is also a parameter in the correlation. The basic correlation relates the drag coefficient, the Mach number, and the integral mean slope IMSA of an equivalent body of revolution with the same area distribution as the configuration of interest downstream of the metric break station using a relationship based on transonic similarity theory. Other parameters which affect the correlation are the interfairing type, the tail type, and the nozzle type. The correlation shown in figure 55 applies for configurations with horizontal interfairings and a single vertical tail and is independent of nozzle spacing. A linear interpolation and extrapolation for equivalent base area ratios other than those presented in the figure is employed.

For convergent and convergent-divergent nozzle installations the drag parameter, K_2, which is the increment in drag from design-pressure-ratio operation to operation at a higher pressure ratio, is shown in figure 56 as a functon of nozzle underexpansion loss. The drag increment, which is normalized by the ideal thrust, is dependent upon both the Mach number and the shroud-exit to metric-break area ratio. This correlation is a function of nozzle type and of nozzle power setting.

Jet-off boattail drags can be computed using the correlation results typical of figure 57. In this case, the increment in drag from jet-off operation to operation at the nozzle design pressure ratio for various nozzle lateral spacings and for various Mach numbers are presented. The drag increment is presented in terms of an increment in drag coefficient referenced to the twin-nozzle shroud exit area and is correlated as a function of boattail trailing-edge angle β at the nozzle exit.

Supersonic flow: Boattail-drag coefficients based on maximum area for a supersonic external flow are computed from the following equation

$$\left.\begin{aligned} C_D &= \hat{C}_{D_{EB}} \frac{\hat{C}_D}{\hat{C}_{D_{EB}}} \frac{A_p}{A_m} + K_3 \frac{p_e - p_L}{p_\infty} \frac{A_{so}}{A_m} \frac{p_\infty}{q_\infty} \\ K_3 &= \frac{\Delta D}{(p_e - p_L)A_{so}} \end{aligned}\right\} \tag{27}$$

where the first term is the jet-off drag and the second term is the increment in drag from jet-off to jet-on operations. The equivalent-body drag is obtained by entering the method-of-characteristics boattail-drag correlation curves presented in figure 58 with a Mach number and IMS. A subsequent correlation such as figure 59 is used to calculate the ratio of jet-off drag to equivalent body drag as a function of Mach number and vertical stabilizer type. For jet-on operation, K_3, which is the increment in drag from jet-off operation normalized by the product of the nozzle shroud external cross-sectional area at the nozzle exit and the difference between nozzle internal exit pressure and the local boattail surface pressure (assuming no flow separation) is obtained from another correlation shown in figure 60 as a function of nozzle mean-boattail angle. The mean boattail angle used is the mean angle over a distance equal to one-third the nozzle exit radius measured from the nozzle exit. This length was selected as being representative of the flow separation length. The local boattail flow properties are obtained from a method-of-characteristics solution. Thus, K_3 is the increment in drag from jet-off operation to operational conditions at which separated flow occurs due to plume effects. It has been observed that little or no separation occurs for $(p_e - p_L)/q_L < 1.4$. Therefore, the correlation results presented in figure 60 are restricted to pressure coefficients greater than 1.4.

Boattail friction drag.- The required input for computation of the boattail friction drag is the boattail length (L_{BT}), the wetted surface area ($A_{W_{BT}}$), and either the momentum thickness (θ) at the start of the boattail or an effective flat plate length (L_{eff}) upstream of the start of the boattail. With these inputs, an average boattail skin friction coefficient is computed by use of Sivells-Payne correlation (ref. 161) which, when combined with the wetted area, yields the friction drag as discussed below.

With an input momentum thickness at the start of the boattail the reference-length Reynolds number, R'_{e_1}, is obtained by iterative solution of the following equation

$$R_{e_\theta} = \frac{\mu'_1}{\mu_1} (0.044\ R'_{e_1})/(\mathrm{Log}_{10}\ R'_{e_1} - 1.5)^2 \tag{28}$$

where the primed quantities denote values evaluated at the reference temperature, T'_1, which is obtained from the following equation

$$T'_1 = T_1 \left[1 + 0.035\ M_\infty^2 + 0.45 \left(\frac{T_{aw}}{T_1} - 1\right)\right] \tag{29}$$

where

$$T_{aw} = T_1 \left[1.0 + \left(\frac{\gamma-1}{2}\right)(0.89)M_\infty^2\right] \tag{30}$$

If an effective flat plate length upstream of the boattail is input, the reference Reynolds number is obtained from the following equation

$$R'_{e_1} = \frac{\rho'_1 U_\infty L_{eff}}{\mu'_1} \tag{31}$$

The local skin friction correlation equation taken from reference 161 is

$$C_{f_1} = \frac{\left[0.088 \left(\mathrm{Log}_{10} R'_{e_1} - 2.3686\right)\right] T_1}{\left(\mathrm{Log}_{10} R'_{e_1} - 1.5\right)^3 T'_1} \tag{32}$$

The local skin friction coefficient at the end of the boattail is computed in a manner similar to that described above except that the length employed in the computation of the reference-length Reynolds number is

$$L_2 = L_{eff} + L_{BT} \tag{33}$$

If the momentum thickness Reynolds number is input, the effective flat plate length at the start of the boattail is computed as follows:

$$L_{eff} = \frac{\mu_1 R_{e_1}}{\rho_1 U_\infty} \tag{34}$$

The skin friction drag coefficient based on maximum area is

$$C_{D_f} = \frac{\left(C_{f_1} + C_{f_2}\right)}{2} \frac{A_{W_{BT}}}{A_m} \tag{35}$$

Annular base drag.- The annular base pressure for a subsonic external flow is computed from the following modification (developed in ref. 44) of the Brazzel-Henderson base pressure correlation (ref. 66):

$$\frac{p_b}{p_\infty} = \frac{0.9 + 0.0167(R_{m_f})}{0.94 + 0.06(A_{so}/A_m)} \tag{36}$$

where R_{m_f} is the nozzle-exit to free-stream momentum ratio, defined as

$$R_{m_f} = \frac{(\dot{m}V)_e}{(\dot{m}V)_\infty} = \frac{\gamma_e \, p_e \, A_e \, M_e^2}{\gamma_\infty \, p_\infty \, A_m \, M_\infty^2} \tag{37}$$

For a supersonic external flow, the following base pressure correlation developed by Brazzel-Henderson is also employed.

$$\frac{p_b}{p_\infty} = \left[\frac{T_e}{T_e^*}\right]\left[\frac{3.5}{0.5 + 3.0\ A_{so}/A_m}\right]\left[0.19 + 1.28\left(\frac{R_{m_f}}{1 + R_{m_f}}\right)\right]$$
$$+ 0.047(5-M_\infty)\left[2\left(\frac{\Delta X_e}{D_m}\right) + \left(\frac{\Delta X_e}{D_m}\right)^2\right] \tag{38}$$

The first term on the right side of Eq. (26) normalizes the jet temperature to the jet temperature of a sonic nozzle. The second term corrects for boattail effects, and the third term is a correlation based on the ratio of nozzle-exit momentum flux to free-stream momentum flux. A nozzle-position (relative to the end of the boattail) correction is obtained by the fourth term.

Comparison with data.- An independent investigation (ref. 41) indicates that the twin-nozzle afterbody-drag performance method reasonably predicts the trends and absolute levels of data for a configuration similar to those used for the original Calac correlation. The evaluation model was a twin-jet air superiority fighter tested in the AEDC PWT 16T facility.

One significant difference exists between the model and the model as defined for the computer program. The model has intermediate spacing of the nozzles and twin vertical tails, whereas for intermediate nozzle spacing, the computer model is limited to a single vertical tail. No accurate assessment has been made of the effects of this difference. It is known, however, that tail surfaces do significantly affect the afterbody flow field.

Another difference between the model and the model defined for the computer program is that the model nozzle lateral spacing falls between the values for narrow and intermediate spacing. The empirical data chosen for the calculations were those closest to the model configuration. The empirical correlations are based on data that is limited in the 0.9 to 1.2 Mach number range. The predicted afterbody drags, therefore, for this Mach regime should be used with caution. Figure 61 provides a comparison between the measured and predicted values of drag coefficient for the cruise nozzle at nozzle pressure ratios of 3.3 and 4.9. Excluding the Mach 0.9 to 1.2 range, the predicted values of drag coefficient are in reasonable agreement with the measured values. A comparison is made of the measured and predicted drag for the reheat nozzle at nozzle pressure ratios 4.2, 5.2 and 7.8 in figure 62. The results are similar, but especially good at a nozzle pressure ratio of 4.2. This is not unexpected since the problem of aft-end closure has been lessened in the reheat mode. Reference 41 concludes that a need exists for more test data to fully evaluate this prediction technique and an extension of the empirical data base to include closely spaced nozzles with dual vertical tails. This comparison is discussed further in the next section where the Calac method is compared with an extended version of the method.

6.2.2.3 NADC prediction technique for twin jet fighter-type aircraft

Description.- The NADC prediction technique (ref. 143) is an extension of the Calac technique. The method was developed by expanding the Calac aft-end drag data base to include data from models of other existing twin-jet fighter-type aircraft. Parametric investigations were then conducted to determine if the existing Calac aft-end drag parameters were all inclusive and could account for the inherent drag variations of the added fighter-aircraft models. Finally, a new drag parameter dependency relationship was derived for the important parameters. The derived relationship is

$$C_{D_{NADC}} = C_{D_{CALAC}} + \sum_{i=1}^{N} \alpha_i X_i \tag{39}$$

where α_i are coefficients determined by the statistical analysis and X_i are the various parameters including NPR, and various similarity relations, and combinations of area ratios, Mach number and Reynolds number listed in Table X. The extended correlation was found to provide a significant error reduction from the Calac correlation. An asset specifically designed into the method is that the data base can be continually expanded to include additional twin-jet aft-end drag data.

The limitations of the NADC prediction technique are that the method is dependent on wind-tunnel data quality and, since it is based on the Calac method it is applicable to the same limited class of configurations. Also, the method does not account for wind-tunnel to full-scale flight Reynolds number variations.

The Calac data base consisted of data from wind-tunnel models which had the horizontal and vertical stabilizers mounted separate from the afterbody force balance so that only the tail interference effects on the afterbody drag were directly measured. Some of the data considered in the NADC correlation procedure had the tails mounted directly onto the afterbody so that the measured drag included the total drag of the tails. Thus, one of the steps in the NADC data-correlation procedure which may produce some error in the predictions results from the necessity of subtracting from the experimentally measured afterbody drag an estimated value of drag of the tails in order to include only the tail interference effect in the afterbody drag correlation.

Evaluation of the prediction method.- In order to evaluate the accuracy of the prediction method as a design tool, some afterbody drag predictions were compared with experimental results for two configurations that were not included in the correlation data base. One of the configurations (ref. 32) was that analyzed peviously by Everling (ref. 41) who compared the data with predictions made by the Calac version of the program. That configuration had tails mounted on plates attached to the forebody, separate from the afterbody force balance. Thus, only the tail interference effects should be present in the data, and the predictions should be directly comparable. The other configuration (ref. 262) is more difficult to compare since data are available only for the cases of tails on or tails off. No data were obtained for afterbody drag in the presence of the tails but not including their drag for direct comparison with the prediction. The results of the tests described in reference 262 provide a qualitative evaluation of the prediction method.

The independent investigation by Everling (ref. 41) of the data of reference 32 indicated that the Calac twin-nozzle/afterbody drag performance method reasonably predicted the trends and absolute levels of data for a configuration similar to those used for the original Calac correlation. The evaluation model was a twin-jet air-superiority fighter tested in the AEDC PWT 16T facility.

As mentioned previously, some of the data used by the NADC in extending the experimental data base had the tails attached to the afterbody balance. The tail profile drag for such cases was estimated and subtracted from the measured drag in order to produce afterbody drag data consistent with that in the Calac data base. The accuracy of such adjustments is unknown.

Figure 63 shows a comparison between the measured and predicted values of drag coefficient. Figures 63(a) and (b) show the comparison for the cruise nozzle at nozzle pressure ratios of 3.3 and 4.9. Predicted values are shown for both the basic Calac program and the NADC modified program. The NADC adjustment gives a slightly improved prediction for the mid-transonic range of Mach numbers while the Calac prediction is better for low and high Mach numbers. Similar results are achieved for the reheat nozzle as shown in figures 63(c), (d), and (e).

Figure 64 shows the drag coefficients on a wind tunnel model of the F-18 aircraft, described in reference 262. Those data are similar to the previous data in the sense that the model has twin tails and narrow-to-wide nozzle spacing, whereas the Calac data base provides for twin tails only for the wide nozzle spacing.

One aspect of the tests reported in reference 262 was the investigation of the effect of removing the tails from the model. This effect is indicated in figure 64 where the drag with tails removed is seen to be signficantly lower than with the tails attached to the afterbody (and to the afterbody balance) for both the cruise nozzle at M_∞ = .6 and .9 and the maximum reheat nozzle at M_∞ = 1.6 and 2.0. The prediction method, which is based on data that includes, presumably, only the tail interference effects (and not the drag of the tails themselves), would be expected to yield a drag value nearer the tails-off value than the tails-on value. As shown in figure 64 that expectation is met by the Calac prediction with the exception of the case for M_∞ = 0.9 for the cruise nozzle (fig. 64(b)), but the NADC prediction is not so consistent.

A more exact evaluation of the data to determine the actual interference effect of the tails on the afterbody drag requires an accurate evaluation of the tail profile drag and is beyond the scope of the present investigation.

The comparisons shown in figure 63 indicate that for configurations that closely resemble those in the Calac data base, the Calac prediction may be better than the NADC prediction except for low supersonic Mach numbers. The comparisons shown in figure 64 provide no quantitative basis for choosing either method. It would be expected that the drag for configurations that more closely resemble those that were added to the data base by the NADC would be more accurately predicted by the NADC version of the program.

6.3 Theoretical Prediction Methods

In general, the interference flow fields associated with installation of the propulsion system in the airplane are dominated by viscous effects such as boundary-layer separation and jet-exhaust plume entrainment. Existing analytical attempts to predict these interference effects are limited to specific effects for simple configurations such as isolated axisymmetric nozzles. Generalizations are often made from these simple shapes to more complex shapes using the concept of an equivalent body of revolution. This technique is found to be unsatisfactory except for small deviations from symmetry. In this section, the general problem of predicting afterbody flow fields will be described followed by a discussion of the status of the theoretical prediction technology.

6.3.1 Description of problem

The usual approach for calculating the flow over boattails is to use the technique of dividing the flow field into a number of analytical regions. A typical breakdown of these regions is shown in figure 65. Included are an inviscid external flow (region I), inviscid jet plume (region II), and viscous region (region III), which includes boundary layers on the boattail and inside the nozzle and the mixing layer between the jet and the external flow. The viscous region may be further divided into attached boundary layer and separated boundary layer regions. Several calculative techniques have been developed which show promise as engineering-type prediction methods. At the pesent time, no generalization of analytical prediction methods to non-axisymmetric nozzles, or to full aircraft configurations has been made.

With regard to the exhaust plume, two physical effects have been identified by Bergman (ref. 6). The first is a displacement outward of the external flow streamlines caused by the shape of the plume. Outward displacement of the streamlines results in stronger flow recompression on the boattail and has a beneficial effect on the drag, as shown in figure 66. The shape of the exhaust plume is a function of nozzle pressure ratio for fixed free-stream conditions. The second effect, entrainment, begins when the exhaust plume velocity is approximately equal to free-stream velocity. This effect increases boattail drag by increasing the velocity of the flow over the boattail and effectively lowering the boattail pressure. The net effect on boattail drag is the sum of the two effects.

Increasing exhaust jet temperature has been found to decrease the drag for fixed nozzle pressure ratio. This effect is caused by greater spreading of the hot plume than the cold plume. The effect of exhaust plume temperature on entrainment is not known.

It must be noted that many of the methods to be discussed in this section contain certain empirical features, and therefore might be considered semi-empirical rather than theoretical. The definition of a theoretical prediction method is considered to include methods wherein empirical techniques may be used for certain specific features such as prediction of the separation point location, but the basic calculative method is a solution of the theoretical governing equations of the flow field. The term empirical prediction methods is thus reserved for those methods based primarily on correlation of experimental data.

6.3.2 Status of theoretical prediction technology

A summary of the status of current technology for predicting drag on axisymmetric nozzle boattails is presented in Table XI. In that table, the factors that must be accounted for are listed in the left hand column, the pertinent reference numbers from the afterbody drag reference list are listed at the top and an X is placed in the appropriate box denoting whether the prediction method accounts for that factor. A blank box in the column for a certain reference means that reference does not treat the corresponding factor. The table reveals that several methods exist for accounting for boundary layers, including separated boundary layers, and several methods exist for accounting for plume shape. Exhaust-plume entrainment is not accounted for in an adequate manner by any existing techniques. Those methods listed as accounting for entrainment are first approximations and have not developed a viable entrainment model.

The theoretical prediction methods fall naturally into three basic categories depending on whether the flow conditions are subsonic, transonic, or supersonic. Within each of those categories another major subdivision is between those methods which treat only attached flow and those which also treat separated flows. The individual methods in each of these categories and subdivisions will be discussed in the following sections.

First, however, it is noted that a program was initiated by the NASA Langley Research Center in June 1976 to assess the state-of-the-art for predicting pressure distributions and drag of boattail nozzles. The objective of the program was to compare available analytical and empirical methods with one set of experimental data so the relative merits of the various methods could be easily assessed. The results were subsequently distributed to interested parties (ref. 8.10). The prediction methods that were applied to the prescribed data set included those described in references 136, 200, 210, 211, 212, 217, 227, and 294. Other investigators have also recently used the same data for comparison (refs. 264, 300). All of the original groups of methods predicted the afterbody drag poorly for subsonic and transonic flows for both an afterbody with no separation and for one with extensive separated flow. The one method that was applicable to supersonic flows, that of Holst (ref. 210), was in good agreement with experimental integrated pressure drag on an afterbody with extensive separation. The prediction methods will now be discussed individually in the following sections.

6.3.2.1 Subsonic afterbody drag calculative methods

The most complete theoretical method for subsonic axisymmetric boattail drag with attached flow is a method produced by the Lockheed California Company (ref. 48).

The method predicts the drag of arbitrary axisymmetric boattail contours through use of the subsonic potential flow method of Smith and Pierce (ref. 164) combined with approximate exhaust-plume and integral-boundary-layer calculative methods. Mutual interaction effects between the external flow and the exhaust flow and between the external flow and the boundary layer are treated. The computer program is equipped to handle convergent, convergent-divergent, and plug-type nozzles. The method is limited to subsonic free-stream Mach numbers below that for which supercritical flow would occur over the boattail, and to configurations for which no boundary-layer separation occurs. Jet-plume mixing is not treated.

Comparisons with data shown in figures 67-69 indicate the method produces good agreement with the data on the conical afterbody of reference 134 when the boundary layer is accounted for (fig. 67). For convergent-divergent and plug-nozzle-boattail configurations (figs. 68 and 69), the pressure distribution trends are properly predicted, but the absolute pressure levels are not predicted very well, especially in the recompression region near the nozzle-boattail trailing edge.

Another method for calculating the subsonic drag of axisymmetric boattails is that of Rom and Bober as described in reference 99. That reference accounts for the boundary layer on the boattail but does not account for jet plumes. Instead, an approximate method is used to account for the flow in the base region, corresponding to jet-off conditions. Separation of the boundary layer is assumed to occur only at the boattail base. Separation on the boattail is not treated.

A calculative method including provision for separation on the boattail was developed by Presz (ref. 253, 80). In that method, the separated region is modeled as a conical dividing streamline surface placed between the separation point on the boattail and the point of reattachment on a solid cylindrical sting. An empirical approach based on an integral boundary layer method is used to determine the location of the point of separation and the angle of divergence of the dividing streamline surface from the boattail surface. In Presz's method, the subsonic potential flow theory of Smith and Pierce is then used to calculate the pressure distribution on an equivalent body consisting of the real body and the conical separation surface. Comparison with data indicates the approach gives a reasonable approximation for the afterbody pressure distribution and drag. Typical comparisons between the theory and data are shown in figures 70 and 71.

An improved version of the method of reference 253 was developed by Presz (refs. 264, 265) by relaxing the requirement that the separation surface be conical and using the boundary-layer displacement thickness to modify the body shape. Before separation and after reattachment, the modified body shape is the actual body contour plus the displacement thickness. In the separated region, the shape is determined by adding the displacement thickness to the dividing streamline determined by a discrete control volume analysis. A jet-plume entrainment model is also included to account for changes in the inviscid flow field due to effects of jet entrainment on the dividing streamline. Comparisons with experimental pressure data on several circular-arc boattails (figs. 72-76) indicate that the method accurately predicts the pressure distribution for bodies with stings on which no separation occurs (fig. 72) or for moderately separated flows (fig. 73). For sting-mounted models with more extensive separation, the comparison is not so good (fig. 74). For models with jets and separated flow, the calculative method of reference 264 appears to be unable to predict the constant pressure that occurs in the separated region (figs. 75 and 76). The errors in the pressure predictions result in fairly large errors in drag as shown by the drag-coefficient values listed in figures 72-74.

Presz's results from reference 253 were used by Reubush and Putnam in reference 136 as a basis for a correlation which gives the divergence angle of the dividing streamline surface as a function of the Mach number at the separation point. The conical separation surface is then used as the solid boundary and an attached boundary layer is calculated for the entire length of the augmented body plus the sting. The subsonic potential flow method of Hess and Smith (ref. 162) is used to calculate the external flow. Comparisons with experimental data indicate good results can be achieved with this technique if an accurate separation prediction is used.

Incorporation of exhaust-plume entrainment into subsonic afterbody flows is discussed in references 297, 298, and 299 where a modular approach is taken to couple the viscous and inviscid processes. Separation of the flow over the afterbody is not considered.

6.3.2.2 Transonic afterbody drag calculative methods

The theoretical methods available for transonic speeds fall naturally into the same two subcategories as for the subsonic methods. Namely, those in which boundary-layer separation on the boattail is treated and those in which it is not. Furthermore, the lack of accurate shock-wave-boundary-layer interaction theories effectively limits these prediction methods to subcritical free-stream Mach numbers or to Mach numbers such that only very weak shocks occur on the body.

Grossman and Melnik (ref. 51) describe a method in which the drag for arbitrary axisymmetric boattail contours is calculated including mutual interaction effects between the external flow, the jet plume and attached-boattail boundary layer. A calculative method like that of South and Jameson used for the external flow is applicable to both purely subsonic and transonic flows. However, the computer programs for the jet plume needed for application of the method are not generally available.

A more readily available method is described in reference 34 by Chow and Bober, which accounts for the mutual interaction between attached boundary layers and subsonic or transonic external flow, but approximates the jet plume as a solid boundary. The full transonic potential equation is used, including boundary-layer effects, yielding good agreement with the experimental pressure distribution for the conical boattail of reference 141. Some examples are shown in figure 77.

The method of references 217 and 252 is similar to that of reference 34 in that the full transonic potential equation is used in conjunction with a boundary-layer method for attached flows. In addition, a simplified plume entrainment model is described which yields qualitatively satisfactory results.

In reference 43, the Spreiter-Alksne method of local linearization (ref. 165) is used with a turbulent-boundary-layer method and the method of characteristics to study plume-shape and afterbody-shape effects. The method is limited to slender bodies and separation is not accounted for.

Several methods have been developed for transonic flows with separation. In reference 212, Yaeger describes a method which is a modified version of that described by Presz and by Presz and Pitkin (refs. 253, 80). It is applicable to bodies with stings and to slightly supercritical flows for which no significant shock-wave-boundary-layer interaction occurs. Some insight into the effects of strong shock-wave-boundary-layer interactions is provided by an analytical study described by Wilmoth in references 211 and 274 where the applicability of Presz's method of reference 253 is shown to be limited to free-stream Mach numbers below about 0.7. Results of that study are shown in figure 78 where the variation of the discriminating streamline separation angle is found to depend strongly on the local Mach number at separation. This also would appear to limit Yaeger's method (ref. 212) to the same Mach-number range since Yaeger employs similar analytical techniques to those used by Presz and restricts his analysis to flows with negligible shock-wave-boundary-layer interaction.

In references 27 and 227, another type of approach is used by Calarese to study the effects of mass and energy injection on boattail drag. An iterative procedure is used whereby viscous effects are added to the inviscid solution of the nonlinear small-perturbation equation. Jet effects are accounted for through empirical correlation and boattail separation is treated with a Korst (ref. 160) base-flow type of analysis. The method is shown to provide good agreement with data for attached flows but only fair agreement for separated flows.

Another different approach is described by Cosner in reference 209. In that approach, separated boundary layers are calculated using an empirical technique to extend the calculation past separation and reattachment points. Jet-plume mixing is also handled in an approximate way. Results presented indicate the method, still in a preliminary state of developement, is not very accurate for flows with extensive separated regions.

In the method of references 218, 300, and 301, Kuhn has employed many of the principles developed in several of the other methods. The full-transonic-potential-equation solution method of South and Jameson is used allowing calculation of flows over non-slender bodies and steep boattail angles. An integral-boundary-layer approach is used whereby both attached and reversed flows are calculated for bodies with solid stings. The separation and reattachment points are calculated as a part of the interaction between the boundary layer and the inviscid flow. An entrainment model is included to account for exhaust-jet effect. Comparisons with data for separated and unseparated flows indicate the method provides good predictions of the afterbody pressure distribution and drag (figs. 80 through 87) even into the region of transonic drag rise, although predicted drags for low-subsonic unseparated flows (fig. 85) are high.

The jet entrainment model used in reference 300 appears to provide fair agreement with data although the accuracy of the drag prediction seems to be a function of the free-stream Mach number as well as the nozzle pressure ratio (figs. 86 and 87).

6.3.2.3 Supersonic afterbody drag calculative methods

Supersonic afterbody drag methods are generally of three types. First are methods applicable to predicting boattail drag with jet plumes or solid plume simulators. Next are methods for predicting base drag. Finally, some methods are available for calculating optimum (minimum-drag) boattail shapes. The first two types consider viscid-inviscid interactions while the third type of method considers only inviscid flows. No comprehensive theoretical method has been found which includes both boattail and base drag.

For calculating afterbody boattail pressure drag in supersonic flow, two methods are described in references 49 and 210. In reference 49, Glasgow, et al., couple the method of characteristics with an attached-boundary-layer method supplemented by approximate methods of accounting for either plume or shock-induced separation based on the correlations of

Bonner and Nixon (ref. 26) and Brazzel and Henderson (ref. 66). Predictions are accurate for cases with no separation, but the approximate theories do not adequately account for the complex interference effects accompanying flow separation on the boattail. A computer program for the CDC 6600 computer is available from AFFDL.

Holst, in the method of reference 210, employs a more fundamental approach by solving the compressible Navier-Stokes equations in the vicinity of the boattail for axisymmetric afterbody-boattail configurations with solid-sting plume simulators. Comparisons with data for pressure distributions on boattails with extensive separated regions are good.

Another method employing a solution of the Navier-Stokes equations was demonstrated by Mikhail, Hankey, and Shang (ref. 267). Their method was applied to an axisymmetric boattail with jet exhaust. Although the method is not a fully developed design technique, it demonstrates that such a complex flow can be computed successfully, and provides a design engineer with good estimates for the surface pressure distribution and skin-friction forces. The method was not demonstrated for flows with separation on the boattail.

A Navier-Stokes solution technique that includes separated flows is described by Forester in reference 296. Progress is reported on development of a computer program with emphasis on computational efficiency and accuracy.

Many methods exist for calculating base-region flow properties. A review of various methods, including those of Korst (ref. 160) and Alber (ref. 184) is presented by Peters and Phares in reference 232 where an analytical model for planar and axisymmetric supersonic turbulent near-wake flows is presented. That model couples an integral form of the boundary-layer equations and the rotational method of characteristics. The base pressure is obtained by an iterative procedure. The method is designed to handle base bleed of a gas different from the outer-stream gas but the calculative technique has only been developed for single gas flows. The model is shown to adequately predict the effect of free-stream Mach number and initial boundary layer on the planar base pressure. Axisymmetric base pressure and flow-field structure are reasonably well predicted for free-stream Mach numbers greater than 2.0, but the turbulent transport model used yields only fair results for Mach numbers less than 1.7. The effect of base bleed on the axisymmetric base pressure is well predicted.

Another base flow analysis is presented in reference 117. In that method, Dixon, et al., extend Korst's theory (ref. 160) to treat base flow on an axisymmetric afterbody with a single operating exhaust nozzle. The flow around the afterbody and in the jet is supersonic with turbulent axisymmetric mixing occurring along the separated flow boundaries. Initial boundary layers are neglected and an empirical spread-rate parameter is used. A complete description of the base flow is obtained from the analysis permitting the prediction of base pressure and other flow parameters of interest. Results obtained from a parametric study illustrate the influence on the base drag of free-stream Mach number, exhaust-jet total pressure, and base, boattail and nozzle geometry.

Another more advanced application of Korst's method is presented in reference 220, where Bauer and Fox apply Korst's method to estimate the bulk base flow properties of nozzle-afterbody configurations with a supersonic jet and supersonic free-stream separated by a finite area base. Initial boundary layers are included as well as dissimilar thermodynamic properties of the two streams and a third base-bleed gas. The inviscid flows are computed by the method of characteristics. The turbulent-mixing analysis uses the turbulent-kinetic-energy method. Comparisons with data indicate the method tends to overpredict the base pressure due to use of too small a mixing rate.

Methods for determining optimum body shapes are described in references 231, 106, 129, 146, 223, and 284. Reference 231 is a survey of the variational problems relative to wings, fuselages, wing-fuselage combinations and nozzles in supersonic, hypersonic, and free-molecular flows. Within this broad scope of applications, it is an important reference on the calculus of variations as applied to the kind of variational problems associated with optimizing afterbody shapes.

6.4 Experimental Data

In Table XII the parameters associated with each Primary Data Source of the afterbody/airframe interaction data base are listed. This table provides a means for selecting particular references from a group of references which have been chosen for an effect from Table II. Numbers appearing in columns 2 and 3 of Table XII refer to Notes to Table XII following the table. These Notes explain the various types of configurations and data presented in the Primary Data Sources. The Notes are very general with respect to test model and data presented, since a detailed list could entail an almost endless list of configurations and types of data. For example, a reference which is indicated as having tested a twin-engine aircraft configuration may have tested this configuration with tails metric, tails nonmetric, or tails removed. The more specific types of configurations tested are not indicated in Table XII, or in the Notes to Table XII, but could be found by further investigation of the particular reference. In the same manner, the types of data presented in the Notes are general, and the list is not intended to be all-inclusive. The types of data presented for each reference are those types which would be most helpful to someone investigating afterbody/airframe drag. Other types of data which are not directly associated with this subject are not included in the Notes. With respect to the afterbody/boattail/nozzle drag coefficient and pressure coefficient distribution, a special note should be made. This data category is used to indicate that data is presented for either the entire afterbody/boattail/nozzle section or for a single element of this section, such as the nozzle. Also, the drag coefficients were obtained using drag balance measurements or by integrating pressures, and may or may not include base drag or friction drag.

It should also be noted that the afterbody section of the models tested was that part of the configuration either aft of the maximum area station or aft of the metric-break station. A dictionary of the shorthand configuration classification scheme used in columns 8 through 12 of Table XII is presented in Table XIII.

The usefulness of the experimental data base lies in the degree to which it can be used to extend the range of applicability of prediction methods, both theoretical and empirical. Much of the data listed has been included in one or more of the correlations discussed in section 6.2. The remaining data may be useful for estimating effects not included in the prediction methods. Two areas in which such extensions are particularly needed are discussed in the following sections. These are Reynolds-number effects and problems of scaling from wind-tunnel data to full-scale flight. The adequacy of the data base for prediction of these effects is discussed.

6.4.1 Reynolds-number effects on afterbody drag

No clear and definite conclusion can be drawn from the existing literature about the effect of scaling from wind-tunnel to full-scale flight Reynolds numbers. Tests conducted by NASA and by AEDC over a wide range of Reynolds numbers indicate that for isolated afterbodies (no interfering surfaces such as wings, tails, etc.) large effects are produced on pressure distributions over boattailed afterbodies but the compensating effect of increased expansion over one part of the body and increased compression over the rest of the body combine to result in little, if any, change in the net afterbody pressure drag. The high sensitivity of the calculated pressure drag to errors in the measured pressure does not appear to be a problem since great care has been taken in the experiments to minimize such errors.

The difficulty in evaluating Reynolds-number effects, or more specifically wind-tunnel to full-scale-flight-scaling effects seems to be in interpreting apparently conflicting results. To date, several experiments have been performed in wind tunnels covering a wide range of Reynolds number from values characteristic of wind-tunnel models to values characteristic of full-scale flight. Those tests indicate no Reynolds-number effect or very slight effects for isolated axisymmetric afterbodies and for the same bodies with wings added. On the other side some tests in which measurements were made both on models in a wind tunnel and on a full-scale model in flight indicate very significant Reynolds-number effects (ref. 127) while other tests indicate wind-tunnel and flight data have similar levels of afterbody/nozzle drag for Mach numbers below the nacelle drag-divergence Mach number (ref. 268). For higher Mach numbers, the drag was found in reference 268 to be lower for flight conditions for wind-tunnel conditions.

The problem lies in isolating the effects of Reynolds number from those due to many other factors, such as: accurate geometrical duplication between wind-tunnel and flight-test models, surface conditions, attitude, control deflections, instrumentation accuracy, model support and tunnel-wall interference, turbulence, propulsion simulation, heat transfer, and possibly noise.

To date, no reliable wind-tunnel-to-flight correlations have been made for real configurations of the type of interest herein. The few tests that have been performed have produced inconclusive results due to unanswered questions. For example, Martens (refs. 68 and 215) described wind-tunnel and flight-test results for the F-15. The data are inconclusive with regard to Reynolds number effects due to the inclusion of ventral fins on the wind-tunnel model but not in flight. Also, the question of hot-jet simulation by cold-gas jets was not considered in the tests.

6.5 Concluding Remarks

Evaluation of the adequacy of the data base for the prediction of afterbody drag leads to the following conclusions:

1. Although a number of systematic studies resulting in the development of empirical methods have been reported, there remain a number of unanswered questions. Perhaps the most important is that of the applicability of the results to flight Reynolds numbers. The experimental data on which the empirical methods are based were gathered at the relatively low Reynolds numbers provided in wind tunnels and therefore may not adequately reflect the viscous effects at flight conditions. Since conflicting results have been published regarding the effects of Reynolds number, this problem needs attention.

2. Although the number of configuration variables that have been tested is sizable, very little data are available for two-dimensonal exhaust systems. Moreover, most of the available experimental results cover only a small angle-of-attack range, not large enough to encompass the flight envelope of interest.

3. The application of modern theoretical methods to the prediction of afterbody drag has only recently been undertaken. Methods to account for boundary-layer separation and jet entrainment effects for the simplest of afterbody configurations are only now being developed. Methods to account for the complex interactions for real aircraft configurations with multiple exhaust systems have not been developed. In any event, the large computers and long run times required at this stage of development make them unsuitable for use in preliminary design studies.

7. DATA BASE FOR AIRFRAME EFFECTS ON INLET "FREE-STREAM" CONDITIONS AND THE EVALUATION OF ITS ADEQUACY FOR PRELIMINARY DESIGN

The performance of an air induction system can be signficantly influenced by the effects of flow produced by (or resulting from) other elements of the configuration, such as fuselage forebody, canards, etc. If the local flow ahead of the inlet differs significantly from a uniform flow at the free-stream Mach number, then the performance of the installed air induction system would be expected to differ from that which would exist with uniform inlet flow conditions. As part of the development of a rational method of predicting these effects, a knowledge of the flow field produced by forebody fuselage, canards, etc., is needed. The following is directed toward this first step, that is, development of a data base for forebody and forebody-wing effects on local flow conditions in the vicinity of wing-body configurations.

The data base for airframe effects on inlet "free-stream" conditions consists of experimentally determined values and theoretical and empirical methods for predicting local flow quantities in the vicinity of fuselage-alone or wing-body configurations. In the following sections, applicable experimental data are presented and methods for predicting local flow fields about fuselage-alone or wing-body configurations are described. The data base is then evaluated with respect to the requirements placed on the data base.

7.1 Presentation of Data Base

7.1.1 Experimental data

Table XIV describes the Primary Data Sources from Table I which present experimental data for airframe effects on inlet "free-stream" conditions. This table identifies the configuration about which flow-field data was obtained, the range of free-stream parameters, and the types of effects studied.

Column one of this table identifies the reference number of the data report. Columns two, three, and four identify the test configuration, flow-field probe position and type of data obtained, respectively. Definitions of the symbols used in these columns are given in Table XV. A distinction has been made in these tables between a body of revolution and a fuselage with a canopy, so that an evaluation of the experimental data base with respect to "real" versus "simplified" configuration effects can be made. The probe-position column describes the locations at which data was taken. For example, $F_{s,a}$ indicates that data was obtained near the side of the fuselage and ahead of the wing, while W_{sh} indicates that data were taken under the wing at positions aft of the wing leading edge. It is noted here that data obtained at positions which are more than a body diameter away from the fuselage surface are indicated with W_a or W_{sh}. The definitions in Table XV of the type of data obtained are self-explanatory.

Columns five through eight of Table XIV identify the ranges of Mach number, unit Reynolds number, angle of attack and angle of sideslip covered for each experimental investigation. The remaining columns indicate various effects for which parametric studies may have been carried out experimentally. A check (✓) in any one of these columns indicates that data was taken to determine the effect of that parameter on one or more flow-field quantities. With respect to these effects, a few comments are made here. First, a check in the General Configuration Data column indicates that a large amount of data, or in some cases, all of the data, was taken for a particular configuration. Second, a check in the Protuberance column indicates that data showing the effects of strakes, canards, or missile components on flow-field quantities were presented. The effects can be due to the addition of these components to a given configuration or to a parametric change of one or more of these components.

7.1.2 Prediction methods

Empirical and theoretical methods from Table I which predict flow fields in the vicinity of body-alone or wing-body configurations are grouped in Table XVI according to the type of flow equations solved (unsteady Euler equations; linearized, compressible, steady potential flow equations; etc.) or the type of method used (transonic equivalence rule, far-field matching, etc.). Each method is then further categorized by the type of flow field for which the method is applicable (axisymmetric or three-dimensional), and the speed range (subsonic, transonic, supersonic) for which the method applies. With respect to the "type of flow field" category, two-dimensional methods, per se, were not included in the data base. However, several methods listed are applicable to both 2-D and axisymmetric configurations (refs. 312, 314, 324), and a few 3-D methods involve solving 2-D equations after assumptions are made about the flow (refs. 34, 292).

Table XVII presents the major features of each method shown in Table XVI. This table is arranged by groups in the same manner as was done in Table XVI. This allows one to compare methods within the same group with respect to the basic assumptions, numerical techniques, body modeling techniques, etc. Details concerning particular aspects of methods whose main features are similar or identical (refs. 151 and 306, or 152 and 305, for example) are not presented in this report, since such a task is beyond the scope of the present work. The last name of the first author of a reference is also included after each reference number in Table XVII.

It should be noted at this point that while a large number of methods for predicting forebody and forebody-wing effects are listed in Tables XVI and XVII, these tables surely do not include all methods for predicting such effects. An attempt has been made to include representative examples for each of several groups of methods, and to include the "best known" and most up-to-date methods within each group. Also, as was noted in section 5.1.3, an analysis of various boundary-layer methods is not presented in this report, although some methods include boundary-layer techniques (e.g., refs. 292, 312, 314, 374, 383, 393) as a part of their solution.

7.2 Evaluation of Data Base

7.2.1 Requirements

The local flow field entering an installed inlet is dependent on an array of parameters. These parameters include nose and fuselage geometry (shape and length), wing geometry (leading edge sweep, flap deflection and thickness), canopy size and shape, protuberances (strakes, canards, and missile components), inlet position (side mounted, fuselage-shielded, or wing-shielded), and free-stream Mach number, angle of attack and angle of sideslip. In the preliminary design process, studies of the effects of several geometric parameters on the flow field generated by each configuration are made over a range of free-stream parameters corresponding to various aircraft missions. The main thrust of these studies is usually to define the configuration for which forebody or forebody-wing effects on local inlet flow-field quantities are most favorable, thereby resulting in high inlet total pressure recovery and low inlet distortion, for a variety of missions or a specified mission. Therefore, as previously discussed in section 5.2.1 with respect to inlet external drag, the data base for forebody and forebody-wing effects on inlet "free-stream" conditions must also satisfy the requirements of breadth, ease of application, and accuracy.

In the following sections, the experimental-data and prediction-methods data base for forebody and forebody-wing effects on inlet "free-stream" conditions is evaluated with respect to these requirements. As previously mentioned in the discussion of the inlet and afterbody drag data bases, the accuracy of all the assembled experimental data has not been evaluated.

7.2.2 Experimental data

The manner in which forebody and forebody-wing effects are often studied experimentally is by starting with a "basic" configuration and perturbing about this configuration over a specified range of free-stream Mach number, angle of attack and angle of sideslip. The "basic" configuration is arrived at through configuration definition studies for which certain mission requirements must be met.

A good example of this kind of study is presented in reference 10 (Project Tailor-Mate). After initial configuration-selection studies were made based on specific mission requirements, five "basic" configurations were chosen for further study. These configurations included two fuselage side-mounted inlet designs (two-dimensional inlets), and two under-wing inlet designs (two-dimensional and axisymmetric inlets). Flow-field data, which consisted of local Mach number, angle of attack, angle of sideslip, and total pressure ratio, were obtained at several candidate inlet axial positions for each basic configuration, after which parametric studies were carried out at the most promising inlet station for each configuration. Final results indicated that for the desired mission requirements, shielded-inlet locations offered better flow-field characteristics than fuselage side-mounted inlet locations. References 22, 34, 280 and 322 contain similar systematic studies of the type described in reference 10.

The remainder of the experimental data base is made up of less comprehensive studies. Thus, there exist experimental data only for a few of the many interesting combinations of the governing parameters. Indeed, considering the large number of geometric and free-stream parameters that affect the nature of the flow in the vicinity of a forebody and forebody-wing configuration, it is obvious that an experimental data base could never be complete for design in itself.

However, the experimental data base can be useful as a preliminary design tool as follows. As a part of a preliminary design process for determining candidate inlet positions for a particular configuration, it is necessary to determine regions of reasonably uniform local flow about the configuration. Experimental flow-field data showing the effect of various configuration parameters, such as fuselage shape, canopies, etc., on local flow-field gradients in various regions of interest are found in the experimental data base. Since parametric studies are carried out in a number of experimental programs for several types of wing-body configurations, general trends can be discerned, such as, the presence of high local-flow gradients in the vicinity of sharp corners. The experimental data base can be used in such a fashion, that is, to determine general trends in flow-field quantities and gradients due to various configuration parameters. The experimental data base is, however, of limited usefulness when it is applied to configurations for which the geometry is markedly different from that of any of the configurations represented in the existing data base.

7.2.3 Prediction methods

A wide variety of methods for predicting flow fields in the vicinity of a forebody or forebody-wing configuration are available. An attempt at evaluating the data base with respect to the methods listed in Table XVI is presented in this section through the use of available data comparisons. For the most part, data comparisons of forebody or forebody-wing flow fields are not given. Rather, comparisons are usually of surface pressure distributions. This gives rise to some difficulty in evaluating some prediction methods, since although a method may predict surface pressures accurately, there is no assurance that adequate prediction of flow fields in the candidate locations of an inlet system follows. For the most part, however, some conclusions can be drawn about methods for which surface pressure data comparisons alone are given.

Empirical methods for predicting forebody and forebody-wing flow fields are given in references 4, 11 and 398. References 4 and 11 both use a combination of theoretical methods and experimental data to obtain angle-of-attack effects on local flow-field quantities at under-wing and under-fuselage positions. As would be expected, these methods will be most successful when applied to configurations which are similar to those from which the data were obtained. Flow-field data comparisons using these two methods, however, could not be found. The method given in reference 398, which utilizes two empirical correlating parameters in conjunction with techniques of potential flow, Prandtl-Meyer expansions and conical shocks, predicts local Mach number, total flow angle, and roll angle (see fig. 88). Due to the assumptions and correlations made in developing this method, it is suggested by the author that its application be limited to axial locations at least one diameter downstream of the nose. Flow-field predictions were made for a 3.0/1 von Kármán ogive at a position 6 diameters downstream of the nose and 1.8 radii from the body centerline and are compared with data from references 399 and 400 in figure 89. Data comparisons for local Mach number, shown in figure 89(a), range from very good ($M_\infty = 4.0$, $\alpha = 10°$) to poor ($M_\infty = 2.0$, $\alpha = 20°$). Comparisons with local total-angle data at $M_\infty = 3.0$ show good agreement over the angle-of-attack range, as do the predicted local roll angle, which is assumed to be independent of M_∞ and α.

The prediction methods listed in the second group in Table XVI are those which solve the incompressible potential flow equations. All of these methods model the body as a distribution of surface singularity panels (i.e., sources, sinks, or vortex quadrilaterals). The panels are represented by plane quadrilaterals (refs. 300, 301, 315, 346), curved quadrilaterals (ref. 302), plane triangles (ref. 315), or conic frustrums (ref. 340), and the singularity strengths either are constant (refs. 300, 301, 315, 346) or vary in some fashion (refs. 302, 340). The best-known of these methods is that of Hess and Smith (refs. 300, 301, 302) which has been developed into a computer program commonly referred to as the Douglas-Neumann Program. Comparisons of predicted and experimental surface pressure distributions on wings of wing-body combinations show excellent agreement using this method. Predicted results of surface pressure distribution on an ogive cylinder were recently obtained by Nielsen Engineering & Research, Inc. using the NSRDC version of the Douglas-Neumann code, and were in good agreement with data over most of the ogive-cylinder. With respect to computer time, reference 301 estimates that a configuration consisting of 950 panels takes about 30 CPU minutes to run on an IBM 360/165, while for the NSRDC program described in reference 397, it is estimated that a 500-panel configuration will take about 5 CPU minutes on the CDC 6600. Flow-field data comparisons could not be located for this method or for any of the other methods in this group. The usefulness of these methods is obviously limited, however, since they are applicable only to incompressible flows.

Group 3 of Table XVI contains those methods which solve the linearized, steady, compressible potential flow equations. Of these, only the method of reference 303 requires that the fuselage shape be axisymmetric. With the exception of reference 318, all of these methods employ singularities to model a wing-body configuration. Flow-field data comparisons were available using the methods of references 303, 304, and 347, and therefore these methods are emphasized in this section.

References 303 and 304 utilize 3-D point sources and sinks along the body centerline and 2-D doublets in the crossflow plane to model circular cross sections. Noncircular cross sections are modeled in reference 304 through the use of polar harmonics in the crossflow plane. A distribution of constant-u-velocity-type panels to model wing loading and a distribution of constant-source-type panels to model wing thickness were used in reference 303, while reference 304 uses three-dimensional source panels to model wing thickness and a vortex-lattice model with imaging to account for wing-body interference.

Wing-body configurations for which flow-field data comparisons were obtained in reference 303 are shown in figure 90. Data comparisons of local upwash and sidewash velocities under the wing of WB1 are presented in figures 91 through 94. Comparisons for WB2 are shown in figures 95 and 96. The trends and magnitudes of the data are, for the most part, predicted well, although the predicted upwash and sidewash in the region of the shock compare poorly with data in some cases.

Predictions of flow fields in the vicinity of a body-alone and a wing-body configuration (see fig. 90(a)) were obtained for $M_\infty = 0.40$ using the method of reference 304. A noncircular addition was attached to the fuselage of the body-alone and wing-body configuration. Crossflow velocity vector plots were obtained for each of these models (see fig. 97). Predicted results agree well with data except in the region of the sharp corner. Data comparisons of local upwash velocity for the body-alone and wing-body configuration with and without noncircular additions are presented in figures 98 and 99. Predicted results agree well with data for the body-alone configuration at both 0° and 6° angle of attack. For the wing-body configuration, the trends of the changes due to the noncircular addition, although not all of the magnitudes of the changes, are predicted using this method.

With respect to computer time, a flow-field traverse of the kind presented in figures 91 through 94 for a simple wing-body configuration can be obtained in approximately 30 CPU seconds on the CDC 6600, using the method of reference 303. Using the method of reference 304, it takes about the same amount of time to calculate cross-flow velocities for twenty cross sections along a wing-body configuration of the kind shown in figure 97(b).

Using the method of reference 347, predicted local upwash and sidewash angles in the vicinity of a fighter-type fuselage and fuselage-wing configuration were compared with data from the Tailor-Mate program (ref. 10). Comparisons are presented in figures 100 and 101 for $M_\infty = .9$

and show good agreement between theory and data at the given survey locations. A drawback in using this method is in setting up the geometry for a complicated configuration. This task involves a great deal of time, since the corner points of each surface panel must be input to the program.

Data comparisons using the other methods of group 3 include surface pressure distributions on body-alone and wing-body configurations. Predicted results are usually in good agreement with data for configurations in which viscous effects are small. A disadvantage of several of these methods is the long computer run times needed to obtain pressure distributions on a complete configuration. For example, the finite-element method of reference 318 requires approximately 775 seconds and 1715 seconds on the IBM 360/50 for typical subsonic (200 elements) and supersonic (556 elements) wing-body configurations, respectively. A typical wing-body configuration consisting of 180 wing panels and 72 fuselage panels requires 15 to 20 minutes on the CDC 6600 using the method of reference 309. Also, the method of reference 350, which is presently being incorporated with the method of reference 348 into a program called PAN AIR (Panel Aerodynamics), has recently been exercised on a light-weight supercruiser configuration (ref. 403). Calculations for this wing-body model required 254 CPU seconds on a CDC 7600 using a sparse panel layout (380 panels) and 914 seconds using a dense panel layout (810 panels).

Group 4 in Table XVI presents the only method found which solves the unsteady, compressible, linearized potential flow equations. This finite-element method, which is presented in reference 319, is an extension of a previously derived method for steady flow (ref. 318). The method is applicable to complex wing-body configurations, but data comparisons using this method could not be found.

References 215 and 290, presented in group 5 of Table XVI, contain methods which predict three-dimensional and axisymmetric flow fields, respectively, about axisymmetric bodies. Both methods employ finite-difference relaxation methods which include mixed-differencing in obtaining solutions to the transonic full potential flow equation (compressible, inviscid, steady). A mixed-difference scheme uses central differencing for locally subsonic flow and upwind differencing for locally supersonic flow. While both of these methods were developed for use in the transonic flow-field range, reference 215 can only be used for subsonic free-stream flows.

Once again, data comparisons are only in terms of surface pressure distributions. Both methods are applicable to blunt and pointed bodies, and comparisons with data indicate that predictions compare well with data except in regions where separation occurs. With respect to computer time, reference 215 indicates that a standard run (5 fine mesh θ = constant planes, 70 z = constant planes, and 40 r = constant surfaces, where θ is the circumferential angle) requires 12 to 15 minutes on the CDC 600. Reference 290 states that a typical subsonic free-stream case runs at about 3300 grid points per second on the CDC 6600 (RUN compiler), while a supersonic free-stream case runs at about 2500 points per second, with the number of iteration cycles required for convergence varying from 50 to 100. As an example for the reference 290 method, a staged missile configuration with a fine grid (9457 mesh points) and a coarse grid (2425 mesh points) required about 6 minutes and 2 minutes, respectively, to obtain a converged solution.

Group 6 presents methods for solving inviscid steady supersonic flow. Most of these methods were developed as a means of solving the blunt-body problem, i.e., a flow condition in which the bow shock is detached. However, these methods are also capable of solving attached bow-shock problems. With the exception of reference 324, all of these methods predict three-dimensional flow fields about general configurations at angle of attack.

Of special interest in this group are the shock-fitting (refs. 152, 289, 305) and shock-capturing (refs. 151, 153, 293, 306) methods. The shock-fitting methods model shocks (bow and embedded) as sharp discontinuities across which the Rankine-Hugeniot equations are applied, while the shock-capturing methods are inherently capable of predicting the location and strength of all shocks. Shock-capturing methods must employ a fine mesh in the vicinity of shocks, due to numerical instabilities near a shock wave. Shock-fitting methods can employ a coarser mesh in the region of a shock, although they are more difficult to program. As can be seen, various tradeoffs exist betwen these two types of methods.

Flow-field data comparisons were presented for many of these methods, although several of the comparisons were made for Mach numbers above the range of interest for supersonic aircraft. Figure 102 presents data comparisons of local Mach number, upwash angle, and sidewash angle in the vicinity of a fuselage configuration using the method of reference 34. This is a reference-plane-type method in which flow properties are calculated for several planes around the periphery of the body, with each plane emanating from the centerline. Two-dimensional, conical or axisymmetric methods are used to obtain flow solutions for each plane, and transverse effects between adjacent planes are accounted for using a wave-interference calculation. Prandtl-Meyer expansions are used to model the effects of a canopy or a fuselage corner. Comparisons of predicted results and data range from good for the local Mach number to poor for the local angle of sidewash.

Data comparisons of shock shape about a blunt-nose space shuttle vehicle using the methods of references 151 and 297 are shown in figure 103. Reference 151 is a shock-capturing method, while reference 297 is a semi-characteristic method. Although the Mach number at which comparisons are made is rather high, some comments can be made with respect to the accuracy of these methods. As can be seen in figure 103, the shock-capturing method shock shapes agree very well with data for both the bow and canopy shocks. The predicted location of the canopy shock is displaced from the experimentally determined location due to slight differences between the actual geometry and the analytical approximation used in the calculations. The semi-characteristic method's predicted bow-shock shape agrees well with data only up to $X/L \simeq .3$, and fails to predict the canopy shock for reasons that are discussed in detail in reference 404. Computation time comparisons using an IBM 360/67 computer were made in reference 404 for a pointed nose configuration at $M_\infty = 5$ and $\alpha = 5°$. The comparisons show that while the shock capturing method (SCT) code is about four times faster than the method of characteristics (MOC) code on a point-for-point basis, the SCT code required approximately 2-1/2 times the total time used by the MOC code to calculate the flow field to a distance one half the body length. This is due to the fact that the SCT code used nearly three times as many radial points and twice as many radial planes as the MOC code.

Data comparisons of local Mach number and local-to-free-stream static pressure ratio in the vicinity of a fuselage configuration using the shock-fitting method of reference 152 are shown in figure 104. Predicted values agree well with data from reference 280 at the axial position of interest. As an example of computation time requirements, surface-pressure distributions were obtained for a complete fighter-type aircraft flying at $\alpha = 6°$ and $M_\infty = 2.5$. This calculation was obtained in 63 CPU minutes on an IBM 370/165 using a 24 x 29 mesh in each cross-sectional plane with a total of 1200 marching steps.

Another method for which flow-field data comparisons exist is that of reference 337. Predicted values of local flow-field quantities are compared with Tailor-Mate data (ref. 10) in figure 105. Comparisons of local Mach number, upwash angle and sidewash angle show good agreement between theory and data, while the experimental results show a wider spread of total pressures than the predicted results. The flow field about the entire Tailor-Mate fuselage was computed in about 5 minutes on a CDC 6600. Flow-field calculations for a simpler fuselage model at an angle of attack of 3.8° and $M_\infty = 2.0$ were reported to have required about 3 minutes.

A few other flow-field data comparisons were available using other methods of group 6, but these comparisons were made for extremely high Mach numbers. These comparisons show good agreement between theory and data for bow-shock static pressure ratio (sphere-cone, ref. 306) and for bow-shock shape (blunt cone, ref. 289). Methods for which only surface-pressure-distribution data comparisons were available, but for which computation time examples were available, are presented in references 153 and 305. A flow-field calculation up to the inlet face of the B-1 aircraft flying at $M_\infty = 2.2$ and $\alpha = 3°$ required 55 minutes on a CDC 7600 using the method of reference 153. Using the shock-fitting method of reference 305, calculation of axial surface pressure distributions at several circumferential positions around a blunt-nose space shuttle required 20 minutes on a CDC 6600 computer. This calculation was carried out using 25 mesh points between the body and shock, 20 points around the body, and 1000 points along the body.

Group 7 in Table XVI contains methods for solving the unsteady Euler equations. Of the four methods shown in this group, only reference 312 does not handle angle-of-attack cases.

Data comparisons utilizing the methods of reference 291 and 373 could not be found, and therefore no conclusions can be drawn about the accuracy of these methods. However, reference 373 does state that a typical blunt-body case, for which calculations can be carried out approximately two nose radii downstream, requires approximately 50 minutes on a CDC 3600.

References 311 and 312 are both shock-capturing methods which utilize an implicit approximate factorization finite-difference scheme to solve the flow equations. Although the method of reference 311 was derived to handle complicated aerodynamic shapes, data comparisons to date have been only for simple axisymmetric shapes. Predicted surface pressure distributions from reference 311 on a parabolic-arc body and a hemisphere-cylinder at transonic Mach numbers and several angles of attack are good agreement with data. Surface pressure distributions on mildly and severely indented bodies at zero angle of attack and high supersonic Mach numbers indicate good agreement between experiment and predicted values from reference 312. With respect to computation time, reference 311 indicates that flow-field calculations about a simple configuration typically require about one hour on a CDC 7600. A comparison of computer times presented in reference 312 shows it to be less than half as fast on a per-point basis as the method of reference 373 for a sphere at M_∞ = 4.9. However, the step size of reference 312 was nearly five times that of reference 373, thereby resulting in a faster convergence to the steady state.

Methods for solving the incompressible and compressible unsteady Navier-Stokes equation are presented in groups 8 and 9, respectively. Reference 316, which proposes two methods of solution for the incompressible case, does not contain data comparisons and therefore will not be discussed further here.

All of the references presented in group 9 can be used to solve for laminar or turbulent flows. The methods presented in references 311 and 312, which have been previously discussed in group 7, make use of the "thin layer" approximation, whereby all viscous terms containing derivatives whose direction is along the body are dropped. This approximation is valid only for high Reynolds number flows. Data comparisons are for surface pressure distributions over a hemisphere cylinder at transonic Mach numbers (ref. 311) and for mildly and severely indented bodies at high supersonic Mach numbers (ref. 312). Predicted values are in good agreement with data in all cases. With respect to computation time, reference 311 reports that for free-stream Mach numbers near unity, a viscous solution for a simple body shape is typically obtained in 2-3 hours on a CDC 7600.

Data comparisons using the method of reference 314 could not be found. However, Kutler (ref. 312) compares his predicted shock shape and surface pressure distribution on a sphere-cylinder with that obtained using the method of reference 314, and the results are in excellent agreement for the case presented. One might make the assumption that since Kutler's results agree well with data for a more complicated configuration (indented body), then most likely his and Viviand's method (ref. 314) agree well with data for a simple sphere-cylinder model.

Data comparisons using the method of reference 383 are available in terms of shock shapes and pitot-pressure profiles. Figure 106 shows good agreement between predicted and experimental results for the outermost shock shape and fair agreement for the inner shock shape for a sharp 10° half-angle cone at $M_\infty = 7.95$ and $\alpha = 24°$. Figure 107 shows predicted and experimental pitot-pressure profiles for a 5° sharp cone at $M_\infty = 1.8$ and $\alpha = 0°$. The results were obtained for a turbulent boundary layer at two circumferential positions. Reference 383 attributes the poor agreement at $\phi = 152°$ to flow reattachment and the resulting complicated flow.

Methods which can be used to solve steady, compressible, viscous, supersonic flow are listed in group 10 of Table XVI. All of these methods solve some form of the Navier-Stokes equations.

References 292 and 374 both make use of Hayes' Equivalence Principle, which relates the steady-state flow field over a slender body to an equivalent time-dependent flow field in one less space dimension. In reference 292, steady, three-dimensional flow is reduced to two-dimensional, time-dependent flow, while reference 374 makes use of the equivalence principle to reduce steady, axisymmetric flow to time-dependent one-dimensional flow. In both references, the axial flow is assumed inviscid. However, axial effects are neglected in reference 292, whereas they are included in reference 374.

Data comparisons from reference 292 of local flow-field quantities for a fuselage configuration at $M_\infty = 2.5$ and $\alpha = 15°$ are shown in figure 108. Local sidewash angle contours indicate that the method gives fairly good results in the lower quadrant, while the predicted location of the canopy shock and the predicted sidewash in the upper quadrant do not agree with the data. The incorrect position of the canopy shock is believed to be due to the equivalence principle approximation of neglecting the velocity perturbation along the free-stream flow direction. The poor agreement between experimental and predicted local Mach number and local upwash angle contours are also attributed to this assumption. Other errors associated with this method are those due to discretization, which has to do with substituting a discrete set of points for the space-time continuum, and neglecting axial viscous effects.

Examples of computation time requirements were also given in this reference. Flow-field calculations for an ogive cylinder at a Mach number of 1.98 and an angle of attack of 10 required 3406 time steps and 10 hours on the UNIVAC 1108. Calculations for the previously mentioned fuselage configuration at $M_\infty = 2.5$ and $\alpha = 15°$ required 2079 time steps and 6 hours on the same machine.

The method of reference 374, which solves for the axisymmetric flow field by iteration, presents data comparisons of shock shapes for a cone-cylinder flare configuration at $M_\infty = 4.54$. Results are presented in figure 109 for the zeroth iterate (inviscid solution) and the first viscous iterate. Each successive iterate after the zeroth requires numerical data from the previous iterate and includes viscous effects. Based on a finite-difference mesh of 50 points, the zeroth iterate results were obtained using 2500 timesteps, while the first iterate required 7000 time steps. These cases required 5 minutes and 40 minutes on the UNIVAC 1108, respectively. As can be seen in figure 109, the first iterate solution cone and flare shock shapes agree well with data, while the method does not predict a separation shock for this iterate. More iterations would be required to determine separation in this region.

Reference 393 uses the parabolic Navier-Stokes marching finite-difference method, in which the streamwise viscous derivatives are neglected. This assumption rules out streamwise separation but allows crossflow separation. Laminar or turbulent boundary layer codes can be incorporated into this method. Predicted surface pressure distributions on an ogive-cylinder at $M_\infty = 3$ and $\alpha = 42°$ are in good agreement with data. Flow-field data comparisons of shock shapes for an ogive-cylinder with the method of reference 297 show good agreement between the two methods. The ogive-cylinder calculations were obtained using 20 circumferential planes and 46 points between the body and shock and required about 1 second per marching step on a CDC 7600.

The method of reference 395 also employs the parabolic Navier-Stokes equations, but uses the "thin-layer" approximation (see discussion in group 9 section) to model viscous effects. Data comparisons of surface pressure distributions on a hemisphere-cylinder at $M_\infty = 1.4$ and $\alpha = 5°$ indicate good agreement between predicted and experimental results.

Groups 11, 12, and 13 contain methods for predicting flows in the transonic Mach number regime. These methods make use of transonic small-disturbance theory (group 11), the transonic equivalence rule (group 12) and a far-field matching method (group 13).

The methods of references 296,298, and 299 were developed using the transonic small-disturbance equation and are applicable to slender body, thin wing configurations under the assumptions of small flow deflections and M_∞ near one. These methods incorporate mixed-difference schemes (see group 5 discussion) and a numerical method based on the relaxation method of Murman and Cole. Reference 298 outlines the basic method and includes results for which both fully conservative and nonconservative differencing was used. Reference 296 uses the inviscid method of reference 298 coupled with a boundary-layer method which accounts for viscous effects on the wing. Reference 299 presents a modified transonic small-disturbance equation which can be used to improve the calculation of shocks due to the wing. Of these references, only reference 298 contains pressure distributions on wing-body combinations. The predicted results, which were obtained for a rectangular-wing-body and a swept-wing-body configuration, varied from fair to good when compared to experimental data. With respect to computation time, only reference 296 contained any useful information. It reported that calculations for a supercritical-wing aircraft at $M_\infty = .90$ and $\alpha = 3.56°$ required about 10 minutes on a CDC 7600.

Reference 341 presents a method which utilizes the well-known transonic equivalence rule, which is summarized schematically in figure 110. As this figure shows, the total solution is composed of the inner solution, the outer limit of the inner solution, and the outer solution. The inner solution accounts for the near-field lift and thickness effects of the aircraft configuration. The outer solution calculates the flow about an equivalent axisymmetric body to obtain far-field effects. Details of the solutions of the inner and outer fields are found in Table XVII.

Data comparisons of flow-field pressures in the vicinity of a "bumpy" axisymmetric body are shown in figure 111 and upwash and sidewash comparisons for a scaled F-16 wing-body configuration are presented in figures 112 and 113. Predicted values of pressure for the bumpy body are in very good agreement with data at all survey locations. Figures 112 and 113 indicate good agreement between predicted and experimental sidewash and upwash except in the region of the wing trailing edge. These discrepancies are associated with discontinuities in the axial area distribution which are not accounted for in the prediction method. Flow-field calculations for wing-body configurations usually require under 30 seconds on a CDC 7600.

The last group in Table XVI presents a far-field matching method for solving transonic flows. A schematic of the method is presented in figure 114 which illustrates the decomposition of the flow field into near-field, mid-field and far-field regions. The method of reference 317 uses the transonic small-disturbance equation in the near-field and middle-field regions. However, the only restrictions made on the inner-field flow equations is that they must reduce to the subsonic Prandtl-Glauert equations in the far-field. Other details of the method can be found in Table XVII. No data comparisons were included in this reference, but some information concerning computation time requirements was included. Calculations of the flow field in the vicinity of a nonlifting rectangular wing of aspect ratio 6 at M_∞ = .82 required 232 CPU seconds. The type of machine used was not given.

Data comparisons of flow fields were also given in reference 10 using a combination of a method of characteristics (MOC) and linear theory. The MOC method, which is restricted to axisymmetric body cases, is supplemented by the linear theory method to calculate the effects of forebody camber and the canopy. Also, a perturbation method is used in conjunction with the $\alpha = 0°$ MOC solution to obtain angle-of-attack effects. The linear theory, which is used exclusively at subsonic speeds, is the method of reference 308, and has been previously discussed.

Flow field data comparisons for a cambered nose fuselage configuration at Mach numbers .90 and 2.5 are presented in figures 115 and 116, respectively. The fuselage cross-sectional shape in the region of interest is also included in these figures. For the subsonic case the total pressure ratio was assumed to be equal to 1.0 for prediction purposes. The subsonic prediction results show the general angle-of-attack trends of the data with respect to local upwash and sidewash angles, although the proper levels and gradients are not always in good agreement. Figure 116(a) indicates fairly good agreement between predicted and experimental total-pressure ratio, while the predicted results show a region of much higher Mach numbers and much lower sidewash angles in the upper part of the grid than those seen in the data. Figures 116(b) and (c) also indicate that the general angle-of-attack and angle-of-sideslip trends seem to be predicted reasonably well.

Figures 117 and 118 present flow-field data comparisons for a wing-fuselage configuration at Mach numbers of .90 and 2.5, respectively. The fuselage, which has a strake attached to it in the region where data was obtained, was represented as a wing with varying leading-edge sweep and with dihedral and camber. Since the linear method did not allow calculation of yawed wings, a special means of obtaining sideslip effects was also devised. Figure 117 shows predicted upwash and sidewash angles to be in rather poor agreement with data, while the predicted local Mach number comparisons are somewhat better. Figure 118 also shows rather poor agreement between experimental and predicted flow-field distributions. The consistent trends in the predicted total-pressure ratios are not seen in the data, and the predicted bow shock is not suggested by the test results. The predicted results also show a region of higher upwash angle on the inboard portion of the grid than those seen in the data.

7.2.4 Concluding remarks

The experimental data and prediction method data base for forebody and forebody-wing effects on inlet "free-stream" conditions has been presented. An evaluation of this data base with respect to completeness, ease of application, and accuracy has led to the following conclusions:

1. Although a few systematic studies for fuselage or wing-fuselage configurations exist (e.g., references 10, 22, 34, 280), the experimental data portion of the data base consists mostly of studies of body-of-

revolution configurations or simple wing-body configurations. Because of this, this portion of the data base is adequate for preliminary prediction only for configurations which are similar to those previously tested. Since the experimental data base for "real" fuselage shapes is very small, the usefulness of this portion of the data base is quite limited.

2. Empirical flow-field methods, as one might expect, are usually only useful for configurations similar to those used in obtaining the method. Also, the empirical methods presented are for bodies of revolution and simple wing-body configurations.

3. As the type of flow and configuration becomes more complicated, the cost of obtaining accurate predictions of flow fields increases. In other words, as the flow equations become more complicated to solve, such as the incompressible, steady, potential flow equations versus the unsteady Euler equations, and as the geometry becomes more complicated, such as a body of revolution versus a fighter-type wing-fuselage configuration, the cost of the computerized prediction methods and the complexity of the associated geometry package will increase. In terms of preliminary design, therefore, a tradeoff exists between cheaper methods which calculate flow fields for simplified configurations and more expensive methods which can be used for complicated geometries. The accuracy gained by using methods capable of handling complicated geometries may indeed be offset by increased costs due to long computer run times.

8. REFERENCES

1. McMillan, O. J., Perkins, E. W., Kuhn, G. D., and Perkins, S. C., Jr.: Data Base for the Prediction of Airframe/Propulsion System Interference Effects. NEAR TR 122, July 1976.

2. Kuhn, G. D.: Computer Programs for Prediction of Nozzle Afterbody Drag of Single and Twin Engine Configurations. NEAR TR 182, Jan. 1979.

3. Godunov, S. K., Zabrodyn, A. W., and Prokopov, G. P.: A Difference Scheme for Two-Dimensional Unsteady Problems of Gas Dynamics and Computation of Flow with a Detached Shock Wave. Cornell Aero. Lab. Transl. by I. O. Bohechevsky, Translated from Zh. Vychisiliteloni Mat. i. Mat. Fiziki, Vol. 1, 1961, p. 1020.

4. Smith, A. and Pierce, J.: Exact Solution of the Neumann Problem-Calculation of Non-Circulatory Plane and Axially Symmetric Flows About or Within Arbitrary Boundaries. Douglas Rept. No. ES26988, Apr. 1958.

5. Hess, J.: Calculation of Potential Flow About Bodies of Revolution Having Axes Perpendicular to the Free Stream Direction. Douglas Rept. No. ES29812, Oct. 1960.

6. Hess, J. and Smith, A.: Calculation of Non-Lifting Potential Flow About Arbitrary Three-Dimensional Bodies. Douglas Rept. No. ES40622, Mar. 1962.

7. Lieblein, S. and Stockman, N. O.: Compressibility Correction for Internal Flow Solutions. J. of Aircraft, Vol. 9, No. 4 Apr. 1972.

8. Stratford, B. S. and Beavers, G. S.: The Calculation of the Compressible Turbulent Boundary Layer in an Arbitrary Pressure Gradient - A Correlation of Certain Previous Methods. ARC R&M No. 3207, Sept. 1959.

9. Stratford, B. S.: The Prediction of Separation of the Turbulent Boundary Layer. J. Fluid Mech., Vol. 5, Part 1, Jan. 1959.

10. Putnam, L. E.: Results of Assessment of State-of-the-Art for Predicting Pressure Distributions and Drag of Boattail Nozzles. NASA/Langley Research Center Memo, Propulsion Aerodynamics Analysis Section, Jan. 1977.

APPENDIX A

REFERENCE LIST FOR INLET/AIRFRAME INTERACTION EFFECTS

I-1. Anderson, W. E., Petersen, M. W., and Sorensen, N. E.: An Evaluation of Transonic Spillage Drag Based on Test Results From Large-Scale Inlet Models. Conference on Aircraft Aerodynamics, NASA SP-124, May 1966.

I-2. Antonatos, P. P., Surber, L. E. and Stava, D. J.: Inlet/Airplane Interference and Integration. AGARD LS-53, Airframe/Engine Integration, May 1972.

I-3. Antonatos, P. P., Richey, G. K. and Klepinger, R. H.: Airframe Propulsion Integration Effects on Vehicle Design. AFAPL-TR-69-103, June 1970.

I-4. Ball, W. H.: Propulsion System Installation Corrections. Vols. I, II, III, and IV. AFFDL-TR-72-147, Dec. 1972.

I-5. Ball, W. H.: Rapid Calculation of Propulsion System Installation Corrections. AIAA Paper No. 74-1174, AIAA/SAE 10th Propulsion Conference, Oct. 1974.

I-6. Ball, W. H. and Ross, P. A.: Experimental Correlation of Installation Effects for Inlet/Airplane Integration. AIAA Paper No. 71-759, AIAA/SAE 7th Propulsion Joint Specialist Conference, June 1971.

I-7. Brazier, M. E. and Ball, W. H.: Accounting of Aerodynamic Forces on Airframe/Propulsion Systems. AGARD CP-150, Airframe/Propulsion Interference, Mar. 1975.

I-8. Callahan, C. J.: An Experimental Investigation of the Component Drag Composition of a 2-D Inlet at Transonic and Supersonic Speeds. AGARD CP-150, Airframe/Propulsion Interference, Mar. 1975.

I-9. Carter, E. C.: Experimental Determination of Inlet Characteristics and Inlet Airframe Interference. AGARD LS-53, Airframe/Engine Integration, May 1972.

I-10. Cawthon, J. A., Crosthwait, E. L., et al.: Supersonic Inlet Design and Airframe-Inlet Integration Program (Project Tailor-Mate). Vols. I, II, and III, AFFDL-TR-71-124, May 1973.

I-11. Crosthwait, E. L., Kennon, I. G., Jr., Roland, H. L., et al.: Preliminary Design Methodology for Air-Induction Systems. SEG-TR-67-1, Jan. 1967.

I-12. Ferri, A.: Engine/Airplane Interference: Definition of the Problem and Related Basic Fluid Dynamic Phenomena. AGARD LS-53, Airframe/Engine Integration, May 1972.

I-13. Fuhs, A. E.: Engine Integration and Thrust/Drag Definition. AGARD LS-53, Airframe/Engine Integration, May 1972.

I-14. Fuller, D. E.: Pressure Distributions for a Rectangular Supersonic Inlet at Subsonic Speeds. NASA rough draft L10424. (See 107 for final version).

I-15. Hand, W. H. and Johnson, R. H.: Propulsion System Integration and Test Program. AFAPL-TR-69-103, June 1970.

I-16. Hartill, W. R.: Test Results of an .07 Scale B-1 External Compression Inlet Drag Model, NASA Ames Test (97)641. North American Rockwell Rept. NA-73-125, Mar. 1973.

I-17. Hartill, W. R., Schoelen, F. J. and Kiser, C. E.: Test Results of an .07 Scale B-1 Mixed Compression Inlet Drag Model, NASA Ames Test (97,11)640. North American Rockwell Rept. NA-72-775, Nov. 1972.

I-18. Hasel, L. E., Weirich, R. C. and Mascitti, V. R.: Assessment of the Effects of Inlet Spillage, Bypass, and Bleed Air on the Performance of Supersonic Cruise Airplanes. Conference on Aircraft Aerodynamics, NASA SP-124, May 1966.

I-19. Hawkins, J. E., Kirkland, F. P. and Turner, R. L.: Inlet Spillage Drag Tests and Numerical Flow-Field Analysis at Subsonic and Transonic Speeds of a 1/8-Scale, Two Dimensional, External-Compression, Varible-Geometry, Supersonic Inlet Configuration. General Dynamics/Convair Rept. No. FZA-467, May 1974.

I-20. Jaarsma, F.: Inlets-Airplane Testing in Transonic Wind Tunnels. AGARD-CP-91-71, Inlet and Nozzles for Aerospace Engines, Sept. 1971.

I-21. Kamman, J. H. and Hall, C. L.: Effects of Selected Design Variables on Three Ramp, External Compression Inlet Performance. NASA CR-2485, Jan. 1975.

I-22. King, L. S.: Investigation, at Inlet Locations, of Fuselage Flow Fields at Transonic and Supersonic Speeds. NASA TN D-7364, Aug. 1973.

I-23. King, L. S. and Schmidt, T. W.: Studies of Aircraft Flow Fields at Inlet Locations. AGARD CP-71-71, Aerodynamic Interference, Jan. 1971.

I-24. Kiser, C. E. and Schoelen, F. J.: Results of the B-1 .07-Scale External Compression Inlet Drag Model Wind Tunnel Test. North American Rockwell Rept. NA-74-159, Dec. 1974.

I-25. Kutschenreuter, P. H.: Force Balance Determination of Supersonic/Hypersonic Combustion-Inlet Performance Levels. J. Aerospace Sci., Nov. 1962, pp. 1389-1390.

I-26. Kutshenreuter, P. H. and Balent, R. L.: Hypersonic Inlet Performance from Direct Force Measurement. J. Spacecraft & Rockets, Vol. 2, No. 2, Apr. 1965, p. 192.

I-27. McVey, F. D., Phillips, E. J. and Rejeske, J. V.: Experimental Investigation of Transonic Inlet Drag. AFAPL-TR-69-103, June 1970.

I-28. Miller, B. A.: Experimentally Determined Aeroacoustic Performance and Control of Several Sonic Inlets. AIAA Paper No. 75-1184, AIAA/SAE 11th Propulsion Conference, Sept-Oct. 1975.

I-29. Mount, J. S.: Effect of Inlet Additive Drag on Aircraft Performance. J. Aircraft, Vol 2, No. 5, Sept-Oct 1965, pp. 374-378.

I-30. Muller, G. L. and Gasko, W. F.: Subsonic-Transonic Drag of Supersonic Inlets. J. Aircraft, Vol. 4, No. 3, May-June 1967, pp. 231-236.

I-31. Neale, M. C. and Armstrong, F. W.: Some Recent Research on Supersonic Intakes at NGTE. AGARD CP-71-71, Aerodynamic Interference, Jan. 1971.

I-32. Osmon, R. V.: Improved method of Spillage Drag Prediction for Two Dimensional Supersonic Inlets. AIAA Paper No. 67-449, AIAA 3rd Propulsion Joint Specialist Conference, July 1967. Also, J. Aircraft, Vol. 5, No. 3, May-June 1968, pp. 254-260.

I-33. Petersen, M. W. and Tamplin, G. C.: Experimental Review of Transonic Spillage Drag of Rectangular Inlets. AFAPL-TR-66-30, May 1966.

I-34. Prokop, C. and Sanator, R. J.: Investigation of Airframe-Inlet Interaction for Supersonic Tactical Fighter Aircraft (U). AFFDL-TR-70-66, Jan. 1970. (Confidential)

I-35. Rejeske, J. V. and Stava, D.: A Test Technique of Inlet/Aircraft Drag Evaluation. AIAA Paper No. 74-1145, AIAA 10th Propulsion Conference, Oct. 1974.

I-36. Richey, G. K., Surber, L. E. and Laughrey, J.A.: Airframe/Propulsion System Flow Field Interference and the Effect on Air Intake and Exhaust Nozzle Performance. AGARD CP-150, Airframe/Propulsion Interference, Mar. 1975.

I-37. Rochow, T. C., Sharp, B. M., and Spong, E. D.: Calculation of Subsonic Inlet Drag. AFAPL-TR-69-103, June 1970.

I-38. Schreiber, L. H.: A Plan for Bookkeeping of the Propulsion and Aerodynamic Elements of Airplane Performance. AFAPL-TR-69-103, June 1970.

I-39. Smith, O. W.: Generalized Method of Predicting Lip-Suction and Spillage Drag Force Coefficients of Isolated Axisymmetric Inlets. General Dynamics AIM No. 185, May 1969.

I-40. Sorensen, N. E., Anderson, W. E. and Wong, N. D.: Performance Summary of a Two-Dimensional and an Axisymmetric Supersonic-Inlet System. Conference on Aircraft Aerodynamics, NASA SP-124, May 1966.

I-41. Stockman, N. O.: Potential and Viscous Flow in VTOL, STOL, or CTOL Propulsion System Inlets. AIAA Paper No. 75-1186, AIAA 11th Propulsion Conference, Oct. 1975.

I-42. Surber, L. E. and Stava, D. J.: Supersonic Inlet Performance and Distortion During Maneuvering Flight. AGARD CP-91-71, Inlets and Nozzles for Aerospace Engines, Sept. 1971.

I-43. Surber, L. E.: Effect of Forebody Shape and Shielding Technique on Two-Dimensional Supersonic Inlet Performance. AIAA Paper No. 75-1183, AIAA/SAE 11th Propulsion Conference, Oct. 1975.

I-44. Thornley, S. A. M. and Carter, E. C.: The Measurement of the Transonic Spillage Drag of a Supersonic Intake. AGARD CP-150, Airframe/Propulsion Interference, Mar. 1975.

I-45. Woollett, R. R., Meleason, E. T., and Choby, D.A.: Transonic Off-Design Drag and Performance of Three Mixed-Compression Axisymmetric Inlets. NASA TM X-3215, June 1975.

I-46. Woollett, R. R., Meleason, E.T., and Choby, D. A.: Transonic Off-Design Drag and Performance of an Axisymmetric Inlet with 40-Percent Internal Contraction on Design. NASA TM X-3042, Aug. 1974.

I-47. Wong, N. D. and Anderson, W. E.: Experimental Investigtion of a Large-Scale, Two-Dimensional, Mixed Compression Inlet System. NASA TN D-7445, Oct. 1973.

I-48. Mascitti, V. R.: Charts of Additive Drag Coefficient and Mass-Flow Ratio for Inlets Utilizing Right Circular Cones at Zero Angle of Attack. NASA TN D-3434, 1966.

I-49. Sibulkin, M.: Theoretical and Experimental Investigation of Additive Drag. NACA Rept. 1187, 1954.

I-50. Wong, N. D. and Anderson, W. E.: Experimental Investigation of a Large-Scale, Two-Dimensional, Mixed Compression Inlet System NASA TN D-6392, June 1971.

I-51. Dobson, M. D. and Goldsmith, E. L.: The External Drag at Subsnic and Supersonic Speeds of Fuselage-Side Intakes for Strike-Fighter Aircraft. ICAS Paper No. 70-49, The 7th Congress of the International Council of the Aeronautical Sciences (Rome, Italy), Sept. 1970.

I-52. McVey, F. D., Rejeske, J. V., and Phillip, J. V.: Experimental Evaluation of Inlet Drag Characteristics in the Transonic Mach Number Regime. AFAPL-TR-68-119, Nov. 1968.

I-53. Rooney, E. C : Development of Techniques to Measure In-Flight Drag of a U.S. Navy Fighter Airplane and Correlation of Flight Measured Drag with Wind Tunnel Data. AGARD CP-124, Aerodynamic Drag, Oct. 1973.

I-54. Black, J. A.: A Wind Tunnel Test of a 0.07-Scale Inlet Drag Model of the B-1 Aircraft at Mach Numbers from 0.60 to 1.60. AEDC-TR-73-188, Nov. 1973.

I-55. Mossman, E. A. and Anderson, W. E.: The Effect of Lip Shape on a Nose-Inlet Installation at Mach Numbers from 0 to 1.5 and a Method for Optimizing Engine-Inlet Combinations. NACA RM A54B09, May 1954.

I-56. Cawthon, J. A., Truax, P. P., and Savage, T. M.: Advanced Inlet Study (Tailor-Mate II). AFFDL-TR-73-72, June 1973.

I-57. Lobert, G. and Thomas, J.: Engine Airframe Interference Problems Peculiar to Aircraft Configurations with Nacelles Mounted Above the Wing. AGARD CP-27, Integration of Propulsion Systems in Airframes, Sept. 1967.

I-58. Rall, F. T., Jr.: Aircraft and Propulsion Operational Considerations Related to Inlet Design. AGARD CP-27, Integration of Propulsion Systems in Airframes, Sept. 1967.

I-59. Fraenkel, L. E.: The External Drag of Some Pitot-Type Intakes at Supersonic Speeds. Part I. RAE Rept. No. 2380, June 1950.

I-60. Tsukahira, T. W., Wong, W. F., Yamada, M., and Hall, G. R.: Supersonic Inlet Investigation. Vols. I, II, and III. AFFDL-TR-71-121, Sept. 1971.

I-61. Tindell, R. H.: F-14 Inlet Maneuvering Capability. AIAA Paper No. 73-1273, AIAA/SAE 9th Propulsion Conference, Nov. 1973.

I-62. Johnson, R. H., et al.: Propulsion System Integration and Test Program (Steady State) Summary. Part I. AFAPL-TR-69-36, Feb. 1969.

I-63. Rejeske, J. V. and Porter, J. L.: Inlet/Aircraft Drag Investigation. AFFDL-TR-74-34, Apr. 1974.

I-64. Johnson, T. J. and Huff, J. N., Jr.. Propulsion System Integration and Test Program (Steady State). Part IV. AFAPL-TR-69-44, June 1969.

I-65. Behal, J. A., Belgen, M. H., and Simons, D. E.: Wind Tunnel/ Flight Data Correlation, Final Report. Vols. I, II, III, and IV. AFFDL-TR-71-105, Oct. 1971.

I-66. Johnson, T. J. and Young, L. C.: Summary of Methods for Calculating Inlet Performance Losses. North American Raviation Rept. TFD-67-767, Aug. 1967.

I-67. Young, L. C.: Design Concepts for Inlets and Exhaust Nozzles. North American Aviation Rept. TFD-64-170, Feb. 1964.

I-68. Syberg, J. and Koncsek, J. L.: Transonic and Supersonic Test of the SST Prototype Air Intake. FAA-SS-72-50, Apr. 1972.

I-69. Syberg, J. and Koncsek, J. L.: Experimental Evaluation of a Mach 3.5 Axisymmetric Inlet. NSA CR-2563, July 1975.

I-70. Syberg, J. and Hickcox, T. E.: Design of a Bleed System for a Mach 3.5 Inlet. NASA CR-2187, Jan. 1973.

I-71. Goldsmith, E. L. and Griggs, C. F.: The Estimation of Shock Pressure Recovery and External Drag on Conical Centre-Body Intakes at Supersonic Speeds. ARC R&M 3035, 1959.

I-72. Moeckel, W. E.: Approximate Methods for Predicting Form and Location of Detached Shock Waves Ahead of Plane or Axially Symmetric Bodies. NACA TN 1921, July 1949.

I-73. Love, E. S.: A Reexamination of the Use of Simple Concepts for Predicting the Shape and Location of Detached Shock Waves. NACA TN 4170, Dec. 1957.

I-74. Brooks, A. J. and Dodd, G. J.: Mixed Compression Air Intakes for Operation at Mach 2.2. Presented at 2nd International Symposium on Air Breathing Engines (Sheffield, England), Mar. 1974.

I-75. Samanich, N. E., Barnett, D. O., and Salmi, R. J.: Effect of External Boundary Layer on Performance of Axisymmetric Inlet at Mach Numbers of 3.0 and 2.5. NASA TM X-49, Sept. 1959.

I-76. McDill, H. E.: Results of a Full Scale B-1 Inlet/Engine Compatibility Test at Subsonic and Supersonic Mach Numbers. AEDC-TR-75-3, Jan. 1975.

I-77. Watne, D. A.: Determination of the Supersnic Additive Drag of Several Similar Inlet Configurations of the Type Used in the F-111. ASD TR-68-50, Nov. 1968.

I-78. Calogeras, J. E. and Meleason, E. T.: Wind Tunnel Investigation of Techniques for Reducing Cowl Drag of an Axisymmetric External-Compression Inlet at Mach 2.49. NASA TM X-1516, Mar. 1968.

I-79. Goldsmith, E. L. and Smith, G. V. F.: The Performance of Some Axisymmetric Isentropic Centrebody Intakes Designed for Mach Numbers of 2.48 and 3.27. ARC R&M 3585, 1969.

I-80. Dobson, M. D.: The External Drag of Fuselage Side Intakes: Rectangular Intakes with Compression Surfaces Vertical. ARC CP-1269, 1974.

I-81. Schulte, H. E.: A Comparison of Approximate Methods of Predicting Shock Detachment Distance for Two-Dimensional Supersnic Inlets. Air Force Institute of Technology, GAE/AE/74S-6, Sept. 1974.

I-82. Bagley, J. A.: Some Aerodynamic Problems of Powerplant Installation on Swept-Winged Aircraft. In: Proceedings, Royal Aeronautical Society, Two Day Convention on Short-Range Transport (London, England), May 1969.

I-83. Neale, M. C.: Aerodynamic Problems of Powerplant Installation. In: Proceedings, Royal Aeronautical Society, Two Day Convention on Short-Range Transport (London, England), May 1969.

I-84. MacMiller, C. J.: Investigation of Subsonic Duct Distortion. AFFDL-TR-69-21, Mar. 1969.

I-85. Muller, G. L. and Gasko, W. F.: Studies of Drag-Reduction Methods for Subsonic Operation of Supersonic Inlets. J. Aircraft, Vol. 4, No. 4, July-Aug 1967, pp. 322-327.

I-86. Moeckel, W. E.: Estimation of Inlet Lip Forces at Subsonic and Supersonic Speeds. NACA TN 3457, June 1955

I-87. Kremzier, E. J. and Campbell, R. C.: Angle-of-Attack Supersonic *Performance of a Configuration Consisting of a Lamp-Type Scoop* Inlet Located Either on Top or Bottom of a Body of Revolution. NACA RM E54C09, May 1954.

i-88. Gnos, A. V.: Performance of a Top Inlet with a Vertical Porous Wedge at Mach Numbers of 1.6 to 2.35. NASA Memo 2-2-59A, May 1959.

I-89. Lazzeroni, F. A. and Pfyl, F. A.: Effect of Boundary-Layer Control and Inlet Lip Shape on the Performance of a Twin-Scoop Air-Induction System at Mach Numbers from 0 to 1.9. NACA RM A55L02, Feb. 1956.

I-90. Crosthwait, E. L.: Pitot Inlet Additive Drag. J. Aircraft, Vol. 7, No. 6, Nov-Dec 1970, pp. 569-570.

I-91. Hube, F. K. and Jenke, L. M.: Wind Tunnel Tests of Supersonic Two-Dimensinal and Half-Axisymmetric Inlet Models in a Non-uniform Flow Field at Mach Numbers from 1.5 through 2.5. AEDC-TR-71-107, May 1971.

I-92. Mascitti, V. R.: An Approximate Solution of Additive-Drag Coefficient and Mass-Flow Ratio for Inlets Utilizing Right Circular Cones at Zero Angle of Attack. NASA TN D-5537, Nov. 1969.

I-93. Steffen, F. W.: Cruise Performance of an Isolated 1.15 Pressure Ratio Turbofan Propulsion System Simulator at Mach Numbers from 0.6 to 0.85. NASA TM X-3064, June 1974.

I-94. Tjonneland, E.: The Design, Development and Testing of a Supersonic Transport Intake System. AGARD CP-91-71, Inlets and Nozzles for Aerospace Engines, Sept. 1971.

I-95. Sussman, M. B., Lamp, G. W. N., Hill, D. J., Bowen, R. R., et al.: A Study of Inlet/Engine Interaction in a Transonic Propulsion Wind Tunnel. Boeing (Commerical Airplne Group) Rept. No. D6-60116, Jan 1970.

I-96. Re, R. J.: An Investigation of Several NACA 1-Series Axisymmetric Inlets at Mach Numbers from 0.4 to 1.29. NASA TM X-2917, Mar. 1974

I-97. Re, R. J.: An Investigation of Several NACA 1-Series Inlets at Mach Numbers from 0.4 to 1.29 and Mass-Flow Ratios Near 1.0. NASA TM X-3324, Dec. 1975.

I-98. Vick, A. R.: An Investigation of Discharge and Thrust Characteristics of Flapped Outlets for Stream Mach Numbers from 0.40 to 1.30. NACA TN 4007, July 1957.

I-99. Dewey, P. E. and Vick, A. R.: An Investigation of the Discharge and Drag Characteristics of Auxiliary-Air Outlets Discharging into a Transonic Stream. NACA TN 3466, July 1955.

I-100. Dewey, P. E.: A Preliminary Investigation of Aerodynamic Characteristics of Small Inclined Air Outlets at Transonic Mach Numbers. NACA TN 3442, May 1955.

I-101. Sorensen, N. E. and Smeltzer, D. B.: Performance Estimates for a Supersonic Axisymmetric Inlet System. AIAA Paper No. 72-45, AIAA 10th Aerospace Sciences Meeting, Jan. 1972.

I-102. Dutton, R. A. and Goldsmith, E. L.: The Drag of Some Wedge Centre-Body Intakes at Mach Numbers of 1.56, 1.86, and 2.14. ARC CP-968, 1967.

I-103. Cubbison, R. W., Meleason, E. T. and Johnson, D. F.: Effect of Porous Bleed in a High-Performance Axisymmetric Mixed Compression Inlet at Mach 2.50. NASA TM X-1692, Nov. 1968.

I-104. Sorensen, V. L.: Computer Programs for Calculating Flow Fields in Supersonic Inlets. NASA TN D-2897, July 1965.

I-105. Smeltzer, D. B. and Sorensen, N. E.: Investigation of a Nearly Isentropic Mixed-Compression Axisymmetric Inlet System at Mach Numbers 0.6 to 3.2. NASA TN D-4557, May 1968.

I-106. Sharp, B. M. and Howe, J. P.: Procedures for Estimating Inlet External and Internal Performance. NWC TP 5555, Apr. 1974.

I-107. Fuller, D. E.: Pressure Distributions for a Rectangular Supersonic Inlet at Subsonic Speeds. NASA TM X-3305, Feb. 1976.

I-108. McVey, F. D., Rejeske, J. V., and Phillips, E. J.: Experimental Evaluation of Inlet Drag Characteristics in the Transonic Mach Number Regime. AFAPL-TR-68-119, Supplement 1, Nov. 1969.

I-109. Trommsdorff, W.: Investigation of Power Plant Inlets. DLR FB 66-34, AAE Library Translation No. 1285, May 1966.

I-110. Goldsmith, E. L.: Boundary Layer Bleed Drag at Supersonic Speeds. RAE TR-66143, Apr. 1966.

I-111. Motycka, D. L., Disabato, V. J., and Andersen, L. Q.: The Use of a Powered Model for Subsonic Nacelle Optimization. ASME Paper No. 72-GT-14, Gas Turbines and Fluids Engineering Conference and Products Show, Mar. 1972.

I-112. Cooper, W. R. and Isely, F. D.: Mini-Inlet Investigation. (U) AFAPL-TR-67-234, July 1967. (Secret)

I-113. Lucas, E. J.: Wind Tunnel Test of a Segmented Engine Inlet at Supersonic Mach Numbers. (U) AEDC-TR-67-139, Apr. 1967. (Confidential)

I-114. Bowditch, D. N., Coltrin, R. E., Sanders, B. W., Sorensen, N. E., and Wasserbauer, J. F.: Supersonic Cruise Inlets, in Aircraft Propulsion. Conference on Aircraft Propulsion, NASA SP-259, Nov. 1970.

I-115. Koenig, R. W.: Inlet Sensitivity Study for a Supersonic Transport. NASA TN D-3881, Mar. 1967.

I-116. Postlewait, J.: Prediction and Measurement of Propulsion System Performance. ASME Paper No. 73-WA Aero 5, Winter Annual Meeting, Nov. 1973.

I-117. Bencze, D. P.: Nacelle-Airframe Interference at Low Supersonic Mach Numbers. AIAA Paper No. 72-1113, AIAA/SAE 8th Joint Propulsion Specialist Conference, Dec. 1972.

I-118. Sorensen, N. E. and Bencze, D. P.: Possibilities for Improved Supersonic Inlet Performance. AIAA Paper No. 73-1271, AIAA/SAE 9th Propulsion Conference, Nov. 1973.

I-119. Shaw, R. J., Wasserbauer, J. F., and Neumann, H. E.: Boundary-Layer Bleed System Study for a Full-Scale, Mixed-Compression Inlet with 45 Percent Internal Contraction. NASA TM X-3358, Mar. 1976.

I-120. Percy, T. G. and Johnson, H. W.: Experimental Investigation at Mach Numbers 1.88, 3.16, and 3.83 of Pressure Drag of Wedge Diverters Simulating Boundary-Layer-Removal Systems for Side Inlets. NACA RM E53L146, Feb. 1954.

I-121. Wilhelm, G. A. and Matthews, J. P.: Trisonic Wind Tunnel Tests of the B-1 0.07-Scale Inlet Drag Model I (Test 1, TWT 242). Vols. I, II, III, IV, and V. North American Rockwell Rept. NA-71-721, Aug. 1971.

I-122. Johnson, T. J.: Test Results of the 0.07-Scale B-1 Inlet Drag Model (TWT 242). North American Rockwell Rept. NA-71-1082, Dec. 1971.

I-123. Kiser, C. E., Johnson, T. J., Manzoku, R. T., and Schoelen, F. J.: Transonic Wind Tunnel Test Results of the 0.07-Scale B-1 Inlet Drag Model (AEDC-TF-305). Rockwell International Corp. Rept No. NA-74-158, Sept. 1974.

I-124. Shaw, R. J., Mitchell, G. A., and Sanders, B. W.: Forward-Slanted Slot Throat Stability Bypass to Increase the Stable Airflow Range of a Mach 2.5 Inlet with 60-Percent Internal Contraction. NASA TM X-2973, May 1974.

I-125. Choby, D. A.: Tolerance of Mach 2.50 Axisymmetric Mixed-Compression Inlets to Upstream Flow Variations. NASA TM X-2433, Jan. 1972.

I-126. Smeltzer, D. B. and Sorensen, N. E.: Analytic and Experimental Performance of Two Isentropic Mixed Compression Axisymmetric Inlets at Mach Numbers 0.8 to 2.65. NASA TN D-7320, June 1973.

I-127. Wasserbauer, J. F., and Choby, D. A.: Performance of a Bicone Inlet Designed for Mach 2.5 with Internal Distributed Compression and 40-Percent Internal Contraction. NASA TM X-2416, Feb. 1972.

I-128. Holdhusen, J. S.: Analysis and Demonstration Techniques for Installation Aerodynamic Effects on High Bypass Turbofans. Reprint of Paper from 32nd Meeting of the AGARD Propulsion and Energetics Panel, Sept. 1968.

I-129. Anderson, B. H.: Design of Supersonic Inlets by a Computer Program Incorporating the Method of Characteristics. NASA TN D-4960, Jan. 1969.

I-130. Anderson, B. H.: Optimization of Supersonic Inlets Using the Method of Characteristics. Symposium on Analytic Methods in Aircraft Aerodynamics, NASA SP-228, Oct. 1969.

I-131. Sorenson, N. E., Latham, E. A., and Morris, S. J.: Prediction of Supersonic and Hypersonic Inlet Flow Fields. Symposium on Analytic Methods in Aircraft Aerodynamics, NASA SP-228, Oct. 1969.

I-132. Anderson, B. H.: Characteristics Study of a Bicone Mixed-Compression Inlet for Mach 1.80 to 2.50. NASA TN D-5084, Mar. 1969.

I-133. Sanders, B. W. and Cubbison, R. W.: Effect of Bleed-System Back Pressure and Porous Area on the Performance of an Axisymmetric Mixed-Compression Inlet at Mach 2.50. NASA TM X-1710, Dec. 1968.

I-134. Adams, C. E. and Hollweger, D. J.: McAir Series VII 1/6 Scale Inlet Test Analysis Report. CDRL Sequence No. A184BA. Vols. I and II, McDonnell Douglas Corp. Rept. No. MDC A0638, Nov. 1970.

I-135. Hollweger, D. J. and Stevens, C. H., Jr.: F-15 McAir Series VIII 1/6 Scale Inlet Test Analysis Report. CDRL Sequence No. A184BA, Vols. I and II, McDonnell Douglas Corp. Rept. No. MDC A1177, Sept. 1971.

I-136. Sonntag, A. H., Laffay, P. J. and Southerland, T. L.: Wind Tunnel Test on the 7.5 Percent Scale F-15 Aerodynamic Drag Model in the AEDC 16 Foot Transonic and Supersonic Facility. Series I, Test TF240 and SF129 (U). McDonnell Douglas Corp. Rept. No. MDC A0624, Oct. 1970. (Confidential)

I-137. Eschweiler, J. C.: F-15 Air Induction and Exhaust System (U). McDonnell Douglas Corp. Rept. No. MDC A1301 (Revised), Apr. 1973. (Confidential)

I-138. Farr, A. P.: F-15 Air Induction and Exhaust System (U). McDonnell Douglas Corp. Rept. No. MDC A0920, Apr. 1971. (Confidential)

I-139. Southerland, T. L.: Supersonic Drag Evaluation Test on the 7.5 Percent Scale F-15 Aerodynamic Drag Model in the AEDC 16 Foot Supersonic Facility, Test SF135 (U). McDonnell Douglas Corp. Rept. No. MDC A1038, Aug. 1971. (Confidential)

I-140. Sorensen, N. E., Smeltzer, D. B., and Cubbison, R. W.: Study of a Family of Supersonic Inlet Systems. J. Aircraft, Vol. 6, No. 3, May-June 1969, pp. 184-188.

I-141. Fukuda, M. K., Roshotko, E., and Hingst, W. R.: Control of Shock-Wave Boundary-Layer Interactions by Bleed in Supersonic Mixed Compression Inlets. AIAA Paper No. 75-1182, AIAA/SAE 11th Propulsion Conference, Oct. 1975.

I-142. Povinelli, L. A.: An Experimental and Analytical Investigation of Axisymmetric Diffusers. AIAA Paper No. 75-1211, AIAA/SAE 11th Propulsion Conference, Oct. 1975.

I-143. Imfeld, W. F.: The Development Program for the F-15 Inlet. AIAA Paper No. 74-1061, AIAA/SAE 10th Propulsion Conference, Oct. 1974.

I-144. Haagenson, W. R. and Randall, L. M.: Inlet Development for the B-1 Strategic Bomber. AIAA Paper No. 74-1064, AIAA/SAE 10th Propulsion Conference, Oct. 1974.

I-145. Hawkins, J. E.: YF-16 Inlet Design and Performance. AIAA Paper No. 74-1062, AIAA/SAE 10th Propulsion Conference, Oct. 1974.

I-146. Reyhner, T. A. and Hickcox, T. E.: A Procedure for Combined Viscous-Inviscid Analysis of Supersonic Inlet Flow Fields. AIAA Paper No. 72-44, AIAA 10th Aerospace Sciences Meeting, Jan 1972.

I-147. Koncsek, J. L. and Syberg, J.: Transonic and Supersonic Test of a Mach 2.65 Mixed-Compression Axisymmetric Intake. NASA CR-1977, Mar. 1972.

I-148. Spong, E. D., Doane, P. M., Rejeske, J. V., and Williams, R. W.: Subsonic Diffuser Designs for Interceptor Applications. Vols. I and II. AFFDL-TR-73-68, June 1973.

I-149. Caughey, D. A. and Jameson, A.: Accelerated Iterative Calculation of Transonic Nacelle Flowfields. AIAA Paper No. 76-100, AIAA 14th Aerospace Sciences Meeting, Jan. 1976.

I-150. Arlinger, B. G.: Calculation of Transonic Flow Around Axisymmetric Inlets. AIAA Paper No. 75-80, AIAA 13th Aerospace Sciences Meeting, Jan. 1975.

I-151. Kutler, P., Reinhardt, W. A., and Warming, R. F.: Numerical Computation of Multishocked, Three-Dimensional Supersonic Flow Fields with Real Gas Effects. AIAA Paper No. 72-702, AIAA 5th Fluid and Plasma Dynamics Conference, June 1972.

I-152. Marconi, F., and Salas, M.: Computation of Three Dimensional Flows About Aircraft Configurations. Comp. Fluids, Vol. 1, No. 2, 1973, pp. 185-195.

I-153. D'Attorre, L., Bilyk, M. A., and Sergeant, R. J.: Three Dimensional Supersonic Flow Field Analysis of the B-1 Airplane by a Finite Difference Technique and Comparison with Experimental Data. AIAA Paper No. 74-189, AIAA 12th Aerospace Sciences Meeting, Feb. 1974.

I-154. Bansod, P.: Supersonic Flow About Ducted Bodies with Subsonic Internal Boundaries. J. Aircraft, Vol. 12, No. 6, June 1975.

I-155. Brown, N., Tindell, R., and Stevens, C.: F-14A 1/7th Scale Inlet-Forebody Wind Tunnel Test Report, Phase IIIA and IIIB. Grumman Rept. No. ASI-33B-R-70-1, Apr. 1970.

I-156. Tindell, R.: F-14A Inlet Status Summary. Grumman Memo No. A51-333-I-70-66, Oct. 1970.

I-157. Yunger, K.: F-14B Air Inlet Performance. Grumman Flight Acceptance Dept. Performance/Propulsion Section Data Release No. FAD-303-I-0-Va. 1272, Aug. 1974.

I-158. Mohl, G. J.: Results of the Static Indraft Inlet Test on a 1/7 Scale F-14 Two Dimensional Inlet at the Grumman, Farmingdale High Speed Facility (GFDT 003). Grumman Rept. No. A51-337-R-69-35, Nov. 1969.

I-159. Brown, N. and Tindell, R: A Comparison of Full Scale and Model Test Results of Steady State and Dynamic Inlet Performance. Grumman Memo No. A51-333-I-69-99 (Technical Information Note #100), Nov. 1969.

I-160. Anderson, O. L.: Finite-Difference Solution for Turbulent Swirling Compressible Flow in Axisymmetric Ducts with Struts. NASA CR-2365, Feb. 1974.

I-161. Allen, R., Chaloff, D., Hayase, G., Hiyama, R., Martindale, C., and Rockwell, H.: A Structural Weight Estimation Program (SWEEP) for Aircraft. Vols. I-XI, ASD/XR 74-10, June 1974.

I-162. Oman, B. H., Pederson, S. K., Karll, N. P., and Real, T. F.: Computer Program to Peform Aircraft Design Synthesis. Vols. I, II, and III. AFFDL-TR-74-35, Apr. 1974.

I-163. Sorensen, N. E., and Smeltzer, D. B.: Investigation of a Large-Scale Mixed-Compression Axisymmetric Inlet System Capable of High Performance at Mach Numbers 0.6 to 3.0. NASA TM X-1507, Feb. 1968.

I-164. Mitchell, G. A., and Davis, R. W.: Performance of Centerbody Vortex Generators in an Axisymmetric Mixed Compression Inlet at Mach Numbers from 2.0 to 3.0. NASA TN D-4675, July 1968.

I-165. Brown, A. C., Nawrocki, H. F., and Paley, P. N.: Subsonic Diffusers Designed Integrally with Vortex Generators. J. of Aircraft, Vol. 5, No. 3., May-June 1968, pp. 221-229.

I-166. Culley, M.: Viscous Interaction in Integrated Supersonic Inlets. Presented at 1st International Symposium on Air Breathing Engines (Marseille, France), June 1972.

I-167. Brown, C. S. and Goldsmith, E. L.: Measurement of the Internal Performance of a Rectangular Air Intake with Variable Geometry at Mach Numbers from 1.7 to 2.5. Part I. ARC CP-1243, Aug. 1971.

I-168. Brown, C. S. and Goldsmith, E. L.: Measurement of the Internal Performance of a Rectangular Air Intake with Variable Geometry at Mach Numbers from 1.7 to 2.5. Part 2 - The Effect of Incidence. ARC CP-1242, Dec. 1971.

I-169. Wasserbauer, J. F. and Choby, D. A.: Mach 2.5 Performance of a Bicone Inlet with Internal Focused Compression and 40-Percent Internal Contraction. NASA TM X-2294, May 1971.

I-170. Cubbison, R. W., Meleason, E. T., and Johnson, D. F.: Performance Characteristics from Mach 2.58 to 1.98 of an Axisymmetric Mixed-Compression Inlet System with 60-Percent Internal Contraction. NASA TM X-1739, Feb. 1969.

I-171. Bowditch, D. N.: Some Design Considerations for Supersonic Cruise Mixed Compession Inlets. AIAA Paper No. 73-1269, AIAA/SAE 9th Propulsion Conference, Nov. 1973.

I-172. Bowditch, D. N., and Anderson, B. H.: Investigation of the Performance and Control of a Mach 3.0, Two-Dimensional, External-Internal-Compression Inlet. NASA TM X-470, June 1961.

I-173. Goldsmith, E. L.: The Effect of Internal Contraction, Initial Rate of Subsonic Diffusion, and Cowl and Centerbody Shape on the Pressure Recovery of a Conical Centerbody Intake at Supersonic Speeds. ARC R&M 3204, Nov. 1956.

I-174. Brown, C. S., and Goldsmith, E. L.: Measurement of the Internal Performance of a Rectangular Air Intake Mounted on a Fuselage at Mach Numbers from 1.6 to 2. Part 4. ARC CP-1291, June 1972.

I-175. Dobson, M. D.: Tests at a Mach Number of 2.0 on a Rectangular, Twin-Duct Air Intake with Variable Geometry, Situated in the Flow Field of a Slender Wing. ARC CP-1122, Dec. 1968.

I-176. Goldsmith, E. L.: Variable Geometry Intakes at Supersonic Speeds - Some Techniques and Some Test Results. AGARD CP-34 Part 1, Advance Components for Turbojet Engines, Sept. 1969.

I-177. Martin, R. A., and Hughes, D. L.: Comparisons of In-Flight F-111A Inlet Performance for On-and-Off Scheduled Inlet Geometry at Mach Numbers of .68 to 2.18. NASA TN D-6490, Sept. 1971.

I-178. Kaldschmidt, G., Syltebo, B. E., and Ting, C. T.: 727 Airplane Center Duct Inlet Low-Speed Performance Confirmation Model Test for Refanned JT8D Engines (Phase II). NASA CR-134534, Nov. 1973.

I-179. Sorensen, N. E. and Gregory, T. J.: Investigation of Modifications of a Twin-Duct Side Inlet Utilizing a Boundary-Layer Removal Slot at Mach Numbers from 1.59 to 2.10. NASA TM X-163, Sept. 1960.

I-180. Smeltzer, D. B., Smith, R. H., and Cubbison, R. W.: Wind Tunnel and Flight Performance of the YF-12 Inlet System. AIAA Paper No. 74-621, AIAA 8th Testing Conference, July 1974.

I-181. Wasserbauer, J. F., Shaw, R. J., and Neumann, H. E.: Minimizing Boundary-Layer Bleed for a Mixed Compression Inlet. AIAA Paper No. 73-1270, AIAA/SAE 9th Propulsion Conference, Nov. 1973.

I-182. Zonars, D.: Problems on Inlets and Nozzles. ICAS Paper No. 70-47, Presented at 7th Congress of the International Council of the Aeronautical Sciences (Rome, Italy), Sept. 1970.

I-183. Nichols, M. R.: Aerodynamics of Airframe-Engine Integration of Supersonic Aircraft. NASA TR D-3390, Aug. 1966.

I-184. Weston, K. c. and Kowalski, K.L.: Experimental Investigation of Extreme Internal Flow Turning at the Cowl Lip of an Axisymmetric Inlet at a Mach Number of 2.95. NACA RM E58A27a, May 1958.

I-185. Mossman, E. A., Lazzeroni, F. A., and Pfyl, F. A.: An Experimental Investigation of the Air-Flow Stability of a Scoop-Type Normal-Shock Inlet. NACA RM A55A13, Apr. 1955.

I-186. Zakharov, N. N.: Investigation of Separated Flow Over Bodies of Revolution in Supersonic Intake Ducts. Presented at 2nd International Symposium on Air Breathing Engines (Sheffield, England), Mar. 1974.

I-187. Campbell, D. H.: F-12 Inlet Develpment. SAE Paper No. 740831, National Aerospace Engineering and Manufacturing Meeting, Oct. 1974.

I-188. Taylor, R. P.: Inlet and Fan Aerodynamics. SAE Paper No. 680711, Aeronautic and Space Engineering and Manufacturing Meeting, Oct. 1968.

I-189. McGregor, I.: A Rig for the Static-Testing of Model Air-Intakes. RAE TR-69251, Nov. 1969.

I-190. Younghans, J. L., Moore, M. T., Collins, T. P., and Direnzi, J. G.: Inlet Flow Fields Simulation Techniques for Engine/ Compressor Testing. Aircraft Eng., Vol. 42, Nov. 1970, pp. 12-17.

I-191. Smith, R. H., and Schweikhard, W. G.: Initial Flight Experience with the XB-70 Air-Induction System. Conference on Aircraft Aerodynamics, NASA SP-124, May 1966.

I-192. Connors, J. F., Wise, G. A., and Lovell, J. C.: Investigation of Translating-Double-Cone Axisymmetric Inlets with Cowl Projected Areas 40 and 20 Percent of Maximum at Mach Numbers from 3.0 to 2.0. NACA RM E57C06, May 1957.

I-193. Christensen, L. L.: Propulsion System Configuration Development for the B-1 Strategic Bomber. AIAA Paper No. 75-1040, Aircraft Systems and Technology Meeting, Aug. 1975.

I-194. Seddon, J.: Boundary-Layer Interaction Effects in Intakes with Particular Reference to Those Designed for Dual Subsonic and Supersonic Performance. ARC R&M 3565, Mar. 1966.

I-195. McGregor, I.: Some Applications of Boundary-Layer Control by Blowing to Air Intakes for VSTOL Aircraft. AGARD CP-91-71, Inlets and Nozzles for Aerospace Engines, Sept. 1971.

I-196. Sears, R. I., Merlet, C. F., and Putland, L. W.: Flight Determination of Drag Normal-Shock Nose inlets with Various Cowling Profiles at Mach Numbers from .9 to 1.5. NACA TR 1281, 1953.

I-197. Anderson, W. E.: Inlet-Drag Studies (U). In: Langley, Ames, Lewis, and Flight Research Center Support of DOD VFAX/FX Projects, NASA SP-78, May 1968. (Confidential)

I-198. Re, R. J. and Wilmoth, R. G.: Performance of an External Compression Inlet of a Variable-Sweep Tactical Fighter Model at Mach Numbers from .5 to 1.3. NASA TM X-1576, May 1968.

I-199. Gregory, N.: On the Static Performance of Two-Dimensional Intakes with Momentum Injection in the Form of Boundary-Layer Control by Blowing. ARC R&M 3656, Feb. 1968.

I-200. Ferri, A. and Nucci, L. M.: Theoretical and Experimental Analysis of Low-Drag Supersonic Inlets Having a Circular Cross-Section and a Central Body at Mach Number of 3.3, 2.75, and 2.45. NACA RM L8H13, Nov. 1948.

I-201. Dobson, M. D.: Wind-Tunnel Tests on a Rectangular, Twin-Duct, Variable-Geometry Air Intake at Supersonic Speeds. Aeronautical Research Council Rept. No. ARC CP-944, 1967.

I-202. Eggers, J. A.: Determination of the Drag of a Wind Tunnel Model Engine Duct by Application of the Momentum Equation. M.S. Thesis, Air Force Institute of Technology, AD-741744, Mar. 1972.

I-203. German, R. C.: The 0.2 Scale B-1 External Compression Inlet Verification Model Test at Transonic and Supersonic Mach Numbers, Phase 2, Final Report, 19 June - 8 Nov. 1973. Rept. No. ARO-PWT-TR-74-28, Aug. 1974.

I-204. Hartley, R. M., Moxley, D. W., Jr., and Ziegler, N. G.: Wind-Tunnel Investigation of Favorable Interference to Increase Lift-Drag Ratios of Supersonic Aircraft. Part II - An Optimized Wing-Body-Inlet Configuration. Rept. No. DTMB-AERO-1063, pt. II, June 1964.

I-205. North American Aviation, Inc.: Aerodynamic Evaluations of the XB-70 Air Induction System. Rept. No. NA-60-1538, Dec. 1960.

I-206. Samanich, N. E.: Pressure Drag of Axisymmetric Cowls Having Large Initial Lip Angles at Mach Numbers from 1.90 to 4.90. NASA Memo 1-10-59E, 1959.

I-207. Sargent, J. C.: Wind Tunnel Test Results of Three Inlets Tested in Lewis Research Center 18-Inch x 18-Inch Wind Tunnel During August, 1959. North American Aviation, Inc. Rept. No. NA-60-377, Mar. 1960.

I-208. Seed, A. R.: Some Factors Affecting the Flow Unsteadiness in Supersonic Intakes. Proceedings of the Symposium on Unsteady Aerodynamics, Tucson, Arizona, Mar. 18-20, 1975, Vol. I, 1975.

I-209. Richey, G. K., Stava, D. J., Brimelow, B., and Bush, H. I.: Airframe-Propulsion Integration for Future Aircraft Systems. SAE Paper No. 680288, May 1968.

I-210. Sorensen, N. E. and Smeltzer, D. B.: Study of Two Axisymmetric Inlets Designed for Mach 3.5. J. Aircraft, Vol. 13, No. 11, Nov. 1967.

I-211. Sajben, M., Chen, C. P., and Kroutil, J. c.: Comparison of Conventional and Force-Based Distortion Index Measurements. AIAA Journal, Vol. 14, No. 10, Oct. 1976.

I-212. Syberg, J. and Koncsek, J. L.: Experimental Evaluation of an analytically Derived Bleed System for a Supersonic Inlet. J. Aircraft, Vol. 13, No 10, 1976.

I-213. Ball, W. H.: Rapid Calculation of Propulsion System Installation Corrections. J. Aircraft, Vol. 13, No. 7, July 1976.

I-214. Wong, W. F.: Application of Boundary Layer Blowing to Suppress Strong Shock Induced Separation in Supersonic Inlets. AIAA Paper No. 77-147, AIAA 15th Aerospace Sciences Meeting, Jan. 1977.

I-215. Reyhner, T. A.: Transonic Potential Flow Around Axisymmetric Inlets and Bodies at Angle of Attack. AIAA Paper No. 77-145, AIAA 15th Aerospace Sciences Meeting, Jan. 1977.

I-216. Sorensen, N. E. and Latham, E. A.: Transonic Performance of an Auxiliary Airflow System for Axisymmetric Inlets. AIAA Paper No. 77-148, AIAA 15th Aerospace Sciences Meeting, Jan. 1977.

I-217. Santman, D. M.: Transonic Performance of a Mach 2.65 Auxiliary Flow Axisymmetric Inlet. NASA CR-2747, Oct. 1976.

I-218. Re, R. J. and Wilmoth, R. G.: Performance of the External Compression Inlet of a 1/6-Scale Model of a Variable-Sweep Tactical Fighter at Transonic Speeds (Phase I). NASA TM X-1804, July 1969.

I-219. Wilmoth, R. G. and Re, R. J.: Performance of the External Compression Inlet of a 1/6-Scale Model of a Variable-Sweep Tactical Fighter at Transonic Speeds (Phase II). NASA TM X-1817, July 1969.

I-220. Burstadt, P. L. and Wenzl, L. M.: A Method to Account for Variation of Average Compressor Inlet Pressure During Instantaneous Distortion Analysis. AIAA Paper No. 76-703, AIAA/SAE 12th Propulsion Conference, July 1976.

I-221. King, R. W. and Neumann, H. E.: A Method of Distortion Pattern Synthesis for High Response Data Screening. AIAA Paper No. 76-704, AIAA/SAE 12th Propulsion Conference, July 1976.

I-222. Motycka, D. L.: Determination of Maximum Expected Instantaneous Distortion Patterns from Statistical Properties of Inlet Pressure Data. AIAA Paper No. 76-705, AIAA/SAE 12th Propulsion Conference, July 1976.

I-223. Runstadler, P. W., Jr., Dolan, F. X., Dean, R. C., Jr.: Diffuser Data Bok. Creare Inc. TN-186, May 1975.

I-224. Kamman, J. H. and Wallace, H. W.: Assessement of Installed Inlet Forces and Inlet/Airframe Interactions. McDonnell Douglas Corp., AFFDL-TR-76-62, July 1976.

I-225. Bower, W. W.: An Analytical Procedure for the Calculation of Attached and Separated Subsonic Diffuser Flows. AIAA Paper No. 74-1173, AIAA/SAE 10th Propulsion Conference, oct. 1974.

I-226. Koch, K. E. and Rees, R. L.: Analysis of Pressure Distortion Testing. NASA CR-2766, Dec. 1976.

I-227. Melick, H. C., Ybana, A. H., and Bencze, D. P.: Estimating Maximum Instantaneous Distortion from Inlet Total Pressure RMS and PDS measurements. NASA TM X-73145, June 1976.

I-228. Merkli, P. E.: Pressure Recovery in Rectangular Constant Area Supersonic Diffusers. AIA Journal, Vol. 14, N. 2, Feb. 1976.

I-229. Harsha, P. T. and Glassman, H. N.: Analysis of Turbulent Unseparated Flow in Subsonic Diffusers. ASME Paper No. 76-FE-26, Gas Turbine and Fluids Engineering Conference, Mar. 1976.

I-230. Tindell, R. H.; Advanced Inlet-Engine matching Technology, Volume I - Aircraft Mission Analysis. Grumman Aerospace Corp. Rept. GAD-321-RT, Nov. 1976.

I-231. Brown, N.: Advanced Inlet-Engine Matching Technology, Volume II- High-Flow Inlet Wind Tunnel Test Results. Grumman Aerospace Corp. Rept. N. GAD-321-RT, Nov. 1976.

I-232. Kamal, W. A., Odukwe, A. O., and Livesey, J. L.: The Effects of "Controlled" Inlet Conditions on the Performance of Conical Diffusers Preceded by Normal Shock Boundary Layer Interaction. 5th Australian Conference on Hydraulics and Fluid Mechanics, Dec. 1974.

I-233. Welge, H. R., Radkey, R. L., and Henne, P. A.: Nacelle Aerodynamic Design and Integration Study on a Mach 2.2 Supersonic Cruise Aircraft. AIAA Paper No. 76-757, AIAA/SAE 12th Propulsion Conference, July 1976.

I-234. Anderson, W. E. and Wong, N. D.: Experimental Investigation of a Large-Scale, Two-Dimensional, Mixed-Compression Inlet System. NASA TM X-2016, May 1970.

I-235. Johnson, R. H.: Inlet Distortion Scaling of Wind Tunnel Model Results. NASA CR-143840, Dec. 1976.

I-236. Reukauf, P. J., Schweikhard, W. G., and Arnaiz, H.: Flight-Test Techniques for Obtaining Comparisons of Wind-Tunnel and Flight Results from Tests on a YF-12 Mixed-Compression Inlet. AIAA Paper No. 74-1195, AIAA/SAE 10th Propulsion Conference, San Diego, CA, Oct. 1974.

I-237. Peake, D. J.: The Use of Air Injection to Prevent Separation of the Turbulent Boundary Layer in Supersonic Flow. ARC CP No. 890, 1966.

I-238. Lauer, R. F., Jr.: Results of a 0.2-Scale B-1 Production Inlet Development and Verification Tests at Subsonic and Supersonic Mach Numbers. AEDC TR-75-57, May 1975.

I-239. Schoelen, F. J., Kiser, C. E., and Mitchell, C. E.: Eleventh Interim Technical Report, Inlet/Nozzle Flight Performance Determination (Wind Tunnel Test Program). Rockwell International NA-76-7, Vol. II, June 1976.

I-240. McGregor, I.: Some Theoretical Parameters Relevant to the Performance of Rectangular intakes with Double-Ramp Compression Surfaces at Supersonic Speeds. RAE TR 71232, Nov. 1971.

I-241. Fisher, S. A., Neale, M. C., and Brooks, A. J.: On the Sub-Critical Stability of Varible-Ramp Intakes at Mach Numbers Around 2. ARC R&M No. 3711, Feb. 1970.

I-242. Svitenko, L. C.: Airframe/Inlet/Powerplant: The Interface Problem. Air Command and Staff College, Air Univ., Maxwell Air Force Base, AL, May 1974.

I-243. Lauer, R. F., Jr.: Results of a 0.15-Scale F-16 Inlet Performance Test at Subsonic and Supersonic Mach Numbers. AEDC-TR-75-123, Sept. 1975.

I-244. Huffman, J. W.: Wind Tunnel Test of a 1/6-Scale F-111 Inlet at the JTF-10A-32 Engine Airflows at Mach Numbers from 1.75 to 2.20. AEDC-TR-68-259, Nov. 1968.

I-245. Sanders, M. E.: Inlet Performance Characteristics of a 1/5-Scale Northrop YF-17 Model at Transonic and Supersonic Mach Numbers. AEDC-TR-74-6, Apr. 1974.

I-246. Riddell, J. F.: Results of a 0.2-Scale B-1 Inlet Verification Model Test at Transonic and Supersonic Mach Numbers. AEDC TR-72-156, Oct. 1972.

I-247. Anderson, C. F. and Jackson, F. M.: Blockage Study of a 1/16-Scale B-1 Inlet Model in the 1-Ft. Transonic and Supersonic Tunnels of the Propulsion Wind Tunnel Facility. AEDC-TR-72-156, Oct. 1972.

I-248. Riddell, J. F.: Blockage Study of a 1/16-Scale F-15 in the 1-Foot Transonic and Supersonic Tunnels of the Propulsion Wind Tunnel Facility. AEDC-TR-71-95, May 1971.

I-249. Kimzey, W. F., Williams, V. O., and Gall, E. S.: Aerodynamic Calibration and Shakedown Testing of the Full-Scale F-15 Aircraft Inlet Simulator. AEDC-TR-72-147, Apr. 1973.

I-250. Graham, F. J.: Results of a 0.1-Scale B-1 Inlet Model Test at Transonic and supersonic Mach Numbers. AEDC-TR-71-219, Oct. 1971.

I-251. Riddell, J. F. and Christenson, R. J.: An Investigation of the Effects of Various Protuberances on the Inlet Performance and Fuselage Pressure Distribution of the 1/6-Scale F-111A Aircraft at Subsonic and Transonic Mach Numbers. AEDC TR-73-33, Feb. 1973.

I-252. Walker, J.: Inlet Performance Characteristics of a Generalized 1/5.2-Scale Aircraft Model at Transonic and Supersonic Mach Numbers. AEDC-TR-76-162, Nov. 1976.

I-253. Smeltzer, D. B. and Sorenson, N. E.: Investigation of a Mixed-Compression Axisymmetric Inlet System at Mach Numbers 0.6 to 3.5. NASA TN D-6078, Nov. 1970.

I-254. Keeney, F. J.: Longitudinal Static Stability and Inlet Drag Characteristics of the McDonnell F-15 Tactical Fighter Aircraft at Mach Numbers of 1.60 and 2.20. AEDC TR-71-100, May 1971. (Confidential)

I-255. Kostin, L: Wind Tunnel Data Analysis March 1975 Test 0.06 Scale Nozzle Afterbody Model. Vol. II. Inlet/Nozzle Flight Performance Determination. Rockwell International Rept. NA 75-809, Feb. 1976.

I-256. Soffker, E. and Renner, A.: Suction Losses of Sharp-Lip Air Intakes. RAE Library Translation 1246, Aug 1967. (DLR FB 65-26, 1965.)

I-257. Culley, M.: A Side Mounted Supersonic Intake and the Problem of Three-Dimensional Boundary Layer Separation. Australian Defense Scientific Service, ARL Mechanical Engineering Rept. 137, June 1972.

I-258. Galigher, L. L.: Wind Tunnel Investigation of a 1/8-Scale AMSA Aircraft-Inlet Model at Transonic and Supersonic Mach Numbers. AEDC TR-67-252, Nov. 1967.

I-259. Keeney, F. J. and Butler, R. W.: Performance Characteristics of a 1/6-Scale F-111A Inlet Model at Supersonic and Transonic Speeds. AEDC TR-67-229, Nov. 1967.

I-260. Lauer, R. F., Jr. and Huffman, J. W.: Supersonic and Transonic Inlet Performance Characteristics of a 1/6-Scale F-111 Model. AEDC TR-67-274, Jan. 1968.

I-261. Baker, D. C.: Wind Tunnel Investigation of a 1/9-Scale Boeing Company AMSA Airplane-Inlet Model at Transonic and Supersonic Mach Numbers. AEDC R-67-231, Nov. 1967.

I-262. McDill, H. E.: Results of a 0.125-Scale RA-5C Inlet Model Test at Transonic and Supersonic Mach Numbers. AEDC TR-70-69, Mar. 1970.

I-263. McDill, H. E. and Huffman, J. W.: Results of a 0.228-Scale RA-5C Inlet Model Test at Transonic and Supersonic Mach Numbers. AEDC TR-69-209, Oct. 1969.

I-264. Huffman, J.W. and Lauer, R. F., Jr.: Performance of a 1/6-Scale F-111A Inlet at Transonic and Supersonic Mach Numbers. AEDC TR-67-90, May 1967.

I-265. McDill, H. E. and Riddell, J. F.: Wind Tunnel Investigation of a 0.10-Scale North American Aviation AMSA Inlet at Transonic and Supersonic Mach Numbers. AEDC TR-67-213, Oct. 1967.

I-266. Hartin, J. P.: Effect of Scale on Supersonic Aircraft Inlet Turbulence in Wind Tunnel Models. AEDC TR-69-170, Oct. 1969.

I-267. Lauer, R. F. and Huffman, J. W.: Inlet Flow Characteristics of a 1/6-Scale F-111A Inlet Model at Transonic and Supersonic Speeds. AEDC TR-67-136, July 1967.

I-268. Grippe, R. P.: Summary of the 1/4-Scale SST Intake/Engine Interaction Test in the AEDC 16 Ft. Transonic Wind Tunnel. Boeing Rept. No. D6A11875-1, May 1970.

I-269. Lauer, R. F. and Huffman, J. W.: Summary of 1/6-Scale Inlet Model Test Results Obtained in Support of the F-111 Development Program. (October 1966 to September 1968.) AEDC TR-68-282, Jan. 1969.

I-270. Shadow, T. O. and Gomillion, G. R.: Wind Tunnel Investigation of the Steady and Unsteady Pressure Environment in the Vicinity of a Normal Shock Located in the Diffuser Section of a Supersonic Inlet Configuration. AEDC TR-69-140, July 1969.

I-271. Lauer, R. F., Jr. and Sanders, M. E.: Steady-State Performance of an Isolated Axisymmetric Inlet with a J85 Engine and Cold Flow Engine Simulators at Mach Numbers from 0.60 to 1.50. AEDC TR-69-260, Dec. 1969.

I-272. Burchfield, C. G.: An Investigation of Inlet and Aircraft Drag on a 7.5-Percent Scale Model of a Twin-Engine High-Speed Fighter Aircraft at Transonic Mach Numbers. AEDC TR-76-79, July 1976.

I-273. Williams, H. J. M.: A Study of the Relation of Engine Stalls to the Total Pressure Dynamic Distortion at the Face of the F-111A/TF-30 Engine. Air Force Institute of Technology, School of Engineering, Thesis for MS Degree, Mar. 1968.

I-274. Keith J. S., Ferguson, D. R., Merkle, C. L., Heek, P. H., and Lahti, D. J.: Analytical Method for Predicting the Pressure Distribution about Nacelle at Transonic Speeds. NASA CR-2217, July 1973.

I-275. Hube, F. K. and Janke, L. M.: Wind Tunnel Tests of Two-Dimensional and Half-Axisymmetric Inlet Models at Mach Numbers 1.5 through 3.0. AEDC TR-70-280, Dec. 1970.

I-276. Stitt, L. E. and Salmi, R. J.: Performance of a Mach 3.0 External-Internal Compression Axisymmetric Inlet at Mach Numbers from 2.0 to 3.5. NASA TM X-145, Jan. 1960.

I-277. Cawthon, J. A.: Design and Preliminary Evaluation of Inlet Concepts Selected for Maneuver Improvement. AIAA Paper 76-701, AIAA/SAE 12th Propulsion Conference, July 1976.

I-278. Neale, M. C. and Lamb, P. S.: Tests with a Two-Dimensional Intake Having All-External Compression and a Design Mach Number of 2.2. ARC CP No. 939, 1967.

I-279. Neal, M. C. and Lamb, P. S.: More Tests with a Variable Ramp Intake Having a Design Mach Number of 2.2. ARC CP No. 938, 1967.

I-280. Prokop, C.: Investigation of the Effects of Airframe Design on Inlet Flow Fields. AFFDL-TR-72-11, Vol. I., Feb. 1972.

I-281. Neale, M. C. and Lamb, P. S.: Tests with a Two-Dimensional Inlet Having All-External Compression and a Design Mach Number of 2.0. ARC CP No. 937, Sept. 1963.

I-282. Griffiths, R. T.: Tests on an Engine Installation for a Slender Gothic Wing at M = 1.82. ARC CP No. 866, 1967.

I-283. Braun, G. W. and Snyder, W. T.: An Experimental Investigation of Shock Wave-Boundary Layer Interaction Dynamics. AFFDL-TR-69-103, Oct. 1969.

I-284. Brown, C. S. and Goldsmith, E. L.: Measurement of the Internal Performance of a Rectangular Air-Intake at a Mach Number of 0.9. ARC CP No. 1346, 1976.

I-285. Mitchell, C. E.: Wind Tunnel Data Report on Series II Tests of a 0.10-Scale AMSA Inlet Model in the North American Rockwell Low Speed Wind Tunnel (U). North American Aviation Rept. NA-67-937, Oct. 1967. (Secret)

I-286. Boman, C. D., Krawitz, G. W., and Barice, W. J., Jr.: Analysis of Results of an Experimental Investigation of the 0.10-Scale Model of the AMSA Air Induction System (U). North American Rockwell Corp. Rept. NA-67-903, Nov. 1967. (Secret)

I-287. Griffiths, R. T.: Tests at M = 1.82 on an Engine Installation with Boundary Layer Diverter for a Slender Gothic Wing. RAE TR-67203, Aug. 1967.

I-288. Goldsmith, E. L. and Brown, C. S.: Some Measurements of the Internal Performance of Two Half-Axisymmetric Air Intakes With Conical Compression Surfaces at Mach Numbers Between 1.8 and 2.5. RAE TR-71058, Apr. 1971.

I-289. Thomas, P. D., Vinokur, M., Bastianon, R. A., and Conti, R. J.: Numerical Solution for Three-Dimensional Inviscid Supersonic Flow. AIAA J., Vol. 10, No. 7, July 1972.

I-290. South, J. C. and Jameson, A.: Relaxation Solutions for Inviscid Axisymmetric Transonic Flow Over Blunt or Pointed Bodies. In.: Proceedings, AIAA Computational Fluid Dynamics Conference, July 1973.

I-291. Li, T. C.: Unsteady Aerodynamics for Advanced Configurations. Part V - Unsteady Potential Flow Around Slender Bodies at Angles of Attack. Technical Documentary Rept. No. FDL-TDR-64-152, Part V, July 1965.

I-292. Walitt, L. and Trulio, J. G.: A Numerical Method for Computing Three-Dimensional Viscous Supersonic Flow Fields about Slender Bodies. NASA CR-1963, Nov. 1971.

I-293. Walkden, F., Laws, G. T., and Caine, P.: A New Shock-Capturing Numerical Method with Application to Some Simple Supersonic Flow Fields. Proceedings, AIAA Computational Fluid Dynamics Conference, Palm Springs, CA, July 1973.

I-294. Ehlers, F. E., Johnson, F. T., and Rubbert, P. E.: Advanced Panel-Type Influence Coefficient Methods Applied to Subsonic and Supersonic Flows. Conference on Aerodynamic Analyses Requiring Advanced Computers, NASA SP-347, Part II, Mar. 1975.

I-295. Presley, L. L.: Computational Methods in Predicting Airframe Propulsion System Interaction. Proceedings of Workshops on Engine-Airframe Integration (Short-Haul Aircraft), May 1977.

I-296. Mason, W., MacKenzie, D. A., Stern, M. A., and Johnson, J. K.: A Numerical Three-Dimensional Viscous Transonic Wing-Body Analysis and Design Tool. AIAA Paper No. 78-101, AIAA 16th Aerospace Sciences Meeting, Jan. 1978.

I-297. Rakich, J. V.: A Method of Characteristics for Steady Three-Dimensional Supersonic Flow with Application to Inclined Bodies of Revolution. NASA TN D-5341, Oct. 1969.

I-298. Bailey, F. R. and Ballhaus, W. F.: Comparisons of Computed and Experimental Pressures for Transonic Flows about Isolated Wings and Wing-Fuselage Configurations. Conference on Aerodynamic Analyses Requiring Advanced Computers, NASA SP-347, Part II, Mar. 1975.

I-299. Ballhaus, W. F., Bailey, F. R., and Frick, J.: Improved Computational Treatment of Transonic Flow about Swept Wings. Advances of Engineering Science, Vol. 4, 13th Annual Meeting of the Society of Engineering Science, NASA CP-2001, Nov. 1976.

I-300. Hess, J. L. and Smith, A. M. O.: Calculation of Nonlifting Potential Flow about Arbitrary Three-Dimensional Bodies. Douglas Aircraft Co. Rept. No. ES-40622, Mar. 1962.

I-301. Hess, J. L.: Calculation of Potential Flow About Arbitrary Three-dimensional Lifting Bodies. Douglas Aircraft Co. Rept. No. MDC-J5679/01, Oct. 1972.

I-302. Hess, J. L.: Status of a Higher-Order Panel Method for Nonlifting Three-Dimensional Potential Flow. Dougls Aircraft Co. Rept. No. MDC-J7714/01, Aug. 1977.

I-303. Dillenius, M.F.E., Goodwind, F.K., and Nielsen, J.N.: Prediction of Supersonic Store Characteristics. Vol. I - Theoretical Methods and Comparisons with Experiment. AFFDL-TR-76-41, May 1976.

I-304. Dillenius, M.F.E., Goodwin, F.K., and Nielsen, J.N.: Extension of the Method for Predicting Six-Degee-of-Freedom Store Separation Trajectories at Speeds up to the Critical Speed to Include a Fuselage with Noncircular Cross Section. Vol. I - Theoretical Methods and Comparisons with Experiment. AFFDL-TR-74-130, Nov. 1974.

I-305. Moretti, G., Grossman, B., and Marconi, F., Jr.: A Complete Numerical Technique for the Calculation of Three-Dimensional Inviscid Supersonic Flows. AIAA Paper 72-192, AIAA 10th Aerospace Sciences Meeting, Jan. 1972.

I-306. Solomon, J. M., Ciment, M., Ferguson, R. E., and Bell, J. B.: Three Dimensional Supersonic Inviscid Flow Field Calculations on Re-entry Vehicles with Control Surfaces. AIAA Paper No. 77-84, AIAA 15th Aerospace Sciences Meeting, Jan. 1977.

I-307. Spreiter, J. R. and Alksne, A. Y.: Slender Body Theory Based on Approximate Solution of the Transonic Flow Equation. NASA Rept. No. 2, 1959.

I-308. Woodward, F. A., Tinoco, E. N., and Larsen, J. W.: Analysis and Design of Supersonic Wing-Body Combinations, Including Flow Properties in the Near Field. Part I - Theory and Application. NASA CR-73106, Aug. 1967.

I-309. Woodward, F. A.: An Improved Method for the Aerodynamic Analysis of Wing-Body-Tail Configurations in Subsonic and Supersonic Flow. Part I - Theory and Application. NASA CR-2228, May 1973.

I-310. Woodward, F. A.: Analysis and Design of Wing-body Combinations at Subsonic and Supersonic Speeds. J. Aircraft, Vol. 5, No. 6, Nov-Dec 1968.

I-311. Pulliam, T. H. and Steger, J. L.: On Implicit Finite-Difference Simulations of Three Dimensional Flow. AIAA Paper No. 78-10, AIAA 16th Aerospace Sciences Meeting, Jan. 1978.

I-312. Kutler, P., Chakravarthy, S. R., and Lombard, C. P.: Supersonic Flow Over Ablated Nosetips Using an Unsteady Implicit Numerical Procedure. AIAA Paper No. 78-213, AIAA 16th Aerospace Sciences Meeting, Jan. 1978.

I-313. Knight, D. D.: Numerical Simulation of Realistic High-Speed Inlets Using the Navier-Stokes Equations. AIAA Journal, Vol. 15, No. 11, Nov. 1977.

I-314. Viviand, H. and Ghazzi, W.: Numerical Solution of the Compressible Navier-Stokes Equations at High Reynolds Numbers with Applications to the Blunt Body Problem. Lecture Notes in Physics No. 59, Proceedings of the Fifth International Conference on Numerical Methods in Fluid Dynamics, 1976.

I-315. Asfar, K. R., Mook, D. T., and Nayfeh, A. H.: Application of the Vortex-Lattice Technique to Arbitrary Bodies. AIAA Paper No. 78-1205, AIAA 11th Fluid and Plasma Dynamics Conference, July 1978.

I-316. Mastin, C. W. and Thompson, J. F.: Three-Dimensional Body-Fitted Coordinate Systems for Numerical Solution of the Navier-Stokes Equations. AIAA Paper No. 78-1147, AIAA 11th Fluid and Plasma Dynamics Conference, July 1978.

I-317. Lee, K. D., Dickson, L. J., Chen, A. W., and Rubbert, P. E.: An Improved Matching Method for Transonic Computations. AIAA Paper No. 78-1116, AIAA 11th Fluid and Plasma Dynamics Conference, July 1978.

I-318. Morino, L., Chen, L. T., and Suciu, E. O.: Steady and Oscillatory Subsonic and Supersonic Aerodnamics around Complex Configurations. AIAA Journal, Vol. 13, No. 3, Mar. 1975.

I-319. Morino, L. and Tseng, K.: Steady, Oscillatory, and Unsteady, Subsonic and Supersonic Aerodynamics (SOUSSA) for Complex Aircraft Configurations. AGARD CP-227, Unsteady Aerodynamics, Sept. 1977.

I-320. Albers, J. A. and Miller, B. A.: Effect of Subsonic Inlet Lip Geometry on Predicted Surface and Flow Mach Number Distributions. NASA TN D-7446, Dec. 1973.

I-321. Morino, L.: A General Theory of Unsteady Compressible Potential Aerodynamics. NASA CR-2464, Dec. 1974.

I-322. Goodwin, F. K.: Data Report for an External Store Test Program using a Generalized Parent Aircraft Model. Vols. I, II, III, and IV. Nielsen Engineering & Research TR 130, Jan. 1977.

I-323. Woollett, R. R. and Connors, J. F.: Zero-Angle-of-Attack Performance of Two-Dimensional Inlets Near Mach Number 3. NACA RM E55K01, Feb. 1956.

I-324. Inouye, M., Rakich, J. V., and Lomax, H.: A Description of Numerical Methods and Computer Programs for Two-Dimensional and Axisymmetric Supersonic Flow over Blunt-Nosed and Flared Bodies. NASA TN D-2970, Aug. 1965.

I-325. Carter, T. D. and Spong, E. D.: High Speed Inlet Investigation. (Final Report for Period April 1975-October 1977) Vol. I. Description of Program and Results. Vol. II. Data Summary. AFFDL-TR-77-105, Nov. 1977.

I-326. Mitchell, G. A.: Experimental Investigation of the Performance of Vortex Generators Mounted in the Supersonic Portion of a Mixed-Compression Inlet. NASA TM X-2405, Nov. 1971.

I-327. Neumann, H. E., Wasserbauer, J. F., and Shaw, R. J.: Performance of Vortex Generators in a Mach 2.5 Low-Bleed Full-Scale 45-Percent-Internal-Contraction Axisymmetric Inlet. NASA TM X-3195, Apr. 1975.

I-328. Smeltzer, D. B. and Sorensen, N. E.: tests of a Mixed Compression Axisymmetric Inlet with Large Transonic Mass Flow at Mach Numbers 0.6 to 2.65. NASA TN D-6971, Dec. 1972.

I-329. Wasserbauer, J. F., Shaw, R. J., and Neumann, H. E.: Design of a Very Low-Bleed Mach 2.5 Mixed-Compression Ilet with 45-Percent Internal Contraction. NASA TM X-3135, Mary 1975.

I-330. Sanders, B. W. and Mitchell, G. A.: Throat-Bypass Bleed Systems for Increasing the Stable Airflow Range of a Mach 2.50 Axisymmetric Inlet with 40-Percent Internal Contraction. NASA TM X-2779, May 1973.

I-331. Coltrin, R. E. and Calogeras, J. E.: Supersonic Wind Tunnel Investigation of Inlet-Engine Compatibility. AIAA Paper No. 69-487, AIAA 5th Propulsion Joint Specialist Conference, June 1969. (Also, NASA TM X-52595.)

I-332. Obery, L. J. and Stitt, L. E.: Perforoance of External-Internal Compression Inlet with Abrupt Turning at Mach Numbers 3.0 to 2.0. NACA RM E57H07a, Oct. 1957.

I-333. Connors, J. F., Lovell, J. C., and Wise, G. A.: Effects of Internal-Area Distribution, Spike Translation, and Throat Boundary-Layer Control on Performance of a Double-Cone Axisymmetric Inlet at Mach Numbers from 3.0 to 2.0. NACA RM E57F03, Aug. 1957.

I-334. Mitchell, G. A. and Cubbison, R. W.: An Experimental Investigation of the Restart Area Ratio of a Mach 3.0 Axisymmetric Mixed Compression Inlet. NASA TM X-1547, Apr. 1968.

I-335. Gawienowski, J. J.: Survey of Local Airflow Characteristics at the Plane of the Cowl Lip of the Left Inlet of a 1/12-Scale Model of the YF-12 Supersonic Aircraft: A Data Report. 2 Volumes. NASA TM X-62483, Nov. 1975.

I-336. Kutler, P., Warming, R. F., and Lomax, H.: Computation of Space Shuttle Flowfields Using Noncentered Finite-Difference Schemes. AIAA Journal, Vol. II, No. 3, Feb. 1973.

I-337. Chu, C. W.: Compatibility Relations and a Generalized Finite-Difference Approximation for Three-Dimensional Steady Supersonic Flow. AIAA Journal, Vol. 5, No. 3, Mar. 1967, pp. 493-501.

I-338. Alford, W. J., Jr. and King, T. J., Jr.: Experimental Investigation of Flow Fields At Zero Sideslip Near Swept- and Unswept-Wing-Fuselage Combinations at Low Speed. NACA RM L56J19, Jan. 1957.

I-339. Carlson, H. W.: Measurements of Flow Properties in the Vicinity of Three Wing-Fuselage Combinations at Mach Numbers of 1.61 and 2.01. NASA TM X-64, Oct. 1959.

I-340. Geissler, W.: Calculation of Potential Flow about Axially Symmetric Fuselages, Annual Profiles and Engine Inlets. NASA TT-F-15213, Dec. 1973.

I-341. Stahara, S. S., et al.: A Rapid Predictive Method for Three-Dimensional Transonic Flow Fields about Parent Aircraft with Application to External Stores. Presented at JTCG Aircraft/Stores Compatibility Symposium, Oct. 1977.

I-342. Perkins, S. C., Jr., Stahara, S. S., and Hemsch, M. J.: Data Report for a Test Program to Study Transonic Flow Fields about Aircraft with Application to External Stores. Vols. I-VI. Nielsen Engineering & Research TR-138, July 1977.

I-343. Perkins, S. C., Jr. and Goodwin, F. K.: Data Report for an External Store Test Program Conducted at Supersonic Speeds. Vols. I-IV. Nielsen Engineering & Research TR-103, Dec. 1975.

I-344. Bergrun, N. R. and Goodwin, F. K.: Data Report for the External Stores Test Program. Vol. I - Summary Report for First Tunnel Energy. Vol. IV - First Tunnel Entry Flow-Field Survey Data. Nielsen Engineering & Research TR-24, Oct. 1970.

I-345. Watson, E. C.: An Experimental Investigation at Mach Numbers from 2.1 t 3.0 of Circular Internal-Compression Inlets Having Translatable Centerbodies and Provision for Boundary Layer Removal. NASA TM X-156, Jan. 1960.

I-346. Maskew, B.: Calculaton of the Three-Dimensional Potential Flow Around Lifting Nonplanar Wings and Wing-Bodies Using a Surface Distribution of Quadrilateral Vortex Rings. Loughborough Univ. of Technology Report TT-7009, Sept. 1970.

I-347. AEDC Three-Dimensional Potential Flow Computer Program. AEDC-TR-75-75, Feb. 1976. Todd, D. C.: Vol. I - Method and Computer Program. Palko, R. L.: Vol. II - Mathematical Modeling, Application and Verification.

I-348. Johnson, F. T. and Rubbert, P. E.: Advanced Panel-Type Influence Coefficient Methods Applied to Subsonic Flows. AIAA Paper No. 75-50, AIAA 13th Aerospace Sciences Meeting, Jan. 1975.

I-349. Ehlers, F. E., Johnson, F. T., and Rubbert, P. E.: A Higher Order Panel Method for Linearized Supersonic Flwo. AIAA Paper No. 76-381, AIAA 9th Fluid and Plasma Dynamics Conference, July 1976.

I-350. Ehlers, F. E., et al.: An Improved Higher Order Panel Method for Linearized Supersonic Flow. AIAA Paper No. 78-15, AIAA 16th Aerospace Sciences Meeting, Jan. 1978.

I-351. Albers, J. A.: Theoretical and Experimental Internal Flow Charactersitics of a 13.97-Centimeter-Diameter Inlet at STOL Takeoff and Approach Conditions. NASA TN D-7185, Mar. 1973.

I-352. Pick, G. S. and Hartley, R. M.: Survey of Three-Dimensional Flow Fields in the Presence of Wings at M = 2.48. 10th Navy Symposium on Aeroballistics, Vol. 3, July 1975.

I-353. Miller, B. A.: Effect of Design Changes on Aerodynamic and Acoustic Performance of Translating-Centerbody Sonic Inlets. NASA TP-1132, Feb. 1978.

I-354. Rizzi, A. W. and Schmidt, W.: Study of Pitot-Type Supersonic Inlet Flowfields Using the Finite-Volume Approach. AIAA Paper No. 78-1115, AIAA 11th Fluid and Plasma Dynamics Conference, July 1978.

I-355. Smith, R. H.: Propulsion-Airframe Interactions Predicability. In Performance Prediction Methods. AGARD CP-242, October 1977.

I-356. Abercrombie, J. M.: Flight Test Verification of F-15 Performance Predictions. In Performance Prediction Methods. AGARD CP-242, October 1977.

I-357. Grelmann, H. W.: YF-17 Full Scale Minimum Drag Prediction. In Performance Prediction Methods. AGARD CP-242, October 1977.

I-358. Webb, T. S., Kent, D. R., and Webb, J. B.: Correlation of F-16 Aerodynamics and Performance Predictions with Early Flight Test Results. In Performance Prediction Methods. AGARD CP-242, October 1977.

I-359. Presley, L. L.: High Angle of Incidence Implications Upon Air Intake Design and Location for Supersonic Cruise Aircraft and Highly Maneuverable Transonic Aircraft. NASA TM 78530, Sept. 1978.

I-360. Presley, L. L.: A Comparison of a Shock-Capturing Technique with Experimental Data for Three-Dimensional Internal Flows. Conference on Aerodynamic Analyses Requiring Advanced Computers. NASA SP-347, Pt. 1, 1975, pp. 623-642.

I-361. Presley, L. L.: Angle-of-Attack Effects on Supersonic Inlet Bleed System Design. AIAA Paper 76-702, AIAA 12th Propulsion Conference, July 1976.

I-362. Presley, L. L.: Internal Flow Calculations for Axisymmetric Supersonic Inlets at Angle of Attack. AIAA Paper No. 75-1214, Sept. 1975.

I-363. Wasserbauer, J. F. and Gerstenmaier, W. H.: Inlet-Engine Matching for SCAR Including Application of a Bicone Variable Geometry Inlet. AIAA Paper 78-961, AIAA/SAE 14th Propulsion Conference, July 1978.

I-364. Savage, T. M. and Porcher, C. E.: A Prediction of the Normal Shock Location for Axisymmetric and Two-dimensional Inlets, and a Method for Calculating Supersonic Additive Drag. General Dynamics, Convair Aerospace Division, MR-P-277, March 1969, revised July 1974.

I-365. Hinz, W. W. and Miller, E. H.: Propulsion Integration of a Supersonic Cruise Strike-Fighter. AIAA Paper No. 79-0100, AIAA 17th Aerospace Sciences Meeting, Jan. 1979.

I-366. Webb, L. D., Whitmore, S. A., and Janssen, R. L.: Preliminary Flight and Wind Tunnel Comparisns of the Inlet/Airframe Interaction of the F-15 Airplane. AIAA Paper No. 79-0102, AIAA 17th Aerospace Science Meeting, Jan. 1979.

I-367. Vadyak, J., Hoffman, J. D., and Bishop, A. R.: Calculation of the Three-Dimensional Flow Field in Supersonic Inlets at Angle of Attack Using a Bicharacteristic Method with Discrete Shock Wave Fitting. AIAA Paper No. 79-0379, AIAA 17th Aerospace Sciences Meeting, Jan. 1979.

I-368. Chu, C. W.: Calculation of Three-Dimensional Supersonic Flow Fields about Aircraft Fuselages and Wings at General Angle of Attack. Northrop Corp. (Aircraft Division) Rept. NOR 72-182, Mar. 1973.

I-369. Weirich, R. L. and Vahl, W. A.: Flow-Field Properties Near an Arrow-Wing-Body Model at Mach Numbers of 1.60, 2.36, and 2.96. NASA TN D-4809, Oct. 1968.

I-370. Hill, W. A., Jr.: Force, Moment, and Flow-Field Characteristics of Two Wing-Body-Nacelle Combinations at Mach Numbers 2 and 3. NASA TM X-111, Jan. 1960.

I-371. Fradenburgh, E. A., Obery, L. J., and Mello, J. F.: Influence of Fuselage and Canard-Type Control Surface on the Flow-Field Adjacent to a Rearward Fuselage Station at a Mach Number of 2.0-Data Presentation. NACA RM E51K05, Jan. 1952.

I-372. Bober, L. J.: Use of Potential Flow Theory to Evaluate Subsonic Inlet Data from a Simulator-Powered Nacelle at Cruise Conditions. NASA TN D-7850, Dec. 1974.

I-373. Moretti, G. and Bleich, G.: Three-Dimensional Inviscid Flow About Supersonic Blunt Cones at Angle of Attack. Vol. I: Numerical Technique for the Three-Dimensional Blunt-Body Problem. Vol. II: Improved Time-Dependent Techniques for the Blunt-Body Problem. Sandia Laboratories Rept. SC-CR-3728, Sept. 1968.

I-374. Walitt, L.: Computation of Steady Axisymmetric Flow using a One-Dimensional Time-Dependent Method. NASA CR-137818, Aug. 1974.

I-375. Babenko, K. I., Voskresensky, G. P., Lyubimov, A. N., and Rusohov, V. V.: Three-Dimensional Flow of Ideal Gas Past Smooth Bodies. NASA TT F-380, Apr. 1966.

I-376. Dobson, M. D.: The External Drag of Fuselage Side Intakes: Semi-Circular Configurations Both with and Without Half Cone Compression Surfaces. RAE TR-72203, Feb. 1973.

I-377. Keeney, F. J.: Inlet-Drag Characteristics of a 7.5-Percent Scale Model of the McDonnell Douglas F-15 Tactical Aircraft at Mach Numbers from 0.60 to 2.20. AEDC TR-70-263, Dec. 1970.

I-378. Bencze, D. P.: Experimental Evaluation of Nacell-Airframe Inteference Forces and Pressures at Mach Numbers of 0.9 to 1.4. NASA TM X3321, Mar. 1977.

I-379. Leamer, P. C. and Kenneen, I. G.: Experimental Investigation of a 0.15-Scale Model of an Underfuselage Normal-Shock Inlet. NASA CR-3049, Oct. 1978.

I-380. Young, L. C.: Variable Inlet Cowl Concept. North American Rockwell Rept. TFD-71-1358, Sept. 1971.

I-381. Olinger, F. V., Shibata, H., and Albers, J. A.: Local Flow Measurements at the Inlet Plane of a 1/2-Scale Model of the YF-12C airplane. NASA TM X-3435, Sept. 1976. (Secret)

I-382. Surber, L. and Sedlock, D.: Effectsof Airframe-Inlet Integration on Half-Axisymmetric and Two-Dimensional Supersonic Inlet Performance. AIAA Paper No. 78-960, AIAA/SAE 14th Joint Propulsion Conference, July 1978.

I-383. McRae, Major D. S. and Hussaini, M. Y.: Numerical Simulation of Supersonic Cone Flow at High Angle of Attack. AGARD CP-247, High Angle of Attack Aerodynamics, Oct. 1978, Paper No. 23.

I-384. Robertson, J. P.: B-1 Status Propulsion System Installation Effects - October 1972. North American Rockwell Rept. TFD-72-1425, Nov. 1972.

I-385. Johnson, T. J.: IP-9 Performance Characteristis for the B-1 External Compression Inlet. Rockwell International Rept. TFD-74-1091, Nov. 1974.

I-386. MacMiller, C. J. and Hurley, O. C., III: B-1 Inlet Performance and Distortion Characteristics During Flight 1-22 Takeoff. Rockwell International Rept. TFD-76-161, Feb. 1976.

I-387. Goldsmith, E. L.: The Problems of Air Intake Testing. RAE TM Aero 1281, Jan. 1971.

I-388. Kutschenreuter, P. H., Jr., Moore, M. T., and Burnett, G. A.: Large Scale Inlet Distortion Investigation. AFFDL TR-70-20, May 1970.

I-389. McDill, H. E., Lauer, R. F., Jr., and Jackocks, J. L.: Results of the Full-Scale F-15 Inlet Engine Compatibility Test at Subsonic and Supersonic Mach Numbers. AEDC TR-72-149, Oct. 1972.

I-390. Kiser, C. E. and Johnson, T. J.: Results of the B-1 .07-Scale External Compression Inlet Drag Model Wind Tunnel Test, TWT 269. North American Rockwell Rept. NA-73-42, Mar. 1973.

I-391. Reyes, C. A., Nixon, J. and Fertig, M.: B-1 Wind Tunnel Test Results - 0.2 Scale External Compression Inlet Verification Model (AEDC SF 164). North Americal Rockwell Rept. NA-74-30, Jan. 1975.

I-392. Cawthon, J. A.: Advanced Inlet/Airframe Integration Concepts. AFFDL TR-77-47, July 1977.

I-393. Rakich, J. V., Vigneron, Y. C., and Agarwal, R.: Computation of Supersonic Viscous Flows Over Ogive-Cylinder at Angle of Attack. AIAA Paper No. 79-0131, 17th Aerospace Sciences Meeting, Jan. 1979.

I-394. Hasel, L. E. and Kouyoumjian, W. L.: Investigation of Static Pressures and Boundary-Layer Characteristics of the Forward Parts of Nine Fuselages of Various Cross-Sectional Shapes at M = 2.01. NACA RM L56I13, Jan. 1957.

I-395. Schiff, L. B. and Steger, J. L.: Numerical Simulation of Steady Supersonic Viscous Flow. AIAA Paper No. 79-0130, AIAA 17th Aerospace Sciences Meeting, Jan. 1979.

I-396. Walker, J.: Documentation of the Phase III 0.192-Scale Northrop/McDonnell-Douglas F-18 Inlet Performance Test at Mach Numbers 0 to 1.55. AEDC TSR-78-P28, Aug. 1978.

I-397. Dawson, C. W. and Dean, J. S.: The XYZ Potential Flow Program. NSRDC Rept. 3892, June 1972.

I-398. Hall, R. B.: The Definition of Tactical Missile Forebody Flow Fields. Presented at 1972 JANNAF Propulsion Meeting (U), Nov. 1972. (Confidential)

I-399. Dunsworth, L. C. and Woodgrift, K. E.: Inlet Technology for Air Launched Missiles. Inlet Configuration Definition Studies. Part II. Aerodynamic Measurements in the Supersonic Flow Field of a Body Composed of 3:1 Von Karman Ogive and Cylinder. AFAPL-TR-72-16, Part II, Apr. 1972.

I-400. Zumpano, F. R.: Inlet Technology for Air-Launched Missiles. Vol. II - Forebody Flow Field Test Results. AFAPL-TR-105, Volume II, Mar. 1972.

I-401. Karanian, A. J. Gadois, S. E., et al.: Investigation of Air Induction System Technology for an Air-Launched Advanced Ramjet Missile (ALARM). Test Data Summary Report (U). NWC-TP-5184, Dec. 1971.

I-402. Karanian, A. J., Gadbois, S. E., and Carlson, P. R.: Investigation of Inlet-Vehicle Installation Interactions for an Air-Launched Advanced Ramjet Missile (U). ALARM Final Report, Vol. II - Detailed Technical Report. UARL Rept. H91065622, Nov. 1969. (Confidential)

I-403. Tinoco, E. N. and Johnson, F. T.: The Application of a Higher Order Panel Method to Realistic Supersonic Configurations. AIAA Paper No. 79-0274, 17th aerospace Sciences Meeting, Jan. 1979.

I-404. Rakich, J. V. and Kutler, P.: Comparison of Characteristics and Shock Capturing Methods with Application to the Space Shuttle Vehicle. AIAA Papr 72-191, Jan. 1972.

I-405. Hess, J. L. and Stockman, N. O.: An Efficient User-Oriented Method for Calculating Compressible Flow About Three-Dimensional Inlets. AIAA Paper No. 79-0081, Jan. 1979.

I-406. Giles, H. L., Brunner, D. W., and Dunn, B. M.: Investigation of Air Induction Systems for Advanced Air-Launched Missiles. Vol. III - Experimental Evaluation of Side-Mounted Inlets for Air-to-Ground Missiles (U). AFAPL TR-70-29, May 1970. (Secret)

APPENDIX B

REFERENCE LIST FOR AFTERBODY/AIRFRAME INTERACTION EFFECTS

A-1. Addy, A. L.: Thrust-Minus-Drag Optimization by Base Bleed and/or Boattailing. J. Spacecraft & Rockets, Vol. 7, No. 11, Nov. 1970, pp. 1360-1362.

A-2. Alber, I. E., and Lees, L.: Integral Theory for Supersonic Turbulent Base Flows. AIAA Paper No. 68-101, AIAA 6th Aerospace Sciences Meeting, Jan. 1968.

A-3. Anderson, R. D., and Martens, R. E.: Exhaust System Interaction Program. AFAPL-TR-73-57, June 1973.

A-4. Benson, J. L., Miller, L. D., and Horie, G.: Theoretical Study of Engine Exhaust Nozzle Airframe Integration. Lockheed Rept. No. LR 20678, Apr. 1967.

A-5. Beheim, M. A, Anderson, B. H., Clark, J. S., Corsen, B. W., Jr., Stitt, L. E., and Wilcox, F. A.: Supersonic Exhaust Nozzles. Conference on Aircraft Propulsion, NASA SP-259, Nov. 1970.

A-6. Bergman, D.: Effects of Engine Exhaust Flow on Boattail Drag. J. Aircraft, Vol. 8, No. 6, June 1971, pp. 434-439.

A-7. Bergman, D.: An Aerodynamic Drag Study of Jet Engine Nozzles. AGARD CP-91-71, Inlets and Nozzles for Aerospace Engines, Sept. 1971.

A-8. Berrier, B. L., and Maiden, D. L.: Effect of Nozzle-Exhaust Flow on the Longitudinal Aerodynamic Characteristics of a Fixed-Wing Twin-Jet Fighter Airplane Model (U). NASA TM X-2389, Oct. 1971. (Confidential)

A-9. Berrier, B. L. and Mercer, C. E.: Off-Design Performance of Two Isentropic Plug Nozzles Designed for a Pressure Ratio of 16.5. NASA TN D-3852, Mar. 1967.

A-10. Berrier, B. L.: Effect of Plug and Shroud Geometry Variables on Plug-Nozzle Performance at Transonic Speeds. NASA TN D-5098, Mar. 1969.

A-11. Berrier, B. L., and Wood, F. H., Jr.: Effect of Jet Velocity and Axial Location of Nozzle Exit on the Performancg of a Twin-Jet Afterbody Model at Mach Numbers up to 2.2. NASA TN D-5393, Sept. 1969.

Preceding page blank

A-12. Berrier, B. L.: Effect of Nozzle Lateral Spacing on Afterbody Drag and Performance of Twin-Jet Afterbody Models with Cone Plug Nozzles at Mach Numbers up to 2.20. NASA TM X-2632, Dec. 1972.

A-13. Berrier, B. L.: Effect of Nozzle Lateral Spacing, Engine Interfairing Shape, and Angle of Attack on the Performance of a Twin-Jet Afterbody Model with Cone Plug Nozzles. NASA TM X-2724, Aug. 1973.

A-14. Berrier, B. L.: Effect of Empennage Inteference on Single-Engine Afterbody/Nozzle Drag. AIAA Paper No. 75-1296, AIAA/SAE 11th Propulsion Conference, Sept. 1975.

A-15. Ball, W. H.: Propulsion System Installation Corrections. Vol. IV. AFFDL-TR-72-147, Dec. 1972.

A-16. Bittrick, W. C.: Installation Benefits of the Single-Engine Exhaust Nozzle on the YF-16. AIAA Paper No. 74-1101, AIAA/SAE 10th Propulsion Conference, Oct. 1974.

A-17. Staff of the Boeing Company: Exhaust System Interaction Program. Vol. VII. Phase I Rept., Chapt. 7.0, Phase I Test. Rept. No. D162-10467-11, Apr. 1973.

A-18. Staff of the Boeing Company: Exhaust System Interaction Program. Vol. III. Phase I Rept., Chapt. 4.0, Performance Integration Methods. Rept. No. D162-10467-11, Apr. 1973.

A-19. Staff of the Boeing Company: Exhaust System Interaction Program. Vol. IV. Phase I Rept., Chapt. 5.0, Element Performance Prediction Methods. Rept. No. D162-10467-11, Apr. 1973.

A-20. Staff of the Boeing Company: Exhaust System Interaction Program. Vol. XV. Phase II Rept., Chapt. 15.0, Phase I Drag Correlations. Rept. No. D162-10467-11, Apr. 1973.

A-21. Staff of the Boeing Company: Exhaust System Interaction Program. Vol. I. Phase 1 Rept., Chapt. 1.0, Summary. Rept. No. D162-10467-11, Apr. 1973.

A-22. Staff of the Boeing Company: Exhaust System Interaction Program. Vol. XVII. Phase II Rept., Chapt. 17.0, Inputs to the Phase II System Analysis. Rept. No. D162-10467-11, Apr. 1973.

A-23. Staff of the Boeing Company: Exhaust System Interaction Program. Vol. VIII. Phase II Rept., Chapt. 8.0, Summary. Rept. No. D162-10467-11, Apr. 1973.

A-24. Postlewaite, J. E., and Salemann, V.: Exhaust System Interaction Program. AFAPL-TR-73-59, June 1973.

A-25. Staff of the Boeing Company: Exhaust System Interaction Program Handbook. Rept. No. D162-10467, Apr. 1973.

A-26. Bonner, E., and Nixon, J. A.: Wind Tunnel Testing Techniques for Integrated Airframe-Exhaust Nozzle Systems. AFFDL-TR-68-94, July 1968.

A-27. Calarese, W.: An Analytical Method to Compute Viscous-Inviscid Transonic Flow on Axisymmetric Afterbodies Including Jet Effects and Boattail Bleed in Separated Regions. AIAA Paper No. 75-1293, AIAA/SAE 11th Propulsion Conference, Sept. 1975.

A-28. Capone, F. J.: Effects of Nozzle Exit Location and Shape on Propulsion-Induced Aerodynamic Characteristics due to Vectoring Twin Nozzles at Mach Numbers from 0.40 to 1.2. NASA TM X-3313, Jan. 1976.

A-29. Coombes, T. D.: A Model Technique for Exhaust System Performance Testing. AGARD CP-150, Airframe/Propulsion Interference, Mar. 1975.

A-30. Corson, B. W., and Reubush, D. E.: Cascade Plug Nozzle and Convergent Nozle performance Comparison (U). NASA TM X-2617, Aug. 1972. (Confidential)

A-31. Compton, W. B., III: Effects of Jet Exhaust Gas Properties on Exhaust Simulation and Afterbody Drag. NASA TR R-444, Oct. 1975.

A-32. Castells, O. T.: Twin Jet Exhaust System Interaction Test. Vol. I. General Electric Rept. No R72AEG235, Aug. 1972.

A-33. Castells, O. T.: Twin Jet Exhaust System Interaction Test. Vol. II. General Electric Rept. No. R72AEG235, Oct. 1975.

A-34. Chow, W. L., Bober, L. J., and Anderson, B. H.: Numerical Calculation of Transonic Boattail Flow. NASA TN D-7984, June 1975.

A-35. Compton, W. B., III: Effect on Base Drag of Recessing the Bases of Conical Afterbodies at Subsonic and Transonic Speeds. NASA TN D-4821, Oct. 1968.

A-36. Compton, W. B., III and Runckel, J. F.: Jet Effects on the Boattail Axial Force of Conical Afterbodies at Subsonic and Transonic Speeds. NASA TM X-1960, Feb. 1970.

A-37. Compton, W. B., III: Jet Effects on the Drag of Conical Afterbodies at Supersonic Speeds. NASA TN D-6789, July 1972.

A-38. Compton, W. B., III: An Experimental Study of Jet Exhaust Simulation. AGARD CP-150, Airframe/Propulsion Interference, Mar. 1975.

A-39. Corson, B. W., Jr., and Schmeer, J. W.: Summary of Research on Jet-Exit Installations. NASA TM X-1273, Oct. 1966.

A-40. Corson, B. W., Jr., and Runckel, J. F.: Exploratory Studies of Aircraft Afterbody and Exhaust-Nozzle Interaction (U). NASA TM X-1925, Dec. 1969. (Confidential)

A-41. Everling, P. C. and Bowers, D. L.: Evaluation of the Twin Nozzle/Afterbody Drag and Nozzle Internal Performance Computer Deck with ESIT Free Jet Data. AFFDL-TM-74-203-FXM, Oct. 1974.

A-42. Glasgow, E. R. and Santman, D. M.: Aft-End Design Criteria and Performance Prediction Methods Applicable to Air Superiority Fighters Having Buried Engines and Dual Nozzles. AIAA Paper No. 72-111, AIAA/SAE Propulsion Joint Specialist Conference, Dec. 1972.

A-43. Grund, E., Konarski, M., and Presz, W., Jr.: Predicting Airframe/Exhaust Nozzle Interaction at Transonic Mach Numbers. AIAA Paper No. 71-720, AIAA/SAE 7th Propulsion Joint Specialist Conference, June 1971.

A-44. Glasgow, E. R., Santman, D. M., and Miller, L. D.: Experimental and Analytical Determination of Integrated Airframe Nozzle Performance. Vol. I. AFFDL-TR-72-101, Oct. 1972.

A-45. Glasgow, E. R., Santman, D. M., and Miller, L. D.: Experimental and Analytical Determination of Integrated Airframe Nozzle Performance. Vol. II. Operating Manual for Twin-Nozzle/Afterbody Drag and Internal Nozzle Performance Computer Deck. AFFDL-TR-72-101, Oct. 1972.

A-46. Glasgow, E. R., Santman, D. M., and Miller, L. D.: Integrated Airframe-Nozzle Performance for Designing Twin-Engine Fighters. Vol. I. AFFDL-TR-73-71, June 1973.

A-47. Glasgow, E. R., Santman, D. M., and Miller, L. D.: Integrated Airframe-Nozzle Performance for Designing Twin-Engine Fighters. Vol. II. AFFDL-TR-73-71, June 1973.

A-48. Glasgow, E. R., Santman, D. M., and Miller, L. D.: Integrated Airframe-Nozzle Performance for Designing Twin-Engine Fighters. Vol. IV. Operating Manual for Subsonic Axisymmetric Nozzle Boattail Drag Computer Deck. AFFDL-TR-73-71, June 1973.

A-49. Glasgow, E. R., Santman, D. M., and Miller, L. D.: Integrated Airframe-Nozzle Performance for Designing Twin-Engine Fighters. Vol. V. Operating Manual for Supersonic Axisymmetric Nozzle Boattail Drag Computer Deck. AFFDL-TR-73-71, June 1973.

A-50. Glasgow, E. R., Santman, D. M., and Miller, L. D.: Integrated Airframe-Nozzle Performance for Designing Twin-Engine Fighters. Vol. VI. Revised Operating Manual for Twin Nozzle/Afterbody Drag and Nozzle Internal Performance Computer Deck. AFFDL-TR-73-71, June 1973.

A-51. Grossman, B. and Melnik, R. E.: The Numerical Computation of The Transonic Flow Over Afterbodies Including the Effect of Jet-Plume and Viscous Interactions. AIAA Paper No. 75-62, AIAA 13th Aerospace Sciences Meeting, Jan. 1975.

A-52. Galigher, L. L.: Evaluation of the Various Exhaust Nozzles at Free Stream Mach Numbers from 0.6 to 3.0. AEDC-TR-70-256, Dec. 1970.

A-53. Herron, R. D.: Jet-Boundary Simulation Parameters for Under-expanded Jets in a Quiescent Atmosphere. J. Spacecraft & Rockets, Vol. 5, No. 10, Oct. 1968, pp. 1155-1160.

A-54. Hines, B. G., Marsh, W. H., and Wood, R. A.: Twin Jet Installation and Test Technique Improvement Test. General Electric Rept. No. R74AEG201, Jan. 1974.

A-55. Homan, M. L.: Nacelle Afterbody Drag Investigation of a B-1 0.06-Scale Model at Mach Numbers from 0.55 to 2.2 AEDC-TR-72-176, Nov. 1972.

A-56. Kirkham, F. S., Lee, E. E., Jr., and Lauer, R. F., Jr.: Afterbody Drag of Several Clustered Jet-Exit Configurations At Transonic Speeds. NASA TM X-1216, Mar. 1966.

A-57. Klineberg, J. M., Kubota, T., and Lees, L.: Theory of Exhaust-Plume/Boundary-Layer Interactions at Supersonic Speeds. AIAA Paper No. 70-230, AIAA 8th Aerospace Sciences Meeting, Jan. 1970.

A-58. Konarski, M.: Experimental and Analytical Determination of Integrated Airframe-Nozzle Performance. Phase I Summary Report. Pratt & Whitney Aircraft Rept. No PWA-4065, Nov. 1970.

A-59. Staff of Langley Research Center: Wind Tunnel Data, Friend or Foe? July 1975.

A-60. Lauer, R. F., Jr. and Mercer, C. E.: Blow-In-Door Ejector Nozzle Performance Comparison Between Fixed-Open and Free-Floating Door Configurations. NASA TM X-1177, Aug. 1967.

A-61. Laughrey, J. A.: Comparison of Testing Techniques for Isolated Axisymmetric Exhaust Nozzles in Transonic Flow. AIAA Paper No. 75-1292, AIAA/SAE 11th Propulsion Conference, Sept. 1975.

A-62. Lee, E. E., Jr., and Runckel, J. F.: Performance of Closely Spaced Twin-Jet Afterbodies with Different Inboard-Outboard Fairing and Nozzle Shapes. NASA TM X-2329, Sept. 1971.

A-63. Maiden, D. L. and Runckel, J. F.: Effect of Nozzle Lateral Spacing on Afterbody Drag and Performance of Twin-Jet After-body Models with Convergent Nozzles at Mach Numbers Up to 2.2. NASA TM X-2099, Oct. 1970.

A-64. Maiden, D. L., and Berrier, B. L.: Effects of Afterbody Closure and Sting Interference on the Longitudnal Aerodynamic Characteristics of a Fixed-Wing Twin-Jet Fighter Airplane Model (U). NASA TM X-2415, Oct. 1971. (Confidential)

A-65. Maiden, D. L., and Berrier, B. L.: Effect of Airframe Modifications on Longitudinal Aerodynamic Characteristics of a Fixed-Wing, Twin-Jet Fighter Airplane Model (U). NASA TM X-2523, Apr. 1972. (Confidential)

A-66. Brazzel, C. E. and Henderson, J. H.: An Emprical Technique for Estimating Power-On Base Drag of Bodies-of-Revolution with a Single Jet Exhaust. AGARD CP-10, The Fluid Dynamic Aspects of Ballistics, Sept. 1966.

A-67. Maiden, D. L.: Performance of an Isolated Two-Dimensional Variable-Geometry Wedge Nozzle with Translating Shroud and Collapsing Wedge at Speeds up to Mach 2.01. NASA TN D-7906, Apr. 1975.

A-68. Martens, R. E.: F-15 Nozzle/Afterbody Integration. AIAA Paper No. 74-1100, AIAA/SAE 10th Propulsion Conference, Oct. 1974.

A-69. Mercer, C. E., Schmeer, J. W., and Lauer, R. F., Jr.: Performance of Several Blow-In-Door Ejector Nozzles at Subsonic and Low-Supersonic Speeds. NASA TM X-1163, Aug. 1967.

A-70. Mercer, C. E., Pendergraft, O. C., and Berrier, B. L.: Effect of Geometric Variations on Performance of a Twin-Jet Blow-In Door Ejector Nozzle Installation (U). NASA TM X-1633, Aug. 1968. (Confidential)

A-71. Mercer, C. E. and Berrier, B. L.: Effect of Afterbody Shape, Nozzle Type, and Engine Lateral Spacing on the Installed Performance of a Twin-Jet Afterbody Model. NASA TM X-1855, Sept. 1969.

A-72. Mercer, C. E. and Reubush, D. E.: Sting and Jet Interference Effects on Longitudinal Aerodynamic Characteristics of a Twin-Jet, Variable-Wing-Sweep Fighter Model at Mach Numbers to 2.2 (U). NASA TM X-2825, July 1973. (Confidential)

A-73. Mercer, C. E., and Berrier, B. L.: Effect of Plug Base Contour on Performance of a Fully Truncated Plug Nozzle with Translating Shroud. NASA TN D-5655, Feb. 1970.

A-74. Mercer, C. E.: Effect of Jet Convergence Angle on the Performance of Annular Nozzles with Semitoroidal Concave Plugs at Mach Numbers Up to 1.82. NASA TN D-6897, Oct. 1972.

A-75. Norton, H. T., Jr.: Installed Performance Characteristics of a Blow-In Door Ejector Nozzle with Terminal Fairings (U). NASA TM X-1611, July 1968. (Confidential)

A-76. Berrier, B. L.: Propulsion Superintegration = Supercruiser. Paper presented at USAF Super-Cruise Technical Conference, Colorado Springs, CO, Feb. 1976.

A-77. Pendergraft, O. C., Jr.: Performance of a Twin D Nozzle-Afterbody Configuration with Wedge Interfairings at Mach Numbers to 2.2 (U). NASA TM X-2100, Oct. 1970. (Confidential)

A-78. Pendergraft, O. C., Jr., and Schmeer, J. W.: Effect of Nozzle Lateral Spacing on Afterbody Drag and Performance of Twin-Jet Afterbody Models with Convergent-Divergent Nozzles at Mach Numbers up to 2.2. NASA TM X-2601, Oct. 1972.

A-79. Armstrong, R. S. and Miller, S. R.: Subsonic Aerodynamic Performance of Nozzle Installations in Supersonic Airplanes. J. of Aircraft, Vol. 5, No. 3, May 1968, pp. 230-235.

A-80. Presz, W. M., Jr. and Pitkin, E. T.: An Analytical Model of Axisymmetric Afterbody Flow Separation. AIAA Paper No. 75-65, AIAA 13th Aerospace Sciences Meeting, Jan. 1975.

A-81. Presz, W. M., Jr. and Pitkin, E. T.: Flow Separation Over Axisymmetric Afterbody Models. AIAA Paper No. 4-17, AIAA 12th Aerospace Sciences Meeting, Jan. 1974.

A-82. Price, E. A., Jr.: Aerodynamic Characteristics of the B-1 Fuselage Afterbody Including Simulated Jet Exhaust Effects at Mach Numbers from 0.55 to 2.20. AEDC-TR-73-73, Apr. 1973.

A-83. Runckel, J. F., Lee, E. E., and Simonson, A. J.: Sting and Jet Interference Effects on the Afterbody Drag of a Twin Engine Variable Sweep Fighter Model at Transonic Speeds. NASA TM X-755, Jan. 1963.

A-84. Putnam, L. E. and Trescot, C. D., Jr.: Effects of Aft-Fuselage-Mounted Nacelles on the Subsonic Longidutinal Aerodynamic Characteristics of a Twin-Turbojet Airplane. NASA TN D-3781, Dec. 1966.

A-85. Putnam, L. E. and Capone, F. J.: Experimental Determination of Equivalent Solid Bodies to Represent Jets Exhausting into a Mach 2.20 External Stream. NASA TN D-5553, Dec. 1969.

A-86. Putnam, L. E.: Effect of Nozzle Interfairings on Aerodynamic Characteristics of a Twin-Engine Variable Sweep-Wing Fighter Airplane at Mach 0.6 to 2.01 (U). NASA TM X-2769, June 1973. (Confidential)

A-87. Putnam, L. E.: Effects of Modifications and External Stores on Aerodynamic Characteristics of a Fighter Airplane with Variable-Sweep Wing and Twin Vertical Tails at Mach 0.65 (U). NASA TM X-2366, Dec. 1974. (Confidential)

A-88. Re, R. J., Wilmoth, R. G., and Runckel, J. F.: Investigation of Effects of Afterbody Closure and Jet Interference on the Drag of a Twin-Engine Tactical Fighter (U). NASA TM X-1382, June 1967. (Confidential)

A-89. Reubush, D. E.: Effects of Fineness and Closure Ratios on Boattail Drag of Circular-Arc Afterbody Models with Jet Exhaust at Mach Numbers Up to 1.3. NASA TN D-7163, May 1973.

A-90. Reubush, D. E. and Runckel, J. F.: Effect of Fineness Ratio on Boattail Drag of Circular-Arc Afterbodies Having Closure Ratios of 0.50 with Jet Exhaust at Mach Numbers Up to 1.30. NASA TN D-7192, May 1973.

A-91. Reubush, D. E. and Mercer, C. E.: Exhaust-Nozzle Characteristics for a Twin-Jat Variable-Wing-Sweep Fighter Airplane Model at Mach Numbers to 2.2. NASA TM X-2947, June 1974.

A-92. Reubush, D. E.: Experimental Study of the Effectiveness of Cylindrical Plume Simulators for Predicting Jet-On Boattail Drag at Mach Numbers Up to 1.30. NASA TN D-7795, Nov. 1974.

A-93. Reubush, D. E.: The Effect of Reynolds Number on Boattail Drag. AIAA Paper No. 75-63, AIAA 13th Aerospace Sciences Meeting, Jan. 1975.

A-94. Reubush, D. E. and Mercer, C. E.: Effects of Nozzle Interfairing Modifications on Longitudinal Aerodynamic Characteristics of a Twin-Jet Variable-Wing-Sweep Fighter Model. NASA TN D-7817, Feb. 1975.

A-95. Reubush, D. E.: The Effect of Reynolds Number on the Boattail Drag of Two Wing-Body Configurations. AIAA Paper No. 75-1294, AIAA/SAE 11th Propulsion Conference, Sept. 1975.

A-96. Robinson, C. E. and High, M. D.: Exhaust Plume Temperature Effects on Nozzle Afterbody Performance Over the Transonic Mach Number Range. AEDC-TR-74-9, July 1974.

A-97. Robinson, C. E., High, M. D., and Galigher, L. L.: Exhaust Plume Temperature and Reynolds Number Effects on Nozzle Afterbody Performance Over the Transonic Mach Number Range. AIAA Paper No. 74-1148, AIAA/SAE 10th Propulsion Conference, Oct. 1974.

A-98. Roffe, G. and Miller, G.: Similarity Parameters and Their Sensitivity for Transonic Airframe Exhaust Nozzle Interactions. AFFDL-TR-73-9, Jan. 1973.

A-99. Rom, J. and Bober, L. J.: Calculation of the Pressure Distribution on Axisymmetric Boattails Including Effects of Viscous Interactions and Exhaust Jets in Subsonic Flow. NASA TM X-3109, Sept. 1974.

A-100. Rooney, E. C.: Development of Techniques to Measure In-Flight Drag of a U.S. Navy Fighter Airplane and Correlation of Flight Measured Drag with Wind Tunnel Data. AGARD CP-124, Aerodynamic Drag, Oct. 1973.

A-101. Runckel, J. F.: Jet-Exit and Airframe Interference Studies on Twin-Engine-Fuselage Aircraft Installations. NASA TM X-1274, Oct. 1966.

A-102. Sykes, D. M.: Experimental Investigation of Boat-Tailed Afterbodies with Driving Bands in Transonic Flow. RARDE Memo 5/73, May 1973.

A-103. Runckel, J. F.: Interference Between Exhaust Systems and Afterbody of Twin-Engine Fuselage Configurations. NASA TN D-7525, May 1974.

A-104. Sadunas, J. A.: Integrated Scramjet Nozzle/Afterbody Performance Analysis. AIAA Paper No. 75-1297, AIAA/SAE 11th Propulsion Conference, Sept. 1975.

A-105. Salas, M. D.: The Numerical Calculation of Inviscid Plume Flow Fields. AIAA Paper No. 74-523, AIAA 7th Fluid and Plasma Dynamics Conference, June 1974.

A-106. Maise, G.: Wave Drag of Optimum and Other Boattails. J. Aircraft, Vol. 7, No. 5, Sept. 1970, pp. 477-478.

A-107. Schmeer, J. W, Lauer, R. F., Jr., and Berrier, B. L.: Performance of Blow-In-Door Ejector Nozzles Installed on a Twin-Jet Variable Wing-Sweep Fighter Airplane (U). NASA TM X-1383, June 1967. (Confidential)

A-108. Schnell, W. C. and Migdal, D.: An Experimental Evaluation of Exhaust Nozzle/Airframe Interference. J. Aircraft, Vol. 7, No. 5, Sept. 1970, pp. 396-400.

A-109. Schnell, W. C.: F-14A Installed Nozzle Performance. AIAA Paper No. 74-1099, AIAA/SAE 10th Propulsion Conference, Oct. 1974.

A-110. Leonard, J. and Gilbertson, M. W.: B-1 Air Vehicle .06-Scale Nozzle/Afterbody Verification Model Wind Tunnel Test Results (Test No. 1). North American Rockwell Rept. No. NA-74-51, Jan. 1974.

A-111. Stoddart, J. A. P.: Jet Effects on Boattail Pressure Drag at Supersonic Speeds. AGARD CP-91-71, Inlets and Nozzles for Aerospace Engines, Sept. 1971.

A-112. Wilmoth, R. G., Norton, H. T., and Corson, B. W., Jr.: Effect of Engine Interfairing Modifications on the Performance of a Twin-Jet Fighter Airplane Model at Mach 1.2 (U). NASA TM X-1534, Mar. 1968. (Confidential)

A-113. Wynosky, T. A. and Spurrell, R. M.: Exhaust System Interaction Program. Final Progress Report. Pratt & Whitney Aircraft Rept. No. PWA-4745, June 1973.

A-114. Miller, E. H. and Migdal, D.: Subsonic Interference Characteristics of Single and Twin Jet Afterbodies. J. Aircraft, Vol. 7, No. 3, May-June 1970, pp. 261-266.

A-115. Aulehla, F. and Besigk, G.: Reynolds Number Effects on Fore- and Afterbody Pressure Drag. AGARD CP-150, Airframe/Propulsion Inteference, Mar. 1975.

A-116. Brazier, M. and Ball, W. H.: Accounting of Aerodynamic Forces on Airframe/Propulsion Systems. AGARD CP-150, Airframe/Propulsion Interference, Mar. 1975.

A-117. Dixon, R. J., Richardson, J. M., and Page, R. H.: Turbulent Base Flow on an Axisymmetric Body with a Single Exhaust Jet. J. Spacecraft Rockets, Vol. 7, No. 7, July 1970, pp. 848-854.

A-118. Herrick, P. W.: Predicting Propulsion Related Drag of Jet Afterbodies. SAE-751088, National Aerospace Engineering and Manufacturing Meeting, Nov. 1975.

A-119. Glidewell, R. J., and Fanning, A. E.: Twin Jet Exhaust System Test Techniques. AGARD CP-150, Airframe/Propulsion Interference, Mar. 1975.

A-120. Moulden, T. H., Wu, J. M., and Spring, D. J.: On Some Problems Encountered in a Theoretical Study of the External Flow over a Nozzle Configuration in Transonic Flight. AGARD CP-150, Airframe/Propulsion Interference, Mar. 1975.

A-121. Quermann, J. K.: Subsonic Base and Boattail Drag: An Analytical Approach. AGARD CP-150, Airframe/Propulsion Interference, Mar. 1975.

A-122. Reid, J. Mundell, A. R. G., and Crane, J. F. W.: The Subsonic Base Drag of Cylindrical Twin-Jet and Single-Jet Afterbodies. AGARD CP-150, Airframe/Propulsion Interference, Mar. 1975.

A-123. Richey, G. K., Surber, L. E., and Laughrey, J. A.: Airframe/Propulsion System Flow Field Interference and the Effect on Air Intake and Exhaust Nozzle Performance. AGARD CP-150, Airframe/Propulsion Interference, Mar. 1975.

A-124. Robinson, C. E., High, M. D., and Thompson, E. R.: Exhaust Plume Temperature Effects on Nozzle Afterbody Performance Over the Transonic Mach Number Range. AGARD CP-150, Airframe/Propulsion Interference, Mar. 1975.

A-125. Harrington, D. E.: Jet Effects on Boattail Pressure Drag on Isolated, Ejector Nozzles at Mach Numbers from .6 to 1.47. NASA TM X-1785, May 1969.

A-126. Walker, S. C.: Isolating Nozzle-Afterbody Interaction Parameters and Size Effects - A New Approach. AGARD CP-150, Airframe/Propulsion Interference, Mar. 1975.

A-127. Wilcox, F. A. and Chamberlin, R.: Reynolds Number Effects on Boattail Drag of Exhaust Nozzle from Wind Tunnel and Flight Tests. AGARD CP-150, Airframe/Propulsion Interference, Mar. 1975.

A-128. Migdal, D. and Schnell, W. C.: Twin-Jet Airframe/Nozzle Tests for VFAX Applications (U). Grumman Aircraft Engineering Corp. Final Report, Contract No. N00019-68-C-0233, Naval Systems Command, Mar. 1969.

A-129. Friedman, M. D. and Cohen, D.: Arrangement of Fusiform Bodies to Reduce the Wave Drag at Supersonic Speeds. NACA Rept. 1236, 1955.

A-130. Reubush, D. E.: An Experimental Investigation of Jet Plume Simulation with Solid Circular Cylinders. NASA TM X-71963, May 1974.

A-131. Glasgow, E. R. and Santman, D. M.: Aft-End Design Techniques for Twin-Engine Fighters. J. Aircraft, Vol. 11, No. 1, Jan. 1974, pp. 39-44.

A-132. Glasgow, E. R.: Integrated Airframe/Nozzle Performance for Designing Twin-Engine Fighters. J. Aircraft, Vol. 11, No. 6, June 1974, pp. 354-362.

A-133. Swihart, J. M. and Nelson, W. J.: Performance of Multiple Jet Exit Installations. NACA RM L58E01, July 1958.

A-134. Shrewsbury, G. D.: Effect of a Simulated Wing on the Pressure-Drag Coefficients of Various 15° Boattails at Mach Numbers from 0.56 to 1.00. NASA TM X-1662, Oct. 1968.

A-135. Blaha, B. J. and Mikkelson, D. C.: Wind Tunnel Investigation of Airframe Installation Effects on Underwing Engine Nacelles at Mach Numbers from 0.56 to 1.46. NASA TM X-1683, Nov. 1968.

A-136. Reubush, D. E. and Putnam, L. E.: An Experimental and Analytical Investigation of the Effect on Isolated Boattail Drag of Varying Reynolds Number Up to 130×10^6. NASA TN D-8210, May 1976.

A-137. Ferri, A.: Introductory Lecture - Engine Airplane Interference - Definition of the Problem and Related Basic Fluid Dynamic Phenomena. AGARD LS-53, Airframe/Engine Integration, May 1972.

A-138. Aulehla, F. and Lotter, K.: Nozzle/Airframe Interference and Integration. AGARD LS-53, Airframe/Engine Integration, May 1972.

A-139. Jarsma, F.: Experimental Determination of Nozzle Characteristics and Nozzle Airframe Interference. AGARD LS-53, Airframe/Engine Integration, May 1972.

A-140. Fuhs, A.E.: Engine Integration and Thrust/Drag Definition. AGARD LS-53, Airframe/Engine Integration, May 1972.

A-141. Shrewsbury, G. D.: Effect of Boattail Junction Shape on Pressure Drag Coefficient of Isolated Afterbodies. NASA TM X-1517, Mar. 1968.

A-142. Westphal, R. C. and Johnson, R. H.: Propulsion System Integration and Test Progrom (Steady State). Part III - Nozzle Interaction Drag Tests. AFAPL-TR-69-44, June 1969.

A-143. Lee, K. and Franz, J.: An Aftend Drag Data Base and Prediction Technique for Twin Jet Fighter Type Aircraft. NADC Rept. No. NADC-77021-30, June 1977.

A-144. Parthasarathy, K. and Bozzola, R.: The Computation of Steady Exhaust Nozzle Flows by a Time Dependent Method. AIAA Paper No. 76-151, AIAA 14th Aerospace Sciences Meeting, Jan. 1976.

A-145. Langfelder, H.: Low-Drag Installation of Twin Propulsion Nozzles in the Rear of the Fuselage for Transonic and Supersonic Flight. Presented at AGARD Specialist' Meeting on Aerodynamics of Power Plant Installation (Part I), Oct. 1965.

A-146. Adams, M. C.: Determination of Shapes of Boattail Bodies of Revolution for Minimum Wave Drag. NACA TN-2550, Nov. 1951.

A-147. Deep, R. A., Henderson, J. H., and Brazzel, C. E.: Thrust Effects on Missile Aerodynamics. U.S. Army Missile Command Rept. RD-TR-71-9, May 1971. (Supersedes RD-TM-68-8)

A-148. McDonald, H. and Hughes, P.: A Correlation of High Subsonic Afterbody Drag in the Presence of a Propulsive Jet on Support Sting. J. Aircraft, Vol. 2, No. 3, May-June 1965, pp. 202-207.

A-149. Pick, G. S.: Afterbody Drag Evaluation - An Interim Progress Report. Naval Ship R&D Center Rept. No. TM 16-76-32, Nov. 1975.

A-150. Throndson, L. W.: Close-Spaced Nozzles Twin Jet Configuration. AIAA Paper No. 70-934, AIAA 2nd Aircraft Design and Operations Meeting, July 1970.

A-151. Swavely, C. E. and Soileau, J. F.: Aircraft Afterbody/Propulsion System Integration for Low Drag. AIAA Paper No. 72-1101, AIAA/SAE 8th Propulsion Joint Specialist Conference, Dec. 1972.

A-152. Robinson, C. E. and Price, E. A.: Effect of Reynolds Number on the Nozzle Afterbody Peformance of the AGARD Nozzle and B-1 .06-Scale Model at Transonic Mach Numbers. AIAA Paper No. 75-1321, AIAA/SAE 11th Propulsion Conference, Sept. 1975.

A-153. Foss, W. E., Lee, E. E., and Runckel, J. F.: Effects of Boattail Area Contouring and Simulated Turbojet Exhaust on the Loading and Fuselage-Tail Component Drag of a Twin-Engine Fighter-Type Airplane Model. NACA RM L58C04, July 1958.

A-154. Chamberlin, R. and Blaha, B. J.: Flight and Wind Tunnel Investigation of the Effects of Reynolds Number on Installed Boattail Drag at Subsonic Speeds. NASA TM X-68162, 1973.

A-155. Taillon, N. V.: Flight-Test Investigation of the Aerodynamic Characteristics and Flow Interference Effects About the Aft Fuselage of the F-111A Airplane. NASA TN D-7563, Feb. 1974.

A-156. Reshotko, E. and Tucker, M.: Approximate Calculation of the Compressible Turbulent Boundary Layer with Heat Transfer and Arbitrary Pressure Gradient. NACA TN 4154, Dec. 1957.

A-157. Miller, L.E.: Predicting Turbulent Compressible Boundary Layers in Strong Adverse Pressure Gradients. AIAA Paper No. 67-196, AIAA 5th Aerospace Sciences Meeting, Jan. 1967.

A-158. Sasman, P. K. and Cresci, R. J.: Compressible Turbulent Boundary Layer with Arbitrary Pressure Gradient and Heat Transfer. ARL 65-65, Apr. 1965.

A-159. Murman, E. M. and Cole, J. D.: Calculation of Plane Steady Transonic Flows. AIAA Paper No. 70-188, AIAA 8th Aerospace Sciences Meeting, Jan. 1970.

A-160. Korst, H. H.: A Theory for Base Pressures in Transonic and Supersonic Flow. J. Appl. Mech., Dec. 1956, pp. 593-600.

A-161. Sivells, J. C. and Payne, R. G.: A Method of Calculating Turbulent-Boundary-Layer Growth at Hypersonic Mach Numbers. AEDC-TR-59-3, Mar. 1959.

A-162. Hess, J. L. and Smith, A. M. O.: Calculation of Non-Lifting Potential Flow About Arbitrary Three-Dimensional Bodies. Douglas Aircraft Co. Rept. No. ES 40622, Mar. 1962.

A-163. South, J. C. and Jameson, A.: Relaxation Solutions for Inviscid Axisymmetric Transonic Flow Over Blunt or Pointed Bodies. In.: Proceedings, AIAA Computational Fluid Dynamics Conference, Palm Springs, CA, July 1973.

A-164. Smith, A. M. O. and Pierce, J.: Exact Solution of the Neumann Problem. Calculation of Non-Circulatory Plane and Axially Symmetric Flows About or Within Arbitrary Boundaries. Douglas Aircraft Co. Rept. No. ES 26988, Apr. 1958.

A-165. Spreiter, J. R. and Alksne, A. Y.: Slender Body Theory Based on Approximate Solution of the Transonic Flow Equation. NASA Rept. 2, 1959.

A-166. Runckel, J. F.: Aerodynamic Interference Between Exhaust System and Airplane. NASA TM X-66888, Sept. 1970.

A-167. Swihart, J. M., Norton, H. T., Jr. and Schmeer, J. W.: Effect of Several Afterbody Modifications Including Terminal Fairings on the Drag of a Single-Engine Fighter Model with Hot-Jet Exhaust. NASA Memo 10-29-58L, Dec. 1958.

A-168. Nelson, W. J. and Henry, B. Z., Jr.: Jet Effects on Base and Afterbody Drag. NACA Conference on Aerodynamics of High Speed Aircraft, Langley Research Center, 1955.

A-170. Sargent, J. C. and Gunter, J. L.: Nozzle Afterbody Configuration Development for the B-1 Strategic Bomber. J. Aircraft, Vol. 13, No. 2, Feb. 1976, pp. 135-139.

A-171. Mercer, C. E. and Schmeer, J. W.: Transonic Performance of Ejector Nozzles Having Zero Boattail Angle and an Internal Base. NASA TM X-1104, June 1965.

A-172. Moulden, T. H., Wu, J. M., and Spring, D. J.: Flow Field Analysis for a Powered Rocket at Transonic Speeds. Tenth International Symposium on Space Technology and Science, Tokyo, Japan, 1973.

A-173. Wu, J. M., Moulden, T. H., and Spring, D. J.: On Some Studies of Aft-End Design and Its Influence on Plume Induced Separation in Transonic Flight. Eighth JANNAF Plume Technology Meeting, Colorado Springs, CO, July 1974.

A-174. Moulden, T. H., Wu, J. M., and Spring, D. J.: A Flow Field Model for, and Some Studies on the Drag of, an Engine Exhaust System at Transonic Flight Speeds. AIAA Paper No. 74-1175, AIAA/SAE 10th Propulsion Conference, San Diego, CA, Oct. 1974.

A-175. Lee, J. D : An Experimental Study of Boattail Pressures at High Subsonic Mach Numbers and High Reynolds Numbers. ARL TR 75-0014, Mar. 1975.

A-176. Byrd, K. F.: Experimental Investigation of Twin Jet Aircraft/ Exhaust Nozzle Installation Effects. General Electric Rept. R69AE0290, May 1969.

A-177. Spratley, A. V.: An Investigation of Boattail Geometry and Reynolds Number Effects on Forebody and Afterbody Drag at Transonic Mach Numbers. AEDC-TR-76-161, Feb. 1977.

A-178. Blaha, B. J., Chamberlin, R., and Bober, L. J.: Boundary Layer Thickness Effect on Boattail Drag. AIAA Paper No. 76-676, AIAA/SAE 12th Propulsion Conference, Palo Alto, CA, July 1976.

A-179. Peters, W. L. and Kennedy, T. L.: An Evaluation of Jet Simulation Parameters for Nozzle/Afterbody Testing at Transonic Mach Numbers. AIAA Paper No. 77-106, AIAA 15th Aerospace Sciences Meeting, Los Angeles, CA, Jan. 1977.

A-180. Knell, D. M. and Lunn, D.: Effect of Asymmetry of Aerodynamic Nozzles Operating in Near-Critical Conditions. Dept. of Aeronautical Engineering, Bristol University, 1969.

A-181. Henderson, J. H.: Results of a Transonic Wind Tunnel Investigation of Thrust Effects on the Aerodynamics of Long Bow Missile Configuration. U. S. Army Missile Command Rept. RD-TR-73-18, Nov. 1973.

A-182. Henderson, J. H.: Results of Transonic Wind Tunnel Investigation to Determine the Effects of Nozzle Geometry and Jet Plume on the Aerodynamics of a Body of Revolution. U. S. Army Missile Command Rept. RD-72-17, Nov. 1972.

A-183. Burt, J. R.: An Experimental Investigation of the Effects of Rocket Plume Simulators on the Radial and Longitudinal Pressure Distribution of a Sting Mounted Body of Revolution at Transonic Mach Numbers. U. S. Army Missile Command Rept. RD-TR-74-21, July 1973.

A-184. Alber, I.: Integral Theory for Turbulent Base Flows at Subsonic and Supersonic Speeds. Ph.D. Thesis, California Institute of Technology, May 1967.

A-185. Henderson, J. H.: Results of a Transonic Wind Tunnel Investigation of Thrust Effects on the Aerodynamics of Four Longitudinally-Supported Ringtail Missile Configurations. U. S. Army Command Rept. RD-73-15, Oct. 1973.

A-186. Reubush, D. E.: Investigation of Very Low Blockage Ratio Boattail Models in the Langley 16-Foot Transonic Tunnel. NASA TN D-8335, Nov. 1976.

A-187. Vandoorn, J. T. M., Erkelens, L J., Hans, S. O. T. H., and Kho, Y. G.: Comparison of Fokker F-28 Wind Tunnel and Flight Data, A Summary. National Aerospace Lab. Rept. No. NLR-TR-73007-U, Amsterdam, Netherlands, Jan. 1973.

A-188. Sedgwick, T. A.: Investigations of Non-Symmetric Two-Dimensional Nozzles Installed in Twin Engine Tactical Aircraft. AIAA Paper No. 75-1319, AIAA/SAE 11th Propulsion Conference, Anaheim, CA, Sept. 1975.

A-189. Lander, J. A., Nash, D. O., and Palcza, J. L.: Augmented Deflector Exhaust Nozzle (ADEN) Design for Future Fighters. AIAA Paper No. 75-1318, AIAA/SAE 11th Propulsion Conference, Anaheim, CA, Sept. 1975.

A-190. Hiley, P. E., Wallace, H. W., and Booz, D. E.: Study of Non-Axisymmetric Nozzles Installed in Advanced Fighter Aircraft, Anaheim, CA, Sept. 1975.

A-191. Maiden, D. L. and Petit, J. E.: Investigation of Two-Dimensional Wedge Exhaust Nozzles for Advanced Aircraft. AIAA Paper No. 75-1317, AIAA/SAE 11th Propulsion Conference, Anaheim, CA, Sept. 1975.

A-192. Spratley, A. V., Thompson, E. R., and Kennedy, T. L.: Reynolds Number and Nozzle Afterbody Configuration Effects on Model Forebody and Afterbody Drag. AIAA Paper No. 77-103, AIAA 15th Aerospace Sciences Meeting, Los Angeles, CA, Jan. 1977.

A-193. Batiuk, G. and Henderson, J. H.: A Summary of Jet Plume Effects on the Stability Characteristics of a Body of Revolution with Various Fin Configurations at Mach Numbers from 0.2 to 2.3 (Normal Jet Plume Simulator). U. S. Army Missile Command Rept. No. RD-77-12, Dec. 1976.

A-194. Henderson, J. H., Dahlke, C. W., and Batiuk, G.: An Experimental Investigation Using a Normal Jet Plume Simulator to Determine Jet Plume Effects on a Long Slender Rocket Configuration at Mach Numbers from 0.2 to 1.5. U. S. Army Missile R & D Command Rept. No. TD-77-2, Feb. 1977.

A-195. Bencze, D. P.: Wind Tunnel Investigation of Nacelle-Air frame Interference at Mach Numbers of 0.9 to 1.4 - Force Data: Volumes I and II. NASA TM X-62,489, Feb. 1976.

A-196. Bencze, D. P.: Wind Tunnel Investigation of Nacelle-Air-frame Interference at Mach Numbers of 0.9 to 1.4 - Force Data. Volumes I and II. NASA TM X-62, 514, Feb. 1976.

A-197. Reubush, D. E.: Effect of Reynolds Number on Boattail Drag. J. Aircraft, Vol. 13, No. 5, May 1976, pp. 334-337.

A-198. Greathouse, W. K. and Migdal, D.: Optimizing Exhaust/Nozzle/Airframe Thrust Minus Drag. SAE Paper No. 680294, Apr. 1968.

A-199. Richey, G. K., Peterson, M. W., and Price, E. A., Jr.: Wind Tunnel/Flight Correlation on the B-1 Nacelle Afterbody/Nozzle. AIAA Paper No. 76-673, AIAA/SAE 12th Propulsion Conference, Palo Alto, CA, July 1976.

A-200. Putnam, L. E. and Abeyounis, W. K.: Experimental and Theoretical Study of Flow Fields Surrounding Boattail Nozzles at Subsonic Speeds. AIAA Paper No. 76-675, AIAA/SAE 12th Propulsion Conference, Palo Alto, CA, July 1976.

A-201. Goetz, G. F., Young, J. H., and Palcza, J. L.: A Two-Dimensional Airframe Integrated Nozzle Design with Inflight Thrust Vectoring and Reversing Capabilities for Advanced Fighter Aircraft. AIAA Paper No. 76-626, AIAA/SAE 12th Propulsion Conference, Palo Alto, CA, July 1976.

A-202. Martin, T. A. and Brazzel, C. E.: Investigation of the Effect of Low Thrust Levels on the Base Pressure of a Cylindrical Body at Supersonic Speeds. U. S. Army Missile Command Rept. No. RD-TR-70-11, May 1970.

A-203. Craft, J. C. and Brazzel, C. E.: An Experimental Investigation of Base Pressure on a Body of Revolution at High Thrust Levels and Free Stream Mach Numbers of 1.5 to 2.87. U. S. Army Missile Command Rept. No. RD-TM-70-6, July 1970.

A-204. Walker, S. C.: Nozzle-Afterbody Wind Tunnel Test of an Attack Aircraft. Vought Systems Division Rept. No. 2-57110/4R-3165, Apr. 1974.

A-205. Viswanath, P. R. and Narasimha, R.: Base Pressure on Sharply Boat-Tailed Aft Bodies. Dept. of Aeronautical Engineering, Indian Institute of Science, July 1972.

A-206. Reubush, D. E.: Experimental Investigation to Validate Use of Cryogenic Temperatures to Achieve High Reynolds Numbers in Boattail Pressure Testing. NASA TM X-3396, Aug. 1976.

A-207. Robinson, C. E.: Evaluation of Reynolds Number and Tunnel Wall Porosity Effects on Nozzle Afterbody Drag at Transonic Mach Numbers. AEDC-TR-76-70, July 1976.

A-208. Galigher, L. L., Yaros, S. F., and Bauer, R. C.: Evaluation of Boattail Geometry and Exhaust Plume Temperature Effects on Nozzle Afterbody Drag at Transonic Mach Numbers. AEDC TR-76-102, Oct. 1976.

A-209. Cosner, R. R. and Bower, W. W.: A Patched Solution of the Transonic Flowfields About an Axisymmetric Boattail. AIAA Paper No. 77-227, AIAA 15th Aerospace Sciences Meeting, Jan. 1977.

A-210. Holst, T. L.: Numerical Solution of Axisymmetric Boattail Fields with Plume Simulators. AIAA Paper No. 77-224, AIAA 15th Aerospace Sciences Meeting, Jan. 1977.

A-211. Wilmoth, R. G.: Analytical Study of Viscous Effects on Transonic Flow Over Boattail Nozzles. AIAA Paper No. 77-223, AIAA 15th Aerospace Sciences Meeting, Jan. 1977.

A-212. Yaeger, L. S.: Transonic Flow Over Afterbodies Including the Effects of Jet-Plume and Viscous Interactions with Separation. AIAA Paper No.77-228, AIAA 15th Aerospace Sciences Meeting, Jan. 1977.

A-213. Reubush, D. E.: Effect of Reynolds Number on the Subsonic Boattail Drag of Several Wing-Body Configurations. NASA TN D-8238, July 1976.

A-214. Compton, W. B., III: Jet Exhaust and Support Interference Effects on the Transonic Aerodynamic Characteristics of a Fighter Model with Two Widely Spaced Engines. NASA TM X-3424, Dec. 1976.

A-215. Martens, R. E.: F-15 Nozzle/Afterbody Integration. J. Aircraft, Vol. 13, No. 5, May 1976, pp. 327-333.

A-216. Henderson, J. H.: Transonic Wind Tunnel Investigation of Thrust Effects on the Longitudinal Stability Characteristics of Several Body-Fin Configurations (Sting-Mounted Model with Normal-Jet Plume Simulator). TR-RD-75-14, Dec. 1974.

A-217. Yaros, S. F.: Prediction of Pressure Distributions on Axisymmetric Bodies in Transonic Flow. AIAA Paper No. 77-226, AIAA 15th Aerospace Sciences Meeting, Jan. 1977.

A-218. Kuhn, G.D.: Computer Program for Calculation of Separated Turbulent Flows on Axisymmetric Afterbodies. AEDC TR-77-72, June 1977.

A-219. Kuhn, G. D. and Nielsen, J. N.: Prediction of Turbulent Separated Boundary Layers. AIAA Journal, Vol. 12, No. 7, July 1974, pp. 881-882.

A-220. Bauer, R. C. and Fox, J. H.: An Application of the Chapman-Korst Theory to Supersonic Nozzle-Afterbody Flows. AEDC TR-76-158, Jan. 1977.

A-221. Maiden, D. L.: Performance of an Isolated Two-Dimensional Wedge Nozle with Fixed Cowl and Variable Wedge Centerbody at Mach Numbers Up to 2.01. NASA TN D-8218, Sept. 1976.

A-222. Kostin, L.: Wind-Tunnel Data Analysis March 1975 Test, 0.06 Scale Nozzle Afterbody Model. Vol. II. Inlet/Nozzle Flight Performance Determination. Rockwell International Rept. No. NA-75-809, Feb. 1976.

A-223. Viswanath, P. R. and Narasimha, R.: Two-Dimensional Aft Bodies for Minimum Pressure Drag in Supersonic Flow. Indian Institute of Science, Nov. 1976.

A-224. Berrier, B. L. and Staff of Propulsion Integration Section: A Review of Several Propulsion Integration Features Applicable to Supersonic-Cruise Fighter Aircraft. NASA TM X-73991, Dec. 1976.

A-225. Berrier, B. L.: Effect of Nonlifting Empennage Surfaces on Single-Engine Afterbody/Nozzle Drag at Mach Numbers from 0.5 to 2.2. NASA TN D-8326, Feb. 1977.

A-226. Bencze, D. P.: Experimental Evaluation of Nacelle-Airframe Interference Forces and Pressures at Mach Numbers of 0.9 to 1.4. NASA TM X-3321, Mar. 1977.

A-227. Calarese, W.: Analysis of Transonic Viscous-Inviscid Interactions on Axisymmetric Afterbodies with Jet Effects and Boattail Injection in Separated Regions. AFFDL-TR-75-117, Sept. 1975.

A-228. Reid, J.: The Effect of Base Bleed on Plug Nozzles. RAE TR No. 65043, Feb. 1965.

A-229. German, R. C.: Strut Support Interference on a Cylindrical Model with Boattail at Mach Numbers from 0.6 to 1.4. AEDC TR-76-40, May 1976.

A-230. Kayser, L. D.: Effects of Base Bleed and Supersonic Nozzle Injection on Base Pressure. U. S. A. Ballistic Research Laboratories Memo Rept. No. 2456, Mar. 1975.

A-231. Miele, A. (Ed.): Theory of Optimum Aerodynamic Shapes, Academic Press, N.Y., 1965.

A-232. Peters, C. E. and Phares, W. J.: Analytical Model of Supersonic, Turbulent, Near-Wake Flows. AEDC-TR-76-127, Sept. 1976.

A-233. Kurn, A. G.: Observations of the Flow from a Rectangular Nozzle. ARC CP No. 1316, Mar. 1974.

A-234. Pozniak, O. M. and Haines, A. B.: Afterbody Drag Measurement at Transonic Speeds on a Series of Twin and Single Jet Afterbodies Terminating at the Jet Exit. ARC CP 1266, Feb. 1973.

A-235. Rosenthal, G.: Advanced Fighter Technology Integration (AFTI). Phase I, Vol. II, Part II, Appendix I, Phase I Wind Tunnel Data Summary. AFFDL-TR-75-87, Aug. 1975.

A-236. Matz, R. J.: Investigation of Subsonic Annular Nozzles for Engine Exhaust/External Flow Interaction Studies. AEDC TR-76-143, Dec. 1976.

A-237. Peters, W. L.: An Evaluation of Jet Simulation Parameters for Nozzle Afterbody Testing at Transonic Mach Numbers. AEDC TR-76-109, Oct. 1976.

A-238. Harper, L. R.: Description of Tests Carried Out at Rolls-Royce (1971) LTD Bristol Engine Division. Reference I-B, AGARD-AG-208, Improved Nozzle Testing Techniques in Transonic Flow, Oct. 1975.

A-239. Dissen, H. and Zacharias, A.: An Experimental Study of the Influence of the Jet Parameters on the Afterbody Drag of a Jet Engine Nacelle Scale Model. Reference I-C, AGARD-AG-208, Improved Nozzle Testing Techniques in the Transonic Flow, Oct. 1975.

A-240. Edmunds, H. and Riedel, H.: Contribution of the Institute fur Angewandte Gasdynamik of the DFVLR, Porz-Wahn. Reference I-D, AGARD-AG-208, Improved Nozzle Testing Techniques in Transonic Flow, Oct. 1975.

A-241. Rozendal, D., Groothoff, C. C., and Derksen, W. B. G.: Results of NLR Contribution to AGARD Ad Hoc Study. Reference I-E, AGARD-AG-208, Improved Nozzle Testing Techniques in Transonic Flow, Oct. 1975.

A-242. Zonars, D., Laughrey, J. A., and Bowers, D. L.: Effects of Varying Reynolds Number and Boundary Layer Displacement Thickness on the External Flow Over Nozzle Boattails. Reference I-F, AGARD-AG-208, Improved Nozzle Testing Techniques in Transonic Flow, Oct. 1975.

A-243. Compton, W. B., III and Runckel, J. F.: Contribution of the National Aeronautics and Space Administration Langley Research Center. Reference I-H, AGARD-AG-208, Improved Nozzle Testing Techniques in Transonic Flow, Oct. 1975.

A-244. Harper, L. R. and Lewis, W. J.: The Infuence of Model External Geometry. Reference II-A, AGARD-AG-208, Improved Nozzle Testing Techniques in Transonic Flow, Oct. 1975.

A-245. Groothoff, C. C.: Influence of Jet Parameters: Nozzle Thrust and Discharge Coefficients. Reference II-C, AGARD-AG-208, Improved Nozzle Testing Techniques in Transonic Flow, Oct. 1975.

A-246. Dissen, H., Edmunds, H., Riedel, H., and Zacharias, A.: Infuence of Jet Parameters: Boattail Pressure Distribution and Pressure Drag. (Evaluation of preliminary results contributed by the participants in the AGARD ad-hoc study.) Reference II-D, AGARD-AG-208, Improved Nozzle Testing Techniques in Transonic Flow, Oct. 1975.

A-247. Laughrey, J. A. and Richey, G. K.: Data Variance Due to Different Testing Techniques. Reference II-E, AGARD-AG-208, Improved Nozzle Testing Techniques in Transonic Flow, Oct. 1975.

A-248. Aulehla, F. and Besigk, G.: Fore- and Aftbody Flow Field Interaction with Consideration of Reynolds Number Effects. Reference II-F, AGARD-AG-208, Improved Nozzle Testing Techniques in Transonic Flow, Oct. 1975.

A-249. Hiley, P. E. and Wallace, H. W.: Investigation of Non-Axisymmetric Nozzles Installed in Tactical Aircraft. Volume I - Study Results. AFFDL TR-75-61, June 1975.

A-250. Sedgwick, T. A.: Investigation of Augmented Deflector Exhaust Nozzles Installed in Tactical Aircraft. AFFDL TR-75-42, May 1975.

A-251. Price, E. A., Jr.: Aft-Nacelle Axial-Force Characteristics of a 0.06-Scale, Strut-Mounted B-1 Model Including Simulated Primary and Auxiliary Jet Effects at Transonic Mach Numbers. AEDC TR-75-121, Sept. 1975.

A-252. Yaros, S. F.: An Analysis of Transonic Viscous/Inviscid Interactions on Axisymmetric Bodies with Solid Stings or Real Plumes. Ph.D. Thesis, University of Tennessee, Aug. 1977.

A-253. Presz, W. M.: Turbulent Boundary Layer Separation on Axisymmetric Afterbodies. Ph.D. Dissertation, The University of Connecticut, 1974.

A-254. Bergman, D.: A Nozzle/Afterbody Drag Prediction Technique for Isolated Bodies of Revolution at Subsonic Speeds. General Dynamics Report ERR-FW-1634, Dec. 1974.

A-255. Bergman, D. and Lawrence, W. G., Jr.: An Afterbody Drag Approximation Procedure (ADAP) for Engine Exhaust Nozzles. General Dynamics Report No. ERR-FW-1675, Dec. 1975.

A-256. Bergman, D.: Twin Engine Nozzle/Afterbody Drag Prediction Procedure. General Dynamics Report No. ERR-FW-1767, Dec. 1976.

A-257. Richey, G. K., Berrier, B. L., and Palcza, J. L.: Two-Dimensional Nozzle/Airframe Integration Technology - An Overview. AIAA Paper No. 77-839, AIAA/SAE 13th Propulsion Conference, July 1977.

A-258. White, R. and Agrell, J.: Boattail and Base Pressure Prediction Including Flow Separation for Afterbodies with a Centered Propulsive Jet and Supersonic External Flow at Small Angles of Attack. AIAA Paper No. 77-958, AIAA/SAE 13th Propulsion Conference, July 1977.

A-259. Bergman, D., Mace, J. L., and Thayer, E. B.: Non-Axisymmetric Nozzle Concepts for an F-111 Test Bed. AIAA Paper No. 77-841, AIAA/SAE 13th Propulsion Conference, July 1977.

A-260. Pendergraft, O. C.: Comparison of Axisymmetric and Non-Axisymmetric Nozzles Installed on the F-15 Configuration. AIAA Paper No. 77-842, AIAA/SAE 13th Propulsion Conference, July 1977.

A-261. Lee, K. W., and Franz, J. J.: Aftend Drag Data Correlation and Prediction Technique for Twin Jet Fighter Type Aircraft. AIAA Paper No. 76-672, AIAA/SAE 12th Propulsion Conference, July 1976.

A-262. Horimoto, S., Marsh, W. H., Uchida, G., and Tsukahira, T. W.: 0.1 Scale F-18 Nozzle/Aft-end Performance Test Analysis Report, Northrop Corporation, Rept. NOR-77-313, Jan. 1978.

A-263. Price, E. A., Jr.: A Parametric Investigation of the Annular Jet Concept for Obtaining Afterbody Drag Data at Transonic Mach Numbers. AEDC TR-77-104, Feb. 1978.

A-264. Presz, W. M., Jr., King, R. W., and Buteau, J. D.: An Improved Analytical Model of the Separation Region on Boattail Nozzles at Subsonic Speeds. NASA CR-3028, July 1978.

A-265. Presz, W. M., Jr., King, R. W., and Buteau, J. D.: An Analytical Model of the Separated Region on Boattail Nozzles. AIAA Paper No. 78-995, AIAA/SAE 14th Joint Propulsion Conference, July 1978.

A-266. Berndt, D., and Kuchar, A. P.: Non-Axisymmetric Nozzle Configuration Development for a Multimission Cruise Aircraft. AIAA Paper No. 77-843, AIAA/SAE 13th Propulsion Conference, July 1977.

A-267. Mikhail, A. G., Hankey, W. L., and Shang, J. S.: Computation of a Supersonic Flow Field Past an Axisymmetric Nozzle Boattail with Jet Exhaust. AIAA Paper No. 78-993, AIAA/SAE 14th Joint Propulsion Conference, July 1978.

A-268. Richey, G. K., Bowers, D. L., Kostin, L. C., and Price, E. A., Jr.: Wind Tunnel/Flight Test Correlation Program on the B-1 Nacelle Afterbody/Nozzle at Transonic Conditions. AIAA Paper No. 78-989, AIAA/SAE 14th Joint Propulsion Conference, July 1978.

A-269. Nugent, J., Taillon, N. V., and Pendergraft, O. C., Jr.: Status of a Nozzle-Airframe Study of a Highly Maneuverable Fighter. AIAA Paper No. 78-990, AIAA/SAE 14th Joint Propulsion Conference, July 1978.

A-270. Lucas, E. J., Fanning, A. E., and Steers, L.: Comparison of Nozzle and Afterbody Surface Pressures from Wind Tunnel and Flight Test on the YF-17 Aircraft. AIAA Paper No. 78-992, AIAA/SAE 14th Joint Propulsion Conference, July 1978.

A-271. Hiley, P. E., Kitzmiller, D. E., and Willard, C. M.: Installed Performance of Vectoring/Reversing Nonaxisymmetric Nozzles. AIAA Paper No. 78-1022, AIAA/SAE 14th Joint Propulsion Conference, July 1978.

A-272. Kostin, L. C. and Gunter, J. L.: B-1 Nozzle/Afterbody Performance Estimates. TFD-74-72, B-1 Division, Rockwell International Corp., Dec. 1974.

A-273. August, H. and Rynes, D.: B-1 Airplane Aft Fuselage Closure Drag Determined by AEDC Test Data. TFD-71-1542, North American Rockwell, Nov. 1971.

A-274. Wilmoth, R. G.: Computation of Transonic Boattail Flow With Separation. NASA TP-1070, Dec. 1977.

A-275. Abeyounis, W. K.: Boundary-Layer Separation on Isolated Boattail Nozzles. NASA TP-1226, Aug. 1978. (See also: Master's Thesis, George Washington University, May 1977.)

A-276. Robinson, C. E.: Exhaust Plume Thermodynamic Effects on Nonaxisymmetric Nozzle Afterbody Performance in Transonic Flow. AEDC-TR-78-24, Aug. 1978.

A-277. Burt, J. R., Jr.: An Experimental Investigation of the Effect of Several Rocket Plume Simulators on the Pressure Distribution of a Body of Revolution at Free Stream Mach Numbers of 0.9 to 1.2. U. S. Army Missile Command Report RD-TR-70-23, Nov. 1970.

A-278. Burt, J. R., Jr., Henderson, J. H., and Pettis, W., Jr.: The Effects of Three Rocket Plume Simulators on the Aerodynamic Characteristics of Several Missile Configurations. U. S. Army Missile Command Report No. RD-TR-70-20, Sept. 1970.

A-279. White, R. A.: The Calculation of Supersonic Axisymmetric Afterbody Flow with Jet-Interference and Possible Flow Separation. Aeronautical Research Institute of Sweden Technical Note AU-912, Dec. 1974.

A-280. Henderson, J. H.: An Investigation of Jet Plume Effects on the Stability Characteristics of a Body of Revolution in Conjunction with Fins of Various Geometry and Longitudinal Positions at Transonic Speeds (Sting-Mounted Model with Normal Jet Plume Simulator). U. S. Army Missile Command Report TR-RD-75-37, June 1975.

A-281. Edmunds, H. and Riedel, H.: On the Simulation of an Underexpanded Propulsive Jet for the Investigation of the Static Longitudinal Stability of an Axially Symmetric Flight Vehicle in Supersonic Flow. European Space Agency Technical Translation ESA-TT-334, Oct. 1976.

A-282. Hess, J. L. and James, R. M.: On the Problem of Shaping an Axisymmetric Body to Obtain Low Drag at Large Reynolds Numbers. Douglas Aircraft Co. Report No. MDC J6791, Jan. 1975.

A-283. Henderson, J. H.: Investigation of Jet Plume Effects on the Longitudinal Stability Characteristics of a Body of Revolution with Various Fin Configurations at Mach Numbers from 0.2 to 2.3 (Normal Jet Plume Simulator). U. S. Army Missile Command Report TR-RD-76-22, Feb. 1976.

A-284. Fraenkel, L. E.: The Theoretical Wave Drag of Some Bodies of Revolution. ARC RM 2842, May 1951.

A-285. Crane, J. F. W.: The Effect of Base Cavities on the Drag of an Axisymmetric Afterbody with a Sonic Nozzle Between $M_\infty = 0.8$ and 1.3. RAE TR 77144, Sept. 1977.

A-286. Rubin, D. V.: A Transonic Investigation of Jet Plume Effects on Base and Afterbody Pressures on Boattail and Flare Bodies of Revolution. U. S. Army Missile Command Rept. No. RD-TR-70-10, Oct. 1970.

A-287. Dahlke, C. W.: An Investigation of Flow and Stability Characteristics of a Body of Revolution with Fins and Flare in Presence of Plume Induced Separation at Mach Numbers 0.7 to 1.4. U. S. Army Missile Research and Development Command Rept. TD-77-11, May 1977.

A-288. Bowers, D. L.: Application of the Initial Plume Angle Correlation to Correct Nozzle/Aftbody Pressure Drag for Hot Exhaust Gas Effects. AFFDL-TR-76-138, Dec. 1976.

A-289. Henry, B. Z., Jr. and Cahn, M. S.: Preliminary Results of an Investigation at Transonic Speeds to Determine the Effects of a Heated Propulsive Jet on the Drag Characteristics of a Related Series of Afterbodies. NACA RM L55A24a, Mar. 1955.

A-290. Love, E. S.: Initial Inclination of the Mixing Boundary Separating an Exhausting Supersonic Jet from a Supersonic Ambient Stream. NACA RM L55J14, Jan. 1956.

A-291. Norton, H. T., Jr. and Swihart, J. M.: Effect of Hot-Jet Exhaust on Pressure Distribution and External Drag of Several Afterbodies on a Single-Engine Airplane Model at Transonic Speeds. NACA RM L57J04, May 1961.

A-292. Agrell, J. and White, R. A.: An Experimental Investigation of Supersonic Axisymmetric Flow Over Boattails Containing a CenteredPropulsive Jet. Aero. Res. Inst. of Sweden Rept. FFA TN-AU-913, Dec. 1974.

A-293. Calarese, W.: Review of Methods of Solution of Afterbody/ Exhaust Nozzle Flow Fields. AFFDL-TR-74-108, Jan. 1974.

A-294. Keller, J. D. and South, J. C., Jr.: RAXBOD: A Fortran Program for Inviscid Transonic Flow Over Axisymmetric Bodies. NASA TM X-72831, Feb. 1976.

A-295. Hinz, W. W. and Miller, E. H.: Propulsion Integration of a Supersonic Cruise Strike-Fighter. AIAA Paper No. 79-0100, AIAA 17th Aerospace Sciences Meeting, Jan. 1979.

A-296. Forester, C. K.: Numerical Simulation of the Interaction of Jet and Freestream Flows in Engine Exhaust Systems. AIAA Paper No. 78-144, AIAA 16th Aerospace Sciences Meeting, Jan. 1978.

A-297. Wilmoth, R. G., Dash, S. M., and Pergament, H. S.: A Numerical Study of Jet Entrainment Effects on the Subsonic Flow Over Nozzle Afterbodies. AIAA Paper No. 79-0135, AIAA 17th Aerospace Sciences Meeting, Jan. 1979.

A-298. Dash, S. M., Pergament, H. S., and Thorpe, R. D.: A Modular Approach for the Coupling of Viscous and Inviscid Processes in Exhaust Plume Flows. AIAA Paper No. 79-0150, AIAA 17th Aerospace Sciences Meeting, Jan. 1979.

A-299. Dash, S. M. and Pergament, H. S.: A Computational Model for the Prediction of Jet Entrainment in the Vicinity of Nozzle Boattails (The BOAT Code). NASA CR-3075, Aug. 1978.

A-300. Kuhn, G. D.: Computer Program for Calculation of Separated Turbulent Flows on Axisymmetric Afterbodies Including Exhaust Plume Effects AEDC TR-79-04, Jan. 1979.

A-301. Kuhn, G. D.: Computer Program for Calculation of Separated Turbulent Flows on Axisymmetric Afterbodies Including Exhaust Plume Effects. AIAA Paper No. 79-0303, AIAA 17th Aerospace Sciences Meeting, Jan. 1979.

A-302. Robertson, J. P.: B-1 Status Propulsion System Installation Effects. North American Rockwell Rept. TFD-72-1475, Oct. 1972.

A-303. Capone, F. J., Gowadia, N. S., and Wooten, W. H.: Performance Characteristics of Nonaxisymmetric Nozzles Installed on the F-18 Airplane. AIAA Paper No. 79-0101, 17th Aerospace Sciences Meeting, Jan. 1979.

A-304. Calarese, W. and Walterick, R. E.: Mass Injection and Jet Flow Simulation Effects on Transonic Afterbody Drag. AIAA Paper No. 78-1180, AIAA 11th Fluid and Plasma Dynamics Conference, July 1978.

A-305. Wagner, B. and White, R. A.: Influence of Fundamental Parameters on the Supersonic Base Flow Problem in Presence of an Exhaust Jet. AIAA Paper No. 79-0133, 17th Aerospace Sciences Meeting, Jan. 1979.

A-306. Korst, H. H.: Modeling of Plume Induced Interference Problems in Missile Aerodynamics. AIAA Paper No. 79-0362, AIAA 17th Aerospace Sciences Meeting, Jan. 1979.

A-307. Kuhn, G. D.: Computer Programs for Prediction of Nozzle Afterbody Drag of Single and Twin Engine Configurations. Interim Report, Nielsen Engineering & Research, Inc. TR-182, Jan. 1979.

A-308. Yurchenok, K. E.: Base Pressure and Temperature Behind Axisymmetric Bodies with Interaction Between a Jet and a Supersonic Stream. Fluid Dynamics, Vol. 9, No. 2, Mar.-Apr. 1974, pp. 228-236.

A-309. Tagirov, R. K.: Transonic Flow Around a Solid of Revolution During the Outflow of a Reaction Jet from its Stern Section. Fluid Dynamics, Vol. 9, No. 2, Mar.-Apr. 1974, pp. 243-249.

A-310. Calarese, W. and Walterick, R. E.: Mass Injection and Jet Flow Simulation Effects on Transonic Afterbody Drag. AFFDL TR-78-57, June 1978.

Page Intentionally Left Blank

APPENDIX C

CROSS-REFERENCE BY AUTHOR OF APPENDICES A AND B

In the following list, reference numbers prefixed by "I" are for documents dealing with Inlet/Airframe Interaction Effects (Appendix A), those prefixed by "A" deal with Afterbody/Airframe Interaction Effects (Appendix B).

Abercrombi, J. M.	I-356
Abyounis, W. K.	A-275
Adams, C. E. and Hollweger, D. J.	I-134
Adams, M. C.	A-146
Addy, A. L.	A-1
Agrell, J. and White, R. A.	A-292
Alber, I. E.	A-184
Alber, I. E. and Lees, L.	A-2
Albers, J. A.	I-351
Albers, J. A. and Miller, B. A.	I-320
Alford, W. J., Jr., and King, T. J., Jr.	I-338
Allen, R., Chaloff, D., Hayase, G. Hiyama, R., Martindale, C., and Rockwell, H.	I-161
Anderson, B. H.	I-129 I-130 I-132
Anderson, C. F. and Jackson, F. M.	I-247
Anderson, O. L.	I-160
Anderson, R. D. and Martens, R. E.	A-3
Anderson, W. E.	I-197
Anderson, W. E., Peterson, M. W., and Sorenson, N. E.	I-1
Anderson, W. E. and Wong, N. D.	I-234
Antonatos, P. P., Richey, G. K., and Dlepinger, R. H.	I-3
Antonetos, P. P., Surber, L. E., and Stava, D. J.	I-2
Arlinger, B. G.	I-150
Armstrong, R. S. and Miller, S. P.	A-79
Asfar, K. R., Mook, D. T., and Nayfeh, A. H.	I-315
August, H. and Rynes, D.	A-273
Aulehla, F. and Besigk, G.	A-115 A-248
Aulehla, F. and Lohler, K.	A-138
Babenko, K. I., Voskresenskiy, C. P., Lyubimov, A. N., and Rosanov, V. V.	I-375

Preceding page blank

ORIGINAL PAGE IS
OF POOR QUALITY

Page Intentionally Left Blank

TABLE I.- DATA BASE FOR INLET/AIRFRAME INTERACTION EFFECTS

Effect	References			
	Review Papers	Primary Data Sources	Empirical Prediction Methods	Theoretical Prediction Methods
I. Airframe effects on inlet "free-stream" conditions				
A. Forebody effects	2,5,6,23,36,42,43, 143,145,182,183,233, 242,294,295,310,381, 403,404	10,22,34,56,58,60,62,80,166, 174,179,257,280,322,335,338, 342,343,369,370,394,399,400, 401,402,406	4,11,398	34,151,152,153,215,289, 290,291,292,293,296,297, 298,299,300,301,302,303, 304,305,306,308,309,311, 312,314,315,316,317,318, 319,321,324,336,337,340, 341,346,347,348,349,350, 368,373,374,375,383,393, 395,397
B. Forebody-wing effects	2,5,6,23,36,42,43, 57,144,182,183,233, 242,294,295,310,365, 382,403,404	10,22,34,60,166,175,280,322, 338,339,342,343,344,352,369, 371,406	4,11	151,152,153,289,293,296, 297,298,299,300,301,302, 303,304,305,306,308,309, 311,312,314,315,316,317, 318,319,321,336,337,341, 346,347,348,349,350,368, 393,395,397
II. Inlet drag	143,144,183,193,209, 365	16*,17,24,54,80,121,122,123, 136,139,155,202,255,282,287, 376,390		

*Of the reports listed as containing data for this effect, refs. 16, 17, 24, 54, 121-123, 255, 390 pertain to the B-1. Detailed breakdown of the effects may be possible but requires further analysis to eliminate the effects of the metric partial forebody and stub wing and the use of the "propulsion reference inlets" as the datum for the measurements presented.

Preceding page blank

TABLE I.- (Continued)

Effect	References			
	Review Papers	Primary Data Sources	Empirical Prediction Methods	Theoretical Prediction Methods
II.				
A. External drag	1,2,4,27,44,51,62, 66,67,79,81,82,115, 128,137,145,156,171, 176,187,213,363,372, 380	19,29,30,33,45,46,47,49,52, 55,63,64,71,77,78,79,85,93, 96,97,102,105,107,108,111, 163,192,196,206,224,230,231, 239,254,272,276,332,333,376, 377,378,384,385	4,5,7,10,11,21,29, 32,33,39,49,71,72, 73,81,86,90,92,102, 106,364	19,37,48,52,59,106,149, 150,154,215,274,354,405
B. Bypass drag	2,4,18,67,115,137, 183,213	45,46,62,64,98,99,100,239, 384,385	4,5,11,21,66,106	
C. Boundary-layer-bleed drag	2,4,18,67,115,118, 213	62,64,89,94,98,133,239,384	4,5,11,21,66,106, 110	
D. Interference drag	18,51,82,115,117, 145,176,233	57,63,224,378		
E. Boundary-layer-diverter drag	51	17,89,120,122,239,282	11,106	
III. Inlet internal performance				
A. Total pressure recovery	1,2,4,25,26,40,42, 43,83,101,114,115, 116,118,128,130,131, 132,137,138,140,143, 144,145,156,171,187, 188,208,209,210,212, 213,242,269,277,331, 382	6,8,10,16,17,19,21,28,34,45, 46,47,50,54,55,56,58,60,61,62, 63,64,65,68,69,71,74,75,76, 77,78,79,80,84,87,88,89,91, 94,95,102,103,105,109,113, 119,121,122,123,124,125,126, 127,133,134,135,141,142,147, 148,155,157,158,159,163,164, 165,167,168,169,170,172,173,	4,5,6,7,11,41,70,71, 79,106,146,160,173, 256,320,351,361	59,104,109,129,199,225, 229,256,313,359,360,362, 367,405

TABLE I.- (Continued)

Effect	References			
	Review Papers	Primary Data Sources	Empirical Prediction Methods	Theoretical Prediction Methods
III.				
A. (Continued)		174,175,177,178,179,180,181, 184,185,189,191,192,194,195, 199,200,201,203,205,207,214, 216,217,218,219,223,224,228, 230,231,232,235,237,238,239, 243,244,245,246,249,250,251, 252,253,258,259,260,261,262, 263,264,265,266,267,268,270, 271,275,276,278,279,281,282, 284,286,287,320,326,327,328, 329,330,332,333,351,379,384, 385,386,388,389,390,391,392, 396		
B. Stable mass flow range	1,42,114,138,143, 144,145,156,193,213, 242,331,382	17,21,56,58,60,68,78,88,89, 91,109,119,124,133,134,135, 155,167,168,169,170,174,191, 192,201,214,241,245,252,258, 266,267,268,271,278,281,327, 328,329,330,333,334,389,391	240,334	
C. Distortion	2,40,42,43,101,114, 118,128,132,137,138, 140,143,144,145,182, 208,209,210,269,273, 277,331,382	6,8,10,19,21,28,34,45,46,47, 50,56,58,60,61,64,65,68,69, 74,75,76,78,84,88,91,94,95, 103,105,119,124,125,126,127, 133,134,135,142,147,148,155, 157,158,159,163,164,165,167, 168,169,170,172,174,175,177, 178,179,180,181,191,192,195,	41,70,146,160,211, 220,221,222,226,361	227,359,360,362,367,405

TABLE I.- (Concluded)

Effect	References			
	Review Papers	Primary Data Sources	Empirical Prediction Methods	Theoretical Prediction Methods
III.				
C. (Continued)		201,203,205,207,214,216,217, 218,219,231,235,238,243,244, 245,246,249,250,251,252,253, 258,259,260,261,262,263,264, 265,266,267,268,271,275,276, 278,279,281,282,286,287,326, 327,328,329,330,332,333,353, 386,388,389,391,392,396		
IV. Inlet lift and moment effects	143	16*,17,24,54,57,58,62,87,121, 123,136,139		
A. Due to airflow spillage	2,82,83	21,63,64,224		
B. Due to bypassed air		58		
C. Due to boundary-layer-bleed flow		64		
D. Interference lift and moments	233	62,63,64,204		117
V. Inlet weight	3,114,115,118,143, 144,145,193,242		11,161,162	

*See footnote on page 203.

TABLE II.- DATA BASE FOR AFTERBODY/AIRFRAME INTERACTION EFFECTS

Effect	References			
	Review Papers	Primary Data Sources	Empirical Prediction Methods	Theoretical Prediction Methods
I. Single engine configurations	79,116,120,137,149, 172,173,179			
A. Exhaust plume effects				
1. Nozzle pressure ratio	5,6,7,118,168,179, 200,237,245,246	16,31,36,37,38,44,52,67,74, 89,90,92,142,177,204,208,225, 228,238,239,240,241,275,286, 289,291,292,302	15,58,148,254,255, 256,307	43,48,49,51,209,210,212, 227,264,265,267,297,299, 300,301,306
2. Exhaust temperature	97,124,168,179,237, 246	31,38,96,167,204,208,239,241, 276,289	148,267,288	297
3. Miscellaneous	98,147,174,243,293, 309	37,125,130,171,181,182,183, 185,193,194,216,277,278,280, 281,283,287,304,310	4,211,274	27,34,80,81,136,209,210, 217,218,252,253,290,296, 298,300,301
B. Nozzle type effects	5,39,224			
1. Axisymmetric	6,7,118,179	9,10,16,28,44,52,60,69,70,73, 74,75,142,171,180,182,228	4,15,58,255	
2. Two-dimensional	201	67,180,221,233	255	
C. Base flow effects	1,68,174,305,308	35,122,181,182,202,203,204, 205,206,228,230,285	4,15,66,111,121,122, 148,279	2,99,117,160,184,220,232
D. Empennage effects	14	95,134,135,142,181,193,216, 225,280,283,291		
E. Mach number effects	98,151,168,179	52,89,90,92,102,130,142,152, 167,175,177,178,181,182,185, 186,193,204,225,240,241	4,15,58	43,106,146

TABLE II.- (Continued)

Effect	References			
	Review Papers	Primary Data Sources	Empirical Prediction Methods	Theoretical Prediction Methods
I.				
F. Angle of attack effects		44,142,175,181,182,185,193, 194,216,275,276,291	258	
G. Reynolds number effects	93,95,173,174,192, 197,242,248	124,127,136,152,154,175,177, 178,206,207,213		264,265
H. Boattail shape effects	14,118,179,192,200, 237,242,244	35,37,89,90,92,136,141,142, 175,177,178,204,205,208,213, 221,229,238,240,275,286,289, 291,292	223	43,106,146,223,231,282, 284
II. Drag of twin engine configurations	3,19,21,23,24,41, 103,116,131,261,269	30,46,47,84	18,22,25,45,46,50, 113,143	
A. Exhaust plume effects				
1. Nozzle pressure ratio	42,111,118,138,150, 151,176	11,13,17,32,33,44,46,47,54, 63,72,88,91,100,101,108,119, 128,133,145,214,234,235	4,15,20,256	
2. Exhaust temperature				
3. Miscellaneous	5,76,170,199	8,55,82,83,152,153,155,169		
B. Nozzle type effects	5,39,76,132,138,224			
1. Axisymmetric	118,198,199,295	17,28,32,33,44,46,47,54,62, 68,71,77,88,91,107,108,109, 128,169,214	4,15,20,49	

TABLE II.- (Continued)

Effect	References			
	Review Papers	Primary Data Sources	Empirical Prediction Methods	Theoretical Prediction Methods
II. B.				
2. Two-dimensional	188, 189,190,191,201, 215,249,250,257,259, 260,266,295,303	28,68,271		
C. Nozzle spacing effects	5,42,76,123,132,138, 150,151,166,176,196, 224	12,13,17,40,44,46,47,63,68, 71,78,108,114,128	4,20	
D. Nozzle location effects	166	11,28,44,56,84		
E. Fuselage inter-fairing effects	5,76,118,123,132, 138,150,166,170,176, 224	11,12,13,32,33,40,46,47,62, 86,94,101,108,112,114,128, 153,155,234,262		
F. Empennage inter-ference effects	5,76,123,132,138, 150,151,166,176,201, 215,224	17,32,33,46,47,54,62,68,87, 169,235,262	15,20	
G. Mach number effects	166	8,11,12,46,47,54,55,63,83,91, 133,145,153,169	15	
H. Angle of attack effects		13,32,33,46,47,54,145,155, 235		
I. Reynolds number effects	199	32,33,46,47,54,152,169,235		
J. Boattail shape effects	215,224	71,234		

TABLE II.- (Concluded)

Effect	References			
	Review Papers	Primary Data Sources	Empirical Prediction Methods	Theoretical Prediction Methods
III. Other configurations	268	110,195,196,222,226,251,272, 273		129
IV. Nozzle internal performance	245	180	4,113	144

TABLE III.- REFERENCES ON SPECIAL TOPICS

Topic	Reference List: Inlet/Airframe Interaction (Appendix A)	Reference List: Afterbody/Airframe Interaction (Appendix B)
Thrust-Drag Bookkeeping	2,4,5,7,13,15,38,62,128, 138,355,356,392	3,18,100,116,139,140,198
Test Techniques	7,9,12,13,15,20,25,26,27, 29,31,35,38,44,63,77,84, 114,116,128,176,180,187, 189,190,236,247,248,249, 355,357,366,387	3,7,17,26,29,31,32,33,36, 38,44,53,54,59,61,64,65, 72,79,83,85,92,96,97,100, 119,124,126,139,140,152, 182,186,199,204,205,208, 229,236,237,247,248,263
Wind Tunnel to Flight Comparisons	53,61,65,143,159,176,177, 180,187,191,355,356,357, 358,366	68,100,121,126,127,154, 155,187,199,268,270
Boundary Layer Methods		156,157,158,161,218,219
Inviscid Flow Methods		105,159,162,163,164,165, 218,294

TABLE IV.- DATA FOR INLET EXTERNAL DRAG

				Range of				Data Showing Separate Effects of					
Reference Number	Inlet	Drag Component Presented	Test Configuration	Mach No.	Reynolds No Per Meter ($\times 10^{-6}$)	Angle of Attack, Deg	Angle of Sideslip, Deg	Cowl Shape	Side Plate Shape	Ramp Angle	Capture Area	Varying B.L. Bleed	Varying Bypass Flow
16	$E_rV_{3v2}S_{t,n}B_p 2.2$	1	2	1.55 - 2.2	14.1	1 to 4	0	✓	✓	✓		✓	
17	$M_rV_{2v2}S_tB_pBP2.2$	3	2	0.55 - 2.2	13.4, 20.0	2, 2.5	0	✓	✓	✓		✓	✓
19	$E_rH_{3v2}S_n 2.2$	$C_{D_{EXT}}$	1[4]	0.55 - 1.39	4.9 - 11.5	0	0			✓			
24	$E_rV_{3v2}S_{t,n}B_pBP$	1	2	1.8 - 2.2	N.R.[5]	0.5 to 3.5	0		✓	✓		✓	
29	P_c	$C_{D_{EXT}}$	1	0.3 - 1.25	N.R.	0	0	✓					
30	$M_rH_{1f}S_r$	C_{D_A}	1	0.5 - 1.3	19.4 - 45.0	0	0			✓			
	M_cC_{1f}	C_{D_A}	1	0.5 - 1.3	19.4 - 45.0	0	0			✓			
33	$E_rH_{2v1}S_{t,r,n} 3.0$	C_{D_A}, C_{D_C}	1	0.7 - 1.4	N.R.	0	0	✓	✓	✓			
	$E_rH_{2v2}S_t 2.2$	C_{D_A}, C_{D_C}	1	0.7 - 1.5	N.R.	0	0	✓		✓			
45	$M_cC_{2v2}BP2.5 (30/70)$[37]	C_{D_A}, C_{D_C}	1	0.8 - 1.27	13.8 - 15.4	0 to 10	0						✓
	$M_cC_{1v1}BP2.5 (60/40)$	C_{D_A}, C_{D_C}	1	0.8 - 1.27	13.8 - 15.4	0 to 10	0						✓
	$M_cC_{1v1}BP2.5 (40/60)$	C_{D_A}, C_{D_C}	1	0.8 - 1.27	13.8 - 15.4	0 to 10	0						✓
46	$M_cC_{2v2}BP2.5$	C_{D_A}, C_{D_C}	6	0.8 - 1.27	13.8 - 15.4	0 to 10	0						✓
47	$M_rH_{2v1}S_tBP3.0$	C_{D_A}, $C_{D_{EXT}}$	1	0.6 - 1.28	11.2 - 14.1	0	0	✓					✓
49	P_c	C_{D_A}	1	1.6 - 1.8	N.R.	0	0			✓			
	M_cC_{1f}	C_{D_A}	1	1.6 - 1.8	N.R.	0	0						
52	$E_cC_{1v1} 2.3$	C_{D_A}, C_{D_C}	1	0.7 - 1.05	N.R.	0	0	✓		✓	✓		
	$E_cC_{1v1} 2.7$	C_{D_A}, C_{D_C}	1	0.7 - 1.05	N.R.	0	0	✓		✓	✓		
	$E_cC_{1v1} 3.1$	C_{D_A}, C_{D_C}	1	0.7 - 1.05	N.R.	0	0	✓		✓	✓		
	$E_rV_{2v1} 2.4$	C_{D_A}, $C_{D_{EXT}}$	7	0.7 - 2.0	N.R.	0 to 9	0			✓			
	$M_rV_{1v1} 8$	C_{D_A}, $C_{D_{EXT}}$	1	0.9	N.R.	0 to 6	0	✓	✓	✓			
54	$E_rV_{3v2}S_nB_pBP2.2$	8	2	0.6 - 1.6	N.R.	0.5 to 3.5	0	✓	✓	✓		✓	
55	P_o	$C_{D_{EXT}}$	1	0.7 - 1.5	10.3 - 12.5	0 to 12	0	✓					
63	$E_rH_{3v3}S_nB_{d,p}BP2.5$	C_{D_A}, C_{D_C}, $C_{D_{INT}}$	11	0.6 - 0.9	10.8 - 12.9	0 to 9	0			✓	✓		
64	$E_rH_{3v1}S_tB_{d,p}BP2.5$	$C_{D_{EXT}}$	7	0.6 - 2.2	N.R.	2 to 12	0	✓		✓		✓	
71	$E_cC_{1v1} 1.86, 2.05, 2.35, 2.90$	$C_{D_{EXT}}$	1	1.5 - 3.3	N.R.	0	0	✓					

TABLE IV.- (Continued)

Reference Number	Inlet	Drag Component Presented	Test Configuration	Range of: Mach No.	Range of: Reynolds No. Per Meter ($\times 10^{-6}$)	Range of: Angle of Attack, Deg.	Range of: Angle of Sideslip, Deg	Data Showing Separate Effects of: Cowl Shape	Data Showing Separate Effects of: Side Plate Shape	Data Showing Separate Effects of: Ramp Angle	Data Showing Separate Effects of: Capture Area	Data Showing Separate Effects of: Varying B L Bleed	Data Showing Separate Effects of: Varying Bypass Flow
77	$E_cC_{2v2}B_pS_r2.2$	C_{D_A}	10(12)	1 2 , 2 2	N R	2 , 5 5	0	✓					
78	$E_cC_{1f}B_{d,p}2\ 5$	C_{D_A}, C_{D_C}	I	2 49	N R	0 to 5	0	✓					
79	$M_cC_{1f}2.48$	$C_{D_{EXT}}$	I	2 1 - 3 3	N R	0	0	✓					
	$M_cC_{1v1}3.27$	$C_{D_{EXT}}$	I	2 1 - 3 3	N R.	0	0	✓					
80	$E_rV_{2v1}S_t2\ 41$	9	10	0 6 - 2 0	8 5 - 22 8	0	0	✓	✓	✓			
	$E_rV_{1f}S_t2$	9	10	0 6 - 2 0	8 5 - 22 8	0	0	✓					
85	E_cC_{1f}	C_{D_A}, $C_{D_{EXT}}$	I	0 85	27.1	0	0	✓			✓		
93	P_c	C_{D_A}, C_{D_C}	I	0 6 - 0 85	12 3 - 14 3	0	0	✓					
96	P_c	$C_{D_{EXT}}$	I	0 4 - 1 29	7 4 - 12 2	0	0	✓					
97	P_c	C_{D_C}, $C_{D_{EXT}}$	I	0 4 - 1 29	7 9 - 12 9	0 to 2	0	✓					
102	$E_rH_{1v1}S_t2\ 1$	$C_{D_{EXT}}$	I	1 56 - 2 14	0 235 - 0 294 1 3	0	0			✓			
105	$M_cC_{1v1}B_p3\ 0$	C_{D_A}	I	0 6 - 1 3	6 6	0	0						
107	$E_rV_{2v1}S_{r,t}3\ 3$	C_{D_A}, C_{D_C}, $C_{D_{EXT}}$	I	0 6 - 0 8	N R	0 to 8	0	✓	✓	✓			
108	$M_cC_{1v1}2\ 7$	C_{D_A}, C_{D_C}	I	0 7 - 2 0	N R	0	0						
	$E_rV_{2v1}2\ 4$	C_{D_A}, $C_{D_{EXT}}$	7	0 7 - 2 0	N R	0 to 12	0			✓			
	$E_rV_{1f}S_{t,n}2.0$	$C_{D_{EXT}}$	I	0 7 - 2 0	N R.	0 to 16	0		✓				
	$M_rV_{1v1}S$	$C_{D_{EXT}}$	I	0 7 - 2 0	N R	0	0	✓	✓	✓			
111	P_c	C_{D_A}, C_{D_C}	I	0 7 - 0 9	N R	0	0	✓					
121	$M_1V_{3v2}S_tB_p2.2$	36	2	0 55 - 2 20	N R	0 to 5	0	✓		✓			
122	$M_rV_{3v2}S_{t,n}B_p2.2$	36	2	0 55 - 1 7	N R.	2 , 2 5	0	✓		✓			
123	$E_rV_{3v2}S_{t,n}B_pBP2.2$	14	2	0 6 - 1 4	N R	0 5 to 3 5	0		✓	✓		✓	
136	$E_rH_{3v3}S_nB_{d,p}BP$	15	16	0 6 - 2 2	4 0 - 8 7	-4 to 20	0			✓	✓		
139	$E_rH_{3v3}S_nB_{d,p}$	15	16	1 6	7 4 - 8 2	-2 to 8	0			✓	✓	✓	
155	$E_rH_{3v2}S_nB_d2\ 4$	17	18	0 6 - 2 4	7 4 - 13.1	-4 to 20	-10 to 10	✓					
163	$M_cC_{1v1}B_p3\ 0$	C_{D_A}	I	0 6 - 3 2	6 6	0 to 8	0						
192	$E_cC_{2v1}3\ 0$	$C_{D_{EXT}}$, C_{D_A}, C_{D_C}	I	1 97 - 3 01	8 2	0 15	0	✓					

TABLE IV.- (Concluded)

Reference Number	Inlet	Drag Component Presented	Test Configuration	Range of: Mach No.	Range of: Reynolds No Per Meter ($\times 10^{-6}$)	Range of: Angle of Attack, Deg	Range of: Angle of Side lip, Deg	Data Showing Separate Effects of: Cowl Shape	Side Plate Shape	Ramp Angle	Capture Area	Varying B L Bleed	Varying Bypass Flow
196	P_c	19	20	0 9 - 1 5	14 1 - 30 8	0	0	✓					
206	P_c	C_{D_C}	I	1 9 - 4 9	1 6 - 19 8	0	0	✓			✓		
224	$E_r H_{3v1} B_{d,p} BPS_n$ 2 5	$C_{D_{EXT}}, C_{D_A}, C_{D_C}$	11^{16}	6 - 1 5	5 25 - 15 74	-1 to 17	0			✓	✓	✓	
230	$E_r H_{2f} B_d BPS_n$ 1 6	21	I	2 - 2 0	N R	0	0						
	$E_r H_{2f} B_d BPS_n$ 1 6	21	I^{35}	2 - 2 0	N R	0	0						
231	$E_r H_{2f} B_d BPS_n$ 1 6	19	I^{35}	85	N R	0	0	✓		✓			
239	$E_r V_{3v2} B_p BPS_n$ 2 2	$C_{D_{EXT}}, C_{D_{BL}}, C_{D_A}, C_{D_{BLD}}, C_{D_{BP}}$	2	7 - 1 4	1 64 - 2 4	1 to 4	0			✓		✓	✓
254	$E_r H_{3v3} B_{p,d} S_n$ 2.2	$C_{D_{EXT}}^{22}$, C_{D_A}, 15	16	1 6, 2 2	7 38 - 8 2	-2 to 8	0			✓	✓	✓	
255	$E_r V_{3v2} B_p BPS_n$ 2.2	24	23	7 - 1 4	3.28 - 16 4	-2 to 6	0						
272	$E_r H_{3v3} B_{p,d} BPS_n$ 2 5	15,21	11^{16}	6 - 1 5	8 2 - 13 1	0 to 17	0			✓	✓		
276	$M_c C_{2v1} B_d$ 3 0	C_{D_C}	I	2 0 - 3 0	1 61 - 8 2	0	0					✓	
282	$E_r H_{1f} S_t$ 1 8	26,27, $C_{D_{BLD}}$	25	1 82	5 25	-10 to 10	0						
287	$E_r H_{1f} S_t$ 1 8	26,27	25	1 82	5 25	-10 to 10	0						
332	$M_c C_{1v1} B_d$ 3 0	C_{D_C}	I	2 0 - 1 9	N R	0 to 15	0					✓	
333	$M_c C_{2v1} B_d$ 3 0	$C_{D_{EXT}}^{H}$	I	2 0 - 3 0	8 2	0	0					✓	
376	P_c	9,29	10	6 - 2 0	29 - 8^{30}	0	0	✓					
	$E_c C_{1v1}$	9,29	10	.6 - 2 0	29 - 8^{30}	0	0	✓		✓			
377	$E_r V_{3v3} B_{p,d} S_n$ 2 2	15, $C_{D_{EXT}}, C_{D_A}$	16	6 - 2 2	4 1 - 8 7	-4 to 20	0				✓		
378	P_o	31	I^{32}	9 - 1 4	9 8	0	0	✓					
384	$E_r V_{3v2} S_n B_p BP2$ 2	$C_{D_A}, C_{D_{BP}}, C_{D_{BL}}$	33	2 - 2 2	N R	N R.	N R						✓
385	$E_r V_{3v2} S_n B_p BP2$ 2	34, $C_{D_{BP}}$	2	2 - 2 2	N R	N R	N R						✓
390	$E_r V_{3v2} S_{n,t} B_p$ 2 2	1	2	55 - 1 3	N R	2	0	✓	✓			✓	
	$M_r V_{2v2} S_t B_p BP2$ 2	3	2	55 - 85	N R	2	0						

NOTES TO TABLE IV

1. Sum of external drag, drag due to the boundary-layer control system, drag of the partial fuselage and stub wing, measured relative to a "propulsion reference inlet"
2. Partial fuselage and stub wing included
3. Sum of external drag and drag of partial fuselage and stub wing, measured relative to a "propulsion reference inlet"
4. I denotes isolated inlet test
5. N.R. denotes quantity not reported
6. Inlet tested in isolated configuration and with non-metric wing simulator
7. Inlet tested in isolated configuration and with non-metric forebody
8. Sum of external drag, drag due to the bypass and boundary-layer control systems, and drag of partial fuselage and wing stub
9. Sum of external and forebody drag
10. Tested with metric forebody
11. Full aircraft model with full aircraft on one force balance, one inlet on another
12. Quarter-round inlet of F-111 type
13. Reynolds number range given based on cowl height; cowl height not reported
14. Sum of external drag, drag due to the bypass and boundary-layer control systems, and the drag of the partial fuselage and wing stub, measured relative to a "propulsion reference inlet"
15. Drag of entire airplane model
16. Model of entire F-15
17. Sum of external drag, boundary-layer control drag, forebody and external-store drag
18. Tested with forebody, with and without various external stores
19. Additive drag plus pressure and friction drag of entire model

NOTES TO TABLE IV (Concluded)

20. Flight test of rocket models having common afterbodies

21. Sum of external drag and bleed bypass system drag

22. External drag does not include drag on lower cowl

23. Full B-1 aircraft model with balance installed in one inlet. Metric portion included nozzles and part of wing. Inlet configurations included are: flow through inlet, faired-over inlet w/BLC and bypass, flow through inlet w/ramps installed.

24. Inlet cowl and ramp integrated pressure-area chord force coefficient

25. Inlets mounted at the rear of an uncambered slender gothic wing

26. Sum of external drag and drag on wing

27. Drag increment; drag of wing-and-inlet configuration (minus base drag and inlet internal drag) minus drag of wing-alone configuration

28. Sum of external drag and bleed drag

29. Sum of spillage and interference drag

30. Reynolds number range given based on inlet radius; inlet radius not reported

31. External drag on a nacelle configuration

32. Nacelle configuration

33. Type of configuration tested with inlet is not known.

34. Sum of additive and bleed drag

35. Inlet design includes auxiliary airflow system

36. Sum of external drag, drag due to boundary-layer control system, and drag of the partial fuselage and stub wing

37. Numbers in parenthesis indicate percentage of external/internal contraction

TABLE VI.- CLASSIFICATION OF PARTIAL PREDICTION METHODS BY GEOMETRY AND SPEED RANGE

Quantity Predicted	Inlet Type	Speed Range		
		Subsonic	Transonic	Supersonic
C_{D_A}	Pitot	4,5,7,11,29,90	4,5,7,11,29,90	4,5,7,11,29,49,90
	2-D	4,5,7,11,33	4,5,7,11,33,106	4,5,7,10,11,32,33,364
	Axi	4,5,7,11	4,5,7,11,48,92	4,5,7,10,11,49
$(C_{D_A})_{ref}$	2-D			21,102,106
	Axi			48,71,92,106
$(C_{D_C})_{ref}$	Pitot			59
	2-D			102,106
	Axi			71,106
$\frac{\partial C_{D_{EXT}}}{\partial (MFR)}$	Pitot			59
	2-D			21,102,106
	Axi			71
C_{LS}	Pitot	11,86	11,86	11,86
	2-D	10,11,32	10,11,32	10,11,32
	Axi	10,11,39	10,11,39	10,11,39
K_{add}	Pitot	4,29	4,29	4,29
	2-D	4,33	4,33	4,33
	Axi	4		4
Terminal Normal Shock Position	Pitot			72,73
	2-D			21,32,81,106,364
	Axi			71,364

Page 217 is not available.

TABLE VII.- MAJOR FEATURES OF THE PARTIAL PREDICTION METHODS

Reference		Major Features
4,5,7 (Ball)	C_{D_A}:	one-dimensional momentum method. At critical mass flow, external compression surface contribution taken from data correlations. For subcritical mass flows in a supersonic free stream, the method of ref. 33 is used for 2-D inlets, and another method (referenced in 4) is used for axisymmetric inlets.
	K_{add}:	K_{add} factors for a number of inlets are shown.
10 (Cawthon)	C_{D_A}:	pressure integration along inlet capture streamline. For subcritical mass flows, the methods of refs. 32, 72, and 364 are used.
	C_{LS}:	correlations are given for 2-D and axisymmetric inlets ($MFR_{ref} = 1$). No provision for effects of details of cowl geometry.
11 (Crosthwait)	C_{D_A}:	one-dimensional momentum analysis. Curves given for compression surface contribution. Uses aproach of ref. 72 for normal shock location.
	C_{LS}:	curves given for calculation of C_{LS} depending on detailed cowl geometry ($MFR_{ref} = 1$).
21 (Kamman)	"Pitot-Inlet Analogy"	
	$C_{D_{A_{crit}}}$:	pressure integration along stagnation streamline.
	$C_{D_{C_{crit}}}$:	method not specified.
	$\frac{\partial C_{D_{EXT}}}{\partial (MFR)}$:	uses methods of refs. 59,71,72,102.

TABLE VII.- (Continued)

Reference		Major Features
29 (Mount)	C_{D_A}:	one-dimensional momentum method.
	K_{add}:	for cowls of varying bluntness and external contours.
32 (Osmon)	C_{D_A}:	extends method of ref. 72 for locating terminal normal shock empirically for sidespill; one-dimensional momentum method used for C_{D_A}.
	C_{LS}:	correlations of data from ref. 33 in terms of detailed cowl geometry ($MFR_{ref} \neq 1$).
33 (Petersen)	C_{D_A}:	one-dimensional momentum method. In supersonic flow at subcritical mass flow ratios, a model for supersonic sidespill is included, subsonic and supersonic spillage over the cowl is allowed. No normal shock movement in model. Correlation presented for ramp drag at critical mass flows.
	K_{add}:	curves given for two ramp inlets with varying ramp angles, cowl and sideplate geometry.
39 (Smith)	C_{LS}:	curves given for calculation of C_{LS} depending on detailed cowl geometry ($MFR_{ref} = 1$).
48 (Mascitti)	$C_{D_{A_{crit}}}$:	exact solution for right circular cones at zero angle of attack.
49 (Sibulkin)	C_{D_A}:	one-dimensional momentum method. For subcritical mass flows, the method of ref. 72 is used. For inlets with centerbodies, at critical or supercritical conditions conical flow theory is used.

TABLE VII.- (Continued)

Reference	Major Features
59 (Fraenkel)	$C_{D_{C_{crit}}}$: linear theory, references given in ref. 59. $\frac{\partial C_{D_{EXT}}}{\partial (MFR)}$: analysis ignores details of cowl shape, result is linear variation of $C_{D_{EXT}}$ with MFR.
71 (Goldsmith)	"Pitot-Inlet Analogy" $C_{D_{A_{crit}}}$: pressure integration along stagnation streamline in conical flow solution. $C_{D_{C_{crit}}}$: linear theory. $\frac{\partial C_{D_{EXT}}}{\partial (MFR)}$: extends method of refs. 59 and 72.
72 (Moeckel)	"Continuity" method for location of terminal normal shock.
73 (Love)	Extension of method of ref. 72 to hypersonic Mach numbers
81 (Schulte)	Prediction of location of terminal normal shock in 2-D inlets allowing for sidespill.
86 (Moeckel)	C_{LS}: one-dimensional analysis for uncambered cowls ($MFR_{ref} = 1$), no dependence on detailed cowl geometry.
90 (Crosthwait)	C_{D_A}: empirical relations. No dependence on details of geometry.
92 (Mascitti)	$C_{D_{A_{crit}}}$: approximate solution for right circular cones at zero angle of attack.

TABLE VII.- (Continued)

Reference	Major Features
102 (Dutton)	"Pitot-Inlet Analogy" $C_{D_{A_{crit}}}$: pressure integration along stagnation streamline for 2-D inlets in supersonic flow with wedge shocks attached; with detached wedge shocks, uses method of ref. 59. $C_{D_{C_{crit}}}$: for wedge cowls, and for elliptical contours by Prandtl-Meyer expansion theory. $\frac{\partial C_{D_{EXT}}}{\partial (MFR)}$: extends method of ref. 71 to two-dimensional geometry.
106 (Sharp)	In supersonic flow, uses "Pitot-Inlet Analogy" $C_{D_{A_{crit}}}$: pressure integration along stagnation streamline; supersonic sidespill and sideplate contraction allowed for. $C_{D_{C_{crit}}}$: wave drag calculated using Prandtl-Meyer theory; contributions due to lip bluntness, sideplates accounted for. $\frac{\partial C_{D_{EXT}}}{\partial (MFR)}$: extends analysis of refs. 71 and 102 to multi-ramp 2-D inlets. In transonic flow, 2-D inlets are treated: $C_{D_{A_{crit}}}$ is calculated from one-dimensional momentum analysis with experimental data correlation, used for ramp contribution, $\frac{\partial C_{D_A}}{\partial (MFR)}$ is determined as a function of free-stream Mach number from a correlation of data.
364 (Savage)	Method of locating terminal normal shock from ref. 32 for 2-D inlet; modified version of ref. 72 for axisymmetric inlet.

TABLE VII.- (Concluded)

Reference		Major Features
364 (cont.)	C_{D_A}:	pressure integration along stagnation streamline; for subcritical flow, subsonic contribution calculated by multiplying relevant spillage area by average of pressure behind normal shock and pressure at cowl lip.

TABLE VIII.- CLASSIFICATION OF FLOW-FIELD PREDICTION METHODS BY GEOMETRY AND SPEED RANGE

Solution Method	References	Applicable Geometry			Applicable Speed Range		
		Pitot	2-D	Axi	Subsonic	Transonic	Supersonic
Numerical solution of the unsteady Euler Equations	19 154,354	 ✓	✓	✓	✓	✓	✓ ✓
Finite-difference solution of full potential equation	37,52 149,150,215	 ✓	✓	✓	✓ ✓	✓ ✓	
Finite-difference solution of incompressible potential equation with compressibility correction	52 405	 ✓	✓	✓	✓ ✓	 ✓	
Streamtube curvature	274	✓	✓	✓	✓	✓	

TABLE IX.- MAJOR FEATURES OF THE FLOW-FIELD PREDICTION METHODS

Numerical solution of the unsteady Euler equations

Reference	Major Features
19 (Hawkins)	Explicit finite-difference solution of unsteady Euler equations (Godunov method, ref. 8.3). Boundary condition at inlet duct subsonic-outflow boundary (critical or subcritical flow) fixes axial velocity at one-dimensional ideal value, extrapolates pressure and density. Initial conditions used include free stream, "best guess", and terminal flow fields from previous calculations. Automatic mesh generation is used. Calculations require large computer storage, long run times.
154 (Bansod)	Explicit finite-difference solution of unsteady Euler equations for two-dimensional and axisymmetric blunt-lipped pitot inlets in a uniform supersonic free stream. Upstream boundary is the bow shock. Boundary condition at inlet duct subsonic-outflow boundary is specially treated to enable mass flow ratio and/or the axial velocity component to be specified. Initial conditions used include estimates from previous calculations and/or empirical methods. Stability and accuracy problems encountered for thin lip shapes were stated to be due to treatment of boundary conditions.
354 (Rizzi)	Finite-volume solution of unsteady Euler equations written in integral conservation-law form for a pitot inlet in a supersonic free stream. The body and bow shock fitted mesh adjusts in time to the motion of the captured bow shock. The inlet duct subsonic-outflow boundary condition is a specified static pressure.

Finite-difference solution of full potential equation

Reference	Major Features
37 (Rochow)	Subsonic, compressible, steady potential flow field is solved using iterative finite-difference technique. Supersonic "bubbles" allowed in solution but strong shock waves invalidate potential analysis.

TABLE IX.- (Continued)

Reference	Major Features
52 (McVey)	Another description of the method given in ref. 37.
149 (Caughey)	Finite-difference solution of steady potential equation. Type-dependent differencing used in rectangular computational domain obtained by "nearly conformal" mapping procedure. Accelerated convergence of iteration solution obtained using several schemes.
150 (Arlinger)	Similar to ref. 149 but uses different mapping scheme to achieve computational domain and accelerated convergence schemes not included.
215 (Reyhner)	Line relaxation finite-difference solution of full potential equation in cylindrical coordinate system. Body must be axisymmetric, flow field three-dimensional (with plane of symmetry). Free stream must be subsonic, local flow may be supersonic.
Finite-difference solution of incompressible potential equation with compressibility correction	
52 (McVey)	The incompressible "Douglas Neumann Potential Flow Program" (refs. 8.4-8.6) which uses surface source distributions is used and corrected for compressibility effects using the Prandtl-Glauert, Karman-Tsein, Laitone, or Krahn methods. The Laitone correction is felt to yield best agreement to data.
405 (Hess)	Panel method applicable to three-dimensional pitot inlets (with or without centerbodies) in a subsonic free stream. Geometry must have plane of symmetry. Exact inviscid incompressible solution obtained by linear superposition of solutions for axial flow, simple pitch and yaw, and static operation. Compressibility effects accounted for through Lieblein-Stockman correction (ref. 8.7).

TABLE IX.- (Concluded)

Streamtube curvature

Reference	Major Features
274 (Keith)	The inviscid streamtube curvature technique is coupled via displacement thickness effects with the compressible turbulent boundary layer integral method of Stratford and Beavers (ref. 8.8). Turbulent separation is included via the Stratford criterion (ref. 8.9). The inviscid procedure utilizes automatic grid refinement and a matrix relaxation technique for use in a uniform free stream.

TABLE X.- PARAMETERS USED IN NADC CORRECTION OF CALAC DRAG PREDICTION

Parameter Number	Expression	Definition
1	$\left\{ \frac{\left(\frac{IMSTA}{2}\right)^{5/3}}{\left[(\gamma + 1)M^2\right]^{1/3}} \right\} * \left\{ \frac{LBTA}{DMAX} \sqrt{\left\lvert M^2 - 1. \right\rvert} \right\}^2 * \left\{ \frac{(M^2 - 1)}{\left[(\gamma + 1)\left(\frac{IMSTA}{2}\right) M^2\right]^{2/3}} \right\}$	Similarity relation; pressure
2	$\frac{M^2}{R_e}$	Pressure spreading estimator
3	$\frac{AEXN}{ATHR}$	Nozzle expansion ratio
4	$\frac{ATHR}{AMB}$	Ratio of internal flow area (nozzle throat) to fuselage area (area at metric break station)
5	$\left\{ \frac{\left(\frac{IMSTA}{2}\right)^{5/3}}{\left[(\gamma + 1)\ M^2\right]^{1/3}} \right\} * \left\{ \frac{LBTA}{DMAX} \sqrt{\left\lvert M^2 - 1. \right\rvert} \right\}^2 * \left\{ \frac{M^2 - 1}{\left[(\gamma + 1)\left(\frac{IMSTA}{2}\right) M^2\right]^{2/3}} \right\}^2$	Similarity relation; pressure drag estimator

TABLE X.- (Continued)

Parameter Number	Expression	Definition
6	IMSTA	Integral-mean-slope of aftbody
7	$\dfrac{M}{R_e^{3/2}}$	Boundary layer parameter; estimator of skin friction
8	$\left\{\dfrac{\left(\dfrac{IMSTA}{2}\right)^{5/3}}{\left[(\gamma + 1)\ M^2\right]^{1/3}}\right\} * \left\{\dfrac{(M^2 - 1)}{\left[M^2 \left(\dfrac{IMSTA}{2}\right)\ (\gamma + 1)\right]^{2/3}}\right\}$	Similarity relation; pressure drag estimator
9	$\left\{\dfrac{\left(\dfrac{IMSTA}{2}\right)^{5/3}}{\left[(\gamma + 1)\ M^2\right]^{1/3}}\right\} * \left\{\dfrac{M^2 - 1}{\left[(\gamma + 1)\ \left(\dfrac{IMSTA}{2}\right)\ M^2\right]^{2/3}}\right\}^3$	Similarity relation; pressure drag estimator
10	$\left\{\dfrac{1}{R_e^{5/6}\ \left[(\gamma + 1)\ M^2\right]^{1/3}}\right\} * \left\{\dfrac{(M^2 - 1) R_e^{1/3}}{\left[(\gamma + 1)\ M^2\right]^{2/3}}\right\}^2$	Similarity relation; estimator of effect of boundary layer on external pressure field (displacement effect)

TABLE X.- (Continued)

Parameter Number	Expression	Definition
11	$\dfrac{1}{R_e^{3/2}}$	Boundary layer parameter; estimator of skin friction
12	$\left\{ \dfrac{\left(\dfrac{IMSTA}{2}\right)^{5/3}}{\left[(\gamma + 1)\ M^2\right]^{1/3}} \right\} * \left\{ \dfrac{LBTA}{DMAX} \sqrt{\lvert M^2 - 1.\rvert} \right\}$	Similarity relation; pressure drag estimator
13	$\left\{ \dfrac{\left(\dfrac{IMSTA}{2}\right)^{5/3}}{\left[(\gamma + 1)\ M^2\right]^{1/3}} \right\} * \left\{ \dfrac{LBTA}{DMAX} \sqrt{\lvert M^2 - 1.\rvert} \right\}^2$	Similarity relation; pressure drag estimator
14	$\left\{ \dfrac{\left(\dfrac{IMSTA}{2}\right)^{5/3}}{\left[(\gamma + 1)\ M^2\right]^{1/3}} \right\} * \left\{ \dfrac{LBTA}{DMAX} \sqrt{\lvert M^2 - 1.\rvert} \right\}^3 * \left\{ \dfrac{M^2 - 1}{\left[(\gamma + 1)\left(\dfrac{IMSTA}{3}\right) M^2\right]^{2/3}} \right\}$	Similarity relation; pressure drag estimator

TABLE X.- (Concluded)

Parameter Number	Expression	Definition
15	NPR	Nozzle pressure ratio
16	CD_{CALAC}	Aftend drag; predicted value from CALAC "Twin Jet Aftend Drag and Nozzle Internal Performance Computer Deck"
17	$\frac{ACC}{AMB}$	Ratio of aftend projected areas
18	$\left\{ \frac{\left(\frac{THSTA}{2}\right)^{5/3}}{\left[(\gamma + 1)\ M^2\right]^{1/3}} \right\} \cdot \left\{ \frac{LBTA}{DMAX} \sqrt{\lvert M^2 - 1.\rvert} \right\}^3$	Similarity relation; pressure drag estimator
19	$\frac{AEXN}{ACC}$	Ratio of nozzle projected areas

TABLE XI.- THEORETICAL PREDICTION METHODS

	Effects Treated	27	34	43	48	49	51	80	99	106	117	129	136	146	160	184	209	210	211	212	217	218	220	223	227	231	232	252	253	264	265	267	274	282	284	296	297	298	299	300	301	306
Subsonic	Boundary Layer	✓	✓		✓		✓	✓	✓				✓				✓		✓	✓	✓	✓			✓			✓	✓	✓	✓			✓			✓	✓	✓	✓	✓	
	Separation	✓						✓	✓				✓				✓		✓	✓		✓			✓				✓	✓	✓									✓	✓	
	Plume Shape	✓			✓		✓										✓			✓	✓	✓			✓			✓		✓	✓						✓	✓	✓	✓	✓	
	Entrainment																✓				✓							✓		✓	✓						✓	✓	✓	✓	✓	
	Compressibility	✓	✓		✓		✓										✓		✓	✓	✓	✓			✓			✓	✓	✓	✓						✓	✓	✓	✓	✓	
	Base Flow															✓																										
Transonic	Boundary Layer	✓	✓	✓			✓										✓		✓	✓	✓	✓			✓			✓					✓			✓	✓	✓	✓	✓	✓	
	Separation	✓															✓		✓	✓		✓			✓											✓				✓	✓	
	Plume Shape	✓		✓			✓										✓			✓	✓	✓			✓			✓					✓			✓	✓	✓	✓	✓	✓	
	Entrainment																✓				✓							✓								✓	✓	✓	✓	✓	✓	
	Base Flow														✓																											
Supersonic	Boundary Layer					✓																										✓				✓						
	Separation					✓												✓														✓				✓						
	Plume Shape					✓																										✓				✓						✓
	Entrainment																															✓										
	Base Flow										✓					✓							✓	✓			✓															
	Wave Drag									✓		✓		✓												✓									✓							

TABLE XII.- DATA FOR AFTERBODY DRAG

Reference Number	Test Model	Data Presented	Range of: Mach Number	Range of: Reynolds Number Per Meter, $\times10^{-6}$	Range of: Angle of Attack	Range of: Nozzle Pressure Ratio	Test Parameters: Nozzle Type	Test Parameters: Inter-fairing	Test Parameters: Nozzle Spacing	Test Parameters: Empennage	Test Parameters: Jet Simulation
8	19	21	6-1.3		-3° to 15°	1-7					CG
9	16	1,2,3,4	0 , 5-1 29		0°	1-11	P				HG
10	16	1,2,3,4	0 , 5-1.3	9 71-12.60	0°	1-8	P				HG
11	17	1,2,3,4	.5-2.2	9 51-14 69	0°	1-22	C.CD	HW,O	1.874		CG
12	17	1,2,3	0, 5-1 3,2 2	9 61-12 76	0°	1-20	P	HW,O	1.12,1.61		CG
13	17	1,2,3,11	0-1.3	9 12-12.33	-2° to 8 5°	1-9	P	HW,O	1.12,1 61		CG
14	18	1,2,11	.5-1 2	9.71-12 60	0°	1-6	CD			H,V_1	CG
16	16	1,2	6- 9		0°	1-6	CD				CG
	18	1	.6- 9		0°		CD			H,V_1	CG
17	19	7,11,2,13	7- 975		0°	1-5	C,CD,P	0	1.5-5 72	H,V_1,V_2	CG
28	19	3,4,1,2,12	.4-1 2	8.2-13 12	-2° to 14°	1-10 5	C,2D	0	1 66	H	CG
30	20	12,8,11	55- 85	10 17-12 14	-2° to 6°						
31	16	1,2,11,13	6-1.2	10 07-14 04	0°	1-14	C,CD				CG,HG
32	19	4,12,1,5,13,2	3-1 5	3 28-19 68	-2° to 10°	1-6	CD	0	2 04[30]	H,V_2	CG
33	19	1,13	.3-1 5	3 28-19.68	0°	1-14	C,CD	0	2 04[30]	H,V_2	CG
35	16	1,2,11,9,10	3-1 3	6.56-13 12	0°						
36	16	1,2,13,9	.3-1 3	6 56-13 12	0°	1-13	CD				CG
37	16	1,2,11	1 83, 2 20	14 69,12 20	0°	1-59	CD				CG
38	16	2,13	6- 95,1 2	10 07-14 04	0°	1-12	CD				CG,HG
40	19										
44	19	3,4,11,2	6-1 6, 1 8-2 5	1 64-19.68	0°,6°,9°,12°	1-18	C,CD,E,P	HW,O	1.25,1.625, 2 00	V_1,V_2,H_δ	CG
	16	2,3	6-1 6, 1 8-3 0	8 20,5 25	0° to 6°	1-18	C,CD,E,P				CG
46	19	3,4,11,12,1,8, 6,7,2	.6-1 6	1 97-19 68	0°,3° to 9°	1-22	C,CD,F,P	HW,O	1 25,1 625, 2 00	V_1,V_2,H_δ	CG,S,CG/S
47	19	8,2	6-1.6	1 97-16.40	-3° to 10°	1-13	C,CD,E,P	HW,O	1.25,1.625, 2 00	V_1,V_2,H_δ	S
52	16	3	6-3 0	3 84-8.20	0°	2-19	C,CD,E,P				CG
54	19	4,11,1,5,2	6-1 5	3 28-16 40	-2° to 8°	1-11	P,CD	0	1 52,2 17	H,H_δ,V_2	CG,S

TABLE XII.- (Continued)

			Range of				Test Parameters					
Reference Number	Test Model	Data Presented	Mach Number	Reynolds Number Per Meter, $\times 10^{-6}$	Angle of Attack	Nozzle Pressure Ratio	Nozzle Type	Inter-fairing	Nozzle Spacing	Empennage	Jet Simulation
55	20	2	55-2.2	5.54-8.20	-10 to 6°	1-14	CD	O			CG
56	20	1,2,11,10	.6-1 3	12.46	0°	1-8	E	O	1,.34		HG
62	17	2,11,1,6	.6-1.3,2.01	10 82,13.78	0°	1-20	C,CD	O	52,.68,.81		CG
63	17	1,?,10,3,4	.6-1 3 2 0-2 2	12 23-12 99	0°	1-21	C	HW,O	1 07,1.82		CG
67	16	3,4	.6- 9 2 0-2 2	10 96-13 09	0°	1-21	2D,C				CG
68	19	11,4,1	.6- 9	12 46	0°,6°	1-7	CD,2D	HW	1.1-2 3	H,V_2	HG
	19(FS)	1,2	.6- 9	6 56-15.42	1.19 to 5 49	1.8-3 7	CD	HW			
69	16	3,4,11,2	5-.9 1.15-1 25		0°	1.2-4.6	E				HG
70	17						E				
71	19		6-1 3,2.2								
72	19	12	2.2		-2° to 6°	1-21					CG
73	16	3,9	5-1 3	12 07	0°	1-8	P				HG
74	16	1,2,3,4	5-1 30,1.82		0°	1-23	P				CG
75	16						E				
77	17		0-2 2		0°	1-21					
78	17	2,1,9,3,4	.6-1 3,2 2	10 30-14 01	0°	1-20	C	HW,O	1.17,1 52, 2 32,3 03		CG
82	20	11,12	5-2.2	5 90-13 12	-2° to 5°	1 3-11	C,CD	O		H_δ	CG
83	19	9,12,1,8,11,2	6-1 2	5 67-7 94	0°	1-6	C,CD	O			HG
84	20	12,8	2. 63- 82	16 73-48 54	-2° to 6°						
86	19	12	.6-2 01					HW		V_2,H	
87	19	12	.65-2 01							H_δ,V_2	
88	19										
89	16	1,9,2,4,3,12	.4-1 3	7 87-14.30	-4° to 8°	1-6	C				CG
90	16	1,9,2,4,3	.4-1 3	9 84-14.04	0°	1-6	C				CG
91	19	1,4,2	6-1 3,2 2	9 84-11 81	-2° to 6°	1-21	CD	HW		$H,V_{2\delta},V_2$	CG
92	16	1,2	4-1 3	9 84-14 04	0°	2	C				S,CG

TABLE XII.- (Continued)

			Range of				Test Parameters				
Reference Number	Test Model	Data Presented	Mach Number	Reynolds Number Per Meter, $\times 10^{-6}$	Angle of Attack	Nozzle Pressure Ratio	Nozzle Type	Inter-fairing	Nozzle Spacing	Empennage	Jet Simulation
94	19	11,12,2,1	.6-1 3,2.2	9.84-11 81	0°	1-21	CD	HW		$H,V_{2\delta},V_2$	S,CG
96	16	1,7,2	.6-1 5	3.28-9 84	0°	2-22	CD				CG,HG
97	16	1,2	6-1 5	3.28-9 84	0°	6-12 7	E,CD				CG,HG
100	19(FS)	8,12	.3-2 0			1 4-8	CD	HW		H,V_2	
101	19	1,3,15	1.2		0°	2-4	E	HW		H,V_1	HG
102	16	9,10,2,11,13	.85-1 2		0°		E				
107	19										
108	17	2,4,8	6-1 3,2 2			1-6	C,P,CD,E	HW,O			CG
109	19	1,2,11,8	.7-1 2,2 2			1-10	CD			H,V_2	CG
110	20	3,4	55-2 2	4.26-8 20	-1° to 8°	1-14	CD	O		H_δ	CG
112	19		1 2								
114	17	2,10,9,11	8			3	C	HW,O	2 39,2 92 3 45		
	16	2	8			3	C				
115	16	5,7,8,2,4,11	.5-.85	5.38-18.76							
119	18	11	6-1 6				CD			V_1,H	S,CG
	19	2,11,12	6-1 6		-2° to 6°	1-11	CD			V_1,H_δ,V_2	S,CG
122	16,17	14,9,11	5- 9	4 00-8 20	0°	1-8	C	O	1 75		CG
124	16	7,2	6-1.5	3 28-9 84	0°	6-12 7	CD,E				CG,HG
125	16	13,2,3,4	.6-1 17			1-11	E				CG,S
126	19(FS)	1,11,9	4-.9			1-3 4	C			H_δ,V_1	
	19	1,9	.4- 9			1-4 2	C				CG,HG
127	20	1,2	6,.9	12.73-16.01	0° to 15°	1 9-4 4	C			H,V_1	HG
	20(FS)	1,2	6, 9	5 61-13 51	3° to 12°		C			H,V_1	
128	19	5,3,2	0., 7-2 2	12 14		1.5-2 0	C,CD,F,P	HW,O			
130	16	1,2	4- 9 1 1-1 3	9 84-14.04	0°	2	C				CG,S
133	20	9,11	.6-3 05			1-40	CD	HW,O			CG

TABLE XII.- (Continued)

Reference Number	Test Model	Data Presented	Range of Mach Number	Range of Reynolds Number Per Meter, $\times 10^{-6}$	Range of Angle of Attack	Range of Nozzle Pressure Ratio	Test Parameters: Nozzle Type	Test Parameters: Inter-fairing	Test Parameters: Nozzle Spacing	Test Parameters: Empennage	Test Parameters: Jet Simulation
134	16	5,1,13,2	.56-1.0	11 61-14 92	0° to 6°						S
135	20	1,2,5	56-1 46	11.81-16.27	0° to 8°		C				S
136	16	1,2	6- 9	12 3-319 80	0°		C				S
141	16	1,2,13	56-1 0	11 81-15 09	0° to 8°		C				S
142	19	11,12,1	6, 85,1 27, 1 7,2 0	16 40-30 50	0° to 10°	1-18 5	P,CD	0		H	CG
145	19	13,10,2,1,4	6-1 4 1 8-2 2			2-10	E	0		H,V_1	CG
152	16	1,2	6-1 5	3 28-167.36			CD				CG
	20	2	8-1 4	3.28-16 40		2 2-7 5	CD	0		H_δ	CG
153	19	1,2,9,11,10, 12,8	8-1 05	12 30-12.92		1-7	C	0		H_δ	HG
154	20	1,2	6, 9	12 33-15 78	0° to 15°	1.9-4.4	C			H,V_1	CG,S
	20(FS)	1,2	6, 9	4 23-12 53	6° to 14°		C			H,V_1	
155	19	1	5- 9	9 25-12 14	1 1° to 4 5°	1 5-2 9	E	0		H,V_1	HG
	19(FS)	1,9,13,2	5- 9 1 38-2 01	8 72-14 86	2.1° to 6 7°	1 5-7 5	E	0		H,V_1	
167	18	2,1,12	8-1.1	14.63	0°	2-9	C			H,V_1	HG
168	16	11,9,1,2	6-2 5		0°	1-7 6	CD				CG,HG
169	19	2,1	6-1 5	3.28-19 68	-2° to 10°	1-9 5	CD	0	1.5,1 7,2 1	H_δ,V_2	CG
171	16	4,1,9,2,3	85, 95,1 08	13.12	0°	1-9	CD,E				HG
175	16	1,2	6, 75, 8	17.5-105	0°						
176	19	2,4,11	.5-5 0	N R	0°	3-13	C,CD,E	HW	1 2	H,V_1	CG
177	16	1,2,5,6,7,8	6-1 4	4 82-17.39	0°						
178	16	1,2	.6- 95	N R	0°						
180	20	15	N R.	N R	0°	N R	2D				CG
181	20	12,9	4-1 25	2.3-5 6	-2° to 10°	N.R.	CD				CG
182	16	1,9	7-1 20	N R.	-6° to 6°	N R	CDE				CG
183	16	7,11	9-1 20	.57- 69	-2° to 2°						S, NJS
185	20	9,12	.4-1 20	4 3-8 9	-5° to 6°	N.R.	CD				CG

TABLE XII.- (Continued)

Reference Number	Test Model	Data Presented	Range of Mach Number	Range of Reynolds Number Per Meter, $\times 10^{-6}$	Range of Angle of Attack	Range of Nozzle Pressure Ratio	Test Parameters Nozzle Type	Test Parameters Inter-fairing	Test Parameters Nozzle Spacing	Test Parameters Empennage	Test Parameters Jet Simulation
186	16	1,2	.4-1.05	4.2-24.9	0°						S
192	16	2,6,7,8	6-1.40	4 85-17 25	0°						S
193	20	12	.2-2 3	N R	-4° to 12°						NJS
194	20	12	2-1.5	N R.	-11° to 11°						NJS
195	20	9,12	.9-1.14	9 84	0° to 7°					H	
196	20	1	9-1 14	9 84	0° to 6°					H	
202	16	9	2.5,3.0	3.94-19 68	0°	N R	CD,C				CG
203	16	9	1 57-2 87	6 56	0°	15-1000	CD				
204	18	1,9	.5- 9	5 0-45 0	0°	1 0-4 5	C			H,V_1	HG,CG
	18(FS)	1,9	4- 8	N R.	N R	1-3 2	C			H_δ,V_1	
	16	1	.6-.9	N R.	0°	1-4 5					HG,CG
205	16	9,1	1 36	10 75-55 76	0°						
206	18	1,2	6, 85, 9	55 6-70 3	0°						S
207	16	2	6-1 5	2 69-159.08	0°		C				CG
208	16	2,1	6-1.5	8 2	0°	1-22	C				HG,CG
213	18	1,2	6- 9	13 8-330 0	0°						S
214	19	12,2,11	6-1 2	10 8-12 4	0° to 9°	1-6	CD	HW	4 44,4.55	H_δ,V_1	CG
216	18	12,9,24	.4-1 25	N R	-4° to 12°						NJS
221	16	3,4	6-1 2,2 1	10.14-12 49	0°	1-27	2D				CG
222	20	1,11,14,26	.7-1 4	3.28-16 4	-2° to 6°	N R	CD	O		H_δ,V	CG
225	18	2,22,23,14	5-1 2,2 2	9 28-12.80	0°	1-20	CD			H,V_1	CG
226	20	12,24	.9-1 4	9 8	-1° to 6°	N R				H	
228	16	1	0, 9,2 0	N R	0°	3-16	P				CG
229	16	7,1,9	6-1 4	13 1-16 4	0°						S
230	16	9	2 5,3.,3 5	18 6-21	0°		CD				CG
233	16	15	0, 74	8 9	0°	1-3	2D				CG

TABLE XII.- (Concluded)

Reference Number	Test Model	Data Presented	Range of: Mach Number	Range of: Reynolds Number Per Meter, $\times 10^{-6}$	Range of: Angle of Attack	Range of: Nozzle Pressure Ratio	Test Parameters: Nozzle Type	Test Parameters: Inter-fairing	Test Parameters: Nozzle Spacing	Test Parameters: Empennage	Test Parameters: Jet Simulation
234	16	2,10	7-1.3	N R.	0°	1-5	C				CG
	17	2,1,10	7-1.3	N R	0°	1-7	C		2.75,2.01		CG
235	19	4,8,12	.17-1 6	3 48-26 74	0° to 29°	1-10	C	O		H,V_1	CG
237	16	2	6-1 5	3 28-8 2	0°	0-20	C,CD				CG,HG
238	16	1,2,15	75-.95	N R	0°	1.7-4.7	C				CG
239	16	1,2,13	.2- 6	.48-1 21[29]	0°	1.7-3	CD				CG,HG
240	16	1,15,13	.5- 96	12 8-29.1	0°	1-6 63	C				CG
241	16	1,2,13,4	.8- 96	21.1-26 1	0°	1.5-4 5	C				CG,HG
251	20	27	55-1 60	8.2	-2° to 6°	1-9	CD	O		H_δ,V	CG
262	19	1,2	6-2 0	8 2	0°	0-16	CD	O		H_δ,V_2	HG
271	19	3,2	.9,1 5	N.R.	0°	1-9	2D	HW		H	CG
272	20	11	.3-2 2	N R.	0° to 5°	1-3	CD	O		H_δ,V_1 [31]	
273	20	22	7-2 2	N R	0°		CD	O		H_δ,V_1 [31]	
276	16	1,2	6-1 4	N R	0°	2-6	2D				CG,HG
277	16	1,9	.9-1 2	6.9-8 4	-2° to 2°						NJS,S
278	16	1,12	.8-1 2	14 8-16.7	-4° to 6°						NJS,S
280	16,28	9,12	.4-1 25	N R	-4° to 6°					H,V	NJS
281	16	27,12	4 15	N R	-6° to 14°						NJS,S
283	16,28	12	2-2 3	N R.	-4° to 11°					H,V	NJS
285	16	1,2,10,13	.8-1 3	8.2	0°	1-6	C				CG
286	16	1	5-1 2	4 9-8 2	-2° to 2°	0-160	C,CD				CG
287	16	12	.7-1 4	13 1-17.4	-3° to 6°					H,V	NJS
289	16	9,10,1,8	.8-1 0	11.1-12.8	0°						
291	18	1,2,9,10	8-1 10	N R.	0° to 5°	1-7					HG
292	16	1,2,9,10	2 01,3 27	6 0	0°	1-40					CG
302	16	11	.3-2.2	N R.	N R	1 3-3 4	CD				HG
304	16	1,2,9,10,11	.9, 95	12 3,19 9	0°	2-5	C				S
310	16	1,2,11	.8- 95	12 3,19 9	0°	2-5	C				S

NOTES TO TABLE XII

1. Afterbody/Boattail/Nozzle pressure coefficient distribution
2. Afterbody/Boattail/Nozzle drag coefficient
3. Thrust-minus-drag coefficient, indicates thrust-minus-total drag or thrust-minus-nozzle drag
4. Thrust coefficient
5. Forebody pressure coefficient distribution
6. Forebody drag coefficient
7. Total configuration pressure coefficient distribution
8. Total configuration drag coefficient
9. Base pressure coefficient distribution
10. Base drag coefficient
11. Pressure or drag coefficient increment due to parametric changes - parameters include nozzle pressure ratio, empennage, area distribution on the afterbody, etc.
12. Aerodynamic characteristics - lift or pitching-moment coefficients and increments of lift or pitching-moment coefficients due to parametric changes
13. Boundary-layer data - includes Mach number profiles and stagnation pressure profiles
14. Interference pressure coefficient distribution - based on the pressure coefficient distribution of a reference model
15. Nozzle exhaust flow-field data - includes local Mach number and flow angle
16. Isolated boattail or single engine configuration - no empennage
17. Isolated twin-engine configuration - no empennage
18. Single engine aircraft configuration
19. Twin engine fighter-type aircraft configuration - includes isolated twin-engine afterbody configuration with empennage
20. Other configurations - includes twin-engine aircraft configuration with single engine under each wing, isolated boattail configuration with attached delta wing, etc.

NOTES TO TABLE XII (Concluded)

21. Any quantities not recorded for confidential reports indicates those quantities are confidential information

22. Sum of afterbody, nozzle, and tail drag coefficient

23. Tail drag coefficient

24. Interference coefficients (drag, lift, pitching-moment) based on drag, lift, or pitching-moment coefficients of a reference model

25. Determines shapes of boattail bodies of revolution for $C_{D_{W_{min}}}$

26. Aft-nacelle integrated pressure-area chord force coefficient

27. Axial-force coefficient

28. Isolated boattail with empennage

29. Reynolds number range given based on maximum diameter of body; maximum diameter of body not reported

30. Based on cruise nozzle diameter

31. Horizontal tails attached to single vertical tail

FS: Refers to full-scale configuration

N.R.: Quantity not reported

TABLE XIII.- AFTERBODY CONFIGURATION CLASSIFICATION SCHEME

Configuration Element	Symbols	Definition of Symbols
Interfairing	HW	Horizontal wedge
	O	Other
Jet Simulation	CG	Cold gas
	HG	Hot gas
	NJS	Normal Jet Simulation
	S	Solid Plume Simulator
Empennage	H	Horizontal stabilizer
	V	Vertical stabilizer
Empennage Subscripts	δ	Deflected
	1	Single vertical tail
	2	Twin vertical tail
Nozzle	C	Convergent
	CD	Convergent-divergent
	E	Ejector
	P	Plug
	2D	Two dimensional

TABLE XIV.- DATA FOR EFFECTS OF AIRFRAME ON INLET FLOW QUANTITIES

Reference Number	Configuration	Probe Position	Data Presented	Range of: Mach Number	Range of: Reynolds Number Per Meter ($\times 10^{-6}$)	Range of: Angle of Attack, Deg.	Range of: Angle of Sideslip, Deg.	Data Showing Effects of: General Configuration Data	Nose Shape	Nose Length	Fuselage Shape	Fuselage Length	Canopy Size or Shape	Axial Position Along Body	Wing L.E. Sweep	Wing L. E. Flap Deflection	Protuberances
10	F,WF	$F_{s,a}, F_b, W_{sh}$	$M_L, \alpha_L, \beta_L, P_L$; $\hat{M}_L, \hat{\alpha}_L, \hat{\beta}_L, \hat{P}_L$	.75 - 2.5	4.2 - 13 6	-5 to 25	-8 to 8	✓			✓	✓	✓	✓	✓	✓	✓
22	WF	W_a, W_{sh}	$M_L, \alpha_L, \beta_L, P_L$	8 - 2.5	6 5 - 9 45	-3 to 20	-13 to 13		✓		✓		✓		✓		
34	F,WF	$F_{s,a}, W_{sh}, W_a$	M_L, α_L, β_L	.8 - 2.5	6 5 - 9.45	-3 to 20	0	✓	✓		✓		✓		✓		
80	F	F_s	M_L	1.4 - 2.0	8.5 - 13 4	0	0	✓									
174	F	F_s	$M_L, \alpha_L, \beta_L, P_L$	1.6 - 2 0	-10 7	0 to 12	0	✓									
175	WB	W_a	M_L, α_L, β_L	2 0	9 3	0	0	✓									
179	FI	F_s	$\hat{M}_L$	1 6 - 2.0	8 2	0 to 5	0			✓							
280	WF	$F_a, F_s, sh, W_{sh}, W_a$, F_b, F_t	$M_L, \alpha_L, \beta_L, P_L$	8 - 3 5	6.5 - 9 45	0 to 20	-8 to 8		✓		✓		✓				✓
322	WB	$F_s, F_t, F_a, F_{b,a}, F_{s,sh}$, W_h	$M_L, \alpha_L, \beta_L, V_L, Q_L$	4	11 2	0 to 12	0		✓		✓	✓	✓				
335	WFI	C	$M_L, P_L, \alpha_L, \beta_L$	.9 - 3 0	8 5 - 13 8	-5 to 10	-4 to 4	✓									
338	WB	$F_s, F_b, F_a, F_{b,a}, F_{s,sh}$, W_a, W_{sh}	α_L, β_L, Q_L	13	N R	-8 5 to 16 4	0	✓							✓		
339	WB	W_a, W_{sh}	M_L, α_L, β_L	1 61, 2 01	9 2, 7 5	0, 4, 8	0	✓							✓		
342	WB	F_b, W_a, W_{sh}	$M_L, \alpha_L, \beta_L, V_L, P_L, v_L$	925, 975, 1 025	9 8	-5 to 5	0	✓									
343	WB	F_b, W_a, W_{sh}	$\alpha_L, \beta_L, M_L, V_L, Q_L, v_L$	1 5, 2 0, 2 5	12 1	0, 5	0	✓									
344	WB	W_a, W_{sh}	$M_L, \alpha_L, \beta_L, Q_L, v_L$	25, 7	8.2	0, 6	0	✓									
352	B,WB	$F_s, F_{s,aft}$	P_1, P_L, M_L	2 48	10 0	0	0							✓			
369	WB	$F_t, F_b, F_{s,a}, F_{s,sh}, W_a$, W_h	$M_L, P_L, \alpha_L, \beta_L$	1.6, 2 36, 2 96	9 84	0 to 4	-5 to 5	✓									
370	WB	F_b	$M_L, P_L, \alpha_L, \beta_L$	2 95	18 6	0 to 23	0, 5	✓	✓								
371	WB	F_b, F_s, F_t	P_L, α_L, β_L	2.0	15 3	0 to 6	0									✓	

TABLE XIV.- (Concluded)

Reference Number	Configuration	Probe Position	Data Presented	Range of: Mach Number	Range of: Reynolds Number Per Meter ($\times 10^{-6}$)	Range of: Angle of Attack, Deg.	Range of: Angle of Sideslip, Deg.	Data Showing Effects of: General Configuration Data	Nose Shape	Nose Length	Fuselage Shape	Fuselage Length	Canopy Size or Shape	Axial Position Along Body	Wing L.E. Sweep	Wing L. E. Flap Deflection	Protuberances
394	B_1	F_b, F_s, F_t	p_L	2.01	12.1	-8 to 15	0				✓			✓			
399	B	F_b, F_s, F_t	$M_L, P_L, \epsilon_L, \phi_L$	2.0 - 4.5	35.4 - 51.2	0 to 24	0		✓					✓			
400	B	F_b, F_s, F_t	$M_L, P_L, \epsilon_L, \phi_L$	2.0 - 4.5	17.1 - 21.0	0 to 25	0							✓			
401	B	F_b, F_s, F_t	P_L, M_L, c_L, ϕ_L	2.1 - 4.3	40.7, 81.3	0 to 10	0		✓					✓			
402	B	F_b, F_s, F_t	$P_L, M_L, \epsilon_L, \phi_L$	2.5 - 4.3	39.4 - 59.0	-10 to 10	0	✓						✓			
406	B	F_s	$\hat{M}_L, \hat{\alpha}_L, \alpha_L, \beta_L, P_L$	*	*	*	*	✓									

*Range is confidential

TABLE XV.- SYMBOL DEFINITIONS FOR TABLE XIV

Column Heading	Symbol	Subscripts or Superscripts
Configuration	B: Body of revolution F: Fuselage with canopy I: Installed inlet W: Wing	1: Fuselage with various cross-sectional shapes, no canopy
Probe Position	C: Inlet cowl-lip plane F: Within a body diameter of the fuselage or body of revolution W: Under-wing position	a: ahead of wing aft: aft of wing b: bottom of fuselage s: side of fuselage sh: shielded by wing t: top of fuselage
Data Presented	M_L: Local Mach number P_L: Local to freestream total pressure ratio (p_{T_L}/p_{T_∞}) p_L: Local to freestream static pressure ratio (p_L/p_∞) Q_L: Local to freestream dynamic pressure ratio (q_L/q_∞) V_L: Local to freestream total velocity ratio (V_L/V_∞) v_L: Local perturbation velocities: $\frac{v_L}{V_\infty}$: local sidewash velocity $\frac{w_L}{V_\infty}$: local upwash velocity $\frac{u_L}{V_\infty}$: local velocity component in free-stream direction α_L: Local upwash angle $(\tan^{-1} \frac{w_L/V_\infty}{u_L/V_\infty})$ β_L: Local sidewash angle $(\tan^{-1} \frac{v_L/V_\infty}{u_L/V_\infty})$ ε_L: Local total flow angle (total included angle between the local velocity vector and the vehicle axis, see fig. 88) ϕ_L: Local roll angle (defines the plane in which ε_L is contained, measured relative to the tangent of the arc of radius of the point of interest, fig. 88	$\hat{}$: indicates average local quantity

TABLE XVI.- CLASSIFICATION OF METHODS FOR PREDICTING FOREBODY AND FOREBODY-WING EFFECTS ON INLET "FREE-STREAM" FLOW FIELD

Group	Flow Equations or Type of Method	Type of Solution	Applicable Speed Range		
			Subsonic	Transonic	Supersonic
1	Empirical methods	3-D	4,11[1]		4,11[1],398[1]
2	Incompressible, steady potential flow	3-D	300,301,302,315, 340[1],346		
3	Linearized, steady, compressible potential flow	3-D	304,309,318,347, 348		303[1],308,309,318, 350
4	Unsteady, compressible linearized potential flow	3-D	319		319
5	Full compressible potential flow	3-D		215[1]	
		Axi		290[1]	
6	Steady Euler equations	3-D			34,151,152,153,289, 293,297,305,306,337, 375
		Axi			324[1]
7	Unsteady Euler equations	3-D	291[3],311	291[3],311	291[3],311,373[1]
		Axi			312[1]
8	Unsteady, incompressible Navier-Stokes equations	3-D	316		

[1]axisymmetric fuselage only
[2]slender bodies and thin wings
[3]slender bodies

TABLE XVI.- (Concluded)

Group	Flow Equations or Type of Method	Type of Solution	Applicable Speed Range		
			Subsonic	Transonic	Supersonic
9	Unsteady, compressible Navier-Stokes equations	3-D	311	311	311
		Axi			312,314
		Conical			383
10	Steady, compressible viscous flow	3-D			292[3],393,395
		Axi			374[1]
11	3-D transonic small disturbance theory	3-D		296[2],298[2],299[2]	
12	Transonic equivalence rule	3-D		341[2]	
13	Far-field matching method	3-D		317	

[1]axisymmetric fuselage only
[2]slender bodies and thin wings
[3]slender bodies

TABLE XVII.- MAJOR FEATURES OF METHODS FOR PREDICTING FOREBODY AND FOREBODY-WING EFFECTS ON INLET FLOW FIELD

Group 1.- Empirical Methods

Reference Number	Features of Prediction Method
4 (Ball)	• under-wing configuration - empirical relations based on Prandtl-Meyer relations for a shock under a 2-D wing used to determine effects of angle of attack (supersonic free stream only) • under-fuselage configuration - effects of angle of attack based on experimental data (subsonic and supersonic free stream) • side-mounted configurations - angle-of-attack effects assumed negligible based on data
11 (Crosthwait)	Fuselage Effects: • superpose potential flow solution of Laitone (axial flow) and incompressible slender-body cross-flow theory solution for subsonic flows • combined supersonic/hypersonic similarity rule for supersonic flows ($M_\infty \geq 2$) Wing Effects: • experimental results on a limited number of wings mounted on a circular fuselage are used to determine angle-of-attack effects for subsonic and supersonic flows
398 (Mahoney)	• forebody represented by suitable tangent cone • two correlating parameters, used in conjunction with a conical shock and 2-D Prandtl-Meyer expansions, are employed to determine flow angles at body surface points • potential flow theory used to determine flow angles at off-body points

TABLE XVII.- (Continued)

Group 2.- Incompressible Potential Flow Equations

Reference Number	Features of Theoretical Prediction Method
300,301 (Hess)	• singularity method • non-lifting surfaces modeled using constant-strength source panels on surface (ref. 300) • lifting surfaces modeled using constant-strength source panels and doublet panels on the surface and trailing vorticity (ref. 301) • panels are plane quadrilaterals
302 (Hess)	• replaces plane surface panels having constant source strengths (ref. 300) with curved surface panels having variable singularity strengths
315 (Asfar)	• singularity method • body is modeled using constant-strength source panels on the surface and surface distributions of vorticity (vortex lattice) • panels are plane quadrilaterals and triangles
340 (Geissler)	• singularity method • body modeled using surface distribution of sources, sinks, and vortices • surface of a body of revolution divided into conic frustrums of small axial extension • bodies of revolution only • weighting factors, which are functions of body geometry, are used to combine the singularities
346 (Maskew)	• singularity method • body modeled using surface distribution of quadrilateral vortex rings of constant strength

TABLE XVII.- (Continued)

Group 3.- Linearized, Steady, Compressible Potential Flow Equations

Reference Number	Features of Theoretical Prediction Method
303 (Dillenius)	• singularity method • axisymmetric cross section modeled using 3-D point sources and sinks along body centerline and 2-D doublets in cross-flow plane • wing modeled using constant u-velocity-type panels and constant source-type panels • position of wing leading-edge shock determined using nonlinear correction to linear solution based on wing thickness
304 (Dillenius)	• singularity method • axisymmetric cross section modeled same as that for reference 303 • noncircular cross section modeled using 3-D point sources and sinks along centerline of equivalent body and polar harmonics and 2-D sources in cross-flow plane • wing-fuselage interference modeled using vortex-lattice model with imaging • wing modeled using 3-D source panels on wing surface
309 (Woodward)	• singularity method • constant source distribution on body panels • linearly varying vortex distribution on wing panels
308 (Woodward)	• singularity method • wing modeled using a surface distribution of vorticity and sources

TABLE XVII.- (Continued)

Group 3.- (Continued)

Reference Number	Features of Theoretical Prediction Method
308 (cont.)	• fuselage modeled using line sources and doublets distributed along body centerline • wing-body-interference modeled using a surface distribution of vorticity on the body in the region of influence of wing-body intersection
318 (Morino)	• finite-element method • surface of body divided into small hyperboloidal elements • potential and normal derivative of potential within each element are constant at the element centroid
349,350 (Ehlers)	• singularity method • planar source and doublet panels • source distribution varies linearly, doublet distribution varies quadratically • in reference 349, there is a single quadratic distribution of doublet strength over each quadrilateral panel • in reference 350, each quadrilateral panel is divided into eight triangular subpanels in such a way that all panel edges are contiguous with adjacent panels; separate quadratic distributions over each triangular subpanel are prescribed
347 (AEDC)	• singularity method • configuration modeled using surface distribution of vorticity and sources
348 (Johnson)	• singularity method • curved source and doublet panels • singularity strengths vary as polynomials

TABLE XVII.- (Continued)

Group 4.- Unsteady, Compressible, Linearized Potential Flow Equations

Reference Number	Features of Theoretical Prediction Method
319 (Morino)	• finite-element method

Group 5.- Full Compressible Potential Flow Equations

Reference Number	Features of Theoretical Prediction Method
215 (Reyhner)	• finite-difference relaxation method • mixed-difference scheme • subsonic free stream only (within transonic range)
290 (South)	• finite-difference relaxation method • modified mixed-difference scheme: difference scheme simulates differencing along and normal to local velocity vector • subsonic and supersonic free stream (within transonic range)

TABLE XVII.- (Continued)

Group 6.- Steady Euler Equations

Reference Number	Features of Theoretical Prediction Method
34 (Prokop)	• reference plane-type method (flow properties calculated for several planes around periphery of body, each emanating from centerline) • two-dimensional shock-expansion method; conical method of Ferri, two-dimensional m.o.c. or axisymmetric m.o.c. used to obtain flow solutions for each plane • transverse flow effects between adjacent planes accounted for using a wave-interference calculation which modifies static pressure and streamline direction at each point of interest • effects of canopy and fuselage corner modeled using Prandtl-Meyer expansions
151 (Kutler), 306 (Solomon)	• shock-capturing technique • MacCormack's second-order predictor-corrector method • conservative form of equations of motion • embedded shocks
152 (Marconi), 305 (Moretti)	• shock-fitting technique • MacCormack's second-order predictor-corrector method • non-conservative form of equations of motion • embedded shocks
153 (D'Attorre)	• shock-capturing technique • Lax-Wendroff finite-difference method • conservative form of equations of motion • embedded shocks

TABLE XVII.- (Continued)

Group 6.- (Continued)

Reference Number	Features of Theoretical Prediction Method
289 (Thomas)	• shock-fitting technique • MacCormack's second-order predictor-corrector method • non-conservative form of equations of motion • no embedded shocks
293 (Walkden)	• shock-capturing technique • pseudo method of characteristics method • non-conservative form of equations of motion • embedded shocks
297 (Rakich)	• method of characteristics (reference plane, or semi-characteristic, method) • MacCormack's second-order predictor-corrector used to obtain cross derivatives • embedded shocks
324 (Inouye)	• inverse, integral method (shock shape assumed and equations of motion integrated numerically by finite-difference method to determine corresponding body shape) • predictor-corrector scheme for subsonic and transonic regions • method of characteristics used in supersonic region • iterative process used for embedded shocks
337 (Chu)	• method of characteristics

TABLE XVII.- (Continued)

Group 6.- (Concluded)

Reference Number	Features of Theoretical Prediction Method
337 (cont.)	• bicharacteristic, inverse redundant method (employ governing differential equations along generators of Mach cone through a point in flow) • embedded shocks
375 (Babenko)	• semi-implicit finite-difference scheme • non-conservative form of equations of motion

TABLE XVII.- (Continued)

Group 7.- Unsteady Euler Equations

Reference Number	Features of Theoretical Prediction Method
291 (Li)	• Euler equations are linearized, then reduced to one equation throught the use of a potential function • boundary conditions satisfied at body, then solution worked outward toward infinity
311 (Pulliam), 312 (Kutler)	• shock-capturing technique • conservative form of equations of motion • embedded shocks • implicit approximate factorization finite-difference technique
373 (Moretti)	• four-dimensional method of characteristics used to determine quantities at shock points and body points • time-dependent explicit Lax-Wendroff type numerical scheme used to determine quantities within shock layer

TABLE XVII.- (Continued)

Group 8.- Unsteady, Incompressible Navier-Stokes Equations

Reference Number	Features of Theoretical Prediction Method
316 (Mastin)	• two partially implicit finite-difference formulations of Navier-Stokes equations developed 1. one-step first-order time differencing scheme viscous and pressure terms treated implicitly successive overrelaxation method used 2. two-step projection method pressure equation uncoupled from momentum equation successive overrelaxation method used • body-fitted curvilinear coordinate system used

TABLE XVII.- (Continued)

Group 9.- Unsteady, Compressible Navier-Stokes Equations

Reference Number	Features of Theoretical Prediction Method
311 (Pulliam), 312 (Kutler)	• shock-capturing technique • conservative form of equations of motion • embedded shocks • implicit approximate factorization finite-difference technique (noniterative, alternating direction implicit) • "thin-layer" approximation used to handle viscous effects • high Reynolds number flows only
314 (Viviand)	• shock-fitting technique • MacCormack's second-order predictor-corrector method • non-conservative form of equations of motion • no embedded shocks
383 (McRae)	• conical symmetry assumption applied to full Navier-Stokes equations • shock-capturing technique • MacCormack's second-order predictor-corrector method • weak conservation form of equations of motion • embedded shocks

For refs. 314 and 383: laminar or turbulent boundary layer can be used.

TABLE XVII.- (Continued)

Group 10.- Steady, Compressible, Viscous Flow

Reference Number	Features of Theoretical Prediction Method
292 (Walitt)	• Hayes' Equivalence Principle used to relate the time-dependent 2-D flow to a steady 3-D flow
	• Navier-Stokes equation solved in cross-flow plane using finite-difference method
	• simultaneous solution of laminar boundary layer and inviscid flow field
	• inviscid axial flow, axial effects neglected
	• laminar boundary layer (2-D)
374 (Walitt)	• steady-state axisymmetric flow field made analogous to time-dependent 1-D flow using Hayes' Equivalence Principle
	• "full" Navier-Stokes equations for axisymmetric flow solved by iteration
	• inviscid axial flow, axial effects included
	• turbulent or laminar boundary layer (1-D, corrected for axial symmetry)
393 (Rakich)	• parabolized Navier-Stokes equations (streamwise viscous derivatives neglected; rules out streamwise separation but allows crossflow separation)
	• laminar and turbulent boundary layers
	• implicit factorization method of Beam & Warming used
	• conservative form of equations of motion
395 (Schiff)	• parabolized Navier-Stokes equation
	• "thin-layer" approximation used to handle viscous effects
	• high Reynolds number flows only
	• conservative form of equations of motion

TABLE XVII.- (Continued)

Group 11.- 3-D Transonic Small-Disturbance Theory

Reference Number	Features of Theoretical Prediction Method
298 (Bailey)	• equations derived from transonic small disturbance theory under assumptions of small flow deflections and free-stream Mach number near unity • finite-difference method based on relaxation method of Murman & Cole • shock-capturing technique • mixed-difference scheme • handles subsonic upstream/supersonic downstream and supersonic upstream/subsonic downstream conditions • can use fully conservative or nonconservative differencing
296 (Mason)	• inviscid method is that of references 298,299 • viscous effects on the wing also included
299 (Ballhaus)	• several modified 3-D transonic small-disturbance equations introduced to improve prediction of shocks • other techniques mentioned for reference 298 also apply

TABLE XVII.- (Continued)

Group 12.- Transonic Equivalence Rule

Reference Number	Features of Theoretical Prediction Method
341 (Stahara)	• total solution made up of inner solution, far-field behavior of inner solution, and outer solution • inner solution: - superposition of solutions to thickness and lift problems obtained from 2-D Laplace equation in cross flow plane at each x-station - thickness solution obtained using method of distributed singularities developed by Stocker - lift solution obtained using analytic conformal mapping solution determined by Spreiter for circular body with mid-mounted zero-thickness wings • outer solution: - 3-D nonlinear transonic differential equation is solved - wing-body combination is modeled using a line distribution along body axis of a combination of sources (related to total cross-sectional area, axial lift distribution, and spanwise wing loading) and doublets (related to axial lift distribution) - in thickness-dominated domain, basic nonlinear outer flow determined principally by line source distribution. For this case, governing PDE is nonlinear axisymmetric transonic small-disturbance equation which is solved using a finite-difference successive line over-relaxation procedure which uses Murman-Cole type-dependent difference operators - in lift-dominated domain, nonlinear outer flow determined by line source and line doublet distribution

TABLE XVII.- (Concluded)

Group 13.- Far-Field Matching Method

Reference Number	Features of Theoretical Prediction Method
317 (Lee)	• computational field divided into near-field, mid-field, and far-field regions • near-field equations must reduce to subsonic linearized potential flow equations (Prandtl-Glauert) in far-field region • far-field solution is a linear combination of source distributions at the far-field/mid-field boundary and (for lifting flows), a vortex centered somewhere in the near field • near-field is solved using finite-difference methods • mid-field is solved using finite-element methods • present method solves transonic small-disturbance equation in mid-field and near-field

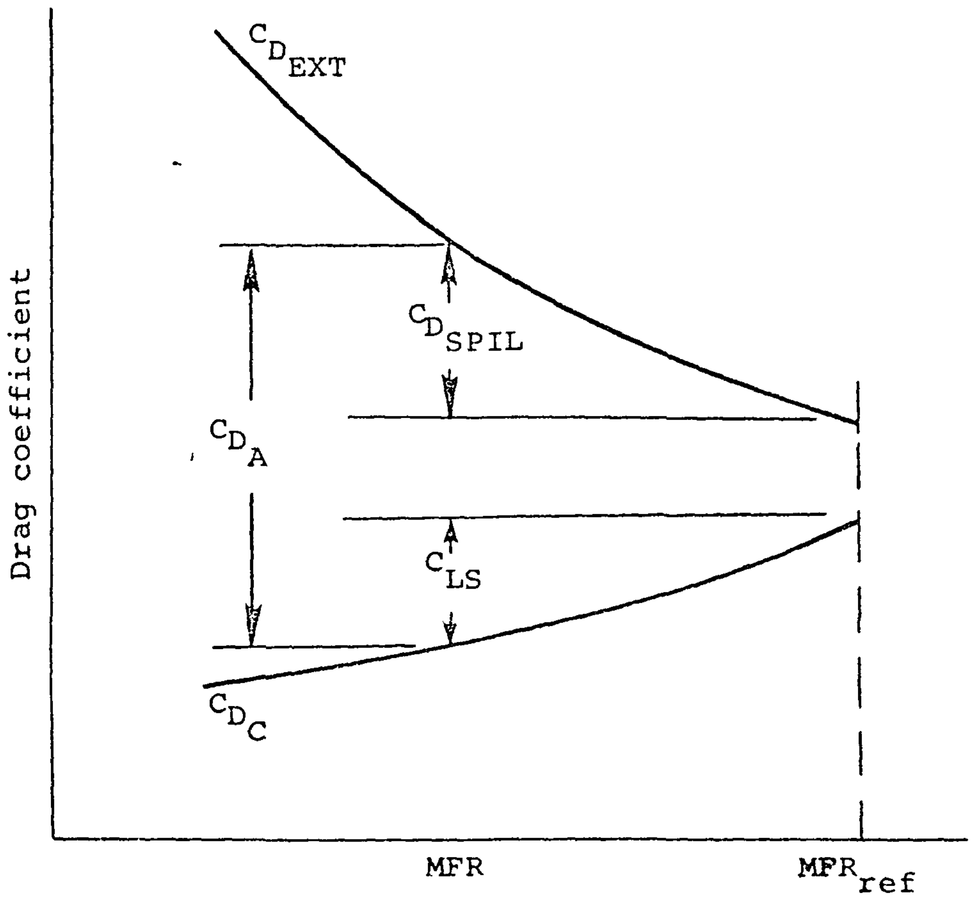

Figure 1.- Inlet external drag terms.

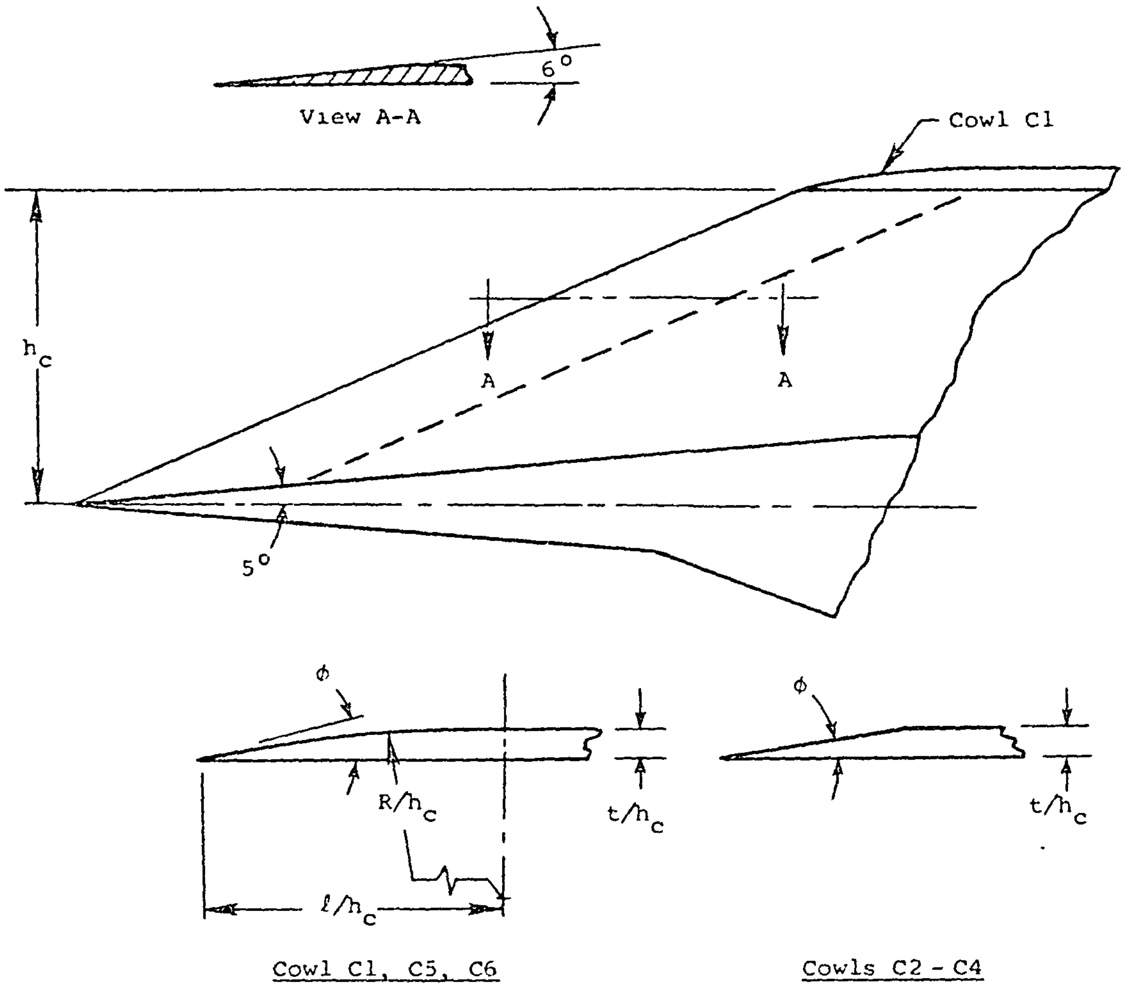

Cowl	ℓ/h_c	R/h_c	t/h_c	ϕ (deg)
C1	1.43	8.22	0.125	10
C2	-	-	0.125	6
C3	-	-	0.125	10
C4	-	-	0.125	15
C5	0.95	3.67	0.125	15
C6	1.90	7.33	0.250	15

(a) Experimental configurations.

Figure 2.- External drag for various cowls from reference 33 (2-D inlet).

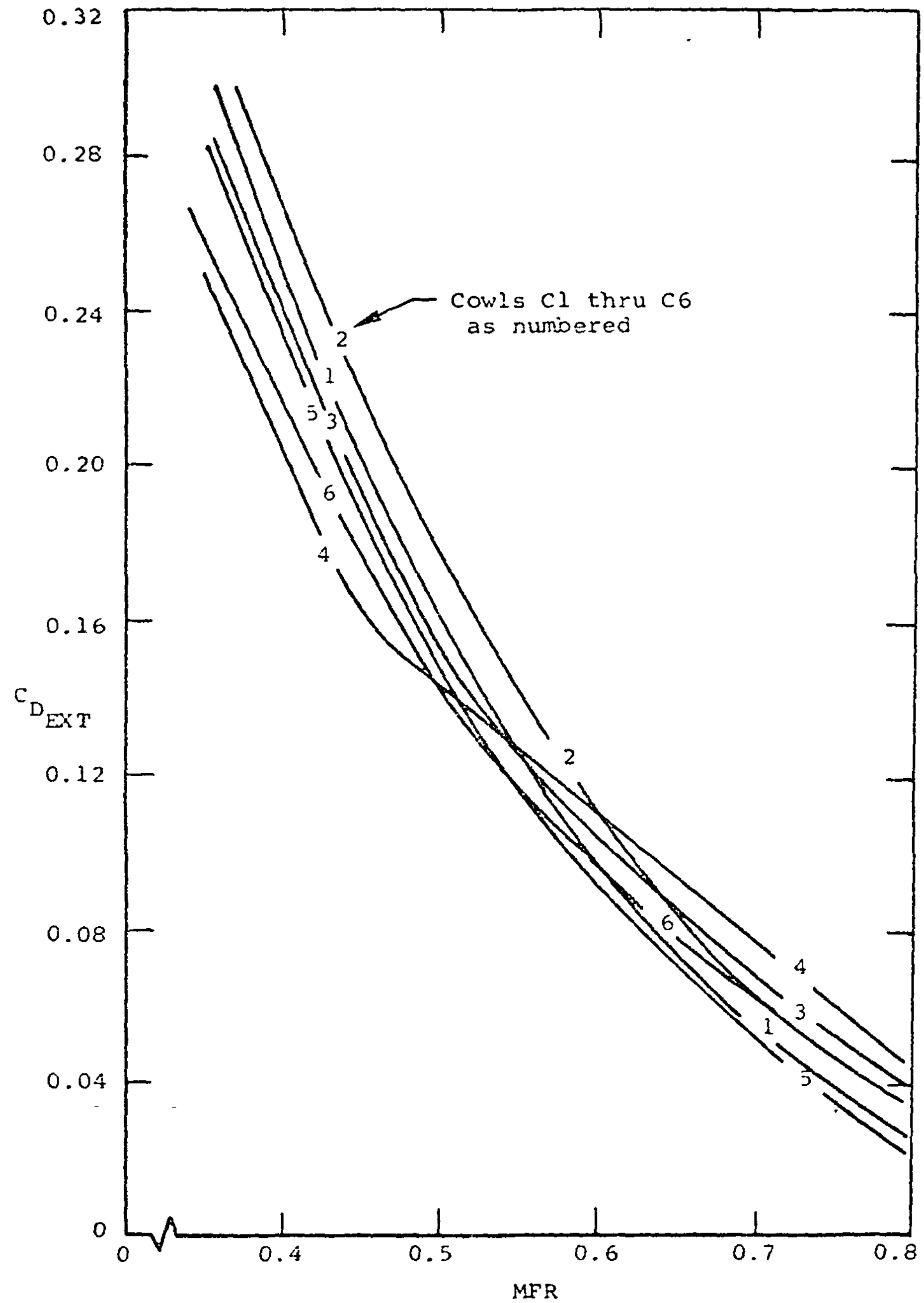

(b) M_∞ = 0.84.

Figure 2.- Continued.

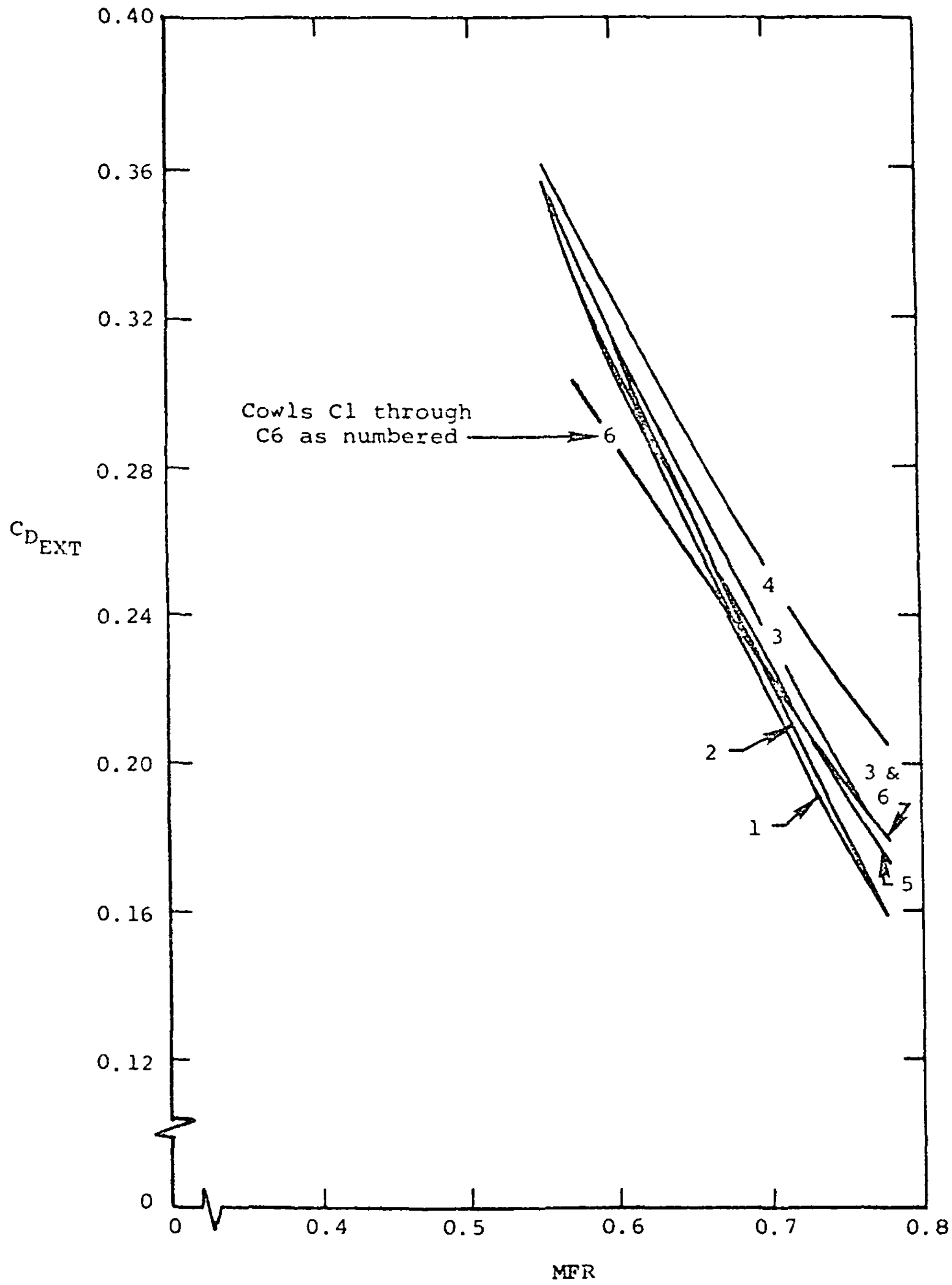

(c) $M_\infty = 1.29$.

Figure 2.- Concluded.

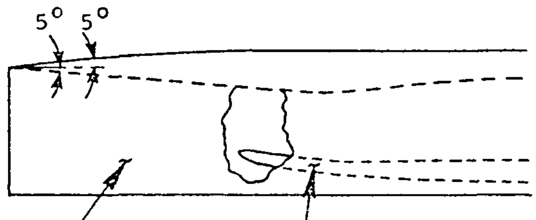

Model assembly. Rectangular sideplate shown.
Alternate sideplate leading edge is swept from
ramp leading edge to cowl lip leading edge.

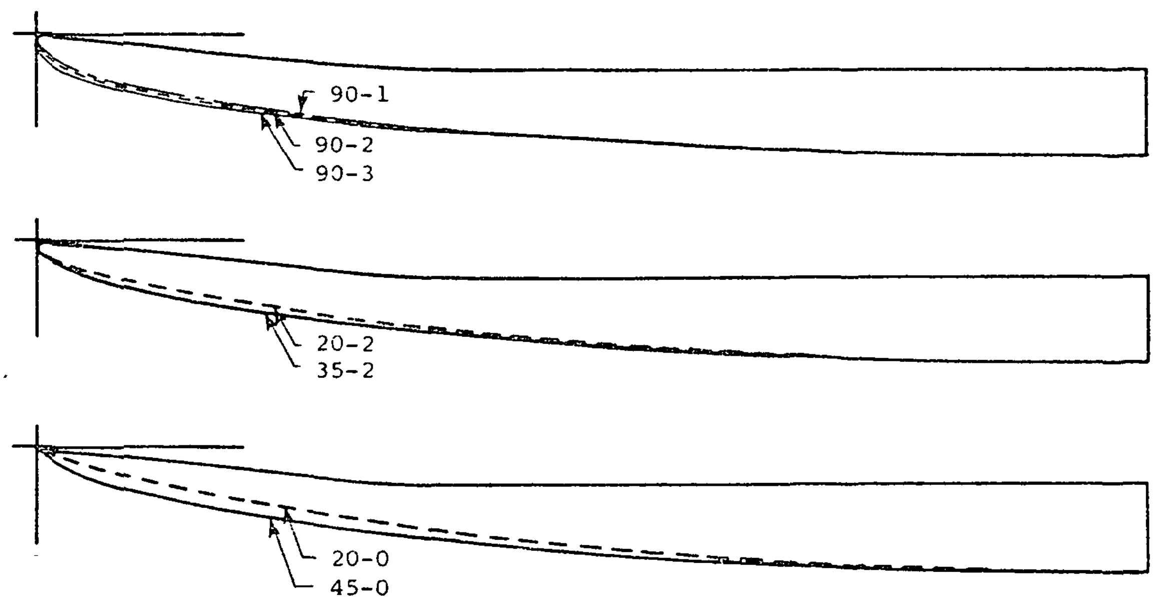

Cowl lip shapes

(a) Experimental configurations.

Figure 3.- External drag for various cowls from
reference 107 (2-D inlet).

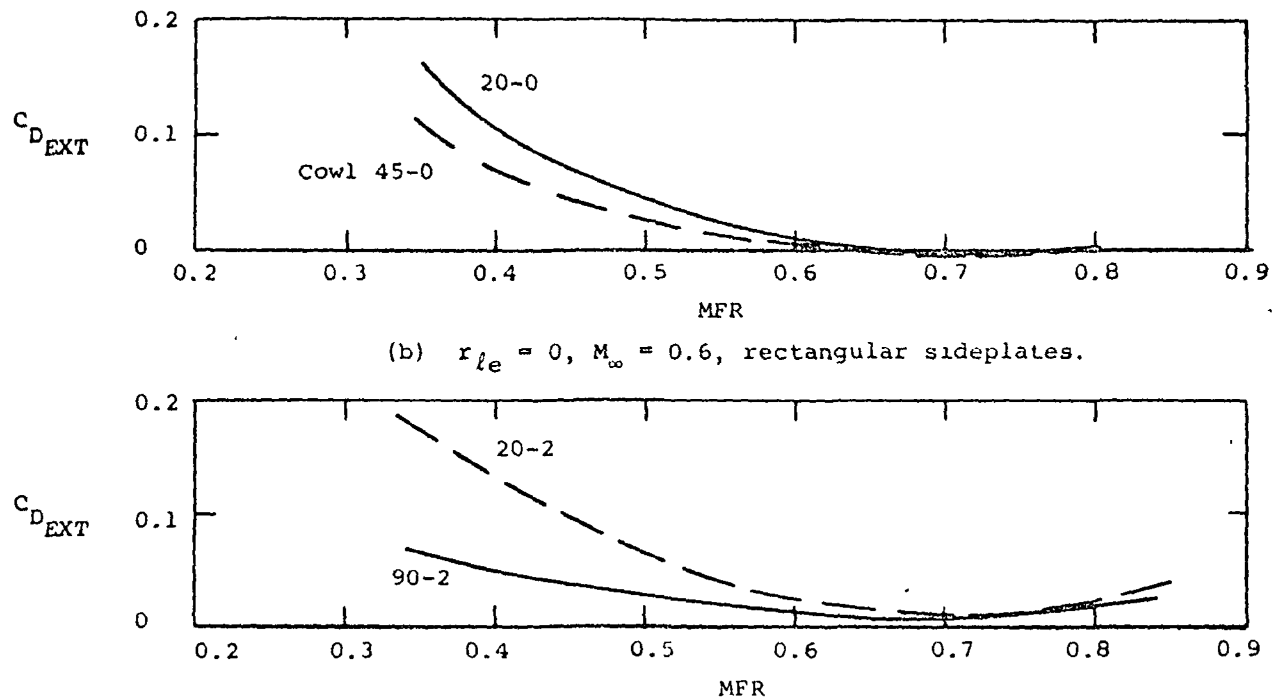

(b) $r_{\ell e} = 0$, $M_\infty = 0.6$, rectangular sideplates.

(c) $r_{\ell e} = 0.254$ cm, $M_\infty = 0.6$, rectangular sideplates.

Figure 3.- Continued.

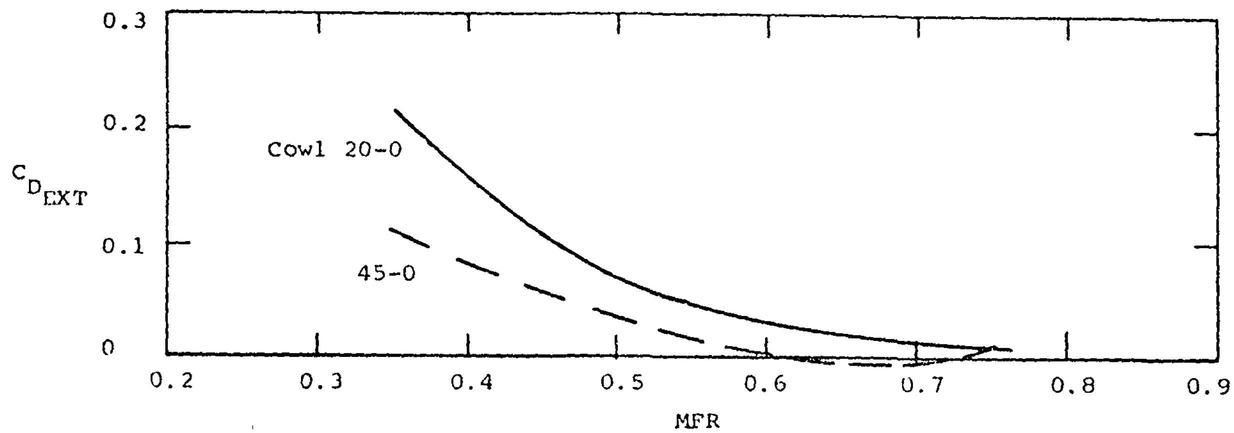

(d) $r_{le} = 0$, $M_\infty = 0.8$, rectangular sideplates.

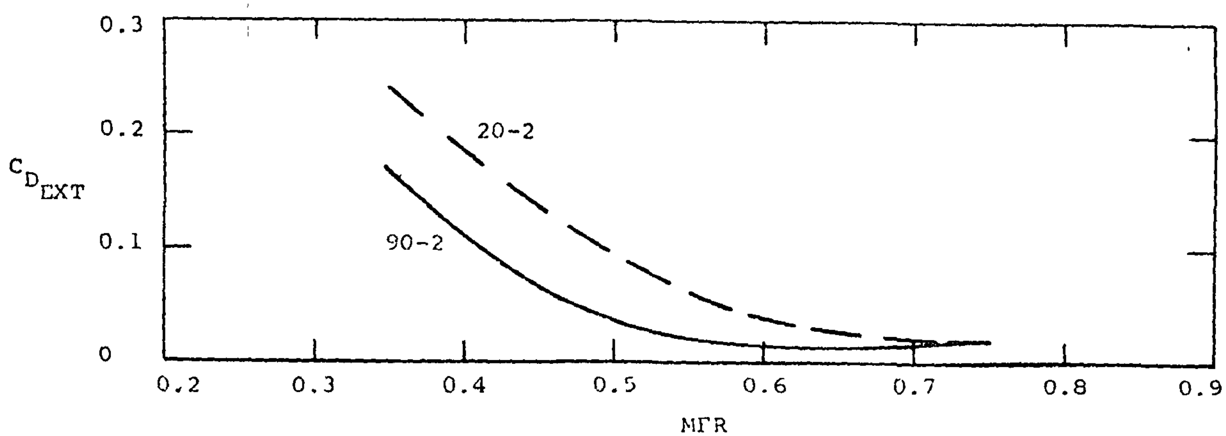

(e) $r_{le} = 0.254$ cm, $M_\infty = 0.8$, rectangular sideplates.

Figure 3.- Concluded.

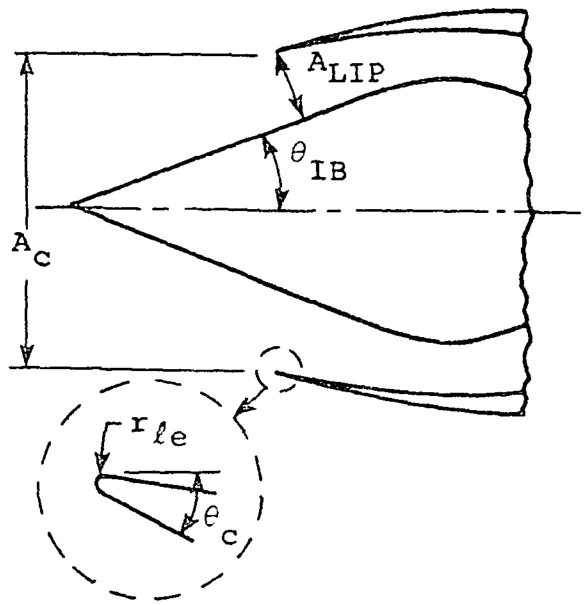

Configuration	θ_c (deg)	$r_{\ell e}$ (cm)	θ_{IB} (deg)	A_{LIP}/A_c
A9 (conical lip)	15	0.020	20	0.619
A18 (elliptical lip)	NACA	0.020	20	0.619

(a) Experimental configurations.

Figure 4.- External drag for two cowls from reference 27 (axisymmetric inlet).

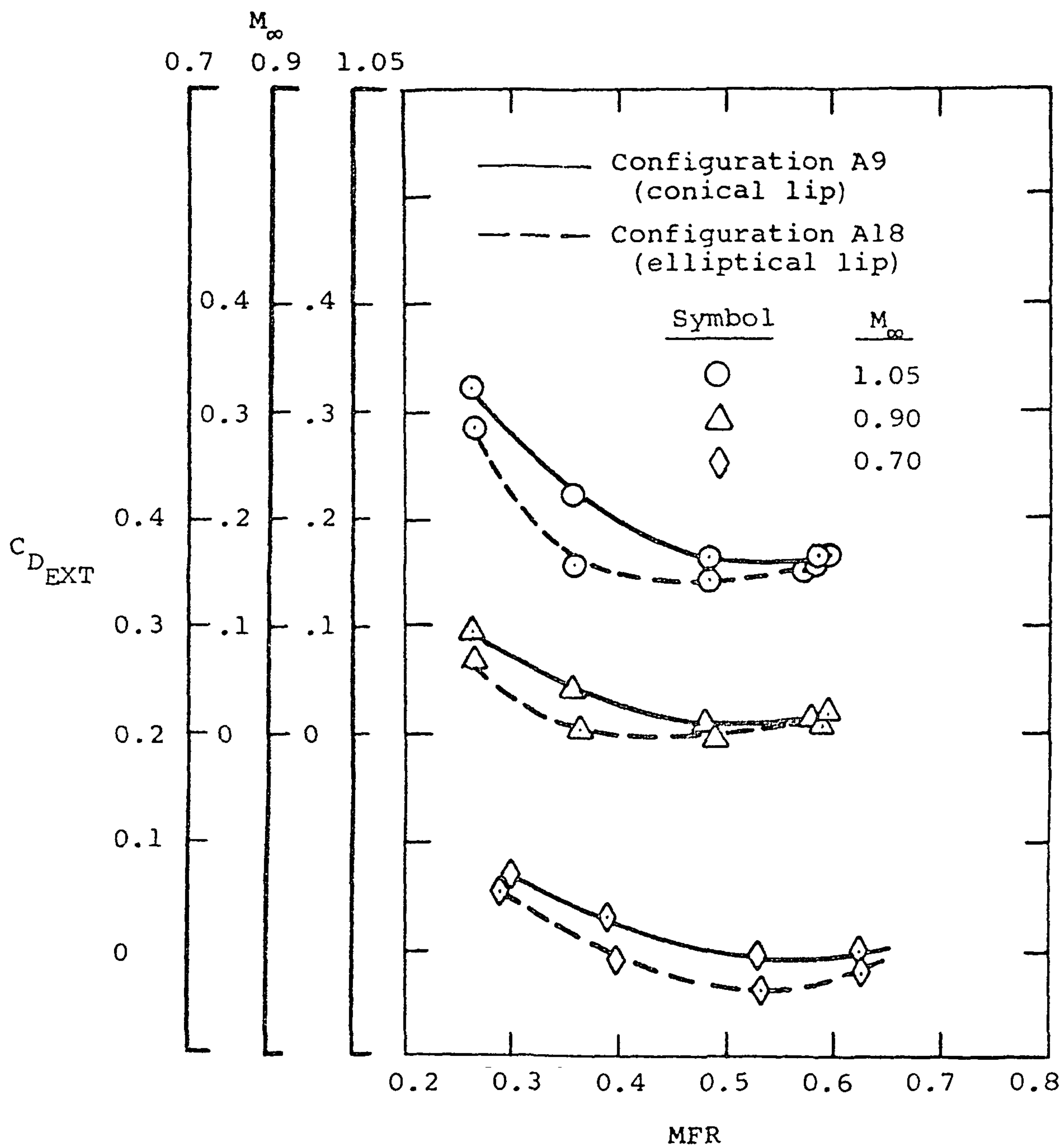

(b) External drag data.

Figure 4.- Concluded.

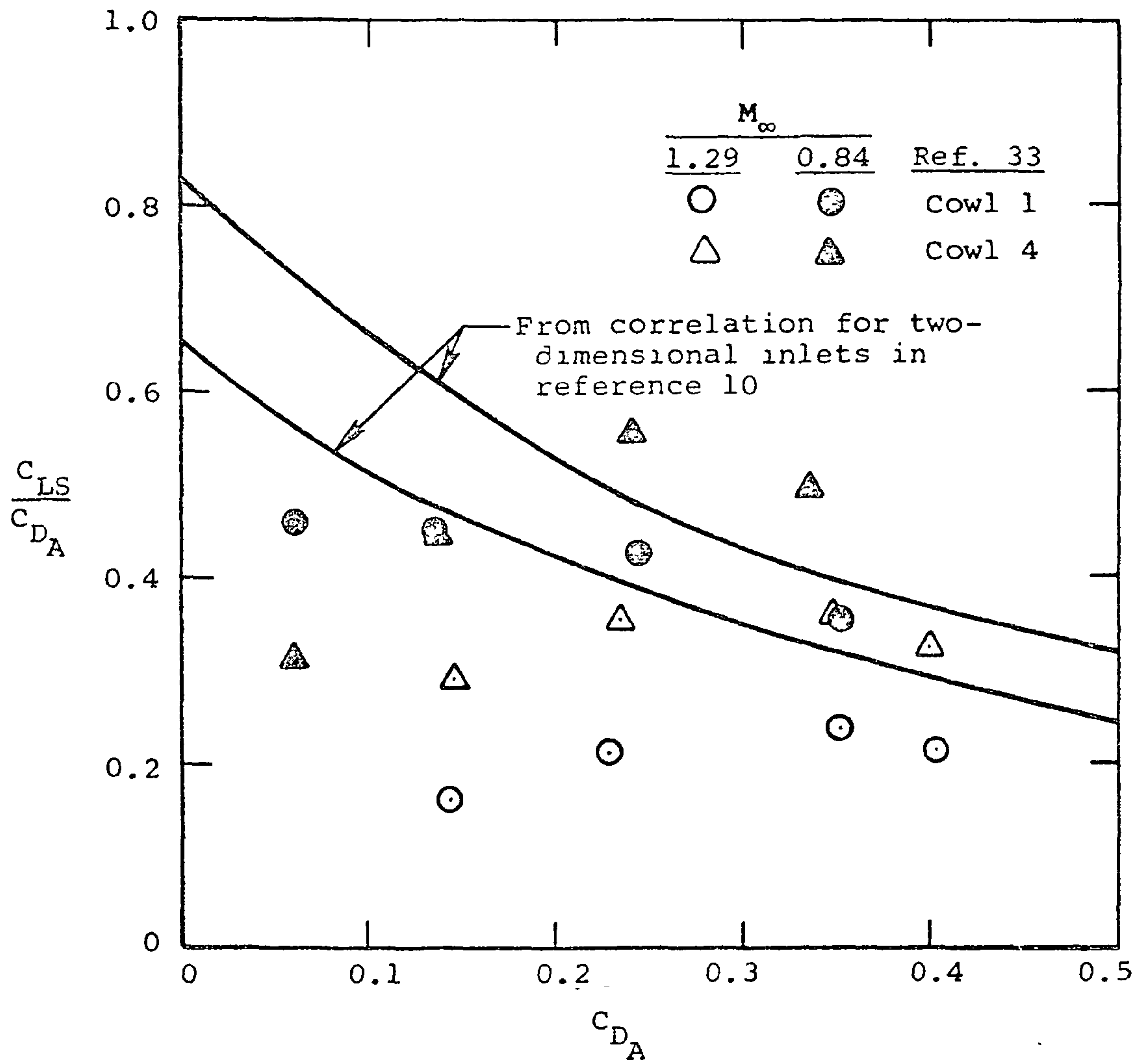

Figure 5.- Comparison of the lip suction correlation of reference 10 with data from reference 33. See figure 2(a) for experimental geometry.

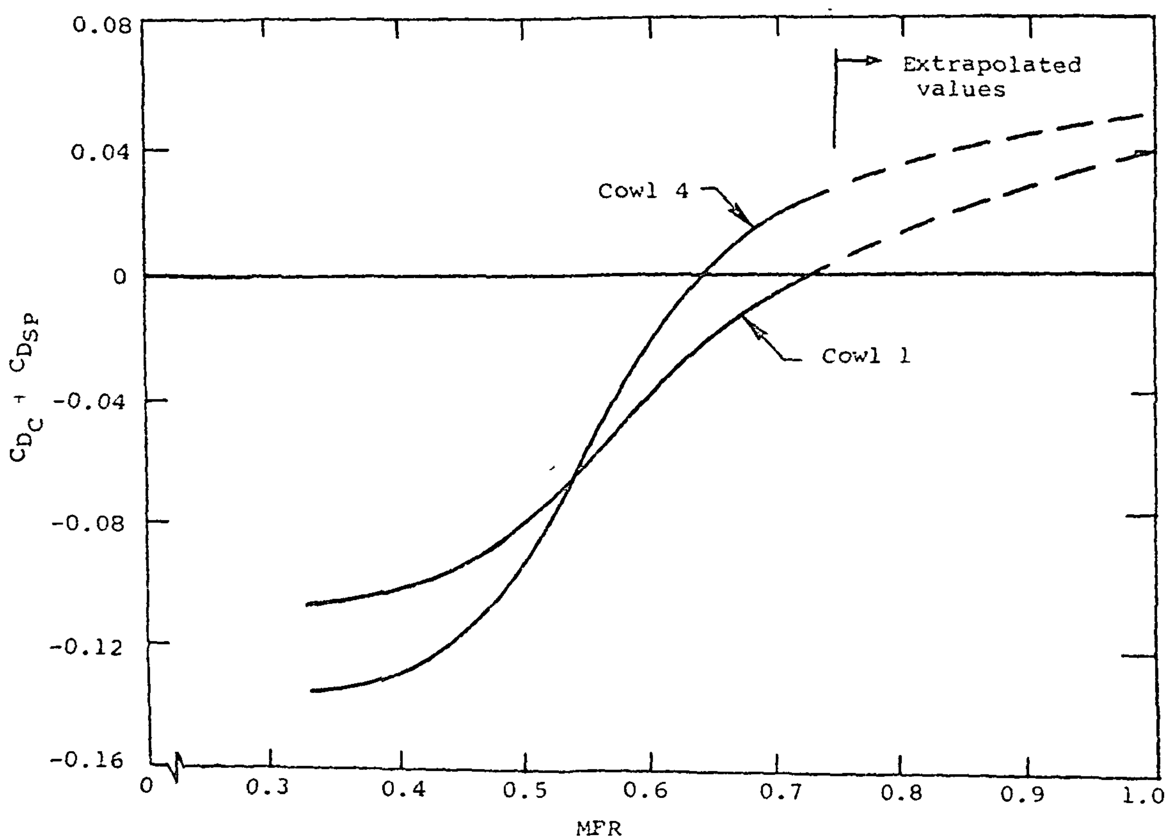

Figure 6.- Extrapolations required to calculate C_{LS} from data of reference 33 ($M_\infty = 0.84$). See figure 2(a) for experimental geometry.

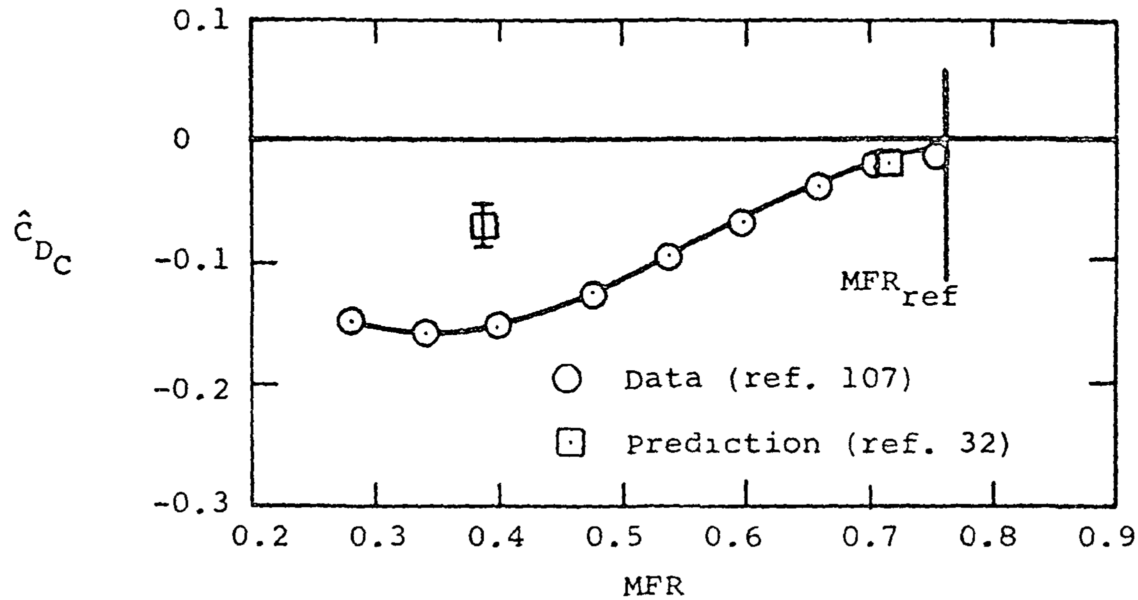

(a) Cowl 90-1, rectangular side plates.

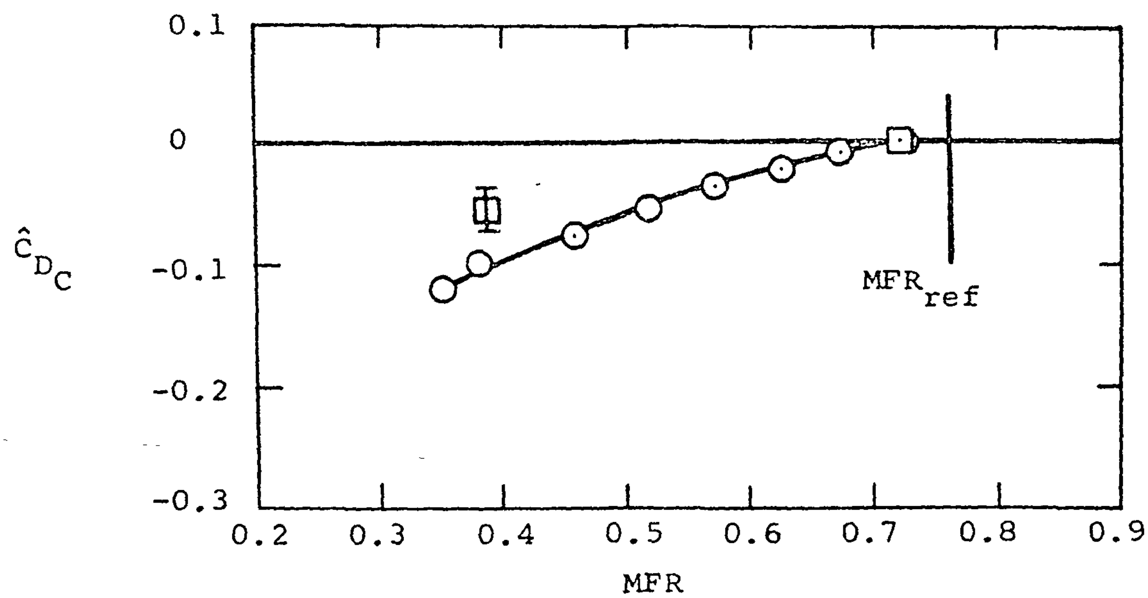

(b) Cowl 90-1, triangular side plates.

Figure 7.- Comparison of lip suction from the method of reference 32 with the data of reference 107; $\alpha = 0$, $M_\infty = 0.8$. See figure 3(a) for experimental geometry.

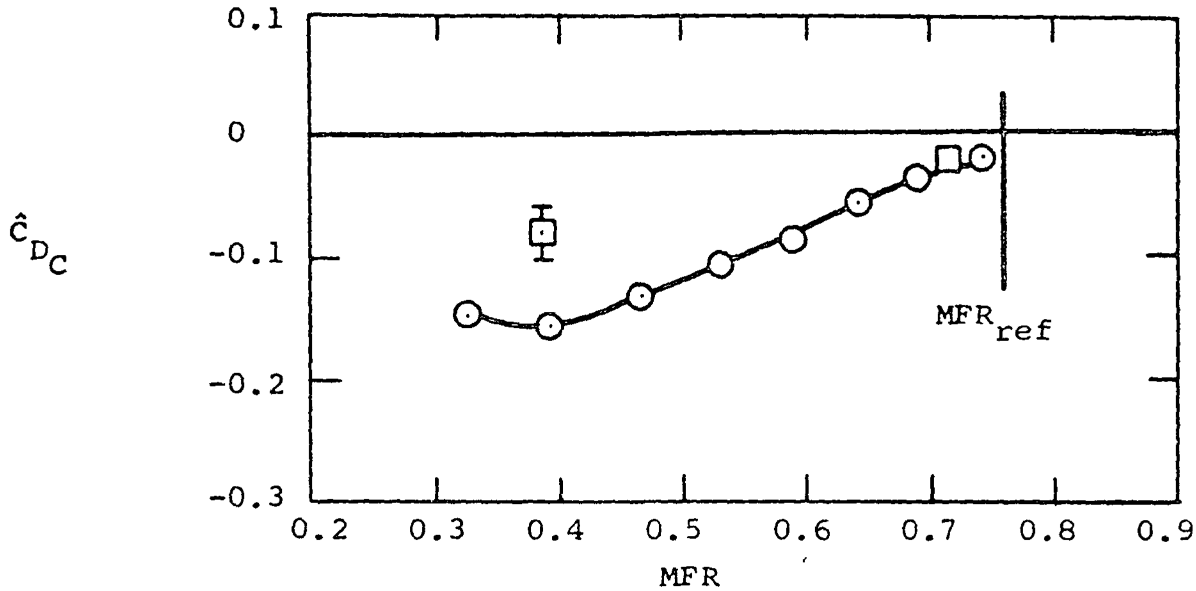

(c) Cowl 90-2, rectangular side plates.

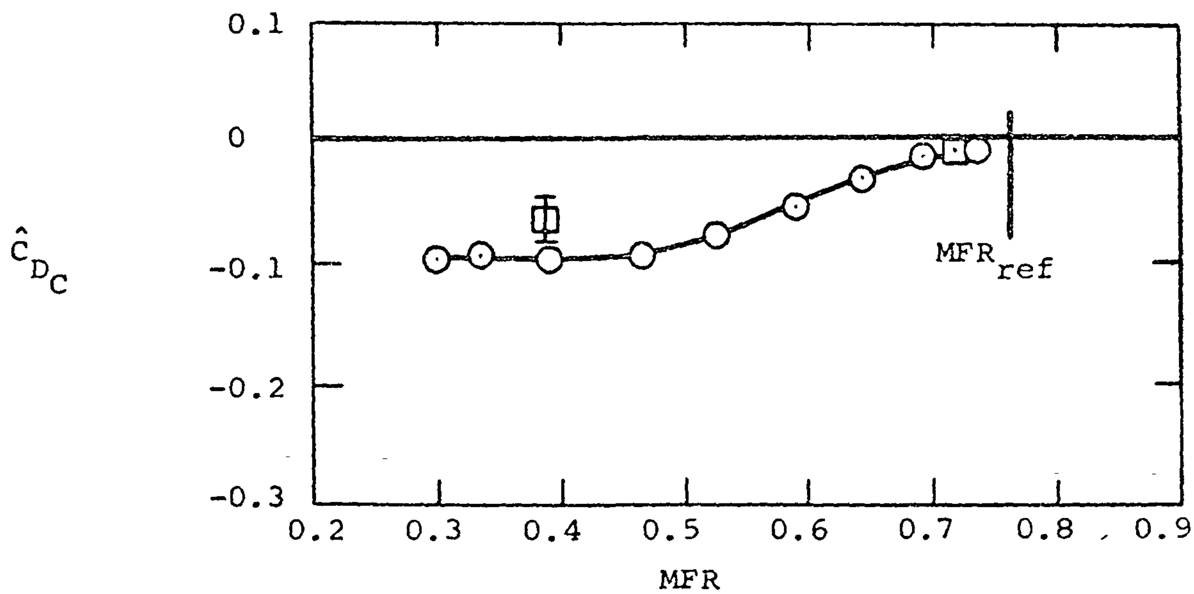

(d) Cowl 20-2, rectangular side plates.

Figure 7.- Concluded.

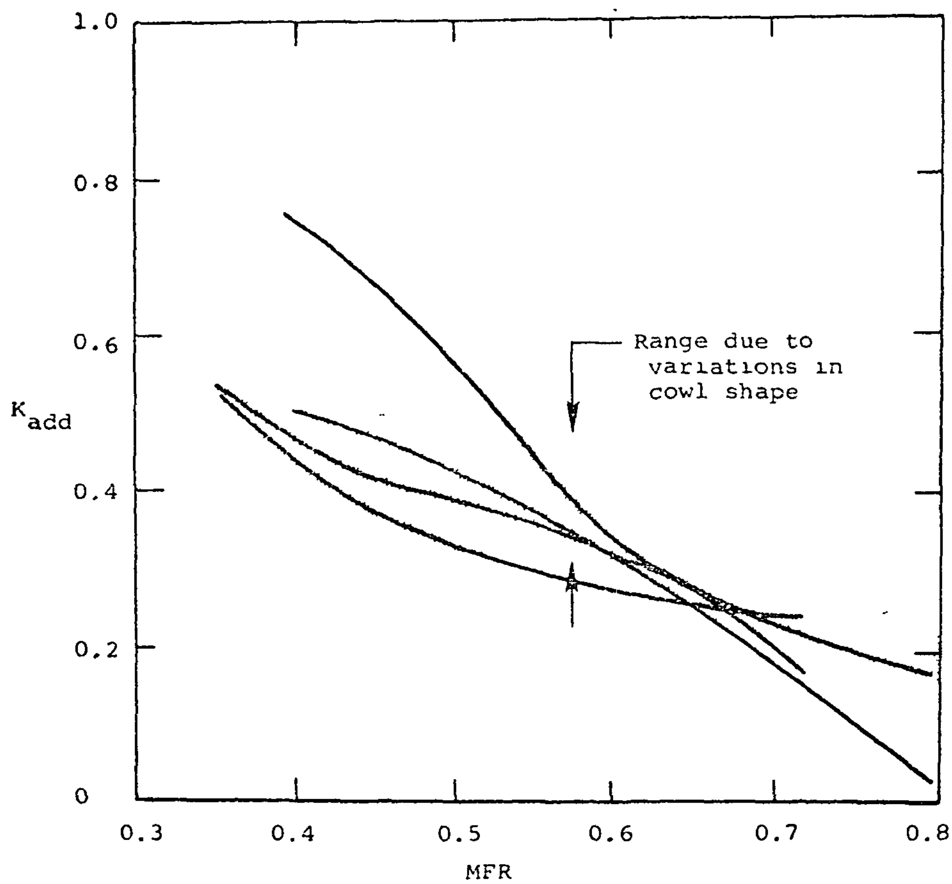

(a) $M_\infty = 0.7$.

Figure 8.- Variation of K_{add} with mass flow ratio from reference 33; two-dimensional, two-ramp, external compression inlets with design Mach number = 3.0.

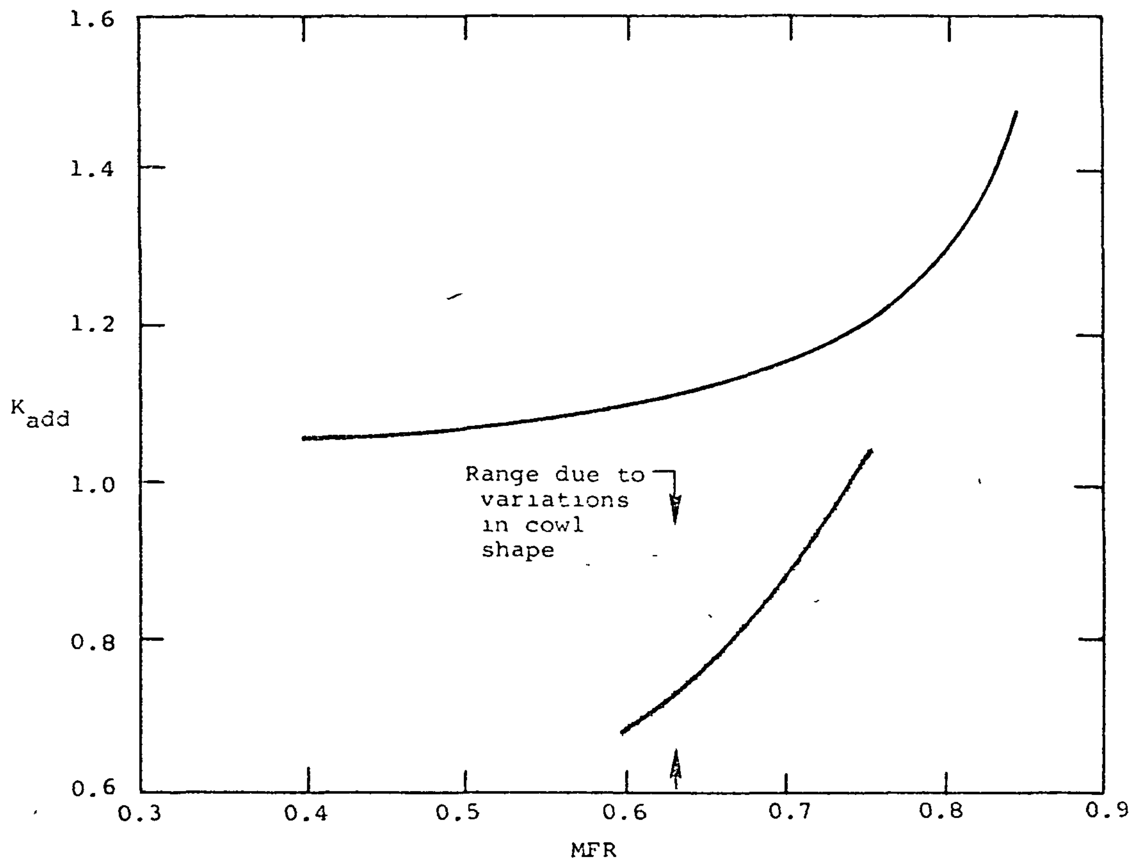

(b) $M_\infty = 1.3$.

Figure 8.- Concluded.

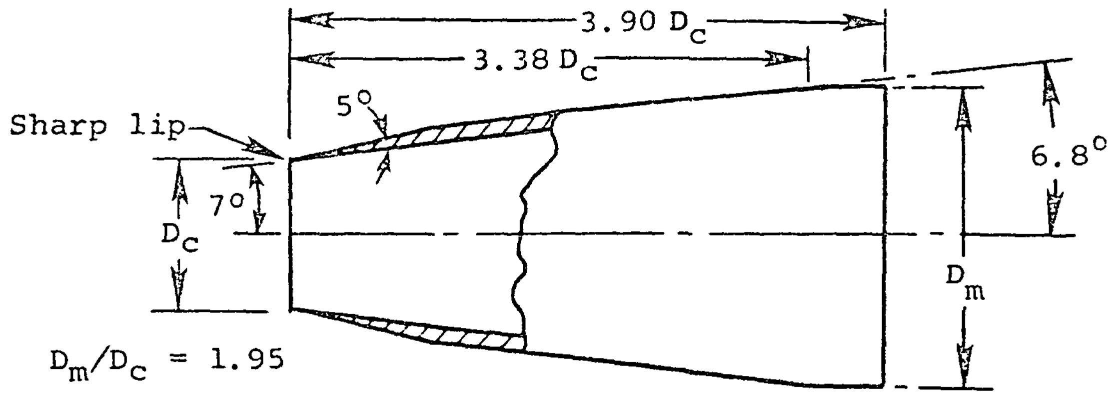

MODEL 25-1

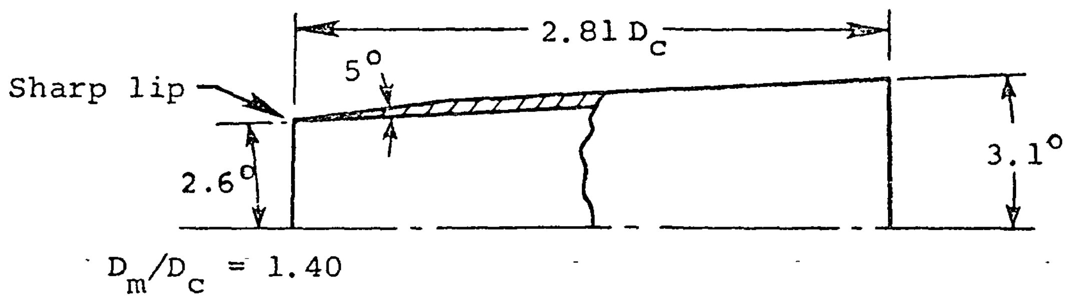

MODEL 50-1

Figure 9.- Experimental configurations (ref. 59) for comparison of experimental and theoretical inlet drag shown in figure 10.

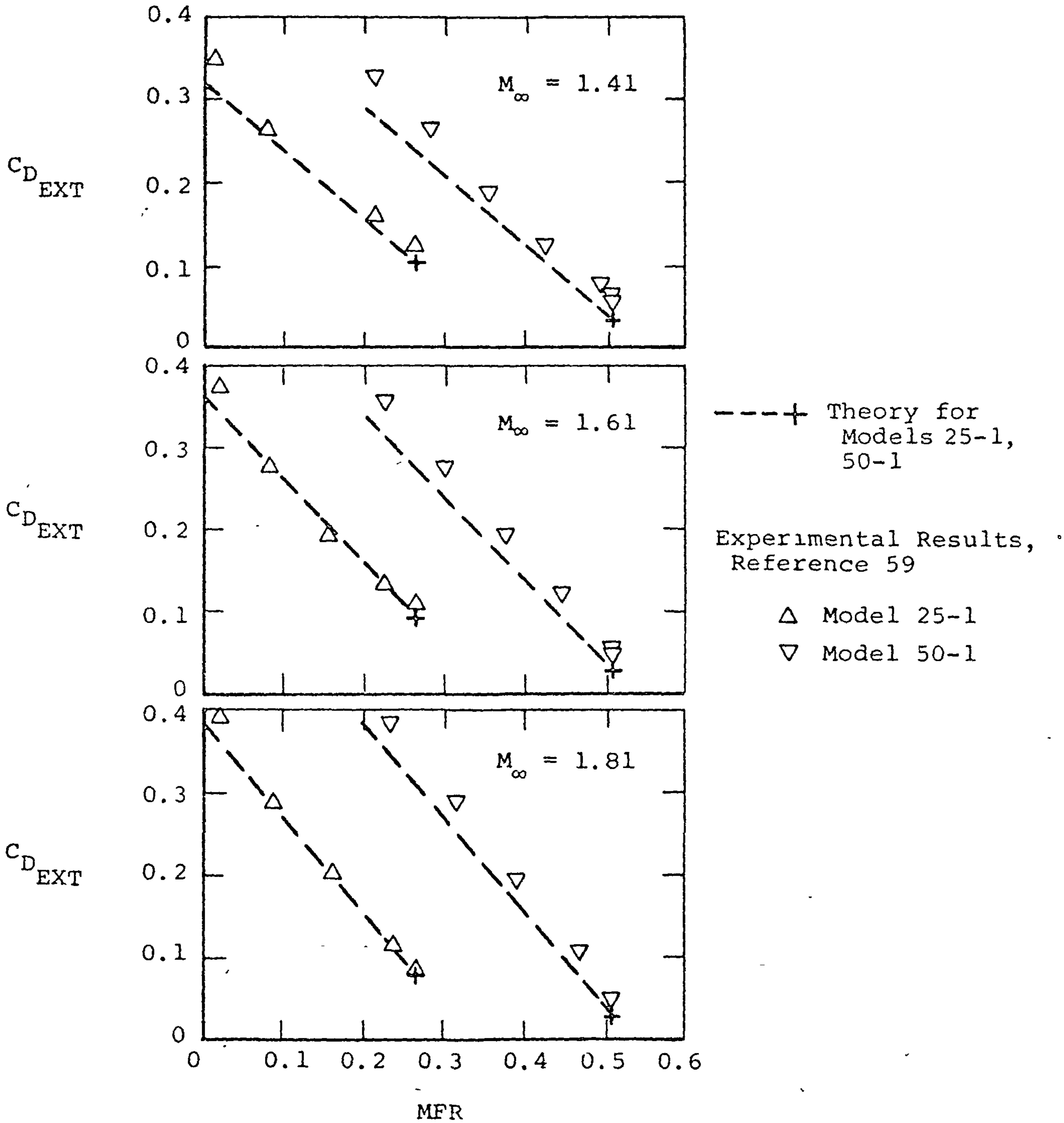

External drag data

Figure 10.- Comparison of experimental and theoretical inlet drag for axisymmetric pitot inlets from reference 21.

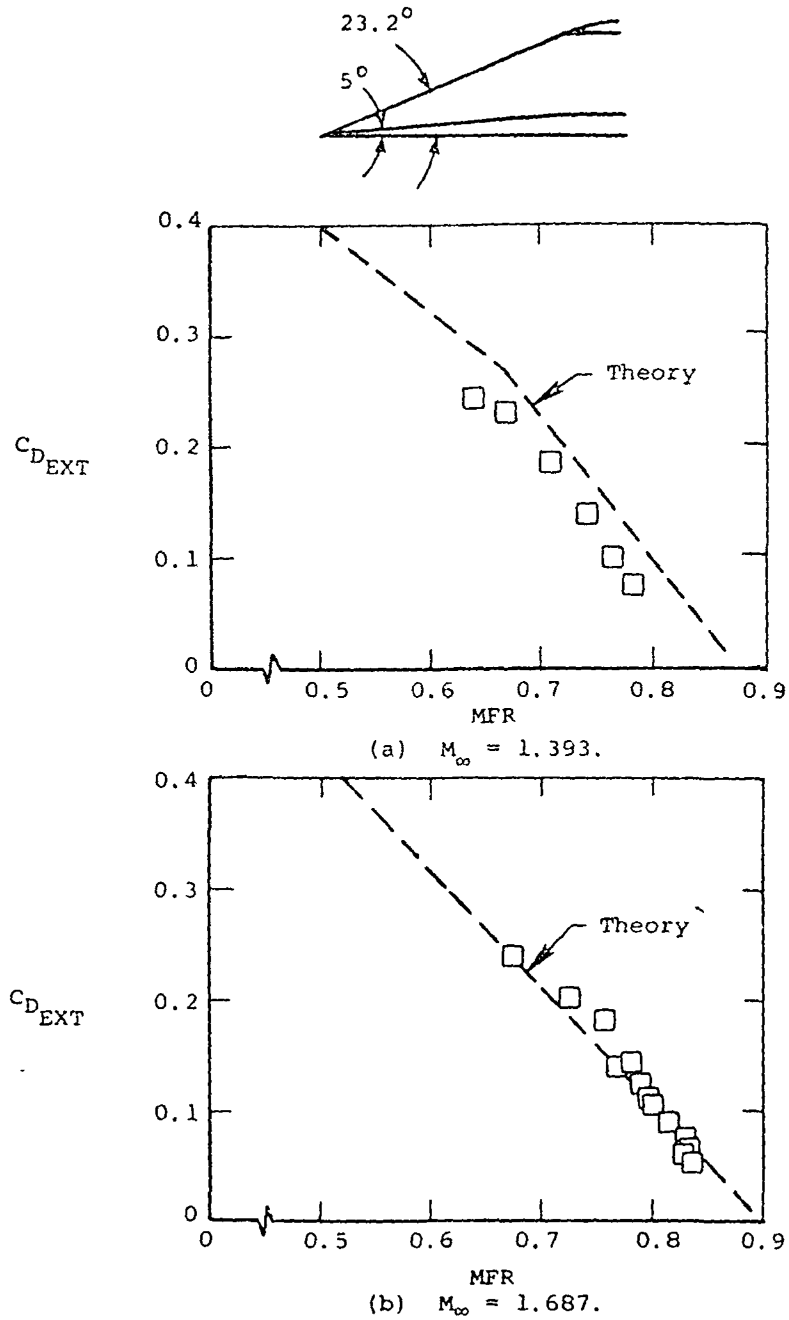

Figure 11.- Comparison of experimental and theoretical inlet drag for a two-dimensional inlet from reference 21. Data from reference 33.

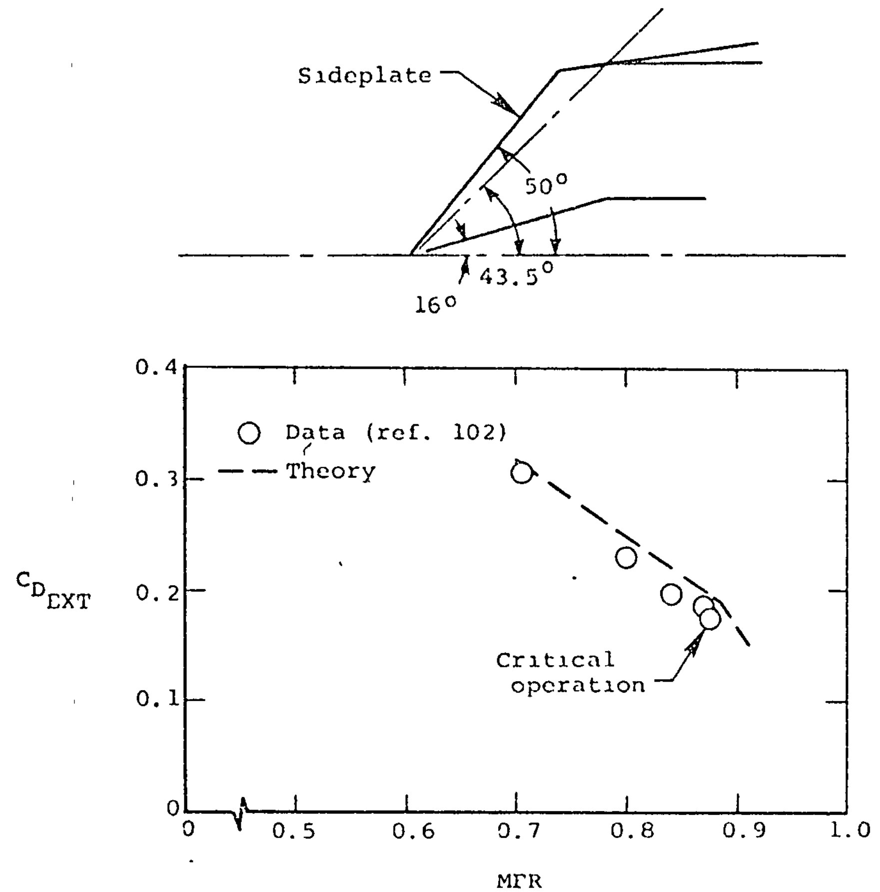

(a) Comparison from reference 21.
Data from reference 102. $M_\infty = 1.86$.

Figure 12.- Comparison of experimental and theoretical inlet drag for a two-dimensional inlet.

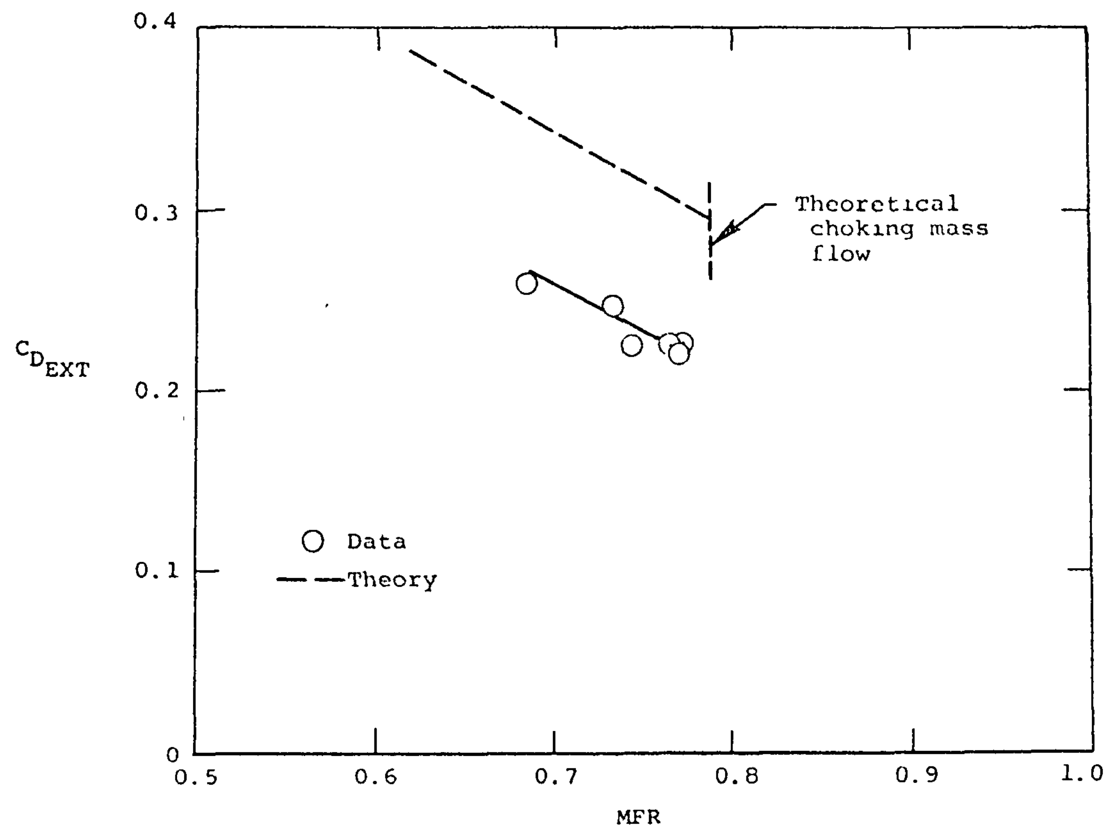

(b) Comparison and data from reference 102. $M_\infty = 1.56$.

Figure 12.- Concluded.

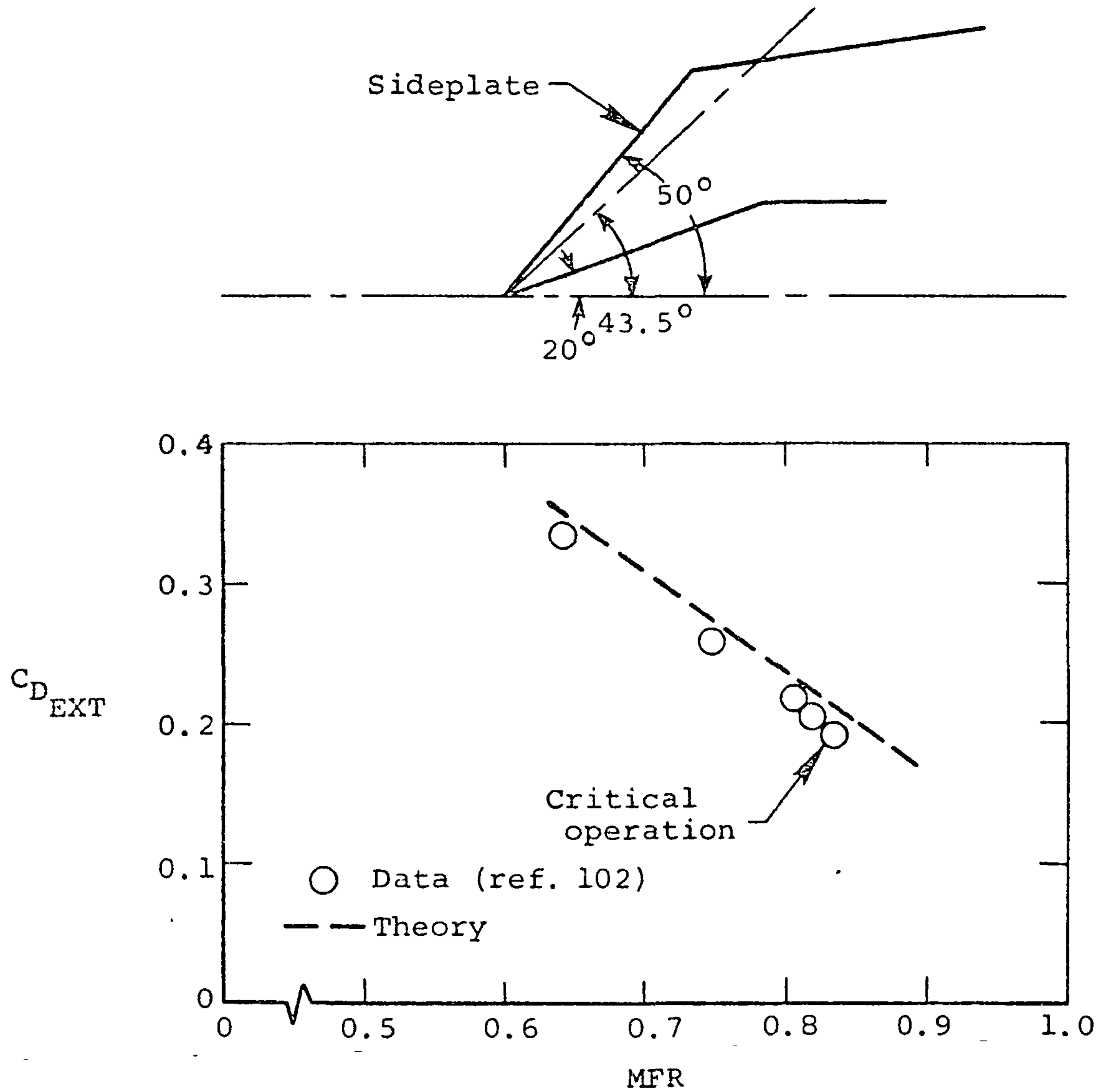

Figure 13.- Comparison of experimental and theoretical inlet drag for a two-dimensional inlet from reference 21. Data from reference 102. $M_\infty = 1.86$.

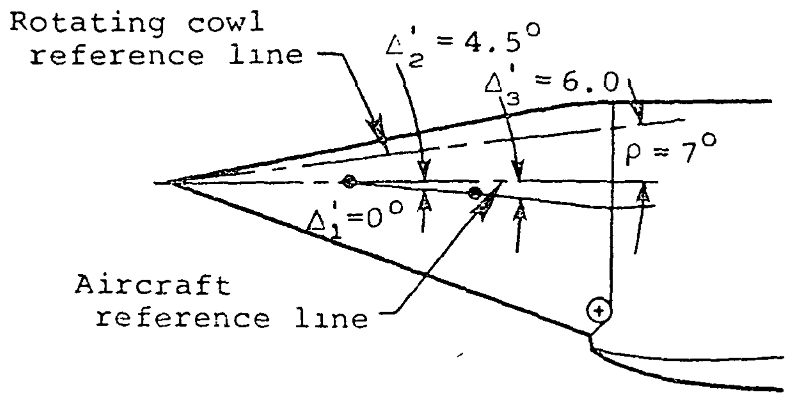

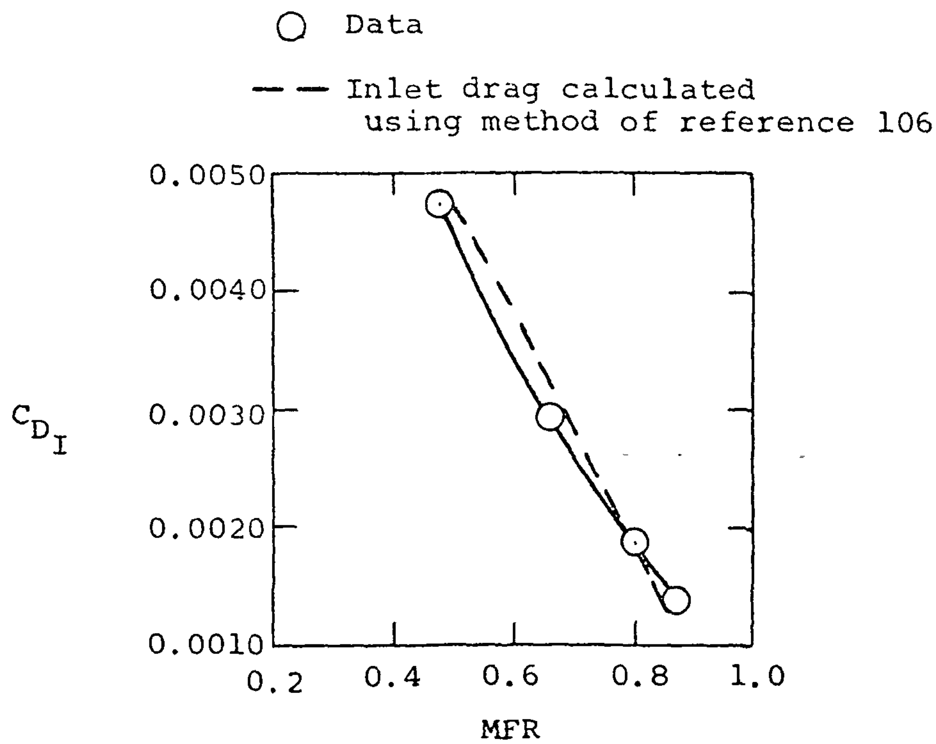

Figure 14.- Comparison of experimental and theoretical inlet drag from reference 224. $M_\infty = 1.5$.

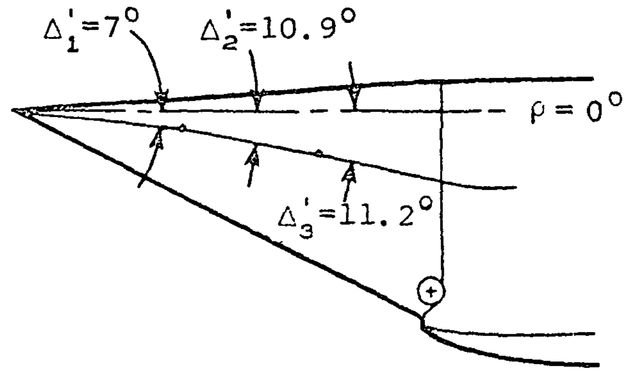

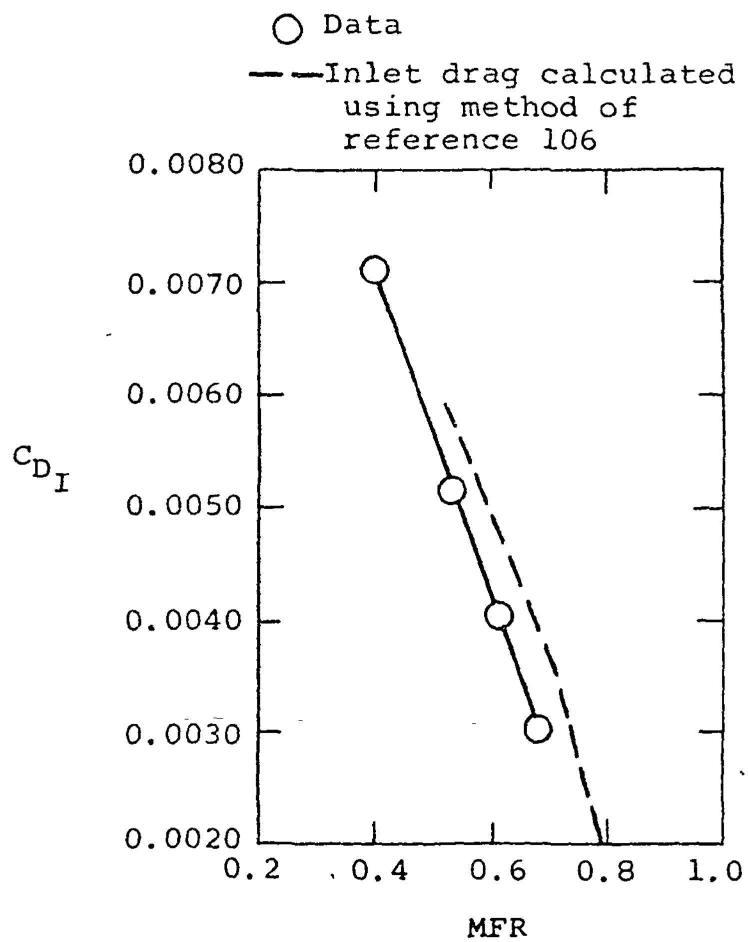

Figure 15.- Comparison of experimental and theoretical inlet drag from reference 224. $M_\infty = 1.5$.

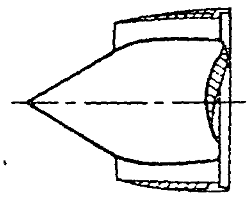

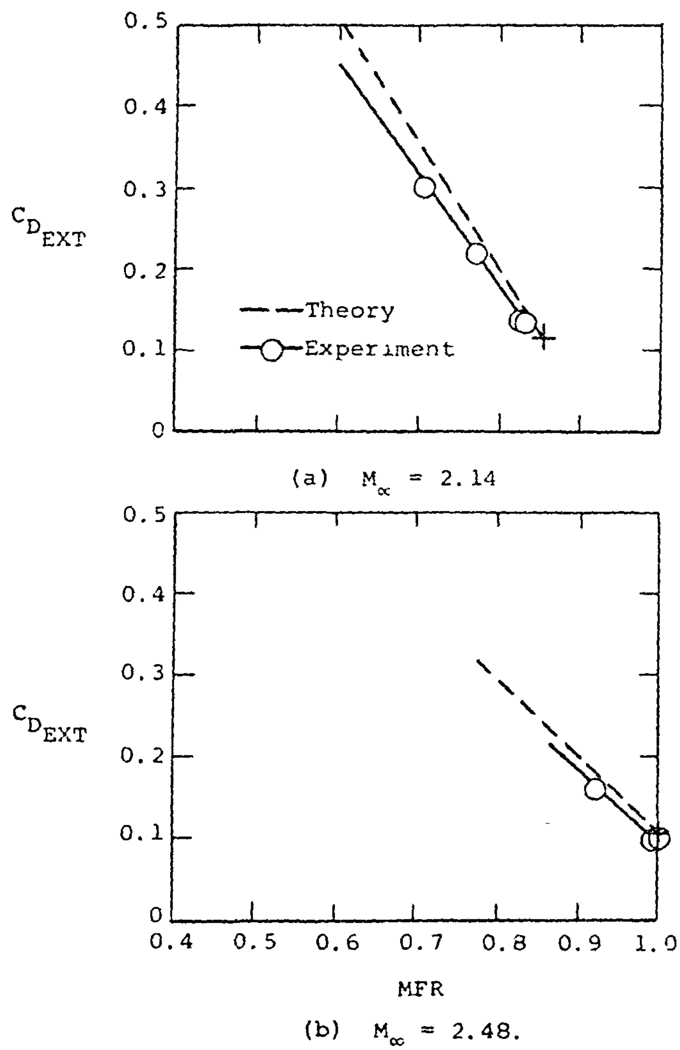

Figure 16.- Comparison of experimental and theoretical inlet drag for SD6 inlet from reference 71.

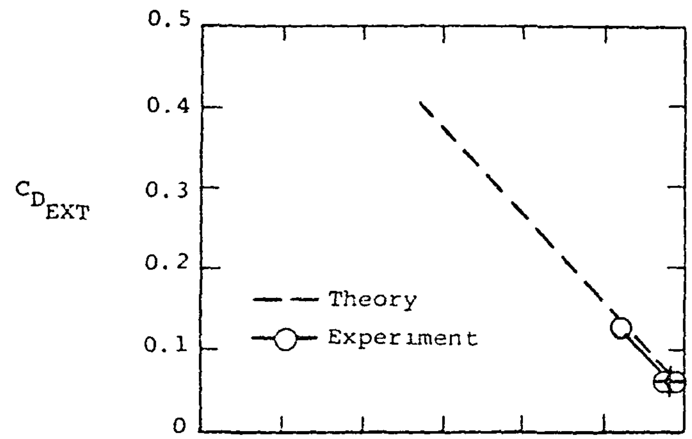

(c) $M_\infty = 2.90$.

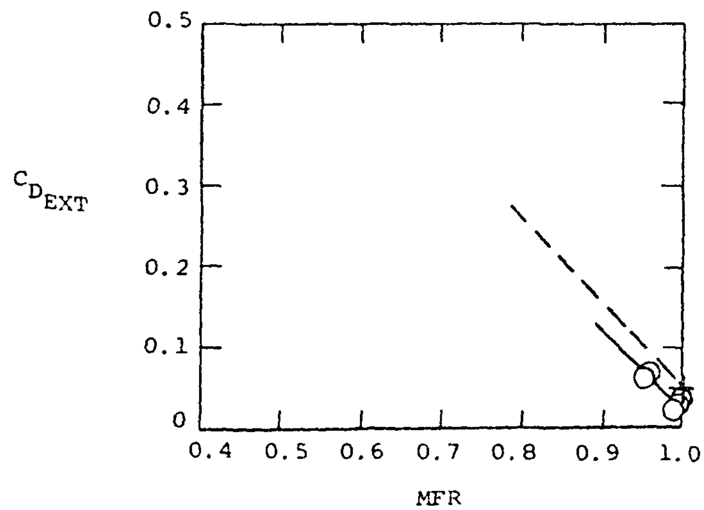

(d) $M_\infty = 3.27$.

Figure 16.- Concluded.

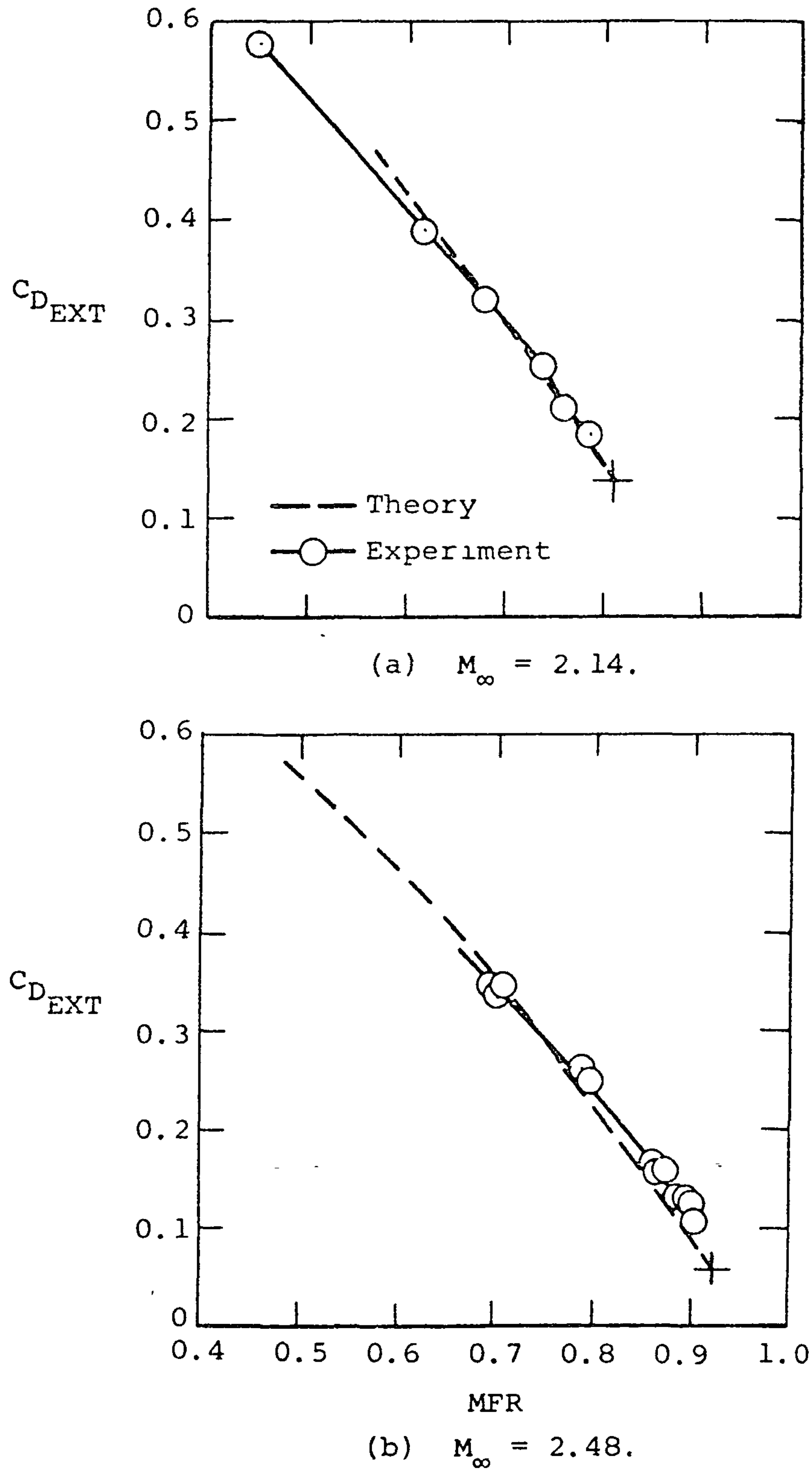

Figure 17.- Comparison of experimental and theoretical inlet drag for SD6 inlet with translated centerbody from reference 71.

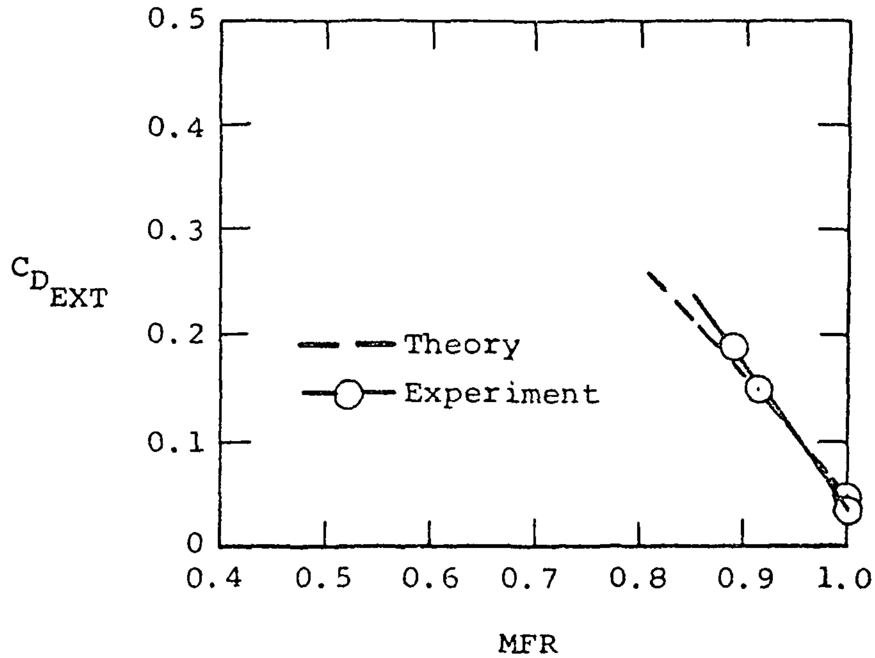

(c) $M_\infty = 2.90$.

Figure 17.- Concluded.

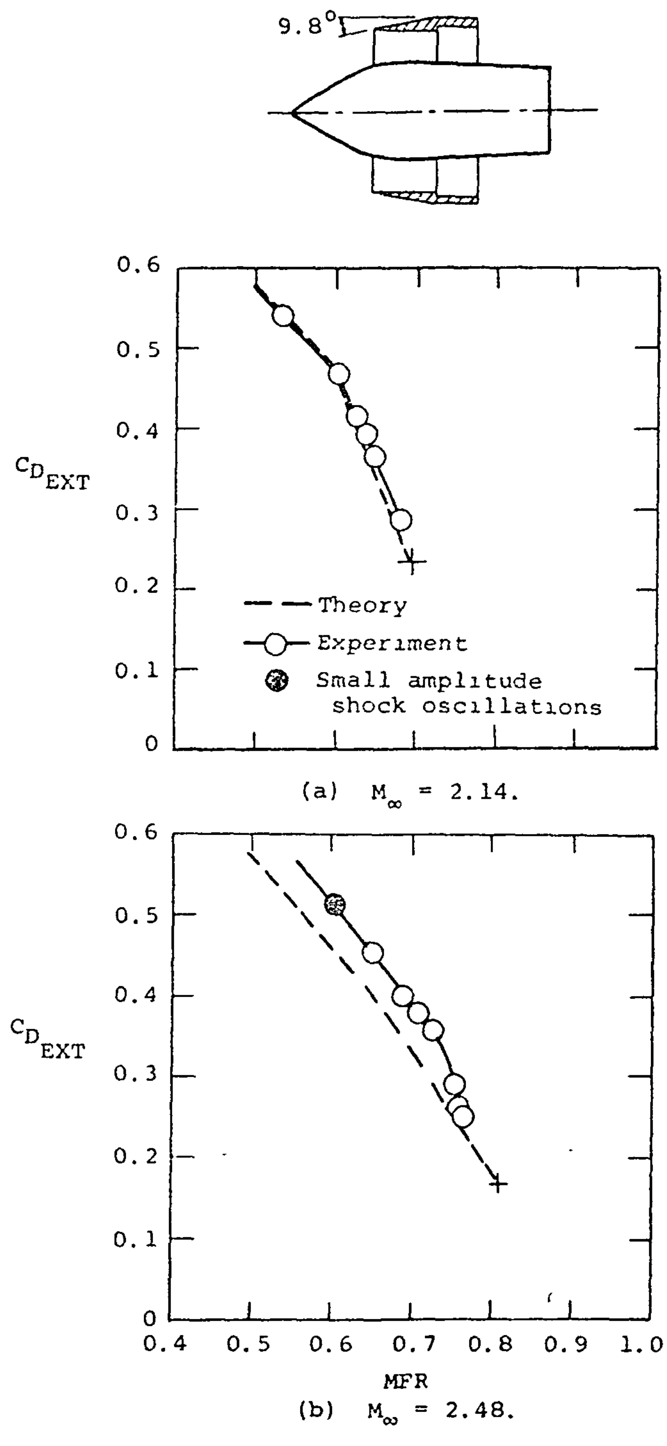

Figure 18.- Comparison of experimental and theoretical inlet drag for 35° III inlet from reference 71.

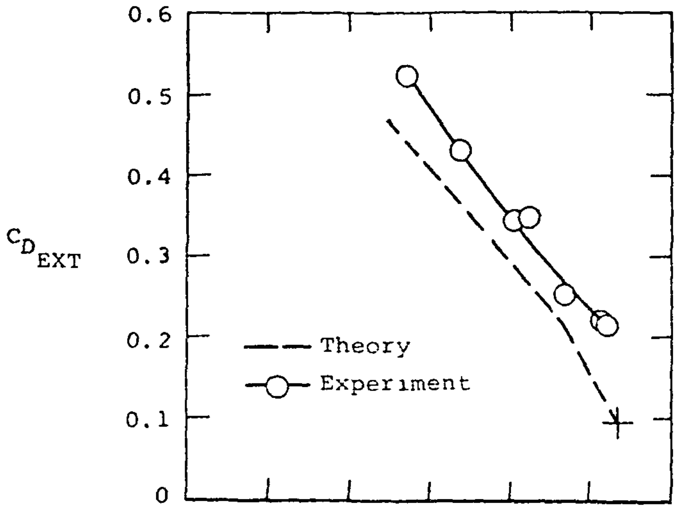

(c) M_∞ = 2.90.

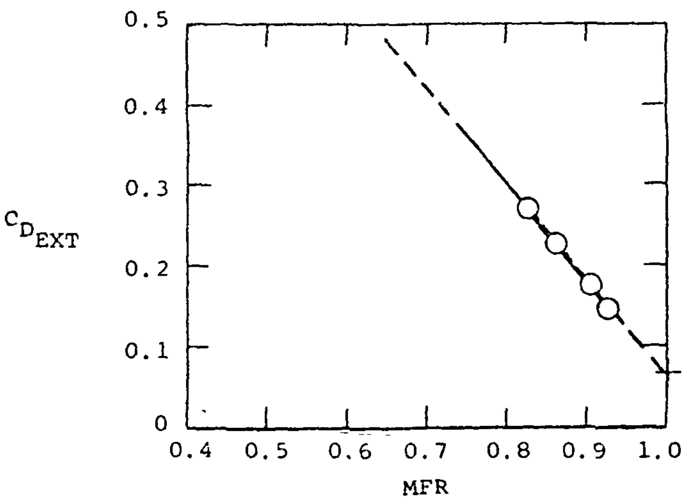

(d) M_∞ = 3.27.

Figure 18.- Concluded.

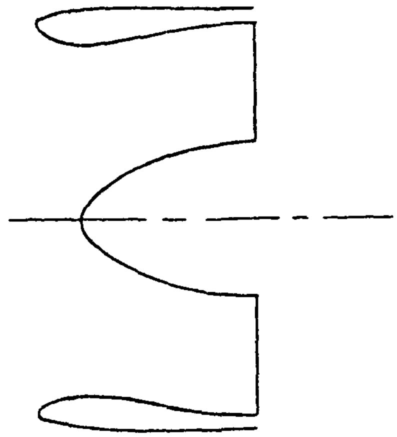

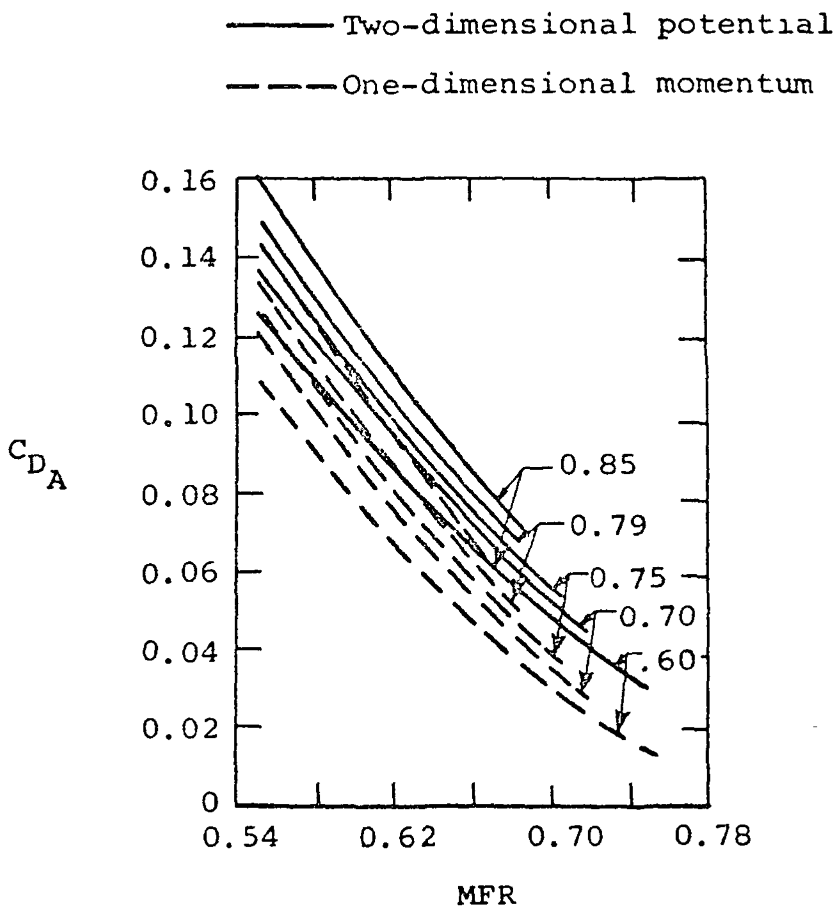

Figure 19.- Comparison of theoretical additive drag values from reference 372.

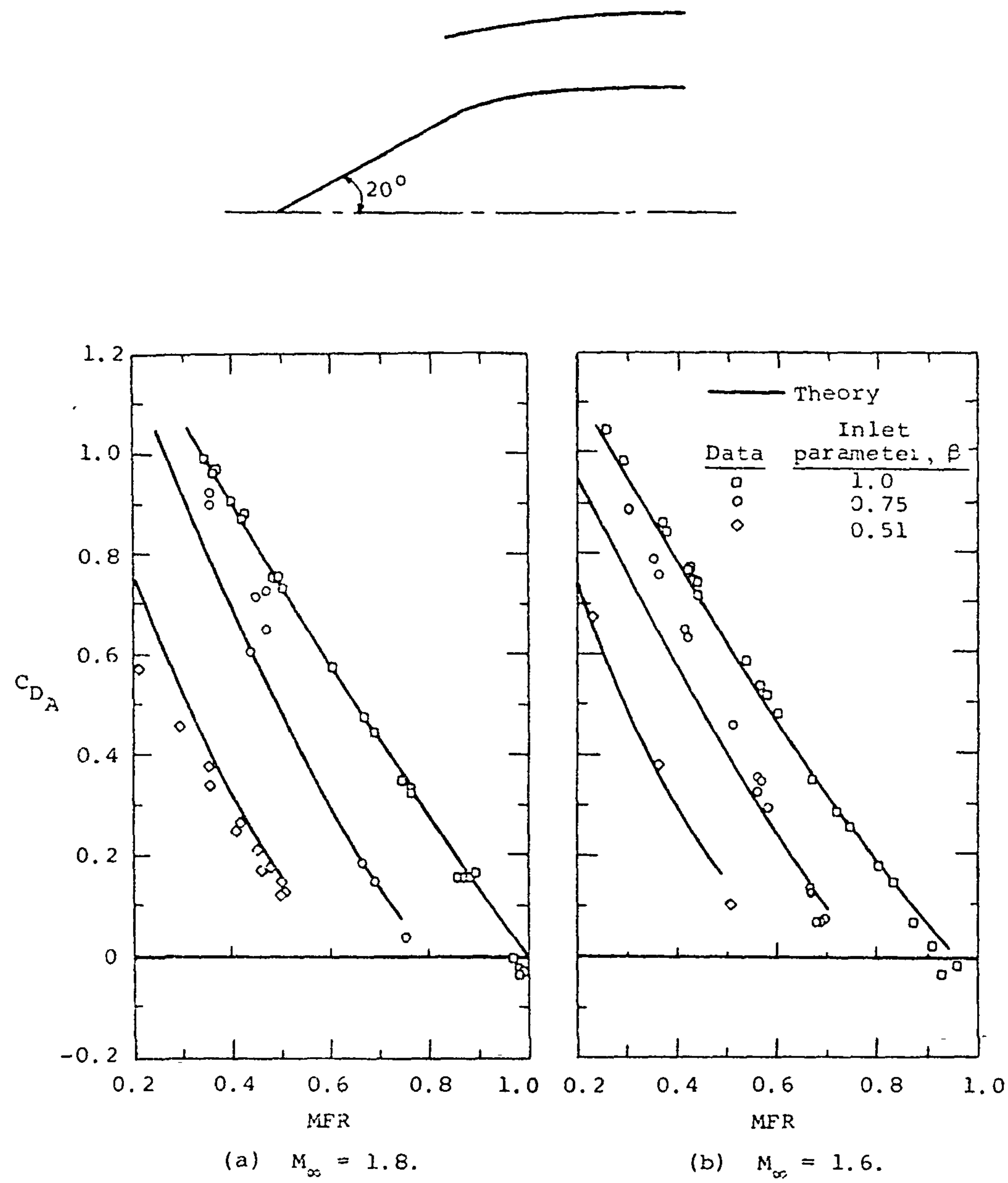

Figure 20.- Comparison of experimental and theoretical additive drag from reference 49.

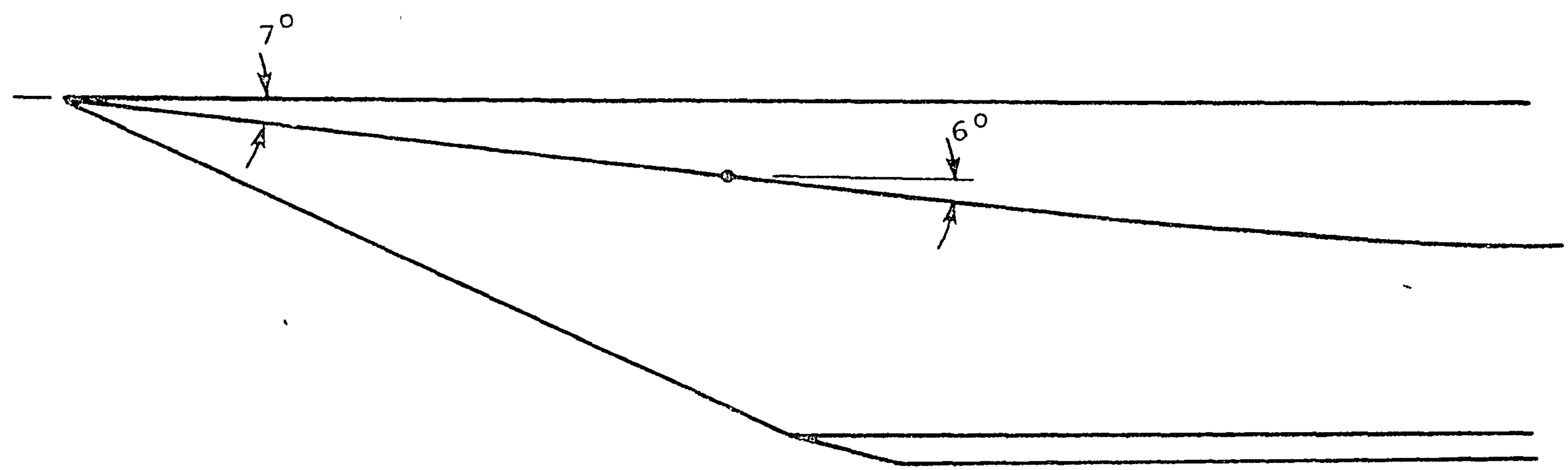

Figure 21.- Inlet geometry from reference 47.

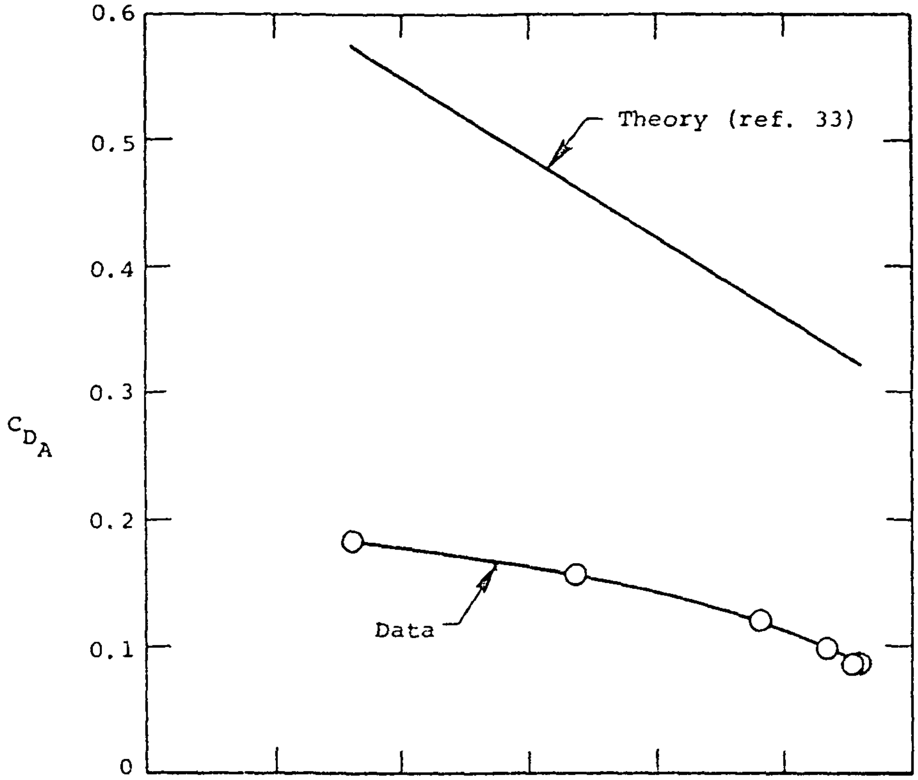

(a) $M_\infty = 1.28$.

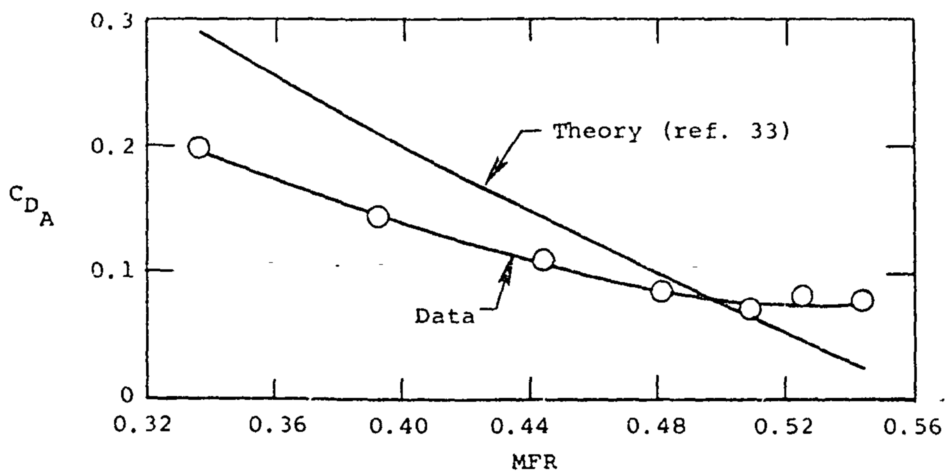

(b) $M_\infty = 0.60$.

Figure 22.- Comparison of experimental and theoretical additive drag from reference 47.

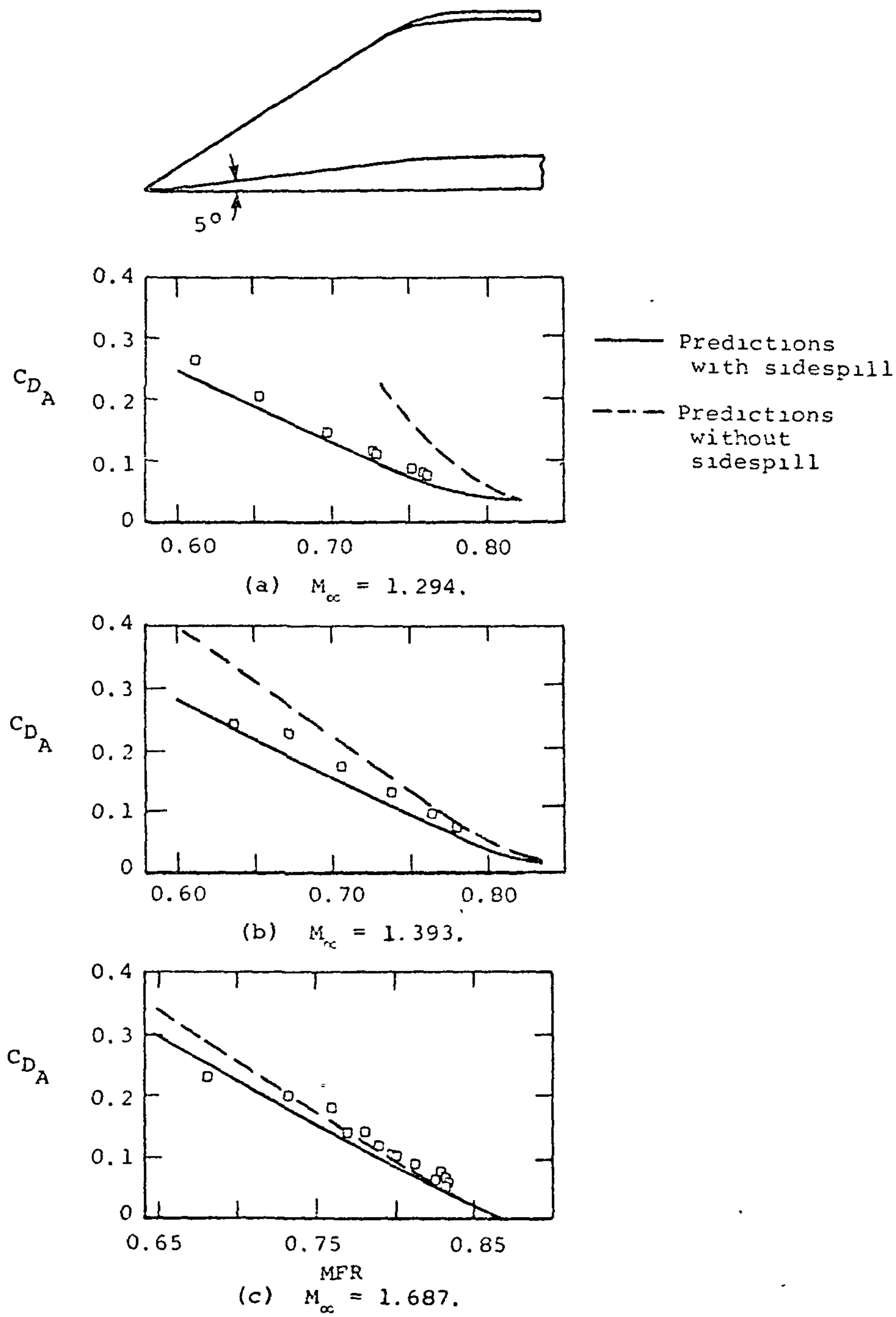

Figure 23.- Comparison of experimental and theoretical additive drag from reference 32. Data from reference 33.

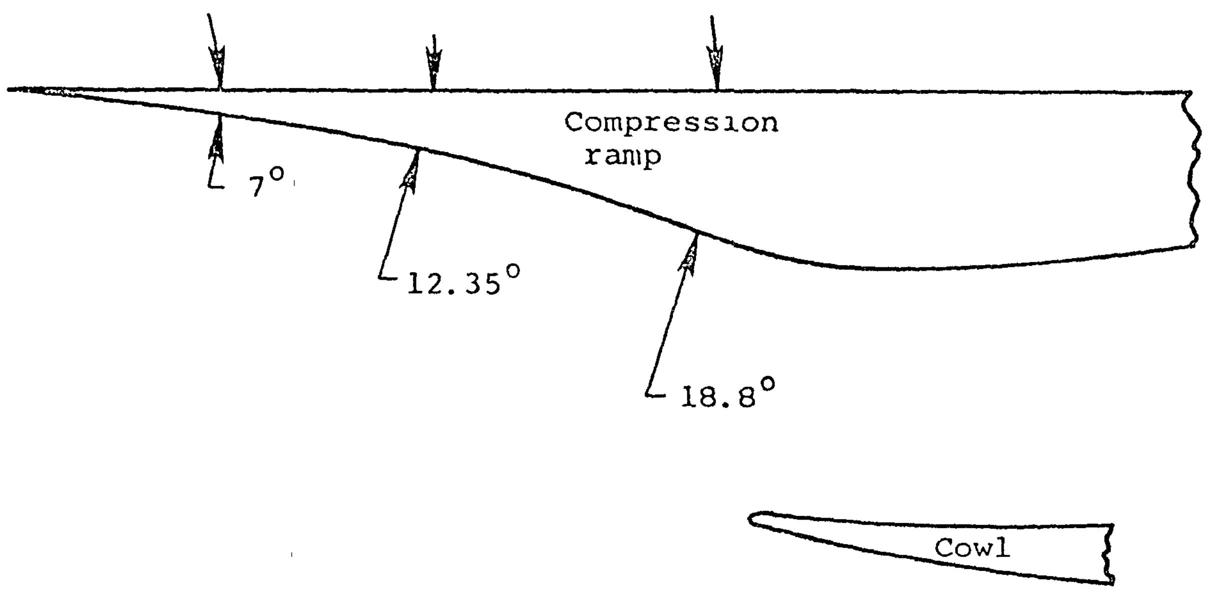

Figure 24.- Two-dimensional inlet geometry for finite-difference calculation of reference 19.

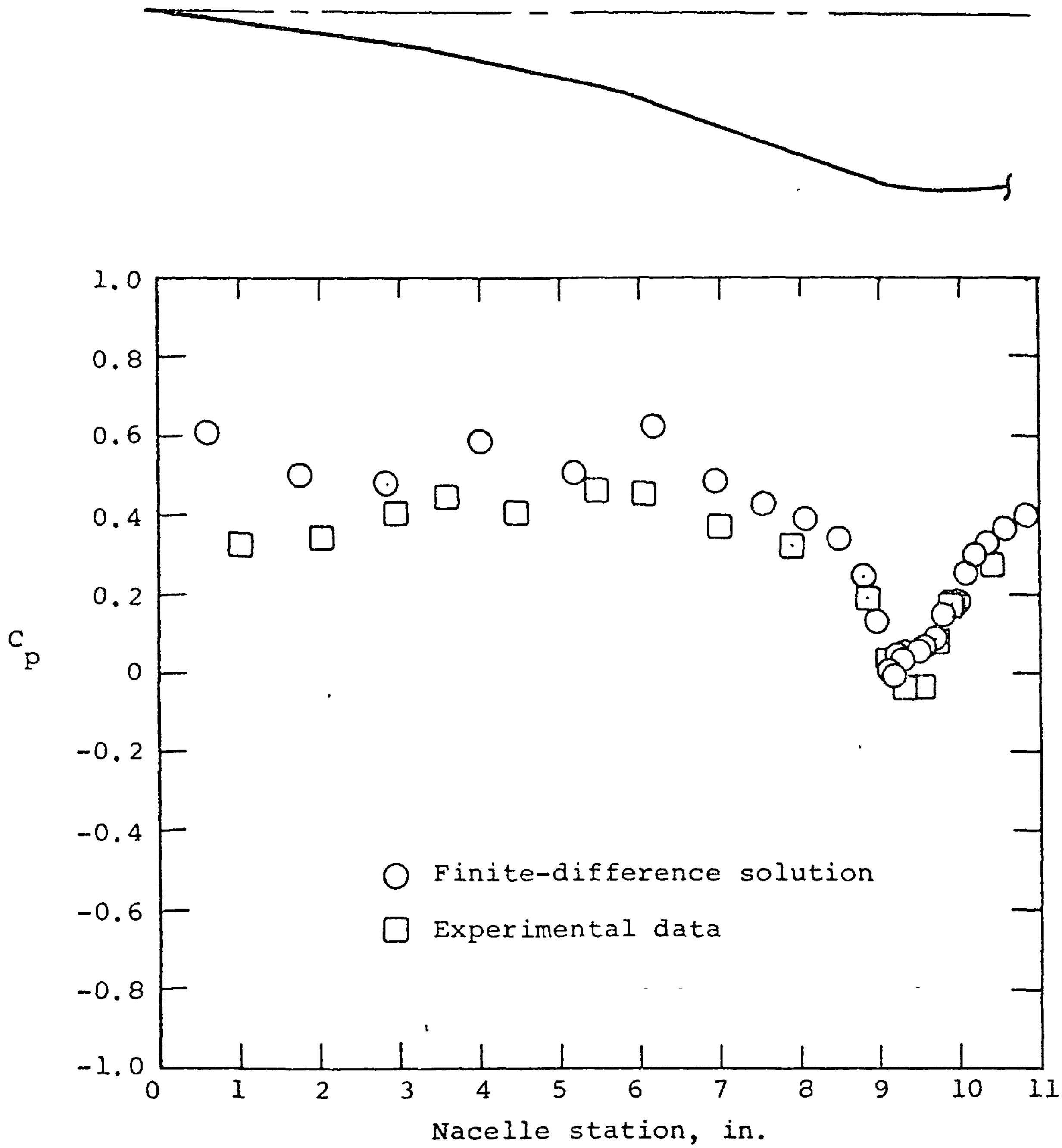

(a) Ramp pressures.

Figure 25.- Comparison of experimental and theoretical surface pressures at $M_\infty = 0.7$, MFR = 0.5 from reference 19.

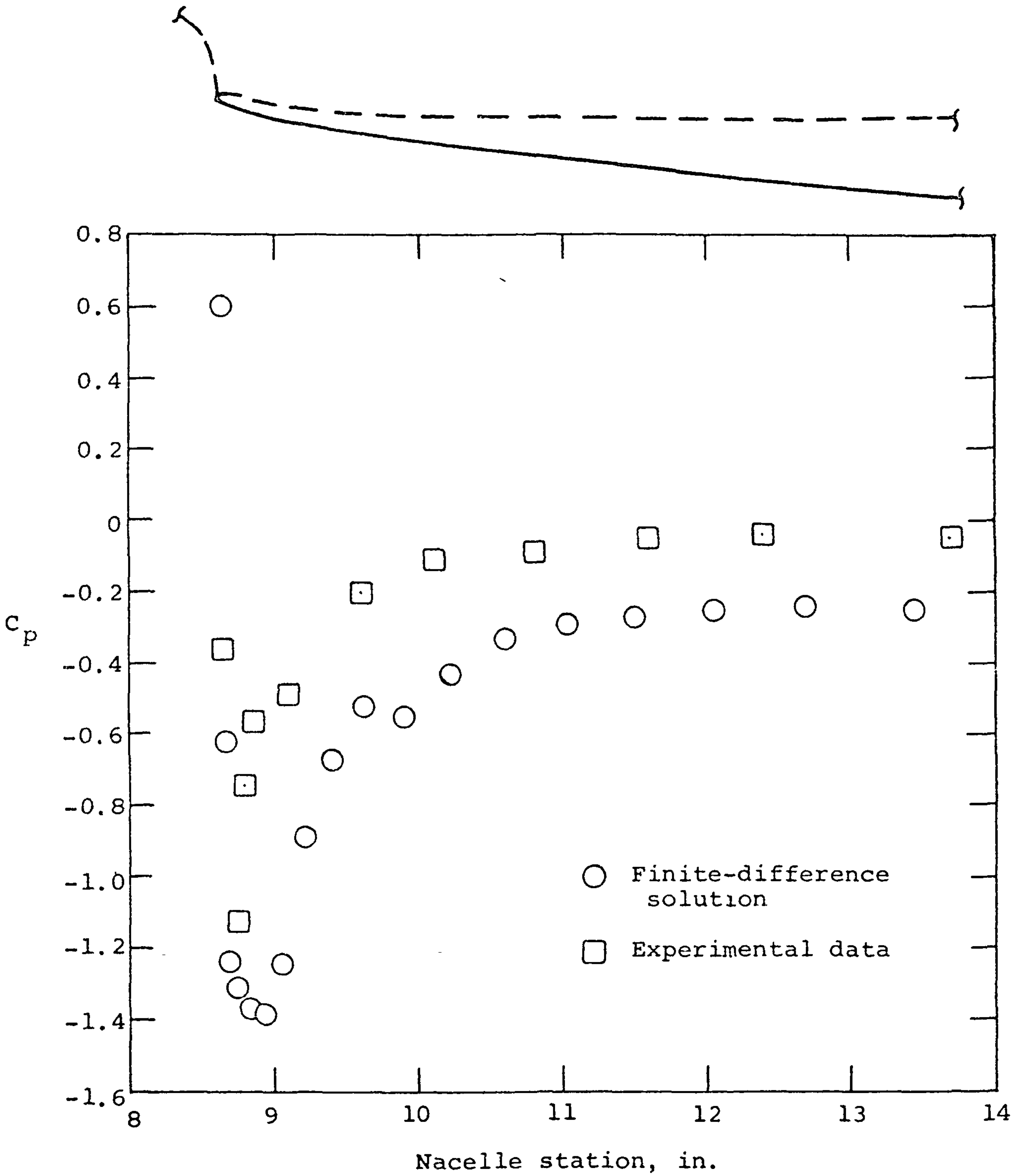

(b) Cowl external pressures.

Figure 25.- Continued.

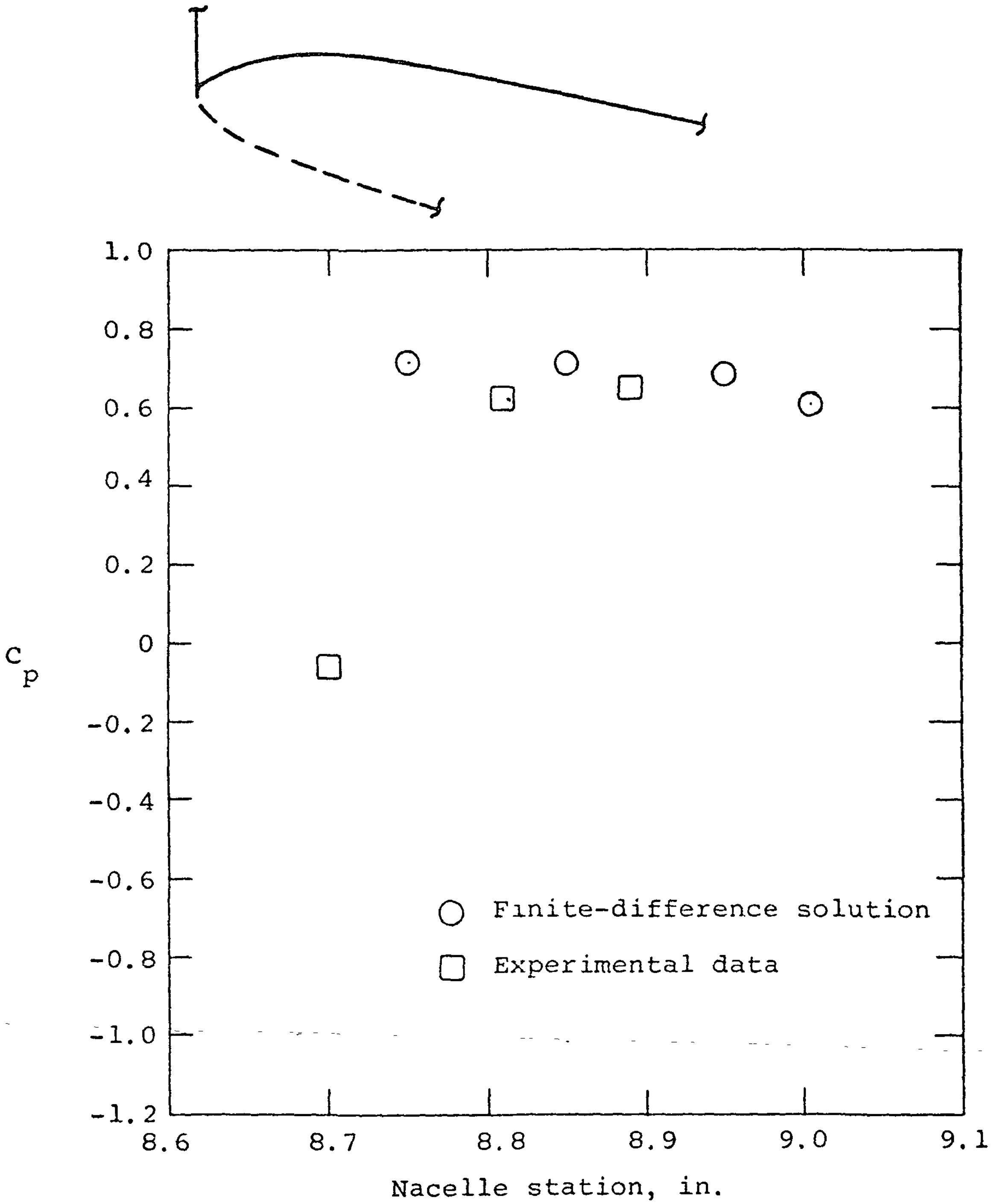

(c) Cowl lip internal pressures.

Figure 25.- Concluded.

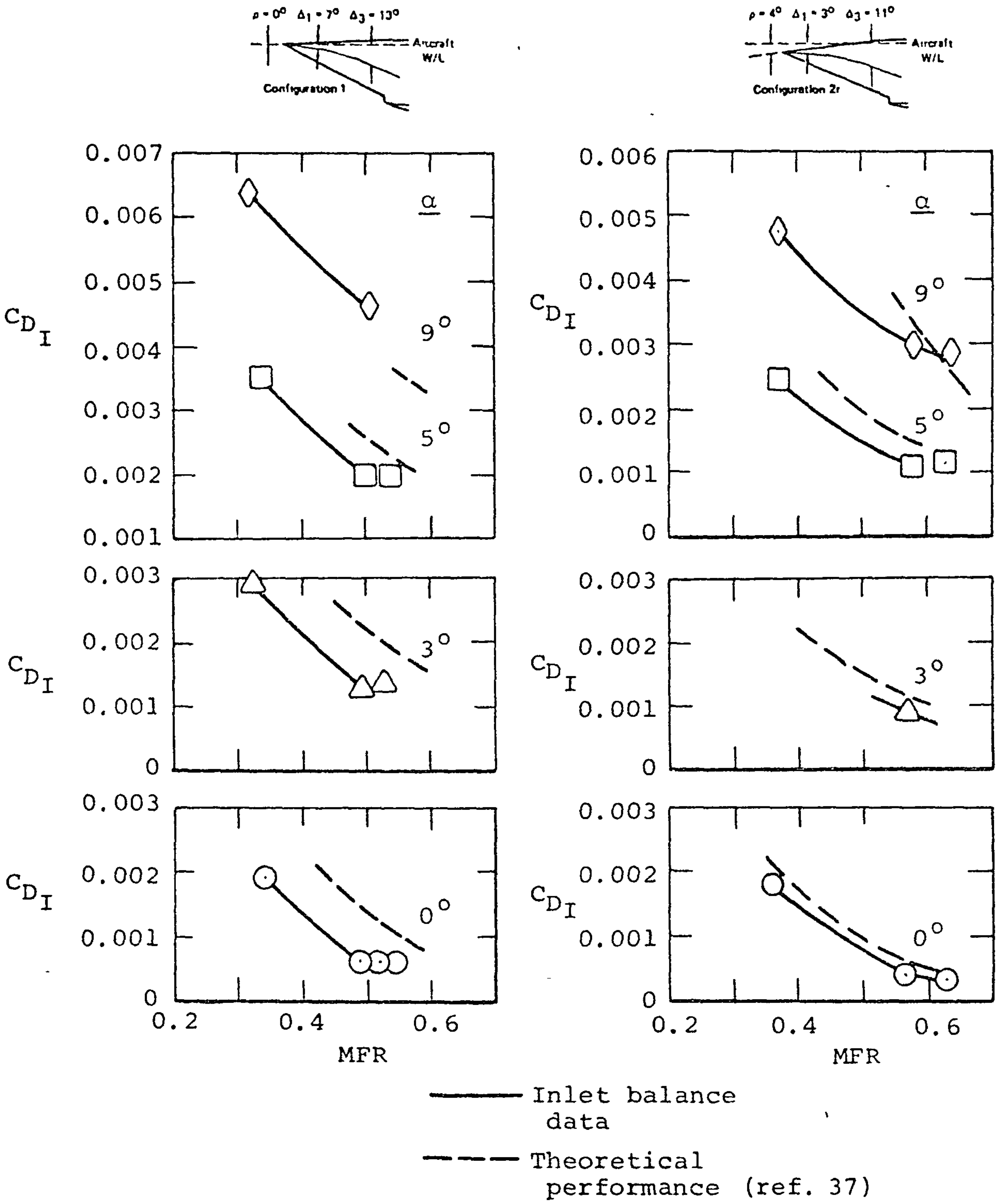

(a) $M_\infty = 0.6$.

Figure 26.- Comparison of experimental and theoretical inlet drag for a 2-D inlet. From reference 63.

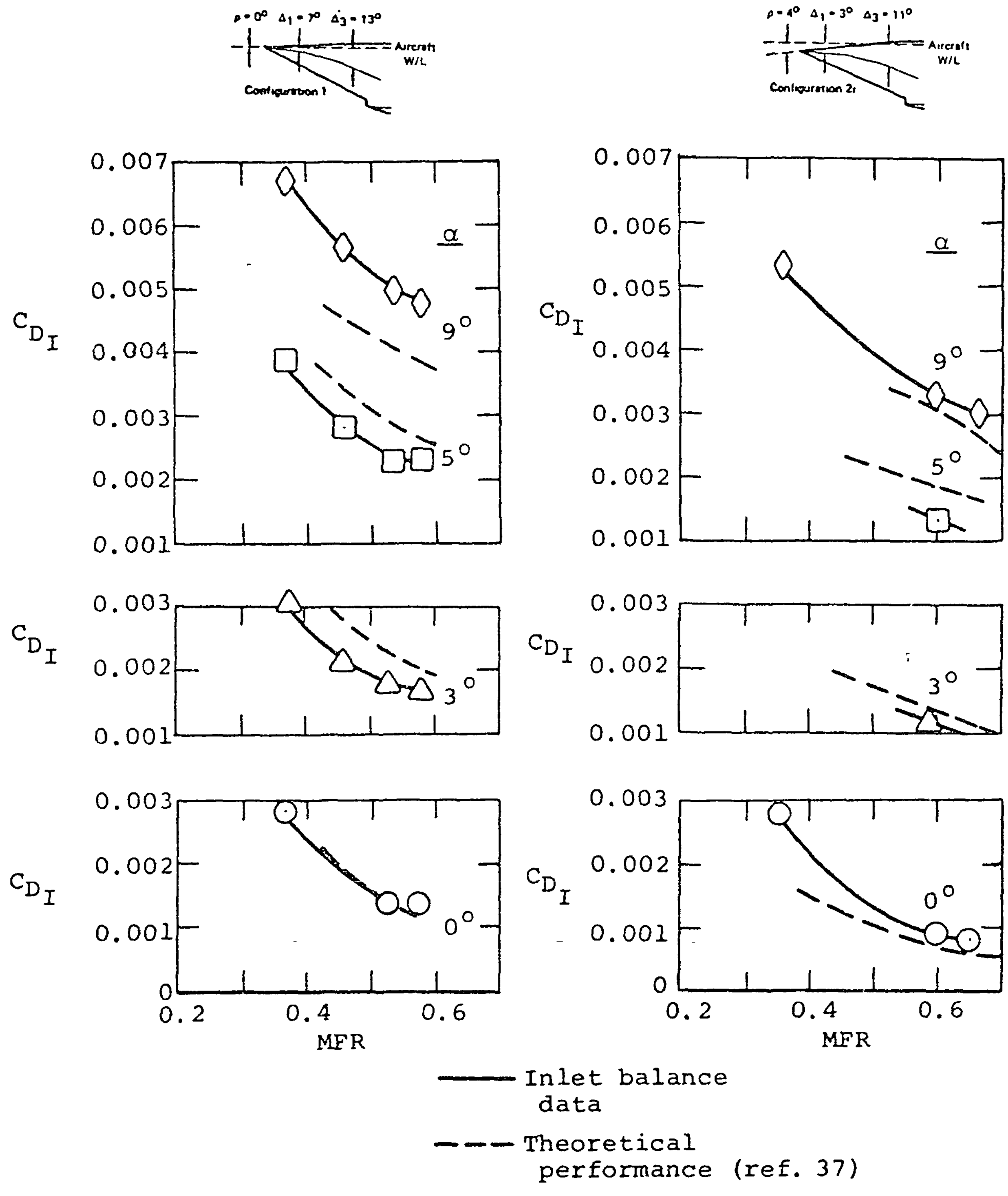

(b) $M_\infty = 0.9$.

Figure 26.- Concluded.

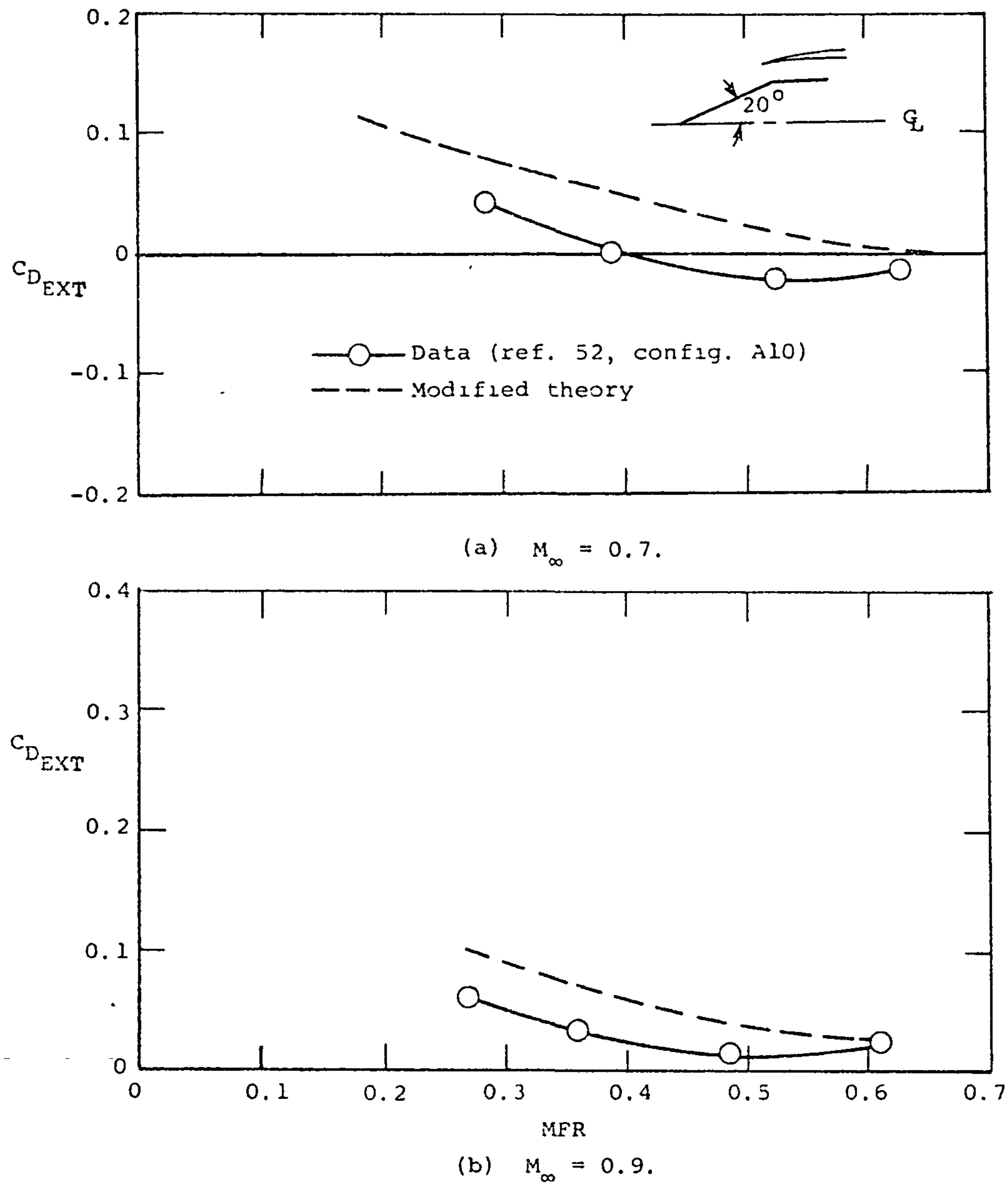

Figure 27.- Comparison of experimental and theoretical inlet drag for an axisymmetric inlet (config. A10, ref. 52). From reference 37.

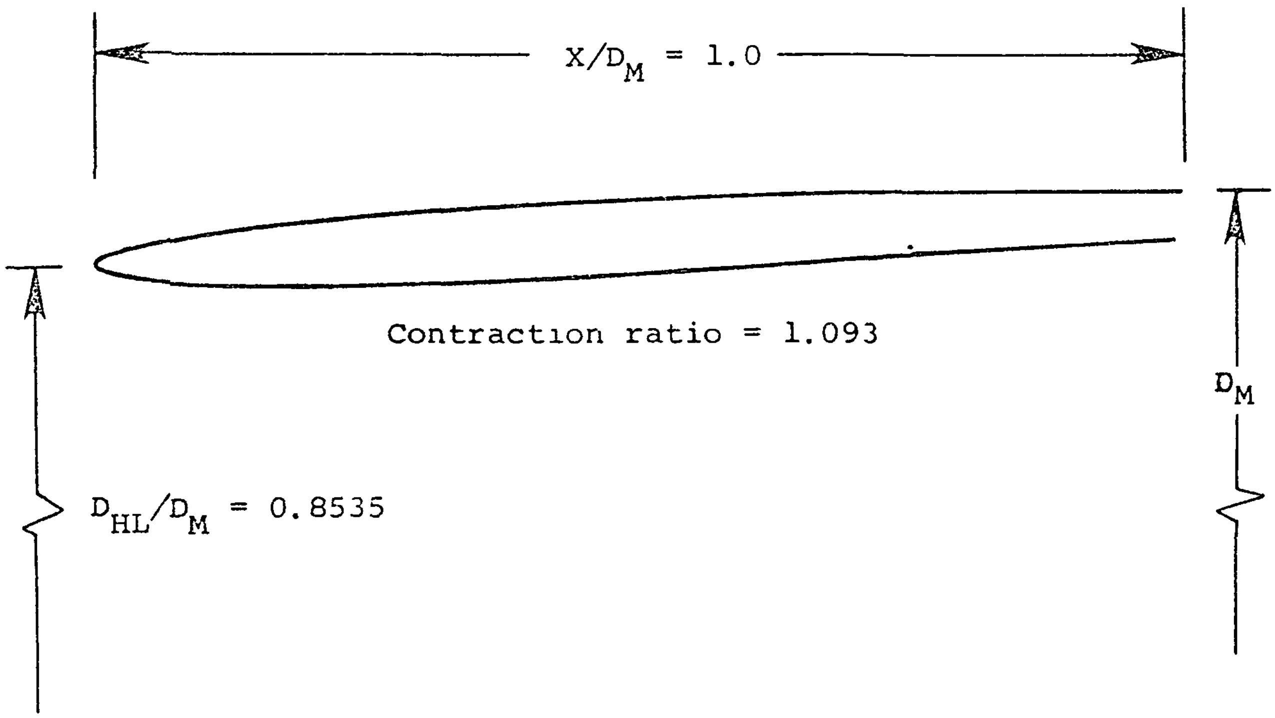

Figure 28.- Pitot inlet geometry for streamtube curvature analysis of reference 274. Identified in reference 274 as NASA 1-85-100 no. 8 inlet, NACA-1 series contour.

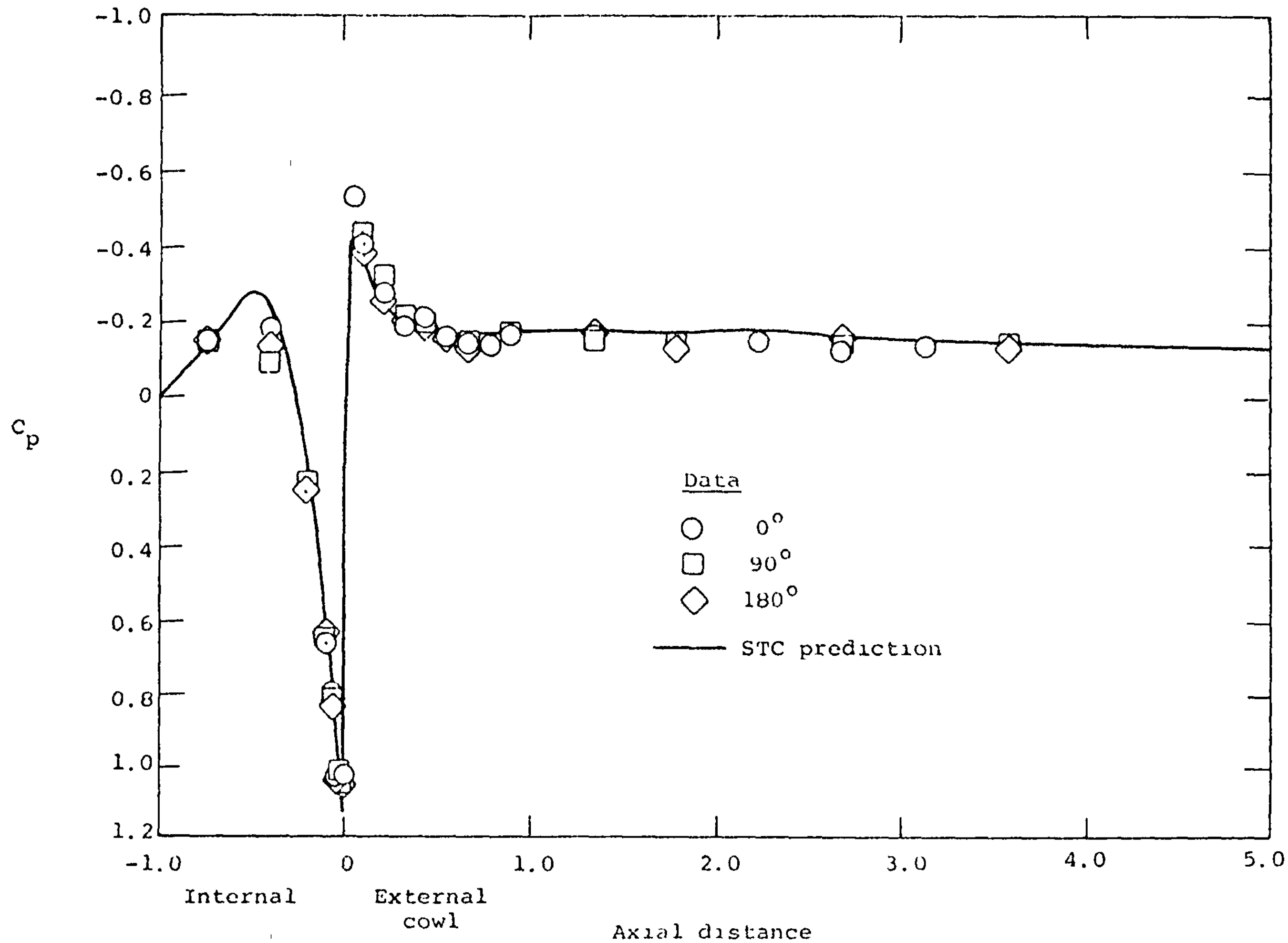

(a) M_∞ = 0.6974, MFR = 0.8715.

Figure 29.- Comparisons of experimental and theoretical surface pressures for the pitot inlet from reference 274.

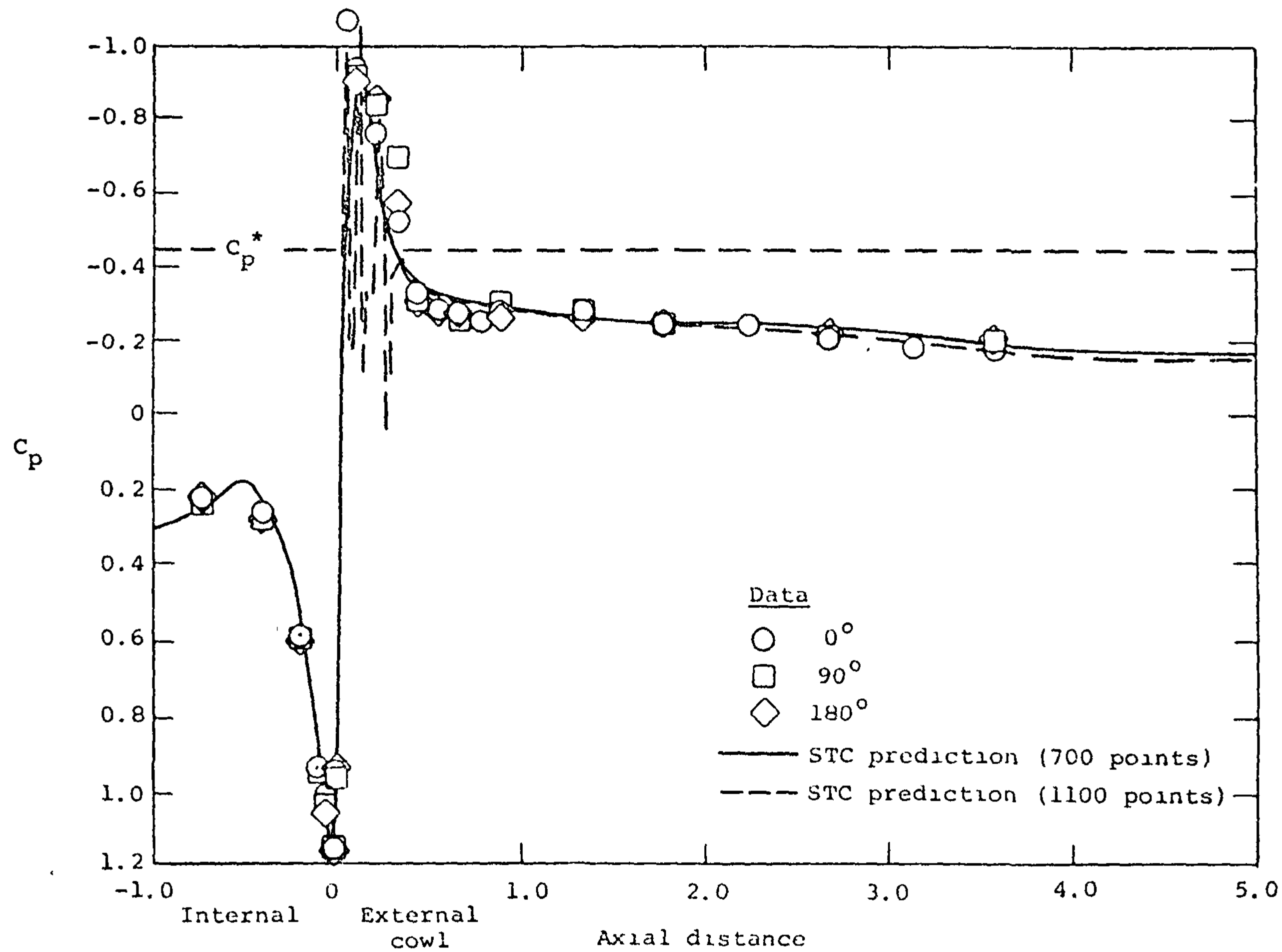

(b) M_∞ = 0.8008, MFR = 0.8093.

Figure 29.- Continued.

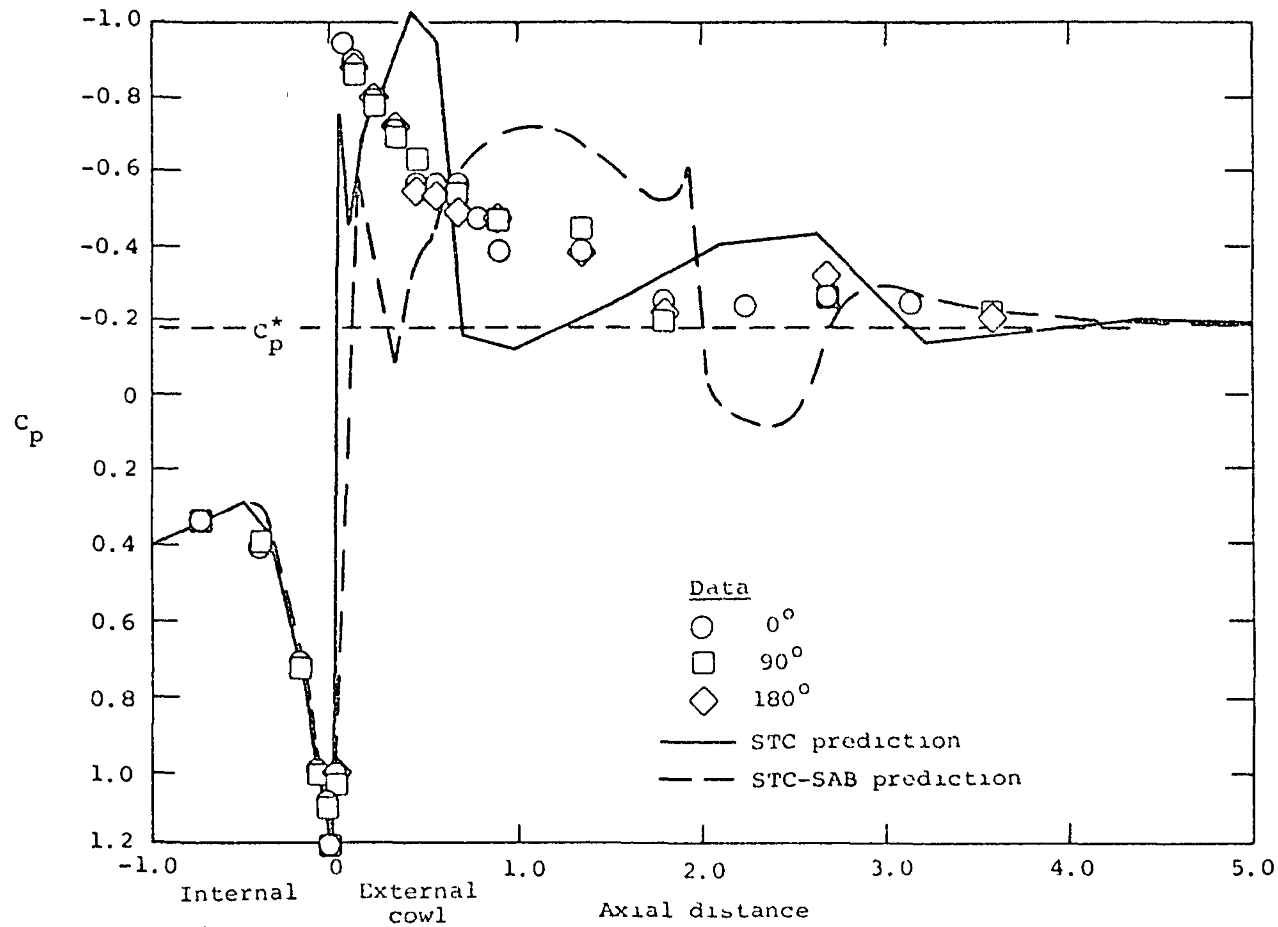

(c) $M_\infty = 0.900$, MFR = 0.8073.

Figure 29.- Concluded.

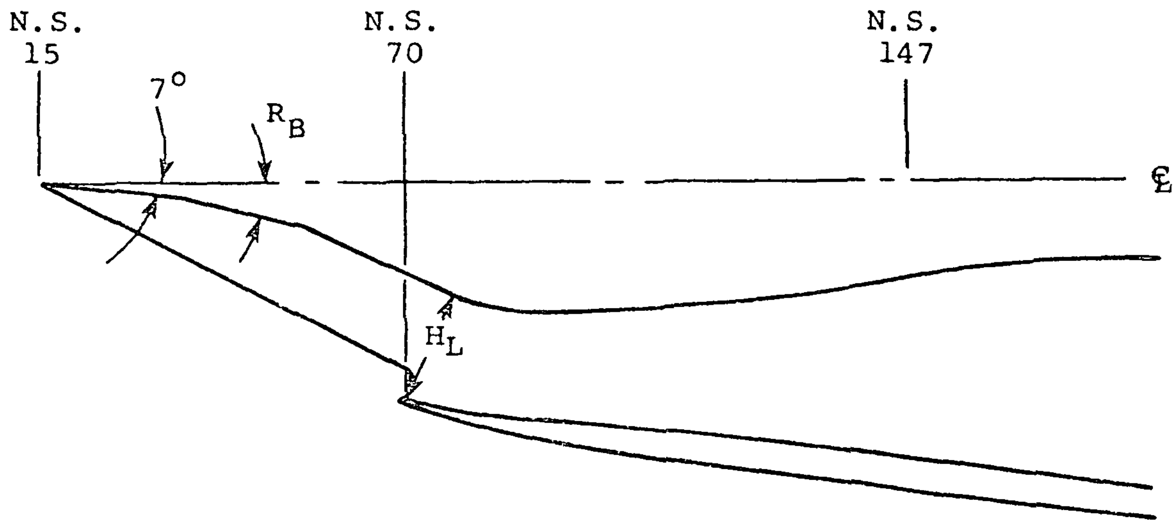

Figure 30.- B-1 external compression inlet geometry from reference 239. Comparisons in following figures use $R_B = 7.2^\circ$, $H_L = 27.3$.

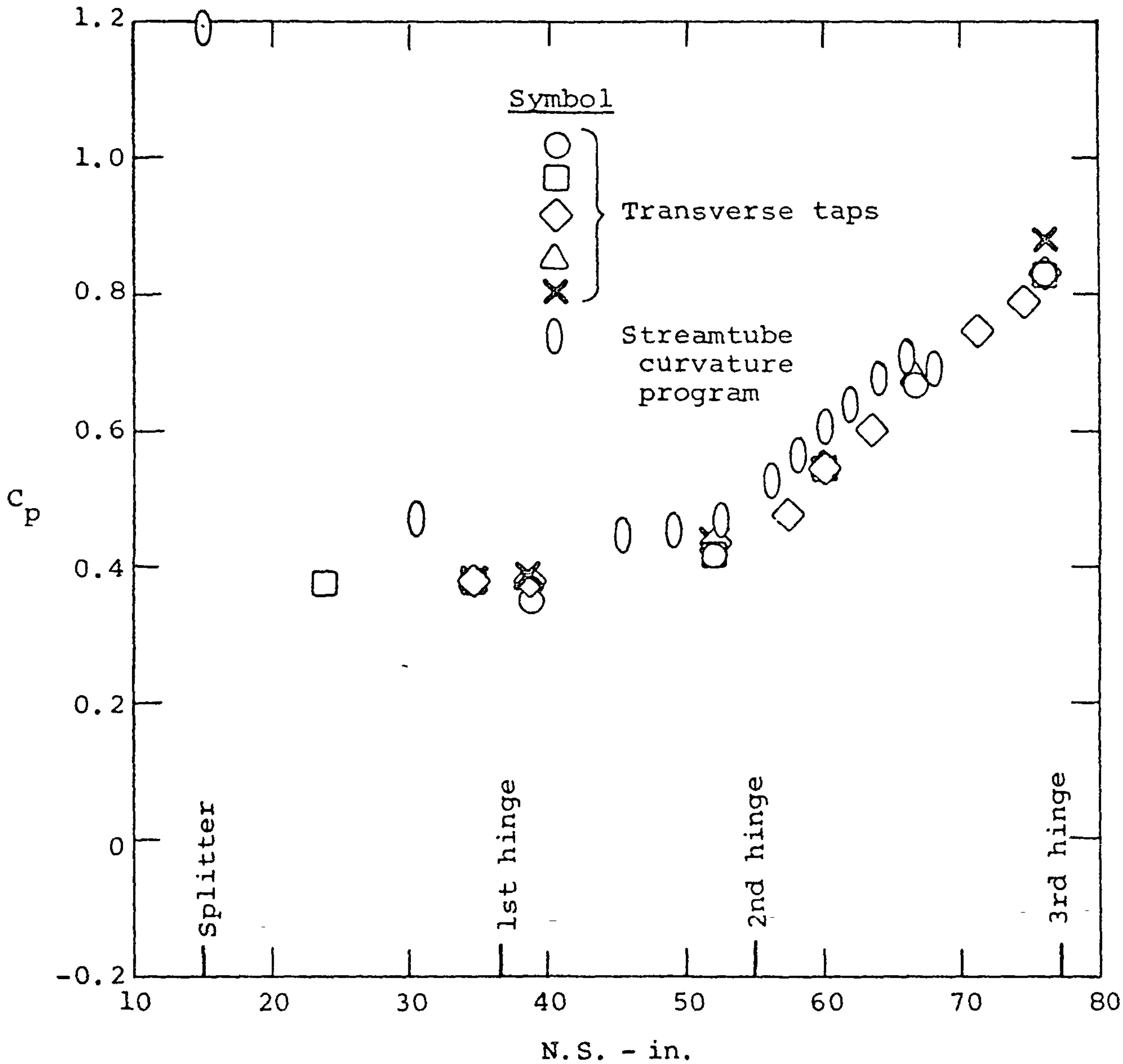

(a) Ramp pressures.

Figure 31.- Comparison of experimental and theoretical surface pressures for the inlet of figure 30 from reference 239. $M_\infty = 0.85$, MFR = 0.55.

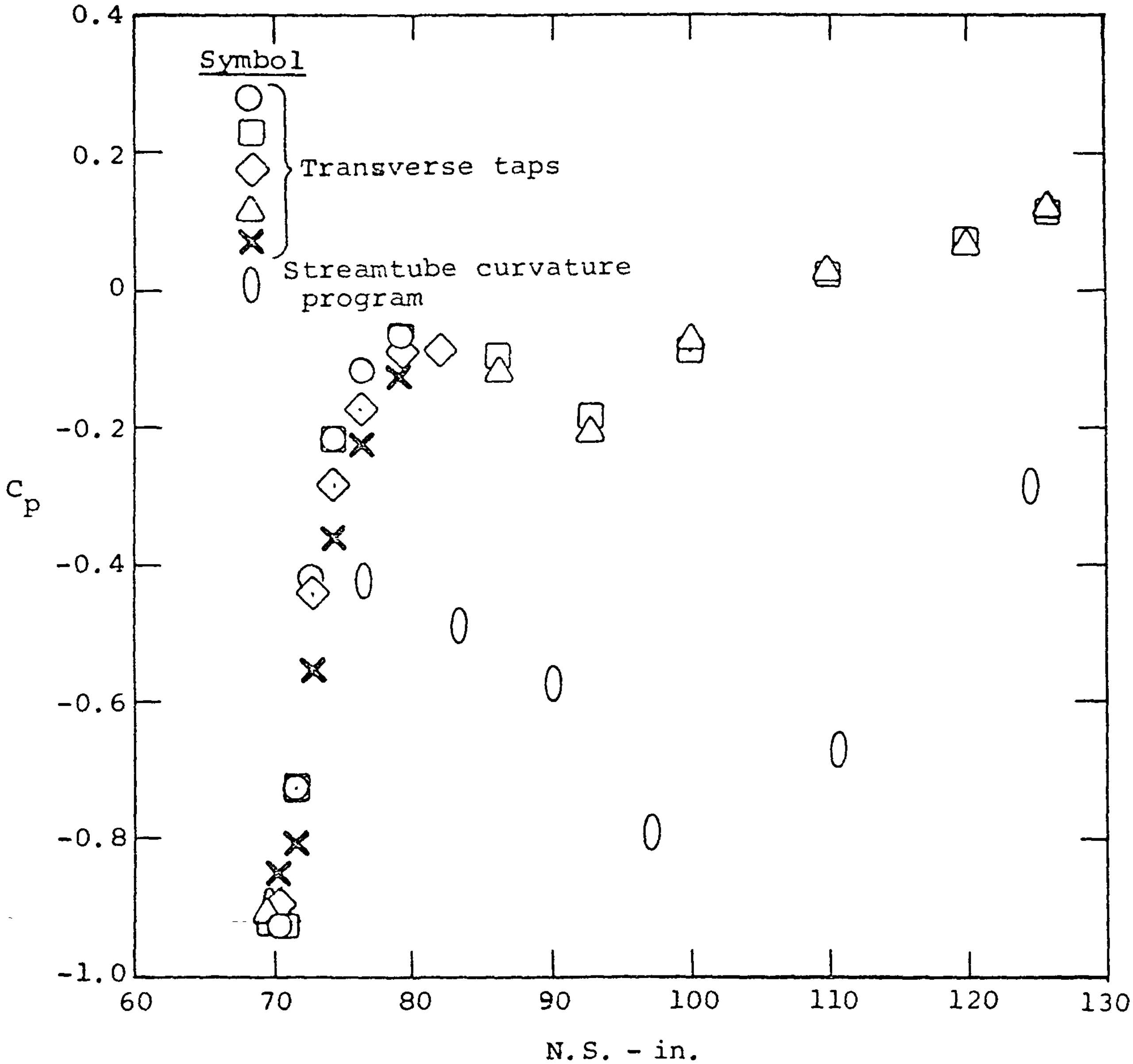

(b) Cowl pressures.

Figure 31.- Concluded.

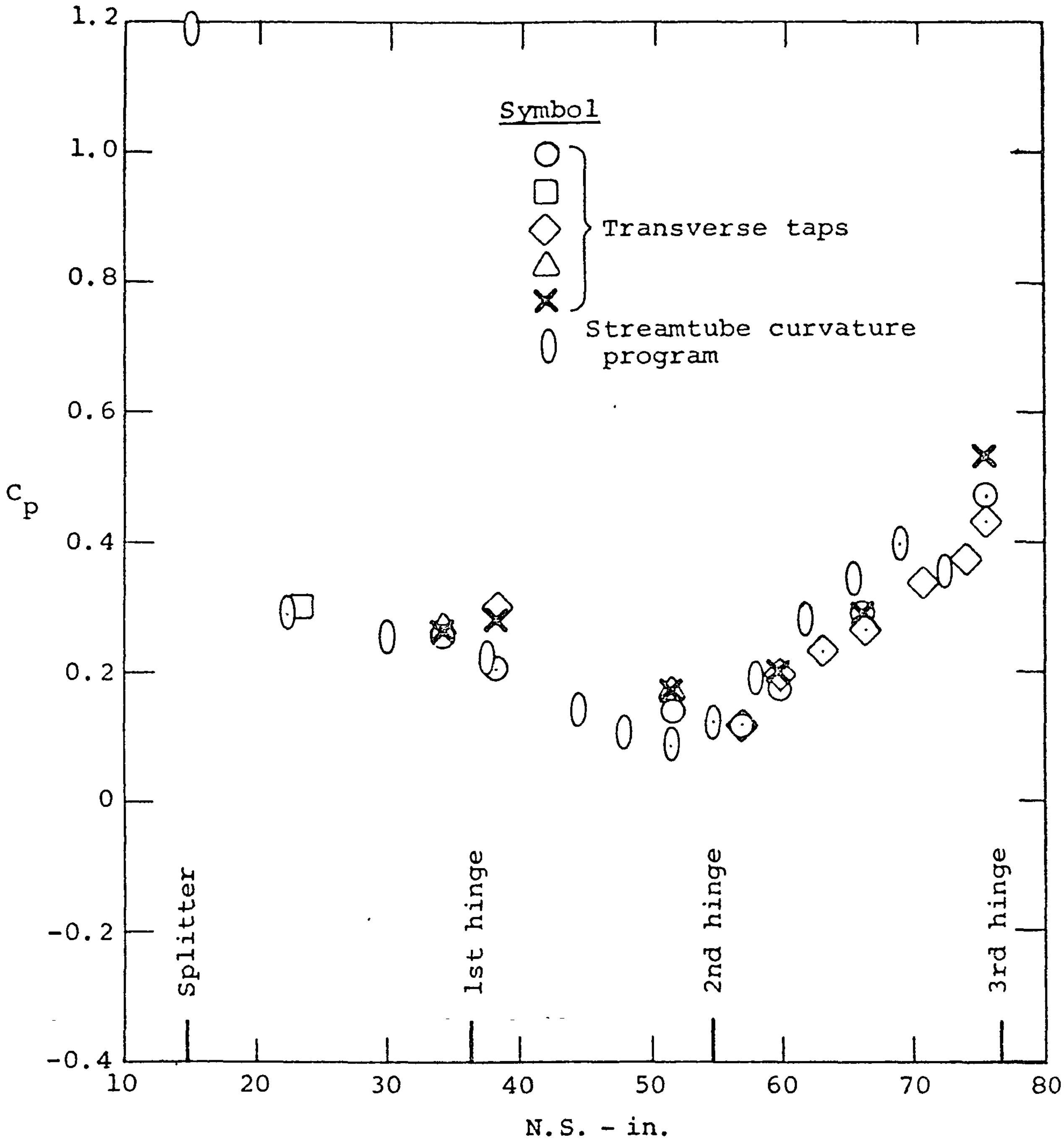

(a) Ramp pressures.

Figure 32.- Comparison of experimental and theoretical surface pressures for the inlet of figure 30 from reference 239. $M_\infty = 0.85$, MFR = 0.75.

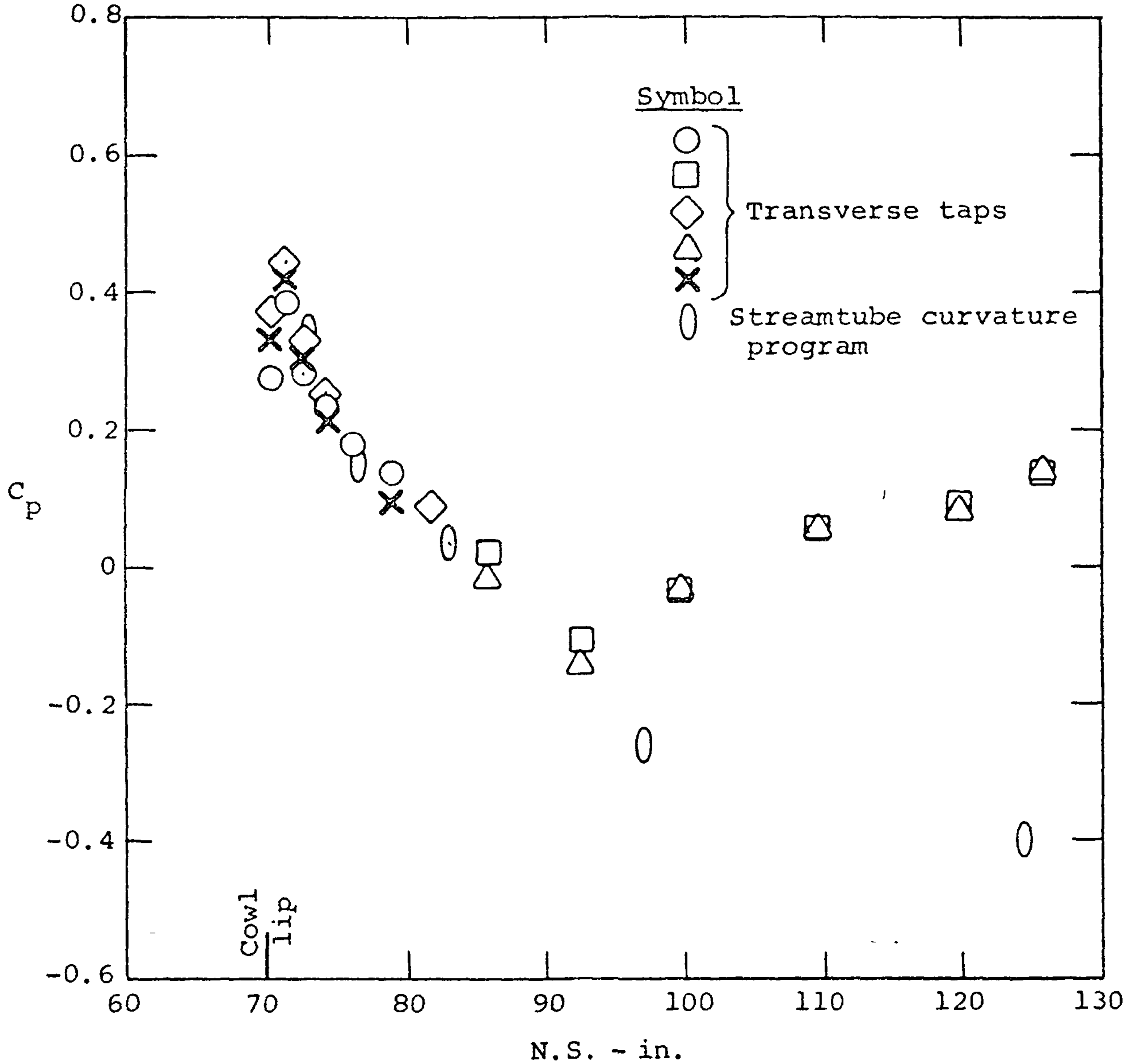

(b) Cowl pressures.

Figure 32.- Concluded.

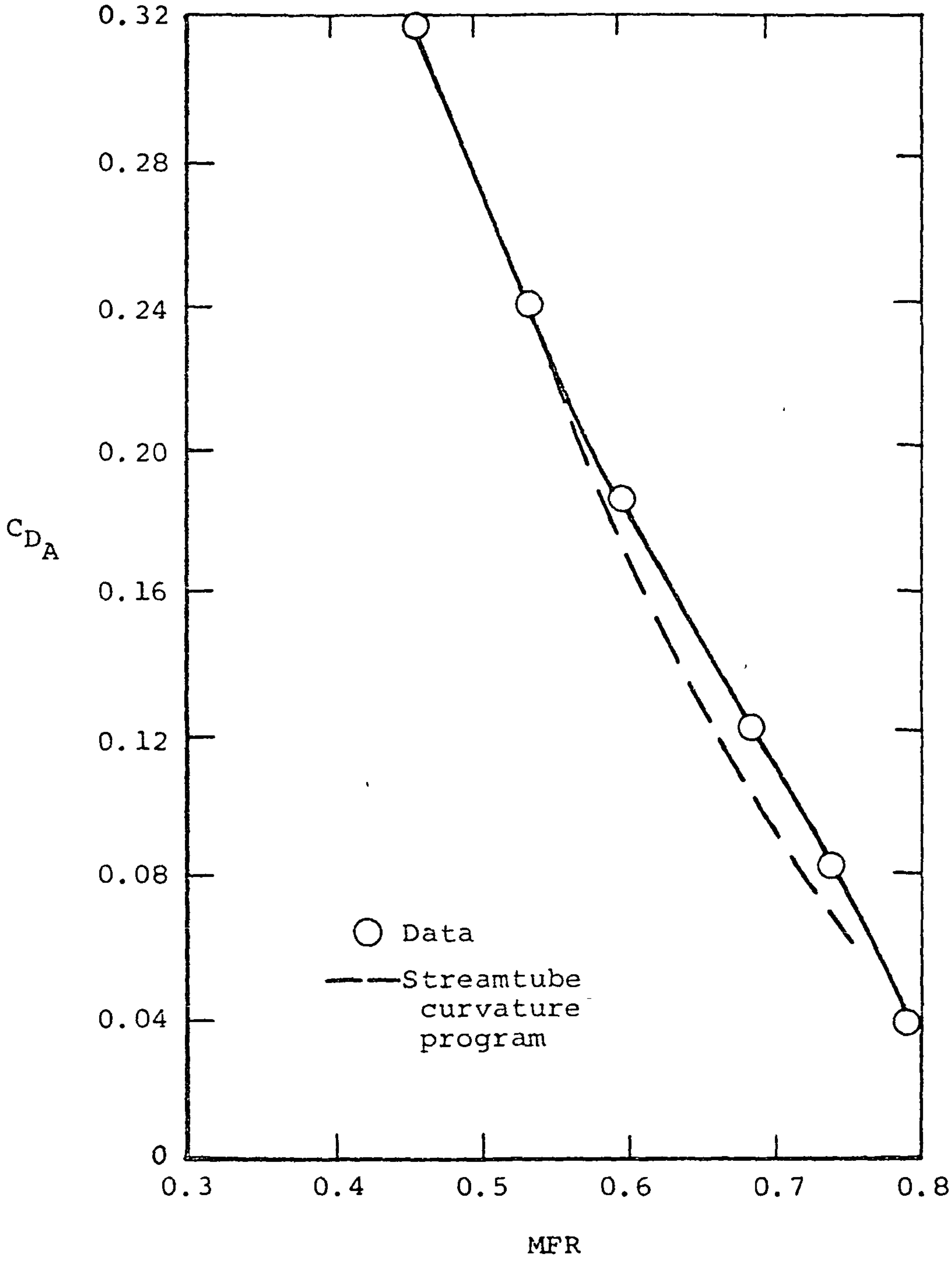

Figure 33.- Comparison of experimental and theoretical additive drag for the inlet of figure 30 from reference 239. $M_\infty = 0.85$.

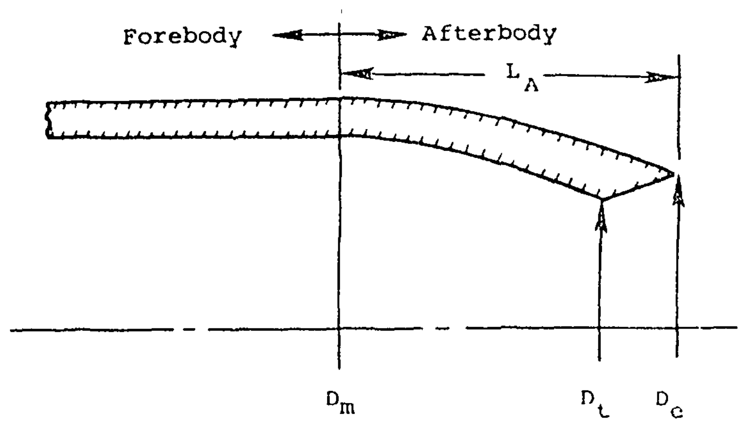

- Fineness ratio, $\overline{FR} = L_A/D_m$
- External area ratio $= A_e/A_m = (D_e/D_m)^2$
- Internal area ratio $= A_e/A_t = (D_e/D_t)^2$

Figure 34 .- Afterbody geometric parameters.

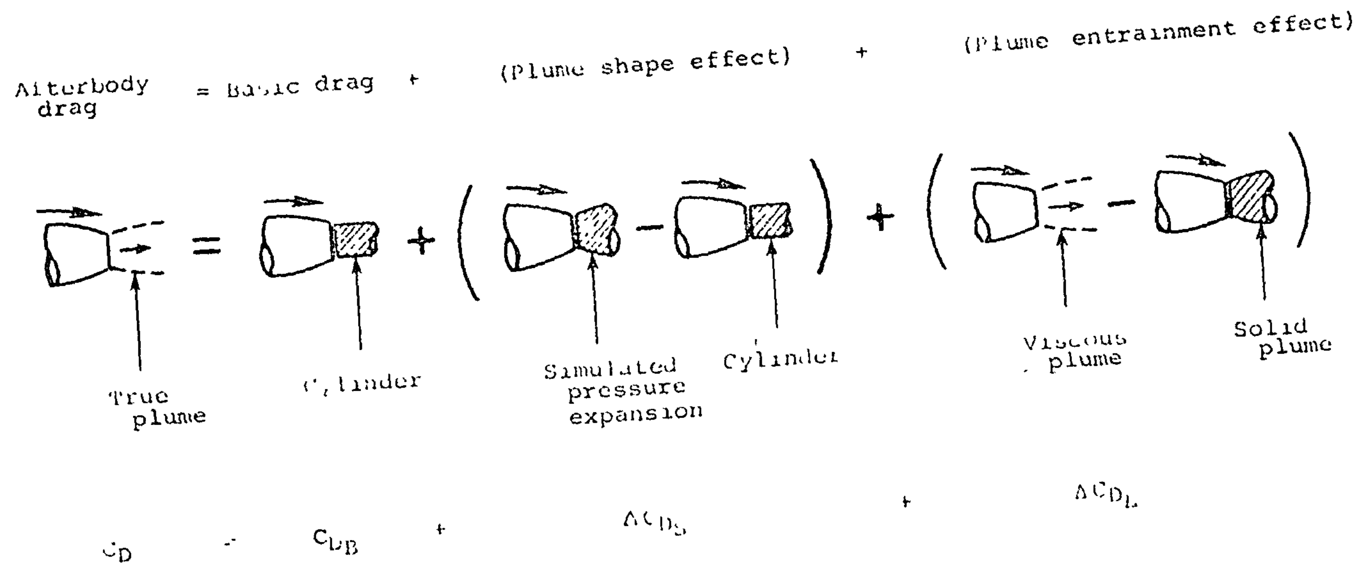

Figure 35.- Afterbody drag components.

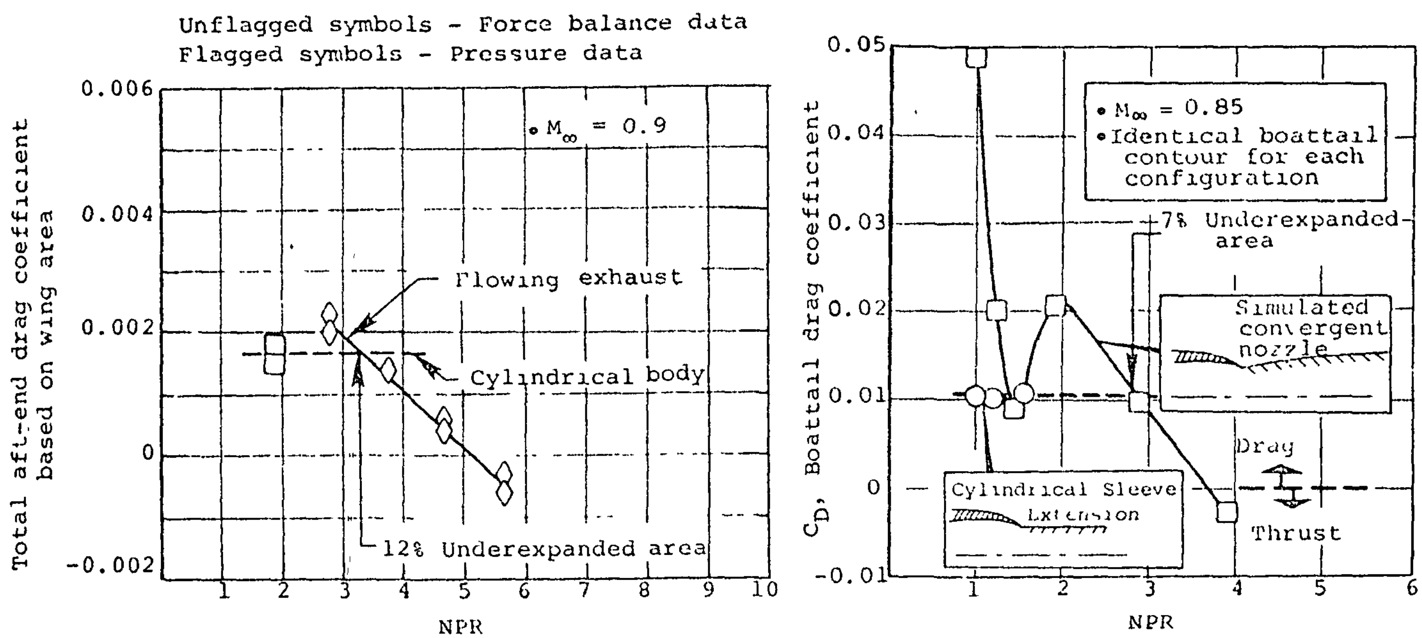

(a) FDL/Lockheed twin-jet installed data, reference 46.

(b) GD Single-engine isolated data; reference 6.

Figure 36 .- Afterbody drag effects of solid cylinders vs true plumes.

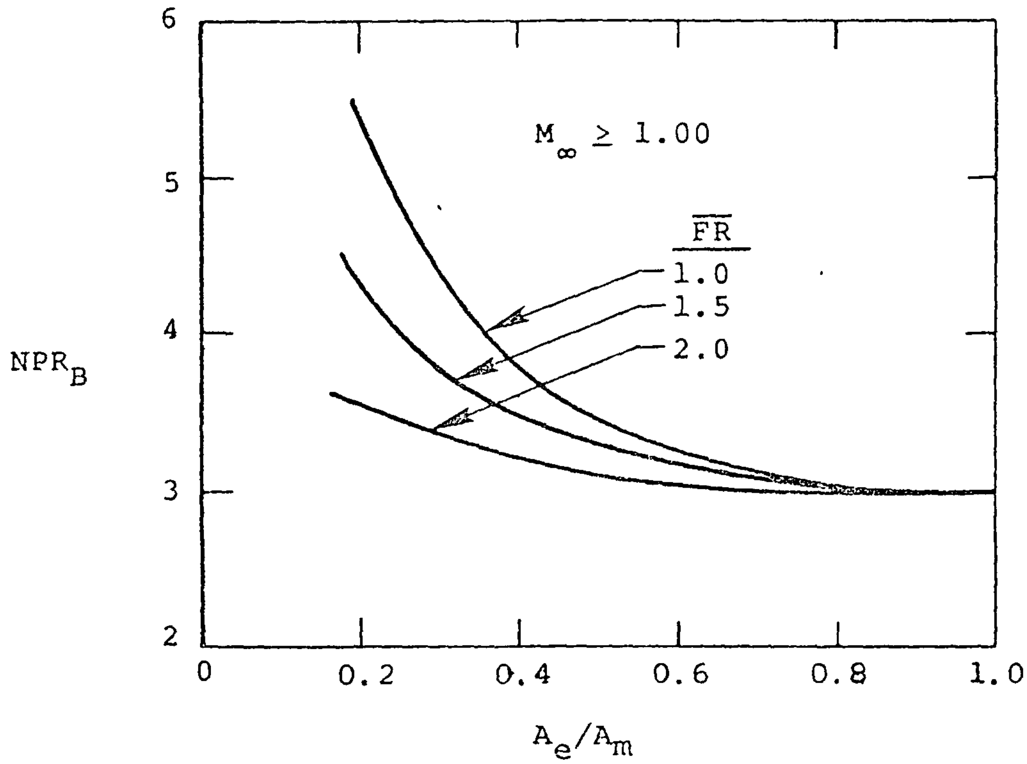

Figure 37. - Basic drag nozzle pressure ratio, NPR_B as a function of boattail geometry.

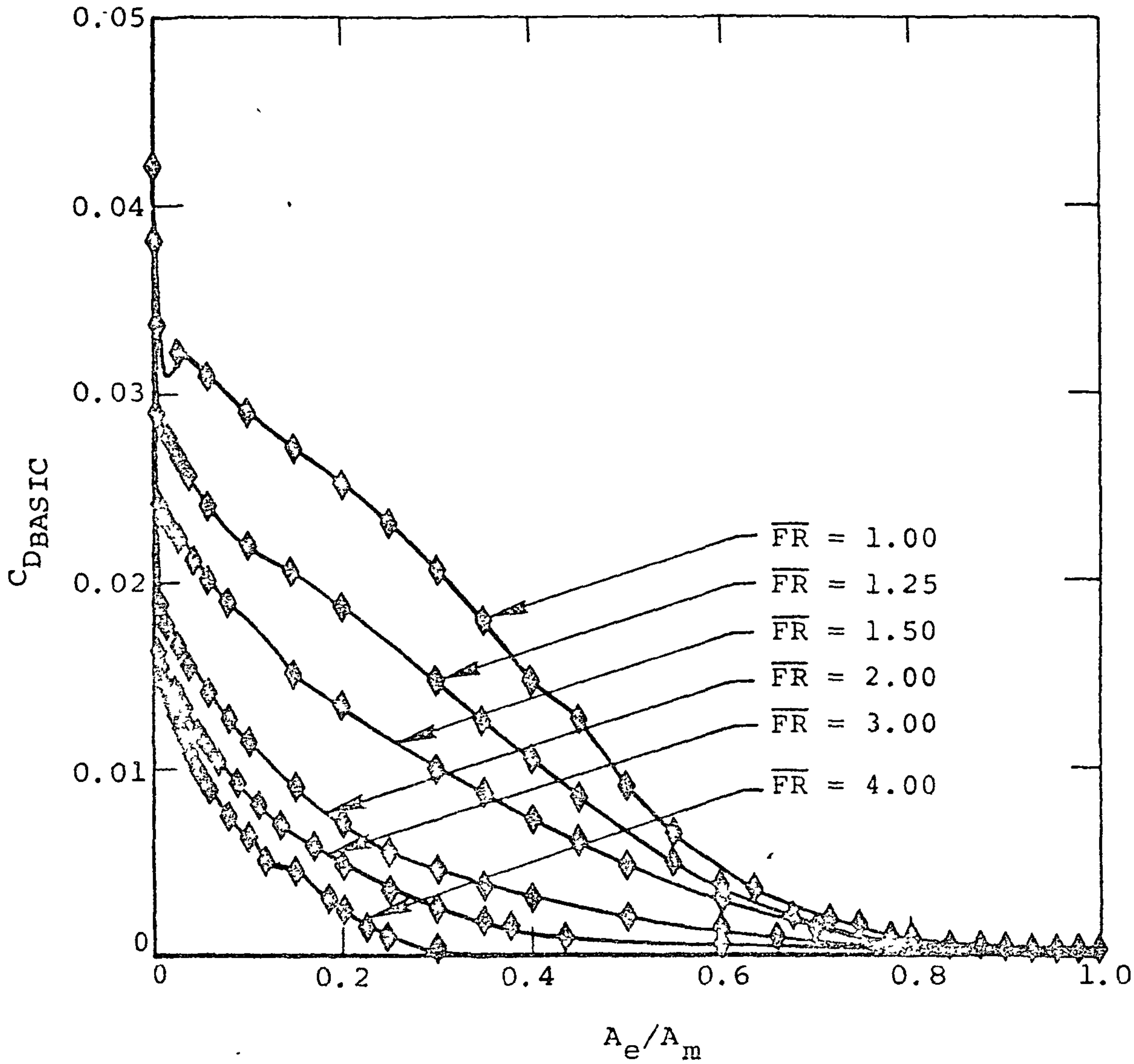

(a) Subsonic ($M_\infty < 0.85$).

Figure 38.- Typical correlations of basic drag.

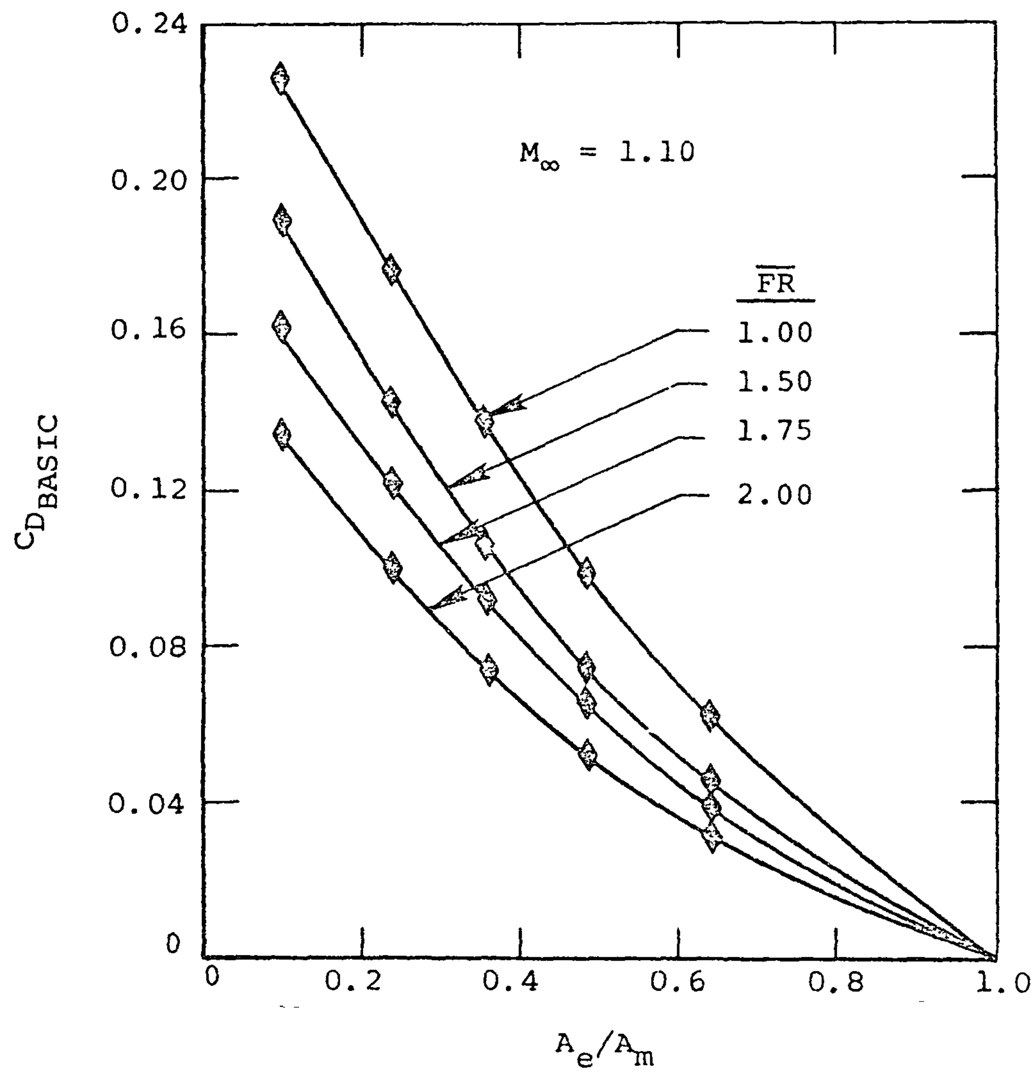

(b) Supersonic ($M_\infty = 1.10$).

Figure 38.- Concluded.

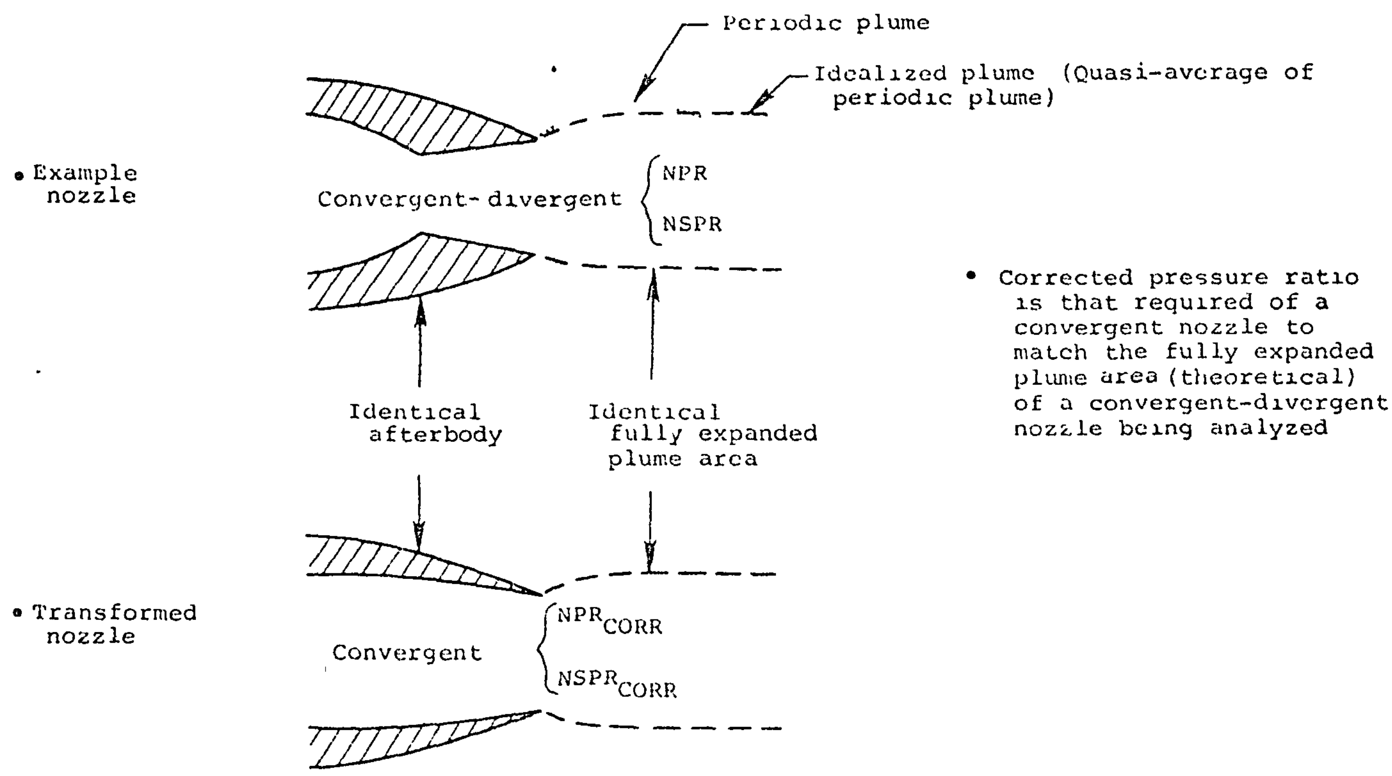

Figure 39.- Corrected pressure ratio definition.

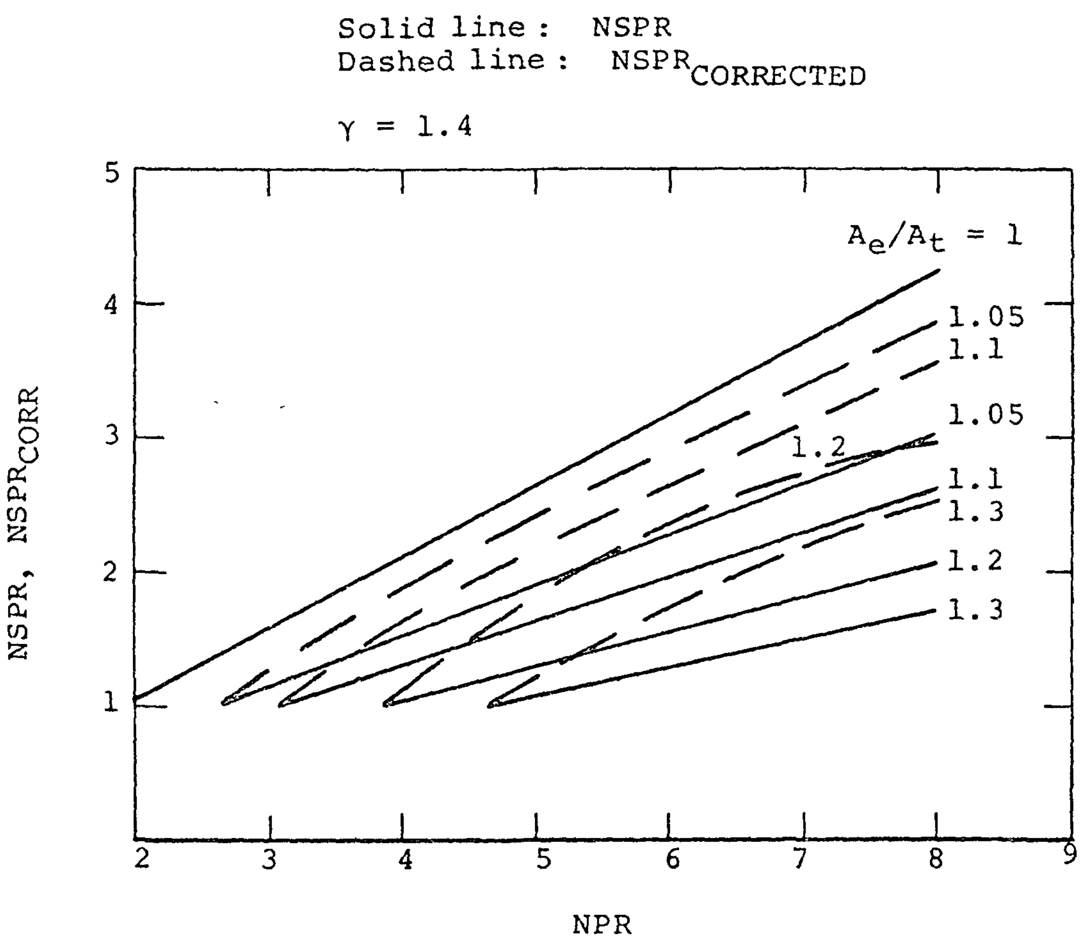

Figure 40.- Example pressure-ratio transforms.

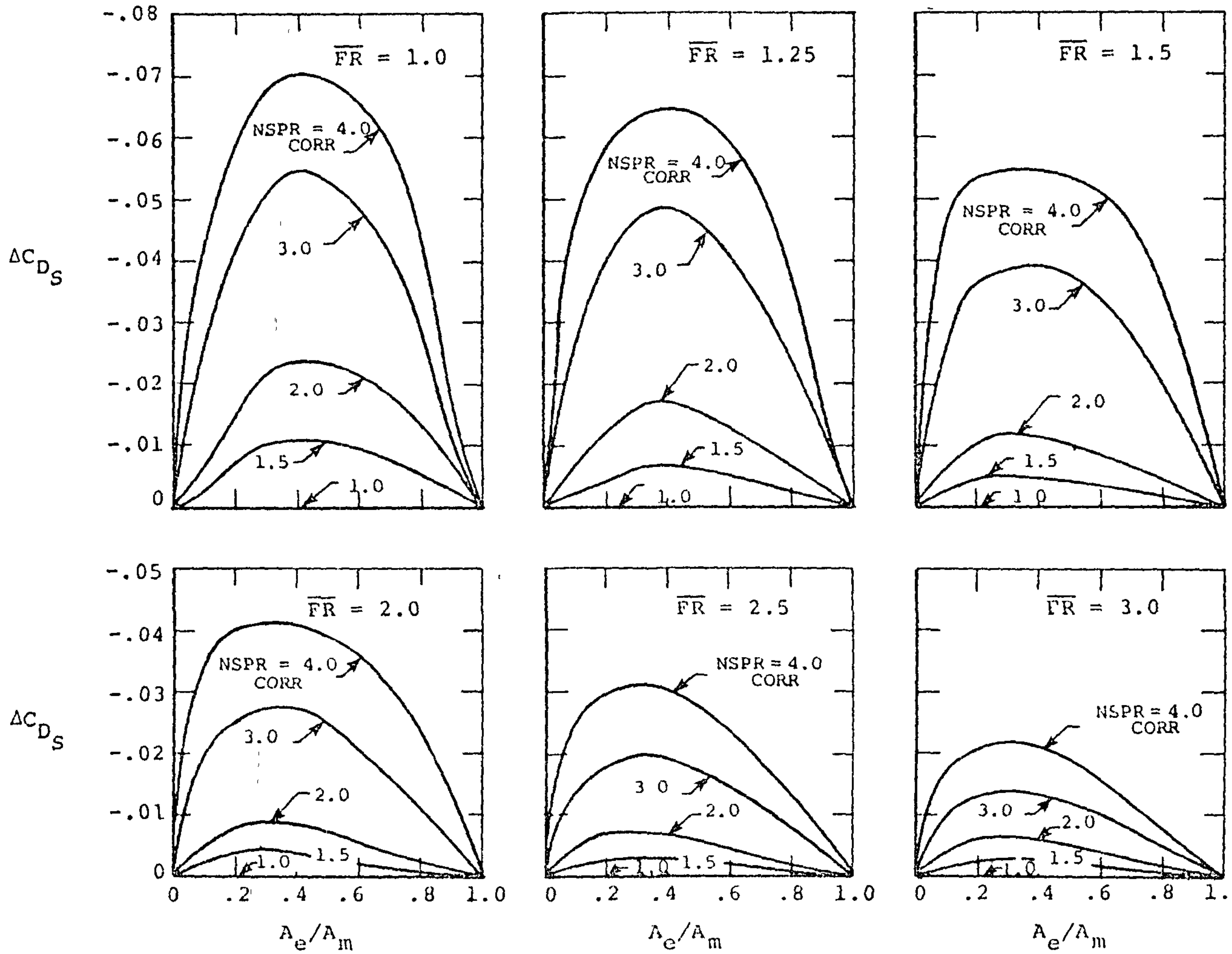

Figure 41.- Plume shape effect on drag.

$$\theta = 1.384\ NSPR_{CORR}\ \frac{\gamma_e}{\gamma_\infty}\left[\frac{1+(M_e-1)^2}{1-(1.176M_\infty-1)^2}\right]$$

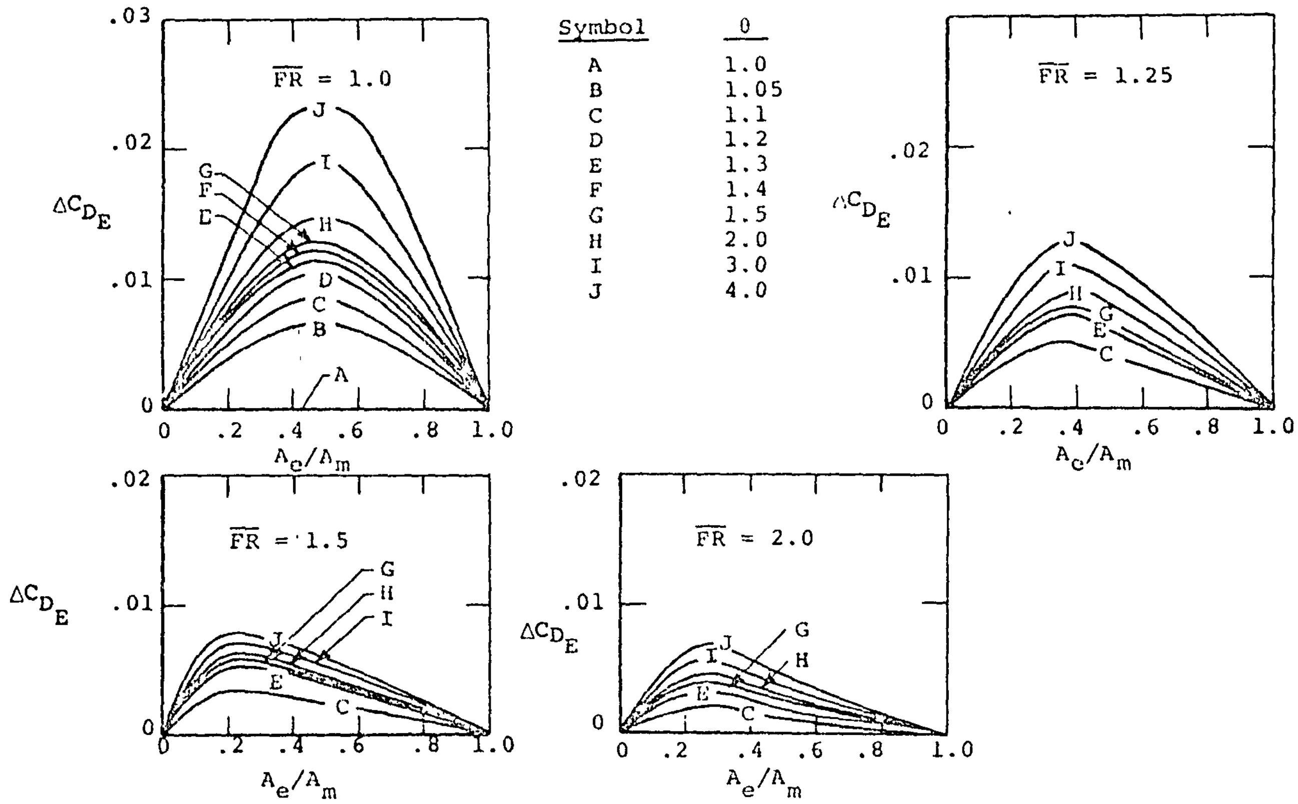

Figure 42.- Plume entrainment effect on drag.

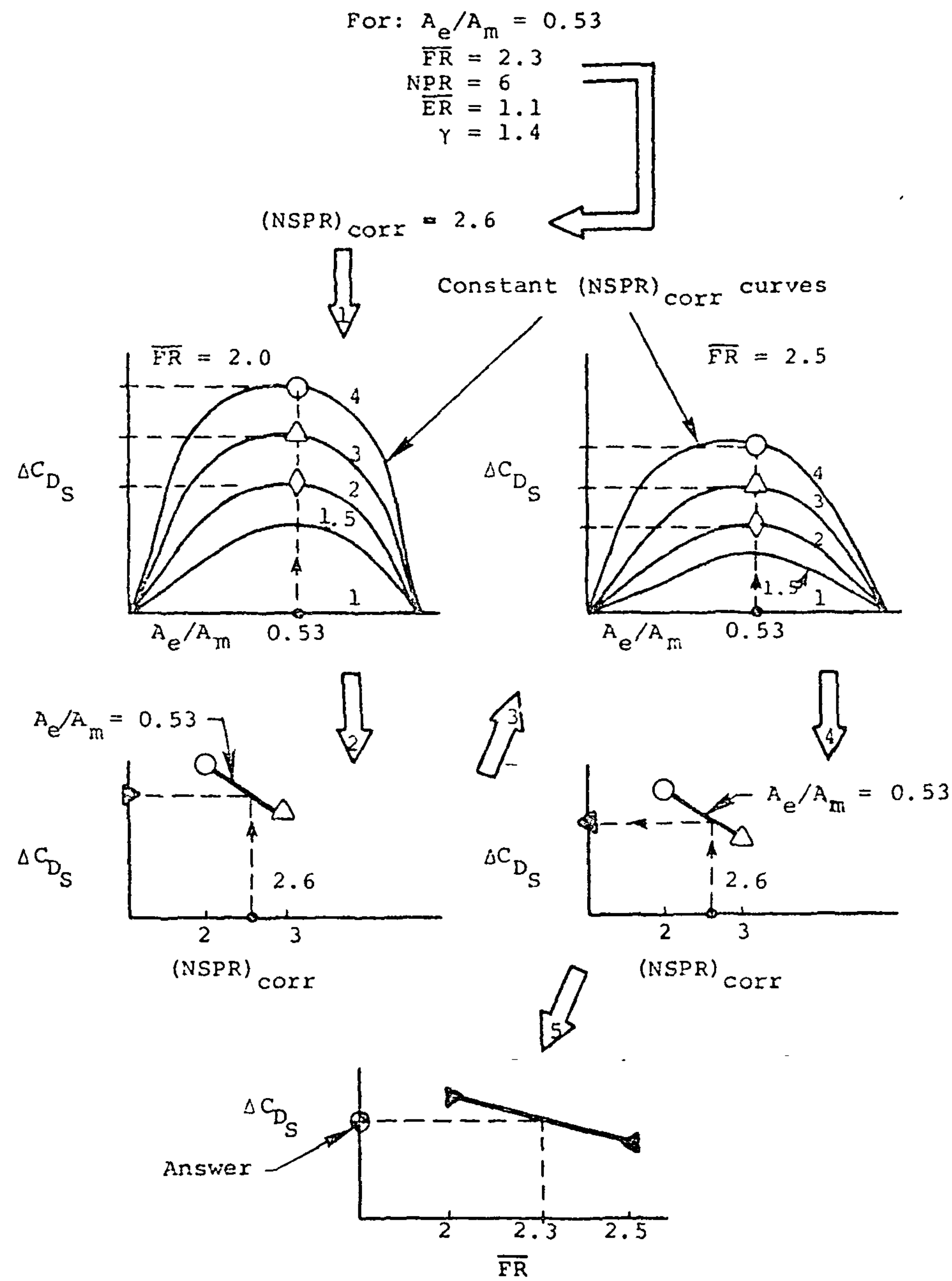

Figure 43.- Example of ADAP interpolation scheme.

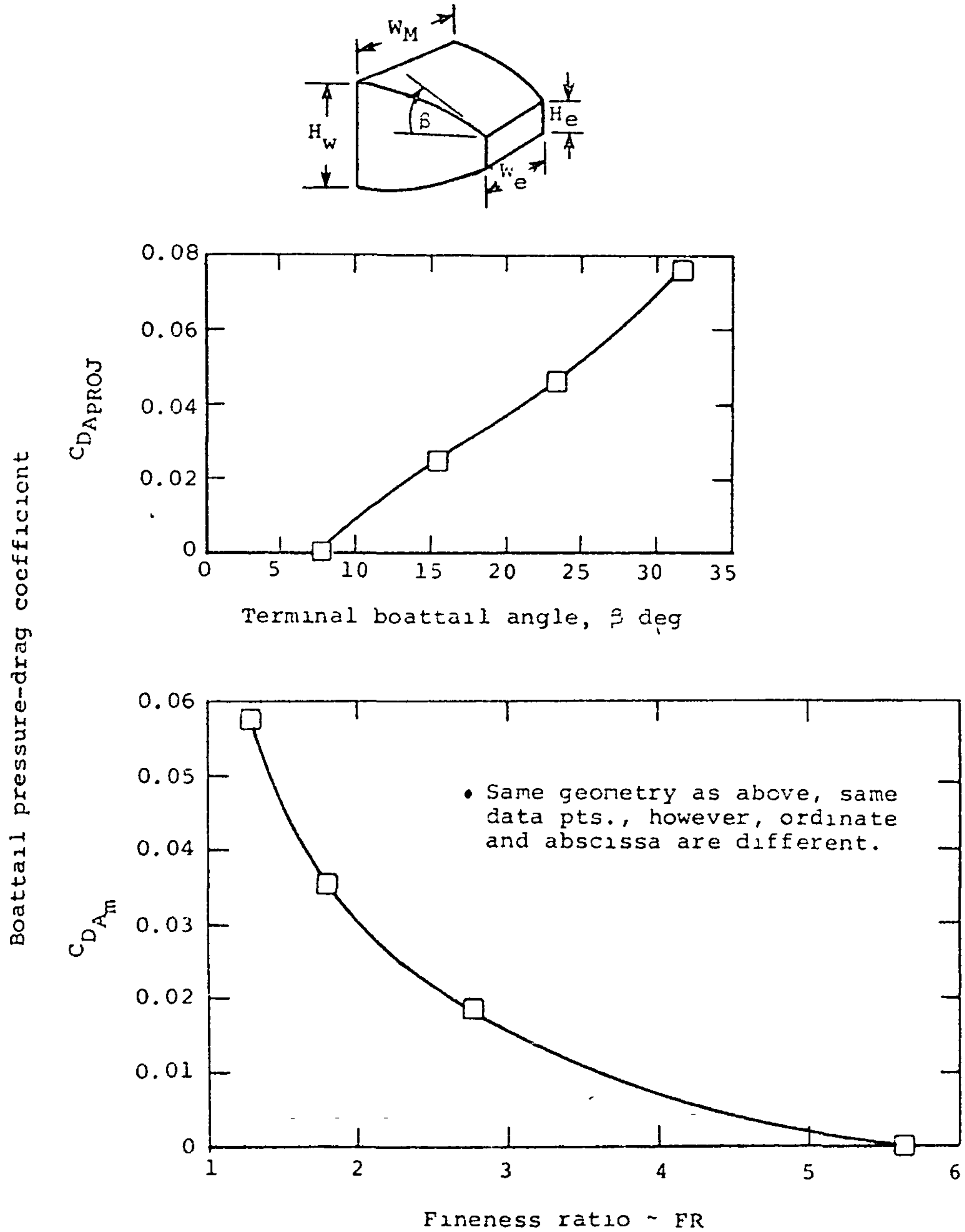

Figure 44.- Nonaxisymmetric nozzle data, $M_\infty = 0.9$, NPR = 2.0, $A_e/A_m = 0.25$.

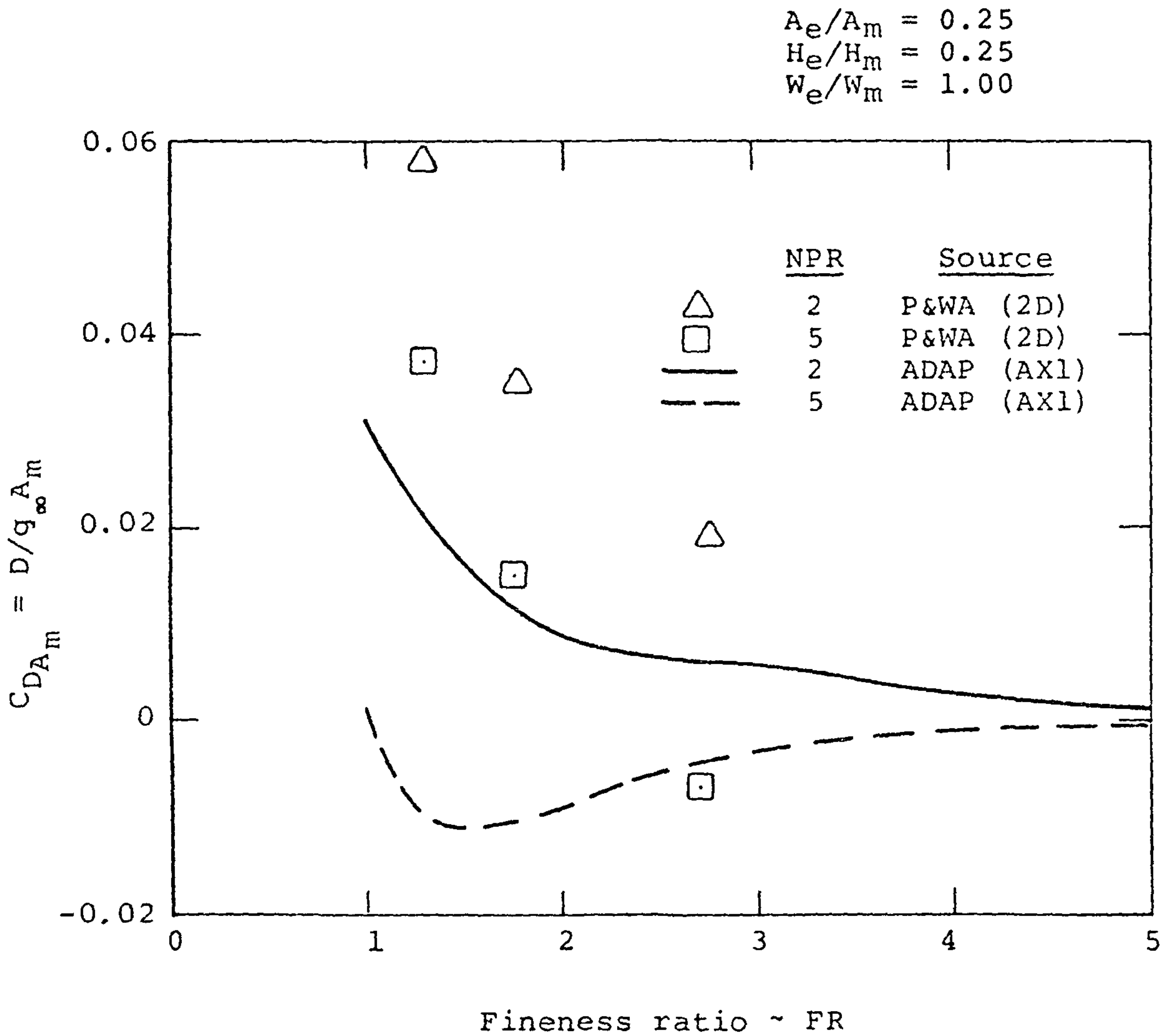

Figure 45 .- Data comparison: 2D nozzle data vs ADAP axisymmetric solution.

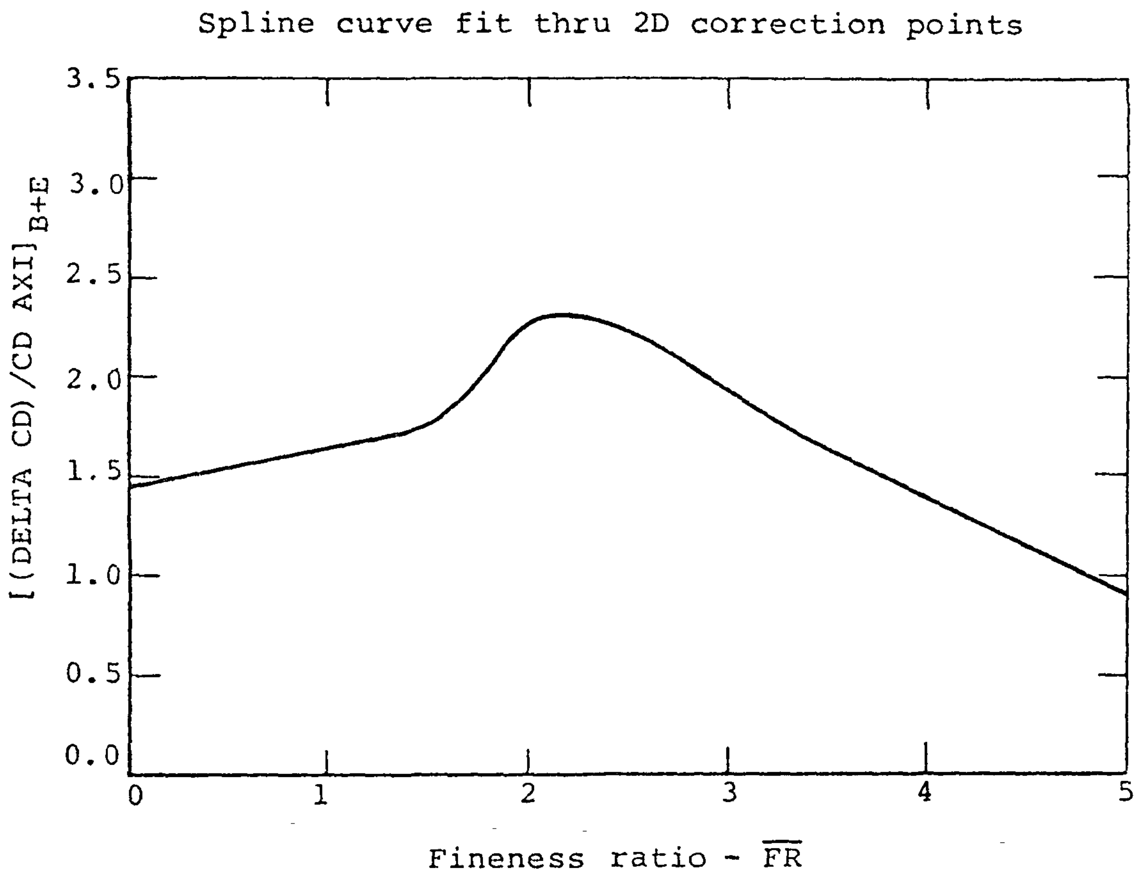

Figure 46.- Two-dimensional effect.

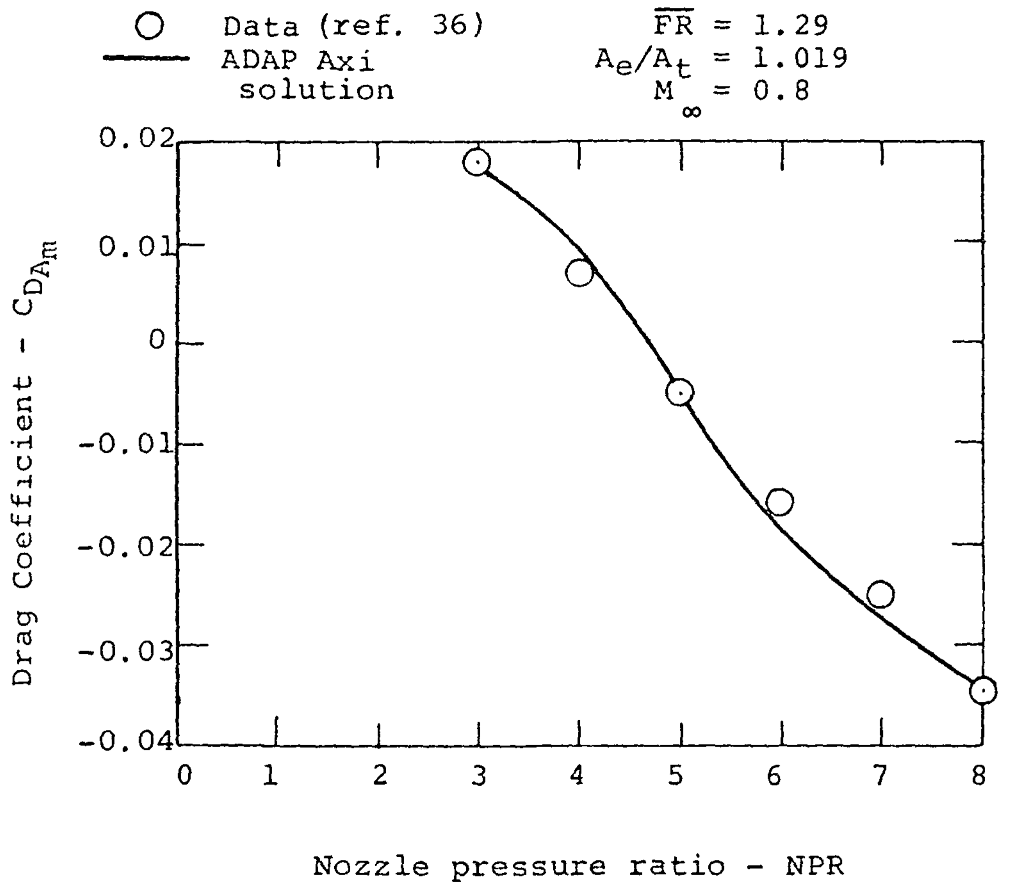

Figure 47.- Example of ADAP drag prediction for axisymmetric nozzles.

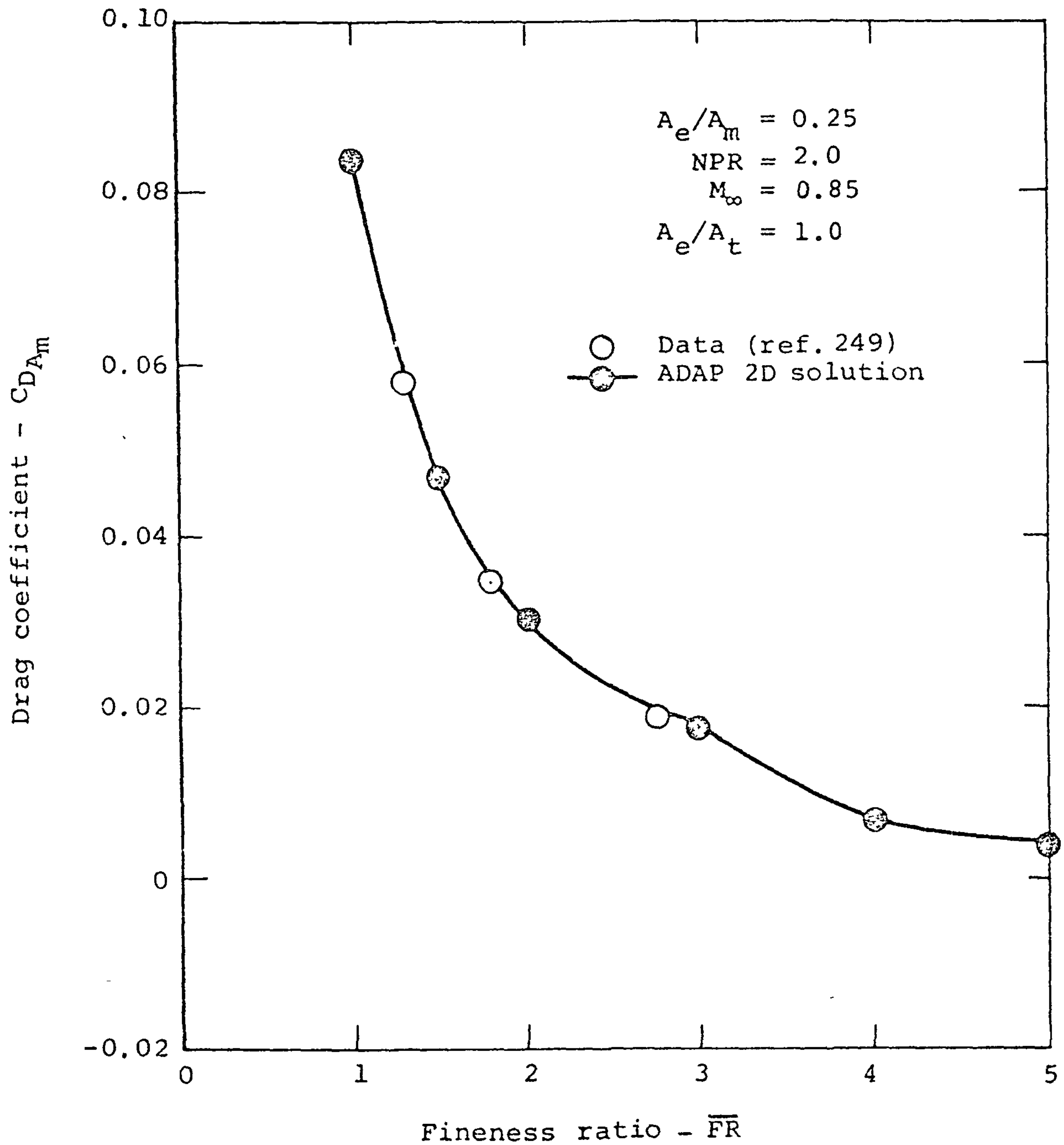

Figure 48.- Example of ADAP drag predictions for 2-D nozzles.

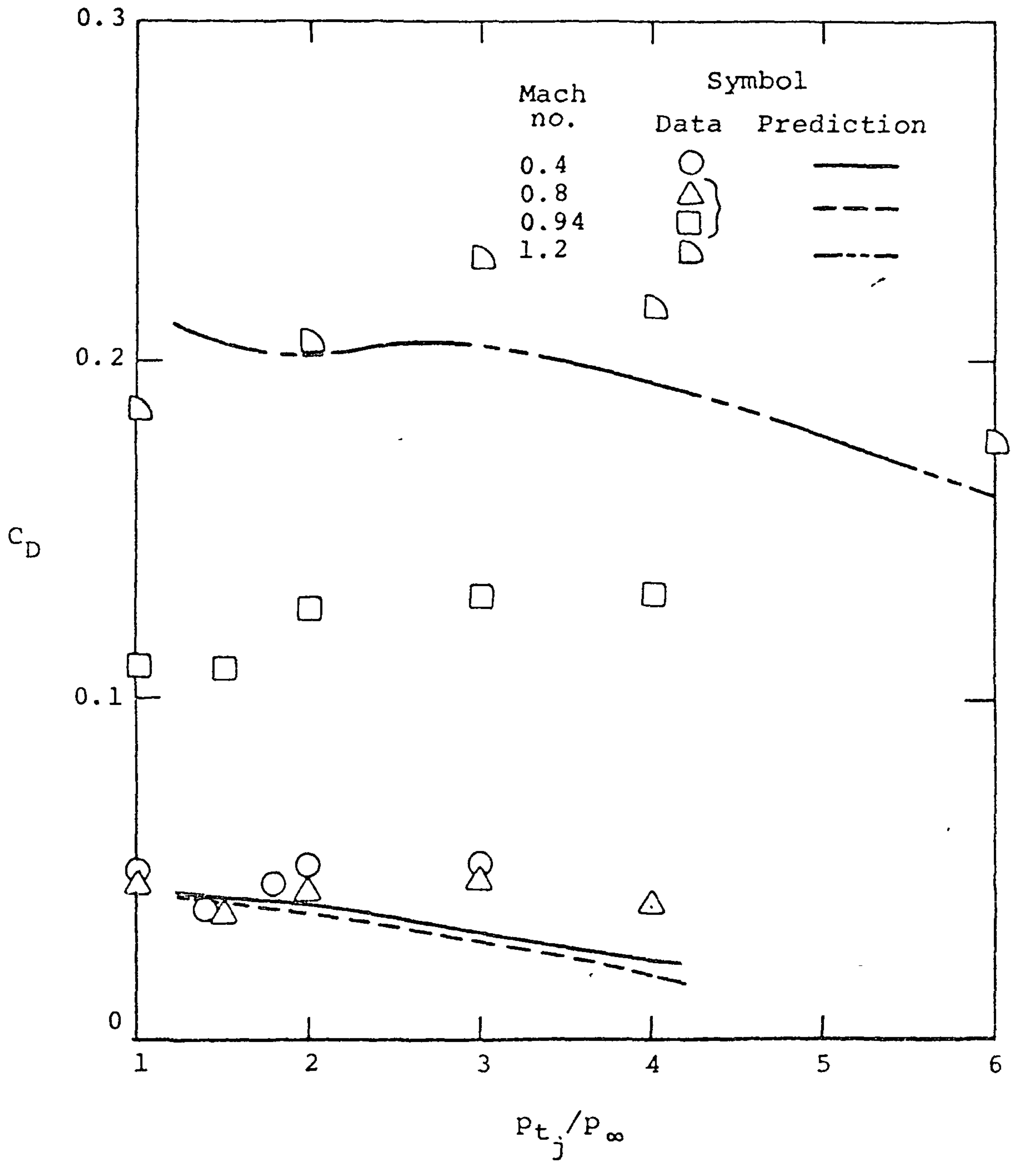

(a) $\overline{FR} = 0.8$, $A_e/A_m = 0.25$.

Figure 49.- Comparison between data and ADAP predicted drag coefficients on several circular arc boattails.

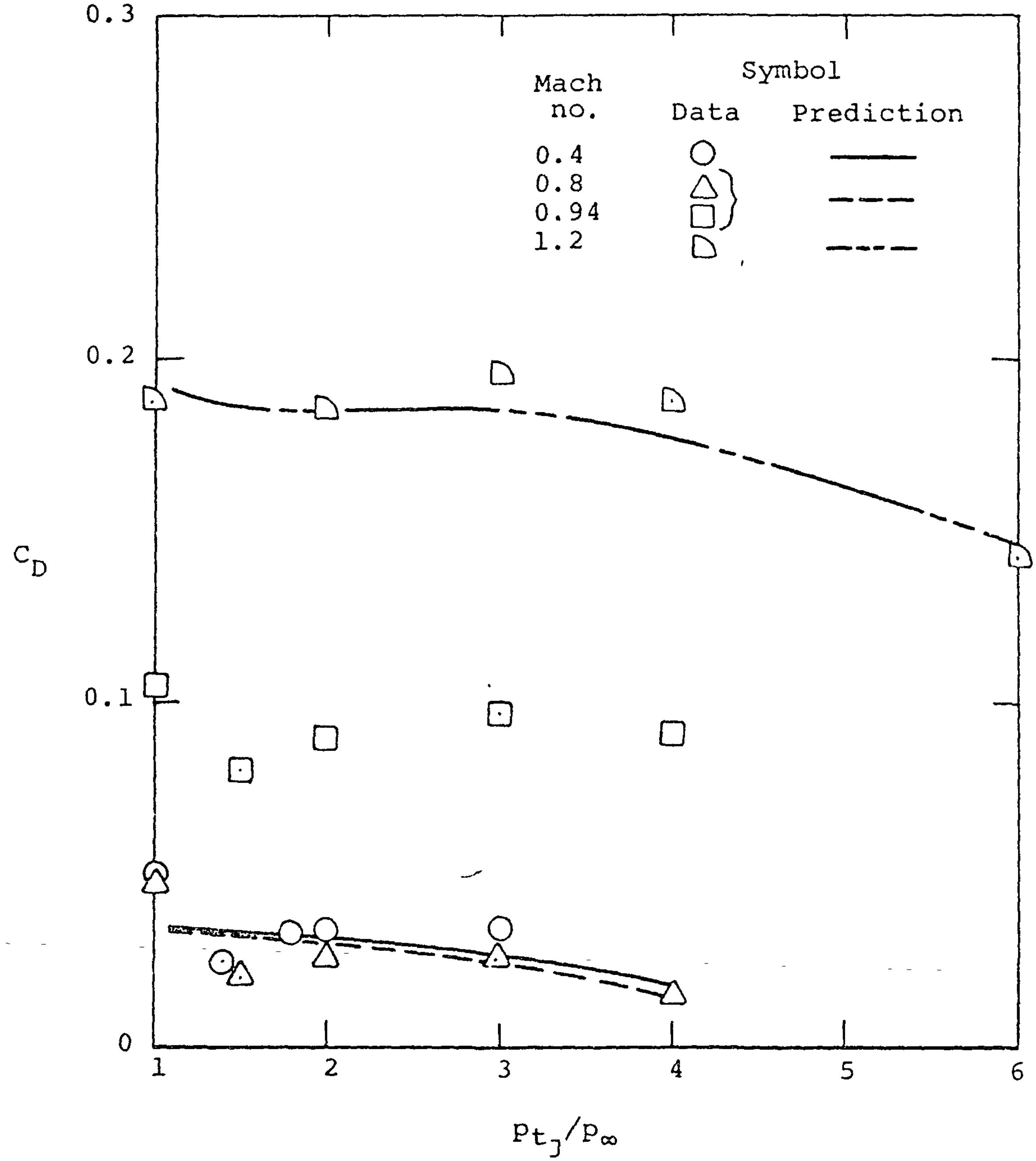

(b) $\overline{FR} = 1.0$, $A_e/A_m = 0.25$.

Figure 49.- Continued.

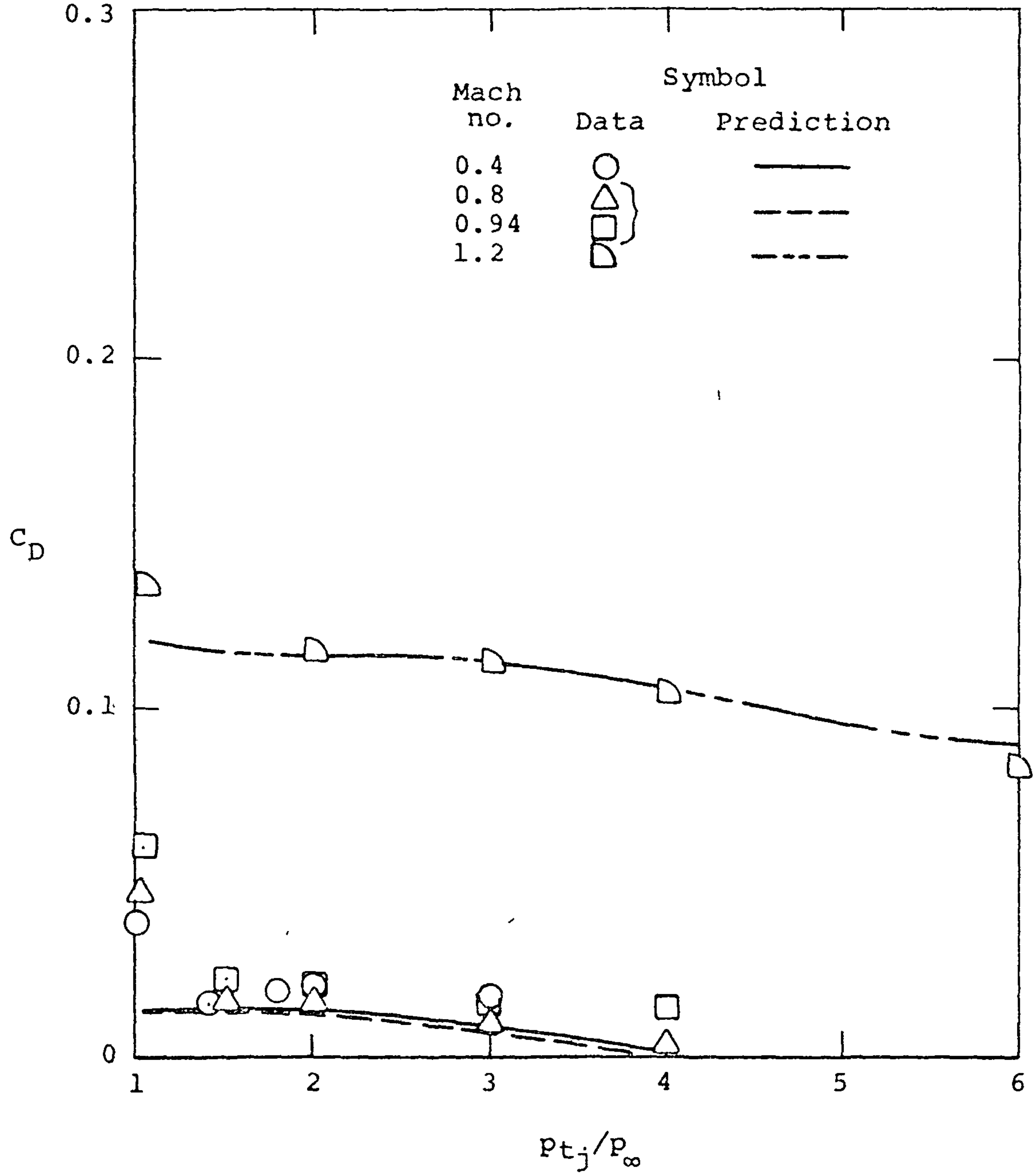

(c) $\overline{FR} = 1.768$, $A_e/A_m = 0.25$.

Figure 49.- Continued.

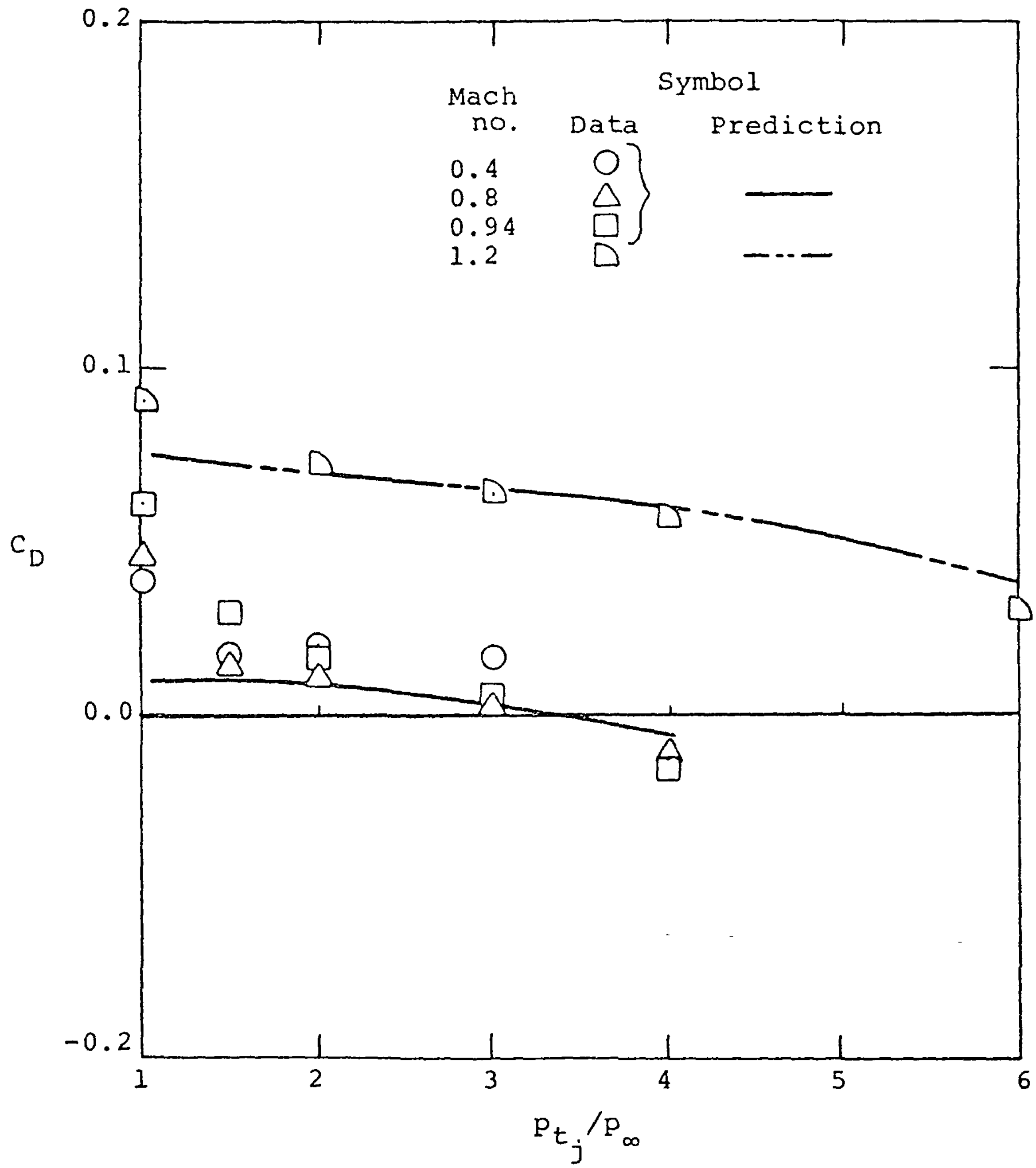

(d) $\overline{FR} = 1.5$, $A_e/A_m = 0.49$.

Figure 49.- Concluded.

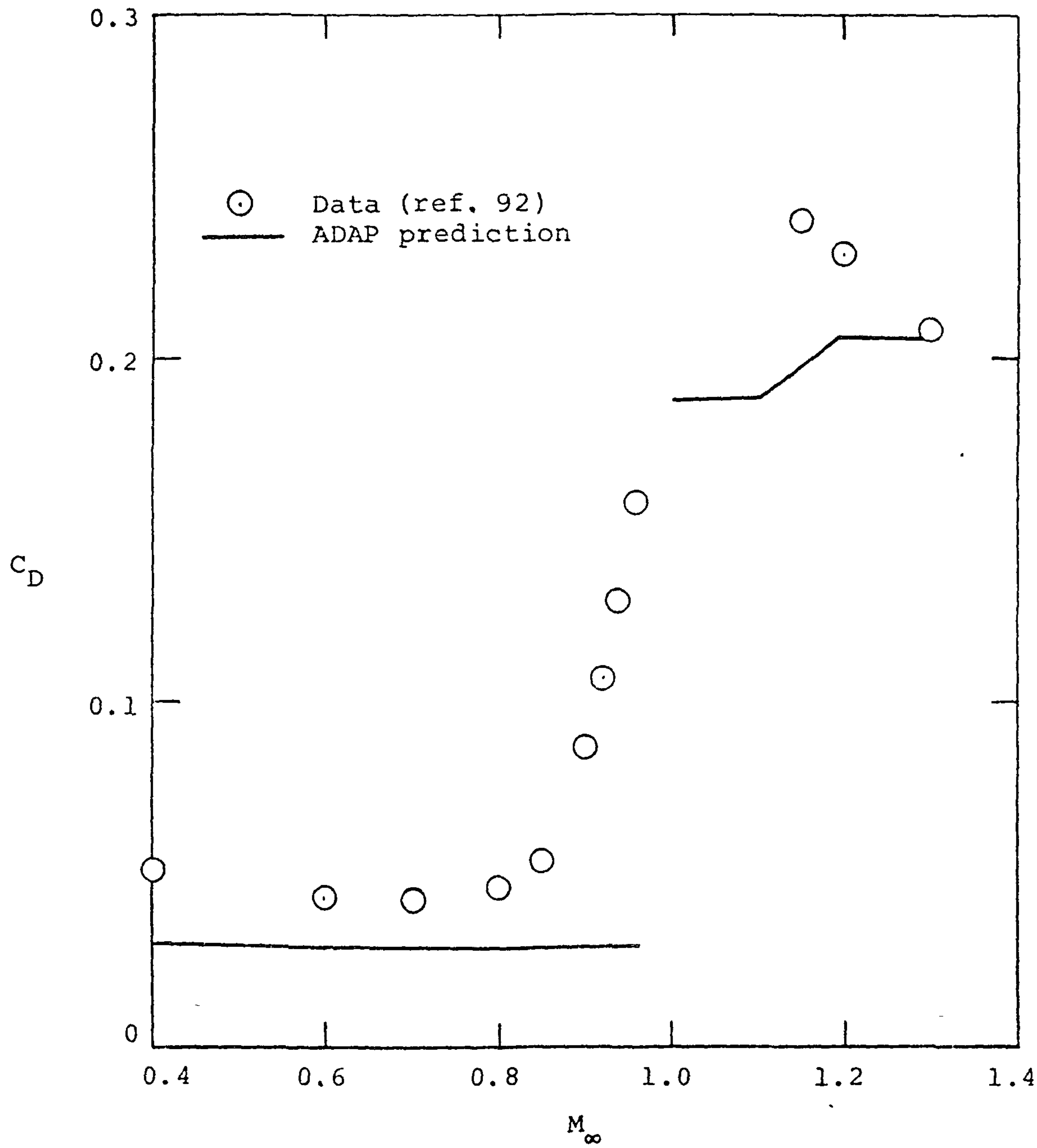

(a) $\overline{FR} = 0.8$, $A_e/A_m = 0.25$.

Figure 50 .- Comparison between data and ADAP prediction for Mach number dependence of boattail-drag coefficients at $p_{t_J}/p_\infty = 3.0$.

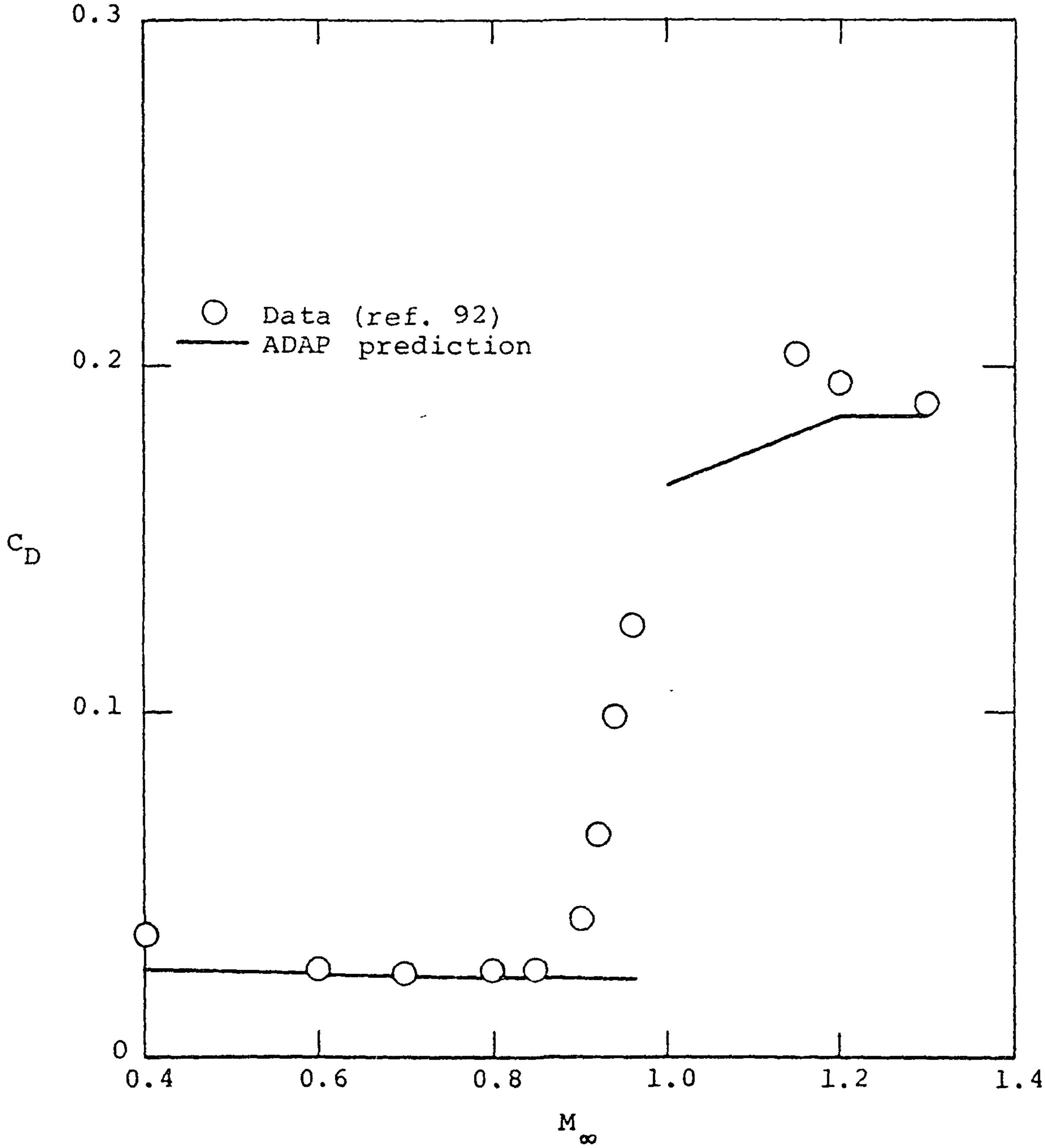

(b) $\overline{FR} = 1.0$, $A_e/A_m = 0.25$.

Figure 50.- Continued.

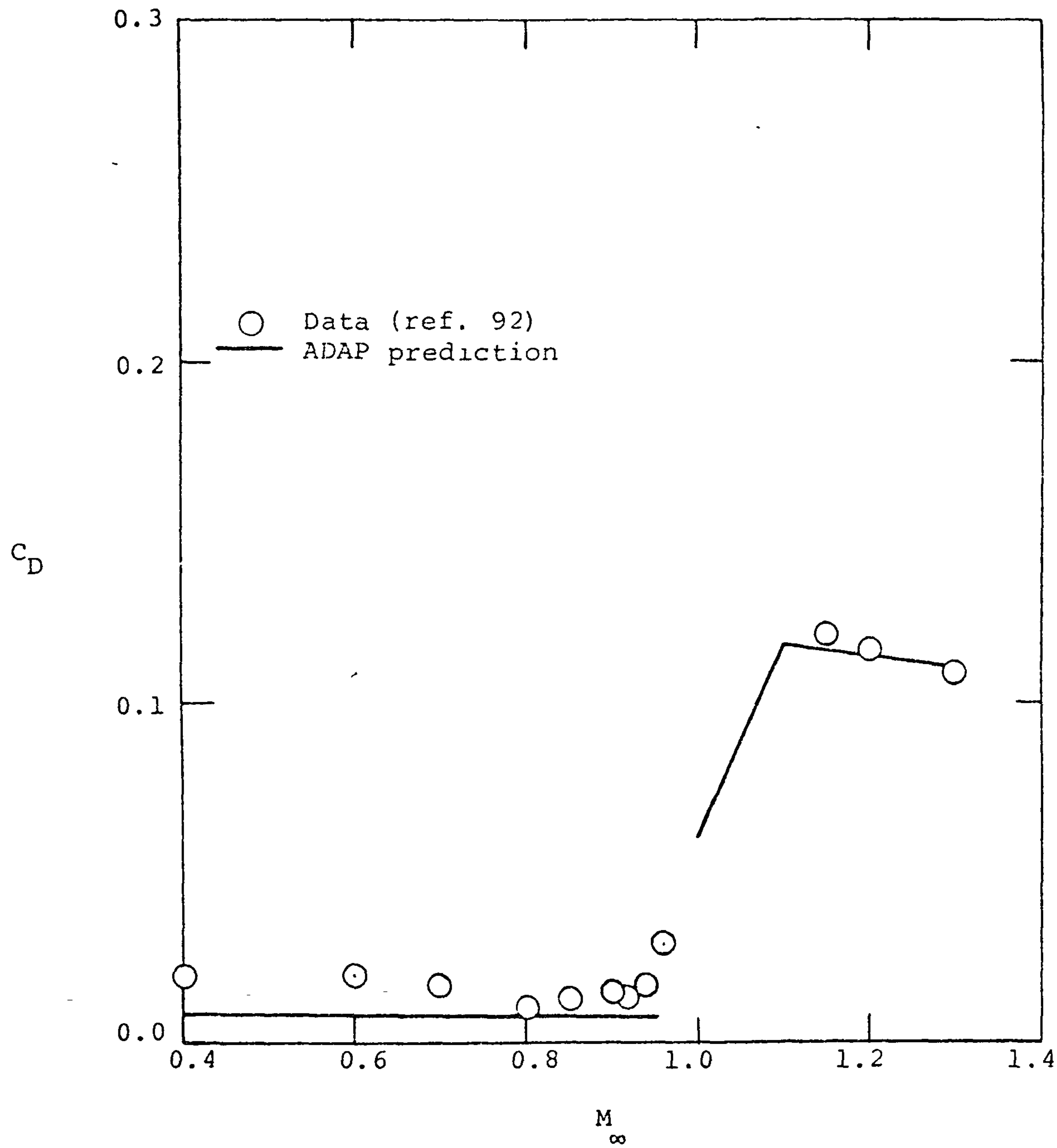

(c) $\overline{FR}$ = 1.768, A_e/A_m = 0.25.

Figure 50 .- Continued.

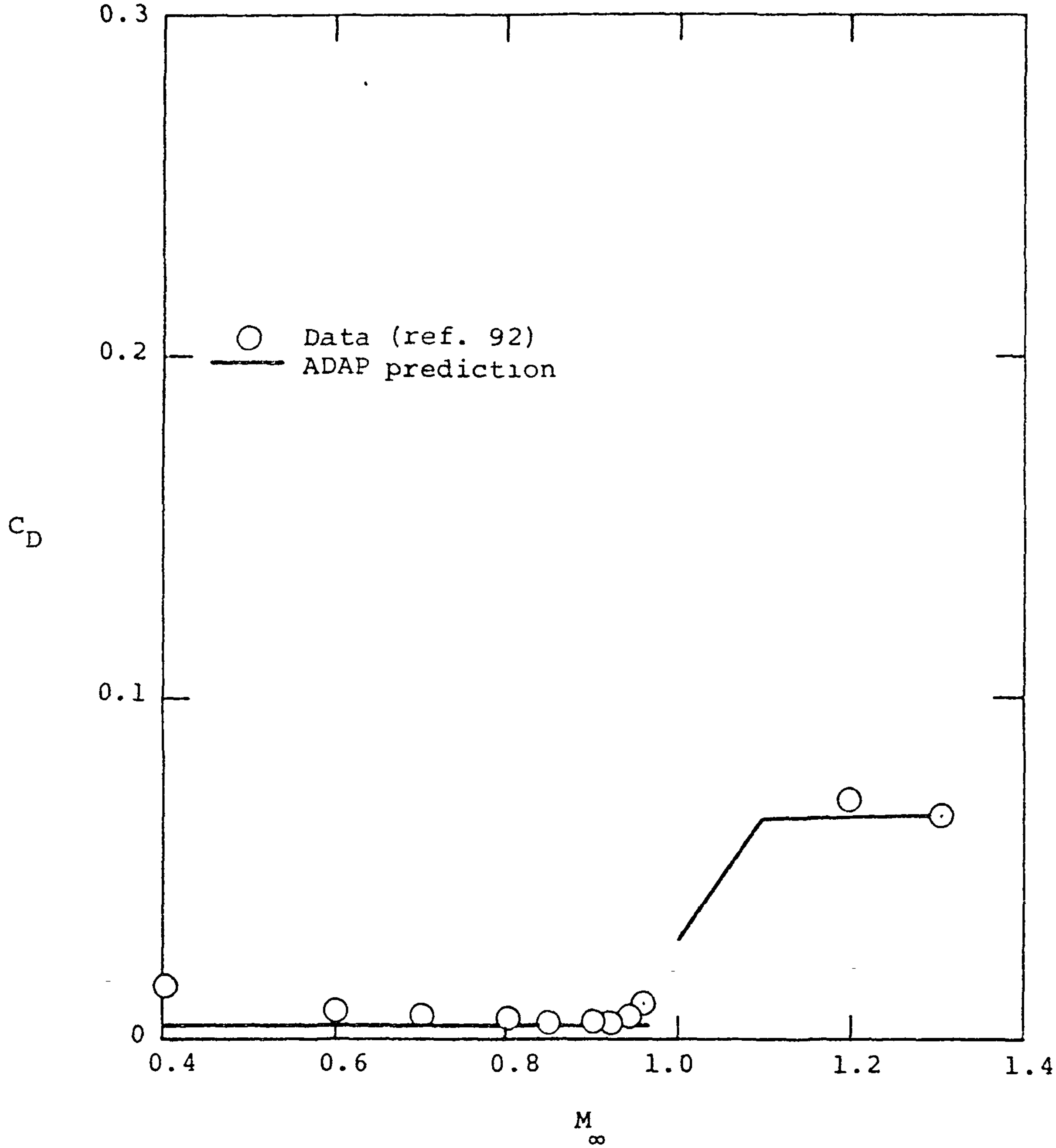

(d) FR = 1.5, A_e/A_m = 0.49.

Figure 50.- Concluded.

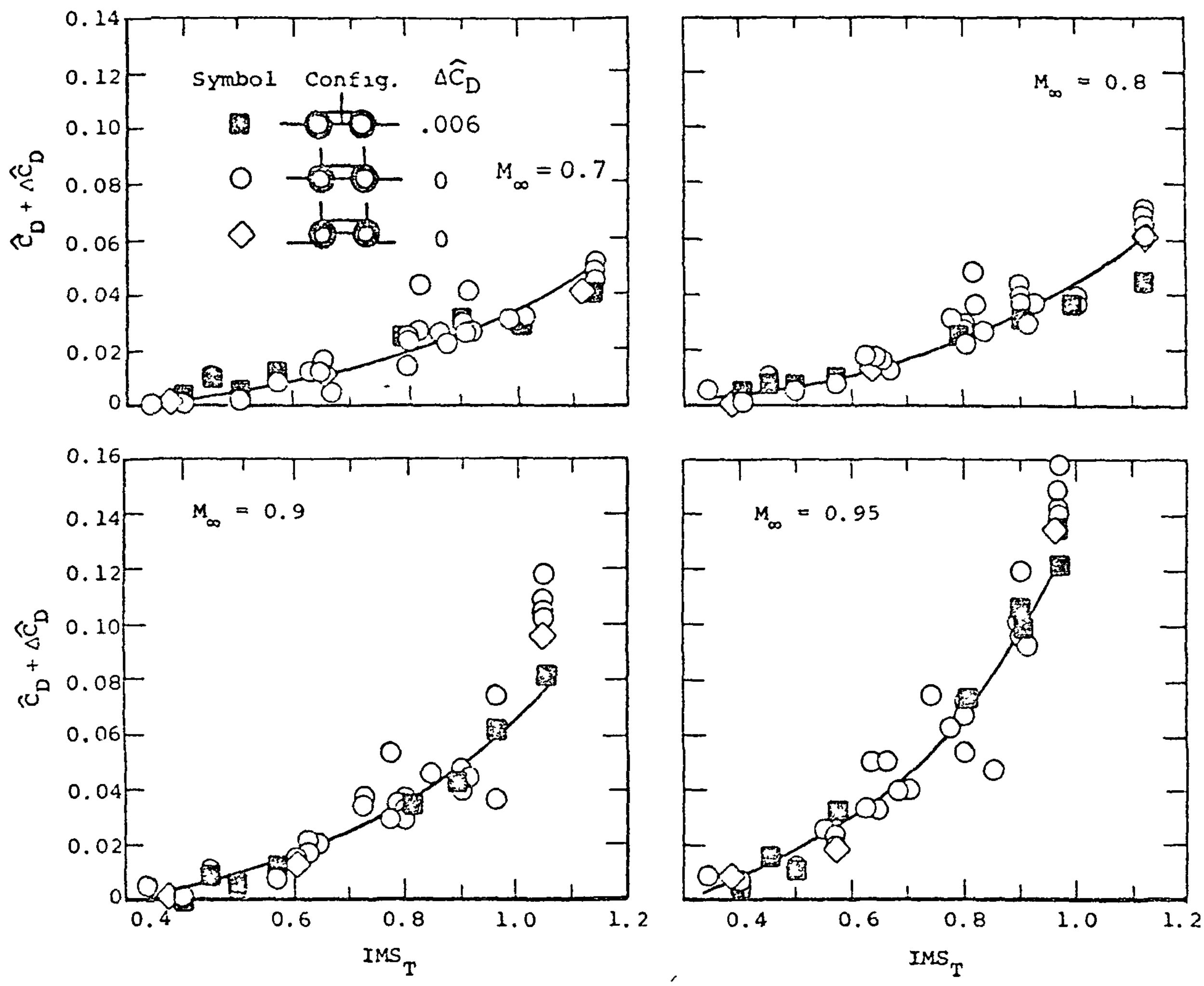

Figure 51.- Combined drag correlation for single and twin vertical configurations.

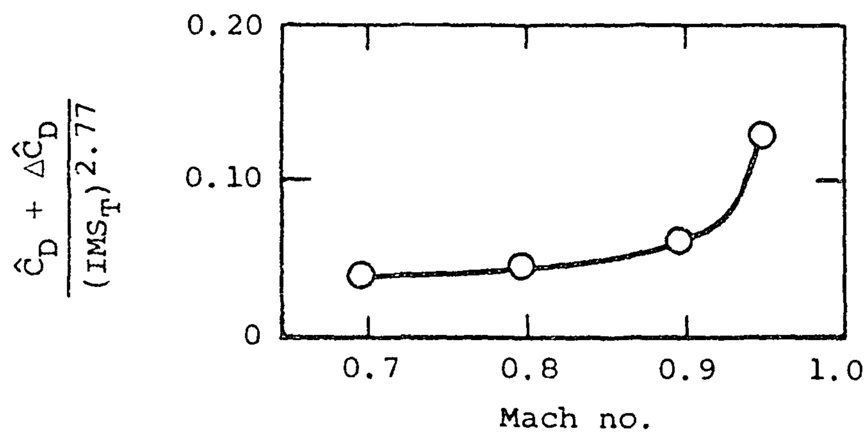

Figure 52.- Final correlation curve for single and twin vertical configurations.

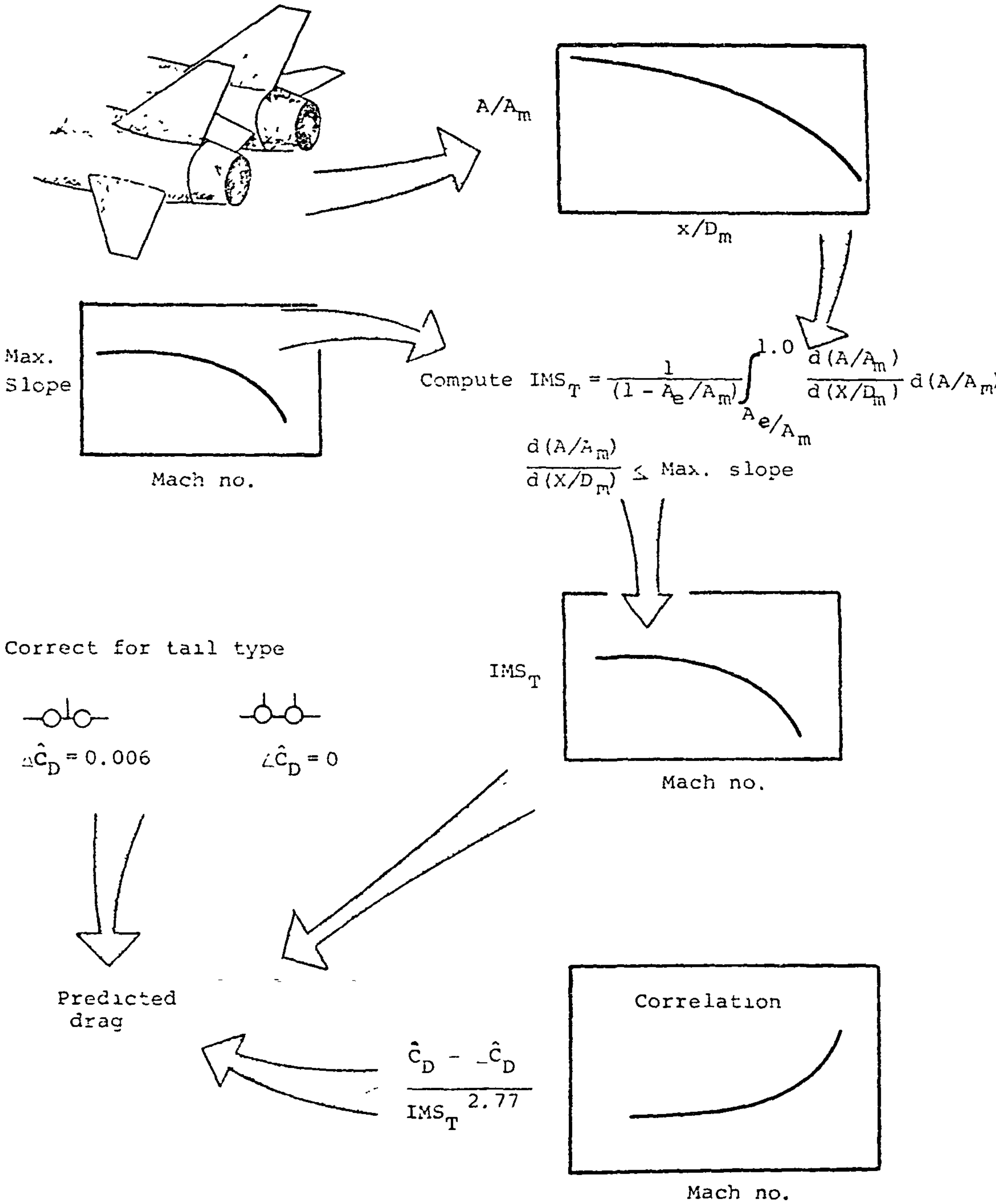

Figure 53.- ESIP drag prediction procedure.

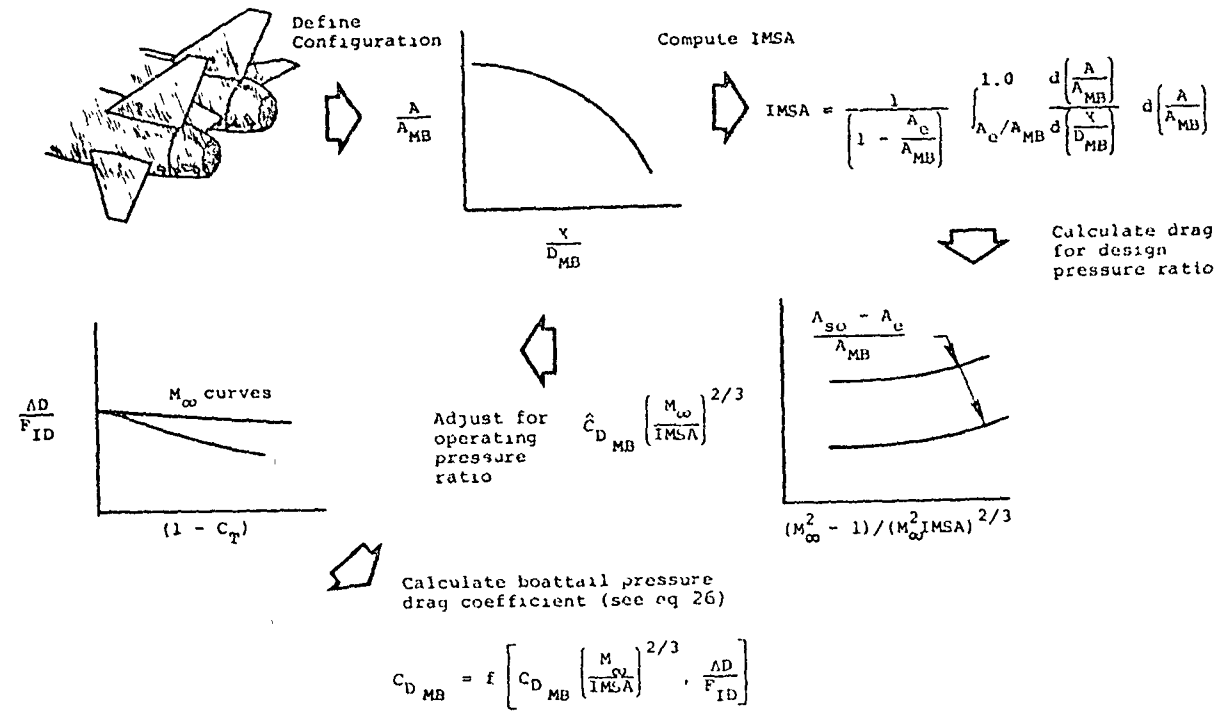

(a) Subsonic flow.

Figure 54.- Schematic of Calac drag prediction procedure.

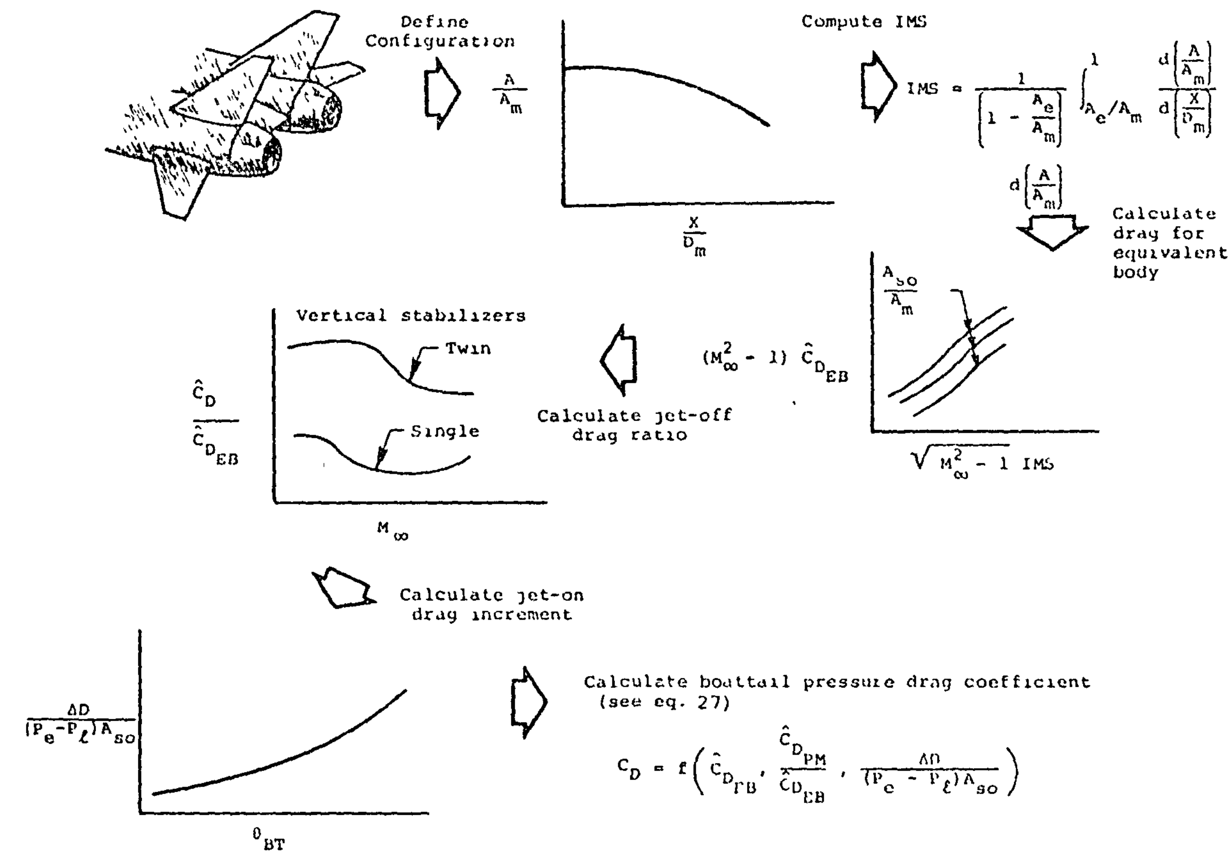

(b) Supersonic flow.

Figure 54.- Concluded.

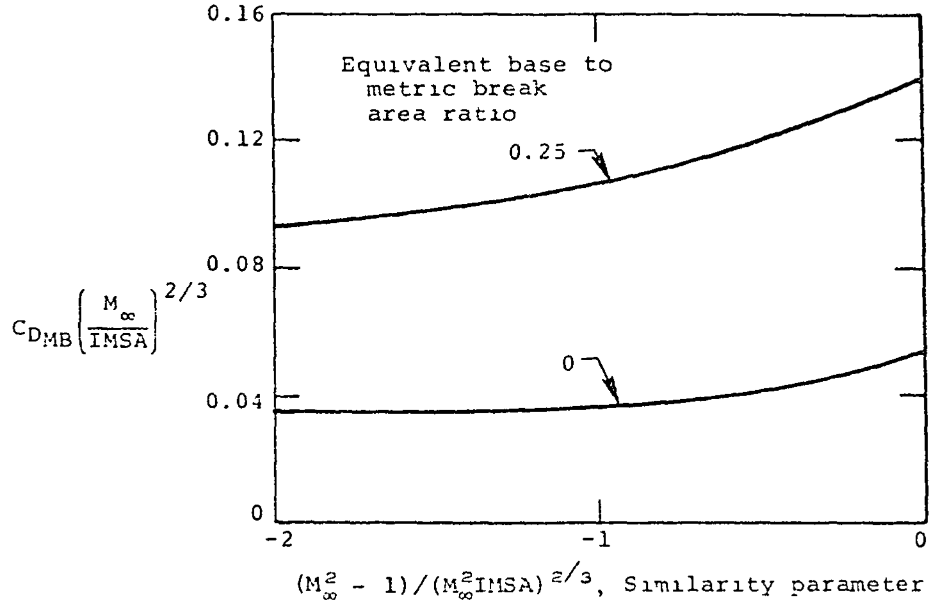

Figure 55.- Transonic similarity correlation of total aft-end pressure drag; single vertical stabilizer and horizontal interfairing.

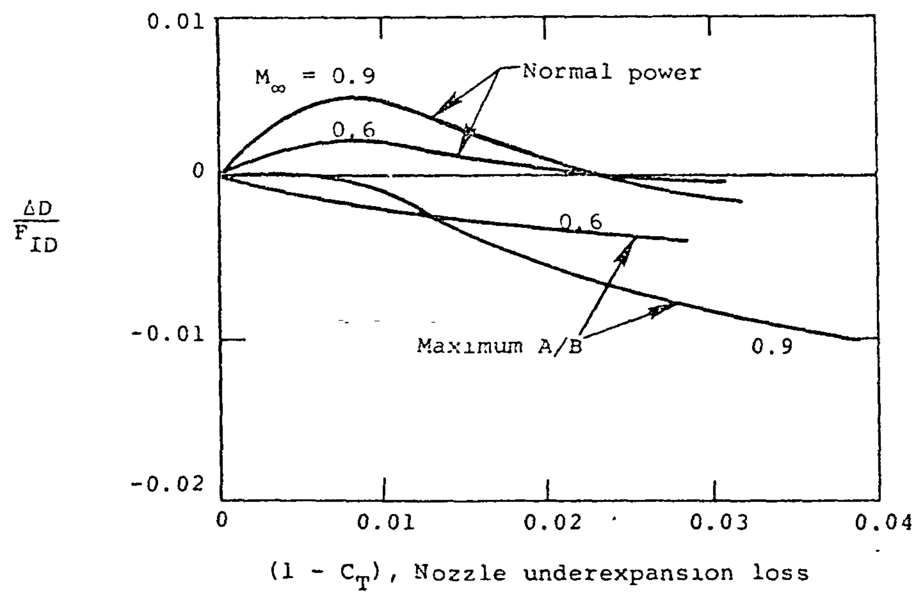

Figure 56.- Correlation of drag increment from design to operating pressure ratio, convergent-flap nozzle.

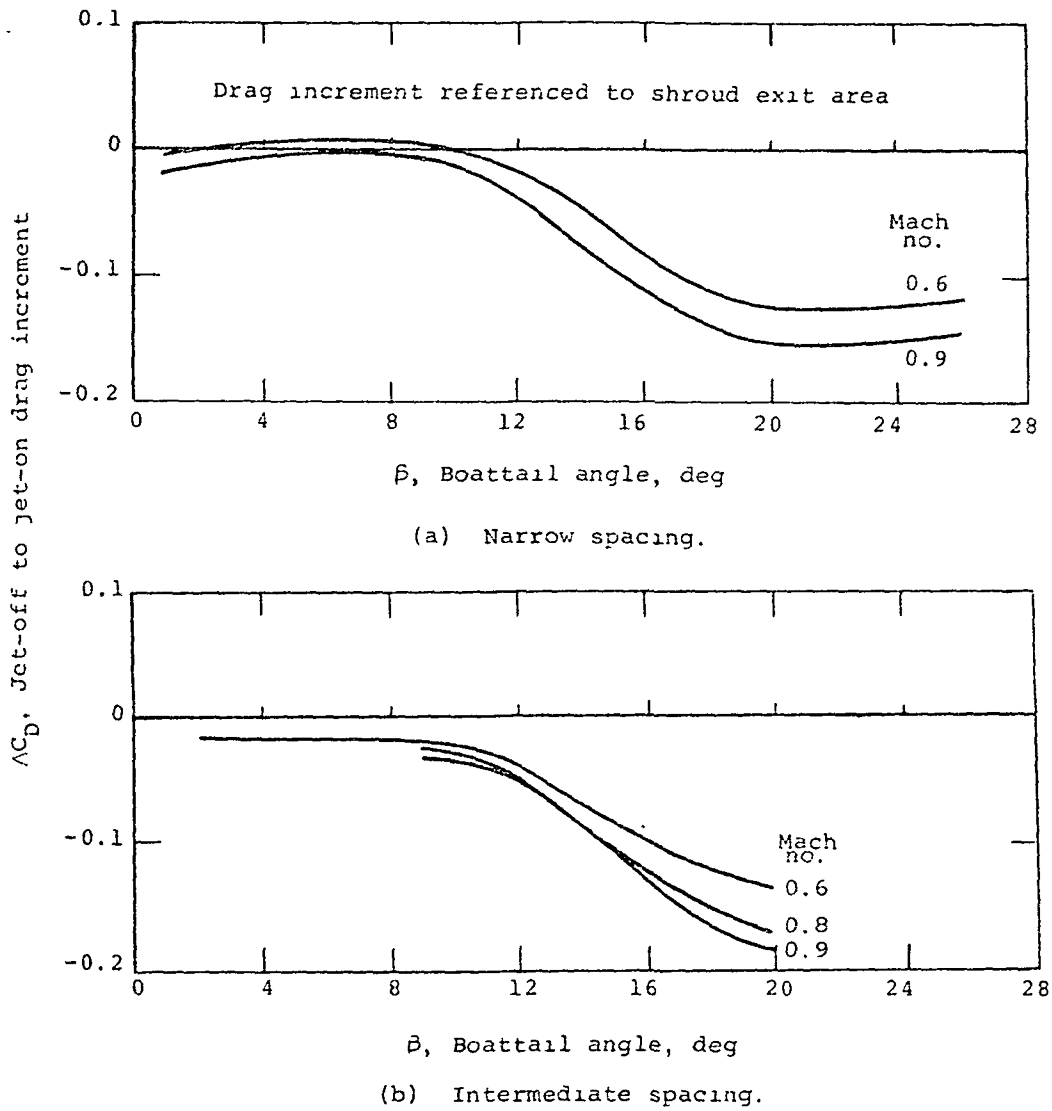

Figure 57.- Correlation of drag increment from jet-off to design pressure ratio.

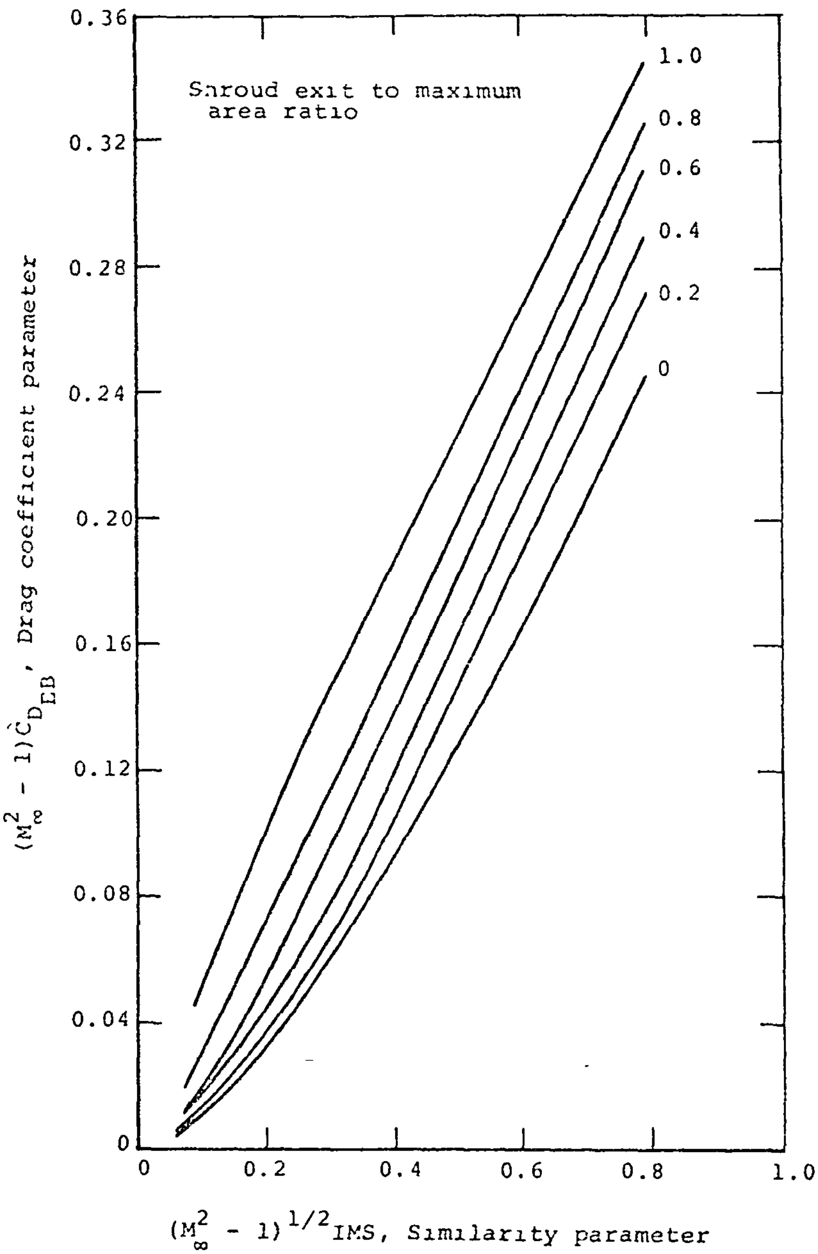

Figure 58.- IMS/supersonic similarity correlation of method of characteristics boattail pressure drag.

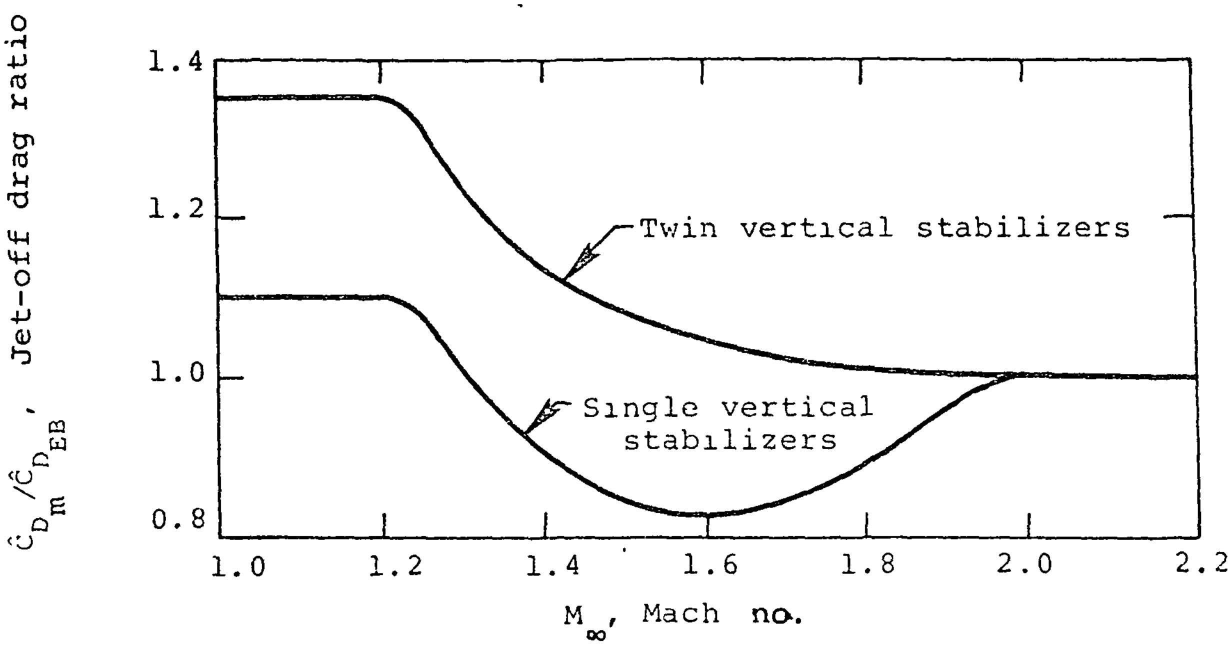

Figure 59.—Equivalent body correlation.

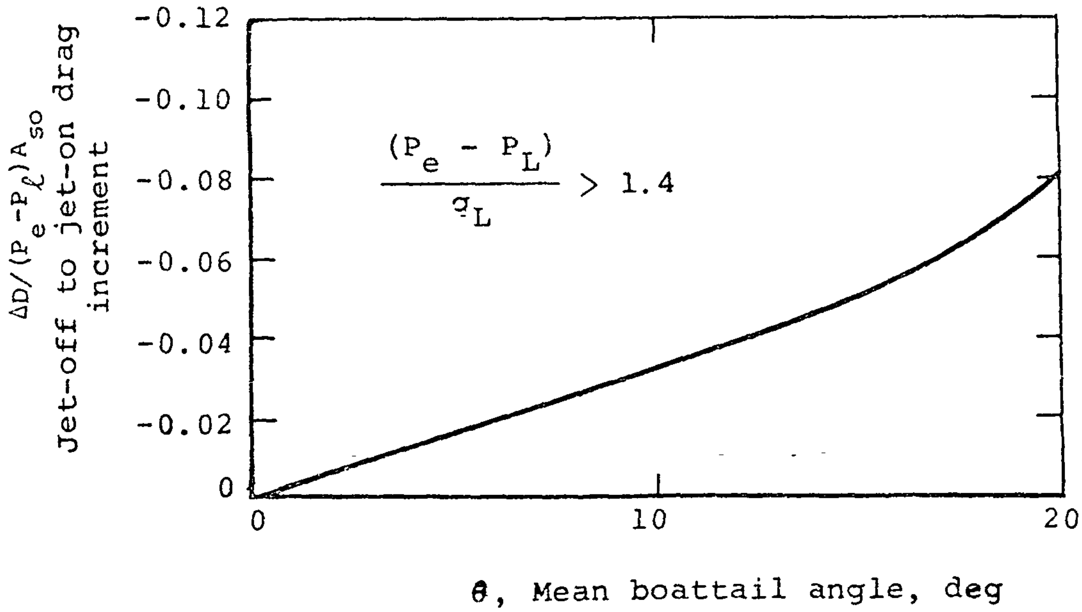

Figure 60.- Correlation of drag increment from jet-off to jet-on operation, supersonic flow.

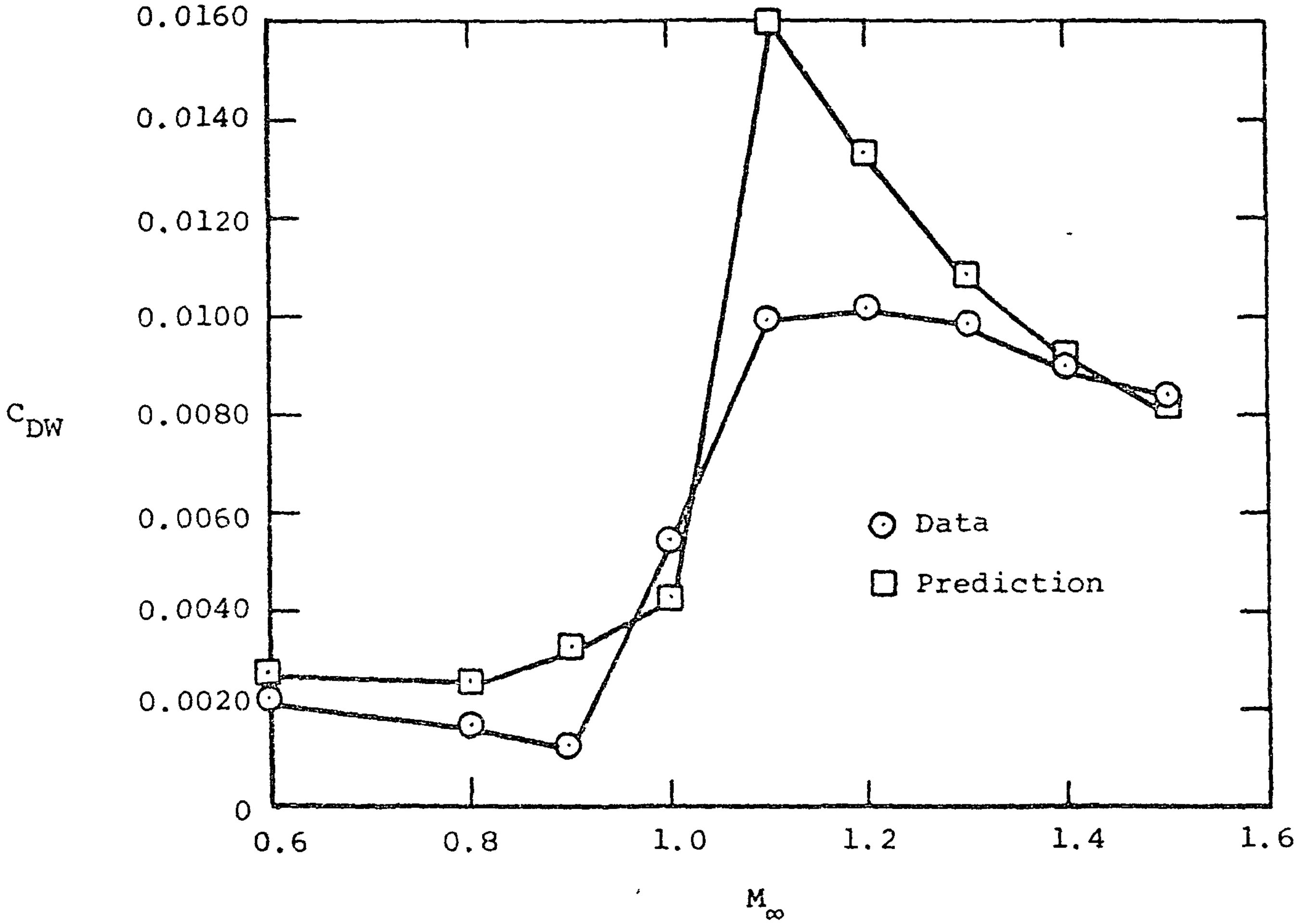

(a) NPR = 3.3.

Figure 61.- Comparison between measured and predicted-drag coefficient for cruise nozzle (ref. 41).

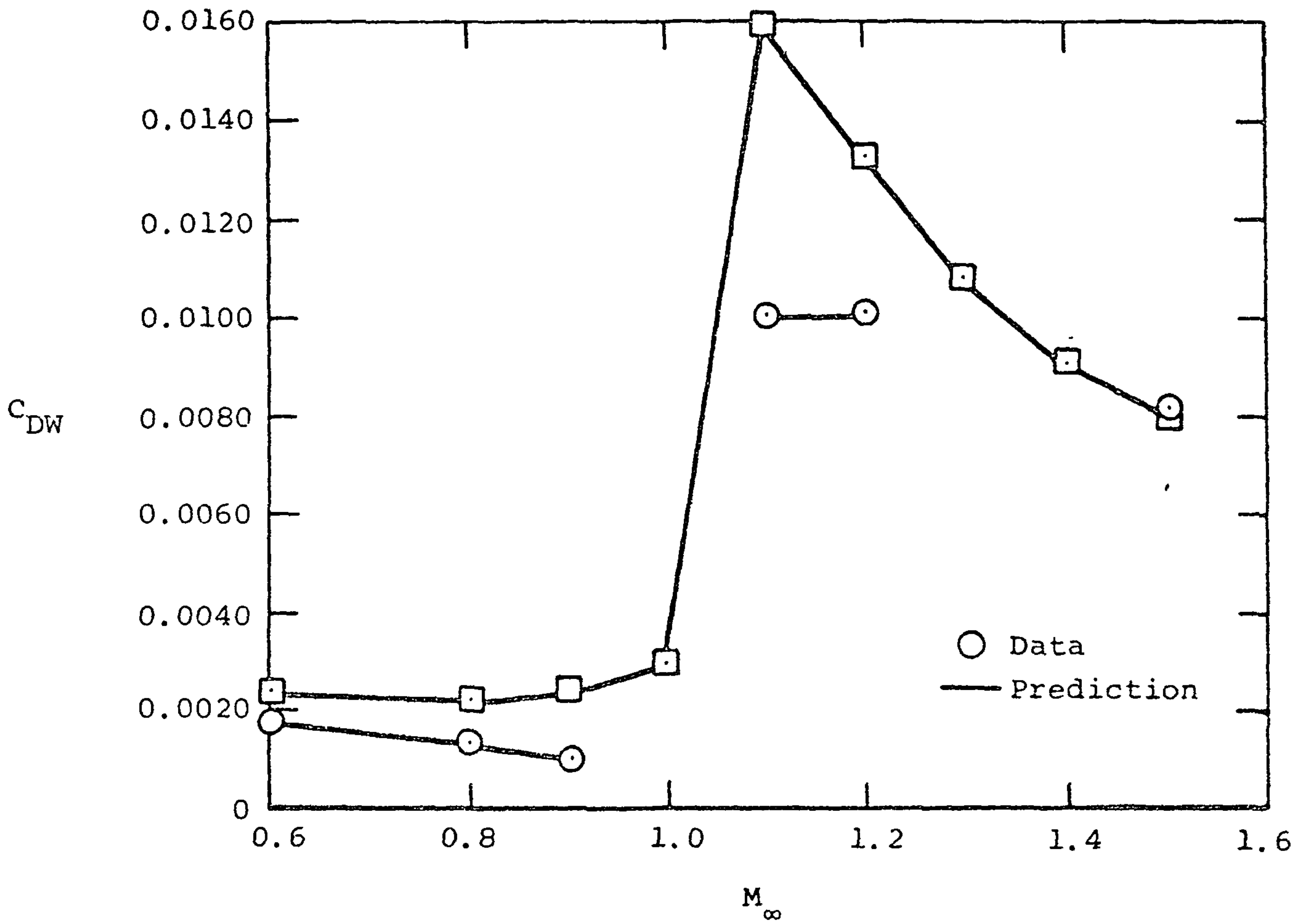

(b) NPR = 4.9.

Figure 61.- Concluded.

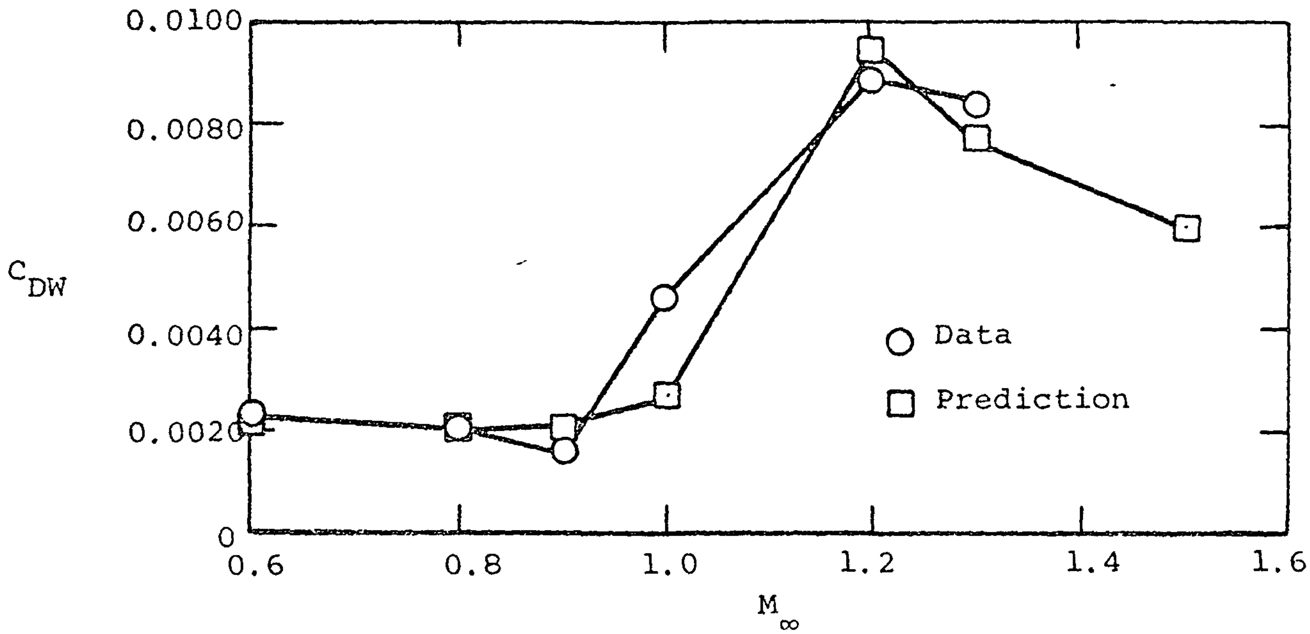

(a) NPR = 4.2.

Figure 62.- Comparison between measured and predicted-drag coefficient for reheat nozzle (ref. 41).

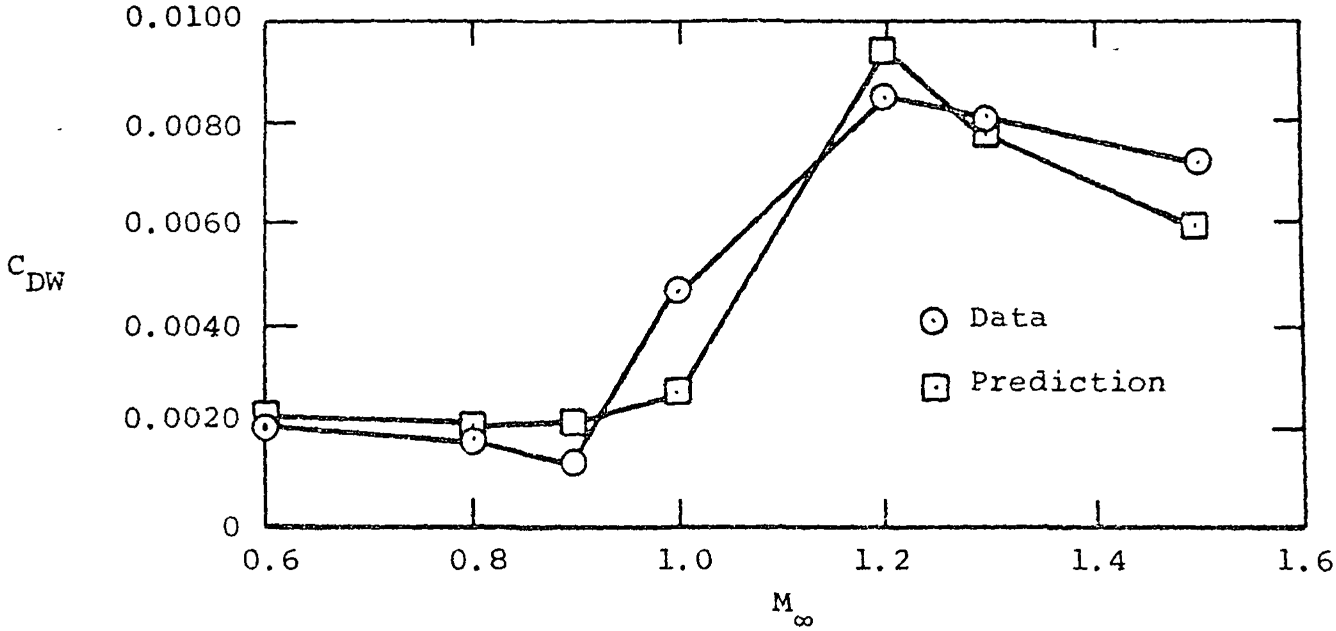

(b) NPR = 5.2.

Figure 62.- Continued.

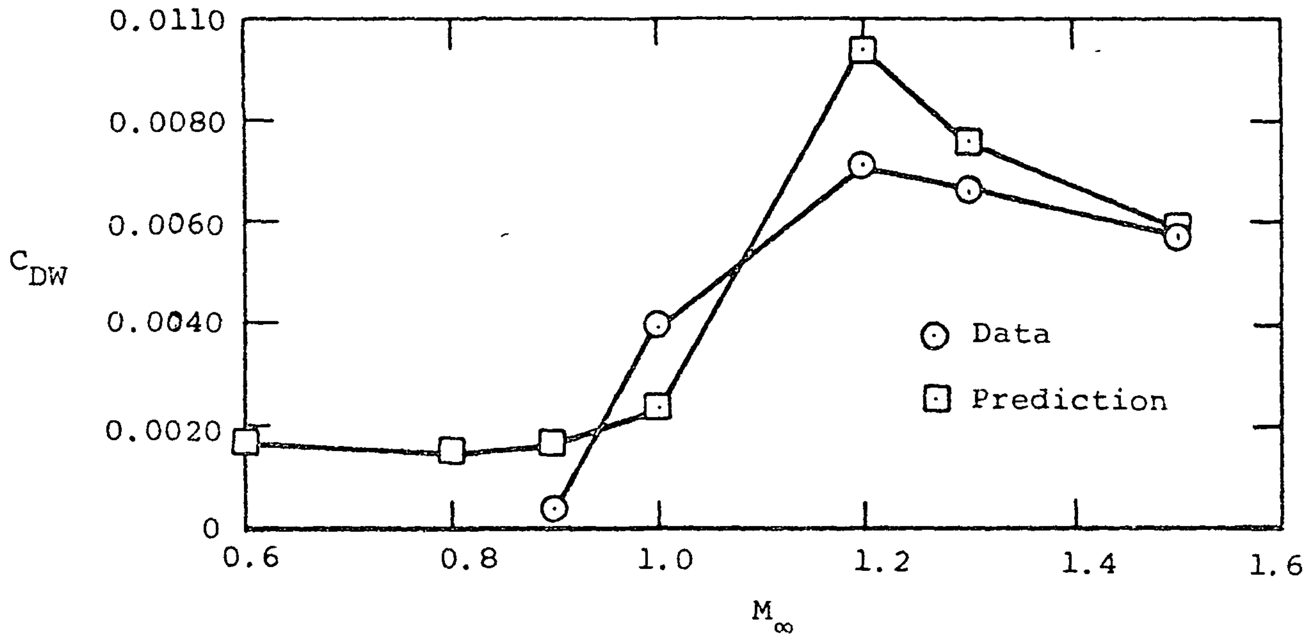

(c) NPR = 7.8.

Figure 62.- Concluded.

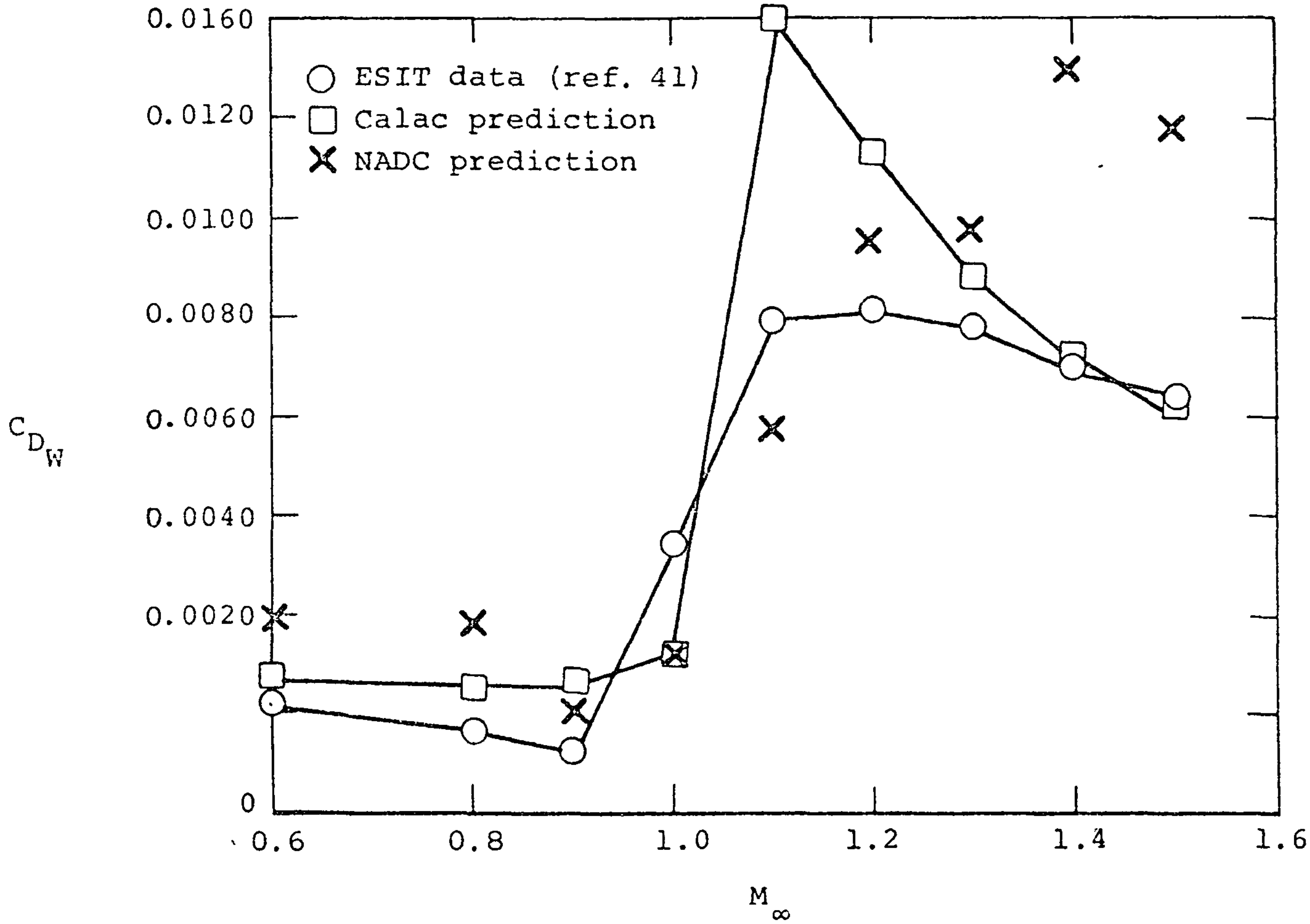

(a) Cruise nozzle, NPR = 3.3.

Figure 63.- Comparison of predicted and measured twin afterbody drag coefficients referenced to wing area.

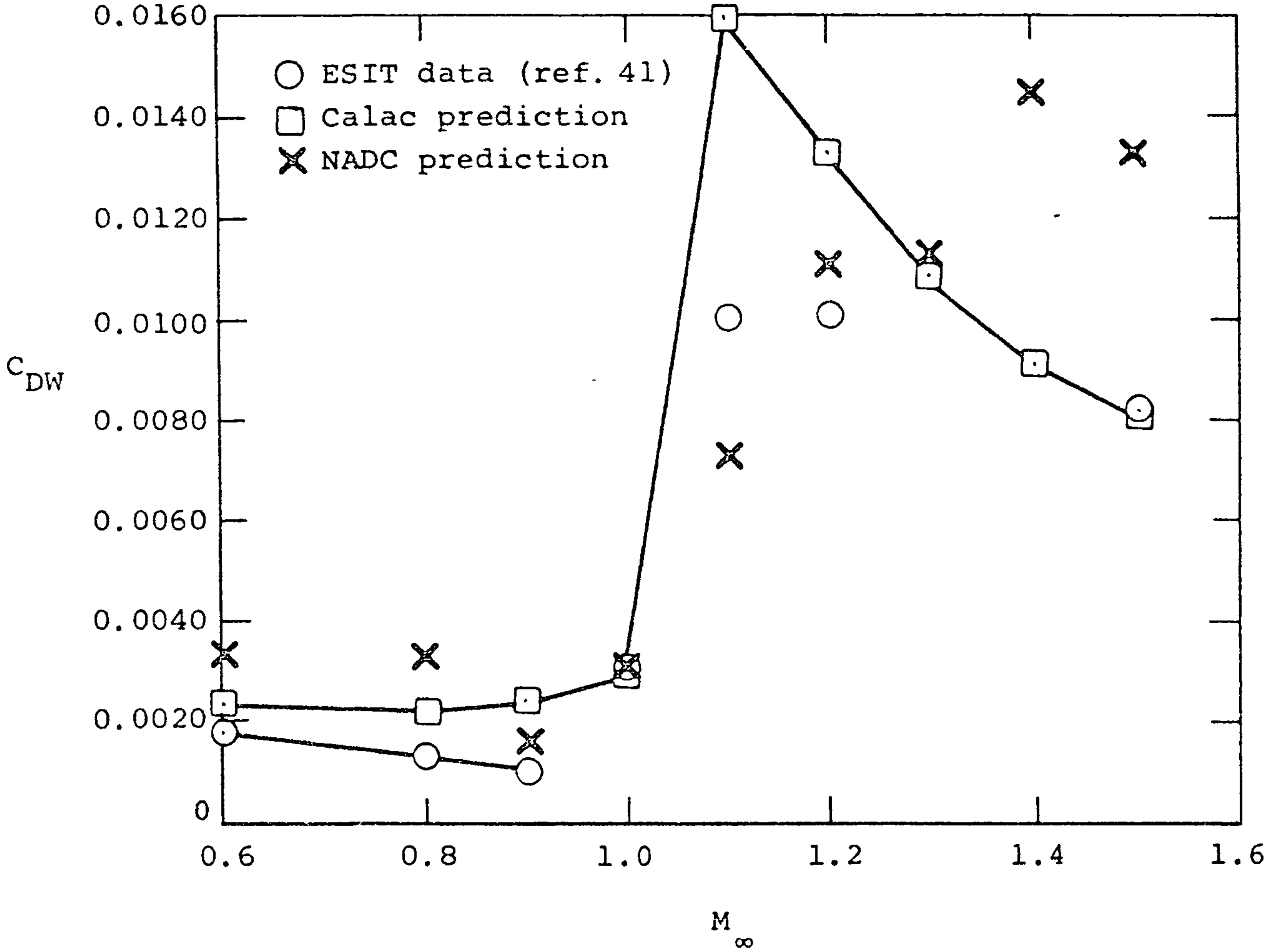

(b) Cruise nozzle, NPR = 4.9.

Figure 63.- Continued.

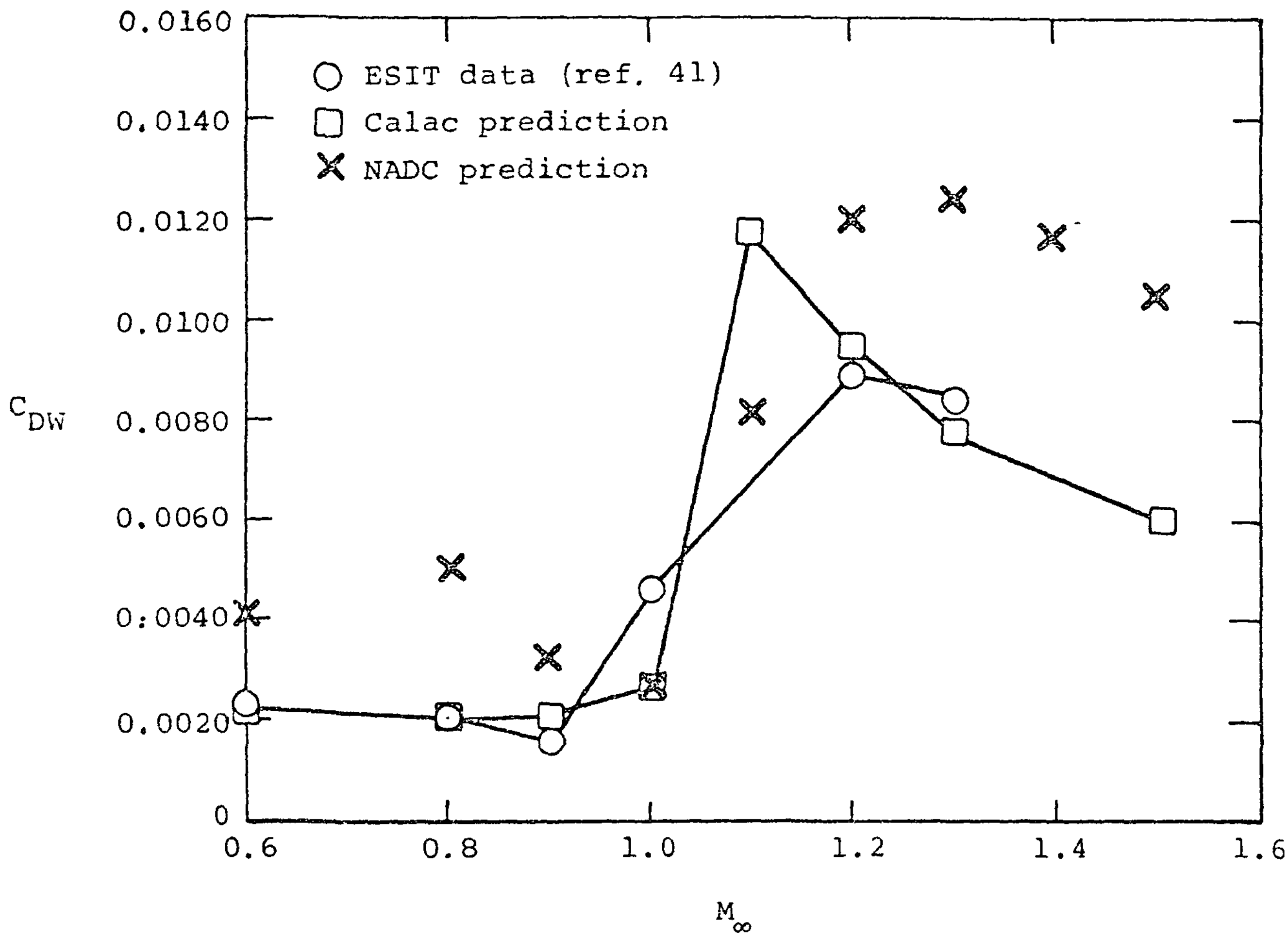

(c) Reheat nozzle, NPR = 4.2.

Figure 63.-Continued.

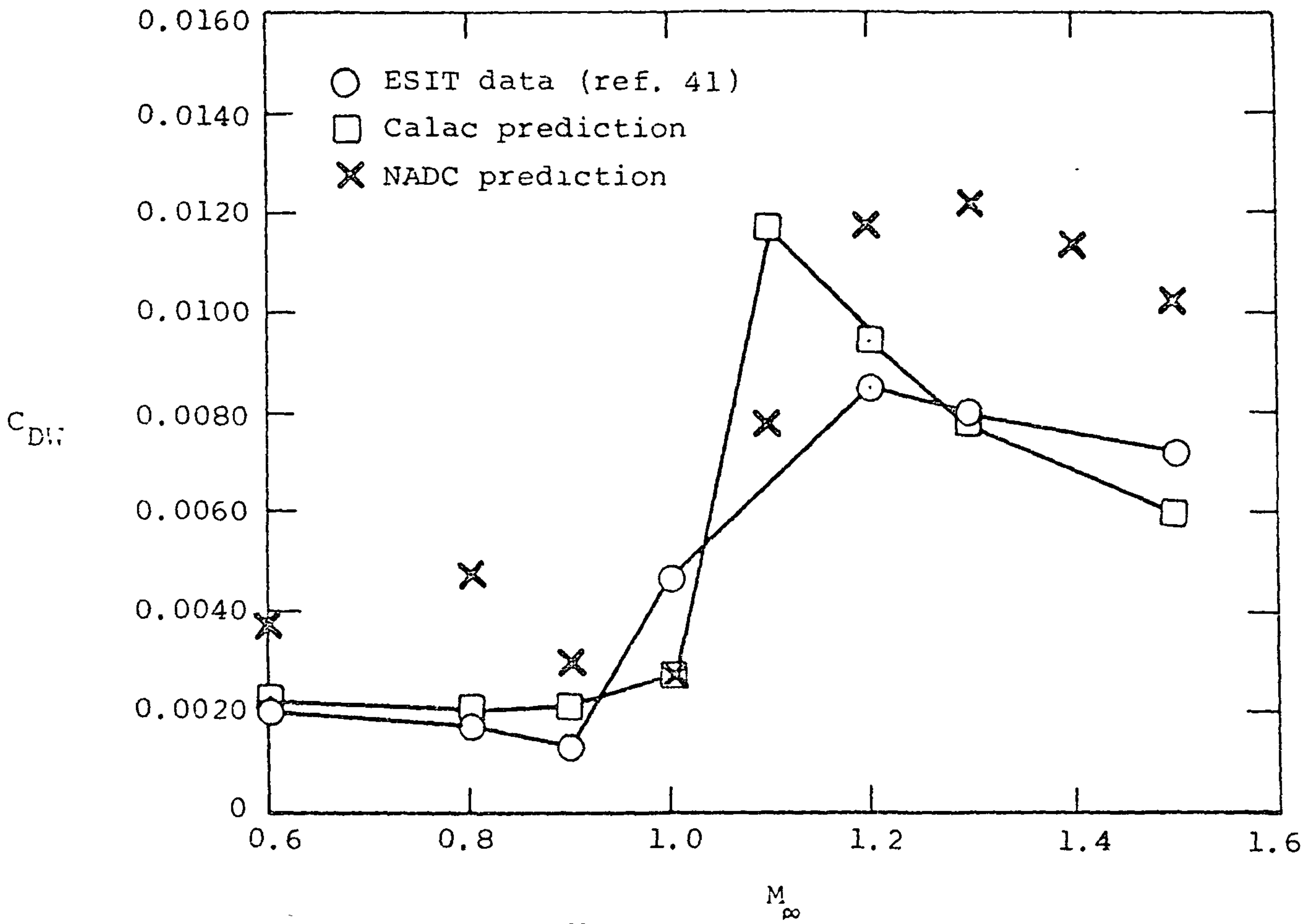

(d) Reheat nozzle, NPR = 5.2.

Figure 63.- Continued.

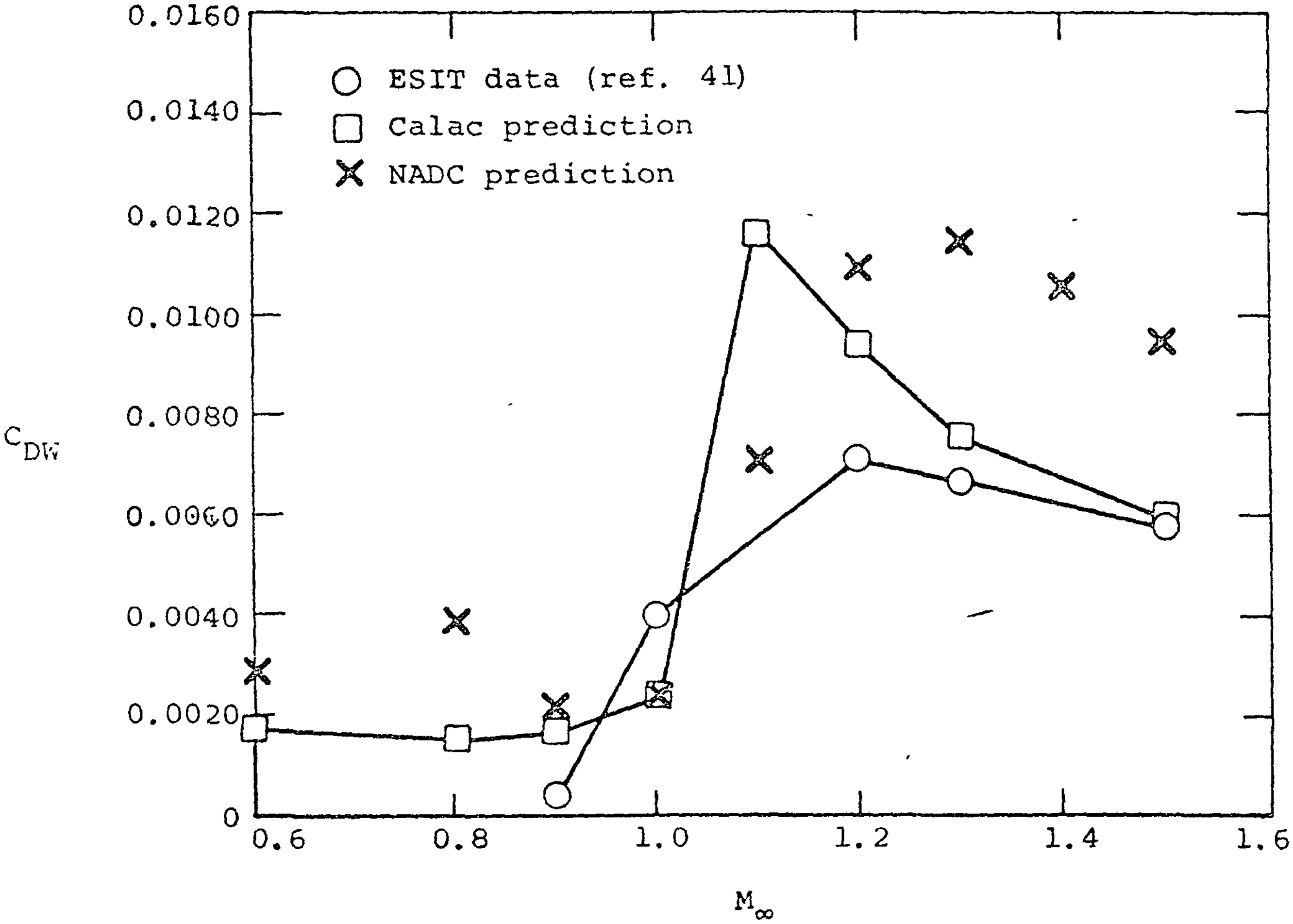

(e) Reheat nozzle, NPR = 7.8.

Figure 63.- Concluded.

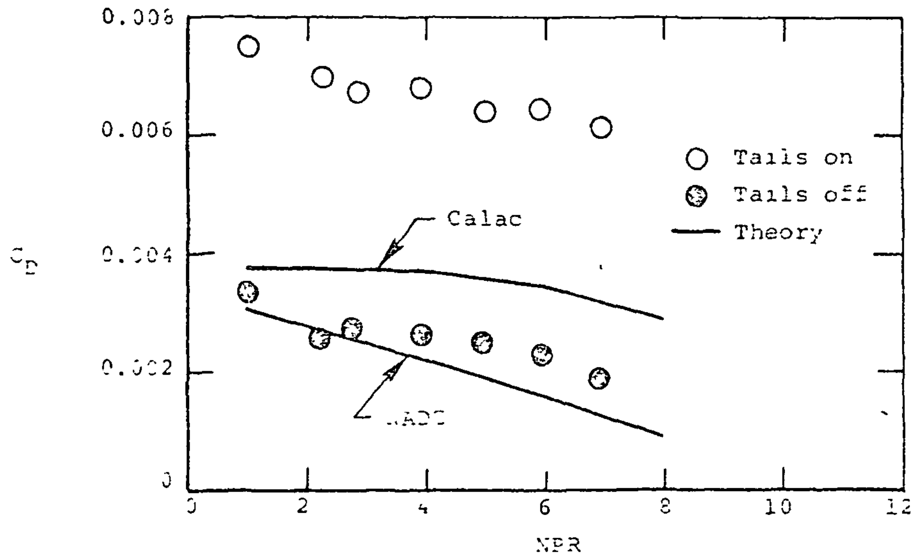

(a) M_∞ = 0.6, cruise nozzle.

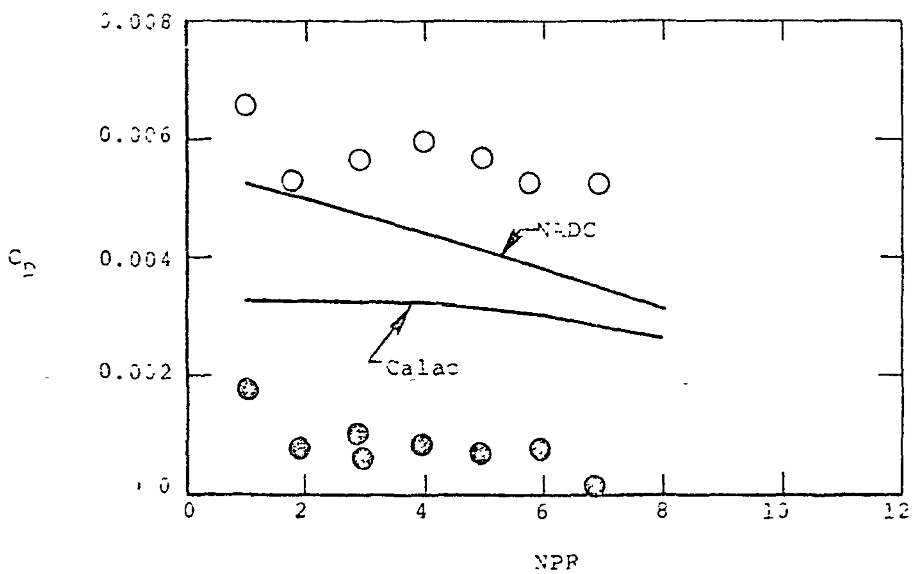

(b) M_∞ = 0.9, cruise nozzle.

Figure 64.-Comparison of predicted and measured afterbody drag on an F-18 model.

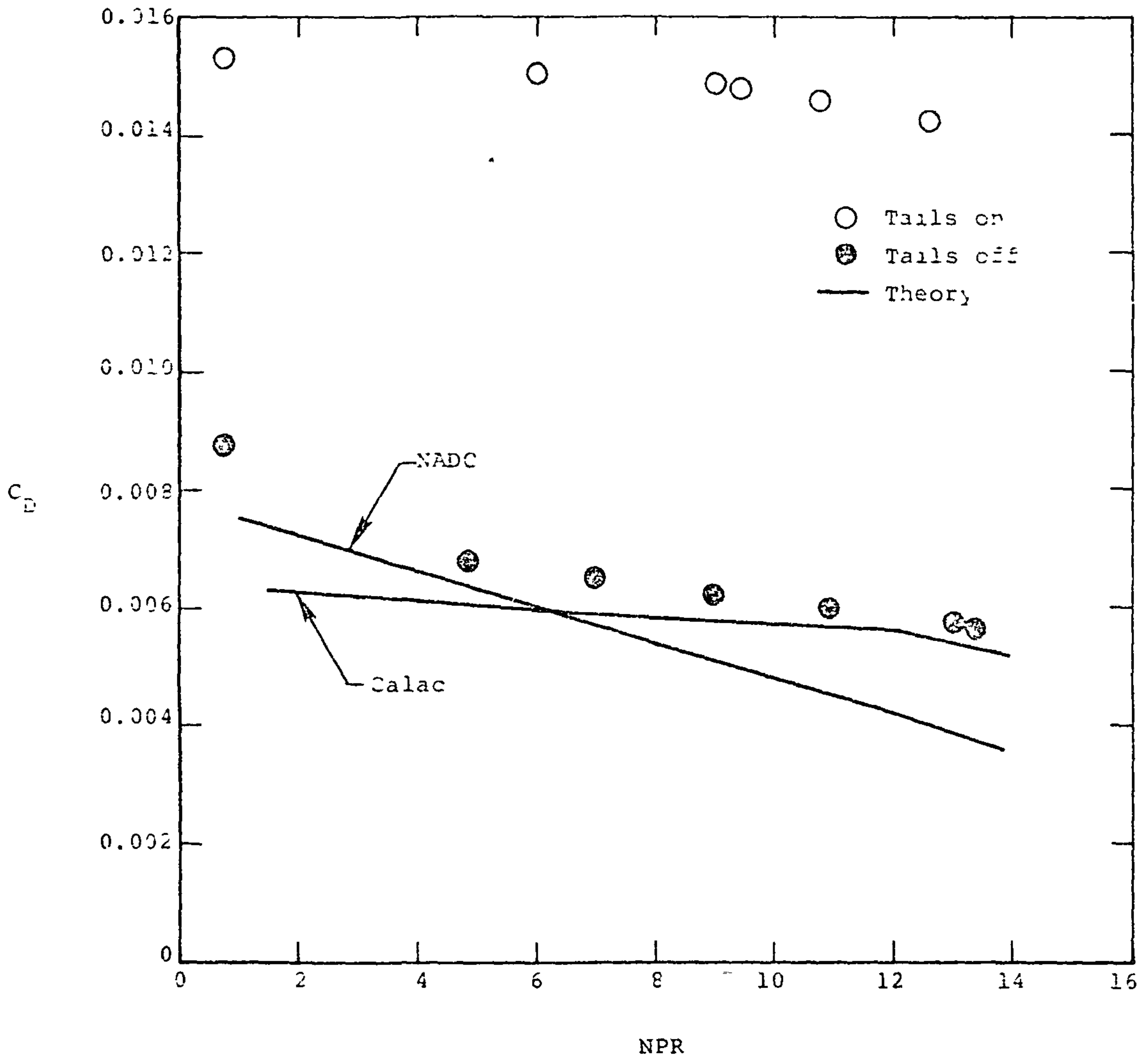

(c) $M_{\infty} = 1.6$, maximum reheat nozzle.

Figure 64.- Continued.

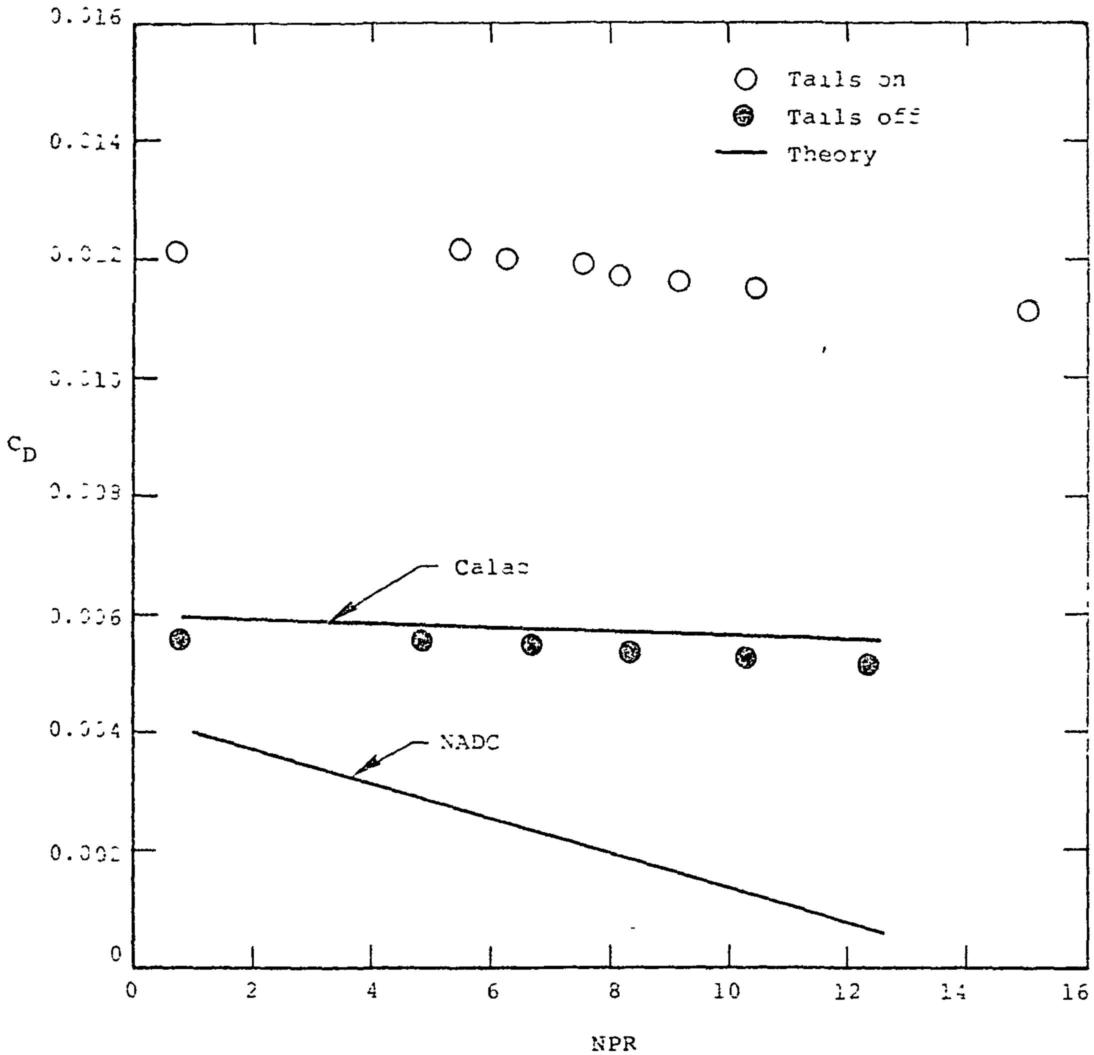

(d) M_∞ = 2.0, maximum reheat nozzle.

Figure 64.- Concluded.

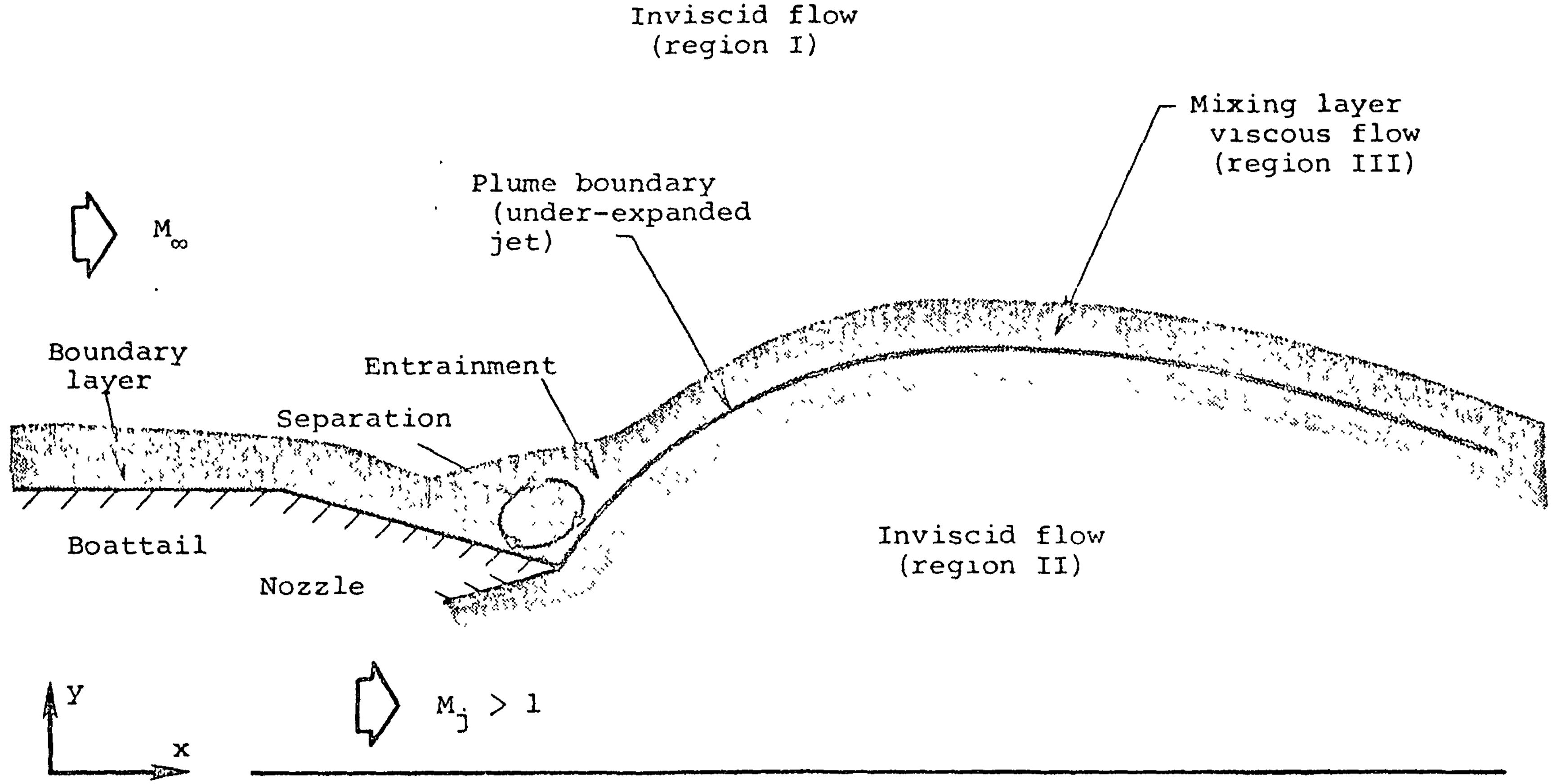

Figure 65 .- Afterbody/nozzle flow-field schematic.

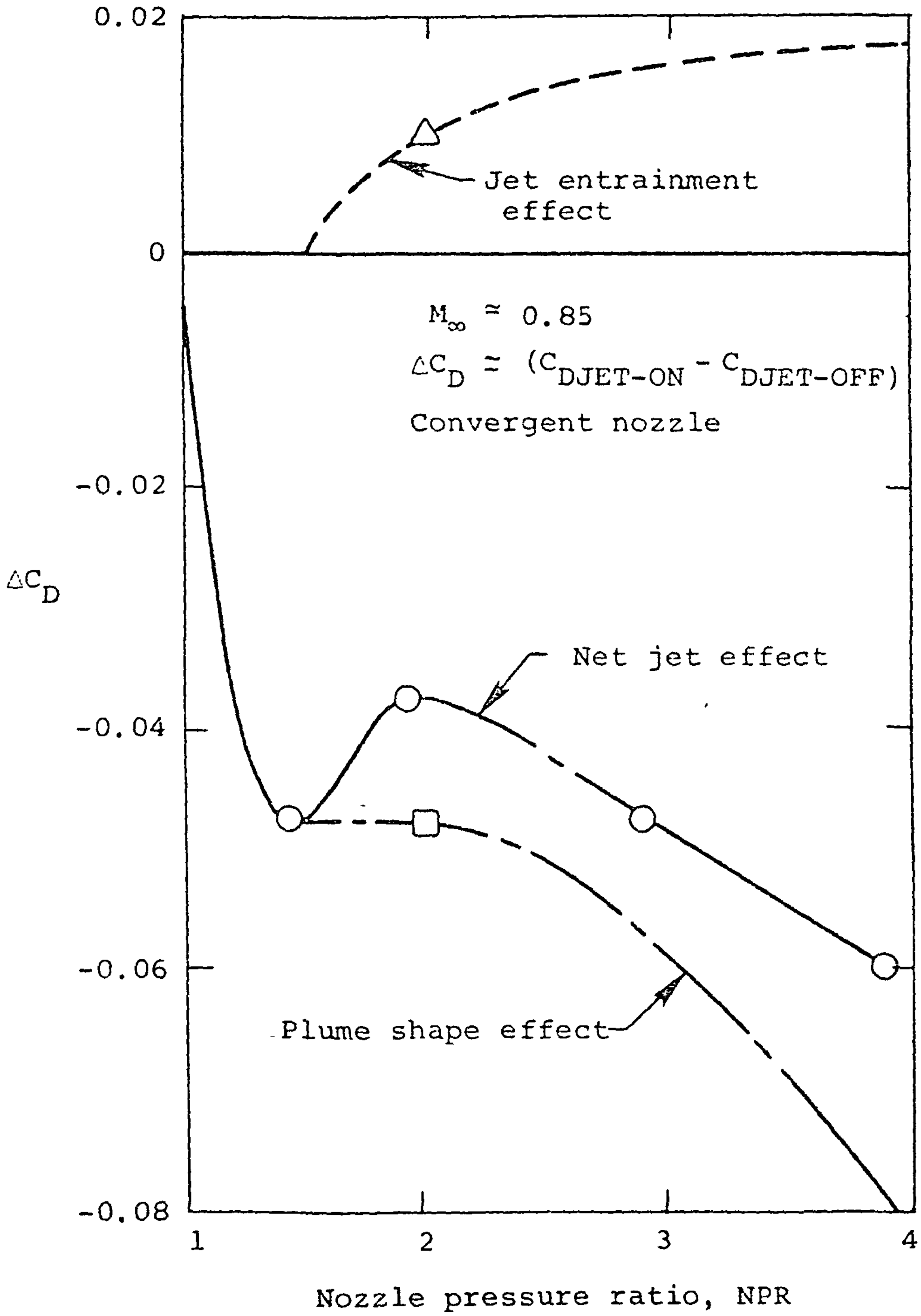

Figure 66.- Qualitative effect of entrainment and plume shape on boattail drag.

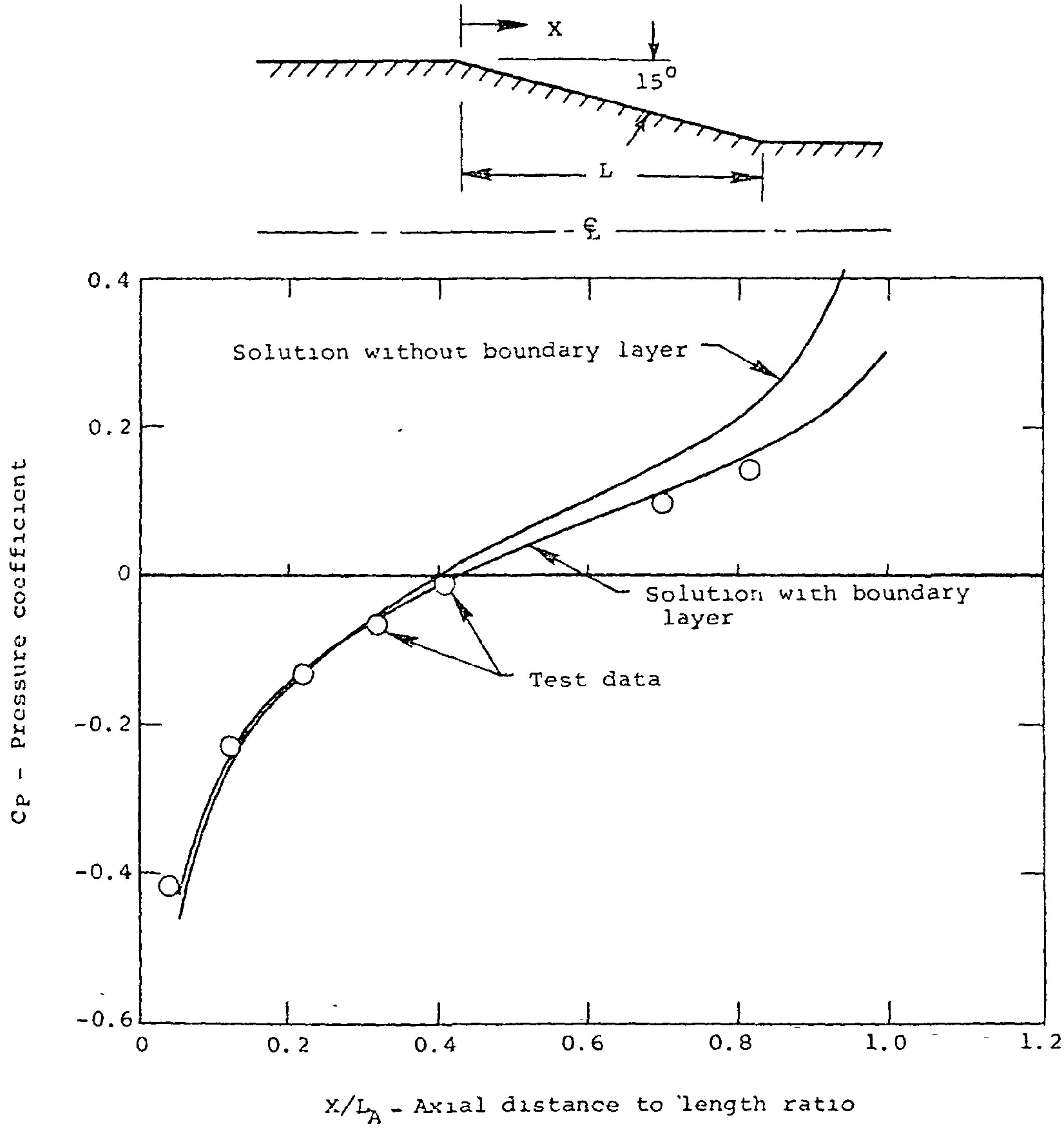

Figure 67.- Comparison of predicted and measured boattail pressure distribution on a conical boattail (ref. 48).

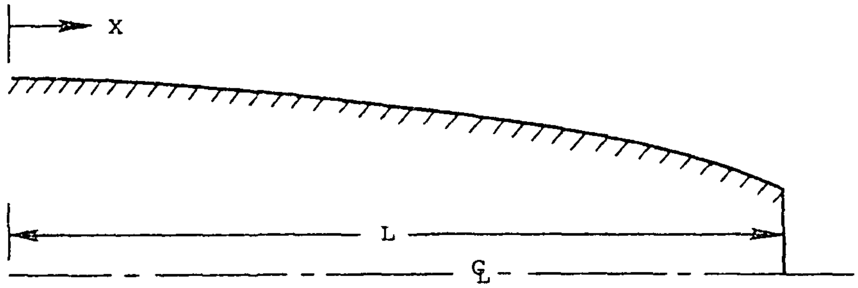

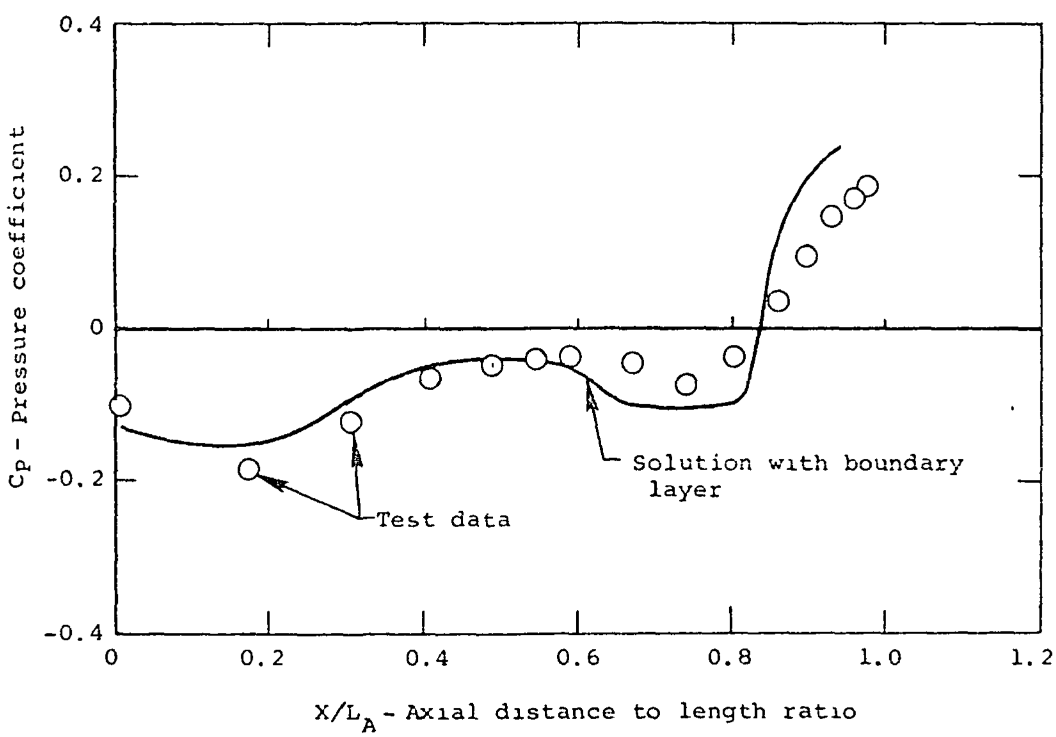

Figure 68.- Comparison of predicted and measured convergent-divergent nozzle boattail pressure distributions (ref. 48). $M_\infty = 0.6$.

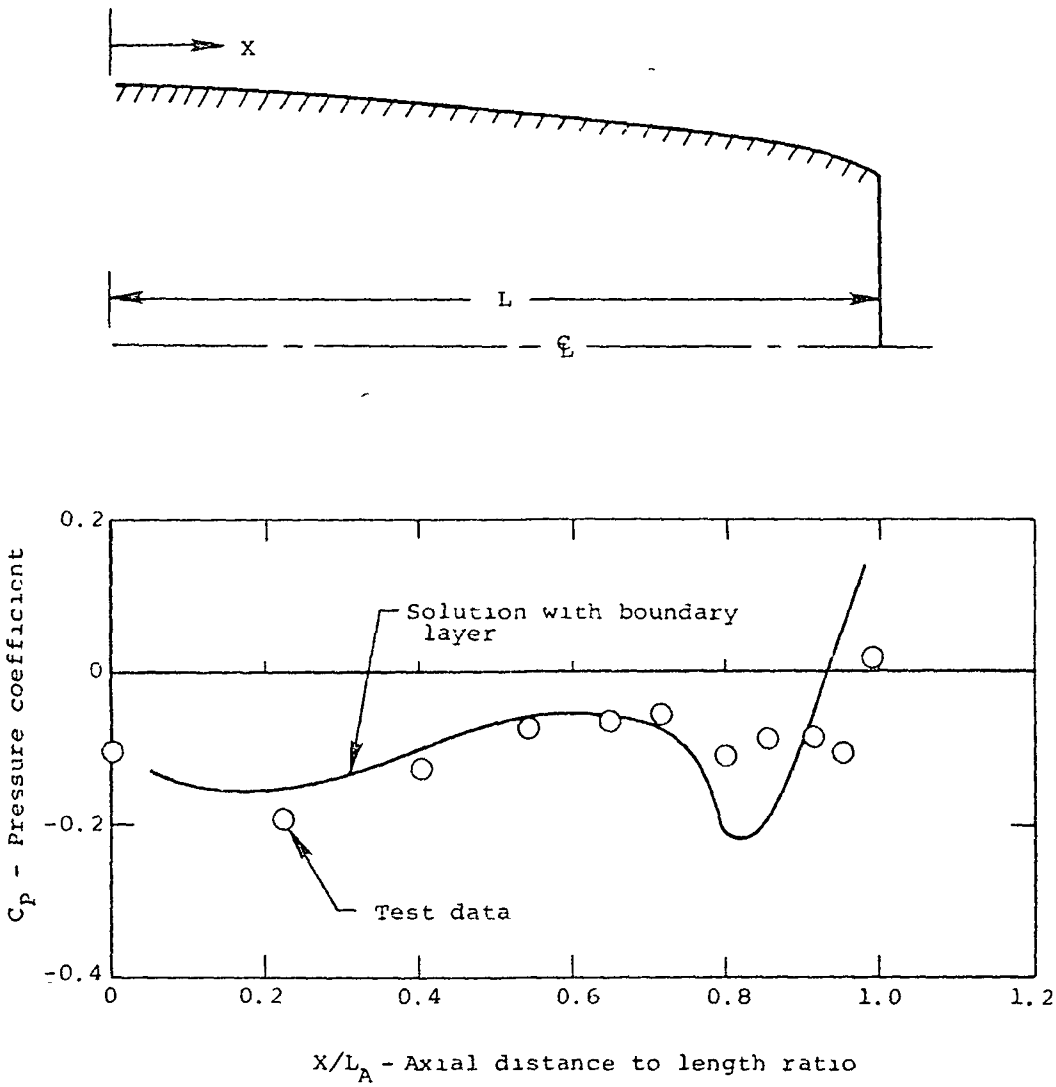

Figure 69.- Comparison of predicted and measured plug nozzle boattail pressure distributions (ref. 48). $M_\infty = 0.6$.

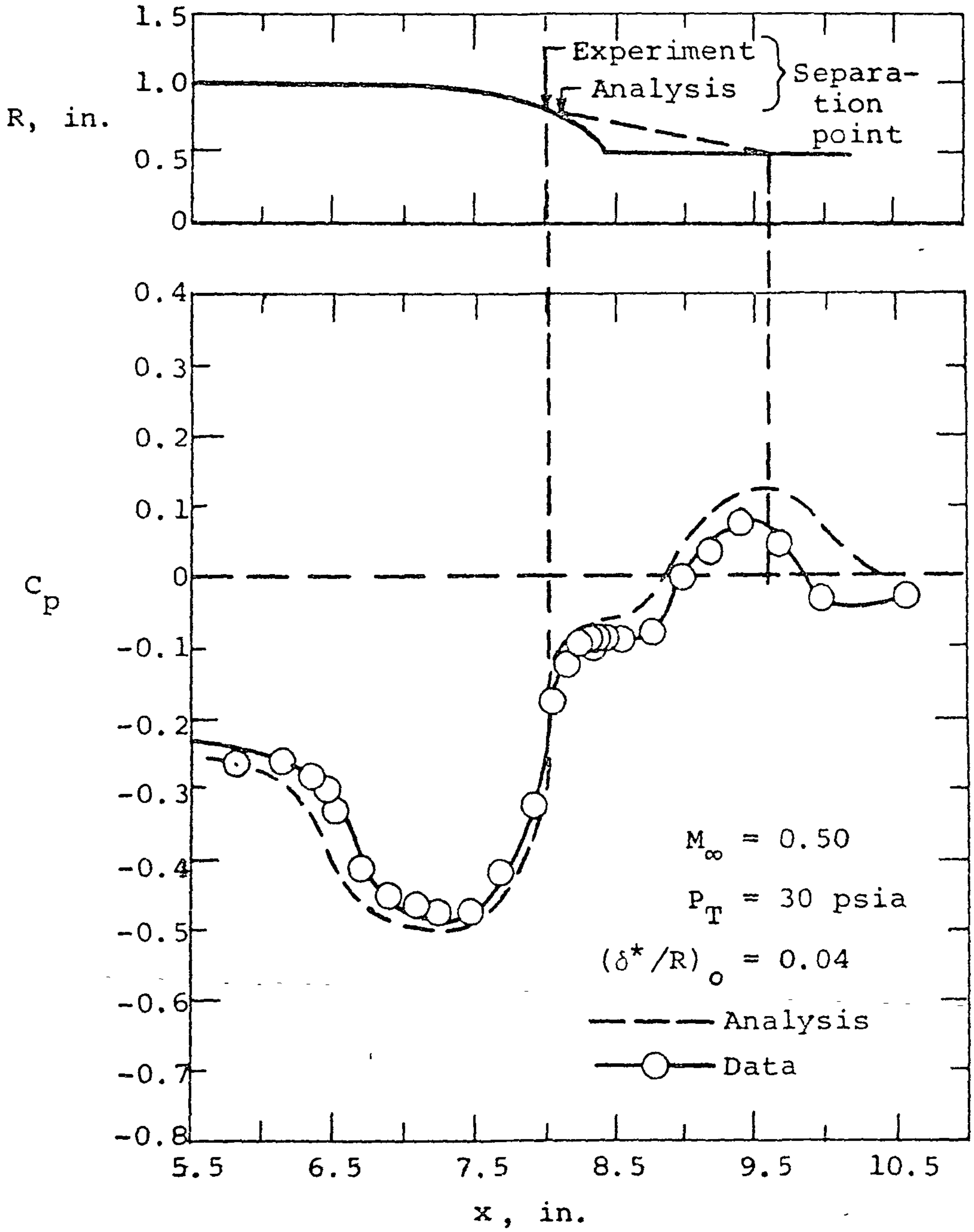

Figure 70.- Comparison of measured pressure distributions on an elliptical afterbody with calculations from the method of Presz (ref. 253).

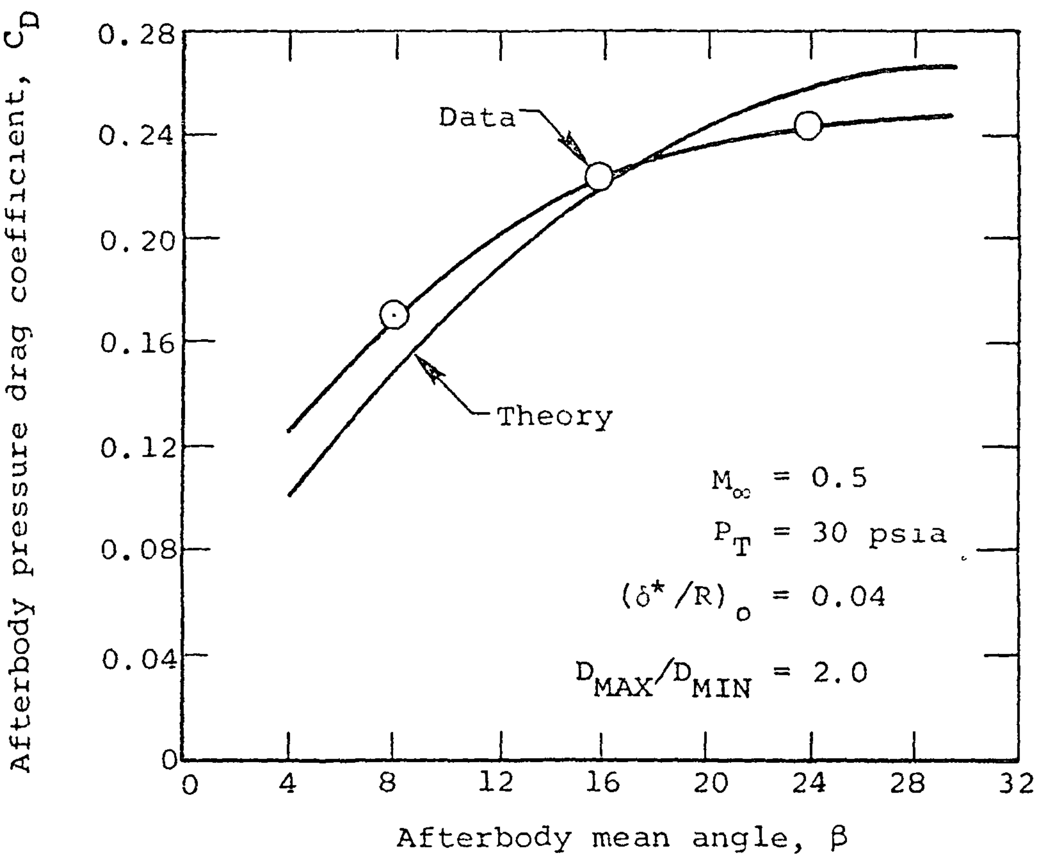

Figure 71.- Measured and calculated pressure drag coefficients of an elliptical afterbody (ref. 253).

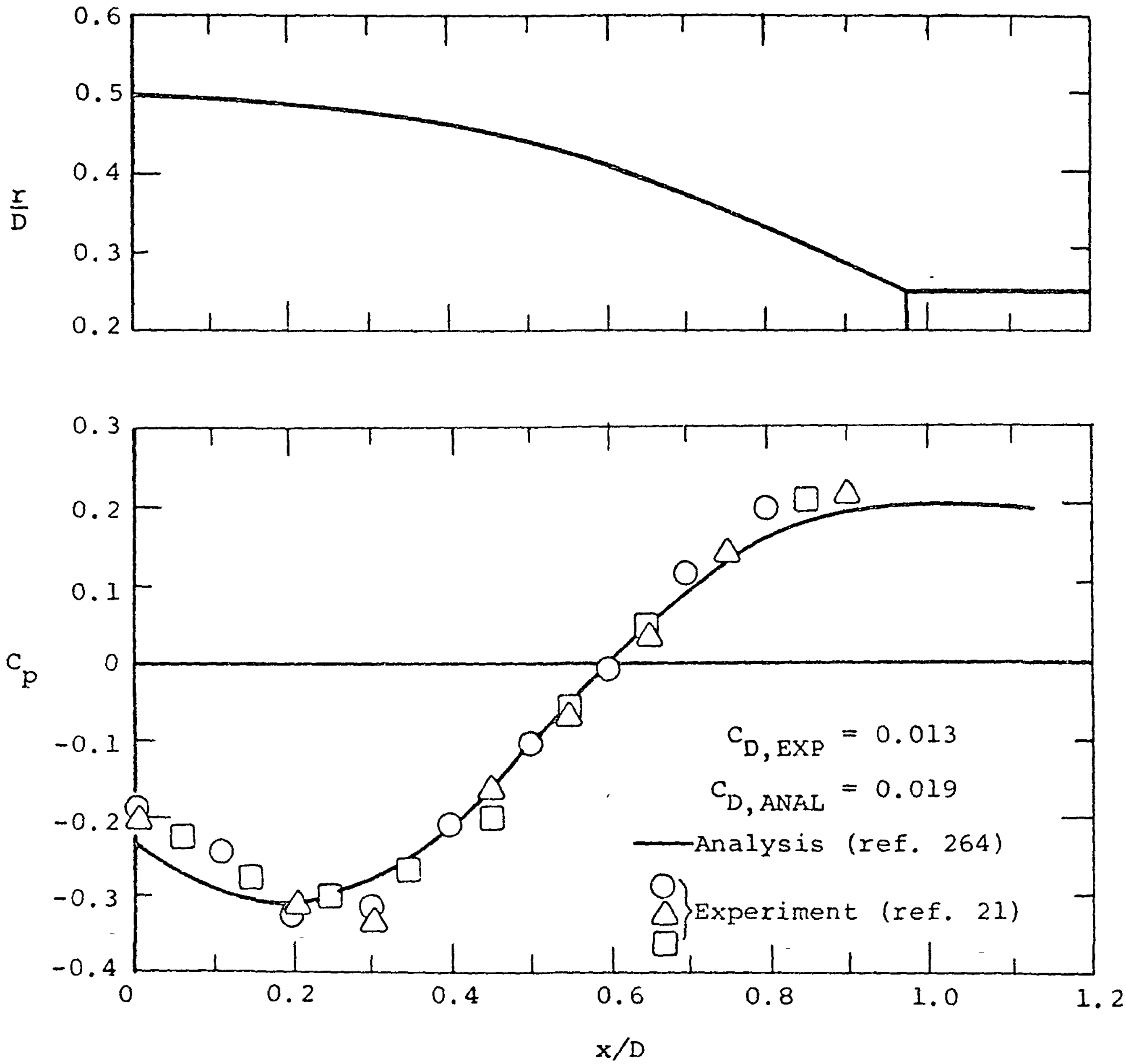

Figure 72.- Comparison of measured and predicted afterbody pressures for a circular arc conical afterbody configuration at $M_\infty = 0.601$ and a Reynolds number of 4.29×10^7.

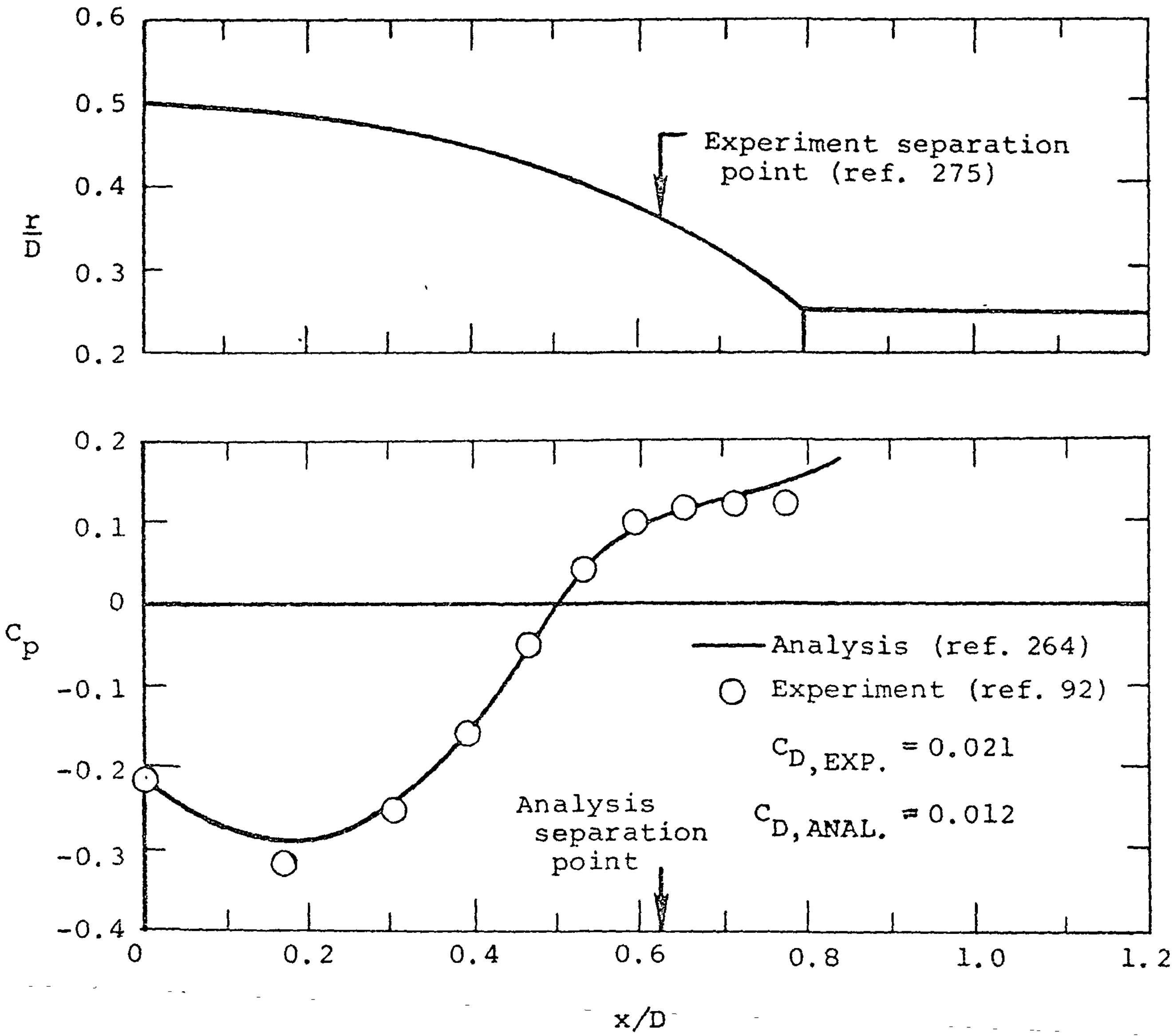

Figure 73.- Comparison of measured and predicted afterbody pressures for a circular arc nozzle configuration at $M_\infty = 0.397$.

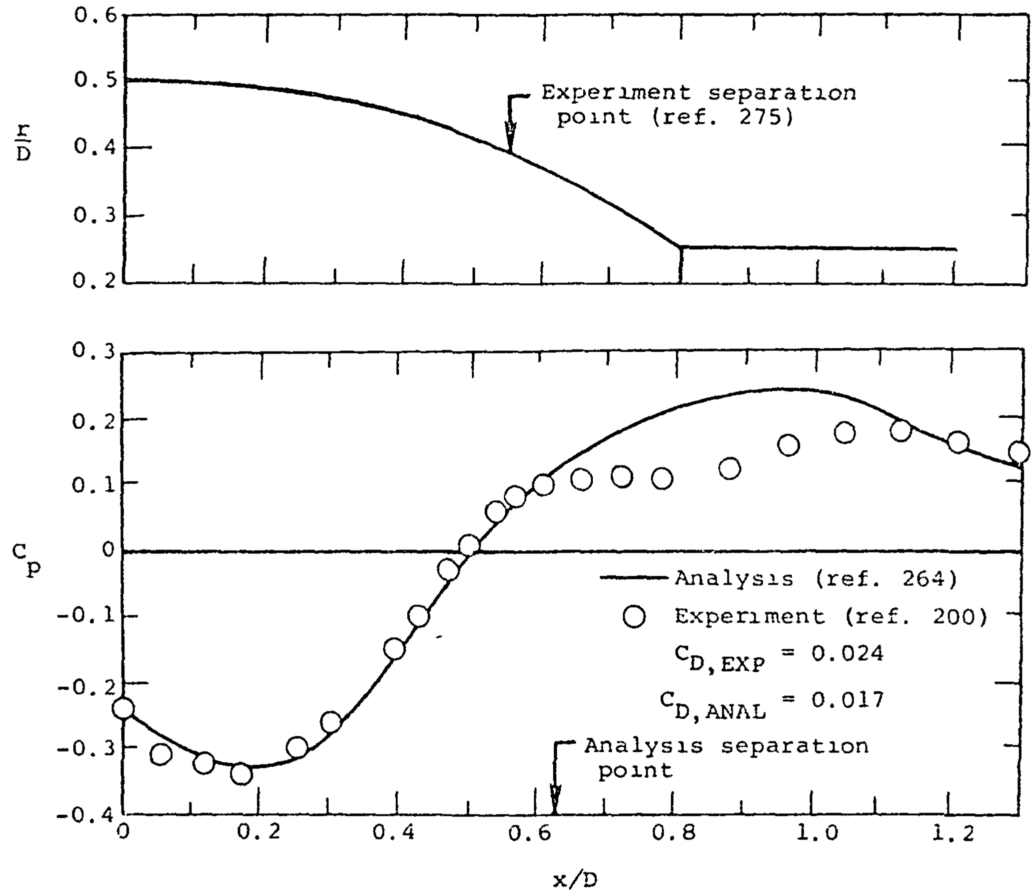

Figure 74.- Comparison of measured and predicted afterbody pressures for a circular arc nozzle configuration at $M_\infty = 0.6$.

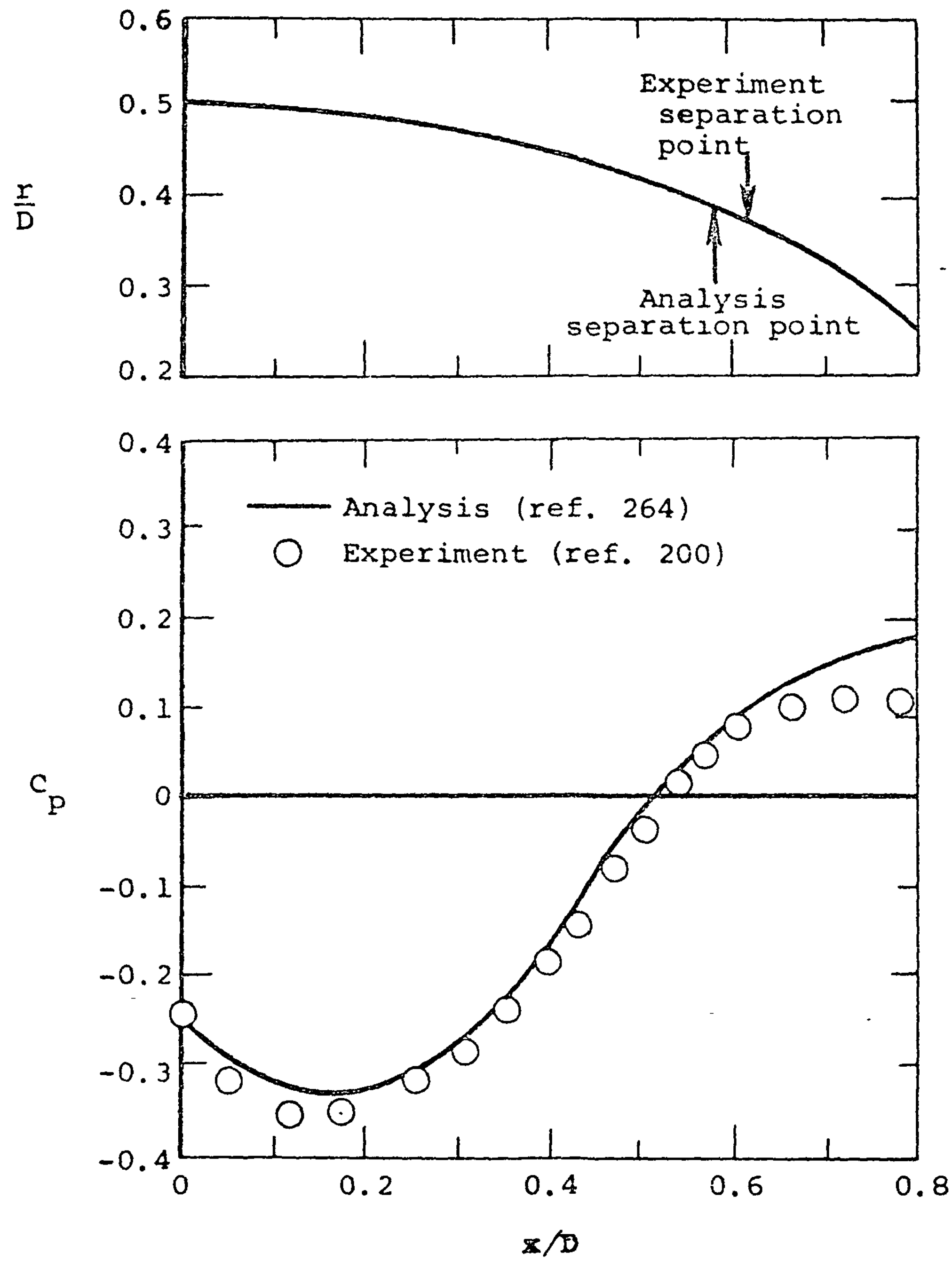

Figure 75.- Comparison of measured and predicted afterbody pressures for a circular arc afterbody at M_∞ = 0.6 and NPR = 2.91.

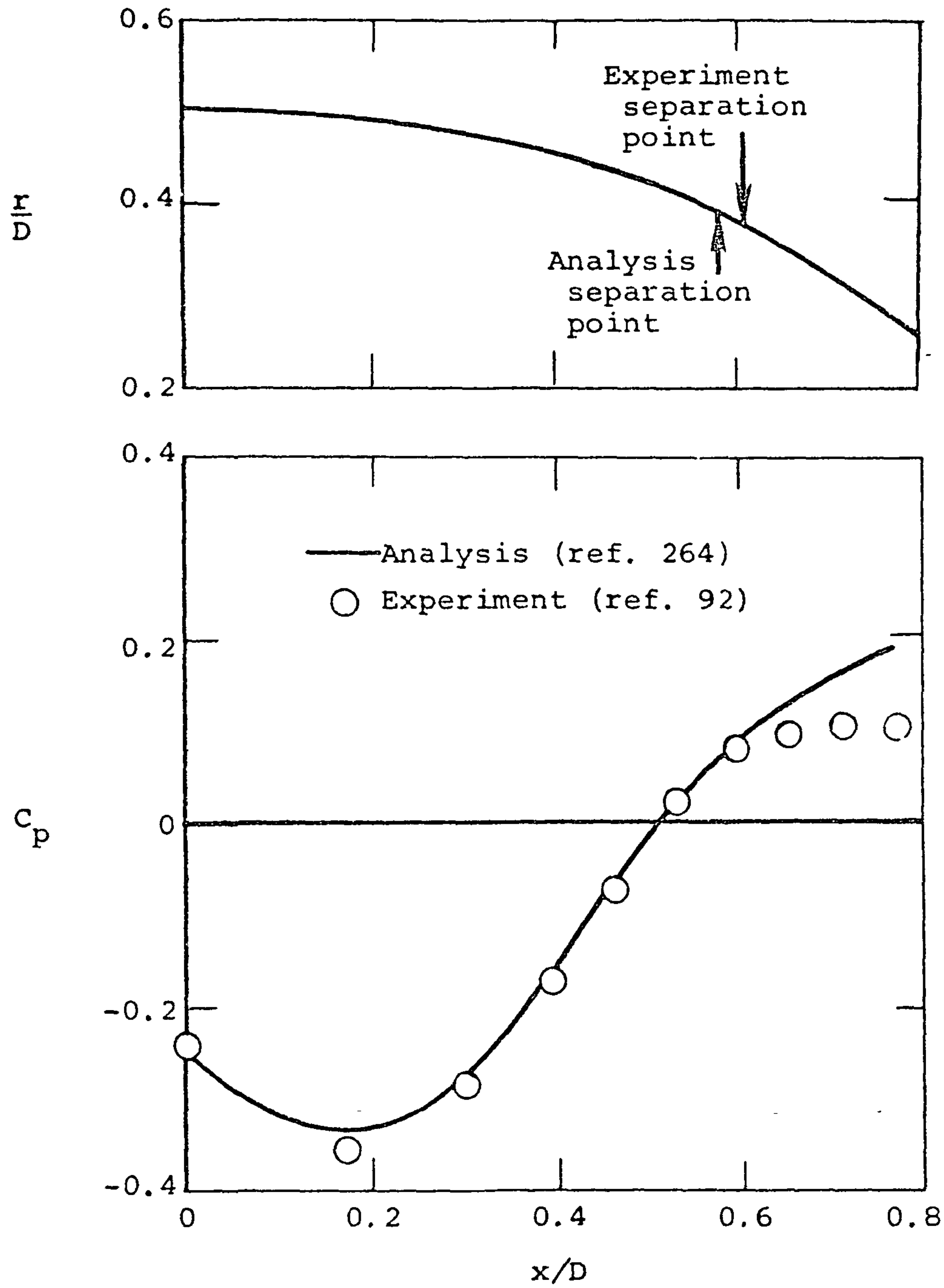

Figure 76.- Comparison of measured and predicted afterbody pressures for a circular arc afterbody at $M_\infty = 0.598$ and NPR = 2.002.

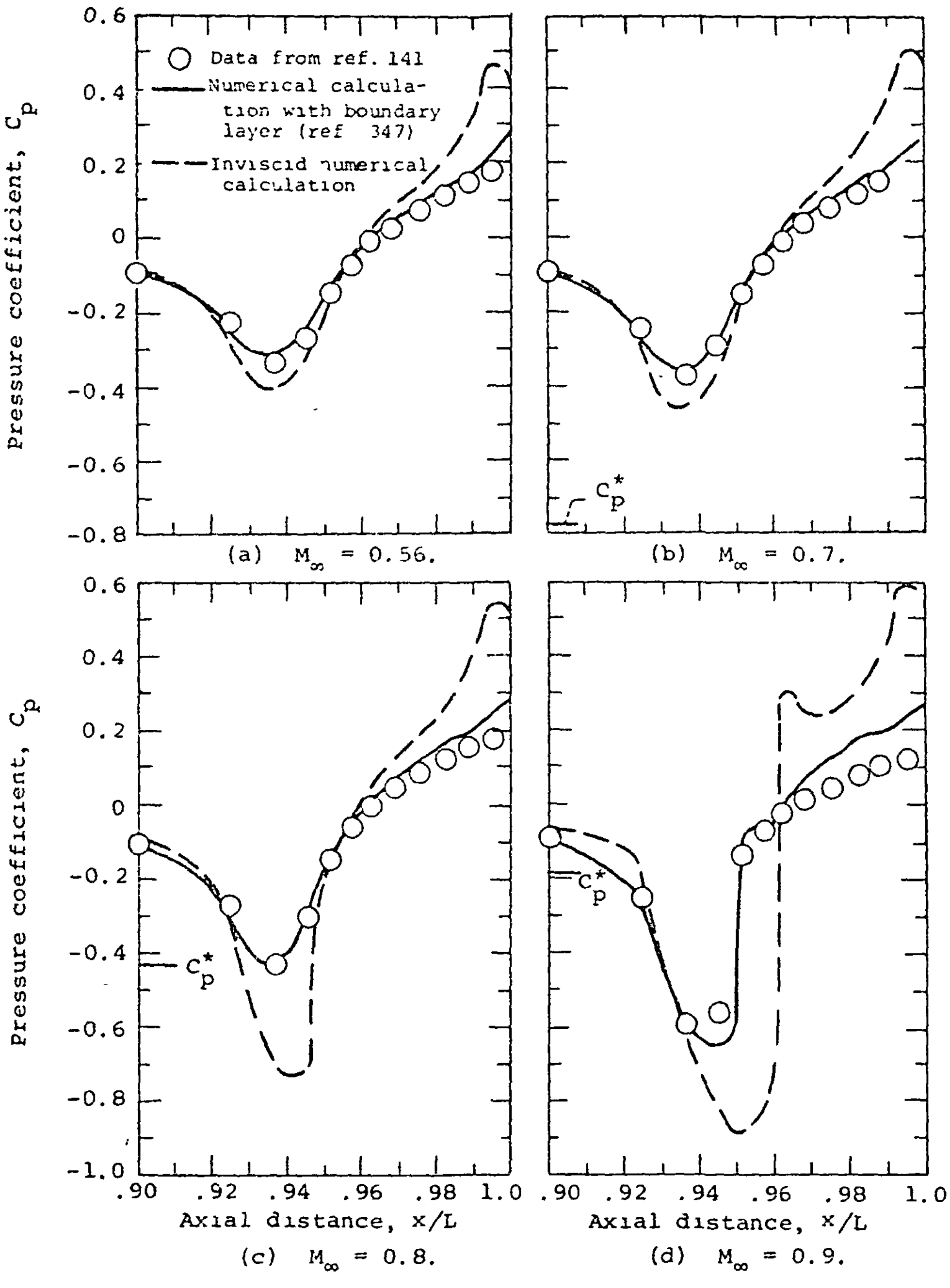

Figure 77.- Comparison of theoretical and experimental boattail pressure distributions.

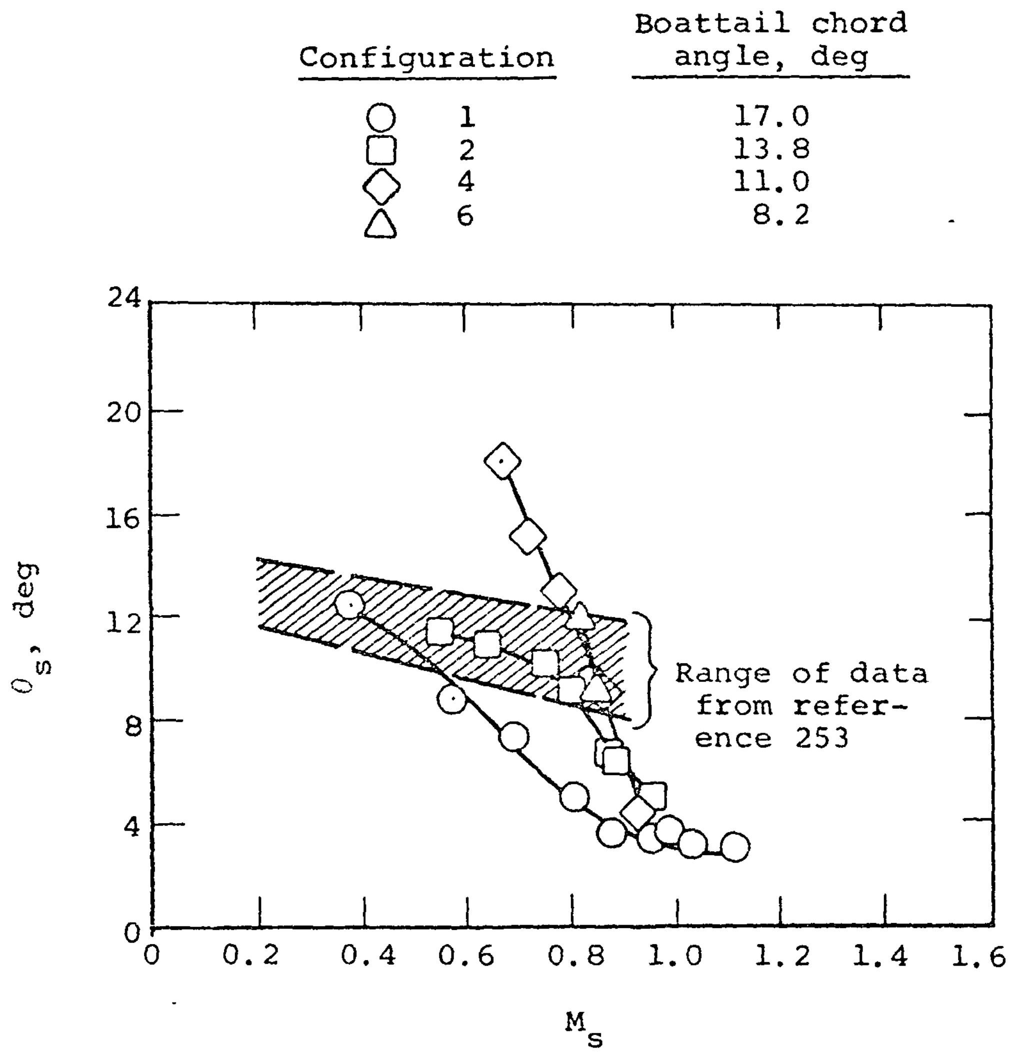

Figure 78.- Variation of discriminating streamline separation angle with local Mach number at separation (ref. 274).

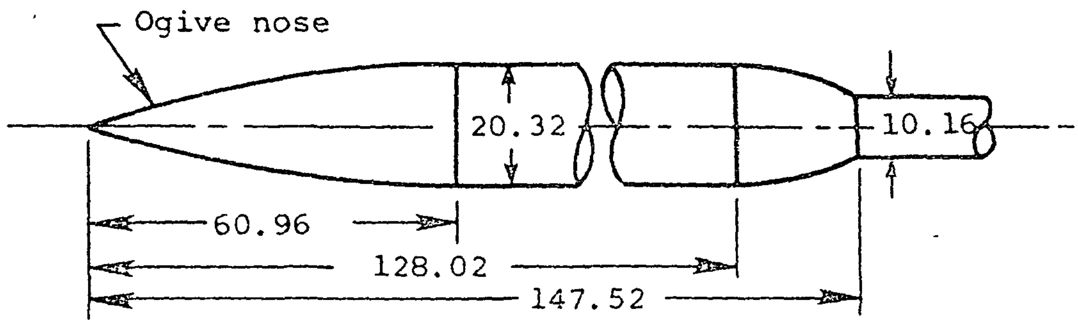

(a) Overall body geometry.

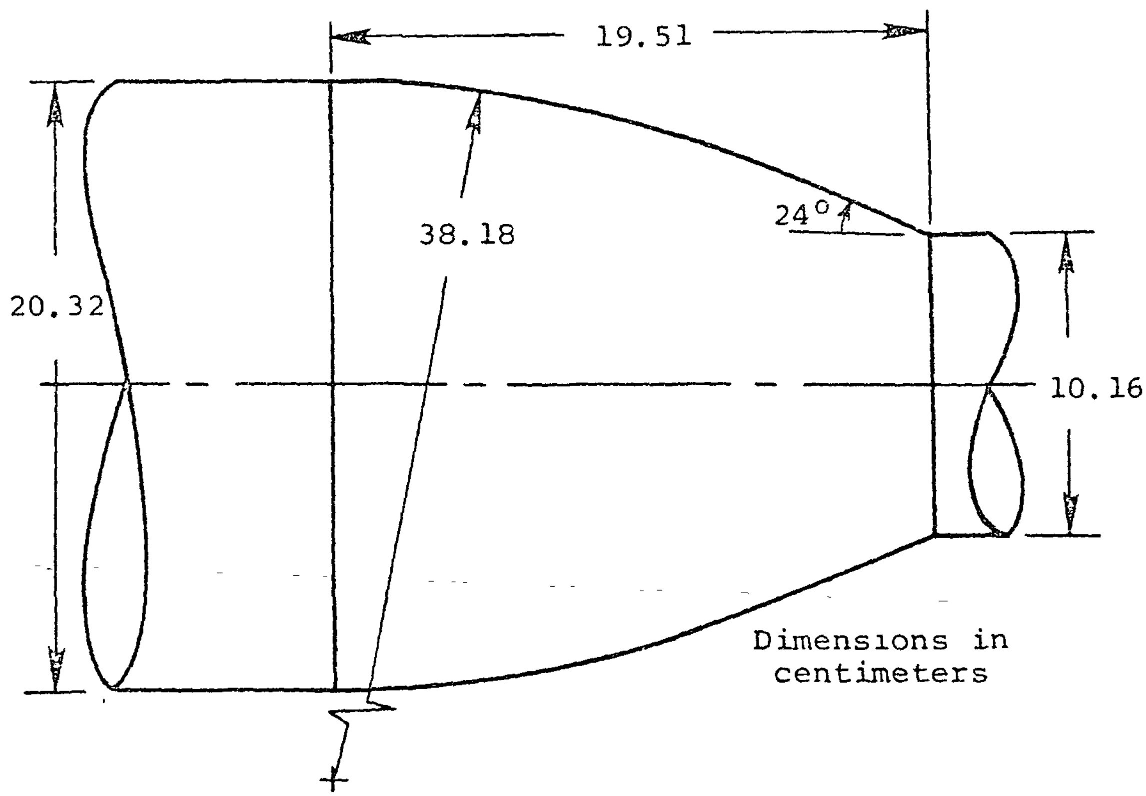

(b) Detailed boattail geometry.

Figure 79.- Body geometry for sample calculation from reference 218.

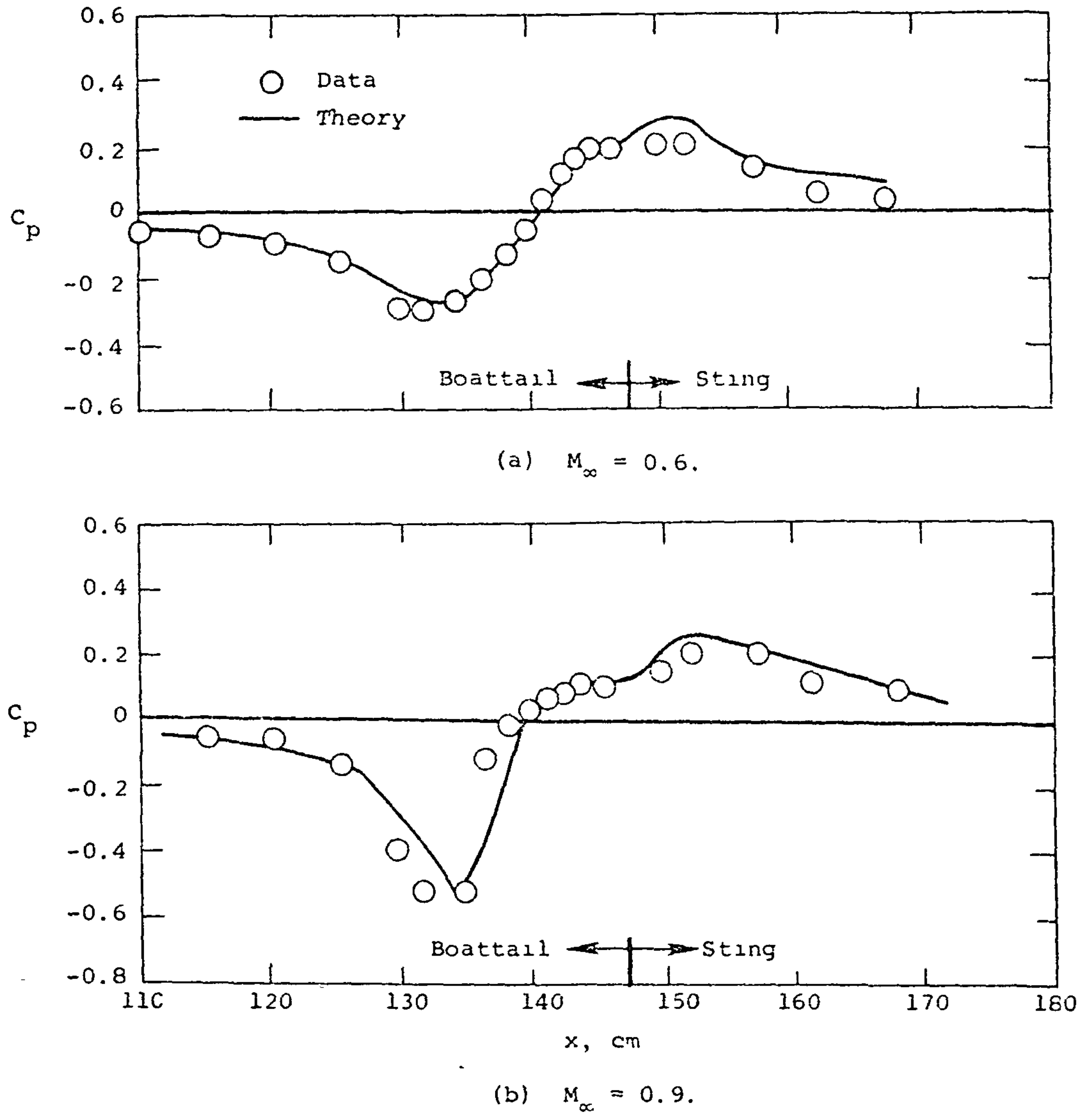

Figure 80.- Comparison of theory with data on a circular arc cone boattail from reference 218.

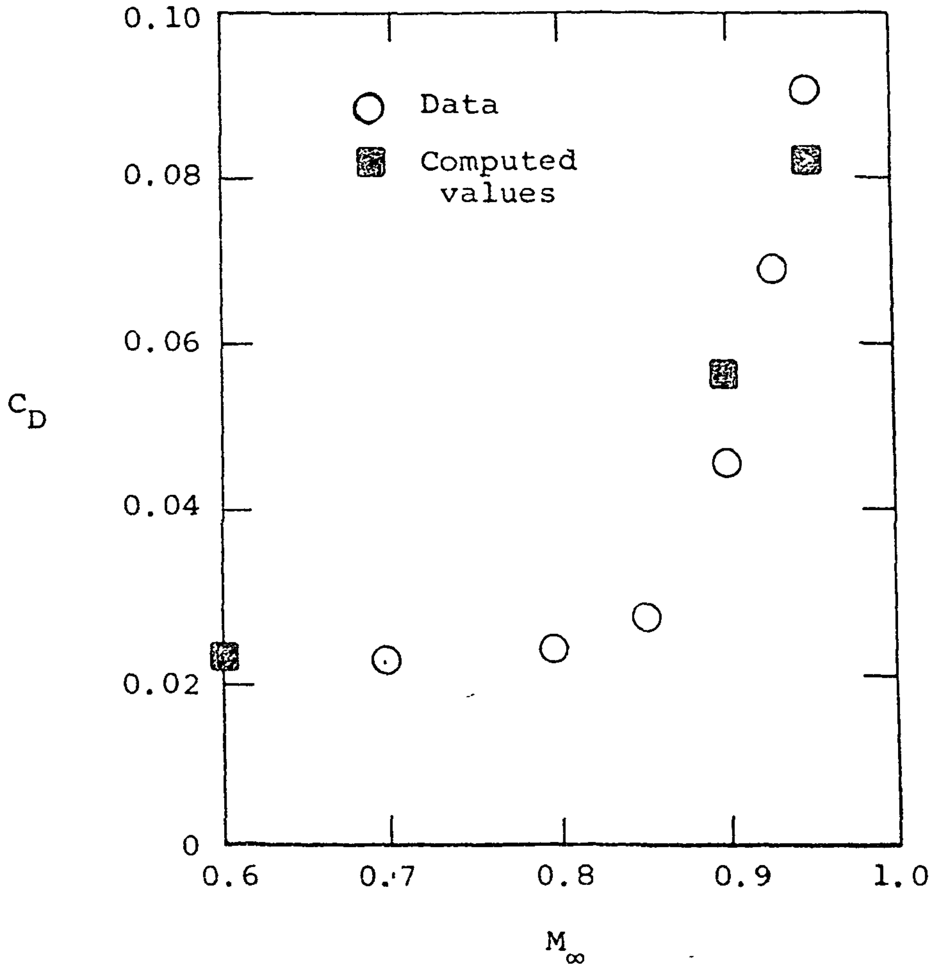

Figure 81.- Comparison of calculated and measured afterbody drag coefficients on the body of figure 79 (ref. 218).

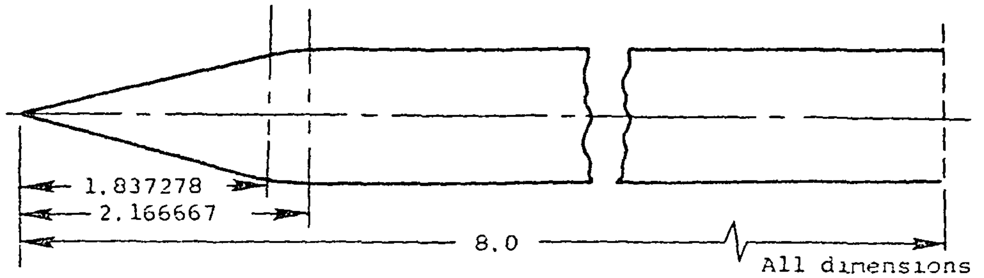

(a) Forebody.

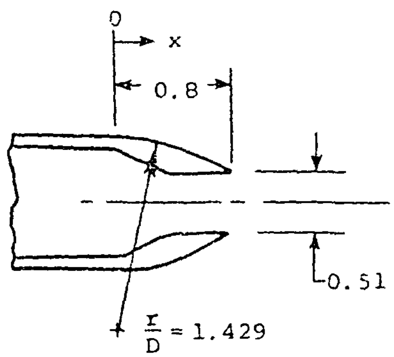

(b) Boattail configuration 1.

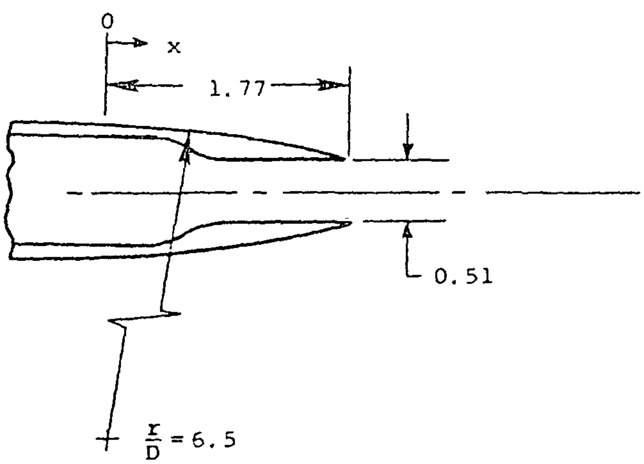

(c) Boattail configuration 2.

Figure 82.- Body with circular arc boattail (ref. 92).

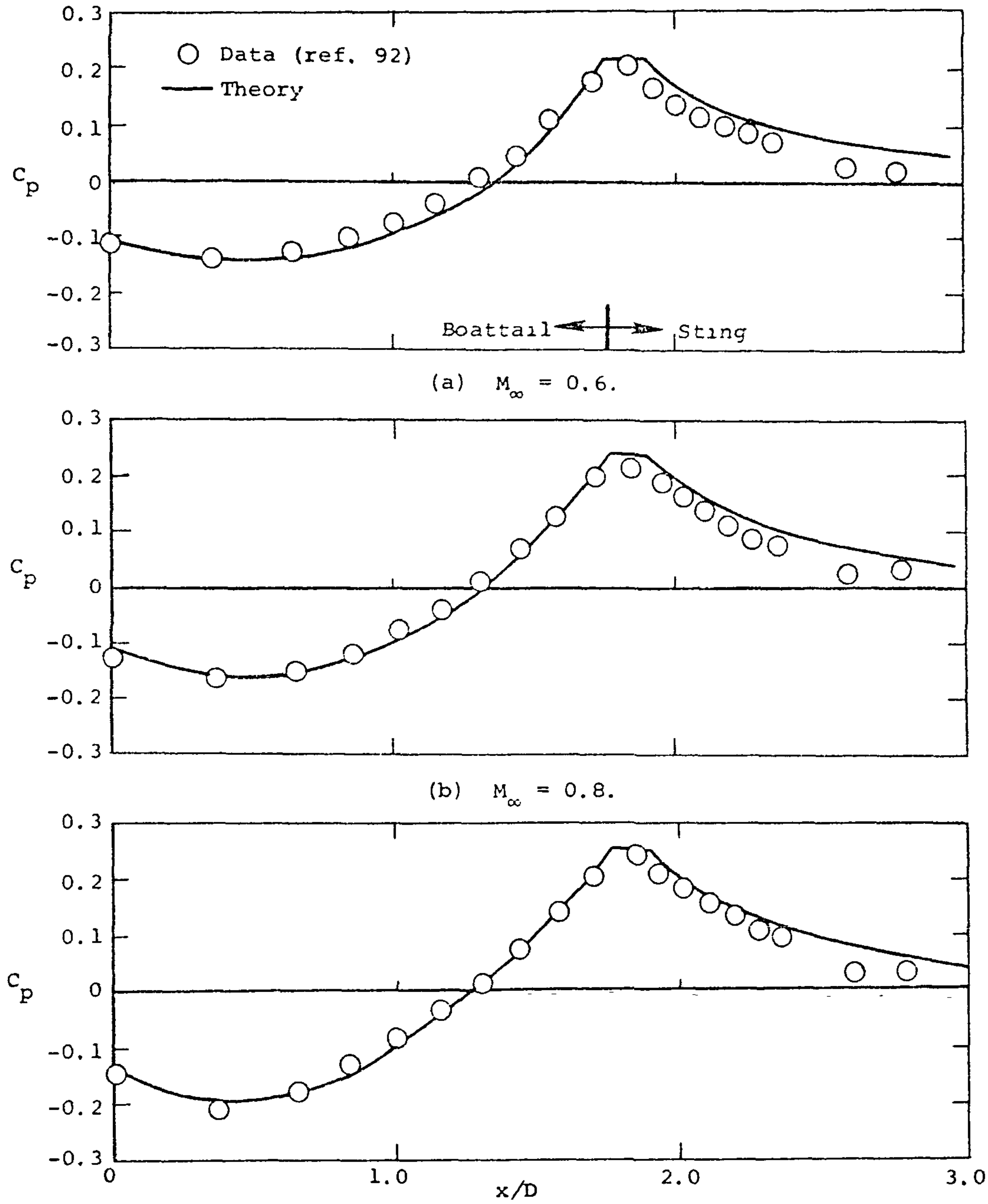

(c) M_∞ = 0.9.

Figure 83.- Comparison between calculated and measured pressure coefficient distributions on boattail-sting configuration 2 (ref. 300).

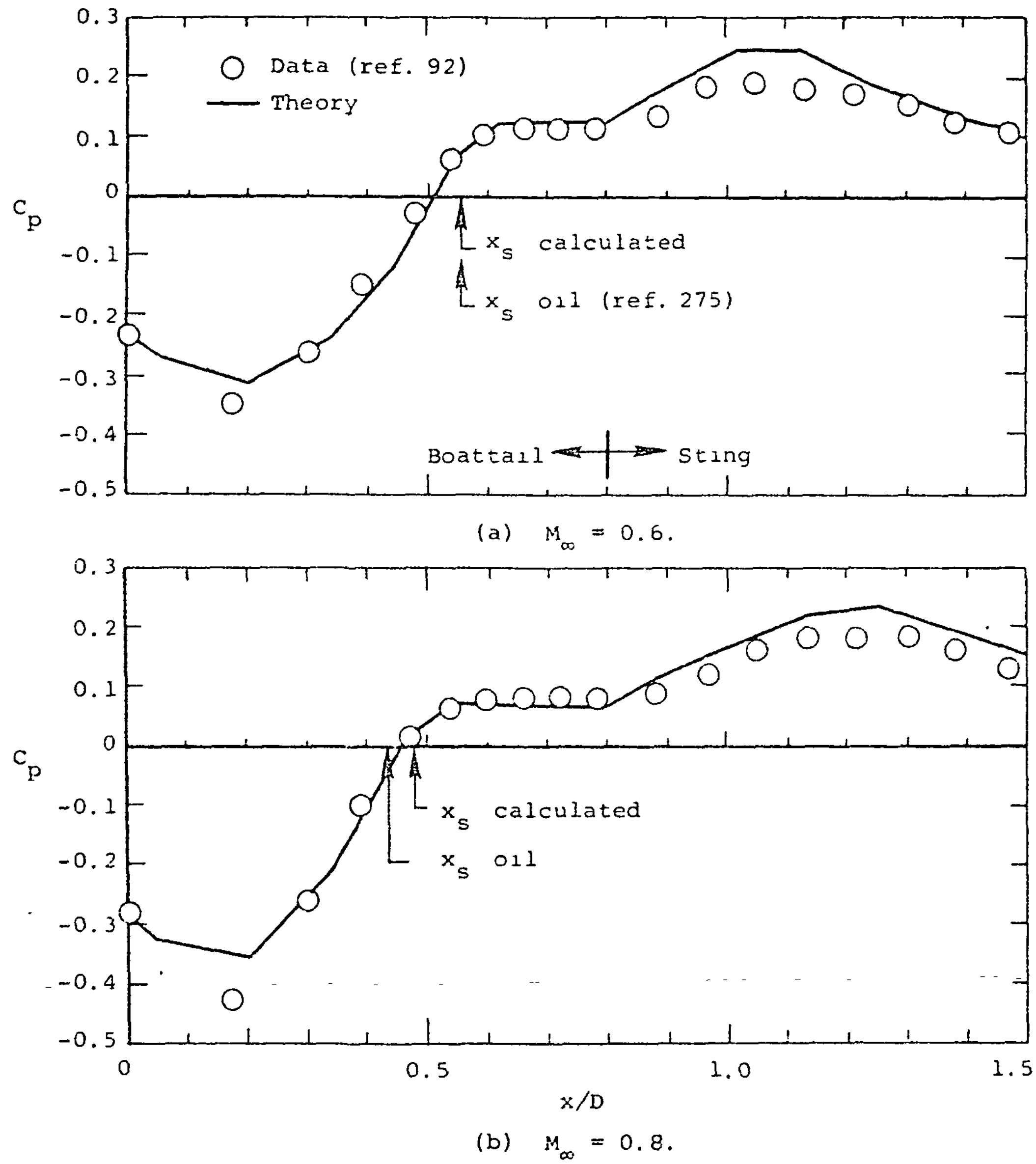

Figure 84.- Comparison between calculated and measured pressure coefficient distributions on boattail-sting configuration 1 (ref. 300).

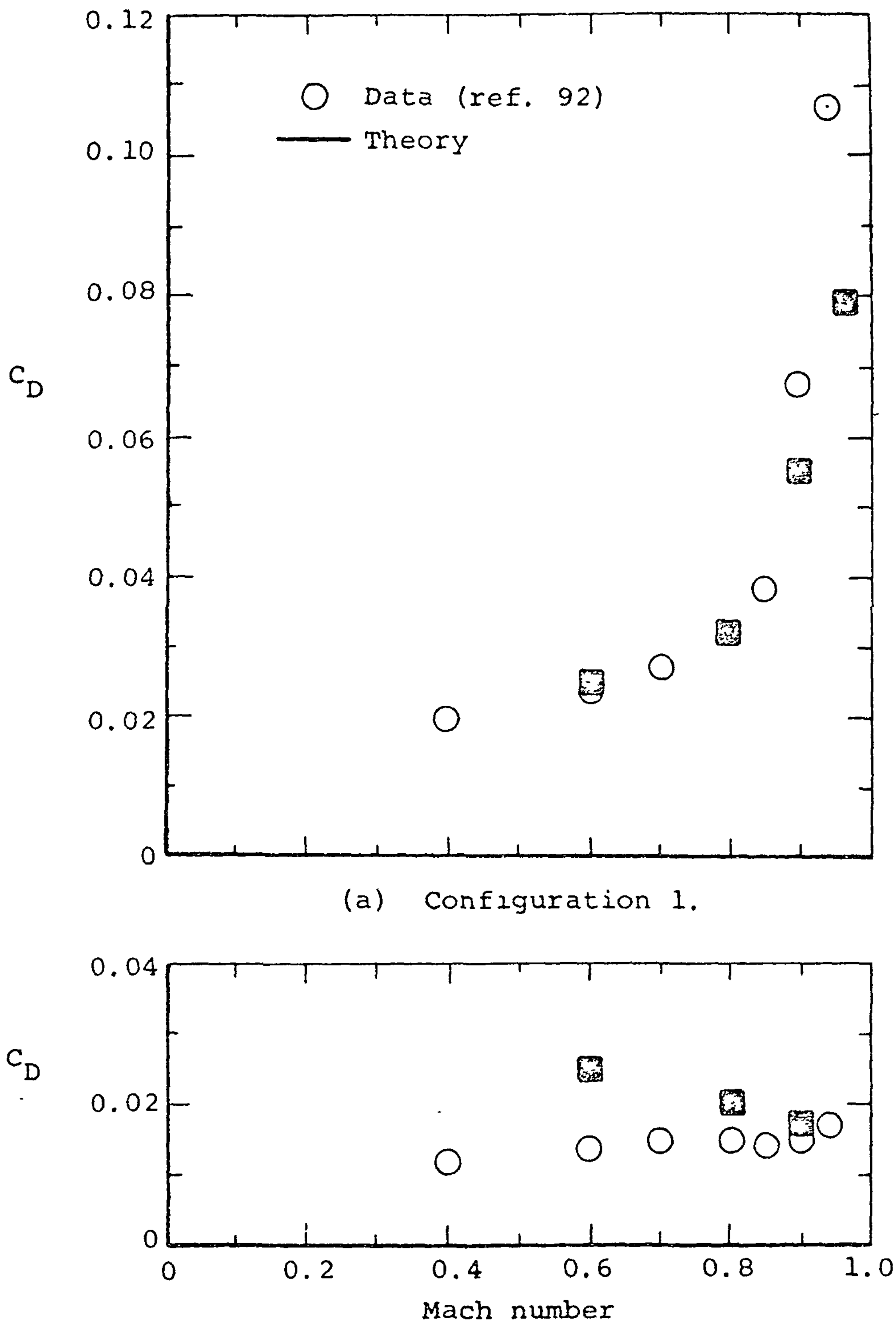

(a) Configuration 1.

(b) Configuration 2.

Figure 85.- Comparison between the theory and experimental data for integrated boattail drag coefficient on boattails with solid plume simulators (ref. 300).

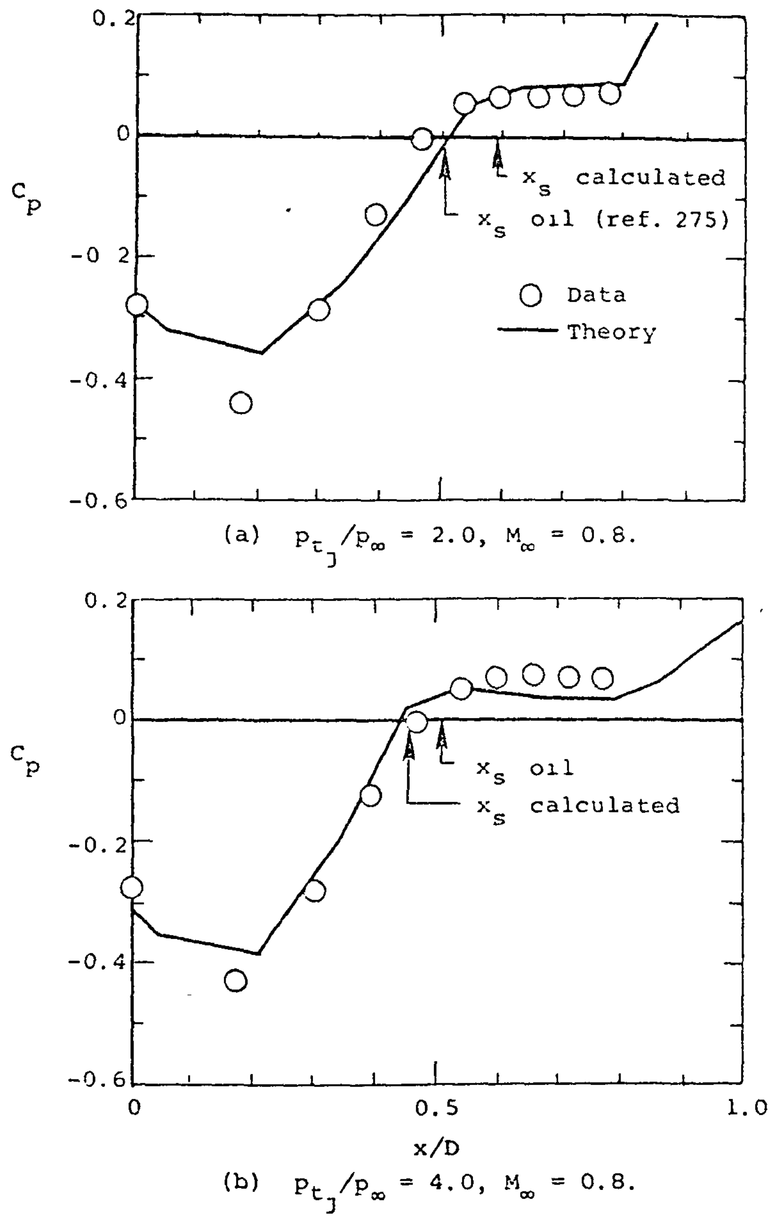

Figure 86.- Comparison between calculated and measured pressure coefficient distributions for separated flow on configuration 1 with exhaust plume simulated by high pressure air (ref. 300).

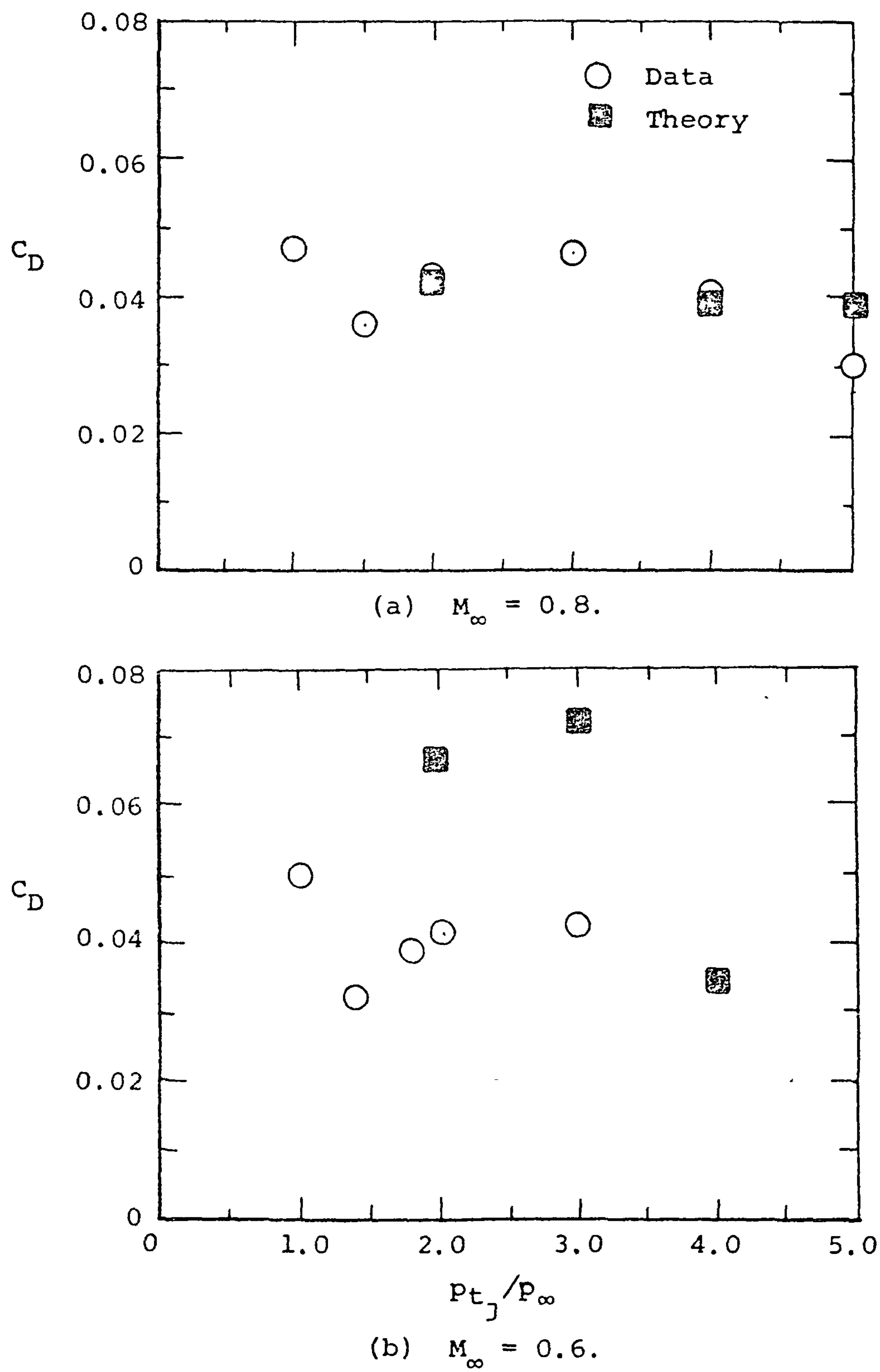

Figure 87.- Comparison of experimental and calculated boattail drag on configuration 1 with plume simulated with high pressure air (ref. 300).

ORIGINAL PAGE IS
OF POOR QUALITY

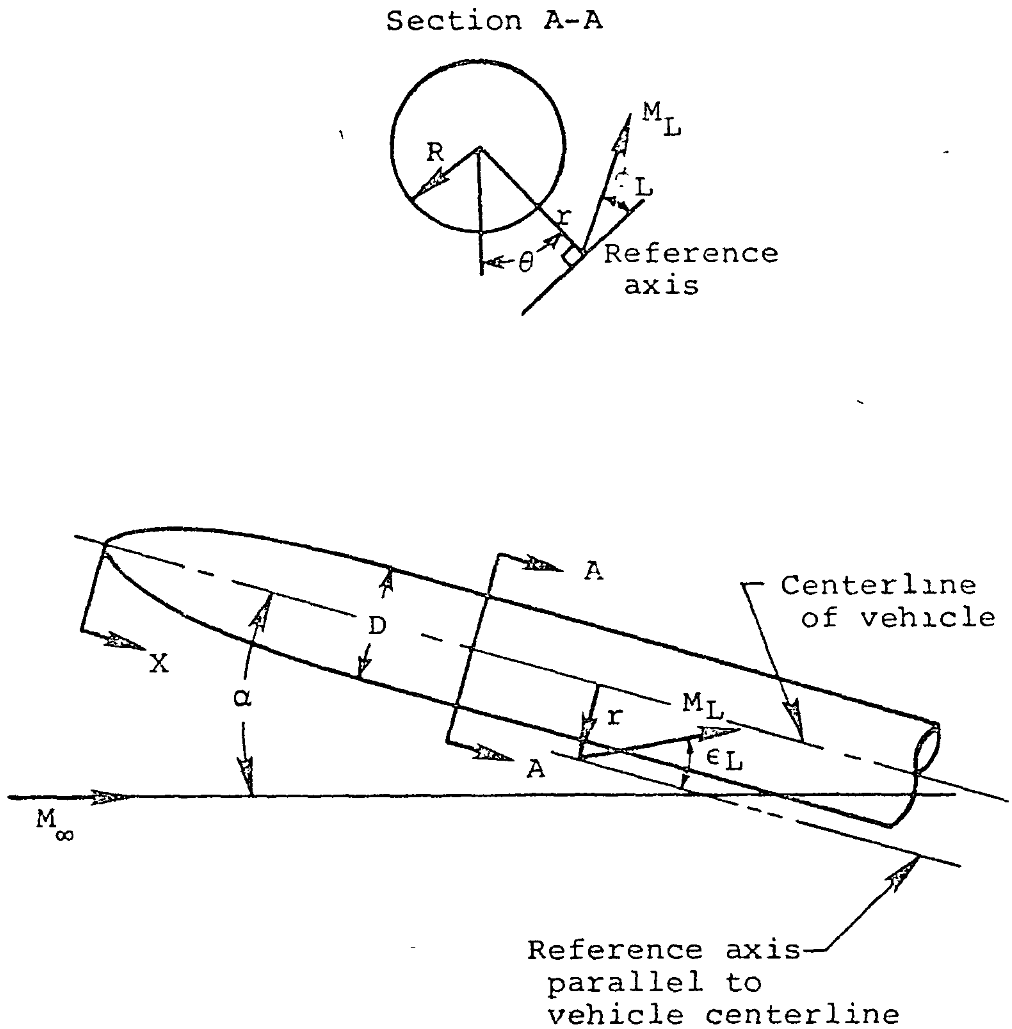

Figure 88.- Definition of flow field geometry.

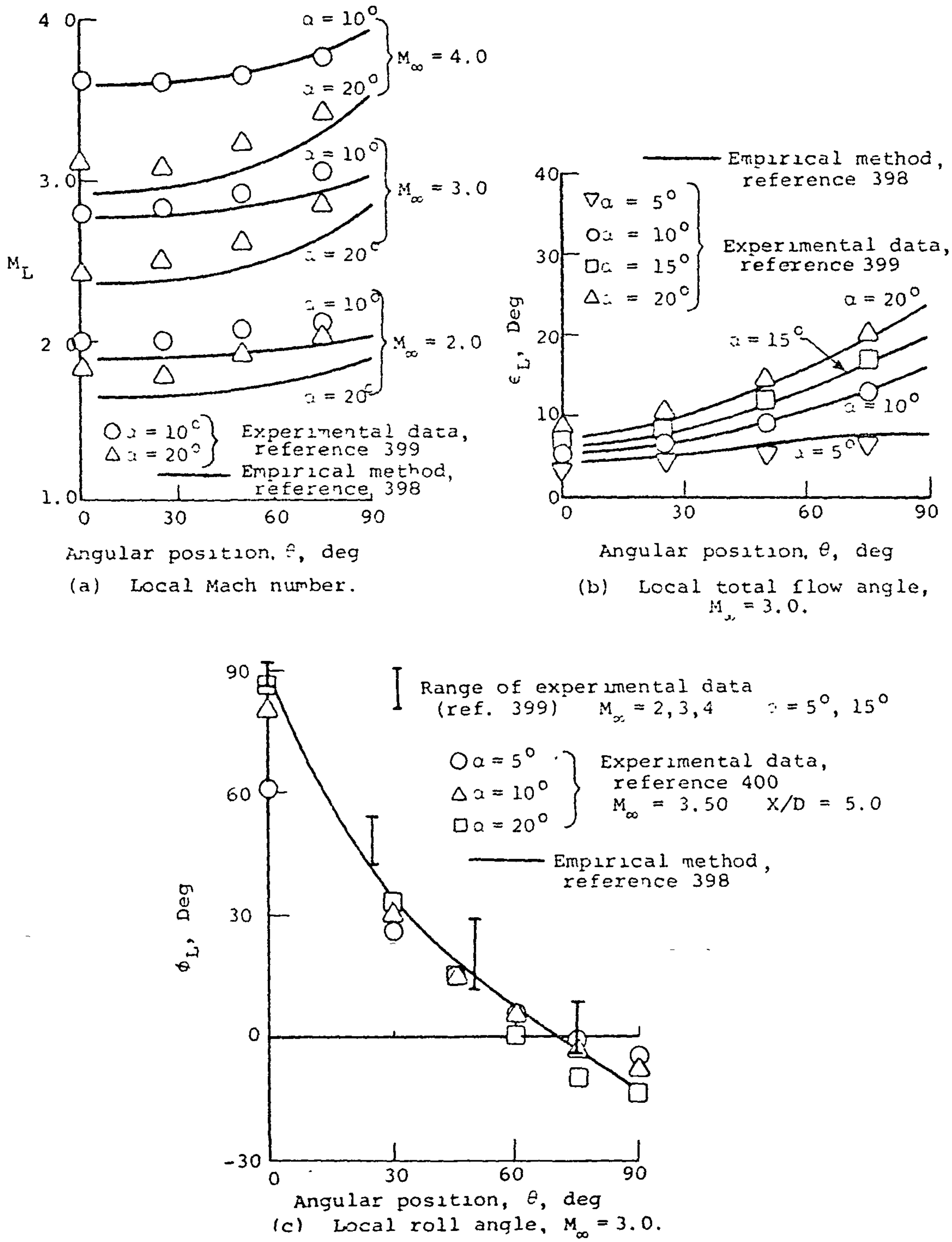

Figure 89.- Data comparisons of local flow quantities at $X/D = 6.0$, $r/R = 1.8$ for a 3.0/1 von Kármán ogive-cylinder.

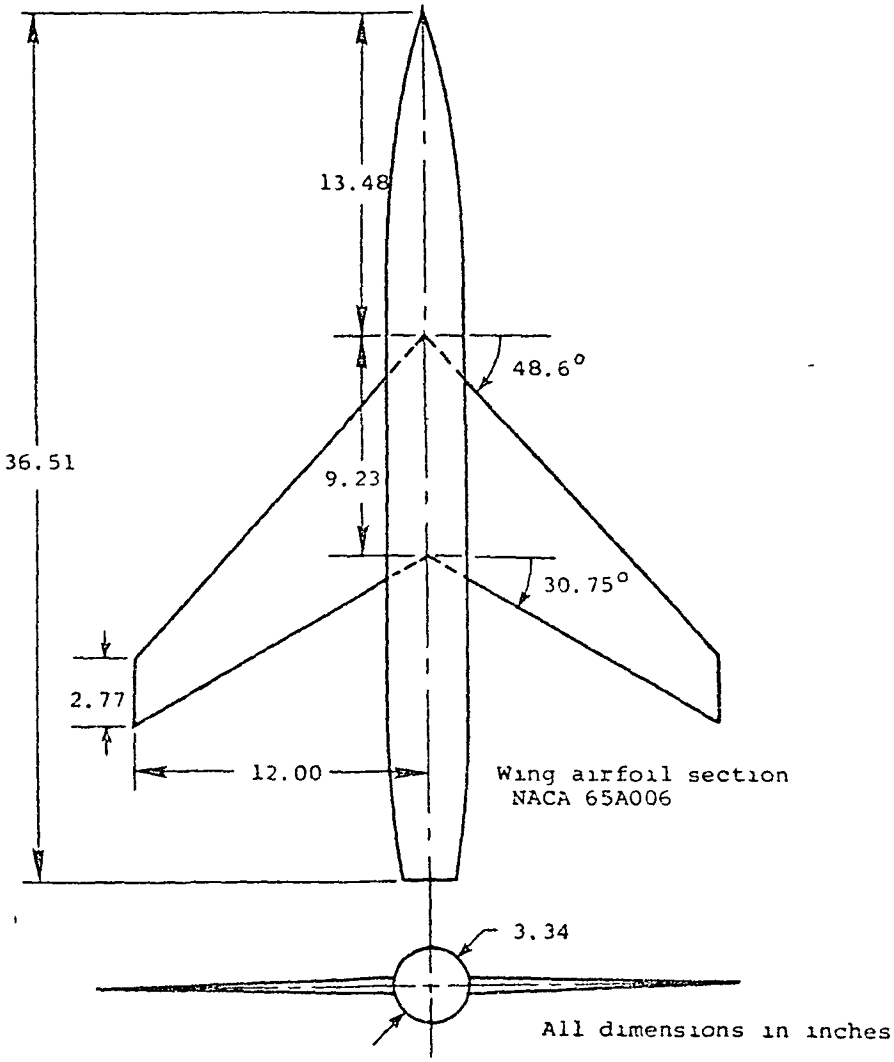

(a) Wing-body configuration 1 (WB1)

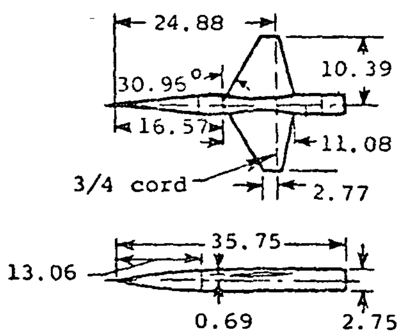

Trapezoidal Wing-Fuselage Configuration

Aspect ratio	3.0
Taper ratio	0.25
Section	4-percent circular arc
Area	1.00 square foot

(b) Wing-body configuration 2 (WB2)

Figure 90.- Wing-body configurations modeled in prediction of local flow fields using method of reference 303.

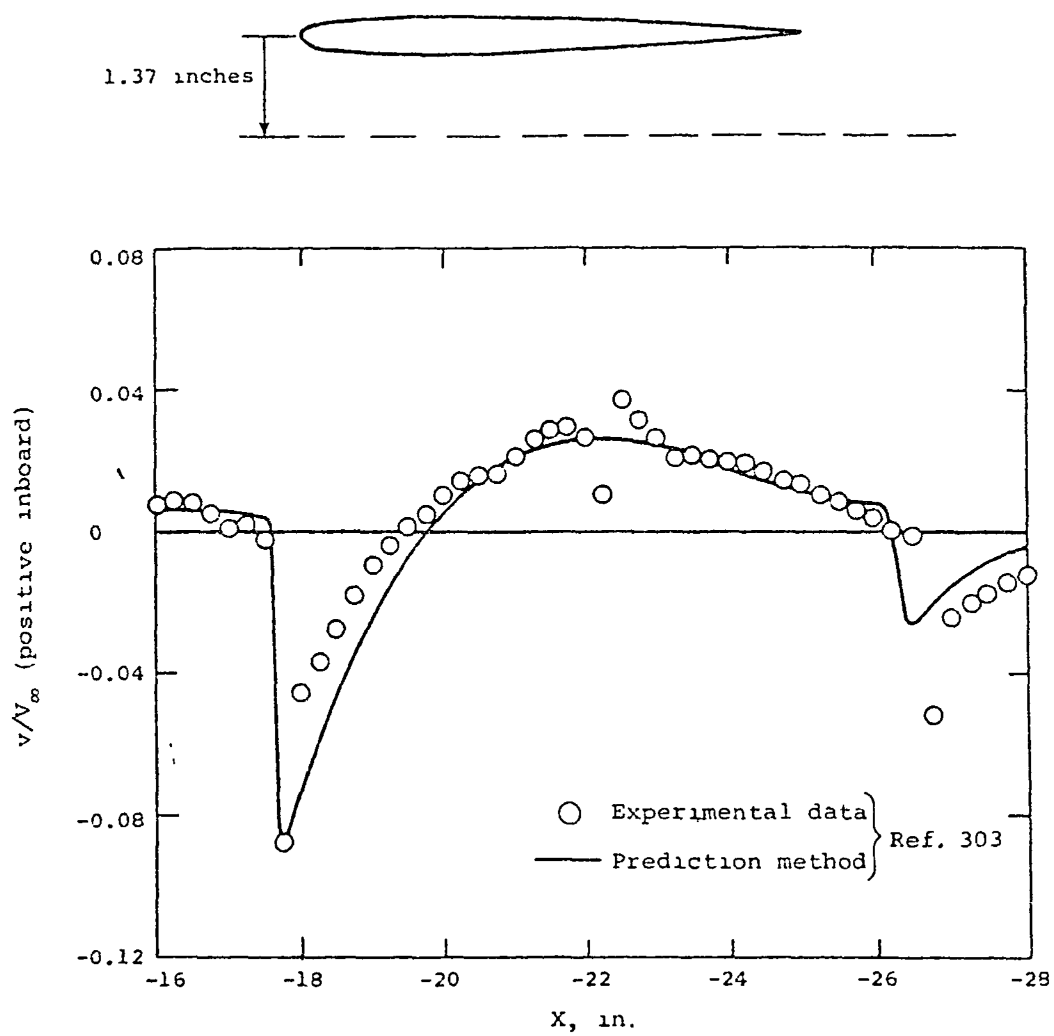

(a) Local sidewash velocity.

Figure 91.- Flow field under the wing of WB1 at the one-third semispan location, $M_\infty = 1.5$, $\alpha = 0^\circ$, $Z = 1.37$ inches.

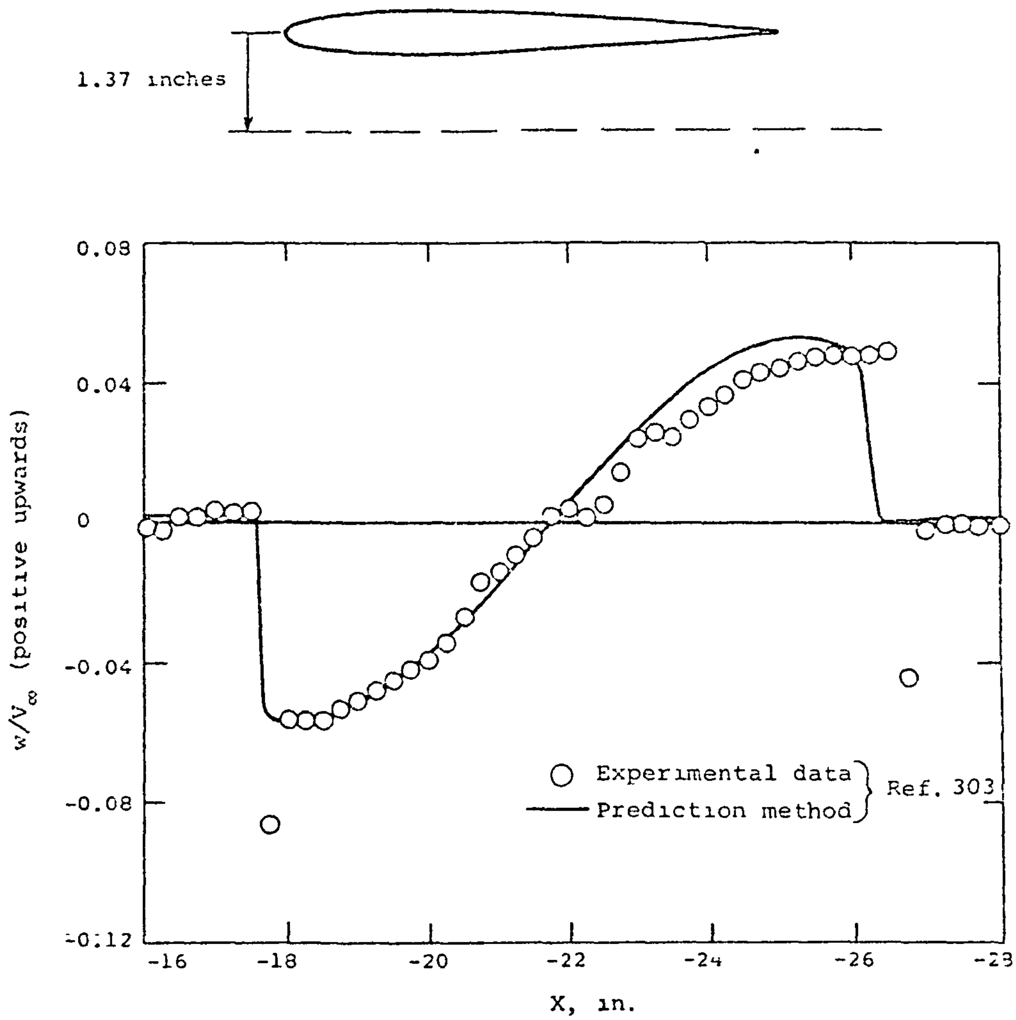

(b) Local upwash velocity.

Figure 91.- Concluded.

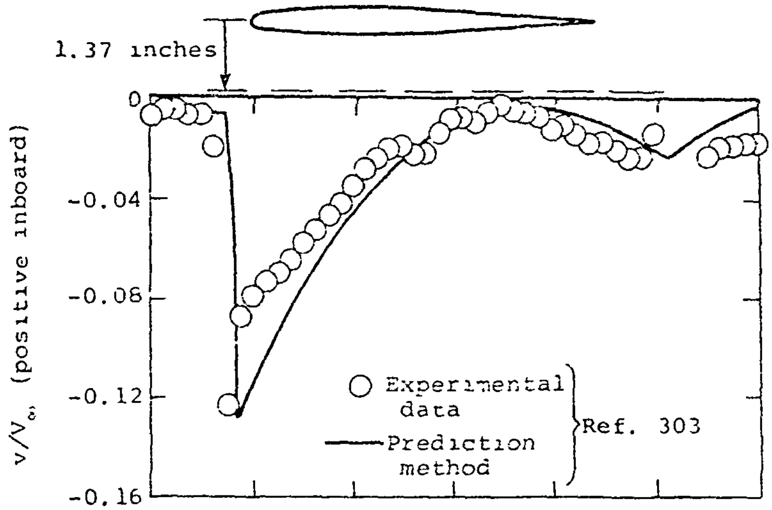

(a) Local sidewash velocity.

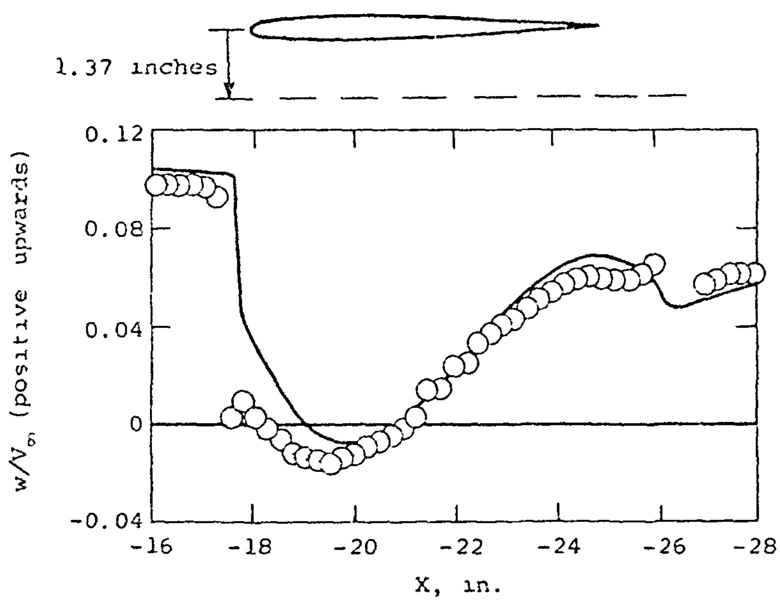

(b) Local upwash velocity.

Figure 92.- Flow field under the wing of W31 at the one-third semispan location, $M_\infty = 1.5$, $\alpha = 5^\circ$, $Z = 1.37$ inches.

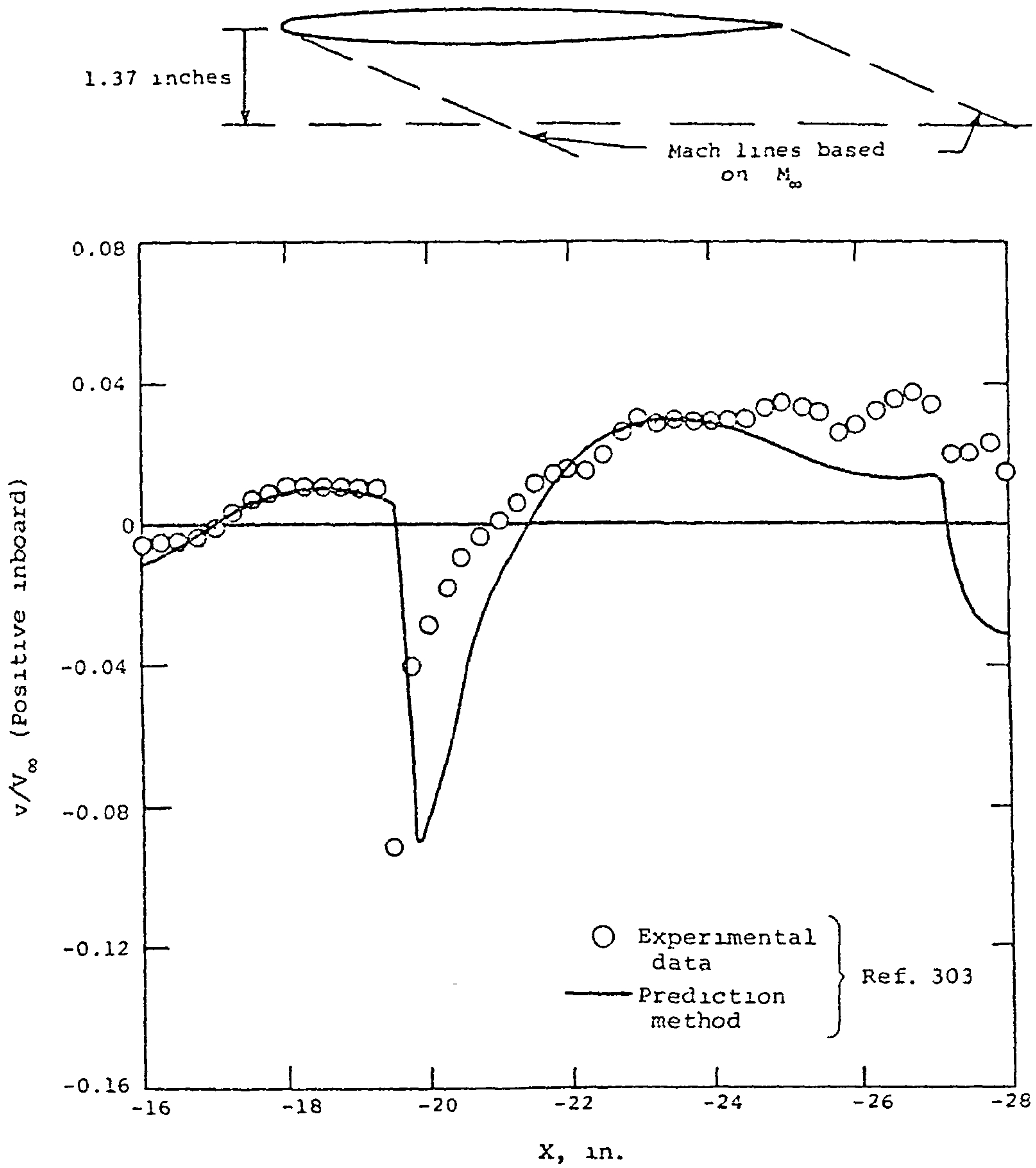

(a) Local sidewash velocity.

Figure 93.- Flow field under the wing of WB1 at the one-third semispan location, $M_\infty = 2.5$, $\alpha = 0^\circ$, $Z = 1.37$ inches.

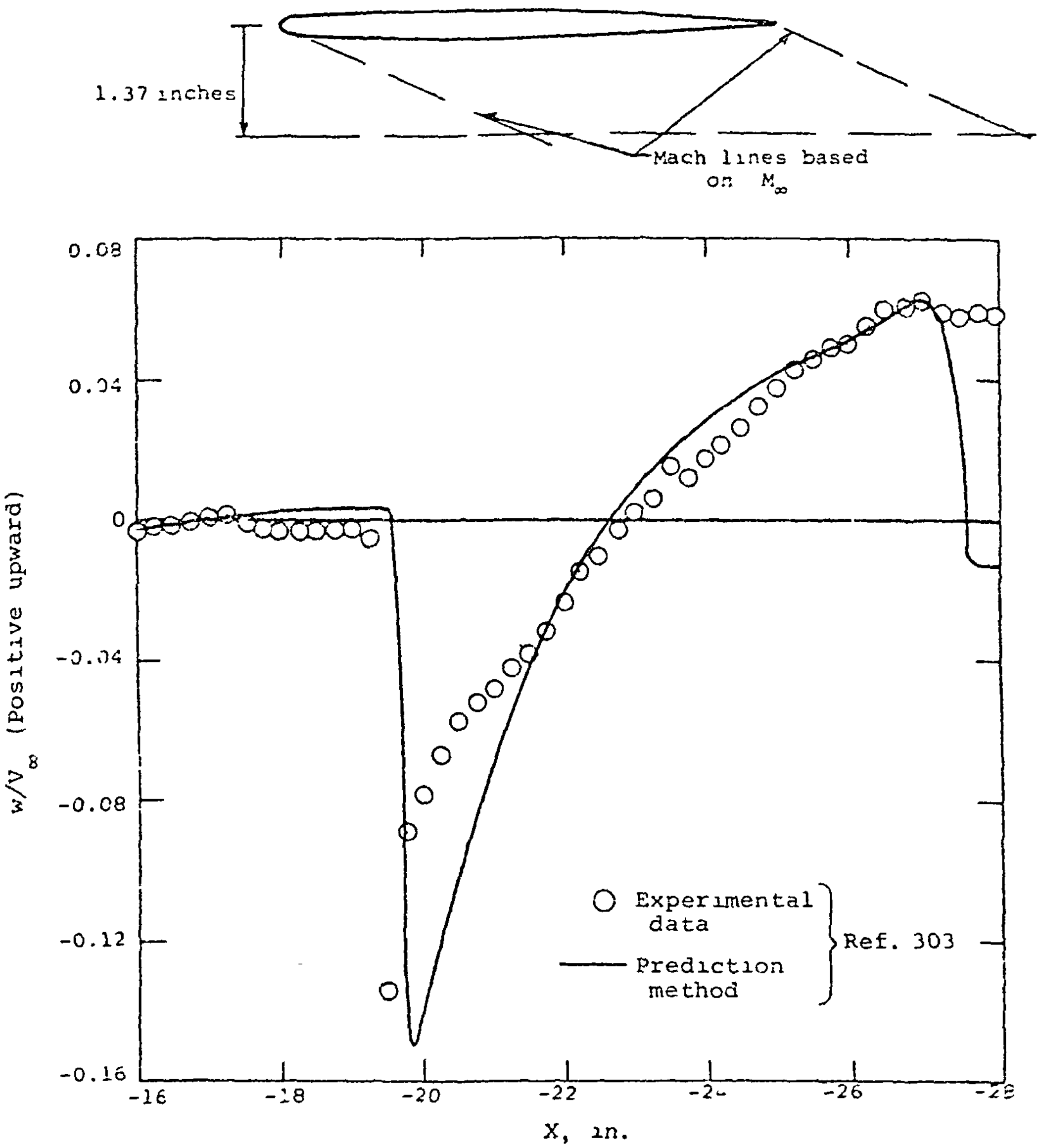

(b) Local upwash velocity.

Figure 93.- Concluded.

C-5

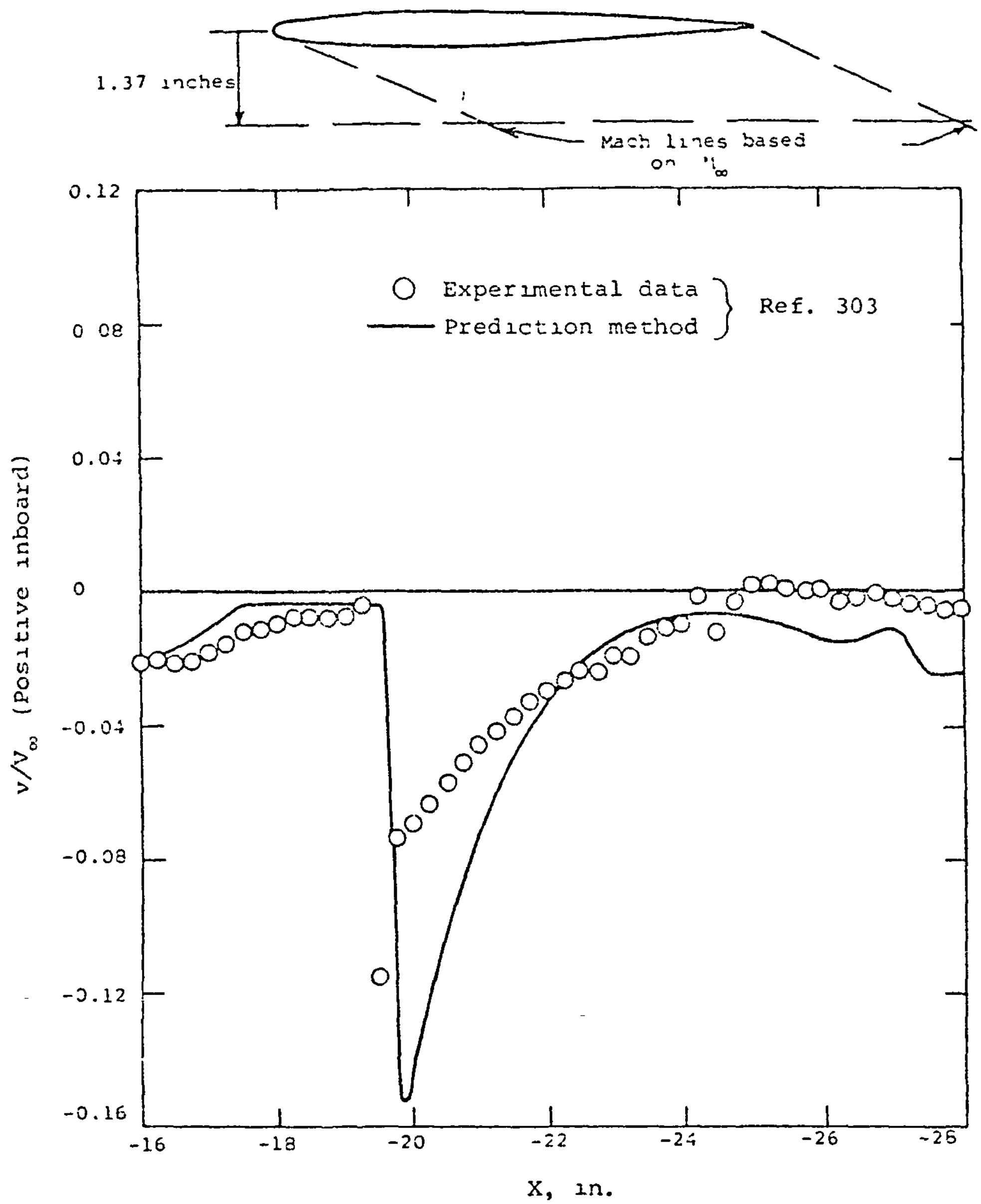

(a) Local sidewash velocity.

Figure 94.- Flow field under the wing of WB1 at the one-third semispan location, $M_\infty = 2.5$, $\alpha = 5^{\circ}$, $Z = 1.37$ inches.

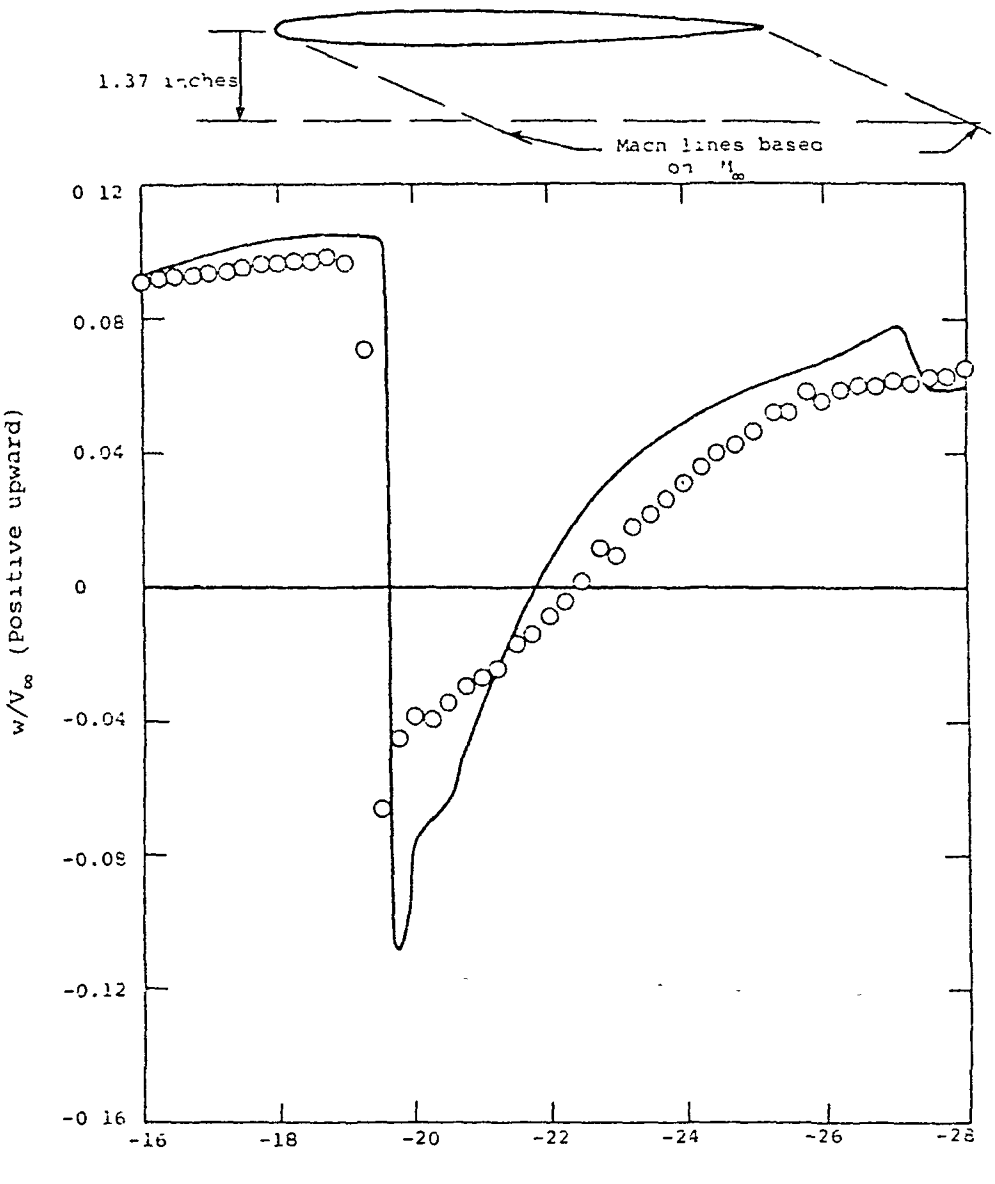

(b) Local upwash velocity.

Figure 94.- Concluded.

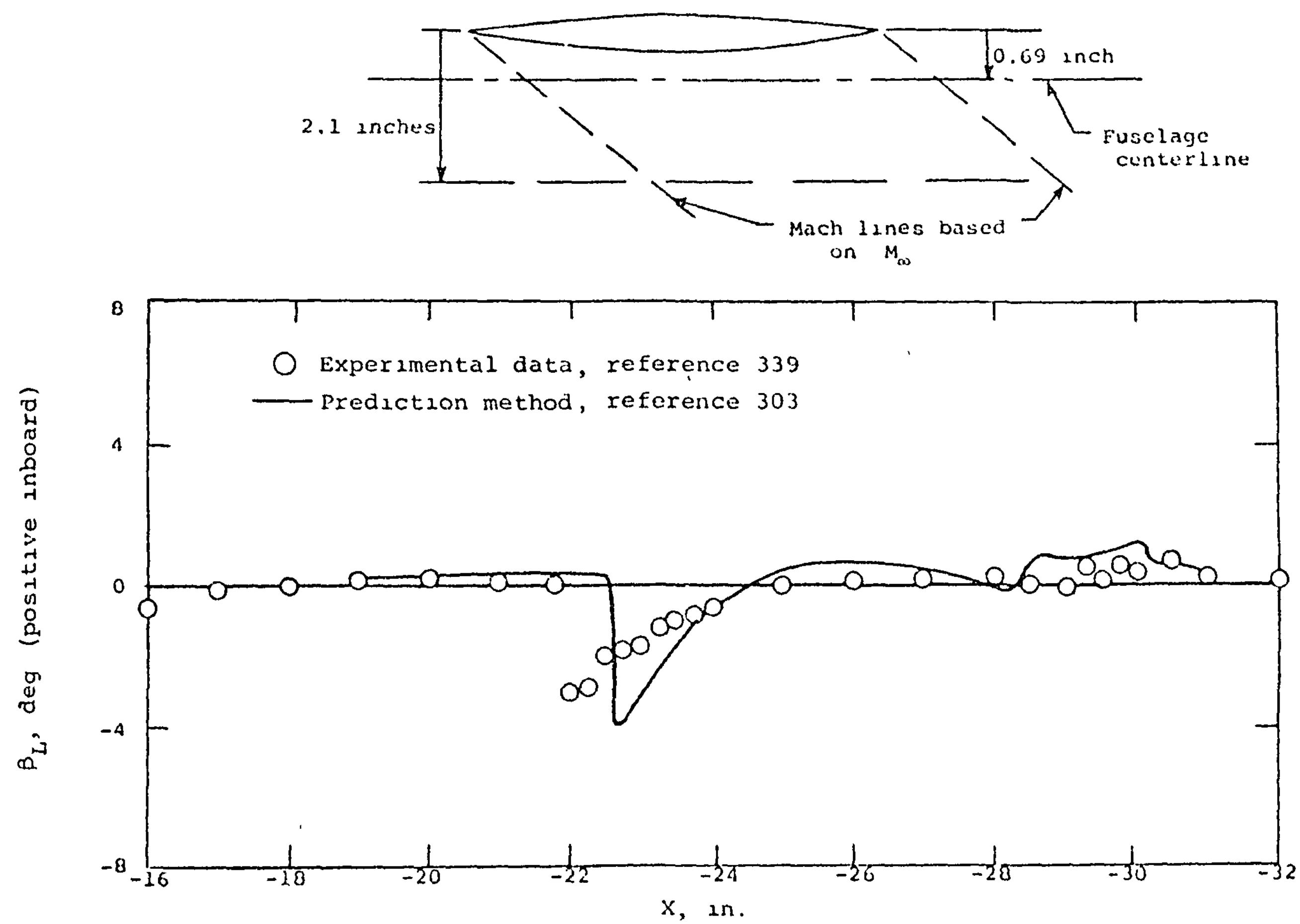

(a) Local sidewash angle.

Figure 95.- Flow field under the wing of WB2 at Y = -6.6 inches, $M_\infty = 1.61$, $\alpha = 0^o$, Z = 1.41 inches.

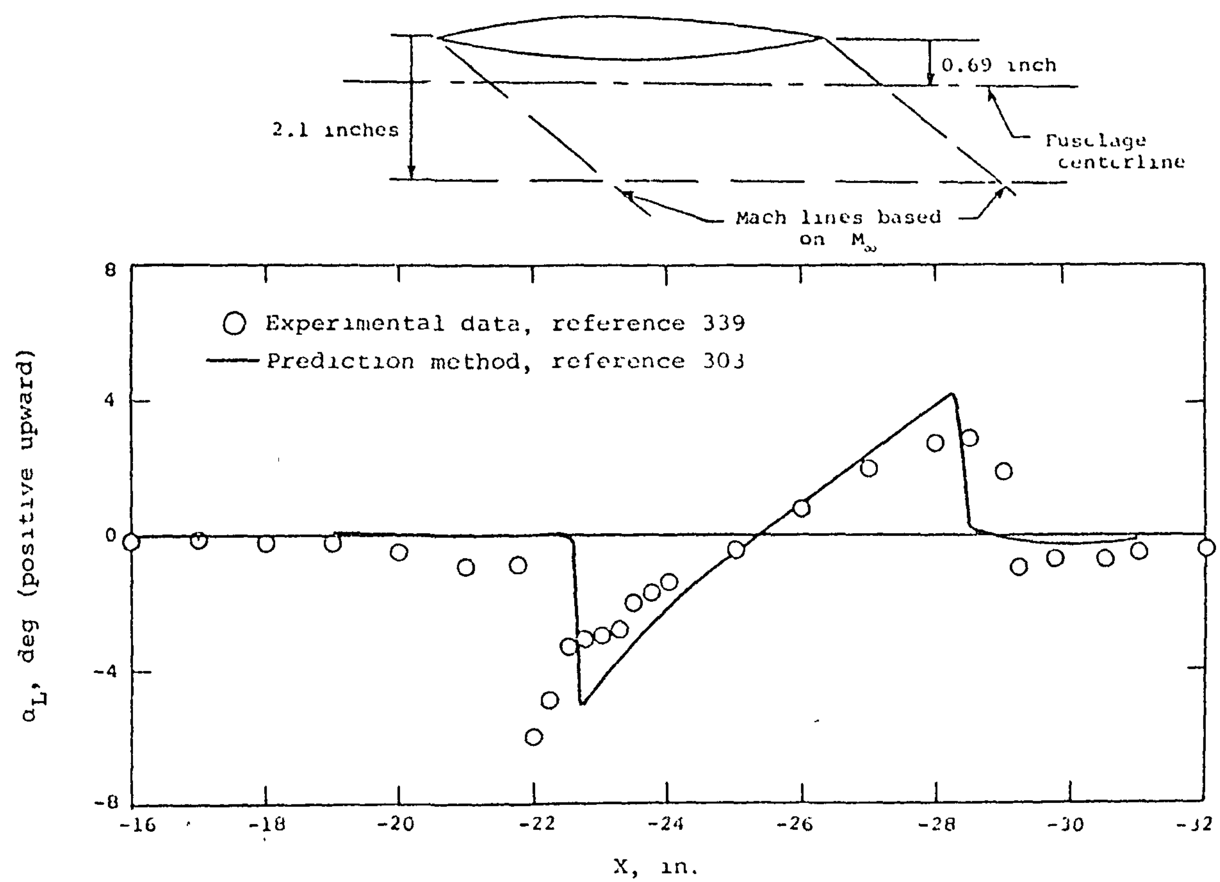

(b) Local upwash angle.

Figure 95.- Concluded.

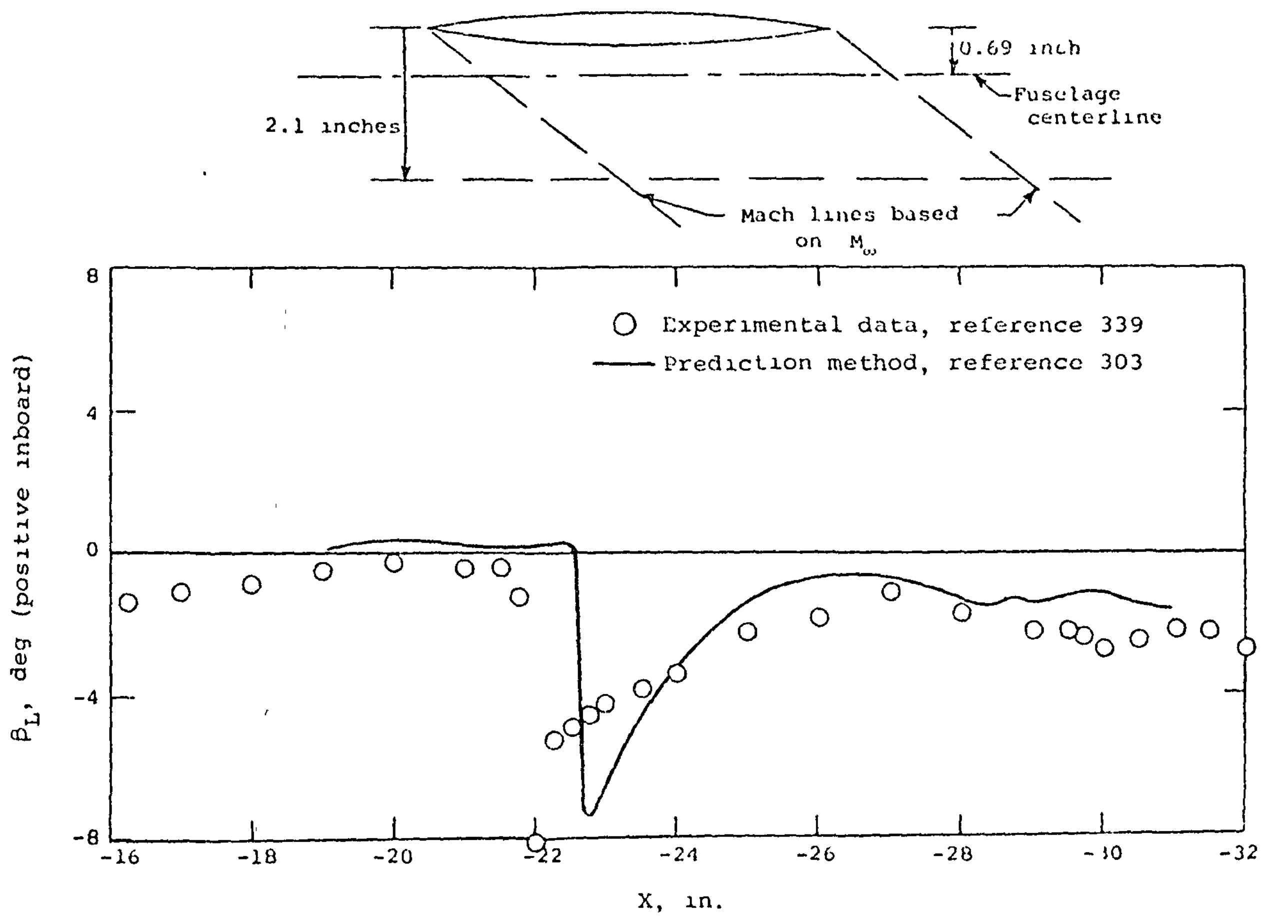

(a) Local sidewash angle.

Figure 96.- Flow field under the wing of WB2 at $Y = -6.6$ inches, $M_\infty = 1.61$, $\alpha = 4$, $Z = 1.41$ inches.

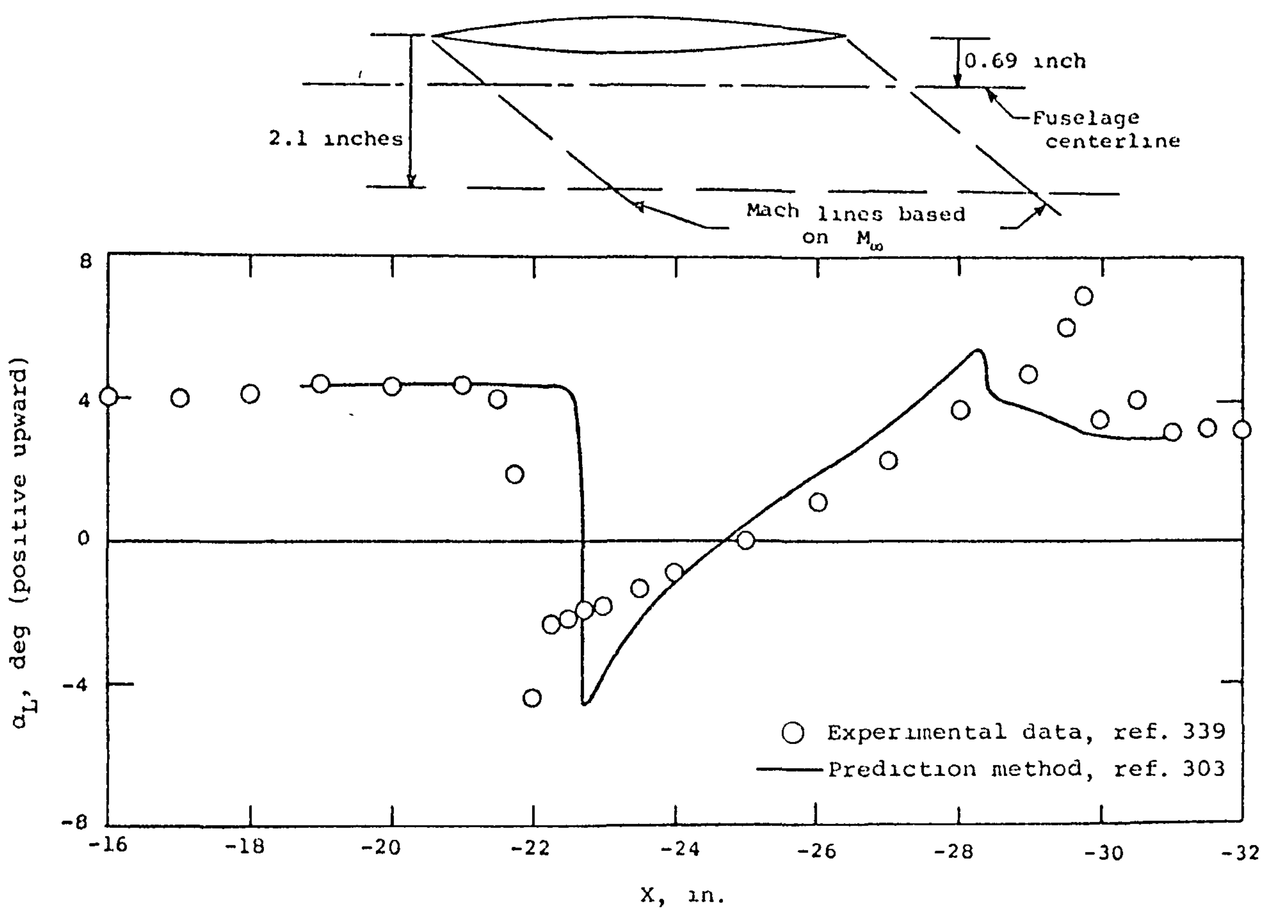

(b) Local upwash angle.

Figure 96.- Concluded.

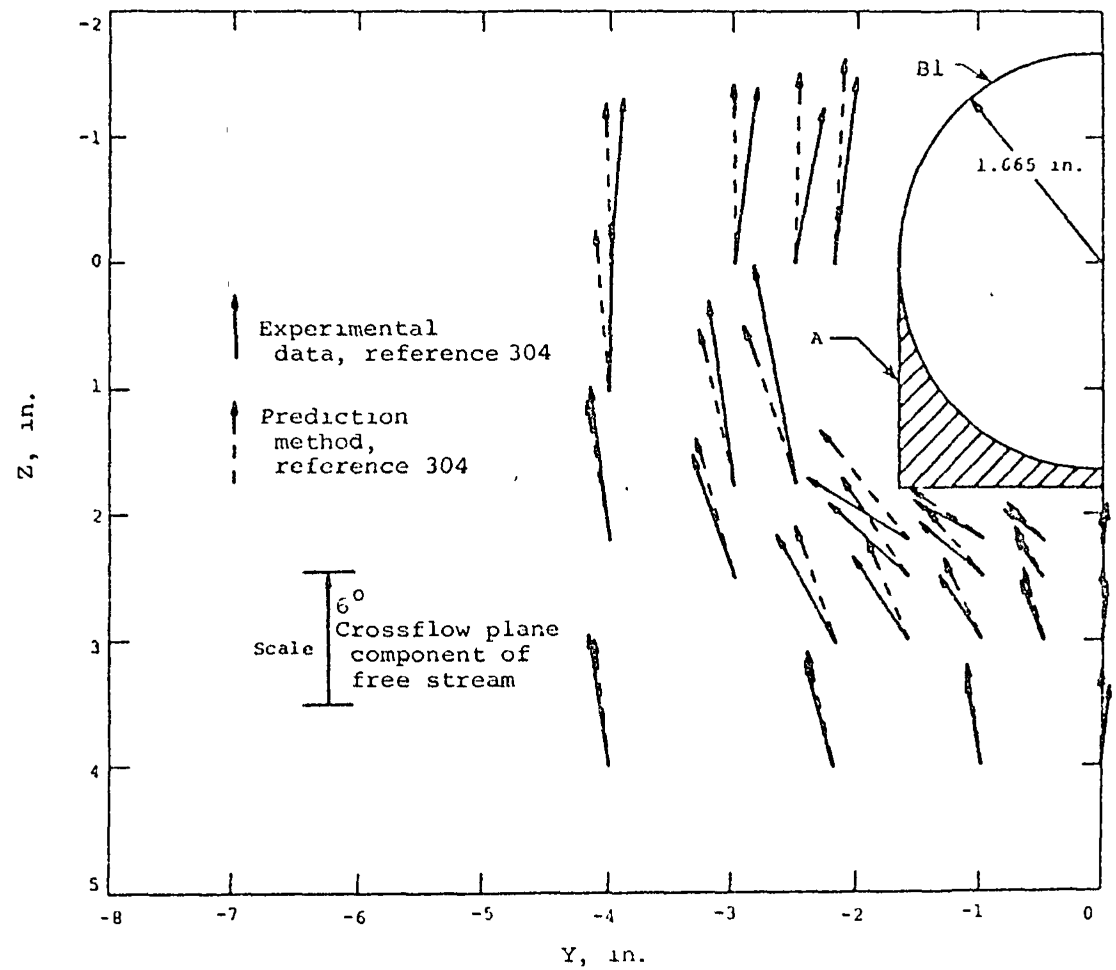

(a) Noncircular fuselage.

Figure 97.- Velocity vector plot in crossflow plane 19.66 inches aft of nose tip, $M_\infty = 0.4$, $\alpha = 6^o$.

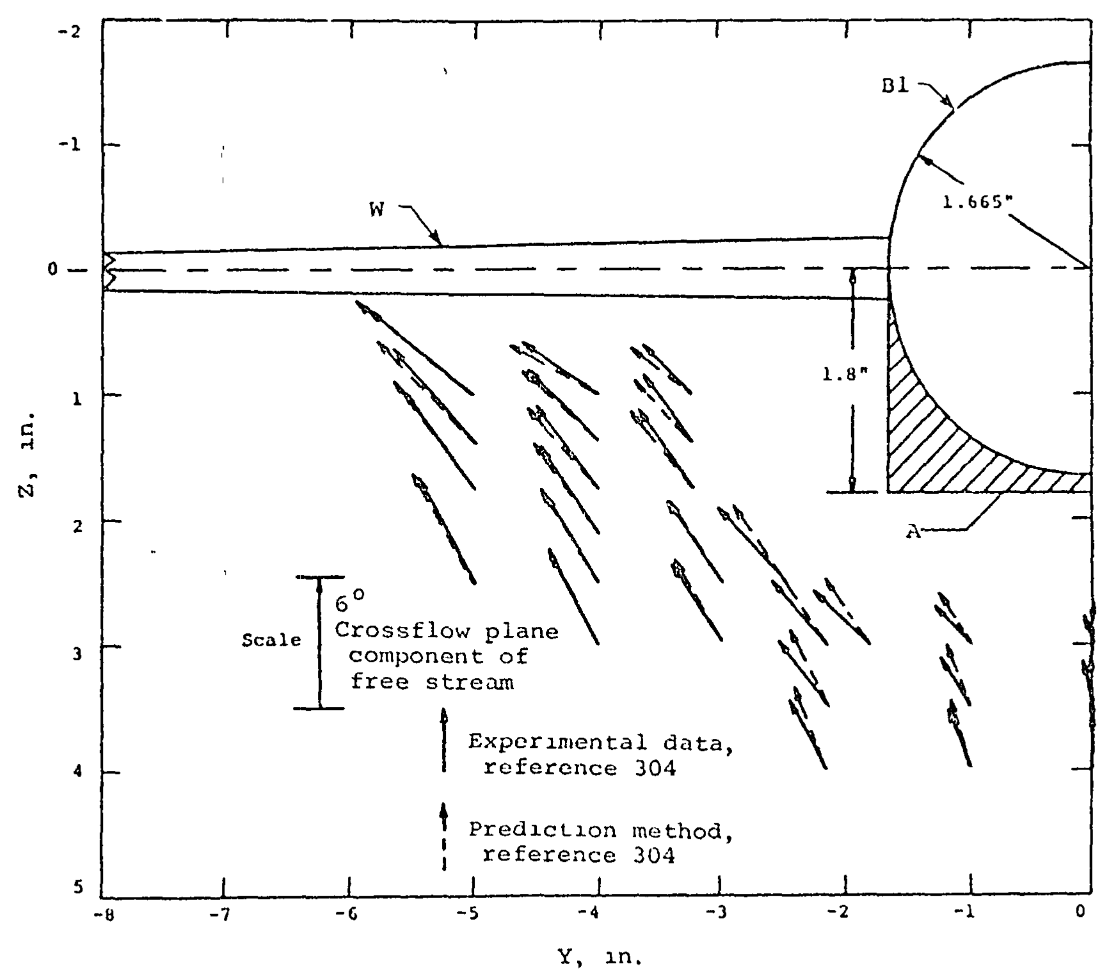

(b) Wing-body model with noncircular fuselage.

Figure 97.- Concluded.

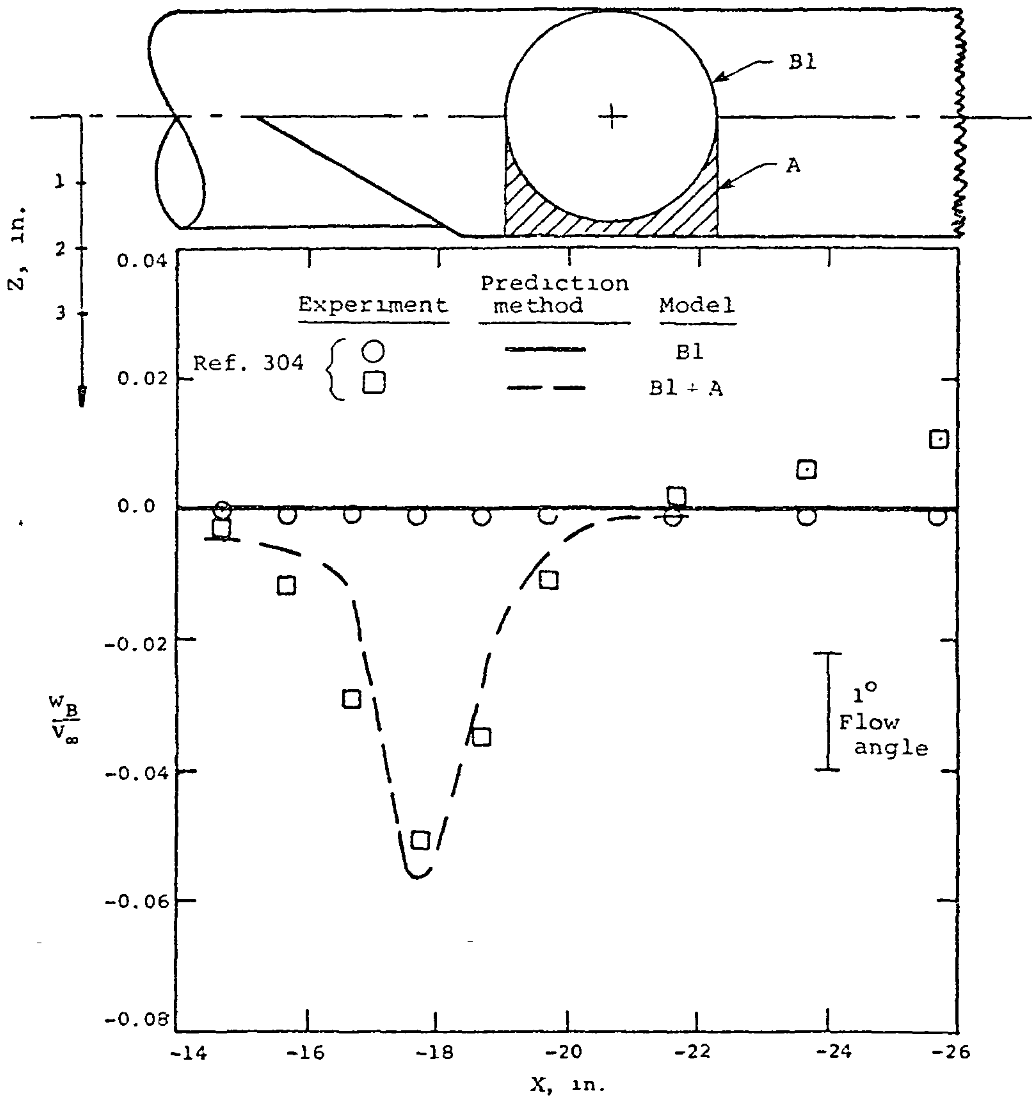

(a) $\alpha = 0°$.

Figure 98 - Distribution of upwash 3 inches under the fuselage centerline for the circular fuselage and for noncircular addition attached to the fuselage, $M_\infty = 0.4$.

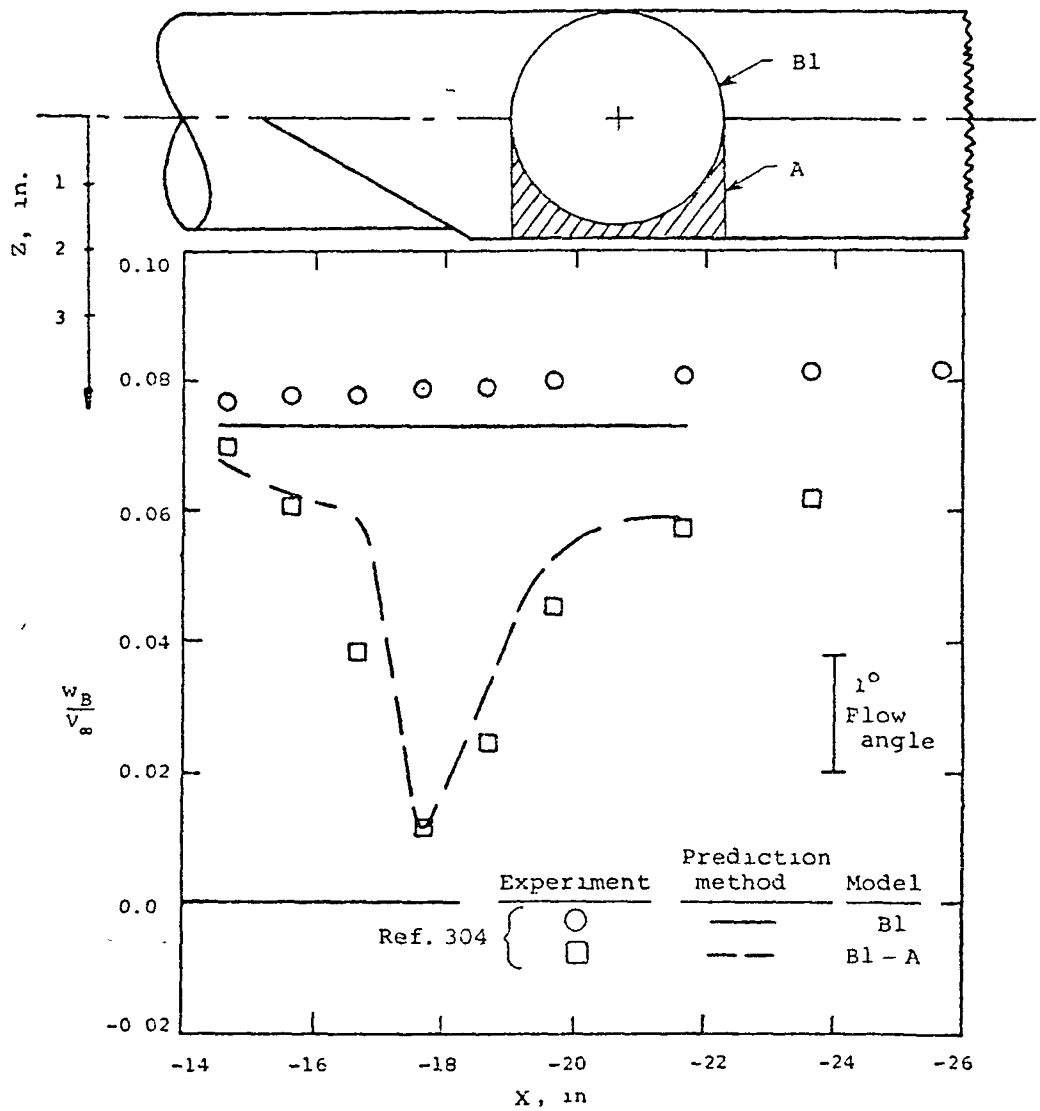

(b) $\alpha = 6°$.

Figure 98.- Concluded.

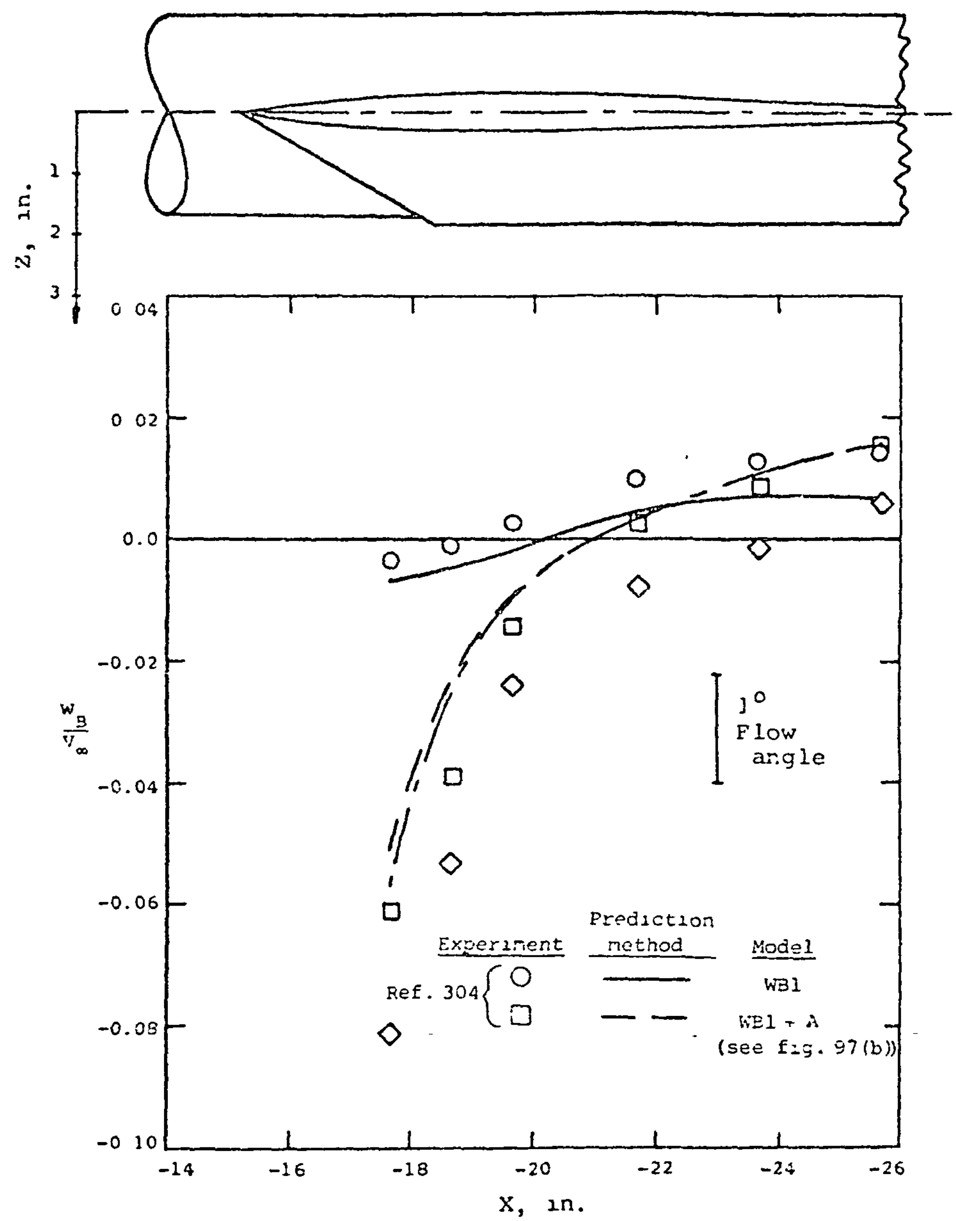

(a) $\alpha = 0°$.

Figure 99.- Distribution of upwash 3 inches under the wing-body fuselage centerline for the circular fuselage and for noncircular addition attached to the fuselage, $M_\infty = 0.4$.

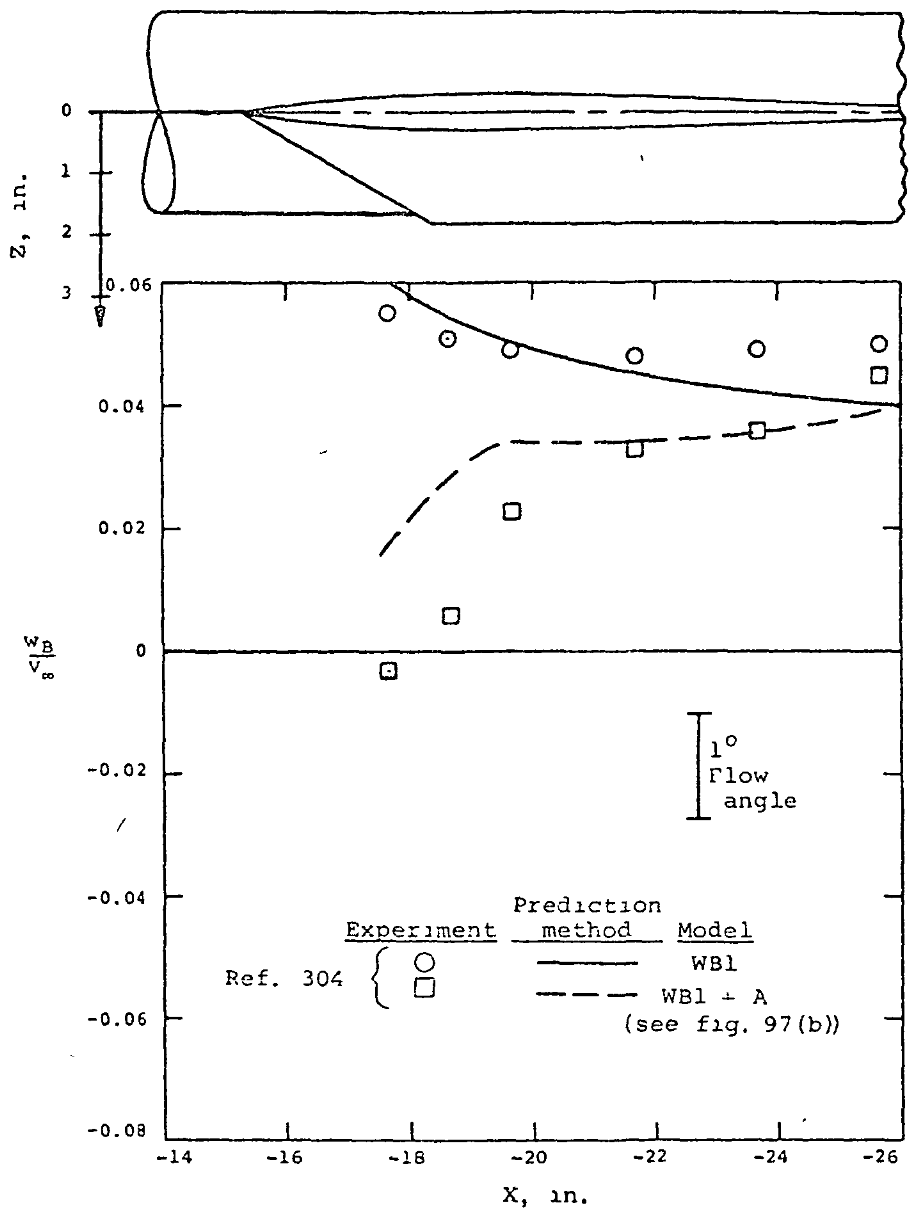

(b) $\alpha = 6°$.

Figure 99.- Concluded.

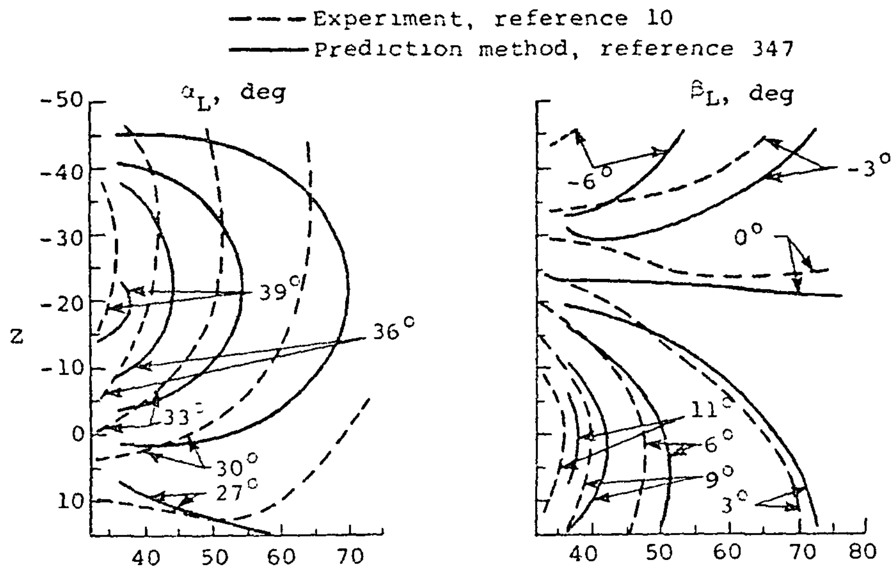

(a) Local upwash angle.

(b) Local sidewash angle.

Figure 100.- Flow field at the side of a fighter-type fuselage, $M_\infty = 0.9$, $\alpha = 25^\circ$.

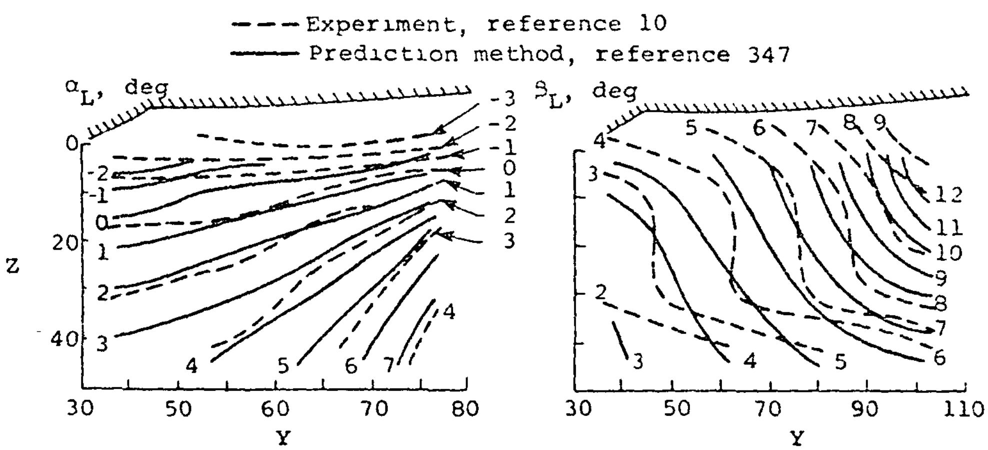

(a) Local upwash angle.

(b) Local sidewash angle.

Figure 101.- Flow field under the wing of a fighter-type wing-fuselage configuration, $M_\infty = 0.9$, $\alpha = 10^\circ$.

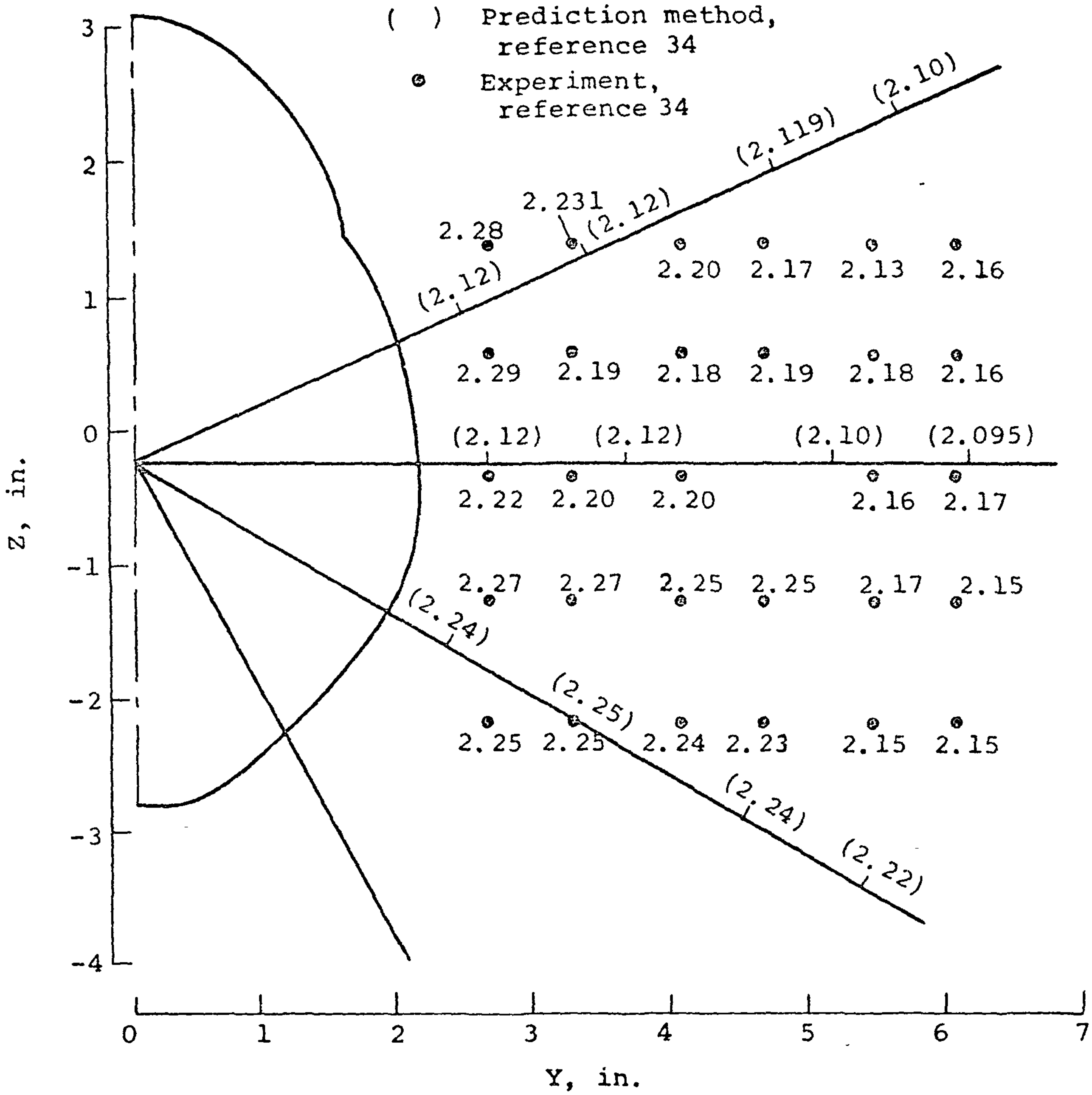

(a) Local Mach number.

Figure 102.- Flow field at the side of a fuselage configuration, $M_\infty = 2.2$, $\alpha = 15^\circ$.

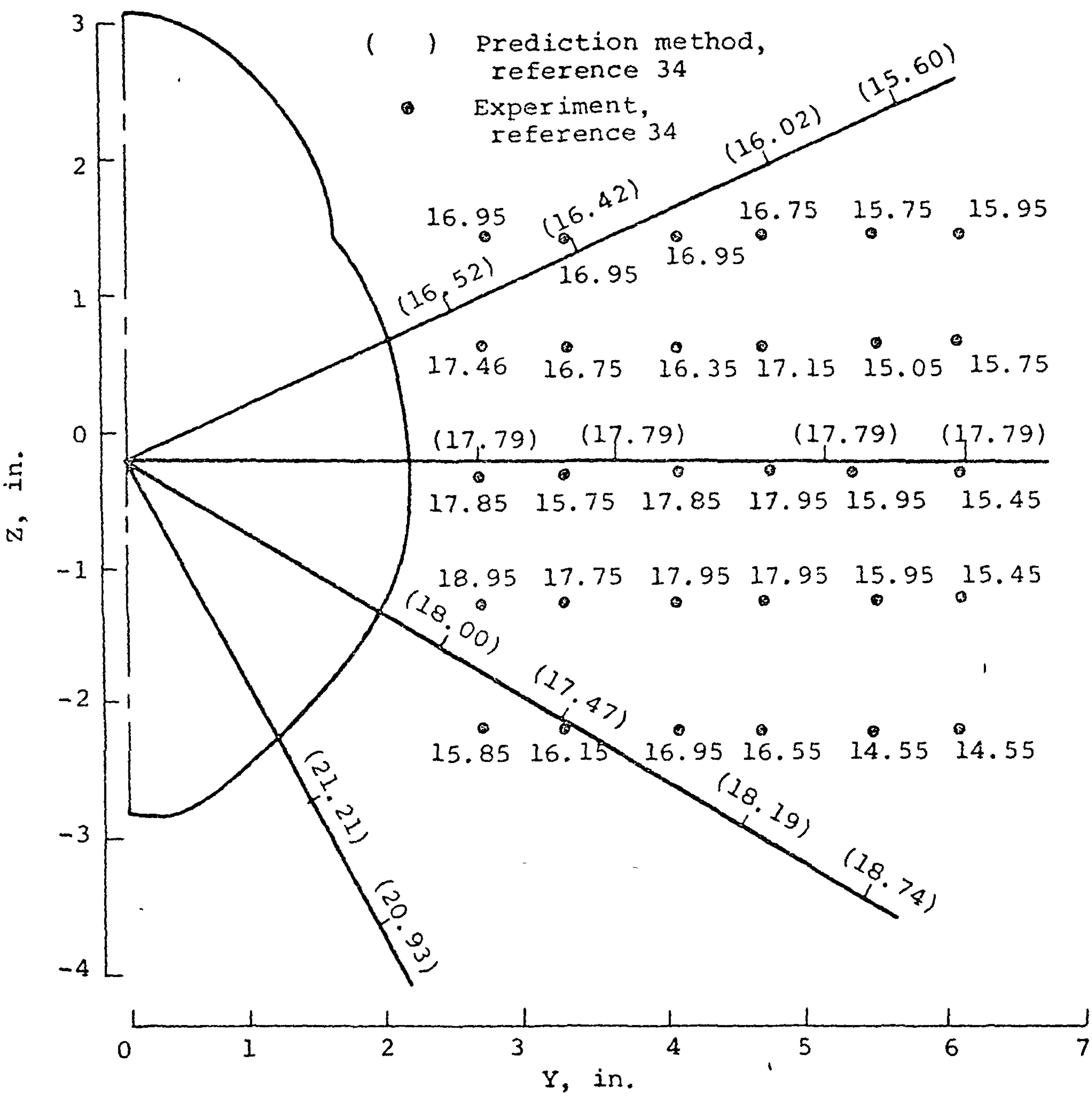

(b) Local angle of upwash.

Figure 102.- Continued.

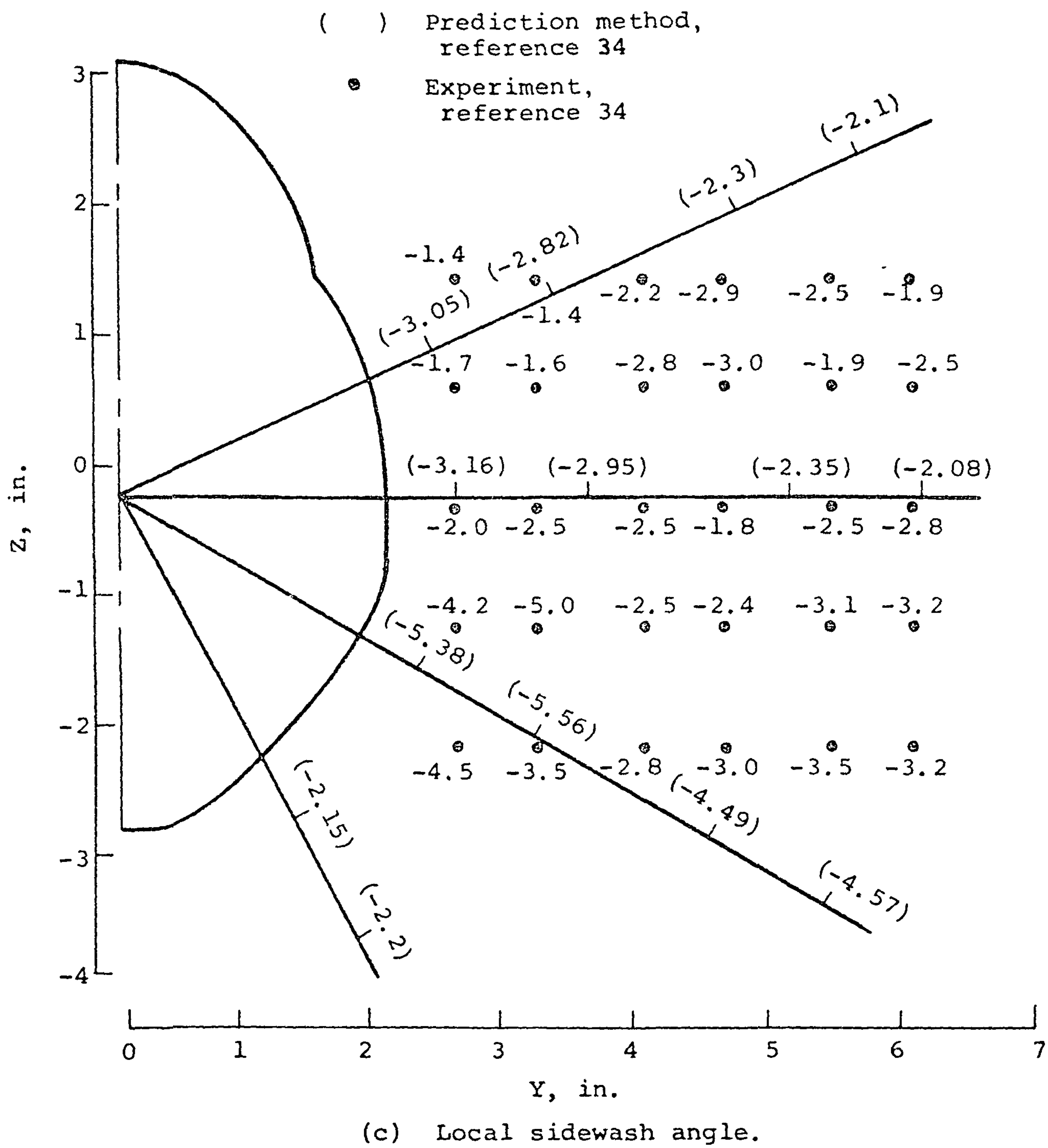

(c) Local sidewash angle.

Figure 102.- Concluded.

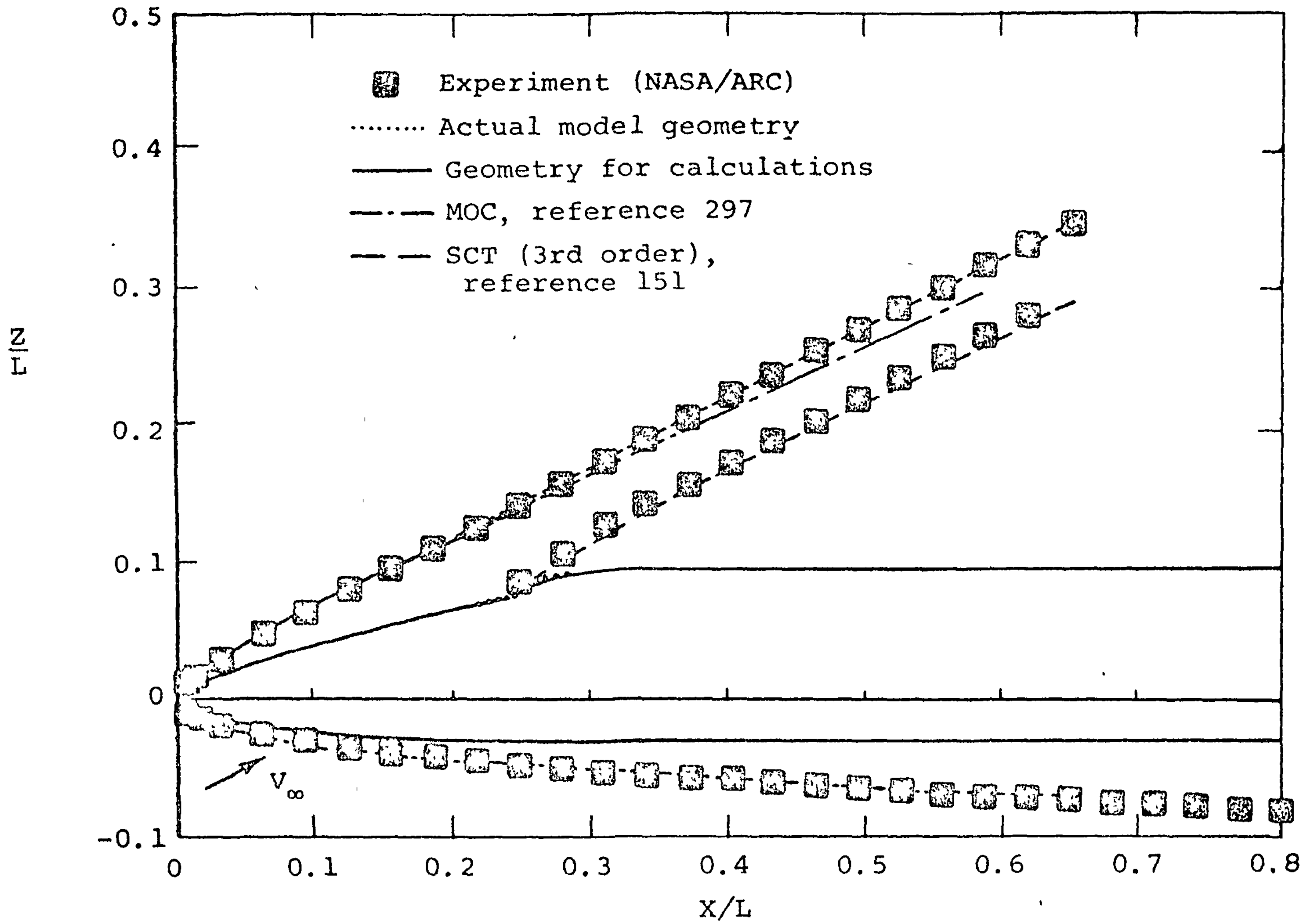

Figure 103.- Shock shape for a blunt nose vehicle, $M_\infty = 7.4$, $\alpha = 15.3^{\circ}$.

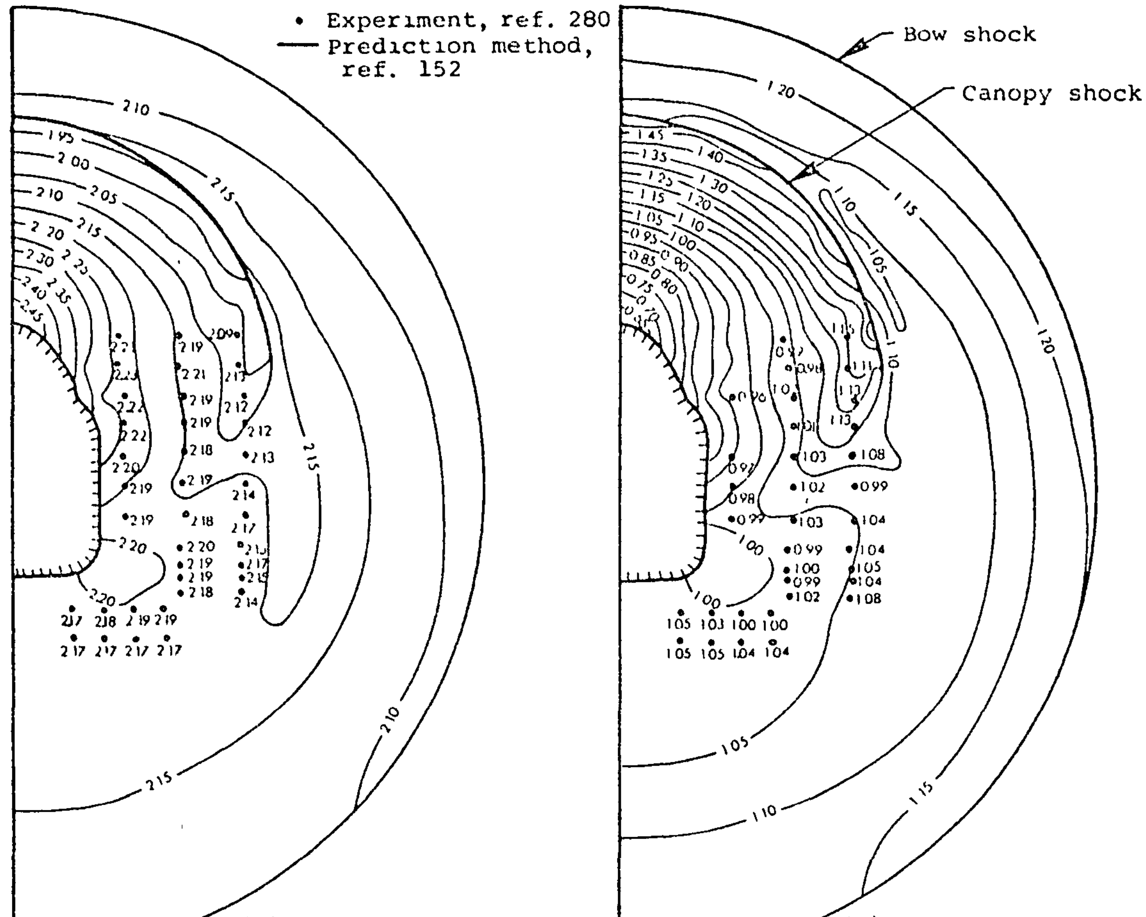

(a) Local Mach number.

(b) Local static pressure ratio.

Figure 104.- Flow field in the vicinity of a fuselage configuration, $M_\infty = 2.2$, $\alpha = 5^\circ$.

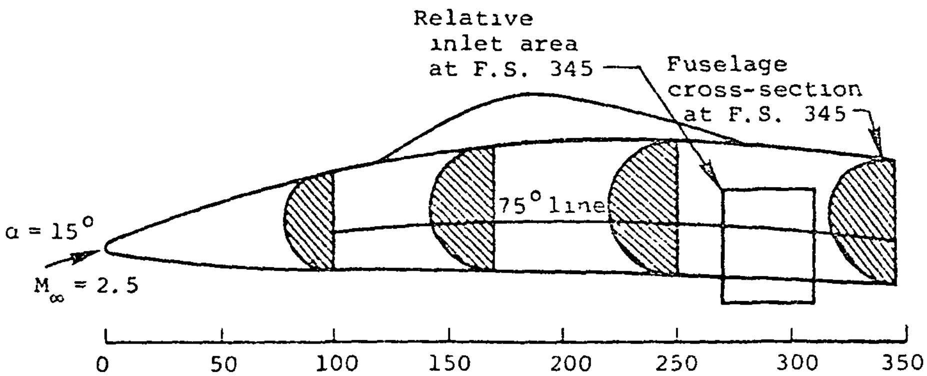

(a) Tailor-Mate fuselage configuration.

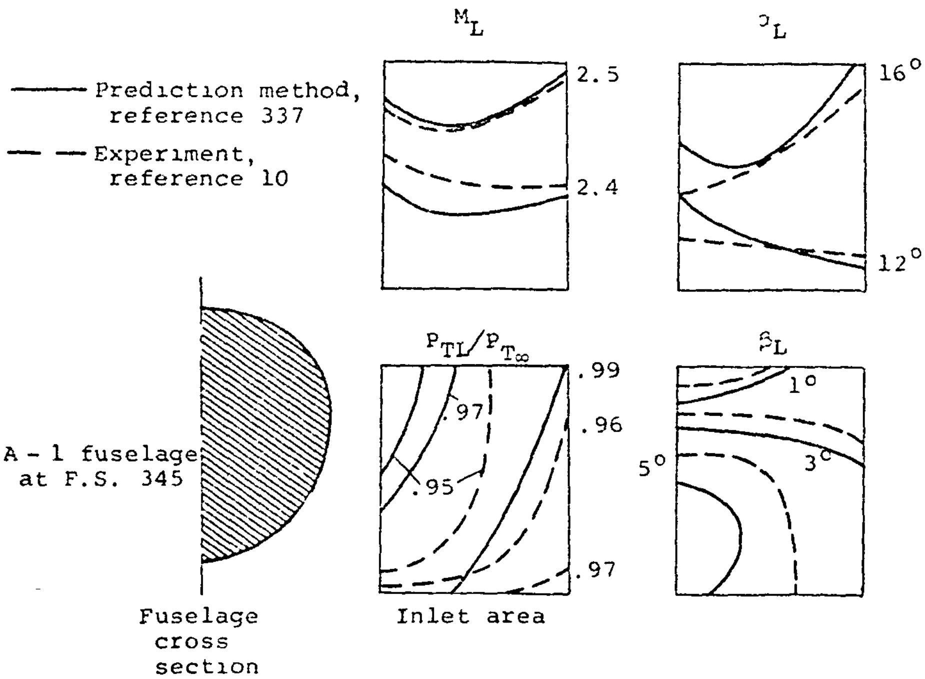

(b) Contour plots of flow properties at inlet face.

Figure 105.- Flow field in the vicinity of the Tailor-Mate fuselage configuration, $M_\infty = 2.5$, $\alpha = 15^\circ$

	Experiment	Prediction method, reference 383
Re_x	3.6×10^5	4.2×10^5
Shock, sonic lines	⊙	———

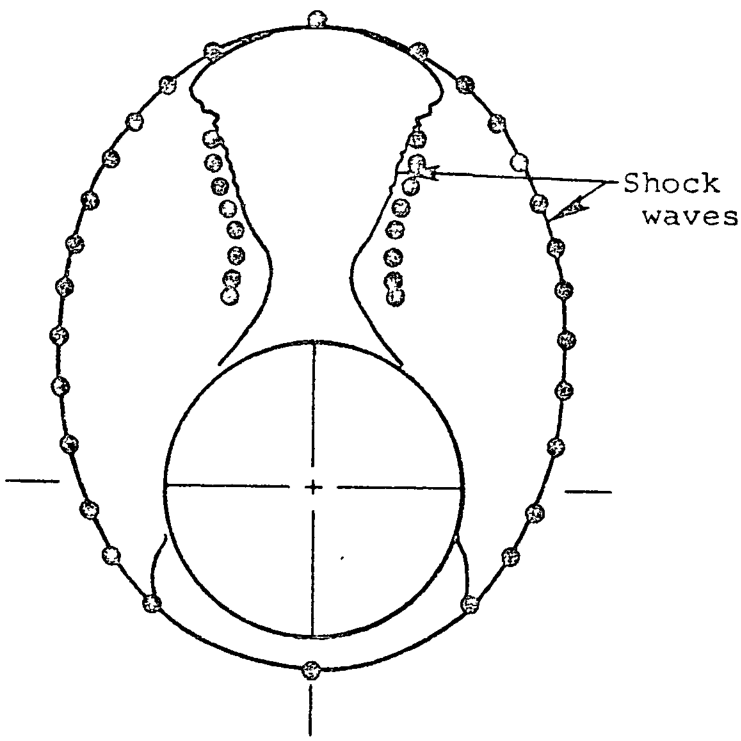

Figure 106.- Comparison of calculated and experimental flow-field features for a sharp 10° half-angle cone, $M_\infty = 7.95$, $\alpha = 24^\circ$.

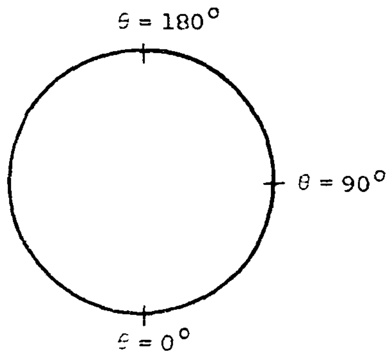

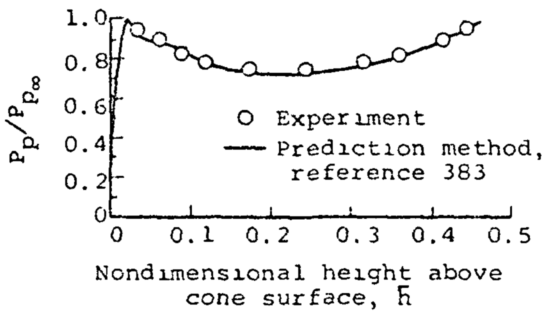

(a) $\theta = 168^\circ$.

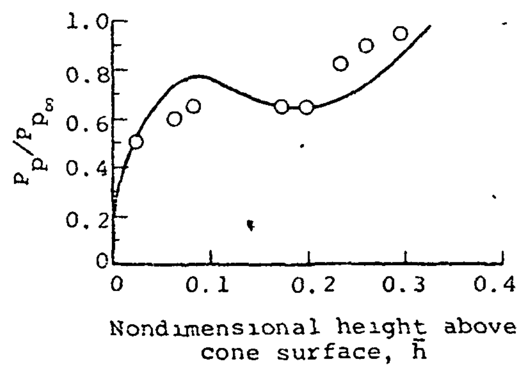

(b) $\theta = 152^\circ$.

Figure 107.- Comparison of predicted and experimental pitot-pressure profiles for a sharp 5° cone, $M_\infty = 1.8$, $\alpha = 12.5^\circ$.

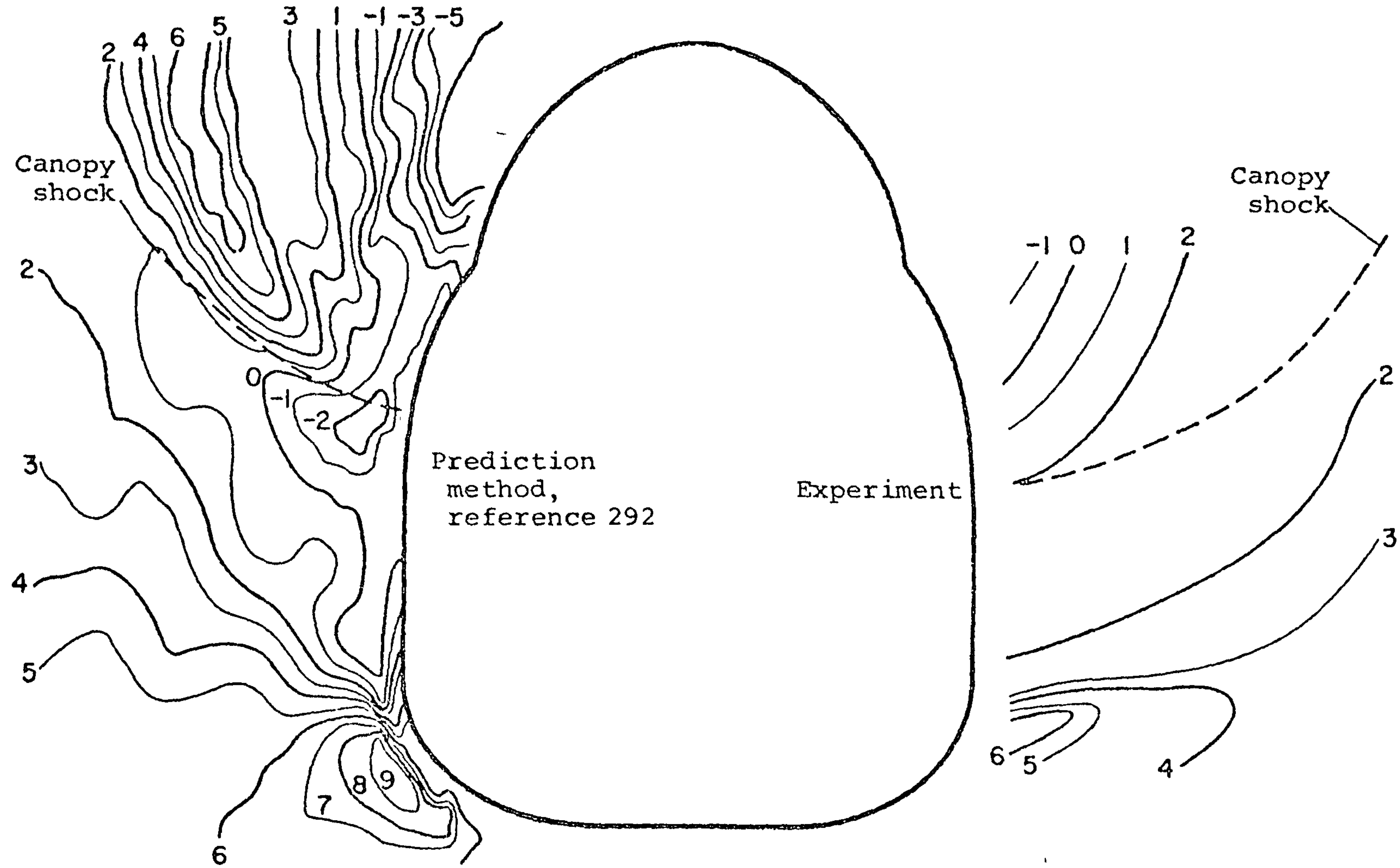

(a) Local sidewash angle, degrees.

Figure 108.- Flow field contours in the vicinity of a fuselage configuration; $M_\infty = 2.5$, $\alpha = 15^\circ$.

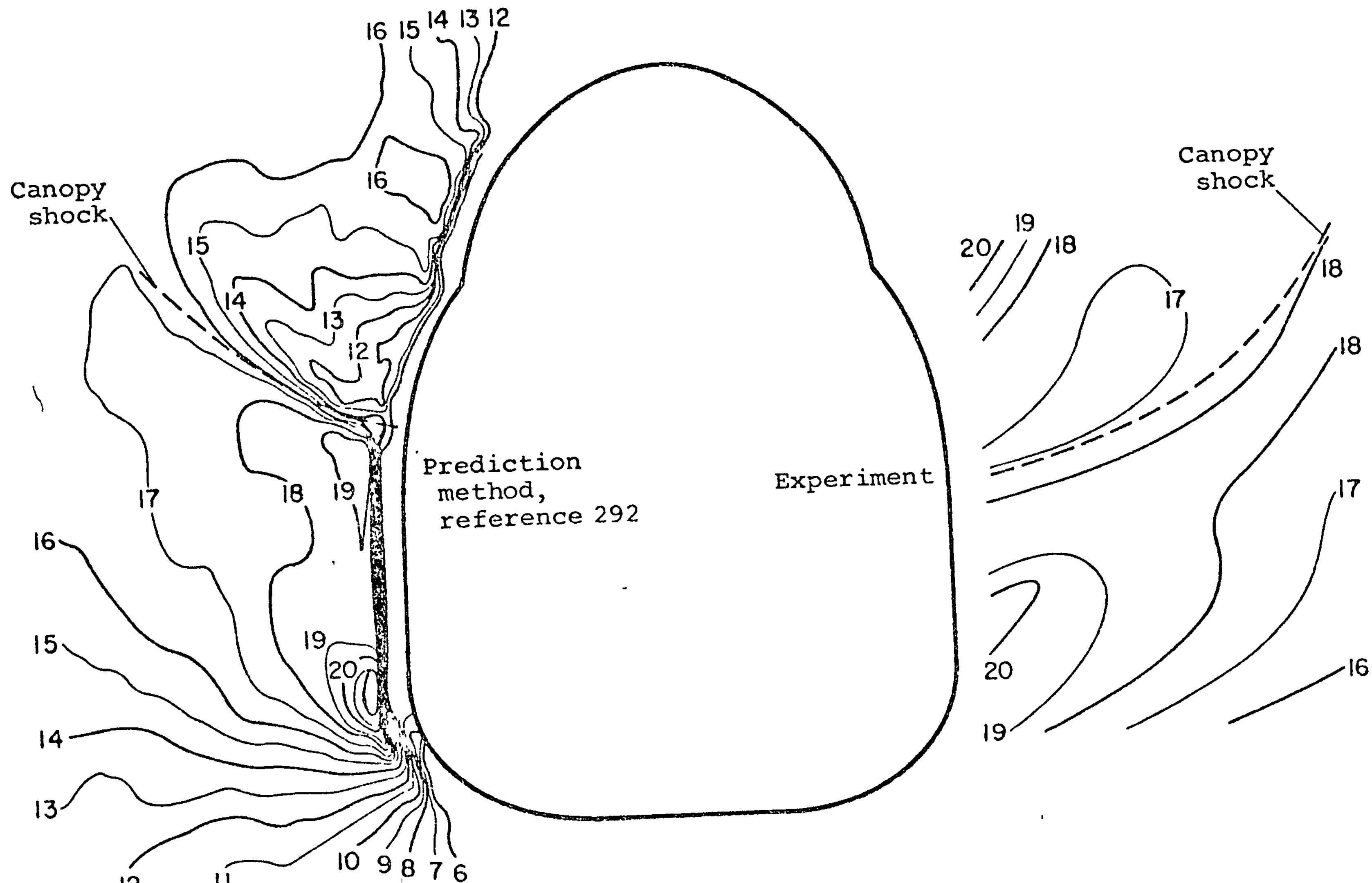

(b) Local upwash angle, degrees.

Figure 108.- Continued.

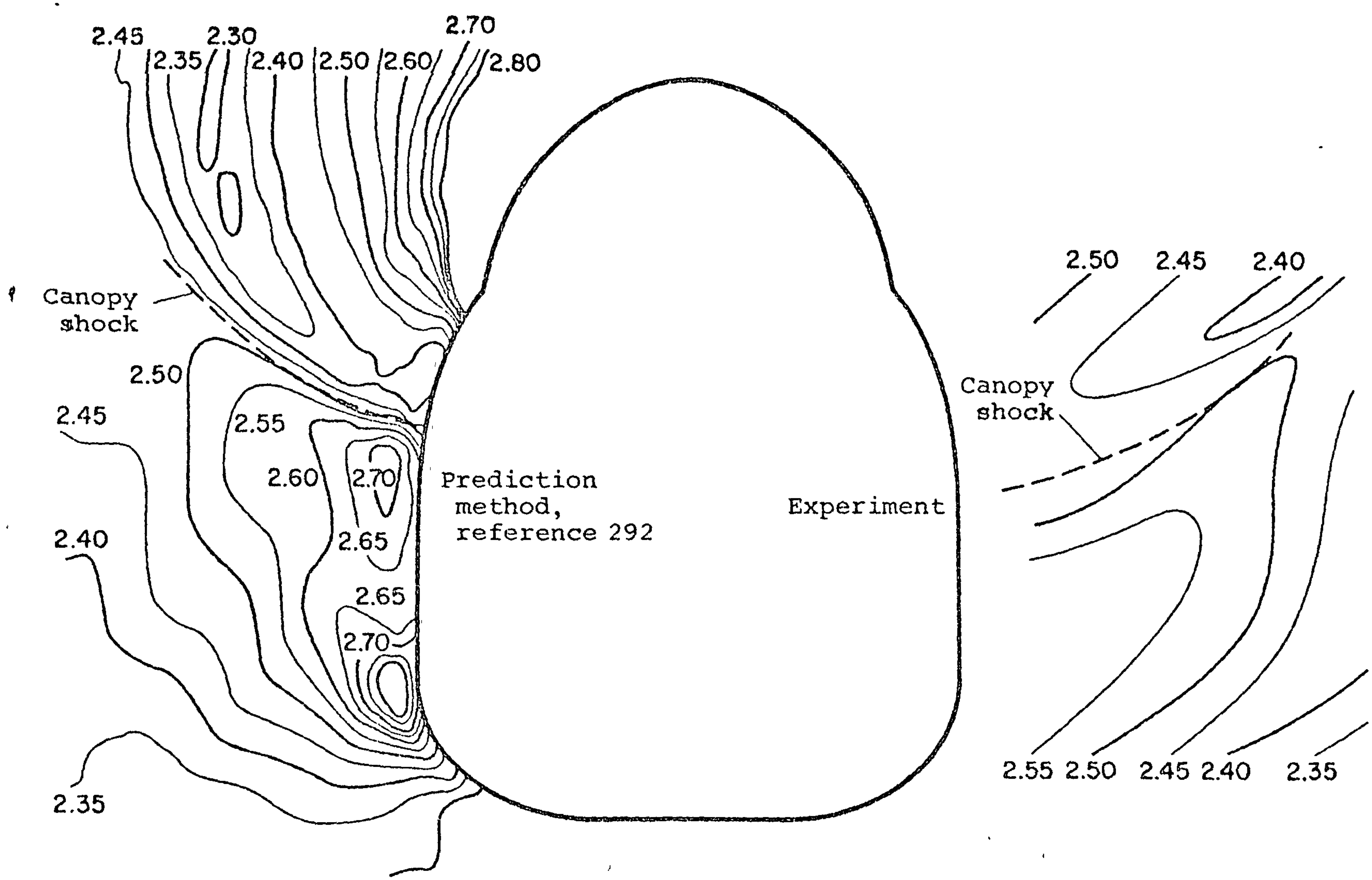

(c) Local Mach number.

Figure 108.- Concluded.

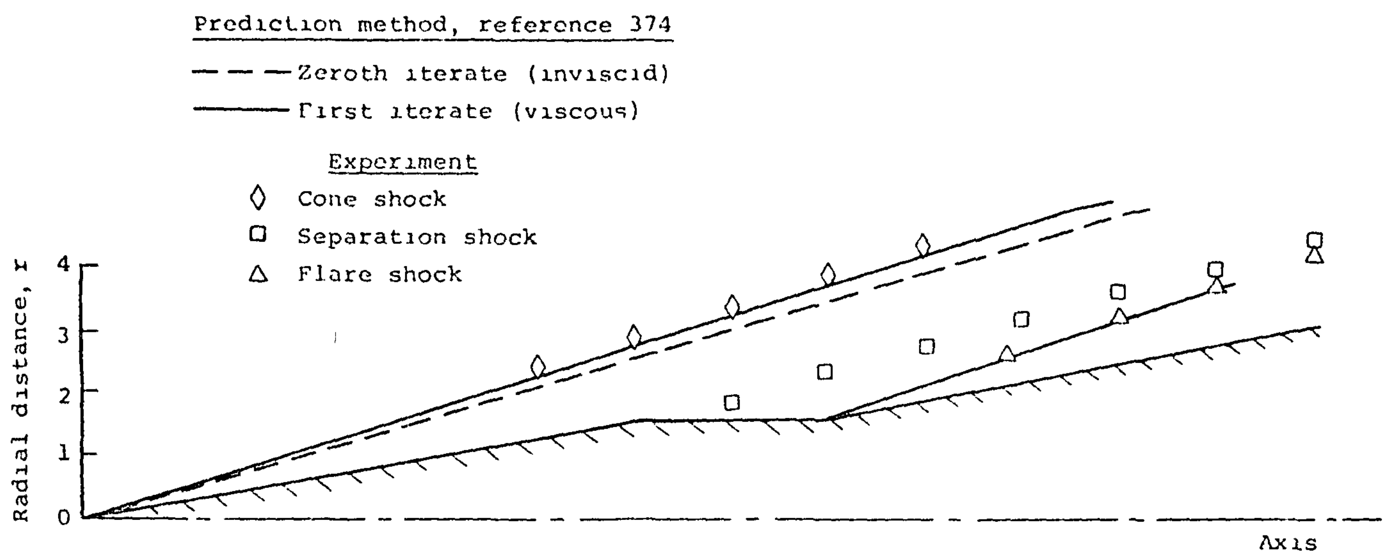

Figure 109.- Shock shapes for a cone-cylinder-flare configuration, $M_\infty = 4.42$, $\alpha = 0^{\circ}$.

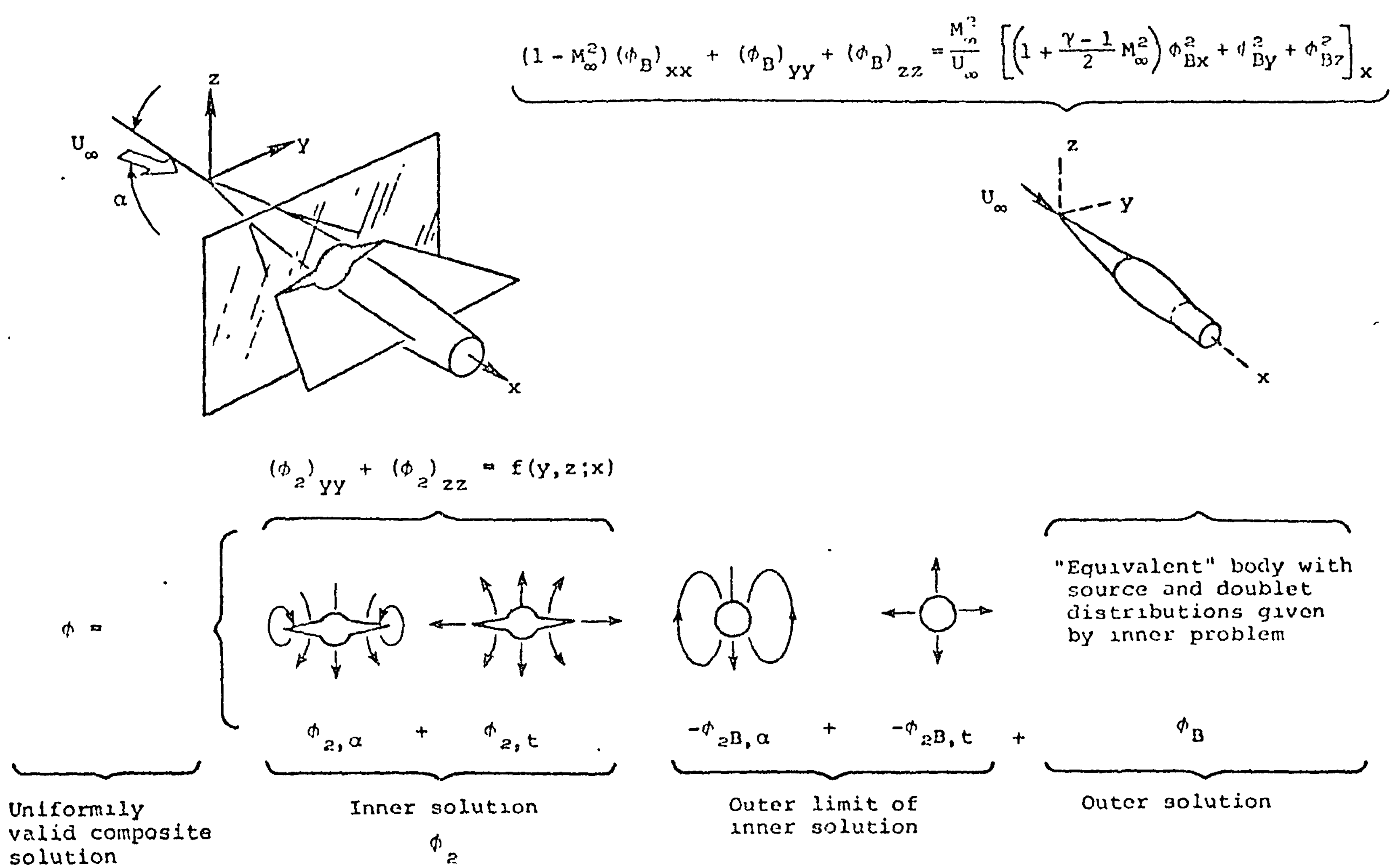

Figure 110.- Schematic representation of transonic equivalence rule (ref. 341) for slender wings and bodies.

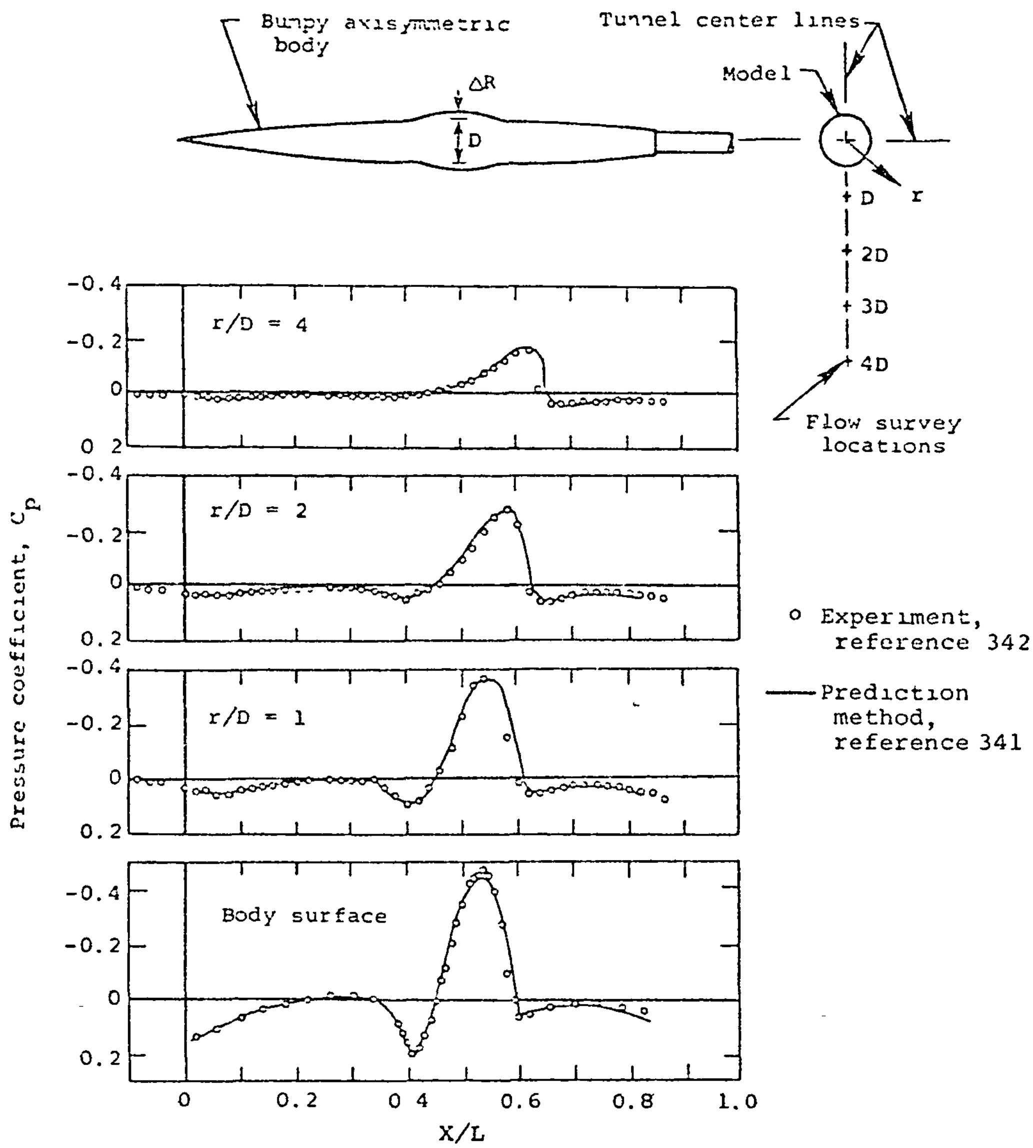

Figure 111.- Body surface and flow-field pressure coefficient in the vicinity of a bumpy axisymmetric body, $M_\infty = 0.975$, $\alpha = 0^o$.

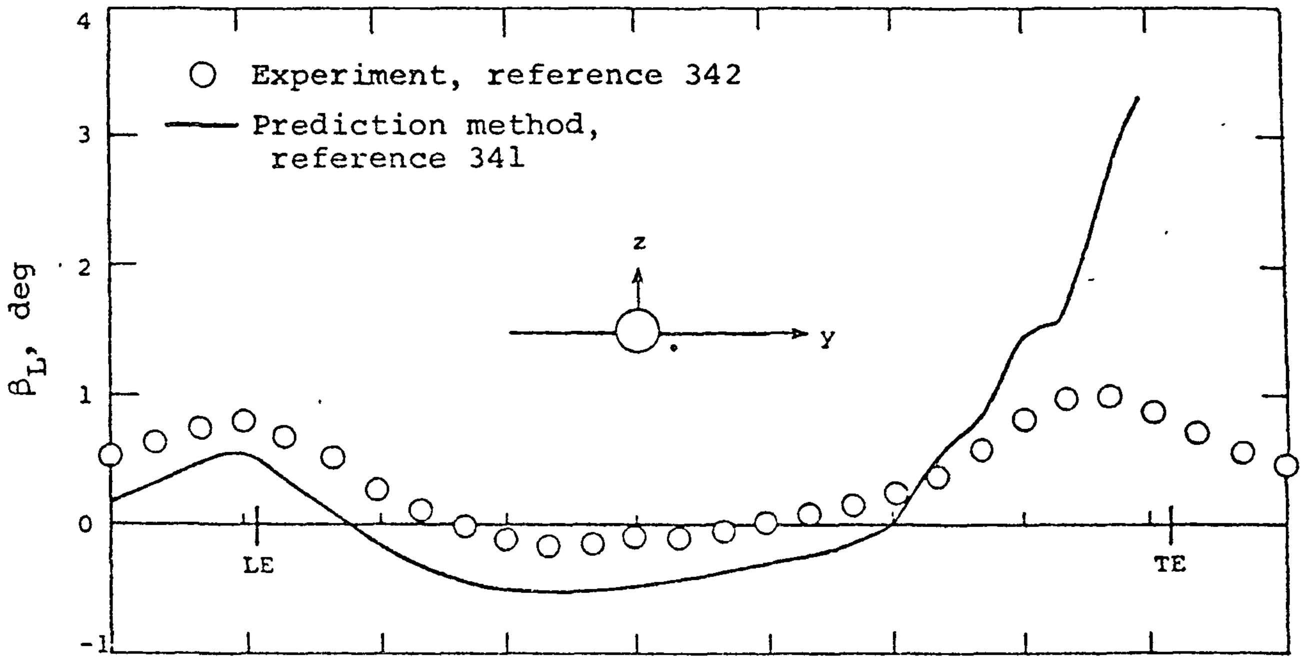

(a) Local sidewash angle, Y = 2.0 in.

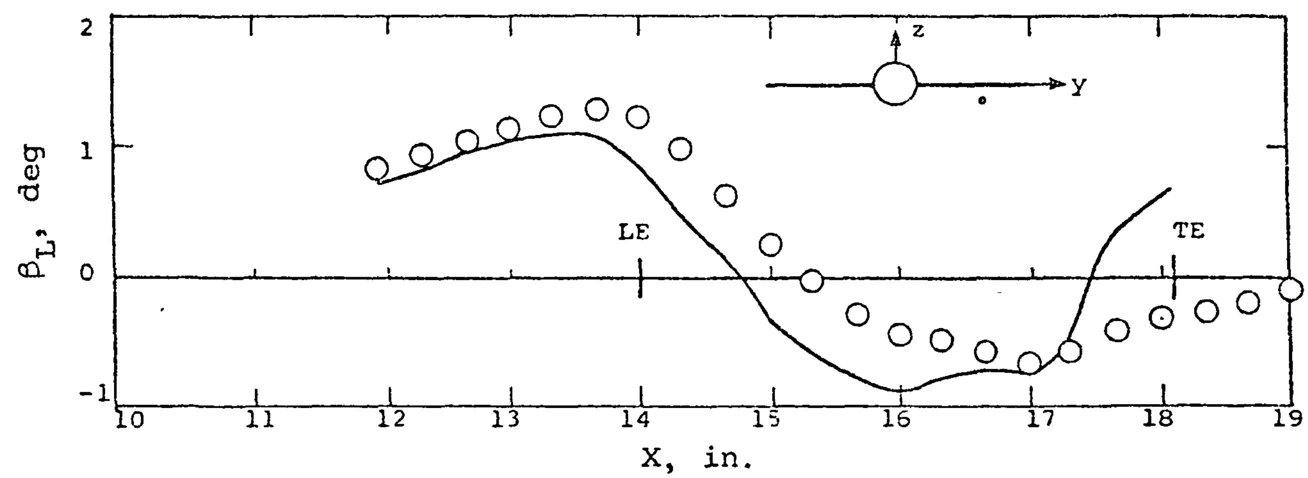

(b) Local sidewash angle, Y = 5.5 in.

Figure 112.- Flow field under the wing of a scaled F-16 wing-body configuration, $M_\infty = 0.925$, $\alpha = 0^\circ$, Z = -1.0 in.

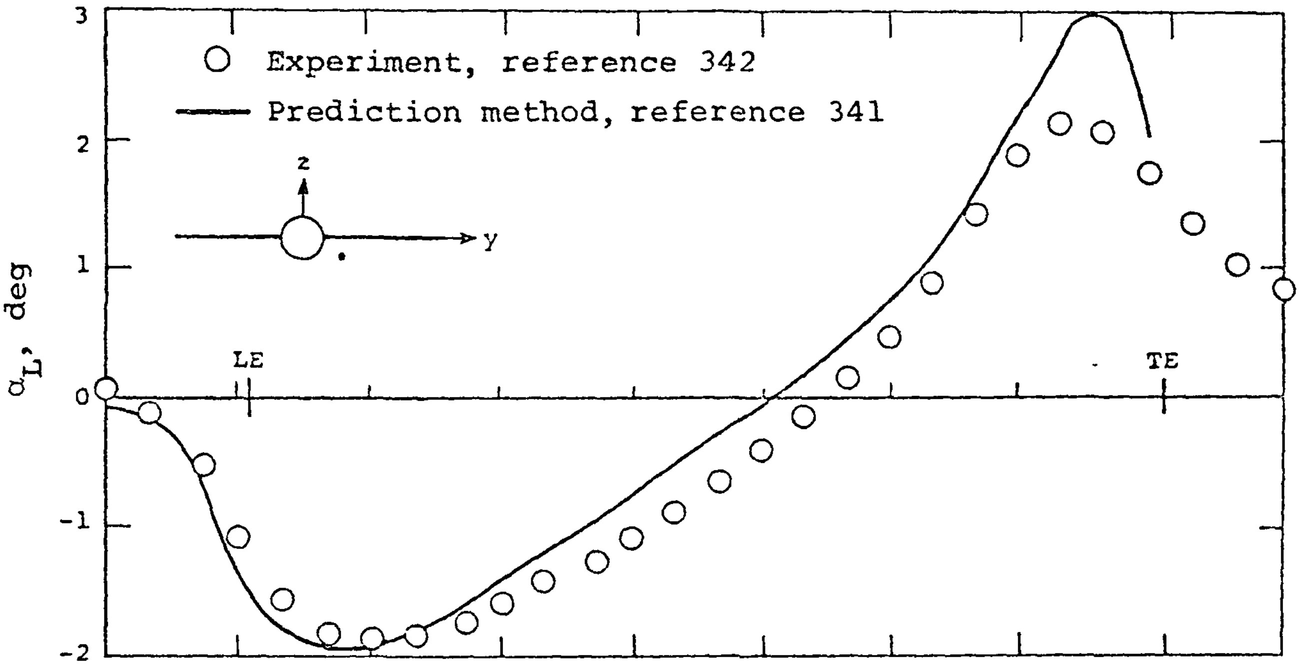

(c) Local upwash angle, Y = 2.0 in.

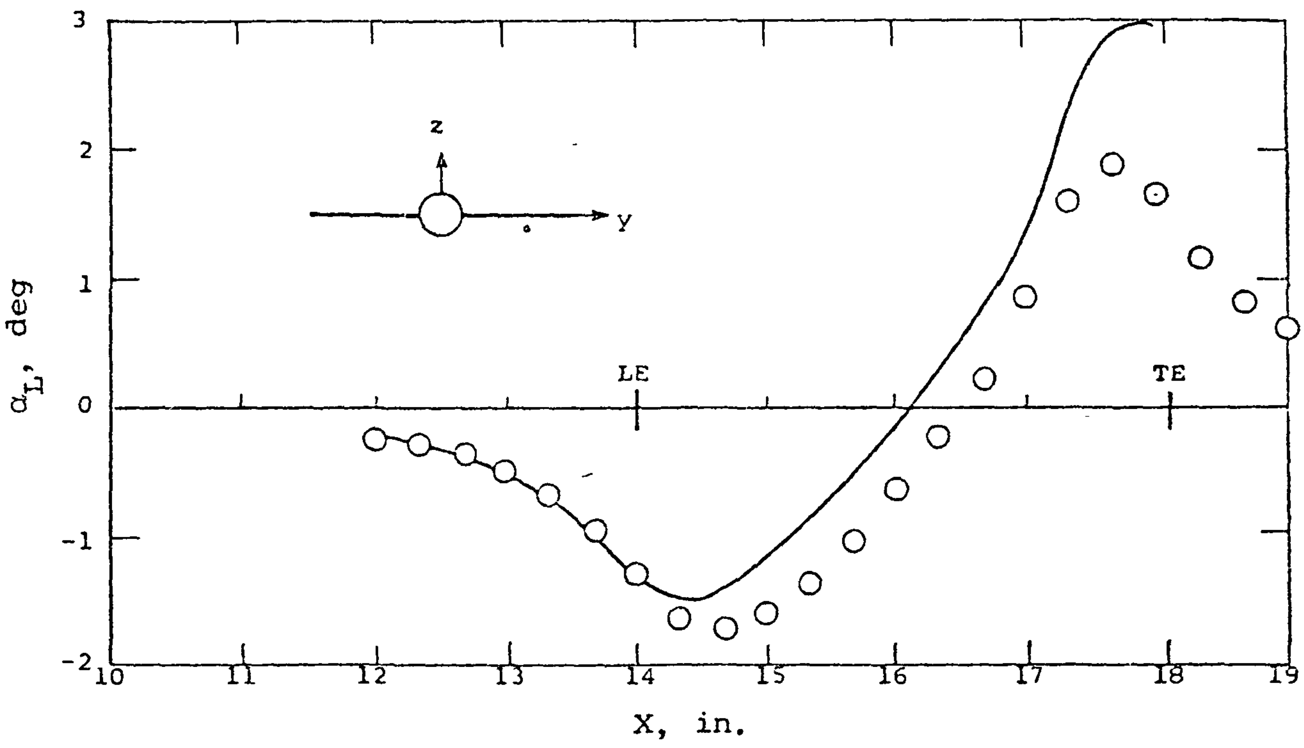

(d) Local upwash angle, Y = 5.5 in.

Figure 112.- Concluded.

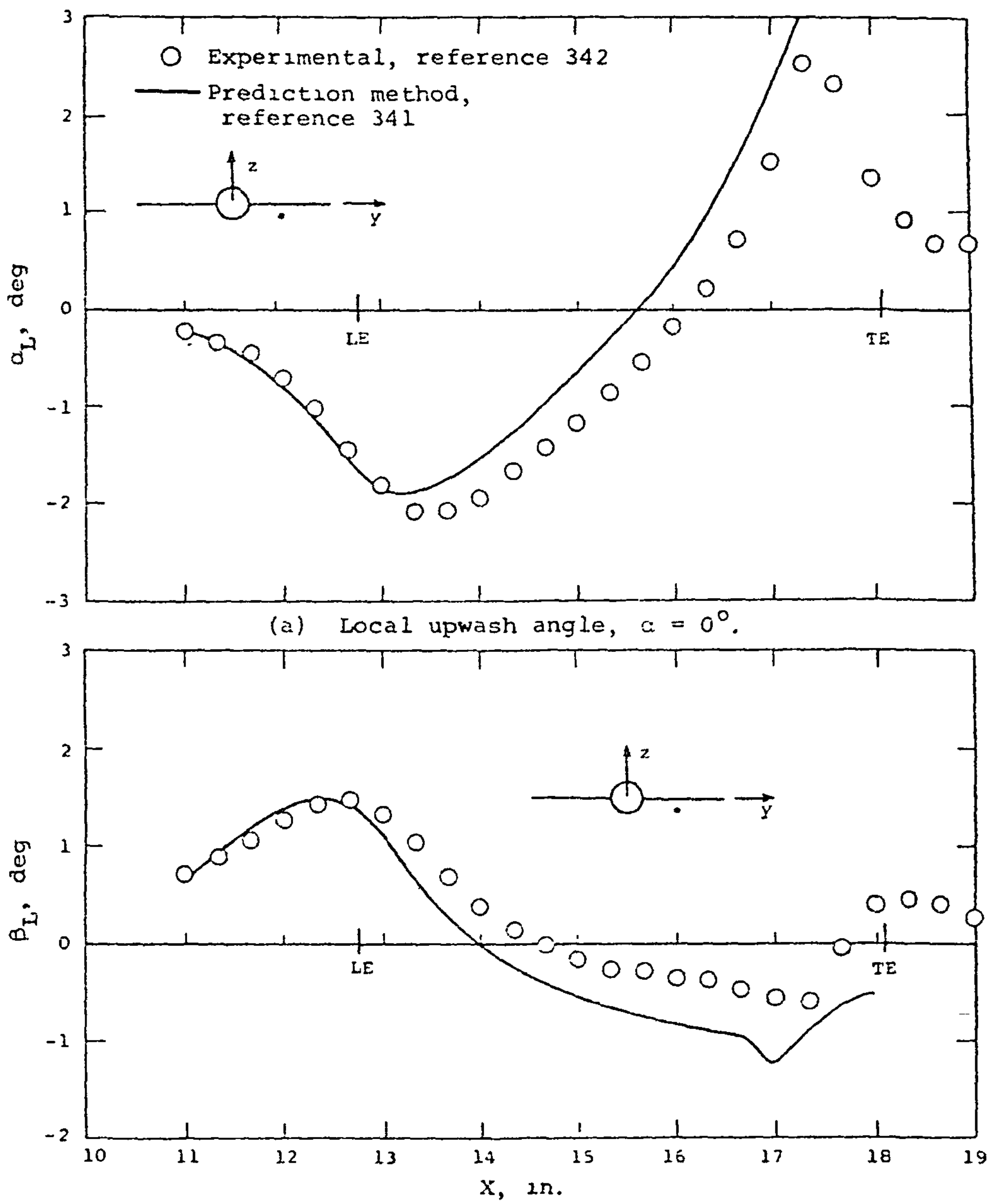

(b) Local sidewash angle, $\alpha = 0^\circ$

Figure 113.- Flow fields under the wing of a scaled F-16 wing-body configuration, $M_\infty = 0.975$, Z = -1 in., Y = 4 in.

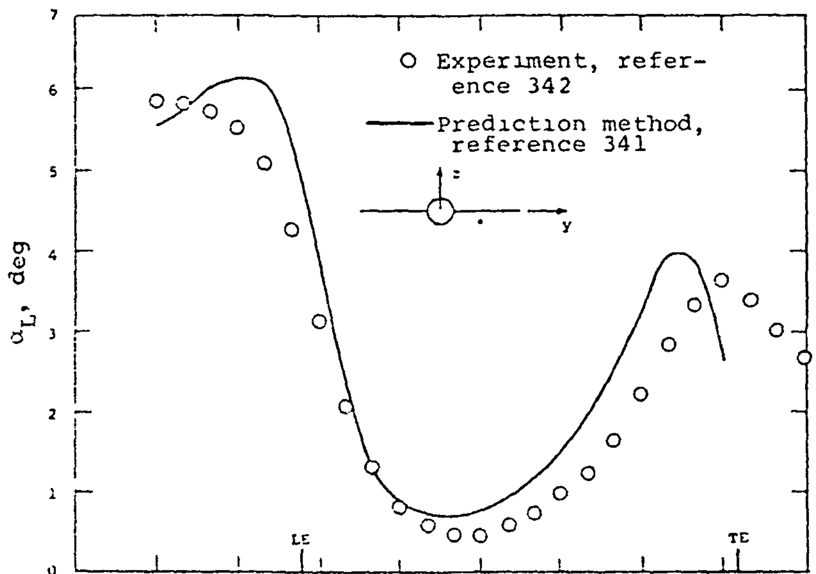

(c) Local upwash angle, $\alpha = 5^{o}$.

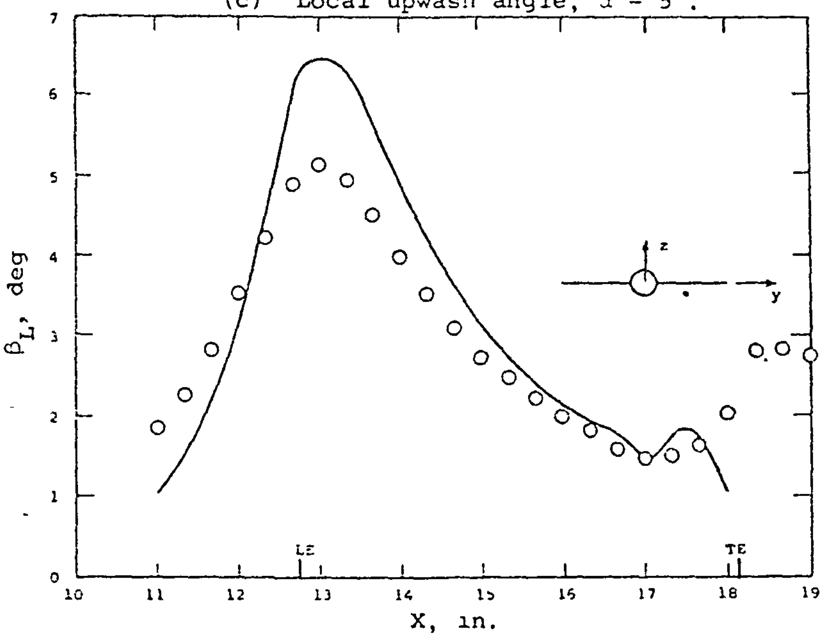

(d) Local sidewash angle, $\alpha = 5^{o}$.

Figure 113.- Concluded.

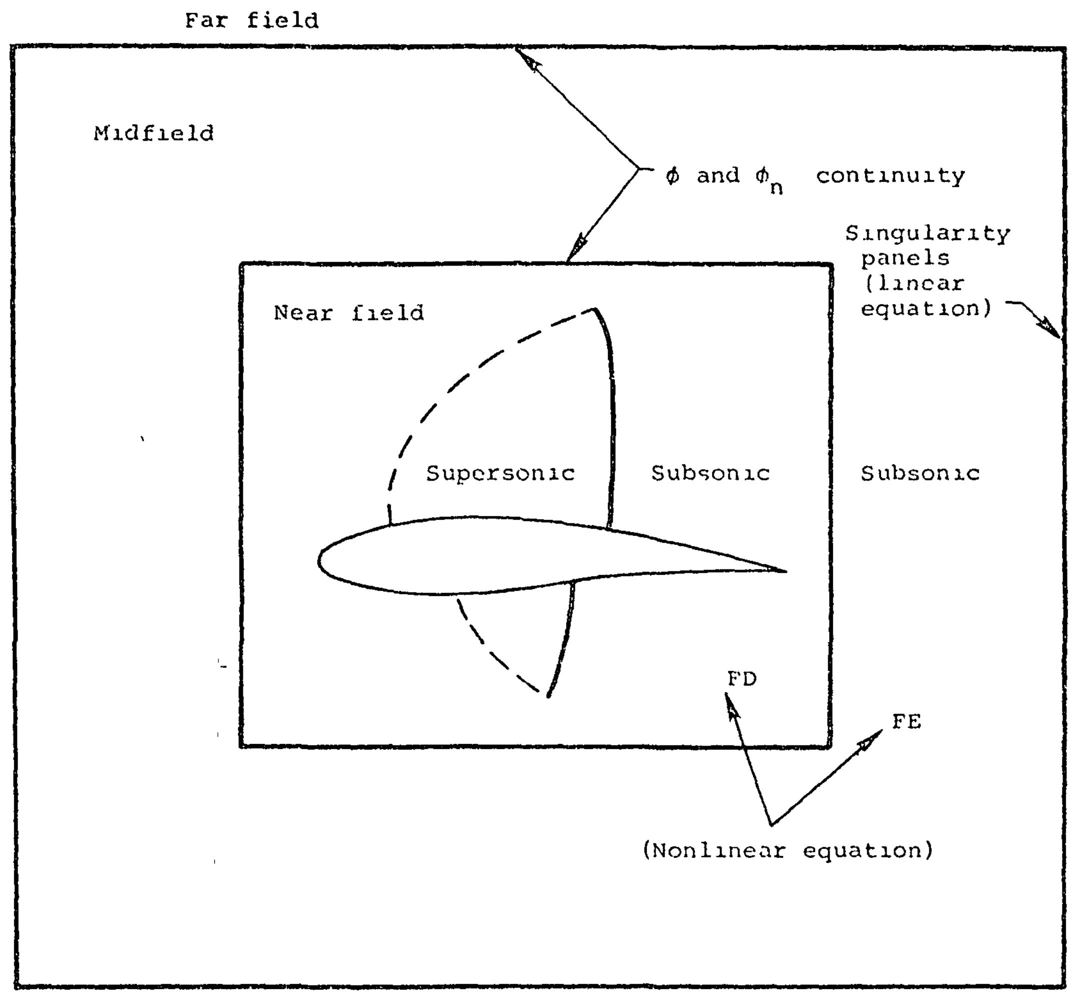

Figure 114.- Schematic representation of flow-field decomposition for far-field matching method (ref. 317).

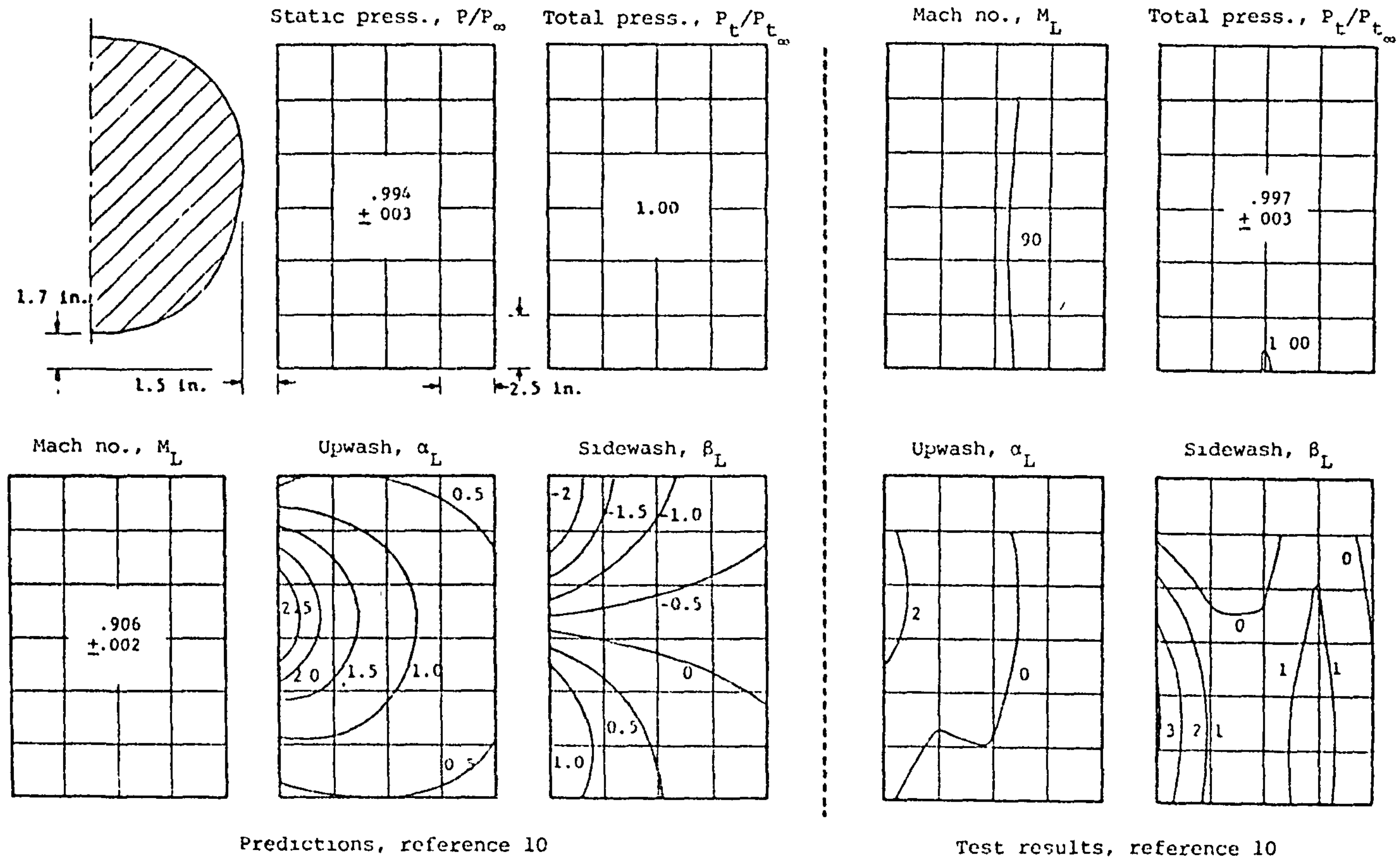

(a) $\alpha = 0^\circ$.

Figure 115.- Flow field at the side of a fuselage configuration, $M_\infty = 0.90$, $\beta = 0^\circ$.

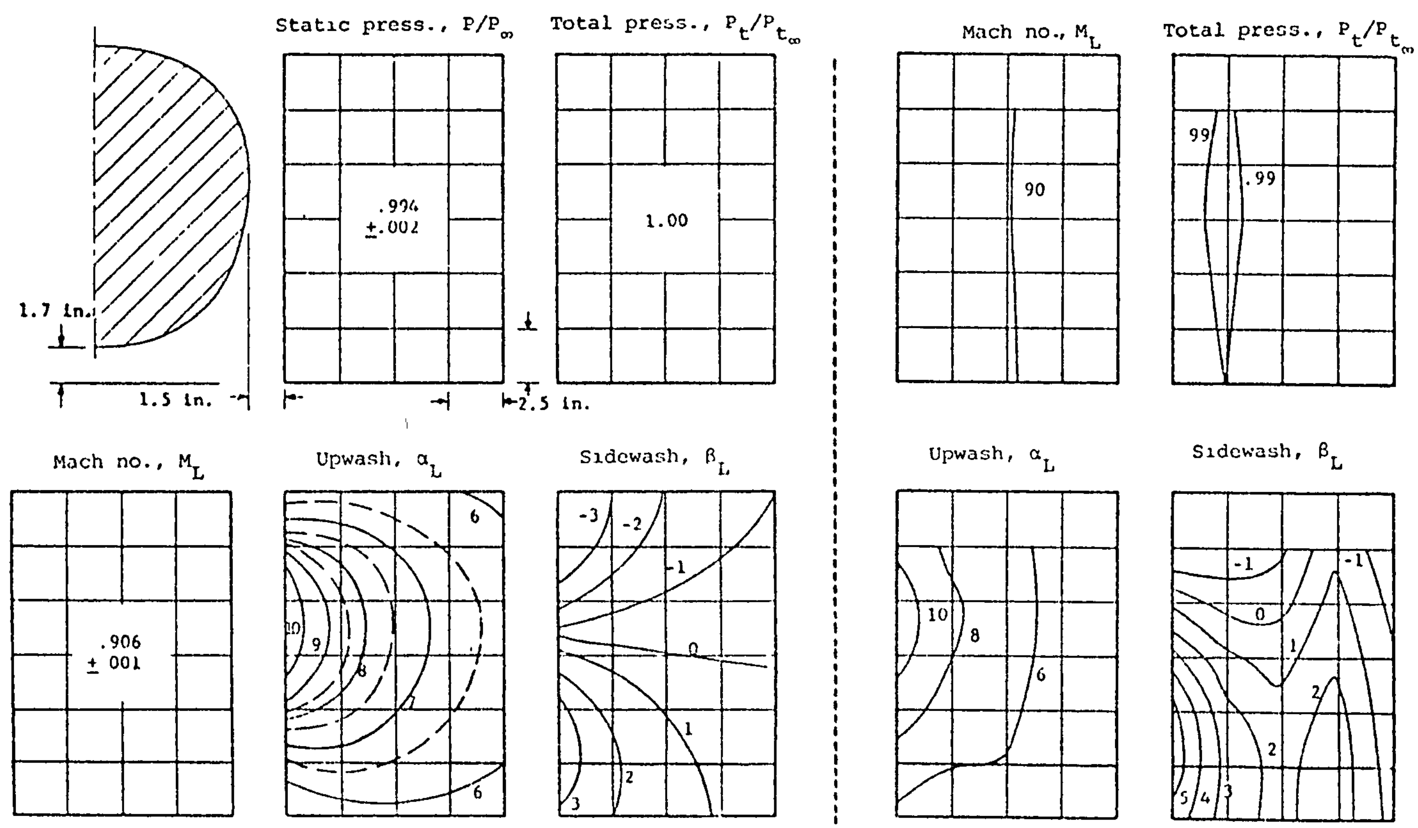

(b) $\alpha = 5^\circ$.

Figure 115.- Concluded.

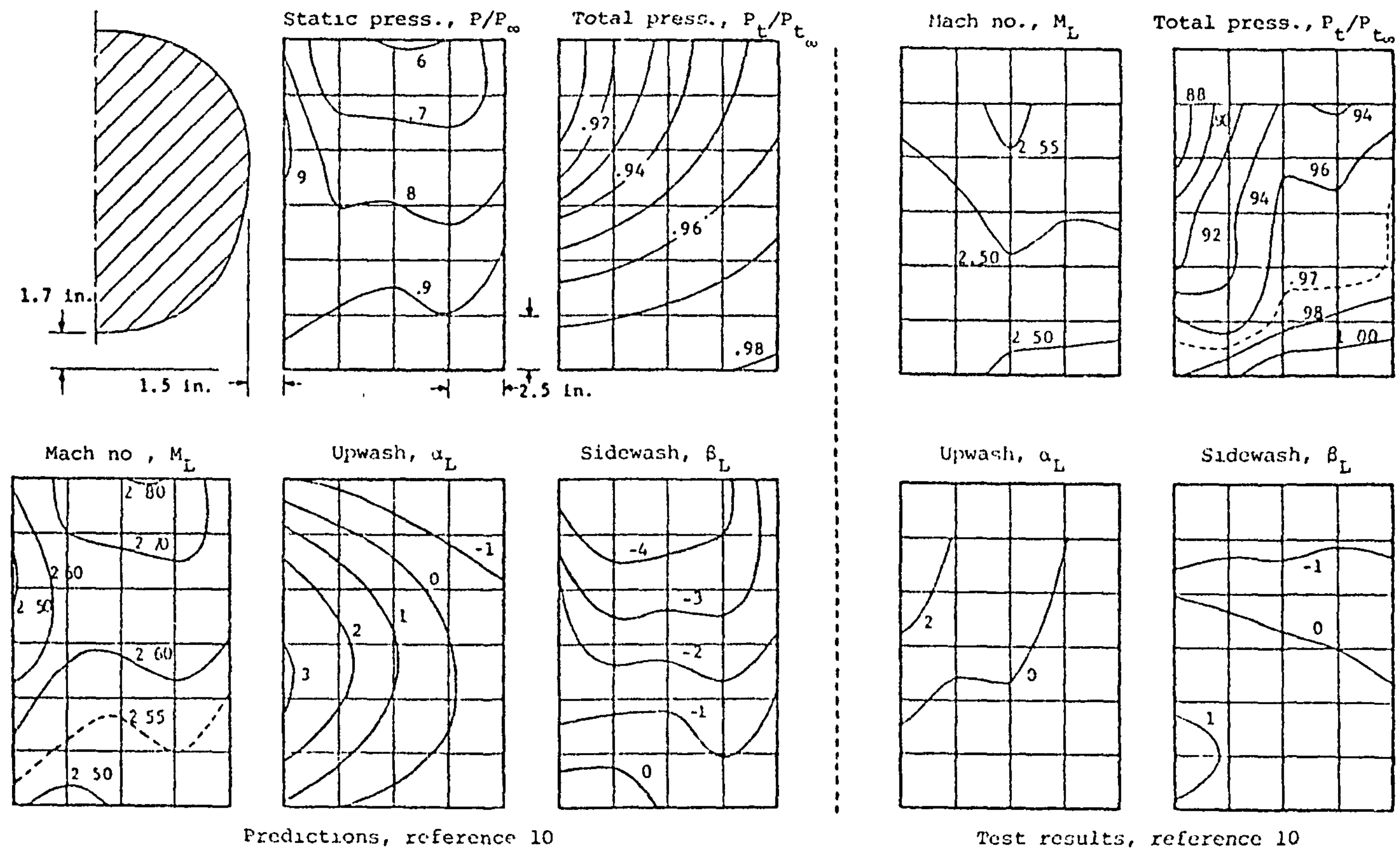

(a) $\alpha = 0^\circ$, $\beta = 0^\circ$.

Figure 116.- Flow field at the side of a fuselage configuration at $M_\infty = 2.5$.

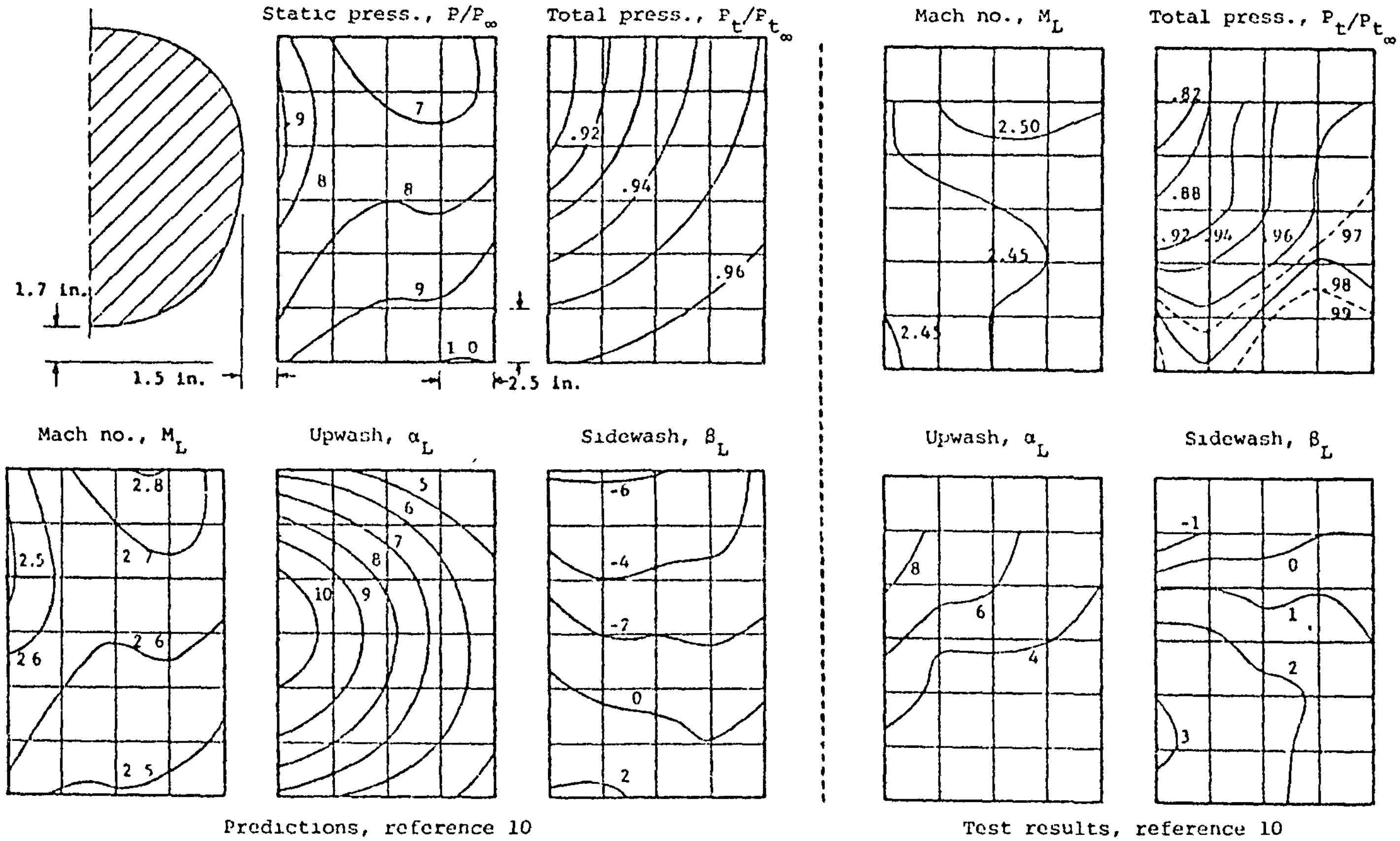

(b) $\alpha = 5^\circ$, $\beta = 0^\circ$.

Figure 116.- Continued.

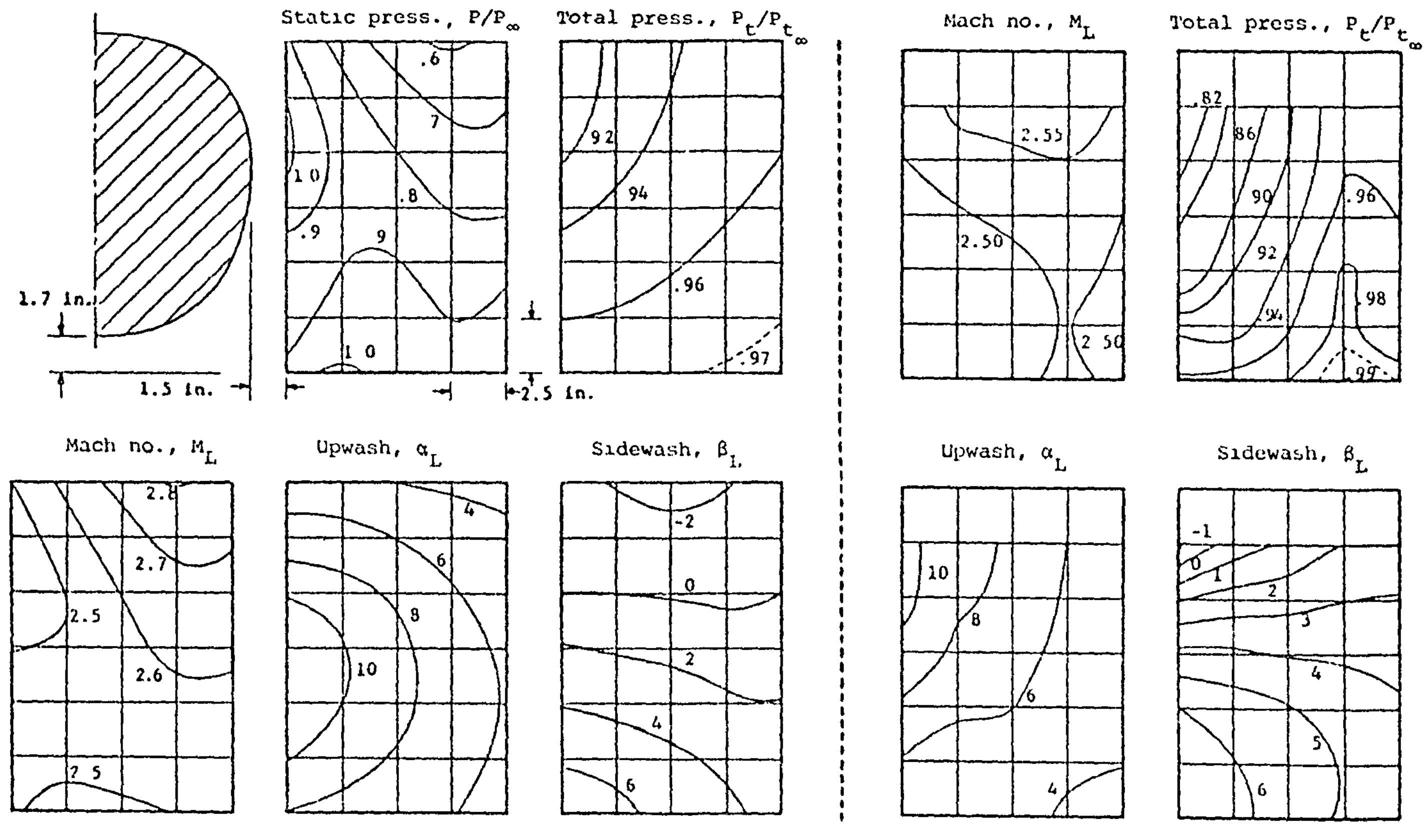

Predictions, reference 10

Test results, reference 10

(c) $\alpha = 5^\circ$, $\beta = 4^\circ$.

Figure 116.- Concluded.

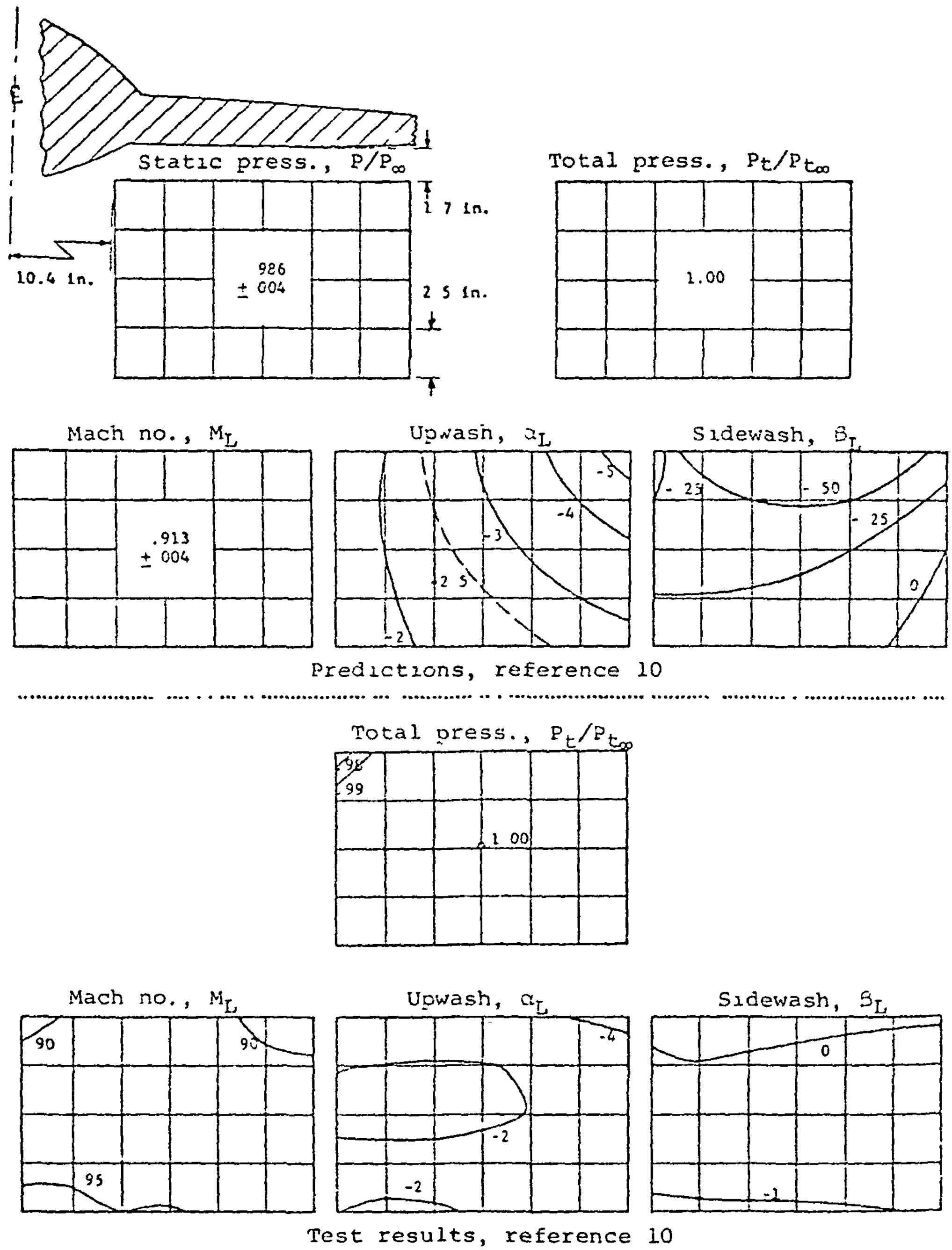

(a) $\alpha = 0^\circ$.

Figure 117.- Flow field under the strake of a wing-fuselage configuration, $M_\infty = 0.90$, $\beta = 0^\circ$.

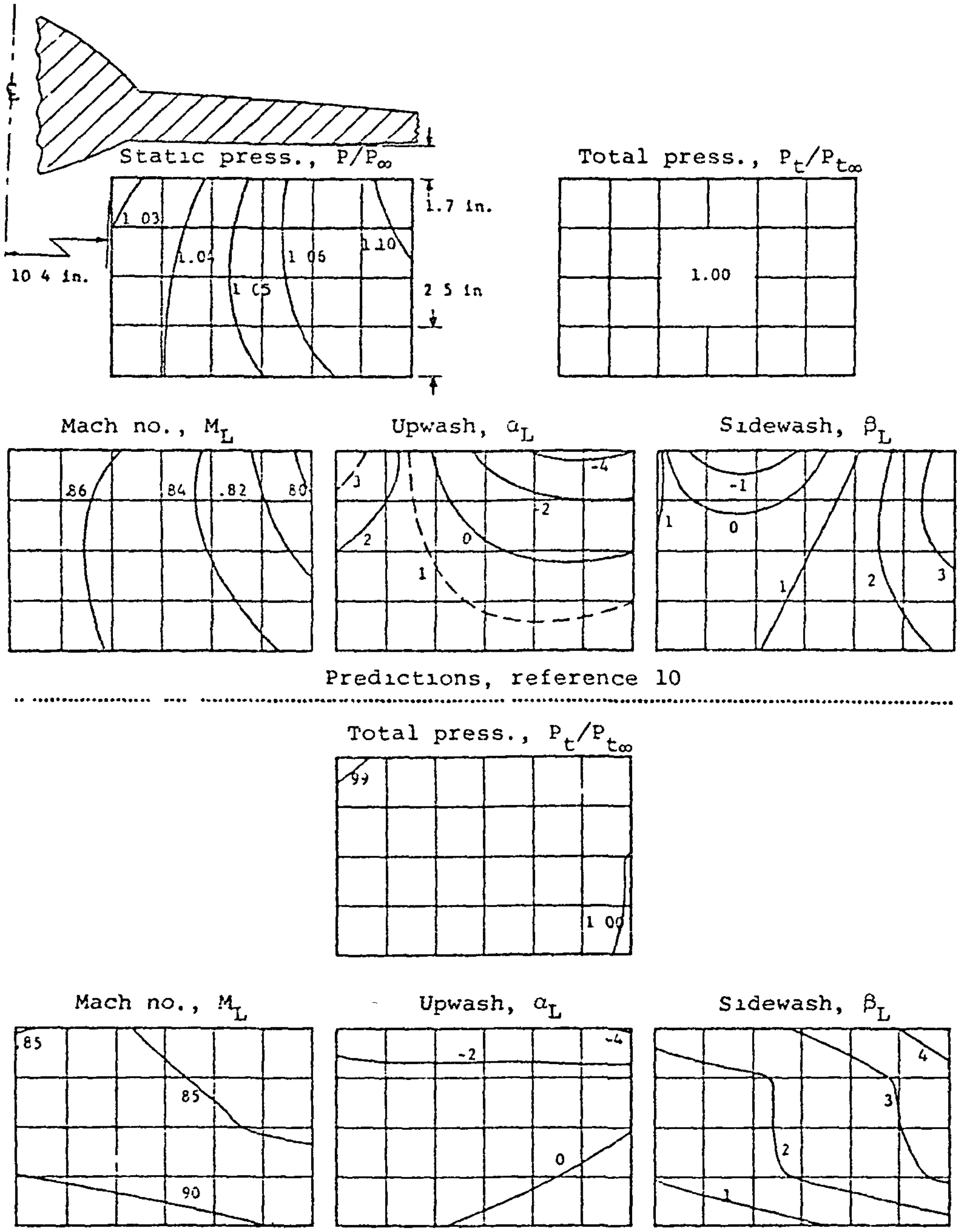

Test results, reference 10

(b) $\alpha = 5^{\circ}$.

Figure 117.- Concluded.

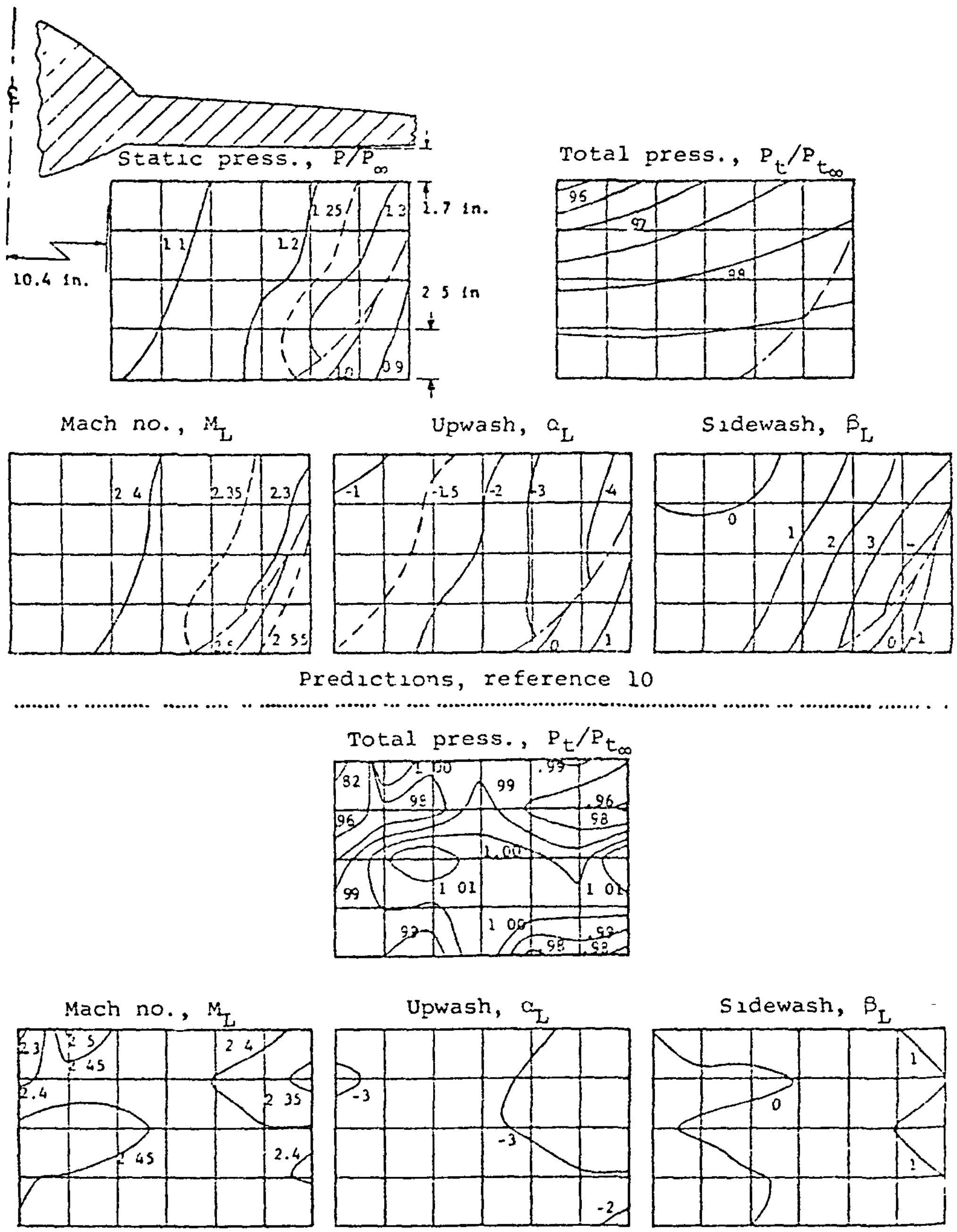

(a) $\alpha = 0^{\circ}$, $\beta = 0^{\circ}$.

Figure 118.- Flow field under the strake of a wing-fuselage configuration, $M_{\infty} = 2.5$.

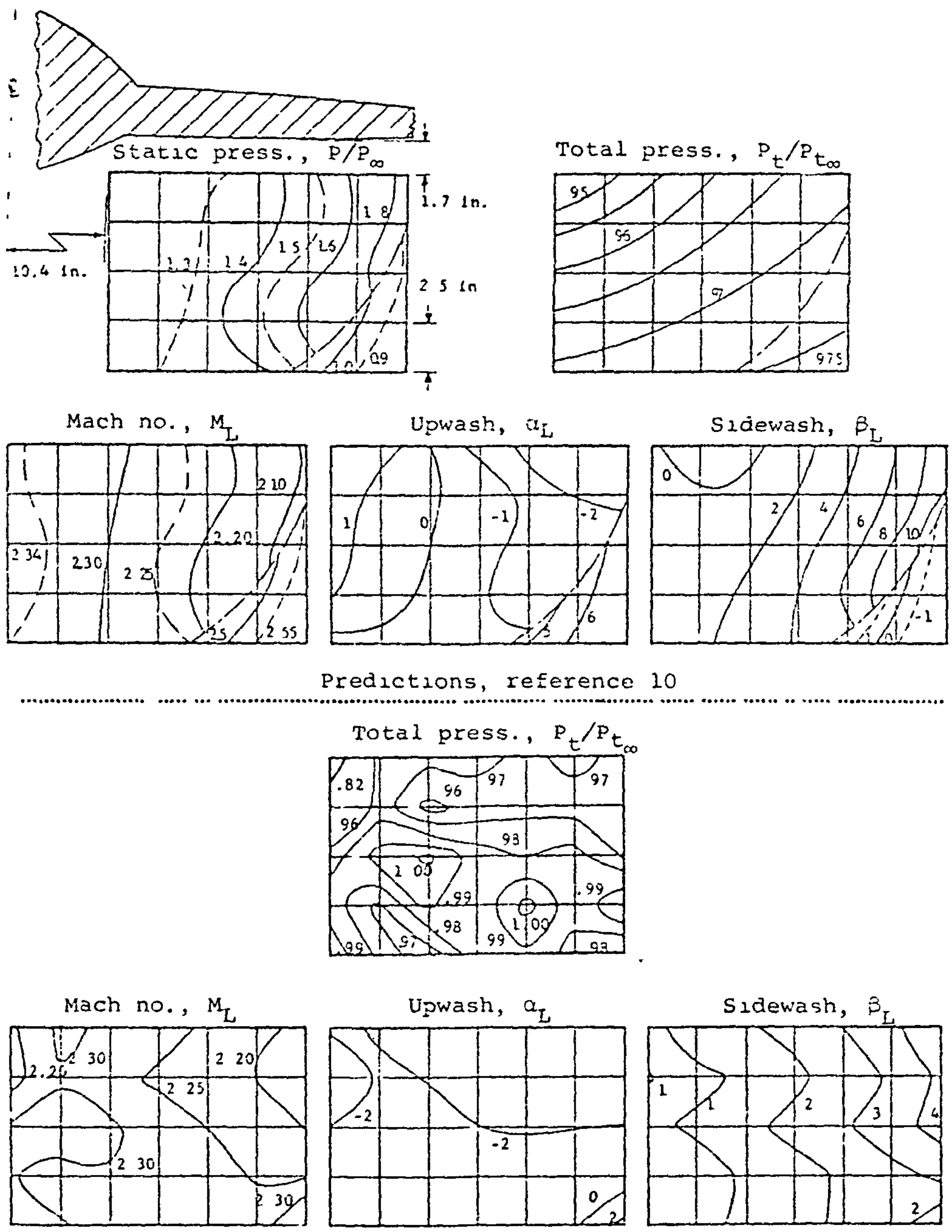

Test results, reference 10

(b) $\alpha = 5^\circ$, $\beta = 0^\circ$.

Figure 118.- Continued.

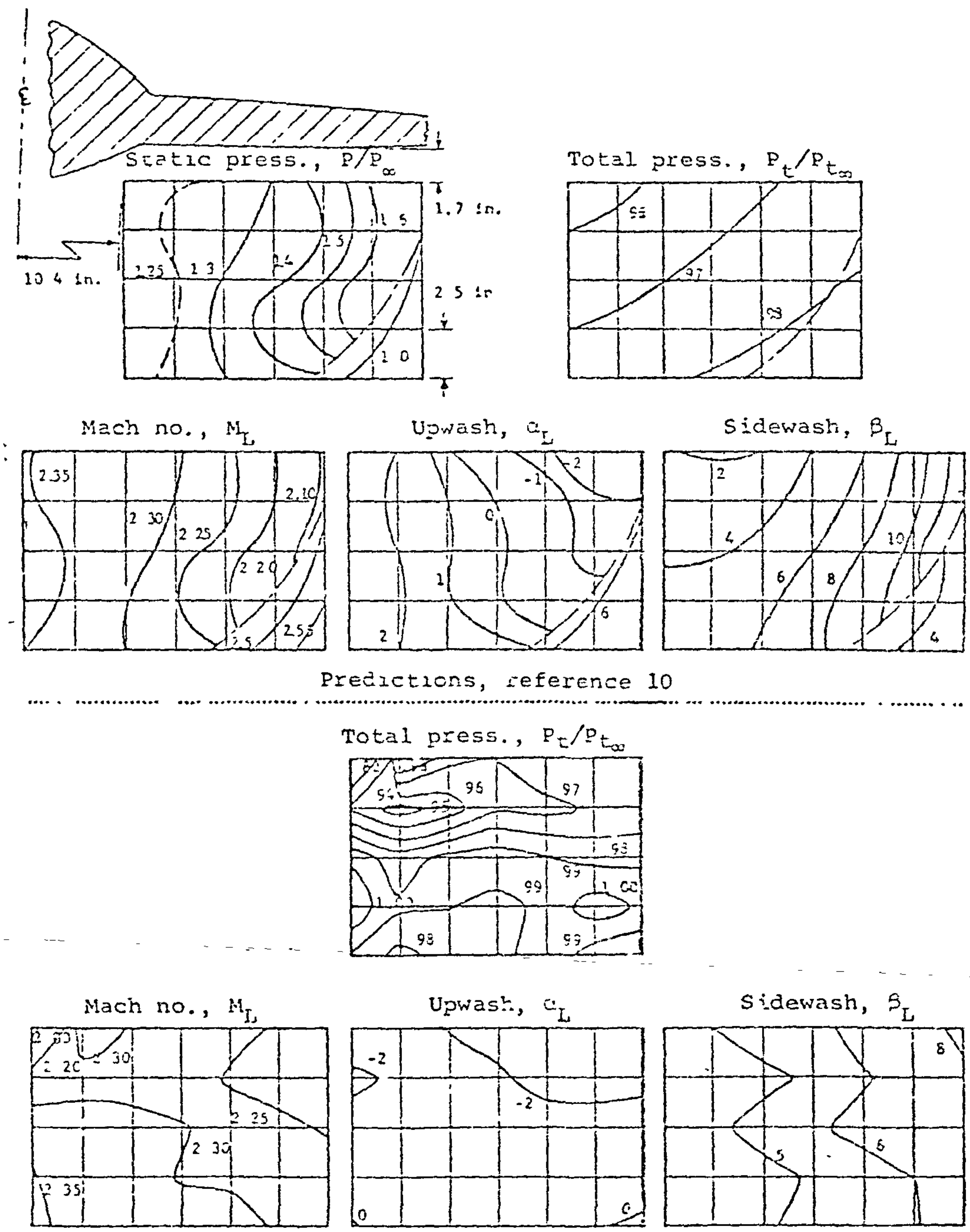

Test results, reference 10

(c) $\alpha = 5^\circ$, $\beta = 4^\circ$.

Figure 118.- Concluded.